Bioresponsive Polymer Therapeutics Containing Coiled-Coil Motifs

Samuel Philip Edward Deacon

M.Pharm. (Hons.) M.R.Pharm.S.

A thesis submitted to Cardiff University in partial fulfilment of the requirements for the degree of Doctor of Philosophy

Centre for Polymer Therapeutics

Welsh School of Pharmacy

Cardiff University

United Kingdom

ProQuest LLC
789 East Eisenhower Parkway
P.O. Box 1346
Ann Arbor, MI 48106-1346

ACKNOWLEDGEMENTS

First and foremost, I would like to express my sincere appreciation to my supervisor Professor Ruth Duncan for her insight, support and passion for this project. I am also indebted to my second supervisor Professor Harm-Anton Klok for his enthusiasm and technical advice in particular with regard to peptide and polymer chemistry. I would like to thank the biotechnology and biological sciences research council (BBSRC) for funding my Ph.D. studentship; it has been a pleasure to have the opportunity to contribute to a very exciting and cutting-edge field of research.

I would also like to thank Bojana Apostolovic whom I met as a collaborator at École Polytechnique Fédérale de Lausanne (EPFL) but in the course of this work has become a great friend. Furthermore, I would like to acknowledge Dr Maria Vicent for her continued support and advice since my M.Pharm. research project, and for the collaboration that she made possible with Professor Antonio Pineda-Lucena and Drs Rodrigo Carbajo and Annie Schott at Centro de Investigacion Principe Felipe (CIPF). My thanks also go to Dr Arwyn Jones and Dr Simon Richardson for their guidance and intellectual support with regard to cell and molecular biology, Dr Konrad Beck for assistance with circular dichroism (CD) spectroscopy and Dr Robert Jenkins and Robin Hicks for their help with mass spectroscopy.

I would like to acknowledge friends and colleagues at the Welsh School of Pharmacy, EPFL and CIPF (past and present): Bal, Catherine, Chris, Danielle, Dejan, Edd, Elaine, Ghaith, Harald, Joe, Keng, Kerri, Francesca, Lucile, Mark, Mat, Monerah, Maarten, Wendy and Wing. It has been a pleasure working and socialising with you all.

Distraction from the highs and lows of research was found in Ju Jitsu culminating in achieving the level of Shodan shortly before the end of this thesis. Thanks go to Sensei's Mark Williams (Smiley) and Rodd Nunn for their fun yet, exceptional teaching, and training partners and friends Tom Hill and Russell Sykes.

The completion of this Ph.D. would not have been possible without the support of truly great friends: Peter Arthure, Nicholas (Mr Chang) Hall, Paul Welford, Gerard Byrne, Chris Robinson and Chris Trapp and the belief and confidence of my whole family, especially, my Mother and Grandmother.

Finally, a very special thank you goes to my fiancée Oriana White for her friendship, unerring support, fun and most importantly her ability to always make me laugh. Not to mention opening my eyes to the delights and charm of Japan.

I have always known
That at last I would
Take this road, but yesterday
I did not know that it would be today

Tsui ni yuku
Michi to wa kanete
Kikishi kado
Kino kyo to wa
Omowazarishi wo

遂に行く
道とは予て
ききしかど
昨日今日とは
思わざりしを

Ariwara no Narihara
9th Century

ABSTRACT

Polyethyleneglycol (PEG) conjugates of peptides, proteins and an aptamer are in routine clinical use as first generation nanomedicines. Here a new family of polymer therapeutics based on PEG conjugates containing a coiled-coil peptide motif as a molecular switch are proposed. The coiled-coil motif is adopted by many naturally occurring proteins/peptides, including transcription factors key to cancer progression (E2F1/AP-1) and Ebola virus proteins (VP35/GP2). These were chosen as the first targets, however there is potentially a much wider role for this novel family of therapeutics.

First studies selected coiled-coil motif peptide sequences (using computational prediction software and published literature) that were then synthesised using a solid phase approach, purified and characterised. To facilitate subsequent PEGylation, peptides were engineered to include an N-terminal cysteine residue. mPEG-maleimide (~5,500 g mol^{-1}) was then conjugated site-specifically *via* the cysteine thiol. A purification method optimised using cation-exchange chromatography enabled the removal of both unreacted mPEG-maleimide and free peptide; purity was $\geq$ 95 % for each conjugate.

Proof of concept was obtained with mPEG-FosW_C, which was designed to inhibit coiled-coil heterodimerisation of native c-Jun and c-Fos proteins (AP-1). ^{1}H, ^{15}N HSQC spectroscopy confirmed target hybridisation of heterodimeric coiled-coils FosW_C : c-Jun and mPEG-FosW_C : c-Jun. In addition, both NMR and CD spectroscopy showed that both heterodimers adopted very similar structures under physiological conditions, irrespective of the presence or absence of PEG. Further studies using fluorescently labelled conjugates investigated cellular uptake in MCF-7 cells, and biological activity was assessed using the MTT assay with and without the use of a cationic transfection reagent.

These studies demonstrate the potential of mPEG-coiled-coil motifs as therapeutic agents. However, demonstrating reproducible biological activity was not possible with the intracellular targets. Investigating the biological activity of the conjugates designed to target the extracellular Ebola virus fusion proteins remains an exciting prospect.

INDEX

		Page No.
Declaration and Statements		i
Acknowledgements		ii
Abstract		iv
Index		v
List of Figures		xiii
List of Tables		xx
Abbreviations		xxii
CHAPTER 1 General Introduction		1
1.1	Introduction	2
1.2	The Coiled-Coil Motif	5
1.3	Nanomedicine and Polymer Therapeutics	19
	1.3.1 PEGylation	23
1.4	Challenges Associated with the Delivery of Polymer-Coiled-Coil Motif Conjugates	26
1.5	Biological Targets	29
	1.5.1 E2F1 and PHB, the Tumour Suppressor Protein	30
	1.5.2 AP-1 Transcription Factor (Jun/Fos)	31
	1.5.3 Ebola Virus VP35 Protein	36
	1.5.4 Ebola Virus GP2 Protein	38
1.6	The Future, from Laboratory to Clinic	39
1.7	Thesis Aims and Objectives	40
CHAPTER 2 Materials and General Methods		44
2.1	Materials and Equipment	45
2.2	General Methods	45
	2.2.1 General Analytical Techniques	45
	2.2.1.1 Determination of Concentration by UV Spectroscopy	45
	2.2.1.2 Agarose Gel Electrophoresis	55

2.2.1.3 SDS-PAGE 56
2.2.1.4 CD Spectroscopy 57
2.2.2 General Chromatography Techniques 58
2.2.2.1 Preparation of Sephadex® G-15 Chromatography Columns 58
2.2.2.2 Use of Sephadex® G-15 and G-25 Media for the Purification and Analysis of OG-labelled conjugates 60
2.2.3 Cell Culture 61
2.2.3.1 Defrosting of Cells 61
2.2.3.2 Cell Maintenance and Passaging 61
2.2.3.3 Counting and Seeding Cells 63
2.2.4 General Biological Assays 63
2.2.4.1 Quantification of Cell Growth Using the MTT Assay 63
2.2.4.2 Determination of Cytotoxicity by the MTT Assay 65
2.2.4.3 Use of Flow cytometry to Measure Cellular Uptake of Fluorescent Probes 65
2.2.5 Statistics 69

CHAPTER 3 Coiled-Coil Peptide Design, Synthesis and Characterisation 70
3.1 Introduction 71
3.1.1 Rational Design, Selection and Prediction of Coiled-Coil Motifs 71
3.1.2 Peptide Synthesis 73
3.1.2.1 Solid Phase Peptide Synthesis (SPPS) 74
3.1.3 Engineered Modifications to Wild-Type Peptide Sequences 81
3.1.3.1 Insertion of Tyrosine as a UV-Chromophore into Peptide Sequences to Aid Characterisation 82
3.1.3.2 N-terminal Cysteine Tagging of Peptides for Site-Specific Conjugation 83
3.1.4 Post-Synthesis Purification and Characterisation of Peptides 84
3.1.4.1 Reverse-Phase High Pressure Liquid Chromatography 84
3.1.4.2 Electrospray Ionisation Time-of-Flight Mass Spectroscopy 84
3.1.5 Experimental Aims 85
3.2 Methods 85

3.2.1 Prediction of Coiled-Coil Motifs Using COILS, Paircoil, LearnCoil-VMF, MultiCoil and Paircoil2 86
3.2.2 Synthesis of Peptides by Fmoc-SPPS 86
3.2.2.1 Distillation of NMP 86
3.2.2.2 Preparation of Reactants and Automated Fmoc-SPPS Protocol 90
3.2.2.3 Resin Cleavage and Removal of Amino Acid Side-Chain Protecting Groups 90
3.2.3 Purification and Analysis of Peptides by RP-HPLC 93
3.2.4 Characterisation of Peptides by ESI-TOF MS 93
3.2.5 TFA/HCl Buffer Exchange 94
3.3 Results & Discussion 94
3.3.1 Prediction of Coiled-Coil Motifs in the Proteins E2F1, PHB, EbVP35 and EbGP2 by computational analysis 95
3.3.2 Design and Synthesis of Coiled-Coil Motif Peptides 99
3.3.2.1 Design and Synthesis of PHB and E2F1 Derived Peptides 99
3.3.2.2 Design/Selection and Synthesis of c-Jun and c-Fos Derived Peptides 111
3.3.2.3 Design and Synthesis of EbVP35 Derived Peptides 117
3.3.2.4 Design and Synthesis of EbGP2 Derived Peptides 119
3.3.3 General Challenges in the Identification of Coiled-Coil Domains 123
3.3.4 Challenges in the Preparation of Synthetic Peptides 126
3.3.5 Conclusions 128

CHAPTER 4 Site-Specific PEGylation 131
4.1 Introduction 132
4.1.1 The Chemistry of PEGylation 132
4.1.1.1 Importance of Site-Specific Conjugation 136
4.1.1.2 Solid and Solution Phase Methodologies for Site-Specific PEGylation 137
4.1.1.3 Ellman's Assay for Free Thiols 140
4.1.2 Assessment of the Methods for Conjugate Purification 144
4.1.3 Use of MALDI-TOF MS for mPEG-Coiled-Coil Motif 144

Conjugate Characterisation
4.14 Use of 2D DOSY for mPEG-Coiled-Coil Motif Conjugate Characterisation 147
4.1.5 Experimental Aims 147
4.2 Methods 148
4.2.1 Synthesis of $Phb_{Y185-214}$-PEG and $EbVP35_{Y88-119}$-PEG Using Solid-Phase C-terminal PEGylation with TentaGel PAP Resin 148
4.2.2 Synthesis of mPEG-$Phb_{CY185-214}$, mPEG-$FosW_C$, mPEG-$EbGP2_{609-630}$ and mPEG-$EbGP2_{CY566-589}$ Using Solution-Phase Thiol-Specific PEGylation with mPEG-MAL 150
4.2.3 Ellman's Assay for Free Thiols 150
4.2.4 Purification of mPEG-Coiled-Coil Motif Conjugates by Cation-Exchange Chromatography 152
4.2.5 MALDI-TOF MS Characterisation of mPEG-Coiled-Coil Motif Conjugates 155
4.2.6 Characterisation of mPEG-$FosW_C$ Using 2D DOSY 155
4.3 Results 157
4.3.1 Preparation of the C-terminal PEG Conjugates: $Phb_{Y185-214}$-PEG and $EbVP35_{Y88-119}$-PEG 157
4.3.2 Preparation of N-terminal mPEG-Coiled-Coil Motif Conjugates Using mPEG-MAL 159
4.3.2.1 Characterisation of mPEG-MAL by SEC and MALDI-TOF MS 159
4.3.2.2 Optimisation of Solution-Phase Synthesis Using mPEG-$EbGP2_{609-630}$ 162
4.3.2.3 Solution-Phase Synthesis of mPEG-$Phb_{CY185-214}$, mPEG-$FosW_C$ mPEG-$EbGP2_{609-630}$ and mPEG-$EbGP2_{566-589}$ 165
4.4 Discussion 182
4.4.1 Comparison of the Relative Merits of the Synthetic Methods Used 182
4.4.1.1 Quality of the mPEG-MAL intermediate and the Challenges of Solution-Phase Synthesis 183
4.4.2 Challenges of characterising mPEG-coiled-coil conjugates 184
4.4.3 Conclusions 186

CHAPTER 5 Investigation of mPEG-Coiled-Coil Motif Target Hybridisation Using Phb : E2F1 and c-Jun:FosW$_C$ as Models: Preparation of Recombinant Targets and Development of Analytical Techniques 187

5.1 Introduction 188

5.1.1 Development of a Method for Recombinant Expression and Purification of Targets rhE2F1 and r-c-Jun/[^{15}N]r-c-Jun 190

5.1.2 Analytical Techniques to Study Target Hybridisation 195

5.1.2.1 CD Spectroscopy 195

5.1.2.2 2D ^{1}H, ^{15}N-HSQC and ^{1}H-NMR Spectroscopy 195

5.1.3 Experimental Aims 197

5.2 Methods 200

5.2.1 Expression of rhE2F1 200

5.2.1.1 Transformation of DH5α and TOP10 *E. coli* with pGEX-KG-(GST)-E2F1 and Plasmid Purification 200

5.2.1.2 Sequencing of the pGEX-KG-(GST)-E2F1 Plasmid 201

5.2.1.3 Sequence Analysis and *In Silico* Construction of the pGEX-KG (GST)-E2F1 Plasmid Map 205

5.2.1.4 Mini-Induction to Test Expression of rhE2F1 205

5.2.2 Expression of r-c-Jun and [^{15}N]r-c-Jun 206

5.2.2.1 Assembly and Characterisation of the cytb5-r-c-Jun Plasmid 206

5.2.2.2 Transformation of BL21-CodonPlus (DE3) *E. coli* with the pET15B-cytb5-ENLYFQGT-r-c-Jun-5 Plasmid 208

5.2.2.3 Expression of cytb5-c-Jun in BL21-CodonPlus (DE3) *E. coli* 208

5.2.2.4 Lysis of BL21-CodonPlus (DE3) *E. coli* by Probe Sonication 209

5.2.2.5 Purification of cytb5-r-c-Jun from Crude Lysate 210

5.2.2.6 Cleavage of cytb5-r-c-Jun Using TEV Protease 211

5.2.2.7 Final Purification and Concentration of r-c-Jun 211

5.2.3 Characterisation of r-c-Jun and [^{15}N]r-c-Jun Peptides by MALDI-TOF MS 212

5.2.4 Preparation of Samples for Target Hybridisation Studies by CD and NMR Spectroscopy 212

5.2.4.1 Characterisation by CD Spectroscopy 212
5.2.4.2 Characterisation by 1D, ^{1}H-NMR and 2D ^{1}H, ^{15}N-HSQC Spectroscopy 213
5.3 Results 214
5.3.1 Recombinant Preparation and Characterisation of rhE2F1 and r-c-Jun 214
5.3.1.1 Characterisation of the pGEX-KG-(GST)-E2F1 Plasmid and Expression of rhE2F1 Protein 214
5.3.1.2 Expression and Characterisation of r-c-Jun and [^{15}N]r-c-Jun Peptides 221
5.3.3 Target Hybridisation Studies 227
5.3.3.1 Preliminary Characterisation by CD Spectroscopy of the Interaction Between Phb and E2F1 Peptides E2F1a and E2F1b 227
5.3.3.2 Characterisation of mPEG-FosW$_C$: c-Jun Target Hybridisation by CD and 1D, ^{1}H-NMR Spectroscopy 231
5.3.3.3 Characterisation of mPEG-FosW$_C$: c-Jun Target Hybridisation Using 2D ^{1}H, ^{15}N-HSQC Spectroscopy 239
5.4 Discussion 243
5.4.1 Comparative Merits of the Model Targets Used to Study Phb : E2F1 and FosW$_C$: c-Jun Hybridisation 248
5.4.2 Challenges of Verifying Coiled-Coil Driven Target Hybridisation 250
5.4.3 Conclusions 252

CHAPTER 6 Investigation of the Cellular Uptake and Cytotoxicity of mPEG-Phb$_{CY185-214}$ and mPEG-FosW$_C$ in MCF-7 Cells *In Vitro* 254
6.1 Introduction 255
6.1.1 Flow Cytometry as a Tool to Study Cellular Uptake of OG-Labelled Conjugates 257
6.1.2 Choice of Fluorescent Probe 257
6.1.3 Methods of Investigating *In Vitro* Cell Viability 260
6.1.4 Transfection of Peptide/Polymer Therapeutics 261

6.1.5 RBC Lysis as a Tool to Study Haematotoxicity 263
6.16 Experimental Aims 263
6.2 Methods 265
6.2.1 Preparation of OG-Labelled Probes 265
6.2.1.1 Synthesis, Purification and Analysis of OG-Labelled Probes 265
6.2.1.2 Effect of OG-Conjugation on Fluorescence Excitation and Emission Spectra 267
6.2.1.3 Effect of pH and Concentration on the Fluorescence Emission Intensity of the OG-Labelled Conjugates 267
6.2.2 Study of Cellular Uptake Using Flow Cytometry 268
6.2.2.1 Cell Uptake Studies Using OG-Labelled Peptides and Conjugates 268
6.2.2.2 Stability of OG-Conjugates Post-Incubation with MCF-7 Cells 269
6.2.3 Assessment of Cell Viability Using the MTT Assay 269
6.2.3.1 Cytotoxicity of $Phb_{185-214}$, $Phb_{Y185-214}$ and mPEG-$Phb_{CY185-214}$ 269
6.2.3.2 Cytotoxicity of $FosW_C$ and mPEG-$FosW_C$ ± Tfx™-50 270
6.2.3.3 Preparation and Reconstitution of Tfx™-50 Reagent 271
6.2.3.4 $FosW_C$ / mPEG-$FosW_C$: Tfx™-50 Complex Preparation 271
6.2.3.5 Assessment of $FosW_C$: Tfx™-50 Molar Ratio and MTT Assay Incubation Time 271
6.2.3.6 Determination of the Optimal $FosW_C$: Tfx™-50 Charge Ratio 273
6.2.3.7 Assessment of the Cytotoxicty of $FosW_C$ /mPEG-$FosW_C$: Tfx™-50 Complexes Using a 2:1 Charge Ratio (1:2.5 Molar Ratio) 273
6.2.4 Investigation of Haemolytic Activity Using the RBC Lysis Assay 273
6.3 Results 275
6.3.1 Synthesis and Characterisation of OG-Labelled Conjugates 275
6.3.2 Cellular Uptake of OG-Labelled Conjugates 284
6.3.3 Biological Assessment 290

6.4 Discussion 297
6.4.1 Challenges of Using Fluorescence to Investigate Cellular Uptake 297
6.4.2 Assessing Biological Activity and the Challenges of Intracellular Delivery of mPEG-Coiled-Coil Motif Therapeutics 305
6.4.3 Conclusions 308

CHAPTER 7 General Discussion 310
7.1 General Discussion 311
7.2 Summary of the Strategy of this Thesis and Key Results, Successes and Challenges 312
7.3 Potential Applications of this Concept 316
7.4 General Conclusions 318

Bibliography 320

Appendix I 345

FIGURES LIST

Page No.

CHAPTER 1 General Introduction

Figure 1.1 Global deaths by cause and UK cancer statistics. 3

Figure 1.2 Polymer coiled-coil-motif target hybridisation. 4

Figure 1.3 Time-line showing the significant events in the converging fields of polymer therapeutics and coiled-coil research. 6

Figure 1.4 Journal articles citing "coiled-coils" from 1978 to 2008. 7

Figure 1.5 Cross sectional and sectional views of (a) a dimeric coiled-coil and (b) a trimeric coiled-coil. 9

Figure 1.6 Helical-wheel illustration of (a) dimeric and (b) trimeric coiled-coils. 10

Figure 1.7 Cartoon to illustrate the cellular locations of the coiled-coil protein targets. 18

Figure 1.8 An overview of endocytic trafficking in non-polarised mammalian cells. 28

Figure 1.9 AP-1 responsive genes in cancer. 33

Figure 1.10 Ebola outbreaks since 1976 and fatality rates for each sub-type. 37

CHAPTER 2 Materials and General Methods

Figure 2.1 The basic principles of RP, SE and Ion-exchange chromatography. 59

Figure 2.2 Elution profiles for OG in Sephadex® G-15 and G-25 columns. 62

Figure 2.3 Scheme to show the mechanism by which soluble MTT is reduced to form the insoluble formazan salt. 64

Figure 2.4 Growth curve for the MCF-7 cell line. 66

Figure 2.5 Flow cytometry dot-plot and acquisition histogram showing the typical distribution of a control cell population. 68

CHAPTER 3 Coiled-Coil Peptide Design, Synthesis and Characterisation

Figure 3.1 The general principles of Fmoc-SPPS. 75

Figure 3.2 The chemical structure of Rink Amide AM Resin. 77

Figure 3.3	Boc and Fmoc protection strategies used in Fmoc-SPPS.	78
Figure 3.4	Coiled-coil prediction for the 437-residue target protein E2F1.	96
Figure 3.5	Coiled-coil prediction for the 272-residue protein PHB.	97
Figure 3.6	Coiled-coil prediction for the 340-residue protein EbVP35.	98
Figure 3.7	Coiled-coil prediction for the 676-residue protein EbGP2.	100
Figure 3.8	Design of E2F1 and PHB-derived peptides for synthesis by Fmoc-SPPS.	103
Figure 3.9	Purification and characterisation of $Phb_{185-214}$.	105
Figure 3.10	Purification and characterisation of $Phb_{Y185-214}$.	107
Figure 3.11	Purification and characterisation of $Phb_{CY185-214}$.	108
Figure 3.12	Purification and characterisation of E2F1a.	110
Figure 3.13	Purification and characterisation of E2F1b.	112
Figure 3.14	Structures of c-Jun:c-Fos and c-Jun:FoW_C coiled-coil complexes.	113
Figure 3.15	Purification and characterisation of c-Jun.	115
Figure 3.16	Purification and characterisation of $FosW_C$.	116
Figure 3.17	Design of the EbVP35 derived peptides $EbVP35_{82-119}$ and $EbVP35_{88-119}$.	118
Figure 3.18	Design of EbGP2 derived peptides.	120
Figure 3.19	Purification and characterisation of $EbGP2_{609-630}$.	122
Figure 3.20	Purification and characterisation of $EbGP2_{CY556-589}$.	124

CHAPTER 4 Site-Specific PEGylation

Figure 4.1	Theoretical coiled-coil motif PEGylation sites.	138
Figure 4.2	Two-step solid phase methodology for the synthesis of C-terminal coiled-coil motif-PEG conjugates.	139
Figure 4.3	Proposed solution phase methodology for site-specific thiol-directed PEGylation.	141
Figure 4.4	Thiol directed conjugation shown with mPEG-MAL.	142
Figure 4.5	Reaction of Ellman's reagent with R-SH.	143
Figure 4.6	Characterisation by MALDI-TOF MS.	145
Figure 4.7	Overview of the experiments conducted in this study.	149
Figure 4.8	Gradient elution method used for cation-exchange chromatography purification and analysis of the mPEG-coiled-	154

coil motif conjugates.

Figure 4.9 Characterisation of crude Phb-PEG by semi-preparative RP-HPLC. 158

Figure 4.10 SEC characterisation of the NOF and Fluka mPEG-MAL intermediates. 160

Figure 4.11 Characterisation by MALDI-TOF of the NOF mPEG-MAL intermediate. 161

Figure 4.12 Rate of PEGylation of $EbGP2_{609-630}$ monitored by Ellman's assay. 163

Figure 4.13 SEC (TSK-gel columns) characterisation of crude mPEG-$EbGP2_{609-630}$. 164

Figure 4.14 SEC (Superdex HR 10/30 column) characterisation of crude mPEG-$EbGP2_{609-630}$. 166

Figure 4.15 Optimisation of conditions for cation-exchange chromatography characterisation. 167

Figure 4.16 Characterisation by cation-exchange chromatography of the peptide $EbGP2_{609-630}$ with decreasing buffer molarity. 169

Figure 4.17 Purification of mPEG-$EbGP2_{609-630}$ by cation-exchange chromatography (MacroCap SP). 170

Figure 4.18 Characterisation of purified mPEG-$EbGP2_{609-630}$ by cation-exchange chromatography and MALDI-TOF MS. 171

Figure 4.19 Purification of mPEG-$FosW_C$ by cation-exchange chromatography (MacroCap SP). 173

Figure 4.20 Characterisation of purified mPEG-$FosW_C$ by cation-exchange chromatography and MALDI-TOF MS. 174

Figure 4.21 Characterisation of mPEG-$FosW_C$ by 2D DOSY. 176

Figure 4.22 Purification of mPEG-$Phb_{CY185-214}$ by cation-exchange chromatography (MacroCap SP). 177

Figure 4.23 Characterisation of mPEG-$Phb_{CY185-214}$ by cation-exchange chromatography and MALDI-TOF MS. 178

Figure 4.24 Purification of mPEG-$EbGP2_{CY566-589}$ by cation-exchange chromatography (MacroCap SP). 180

Figure 4.25 Characterisation of mPEG-$EbGP2_{CY566-589}$ by MALDI-TOF MS. 181

CHAPTER 5 Investigation of mPEG-Coiled-Coil Motif Target Hybridisation Using Phb : E2F1 and c-Jun:FosW$_C$ as Models: Preparation of Recombinant Targets and Development of Analytical Techniques

Figure 5.1	Schematic overview of the three target hybridisation studies conducted.	189
Figure 5.2	The consensus protocol for recombinant protein expression and purification, recommended by Gräslund *et al*, (2008).	191
Figure 5.3	Characteristic CD spectra of common peptide structures.	196
Figure 5.4	Typical 1D ^{1}H-NMR and 2D ^{1}H, ^{15}N-HSQC spectra for a 36-residue peptide.	198
Figure 5.5	pGEX-KG vector map and schematic of pGEX-KG-(GST)-E2F1 sequencing strategy.	202
Figure 5.6	Illustration of the recombinant method used to express peptides r-c-Jun and [^{15}N]r-c-Jun.	207
Figure 5.7	Summary of the experiments conducted towards recombinant expression of the rhE2F1 target protein.	215
Figure 5.8	Characterisation by agarose gel electrophoresis of the pGEX-KG-E2F-1 plasmid.	216
Figure 5.9	Linear alignment of the contiguous pGEX-KG-(GST)-E2F1 plasmid sequence.	218
Figure 5.10	Magnified alignment of the contiguous pGEX-KG-(GST)-E2F1 plasmid sequence.	219
Figure 5.11	Consensus sequence for the pGEX-KG-(GST)-E2F1 plasmid in FASTA format.	220
Figure 5.12	SDS-PAGE characterisation of rhE2F1 expression in BL21 (DE3) pLysS *E. coli*.	222
Figure 5.13	SDS-PAGE characterisation of rhE2F1 expression in BL21 (DE3) pLysS *E. coli*.	223
Figure 5.14	Summary of the experiments conducted towards recombinant expression of the [^{15}N]r-c-Jun target peptide and analysis of target hybridisation with FosW$_C$/mPEG-FosW$_C$.	224
Figure 5.15	SDS-PAGE analysis of the expression of r-c-Jun in BL21-CodonPlus (DE3) *E.coli*.	225
Figure 5.16	SDS-PAGE analysis of the expression of [^{15}N]r-c-Jun in	226

BL21-CodonPlus (DE3) *E.coli*.

Figure 5.17 SDS-PAGE analysis of the TEV cleavage and final purification of [^{15}N]r-c-Jun. 228

Figure 5.18 MALDI-TOF MS characterisation of peptdes r-c-Jun and [^{15}N]r-c-Jun. 229

Figure 5.19 Analysis of $Phb_{185-214}$ and $Phb_{Y185-214}$ thermal denaturation by CD spectroscopy. 230

Figure 5.20 Characterisation of the interaction between $Phb_{Y185-214}$ and target peptides E2F1a and E2F1b using CD spectroscopy. 232

Figure 5.21 Characterisation of [^{15}N]r-c-Jun and synthetic c-Jun at 37 °C and 4 °C using CD spectroscopy. 233

Figure 5.22 Characterisation of mPEG-MAL and mPEG-$FosW_C$ by CD spectroscopy. 235

Figure 5.23 Characterisation of c-Jun : mPEG-$FosW_C$ by CD spectroscopy using a "Tandem Cell". 236

Figure 5.24 Characterisation of c-Jun : $FosW_C$ and c-Jun : mPEG-$FosW_C$ by CD spectroscopy. 237

Figure 5.25 Analysis of the thermal denaturation of c-Jun : $FosW_C$ and c-Jun : mPEG-$FosW_C$ complexes by CD spectroscopy. 238

Figure 5.26 Characterisation of c-Jun : $FosW_C$ and c-Jun:mPEG-$FosW_C$ complexes before and after thermal denaturation and after renaturation (cooling) using CD spectroscopy. 240

Figure 5.27 Characterisation of the thermal denaturation of c-Jun (synthetic), $FosW_C$ and mPEG-$FosW_C$ using 1D ^{1}H-NMR spectroscopy. 241

Figure 5.28 2D ^{1}H, ^{15}N HSQC characterisation of the [^{15}N]r-c-Jun :$FosW_C$ (1:1) coiled-coil complex. 242

Figure 5.29 2D ^{1}H, ^{15}N HSQC characterisation of the [^{15}N]r-c-Jun : mPEG-$FosW_C$ (1:1) coiled-coil complex. 244

Figure 5.30 2D ^{1}H, ^{15}N HSQC characterisation of the [^{15}N]r-c-Jun : $FosW_C$ (1:1) and [^{15}N]r-c-Jun : mPEG-$FosW_C$ (1:1) coiled-coil complexes. 245

Figure 5.31 2D ^{15}N HSQC characterisation of the [^{15}N]r-c-Jun : $FosW_C$ coiled-coil complex at a 1:1 and 1:2 ratios. 246

Figure 5.32 2D ^{15}N HSQC characterisation of the [^{15}N]r-c-Jun : mPEG- 247

$FosW_C$ coiled-coil complex at a 1:1 and 1:2 ratios.

CHAPTER 6 Investigation of the Cellular Uptake and Cytotoxicity of mPEG-$Phb_{Y185-214}$ and mPEG-$FosW_C$ in MCF-7 Cells *In Vitro*

Figure 6.1 Schematic overview of the experiments conducted in this study. 256

Figure 6.2 Possible sites of conjugating OG to peptides $FosW_C$ and $Phb_{Y185-214}$ and reaction scheme for OGSE488-X with a reactive amine side-chain. 259

Figure 6.3 Reconstiution and use of Tfx™-50 reagent. 272

Figure 6.4 Evaluation of reaction efficiency and purity using SEC of OG-labelled conjugates $Phb_{Y185-214}$-OG and mPEG-$Phb_{CY185-214}$-OG. 276

Figure 6.5 Evaluation of reaction efficiency and purity using SEC of OG-labelled conjugates $FosW_C$-OG and mPEG-$FosW_C$-OG. 277

Figure 6.6 Characterisation of OG fluorescence excitation and emission spectra. 279

Figure 6.7 Characterisation of OG fluorescence excitation and emission spectra (continued). 281

Figure 6.8 Overlay of the normalised fluorescence excitation and emission spectra of OGSE488-X and OG-labelled peptides and mPEG-conjugates. 282

Figure 6.9 Determination of the pH sensitivity of OG fluorescence emission before and after conjugation. 283

Figure 6.10 Determination of the pH sensitivity of OG fluorescence emission (continued). 285

Figure 6.11 Uptake of $Phb_{Y185-214}$-OG and mPEG-$Phb_{Y185-214}$-OG relative to mPEG-OG at 37 °C in MCF-7 cells over 5 h. 286

Figure 6.12 Uptake of $FosW_C$-OG, $FosW_C$-OG : Tfx™-50, mPEG-$FosW_C$ OG, mPEG-$FosW_C$-OG : Tfx™-50 and Tfx™-50 alone over the first 2 h of the transfection protocol. 288

Figure 6.13 Change in acquisition pattern of cells and gated population during the course of flow cytometry analysis. 289

Figure 6.14 Cytotoxicity of $Phb_{Y185-214}$ and mPEG-$Phb_{CY185-214}$ relative to mPEG-NH_2 and PEI in MCF-7 cells, over 72 h. 291

Figure 6.15 Cytotoxicity of $Phb_{Y185-214}$ and mPEG-$Phb_{CY185-214}$ relative to mPEG-NH_2 and PEI in MCF-7 cells over 72 h. 292

Figure 6.16 Cytotoxicity of $FosW_C$ and mPEG-$FosW_C$ relative to mPEG-NH_2 and PEI in MCF-7 cells over 72 h. 294

Figure 6.17 Determination of the optimal molar ratio of $FosW_C$: Tfx™-50 over 24 and 72 h in MCF-7 cells using the MTT assay. 295

Figure 6.18 Effect of charge ratio on the cytotoxicity of the $FosW_C$: Tfx™-50 complex in MCF-7 cells using the MTT assay. 296

Figure 6.19 Cytotoxicity of $FosW_C$, $FosW_C$: Tfx™-50 complex, mPEG-$FosW_C$, and mPEG-$FosW_C$: Tfx™-50 complex in MCF-7 cells using the MTT assay. 298

Figure 6.20 Haematotoxicity of the polymer controls, $Phb_{Y185-214}$ and $FosW_C$ peptides and mPEG-$Phb_{Y185-214}$ and mPEG-$FosW_C$ conjugates. 299

Figure 6.21 Structures of 6-carboxyfluorescein and OGSE488-X. 301

Figure 6.22 Possible cellular fates of OG-conjugates and the challenges faced with the use of fluorescence probes. 302

CHAPTER 7 General Discussion

Figure 7.1 Schematic showing selected publications leading to and emanating from this Ph.D. thesis. 313

Figure 7.2 Schematic showing potential research projects that could be conducted as a continuation of this Ph.D. thesis. 317

TABLES LIST

Page No.

CHAPTER 1 General Introduction

Table 1.1	Summary of biological proteins that contain coiled-coil motifs with potential for therapeutic intervention.	12
Table 1.2	Polymer-protein conjugates in the clinic or late stage clinical trials.	21
Table 1.3	AP-1 target genes in tumour development and suppression.	34

CHAPTER 2 Materials and General Methods

Table 2.1	Materials used in this study.	46
Table 2.2	Equipment used in this study.	51

CHAPTER 3 Coiled-Coil Peptide Design, Synthesis and Characterisation

Table 3.1	A summary of the five computational methods available to identify and predict coiled-coil motifs in proteins.	72
Table 3.2	A summary of commonly used side-chain protecting groups	79
Table 3.3	A summary of the usage parameters and URLs for each of the coiled-coil prediction programmes accessed.	87
Table 3.4	Preparation of amino acid solutions for the parallel synthesis of c-Jun, $FosW_C$ and $EbGP2_{609-630}$.	88
Table 3.5	Preparation of reaction solutions for the parallel synthesis of c-Jun, $FosW_C$ and $EbGP2_{609-630}$.	89
Table 3.6	Amino acid coupling protocol for Fmoc-SPPS.	91
Table 3.7	Termination (N-terminal acetylation) protocol for Fmoc-SPPS.	92
Table 3.8	Summary of amino acid sequences for the peptides synthesised in this study.	101
Table 3.9	Pros and cons of the biophysical techniques used to identify and characterise coiled-coil motifs.	125
Table 3.10	Summary of synthesis data for each of the peptides prepared in this study.	129

CHAPTER 4 Site-Specific PEGylation

Table 4.1	Summary of PEG characteristics used in the synthesis of the eight FDA approved PEG-protein conjugates.	134
Table 4.2	Summary of reactants and solvents used in the solution-phase synthesis of the four conjugates listed.	151
Table 4.3	Summary of buffers required for purification, yield and molecular weights for the four conjugates synthesised.	153
Table 4.4	Summary of attempts to acquire MALDI-TOF spectra of mPEG-coiled-coil motif conjugates.	156

CHAPTER 5 Investigation of mPEG-Coiled-Coil Motif Target Hybridisation Using Phb : E2F1 and c-Jun:FosW$_C$ as Models: Preparation of Recombinant Targets and Development of Analytical Techniques

Table 5.1	Characteristics of the primers used to determine the sequence of the E2F1 ORF.	204

CHAPTER 6 Investigation of the Cellular Uptake and Cytotoxicity of mPEG-Phb$_{Y185-214}$ and mPEG-FosW$_C$ in MCF-7 Cells *In Vitro*

Table 6.1	Choice of reagents considered to aid intracellular delivery of FosW$_C$ and mPEG-FosW$_C$.	262
Table 6.2	Summary of reactants used for preparation of the OG-labelled probes.	266
Table 6.3	Characterisation of OG-labelled peptides, polymer and conjugates.	278
Table 6.4	Comparison of c-Fos derived peptide sequences and charges.	307

ABBREVIATIONS LIST

AAA	Amino Acid Analysis
Acm	Acetamidomethyl
ACN	ACetoNitrile
Amp	Ampicillin
ALL	Acute Lymphoblastic Leukaemia
AP-1	Activator Protein-1
BBSRC	Biotechnology and biological sciences research council
BCA	BicinChoninic Acid
Boc	*t*-butoxycarbonyl
Bum	*t*-Butoxymethyl
bZIP	basic Leucine Zipper
C	Cysteine
$CaCl_2.2H_2O$	Calcium chloride
CaH_2	Calcium Hydroxide
Cam	Chloramphenicol
CD	Circular Dichroism
$CHCl_3$	Chlorophorm
CIPF	Centro de Investigacion Principe Felipe
CRUK	Cancer Research UK
cytb5	Cytochrome b_5
Da	Dalton
DBU	1,8-diazabicyclo(5.4.0)undec-7-ene
DCM	DiChloroMethane
ddH_2O	double distilled water
Ddiv	1-(4,4-Dimethyl-2,6-dioxocyclohexylidene3-methylbutyl
DHB	DiHydroxyBenzoic acid
DIVEMA	DIVinylEtherMaleicAnhydride
DMF	DiMethylFormamide
DMSO	DiMethyl SulphOxide
DIPEA	N,N-DiIsoPropylEthylAmine
DOSY	Diffusion Ordered SpectroscopY
DTNB	5,5'-DiThiobis(2-NitroBenzoic acid)

DTT	DiThiolThreitol
ε	Molar extinction coefficient
E2F	E2 Factor
EbVP35	Ebola Viral Polymerase 35
EbGP2	Ebola GlycoProtein 2
E. coli	*Escherichia coli*
EDT	EthaneDiThiol
EDTA	EthyleneDiamineTetraAcetic acid
EMEA	European MEdicines Agency
EMT	Epithelial-Mesenchymal Transition
EPFL	École Polytechnique Fédérale de Lausanne
EPR	Enhanced Permeation and Retention
ESF	European Science Foundation
ESI-TOF MS	ElectroSpray Ionisation Time Of Flight Mass Spectrometry
EtBr	Ethidium Bromide
Et_2O	Diethyl ether
EtOH	Ethanol
ExPASy	Expert Protein Analysis System
F	Phenylalanine
FCS	Foetal Calf Serum
FDA	Food and Drug Administration
FITC	Fluorescein IsoThioCyanate
Fmoc	9-Fluorenylmethyloxycarbonyl
FTIR	Fourier Transform-Intra Red
GP2	Glycoprotein 2
GST	Glutathione-S-Transferase
HCl	HydroChloride
HCTU	2-(6-Chloro-1H-benzotriazole-1-yl)-1,1,3,3-tetramethyl aminium hexafluorophosphate
HEPES	4-(2-HydroxyEthyl)-1-PiperazineEthaneSulfonic acid
HER2+	Human Epidermal growth factor Receptor 2+
HF	Haemorrhagic Fever
HIV	Human Immune deficiency Virus

HOBt	Anhydrous 1-hydroxybenzotriazole
HSQC	Heteronuclear Single Quantum Coherence
IFN	InterFeroN
IMAC	Immobilised Metal Affinity Chromatography
Imd	Imidazole
IPTG	Isopropyl-beta-D-thiogalactopyranoside
IRF-3	Interferon Regulatory Factor-3
K	Lysine
LB	Luria Broth
LDL	Low-Density Lipoprotein
LIC	Ligation Independent Cloning
LPS	LipoPolySaccharide
MALDI-TOF MS	Matrix-Assisted Laser Desorption/Ionisation Time Of Flight Mass Spectrometry
MCS	Multiple Cloning Site
MeOH	Methanol
MOPS	3-(N-MorpholinO) PropaneSulfonic acid
mPEG	monomethoxyPolyEthyleneGlycol
mPEG-NH_2	mPEG-amine
mPEG-MAL	mPEG-maleimide
Mn	Number average molecular weight
MS	Mass Spectrometry
MSR	Macrophage Scavenger Receptor
Mtr	4-Methoxy-2,3,6-trimethylbenzenesulphonyl
Mw	Weight average molecular weight
Mw/Mn	Polydispersity
MW	Molecular Weight
MWCO	Molecular Weight Cut-Off
MS	Multiple Sclerosis
MTT	Methylthiazolyldiphenyl-tetrazolium bromide
NaAc	Sodium Acetate
NaF	Sodium Fluoride
NaI	Sodium Iodide
NCS	NeoCarzinoStatin

NHS	N-hydroxysuccinimide
$^{15}NH_4Cl$	^{15}N Labelled ammonium chloride
NMM	N-MethylMorpholine
NMP	N-MethylPyrrolidone
NMR	Nuclear Magnetic Resonance
NOE	Nuclear Overhauser Effect
NOESY	Nuclear Overhauser Effect SpectroscopY
OD	Optical Density
OGSE488-X	Oregon Green Succinimidyl Ester 488-X
ORF	Open Reading Frame
Par-4	Prostate Apoptosis Response Factor-4
Pbf	2,2,4,6,7-Pentamethyldihydrobenzofuran-5-sulfonyl
PBS	Phosphate Buffered Saline
PCR	Polymerase Chain Reaction
PDB	Protein Data Bank
PEG	PolyEthyleneGlycol
PEI	PolyEthyleneImine
PHB	ProHiBitin
PK	PharmacoKinetic
Pmc	2,2,5,7,8-Pentamethylchroman-6-sulphonyl
rh	Recombinant human
RP-HPLC	Reverse Phase-High Pressure Liquid Chromatography
RBC	Red Blood Cell
RP	Reverse Phase
SARS	Severe Acute Respiratory Syndrome
SCID	Severe Combined ImmunoDeficiency Syndrome
SDS	Sodium Dodecyl Sulphate
SDS-PAGE	Sodium Dodecyl Sulphate-PolyAcrylamide Gel Electrophoresis
SE	Size-Exclusion
SEC	Size-Exclusion Chromatography
SMA	Styrene Maleic Anhydride
SMANCS	Styrene Maleic Anhydride NeoCarzinoStatin
SNARE	Sensitive Factor Attachment Protein Receptor

SPA	Succinimidyl-PropionAte
SPPS	Solid Phase Peptide Synthesis
TBE	Tris-Borate-EDTA
*t*Bu	*t*-Butyl
*t*BuO	*t*-Butoxy
*t*Buthio	*t*-Butylthio
TCEP	tris(2-carboxyethyl)phosphine hydrochloride
TEMED	N,N,N',N'-TEtraMethylEthyleneDiamine
TEV	Tobacco etch virus protease
TFA	TriFluoroacetic Acid
THF	TetraHydroFuran
TIPS	TriIsoPropylSilane
TLC	Thin Layer Chromatograpty
Trt	Trityl
Trypsin-EDTA	Trypsin-0.53 mM ethelenediaminetetraacetic acid 0.05 % w/v
TSP	2,2,3,3-tetradeutero-3-trimethylsilylpropionic acid
UKCCCR	United Kingdom Co-ordinating Committee on Cancer Research
W	Tryptophan
WHO	World Health Organisation
Y	Tyrosine

CHAPTER 1

General Introduction

1.1 Introduction

Worldwide, cancer, with 7.6 million attributed deaths in 2005 is one of the top ten leading causes of mortality (World Health Organisation (WHO) Fact Sheet No. 297, 2006). In the UK alone, over 250,000 people are newly diagnosed with cancer each year (Office for National Statistics, 2008). Most common among these are breast, lung, colorectal, and prostate cancer (**Figure 1.1a**). Although new treatments such as the monoclonal antibody Herceptin® (www.herceptin.com) offer hope to carefully selected Human Epidermal growth factor Receptor 2+ (HER2+) cohorts, astonishingly breast cancer remains the leading cause of death for adult women; for women in their late 30s it is responsible for approximately 10 % of all deaths in high income countries and rises to 14 % for women in their 50s (World Health Statistics, 2008).

Chronic diseases have now overtaken infectious diseases as the leading cause of death globally (Abegunde, 2005) (**Figure 1.1b**). However the "...book has not yet been closed on infectious disease" despite infamous words to the contrary by the then Surgeon General of the United States, William H. Stewart in his 1969 annual report (cited in Nelson, 2003). Of recent concern is the spread of endemic zones of infectious diseases with climate change (Kuhn *et al*, 2005). Pathogens such as Ebola (Peters & LeDuc, 1999), avian influenza (Claas *et al*, 1998; Ungchusak *et al*, 2005), Severe Acute Respiratory Syndrome (SARS) coronavirus (Eichelberger, 2007) and multi-drug resistant bacteria (Enright *et al*, 2002) pose not only a psychological but a real threat to human health. Furthermore, as a result of the recent political climate, infection is not limited only to the 'natural' spread of pathogens but there is also the fear of such agents being used in bio-terrorism (Bray, 2003; Peters, 2005).

The aim of this research was to capitalise on the growing understanding of the regulatory importance of coiled-coil motifs present in many proteins (Lupas *et al*, 1991) and develop a new therapeutic class of conjugates containing coiled-coil peptide motifs as putative molecular switches for a diverse range of pathologies (**Figure 1.2**).

The hypothesis proposed is that polymer-coiled-coil motif therapeutics will be able to dock with target proteins in a highly specific manner and induce a clinically significant biological response. As large, multi-component, macromolecular entities

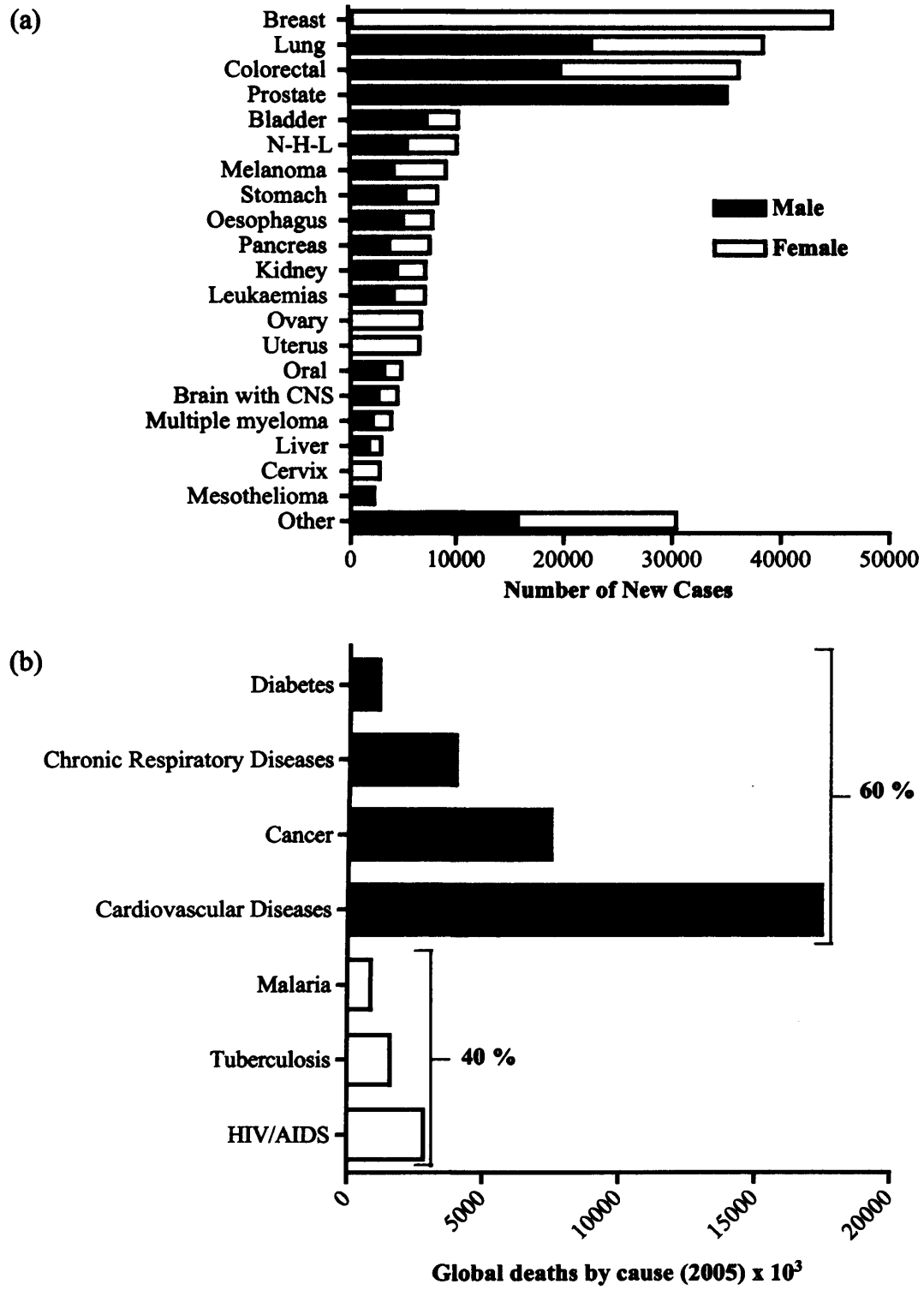

Figure 1.1 Global deaths by cause and UK cancer statistics. Panel (a) The 20 most commonly diagnosed cancers (excluding non-melanoma skin cancer), in the UK, 2004. Adapted from (http://info.cancerresearchuk.org/cancerstats/incidence /commoncancers). Panel (b) shows the total global deaths by cause in 2005, adapted from Abegunde *et al*, (2005), chronic diseases are shown in black, infectious diseases are shown in white.

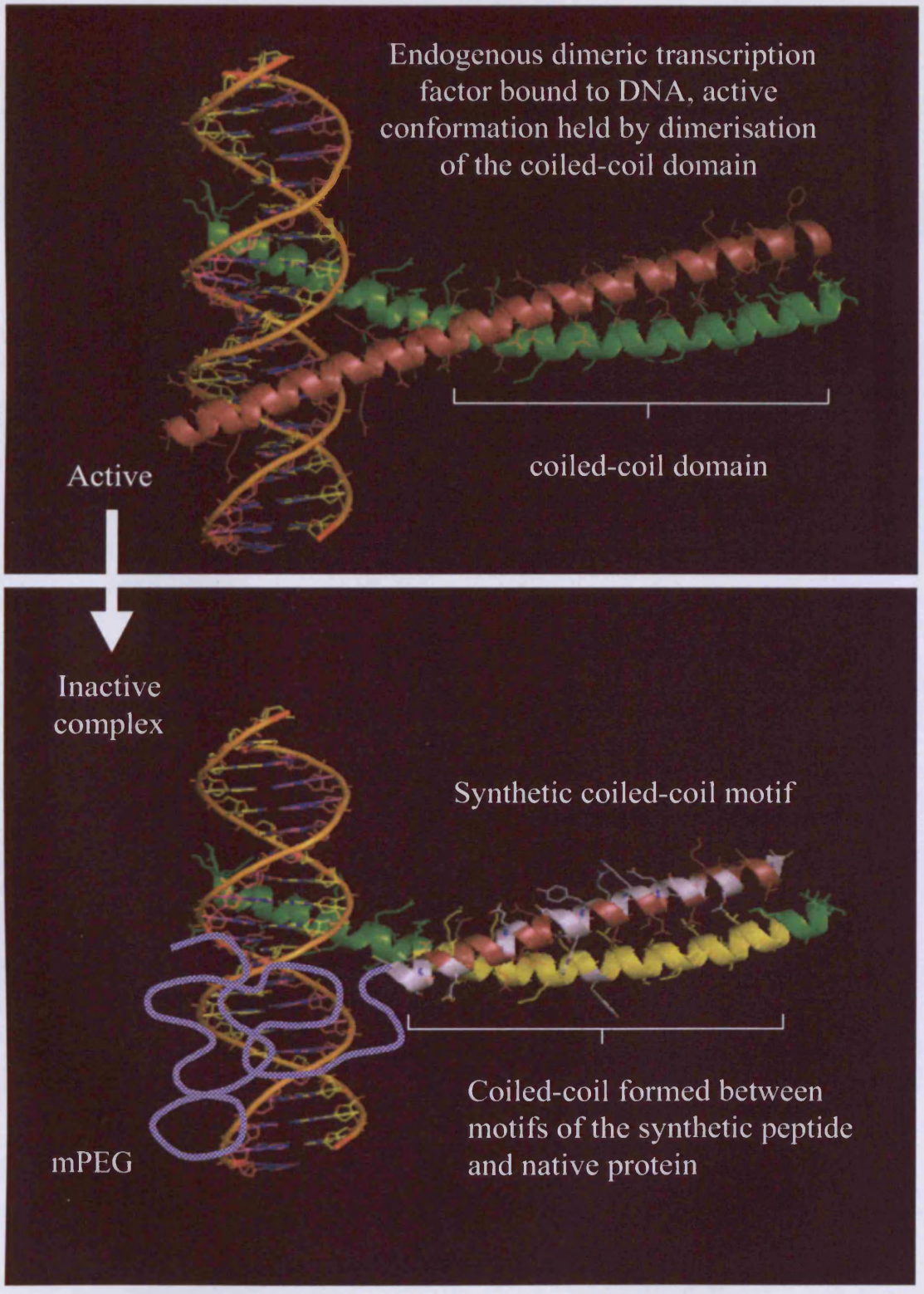

Figure 1.2 Polymer coiled-coil-motif target hybridisation. The proposed mechanism in which a polymer-coiled-coil motif would hybridise to form a heterodimeric coiled-coil to render a coiled-coil protein target inactive. In this instance a dimeric transcription factor is shown. Protein structure file was obtained from the Protein Data Bank (PDB), DOI:10.2210/pdb1fos/pdb, editing and rendering was conducted using MacPyMOL.

these conjugates differ from the small molecules Nobel Laureate, Ehrlich first proposed as drugs 'chemotherapy' towards the end of the 19th Century (http://nobelprize.org/nobel_prizes/lists/all). Although much progress was made in the treatment of disease in the last century the 'magic bullet' as proposed by Ehrlich was not realised until the development of monoclonal antibodies in the 1970s (Kohler & Milstein, 1975). Despite being widely studied over the three decades since, there is still only one nanoparticle, one antibody-drug conjugate and a small number of liposomal products in routine clinical use (reviewed in Duncan, 2005). Polymer therapeutics (Duncan, 2003; Duncan 2006) however, especially PEG-protein conjugates (Davis, 2002; Harris & Chess, 2003; Veronese & Harris, 2008), with at least nine products in the clinic, have proven the most successful first generation nanomedicines (see section 1.3). The key developments in the fields of polymer therapeutics and those of the coiled-coil motif are summarised in **Figure 1.3**.

In order to fully comprehend the rationale for this study, an introduction to the coiled-coil motif, peptide synthesis, polymer-therapeutics, cellular delivery and the biological targets selected for proof of principle research is required. Each of these topics are reviewed and discussed in the following pages.

1.2 The Coiled-Coil Motif

Firstly, it is necessary to define the coiled-coil motif, briefly review its role in the regulation of protein function and explain the rationale for its use as the therapeutic entity.

The coiled-coil motif was first described over 50 years ago (Crick, 1953; Pauling & Corey, 1953). Since then, a large number of proteins have been discovered that either contain coiled-coils or interact *via* the formation of a coiled-coil. It has been estimated that approximately 2 to 3 % of amino acids found in natural proteins form coiled-coil motifs (Berger, 1995; Lupas *et al*, 1991). However, it is now considered likely that these estimates are conservative since they were predicted before genomic sequence data was complete or even available for many species. Whereas pre-1990 the number of published journal articles describing the term "coiled-coil" was less than 80 per year, in the last two decades this has increased rapidly to over 700 articles per year (**Figure 1.4**). In order to identify coiled-coil motifs that may be of interest for

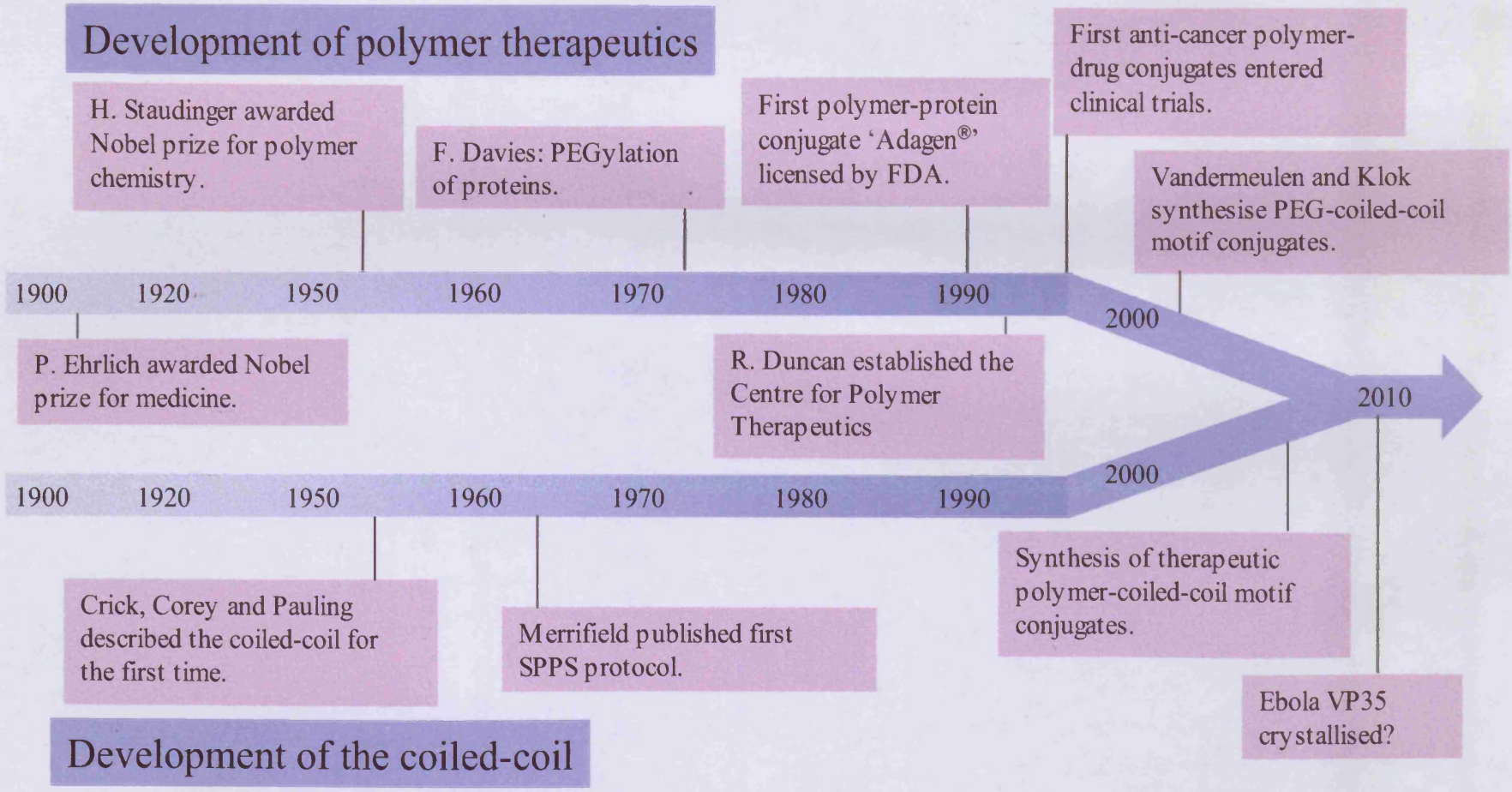

Figure 1.3 Time-line showing the significant events in the converging fields of polymer therapeutics and coiled-coil research.

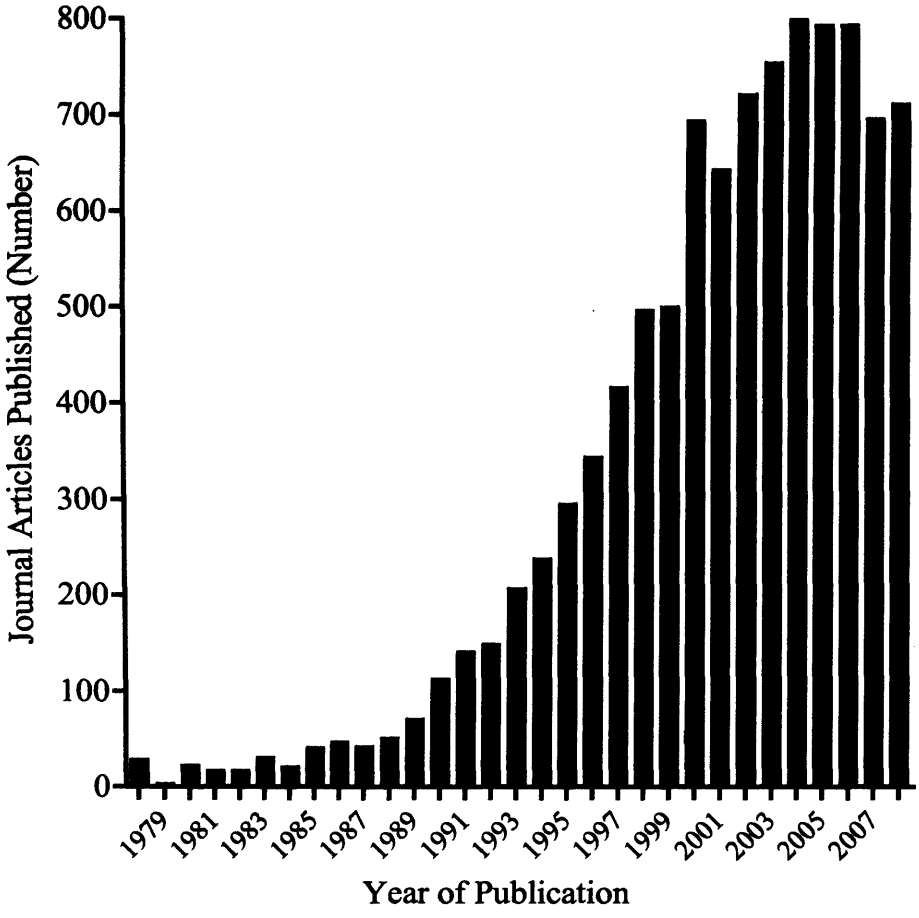

Figure 1.4 Journal articles citing "coiled-coils" from 1978 to 2007. Data obtained using SciFinder Scholar (vMac OSX 07). Before 1978 fewer than 6 articles per year were published.

development as the therapeutic component of a polymer-coiled-coil conjugate one needs to understand, at least in brief the structure of the coiled-coil.

The Molecular Structure of the Coiled-Coil Motif

The coiled-coil is an evolutionarily conserved structural domain consisting of between two and five, amphipathic α-helices (**Figure 1.5**) that wrap around each other to form a supercoil (Lupas *et al*, 1991). The α-helices may be arranged in either a parallel or anti-parallel conformation, and the composition of the domain may be either hetero or homo oligomeric. Most commonly, each α-helix consists of a seven residue (heptad) repeat sequence with each residue denoted a, b, c, d, e, f and g. However, very rarely, 11-residue (undecad) repeat sequences have also been observed (Hicks *et al*, 1997). In these structures, unlike the heptad repeat, the turn of the supercoil is right-handed i.e. the same as the underlying α-helices.

α-Helices with heptad repeats consist, generally, of hydrophobic amino acids at the first (a) and fourth (d) positions. This results in the formation of a hydrophobic seam that winds around each α-helix; it is along this seam that two or more α-helices associate (**Figure 1.6**) thus forming the most entropically favourable structure. Crick referred to the arrangement of hydrophobic amino acid side chains in a dimer as "knobs-into-holes packing" (Crick, 1953). This is the accepted hallmark of a coiled-coil and very accurately described the interaction that is, in part, responsible for the high stability of coiled-coil structures. Further stabilisation of the structure is often the result of amino acids at positions (e) and (g) forming ionic bonds or covalent disulphide bridges. The remaining amino acids (b, c and f) that constitute the heptad are generally polar or hydrophilic residues and thereby increase the solubility of the domain in aqueous environments. For further reading, the structures of coiled-coils have been reviewed previously (Lupas, 1996; Woolfson, 2005), more extensively and in more detail than is intended here.

It is important to note that coiled-coils found in nature often do not fit the mathematically ideal model described (Crick, 1953). For example, lysine, a hydrophilic amino acid, has been found, not uncommonly, to occupy positions (a) or (d) (Lupas *et al*, 1991). Furthermore, hydrophobic amino acids may be present in positions (b, c, e, f or g) thereby resulting in poor aqueous solubility of the peptide (Watanabe *et al*, 2000).

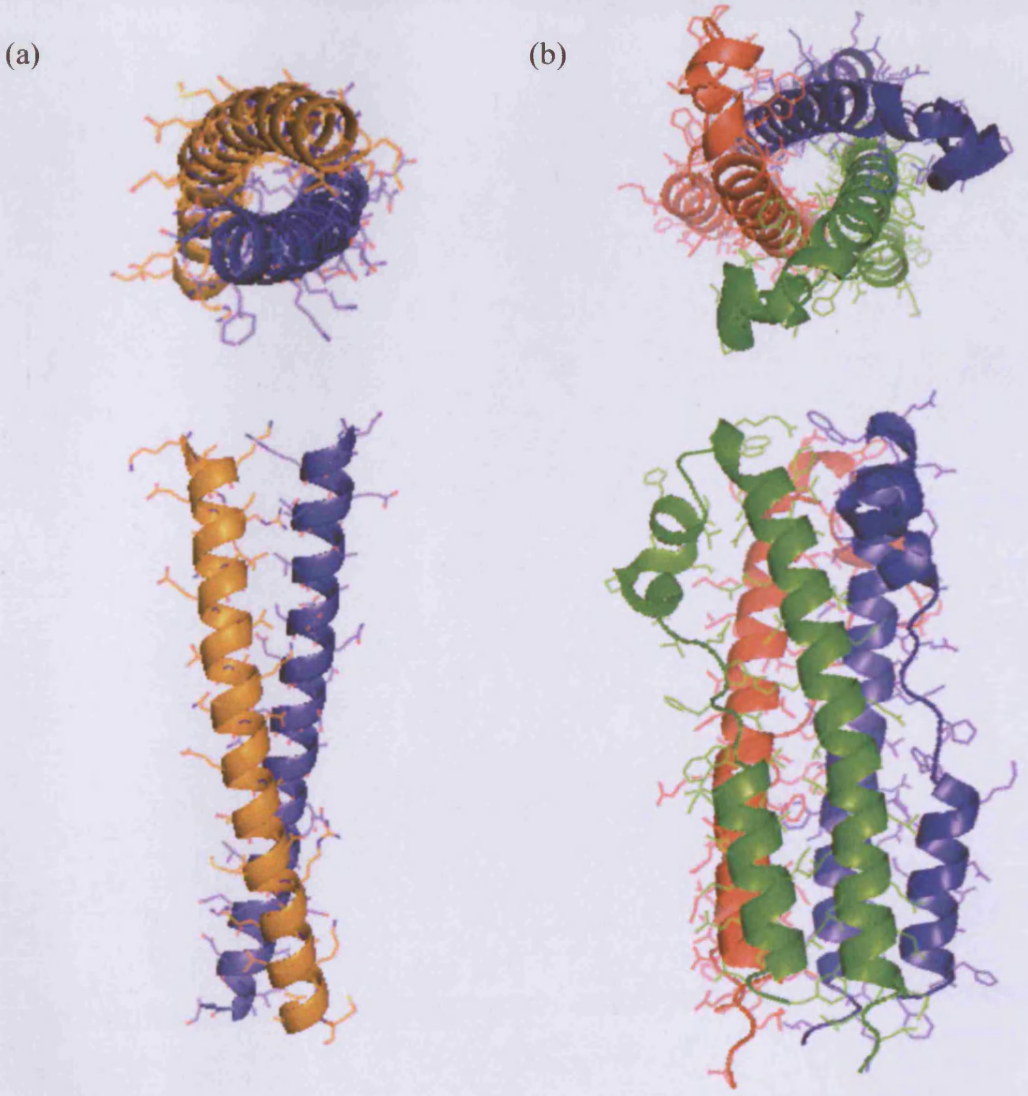

Figure 1.5 Cross sectional and sectional views of (a) a dimeric coiled-coil and (b) a trimeric coiled-coil. Higher order oligomers do exist including tetra and pentameric coiled-coils, however since they do not feature in this thesis they are not shown here. Protein structure files were obtained from the PDB, (a) DOI:10.2210/pdb1fos/pdb and (b) DOI:10.2210/pdb2ebo/pdb, editing and rendering was conducted using MacPyMOL.

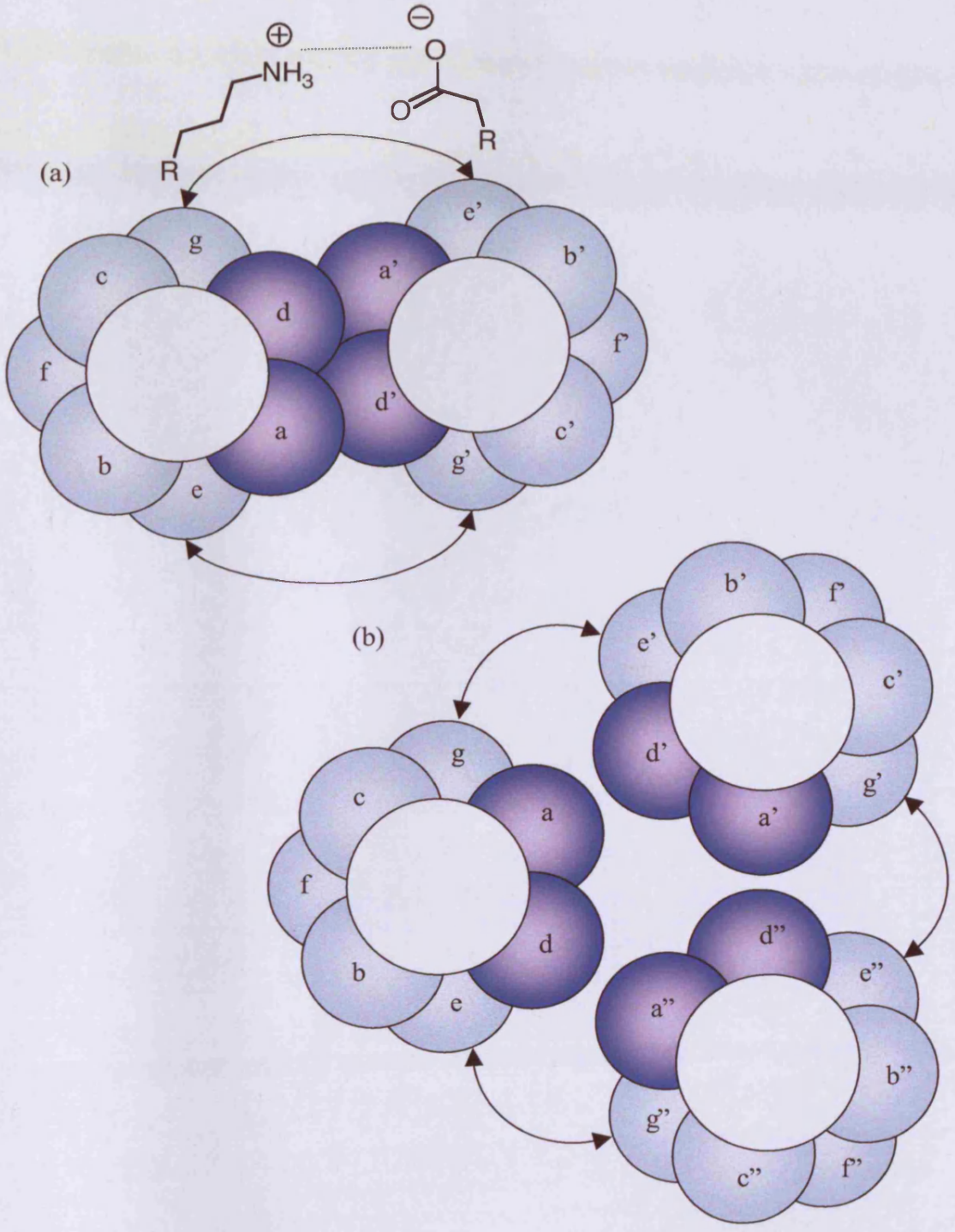

Figure 1.6 Helical-wheel illustration of (a) dimeric and (b) trimeric coiled-coils. The schematic illustration shows the hydrophobic 'seams', depicted in dark blue, while the electrostatic interactions which help to further stabilise the coiled-coil structures are shown with arrows. An example of such an interaction is shown in panel (a) and depicts the ionic bond between charged lysine and aspartic acid side-chains at heptad positions g and e', respectively.

The Role of the Coiled-Coil Motif in Regulation of Protein Function

Many biological signalling networks (Zhang *et al*, 2000), viral docking (Watanabe *et al*, 2000) and intracellular transport processes (Gillingham & Munro, 2003) rely upon protein-protein interactions for regulation including activation or deactivation. Specificity of these interactions is governed by the length and conformation of the interaction domains. The coiled-coil motif was chosen for development as a therapeutic entity because of its ability in nature to mediate highly specific interactions of medical significance, ease of synthesis and structural stability.

Following a review of the literature, a summary of coiled-coil motifs with potential for development as therapeutics is provided in **Table 1.1**. From this summary it is clear that there is a diverse range of diseases in which coiled-coils play a key role in pathogenesis from mediating oligomerisation in cancer (Shaulian & Karin, 2002) and viral infection (Bianchi *et al*, 2005; Reid *et al*, 2005), probing transmembrane pores as antimicrobial agents (Mohanty *et al*, 2003) to mediating Golgin-Rab membrane fusion (Barr & Short, 2003).

Use of the Coiled-Coil as a Therapeutic Entity

Remarkably, considering their functions in high profile diseases such as cancer and human immune deficiency virus (HIV), to date, the author has found few instances whereby a coiled-coil motif has been suggested as a novel therapeutic (Bianchi *et al*, 2005; Mason *et al*, 2006). Usually, where research has identified the coiled-coil motif as an essential component of pathogenesis, authors point towards the development of small molecule inhibitors (Joshi *et al*, 2003). However, it is worthy of note that the concept of using short peptide sequences, sometimes described as "miniature proteins" with therapeutic or structural characteristics comparable with those of the original protein from which they were derived has been discussed previously (Garner & Harding, 2007). Furthermore, coiled-coils have been utilised to stabilise antibody fragments (Arndt *et al*, 2001) and generate pH responsive hydrogels (Wang *et al*, 1999).

The use of the coiled-coil motif as a therapeutic, to drive the oligomerisation of one or more proteins into either an active or inactive complex is new, and in this context they may be considered molecular switches since pharmacological intervention, using a coiled-coil motif may make it possible to turn a pathway on or off with a high degree of specificity. In the clinic, it has been shown that it is possible to competitively inhibit or

Table 1.1 Summary of biological proteins that contain coiled-coil motifs with potential for therapeutic intervention.

Protein	Biological Function	Cellular Location and Structural Summary	Proposed Therapeutic Intervention/Use	References
AP-1	Oncogenic transcription factor	Heterodimeric complex of proteins from the Jun and Fos. Monomeric proteins located in cytosol/nucleus, dimer is formed in nucleus.	Competitively inhibit the formation of the heterodimer and thus down-regulate AP-1 mediated transcription.	Shaulian & Karin, 2002; Eferl & Wagner, 2003; Mason *et al*, 2006
Multi-Drug Resistance Protein A: EmrA (*Escherichia coli - E. coli*)	EmrA binds with TolC to form a complex that acts as an efflux pump. Mechanism of bacterial, multi-drug resistance.	Protein is anchored in cell membrane, whilst coiled coil motif extends into the periplasmic space. 18-residue dimeric/trimeric coiled- coil motif mediates binding with TolC.	Prevent action of efflux pump with a synthetic peptide; increase effectiveness of current anti-biotic therapy.	Borges-Walmsley *et al*, 2003; Zgurskaya & Nikaido, 1999
BRCA1	Binds to JunB to regulate transcription and suppress tumour growth. In various cancers the coiled-coil motif is mutated preventing dimerisation.	34-residue dimeric coiled-coil motif exists in the AD1 domain of BRCA1.	Breast and/or ovarian carcinoma suppression with a synthetic peptide corresponding to AD1 coiled-coil.	Hu & Li, 2002; Hu *et al*, 2000

Table 1.1 Summary of biological proteins that contain coiled-coil motifs with potential for therapeutic intervention.

Protein	Biological Function	Cellular Location and Structural Summary	Proposed Therapeutic Intervention/Use	References
E Colicins 1-9	All bind to *E. coli* outer membrane cobalamin transporter BtuB. Membrane depolarising (1), DNase activity (2, 7, 8 and 9), RNase activity (3, 4, 5, 6).	> 100-residue dimeric coiled coil is part of a tripartite structure consisting of receptor binding, translocation and toxin domains connected by coiled coils.	Delivery of bacteriocidal therapeutics. 'Hair-pin' of coiled-coil may have bacteriocidal activity.	Cao & Klebba, 2002; Mohanty *et al*, 2003
E2 factor (E2F) Transcription Factor Family	DNA transcription factor.	Two pairs of potential heptads exist in a sequence of 54 amino acids in the 'marked box domain' of the protein, separated by a sequence of 20 amino acids. Possibly a dimeric or trimeric coiled-coil. Nuclear.	Suppression of transcription with a synthetic peptide would be a novel treatment for cancer and proliferative disorders.	Joshi *et al*, 2003; Stevaux & Dyson, 2002; Wang *et al*, 1999
Ebola Virus Glycoprotein -2 (GP2)	Drives apposition of host cell and viral membranes to enable virus entry into cell.	Each GP2 protein is composed of a C-terminal and an N-terminal α-helix. The latter drives the formation of a homotrimeric coiled-coil.	Competitive inhibition of GP2 trimerisation using a synthetic coiled-coil motif to inhibit viral fusion.	Watanabe *et al*, 2000.

Table 1.1 Summary of biological proteins that contain coiled-coil motifs with potential for therapeutic intervention.

Protein	Biological Function	Cellular Location and Structural Summary	Proposed Therapeutic Intervention/Use	References
Ebola Virus, Viral Polymerase Protein 35 (VP35)	Interferon (IFN) α and β down-regulation. Coiled-coil domain may mediate viral RNA synthesis.	37 residue trimeric coiled-coil. Following viral infection of cell the coiled-coil motif mediates homo-trimerisation. Cytoplasmic location.	Prevent oligomerisation with an inhibitory, coiled-coil peptide. Previous research has shown that this could decrease VP35 activity by 100 fold.	Basler *et al*, 2003; Basler *et al*, 2000; Reid *et al*, 2005
HIV gp41HR1	HIV gp41 is essential for fusion and entry into host cells.	48-residue trimeric coiled-coil. HR1 is an N-terminal heptad repeat, it mediates trimerisation of gp41.	Coiled-coil peptide has been shown to inhibit fusion of HIV to host cells.	Bianchi *et al*, 2005
Laminins 1-12.	Cell adhesion, e.g. coiled-coil mediated agrin binding.	50-80 residue, parallel trimer is a structural component of laminin protein.	Incorporation into a drug delivery system as a targeting moiety. Immobilise on surfaces to promote cell adhesion.	Rousselle *et al*, 1995; Sanz *et al*, 2003; Tunggal *et al*, 2000
Macrophage Scavenger Receptor (MSR) I & II.	Receptor mediated endocytosis of a range of ligands e.g. lipopolysaccharide (LPS) and low-density lipoprotein (LDL).	22-residue trimeric coiled-coil is located in extracellular component of protein, a decreased pH induces a conformation change to release ligand.	Design of a synthetic system using the pH sensitive coiled-coil to clear LPS from gram – ve bacteria during sepsis.	Frank *et al*, 2000; Suzuki *et al*, 1997

Table 1.1 Summary of biological proteins that contain coiled-coil motifs with potential for therapeutic intervention.

Protein	Biological Function	Cellular Location and Structural Summary	Proposed Therapeutic Intervention/Use	References
P115	Forms a hetero-oligomer with Rab1. The homo-oligomer promotes the formation of syntaxin-5 containing SNARE bundles.	28-residue, parallel dimers exist in four regions of predicted coiled-coil structure between an N-terminal globular head and C-terminal acidic domain. Cytoplasmic location.	Modulate Rab1 signalling. May have potential in treatment of lysosomal storage diseases.	Beard *et al*, 2005
PIGEA-14	Forms homo-oligomers, also hetero-oligomers with polycystin-2 and GM130. It affects the intracellular distribution of polycystin-2.	59-residue coiled-coil. Cytoplasmic location. Approximately half of the protein exists as a coiled coil motif.	Only present in renal tissue, therefore drug targeting potential. Treatment of polycystic kidney disease.	Hidaka *et al*, 2004
Prohibitin (PHB)	Hetero-oligomerisation with all transcriptionally active members of the E2F family (1-5) thus preventing transcription.	41-residue protein, possibly forms a dimer and / or trimer. Cytoplasmic location.	A peptide corresponding to the coiled-coil motif induces apoptosis and growth suppression in cell culture. Novel therapeutic for cancer and proliferative disorders.	Joshi *et al*, 2003

Table 1.1 Summary of biological proteins that contain coiled-coil motifs with potential for therapeutic intervention.

Protein	Biological Function	Cellular Location and Structural Summary	Proposed Therapeutic Intervention/Use	References
Prostate Apoptosis Response Factor (Par-4)	Under expression: cancers of the colon, prostate and kidney. High levels: neurone death, Alzheimer's disease. Forms homo and hetero-oligomers, coiled-coil motif recently shown to be inactive as a tumour suppressor.	38-residue dimeric coiled-coil. Protein is predominantly a coiled-coil at C-terminus. Classified as a leucine zipper.	Treatment of Alzheimer's with a peptide that forms a homo-oligomer, thus preventing pathogenic hetero-oligomerisation.	Guo *et al*, 1998; Chakraborty *et al*, 2001; El-Guendy & Rangnekar, 2003; Guo & Xie, 2004; Xie & Guo, 2005
Stat3	One of a family of latent transcription factors. It has dual functions, acting as a signalling molecule and transcription factor. Forms heterooligomers.	191 residue tetrameric coiled-coil. Cytoplasmic transcription factor containing a coiled-coil motif between the N-terminal domain and DNA binding domain.	Utilisation of nuclear localisation signal.	Ma *et al*, 2003; Zhang *et al*, 2000
TRK-T3	Oncogenic thyroid protein. Oncogenicity is mediated via homo-oligomerisation.	20-30 residue trimeric coiled-coil. Cytoplasmic protein.	Prevent homo-oligomerisation with an inhibitory, coiled-coil peptide.	Greco *et al*, 1998

disrupt coiled-coil oligomerisation by introducing an α-helical peptide with a higher affinity than the wild-type and it has been suggested that the 36-amino acid synthetic anti-HIV peptide Fuzeon (Enfuvirtide) (Fletcher, 2003) inhibits fusion of HIV-1 with $CD4^+$ cells in this way.

The underlying premise of this research is that judicious selection and/or engineering of the coiled-coil sequence will allow design of monomethoxyPEG (mPEG) conjugates that could (i) neutralise infectious diseases (e.g. the Ebola virus) in the circulation, (ii) prevent cellular entry/activity (e.g. HIV or the Ebola virus), or (iii) interrupt nuclear or cytosolic biochemical pathways (e.g. activator protein-1 (AP-1) transcription factor in cancer) (**Figure 1.7**).

A Note on the Nomenclature of Coiled-Coils

Often, in the literature, sequences that form a coiled-coil are referred to interchangeably as peptides or proteins. Since there is not universal agreement as to what defines a polypeptide as a protein or peptide this is not surprising. In this thesis, polypeptides of fewer than 50 amino acid residues are typically referred to as peptides, those that are larger are referred to as proteins. A further point of confusion is that peptides with the propensity to form a coiled-coil are referred to as "coiled-coil peptides" (Joshi *et al*, 2003). In fact, they are α-helical peptides and should only be considered a coiled-coil following homo or hetero-oligomerisation. As such, in this thesis "coiled-coil peptides" are referred to as 'coiled-coil motifs' and the resultant hetero/homo-oligomer a 'coiled-coil' for clarity.

Synthesis of Coiled-Coil Motifs

In order to understand the rationale for the choice of protein targets in section 1.5 from the many summarised in **Table 1.1**, it is important to introduce the principles and limitations of peptide synthesis here. More detail is provided in Chapter 3.

Many methods have been published with respect to the synthesis of peptides and proteins and most, if not all, may be applied to the synthesis of coiled-coil motifs. The advent of solid phase peptide synthesis (SPPS) has made it possible to create synthetic coiled-coils with relative ease. Current protocols however limit the chain length of amino acids synthesised to less than 50 (Chan & White, 2000). Yet, in order to obtain a high yield it is preferable to keep below 40 amino acids. The cost of new therapeutics is an essential consideration that should be borne from the very beginning stages of design

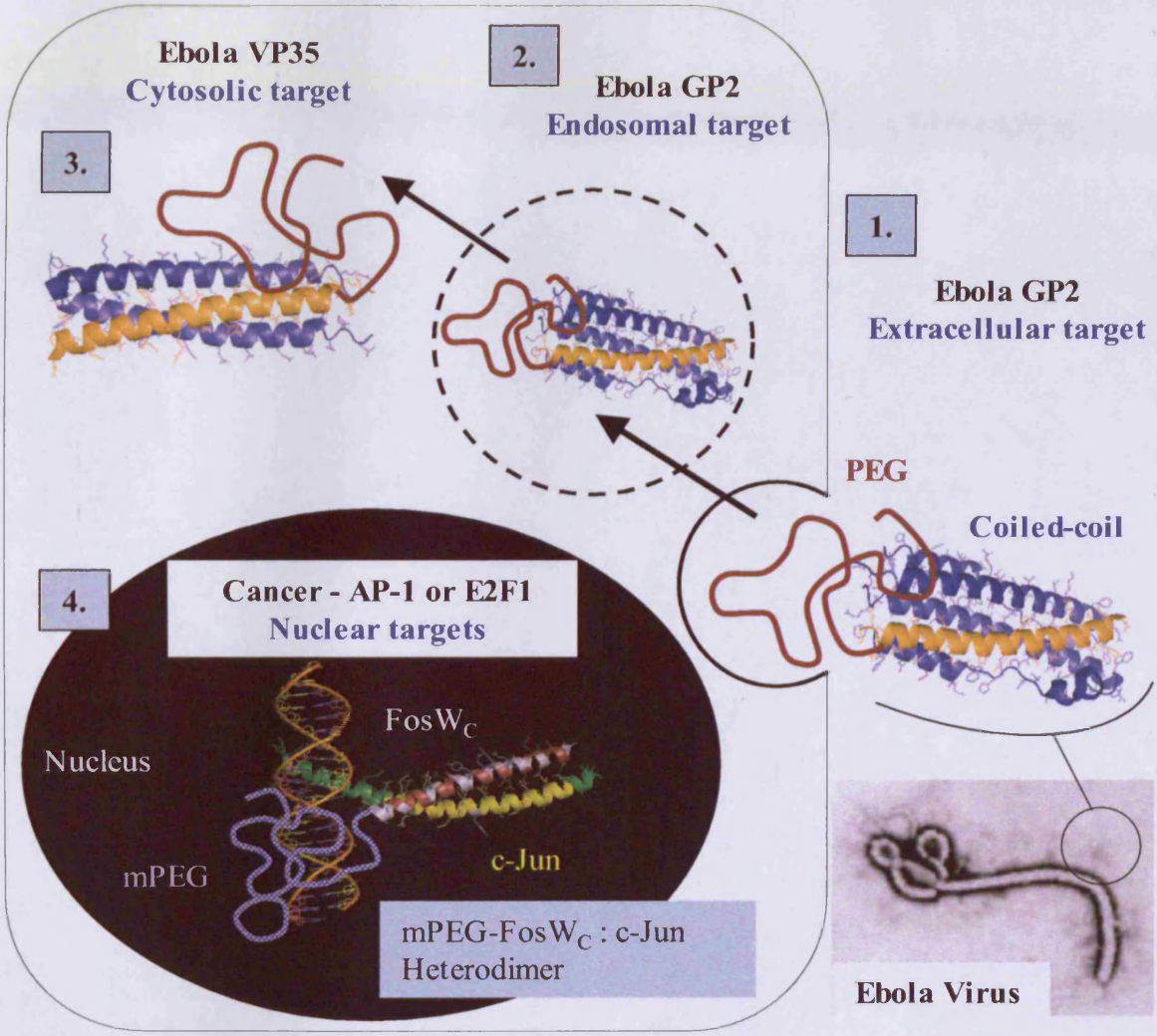

Figure 1.7 Cartoon to illustrate the cellular locations of the coiled-coil proteins targets. The cellular location of the target will influence the design of polymer-coiled-coil therapeutic and design of *in vitro* experiments since local conditions such as pH will vary. Protein structure files were obtained from the PDB, illustrations of EbGP2 and EbVP35 were adapted from DOI:10.2210/pdb2ebo/pdb, while illustration of the nuclear target AP-1 was adapted from DOI:10.2210/pdb1fos/pdb, editing and rendering was conducted using MacPyMOL.

(Sato *et al*, 2006). Therefore when reviewing the targets summarised in **Table 1.1**, a primary consideration was that the sequences chosen for synthesis should be less than 40 residues in length.

Caveats and Limitations of Therapeutic Peptides

As drugs, peptides have inherent limitations including their short plasma half-life, susceptibility to proteolytic degradation and the challenge of delivery to the target (Sato *et al*, 2006). As PEGylation is already a well-established method of improving plasma half-life, biological stability and reducing proteolysis and imunogenicity of covalently bound peptides and proteins this approach has real potential to generate therapeutically useful mPEG-coiled-coil therapeutics (Davis, 2002; Harris & Chess, 2003; Veronese & Harris, 2008). This concept is discussed in the following section.

1.3 Nanomedicine and Polymer Therapeutics

Research emanating from the field of Nanomedicine, has the potential to contribute some of the greatest developments of the 21st Century. In 2005 the European Science Foundation (ESF) Forward Look on Nanomedicine document (ESF, 2005) defined the field of nanomedicine as:

"...the science and technology of diagnosing, treating and preventing disease and traumatic injury, of relieving pain, and of preserving and improving human health, using molecular tools and molecular knowledge of the human body. It embraces five main sub-disciplines which are in many ways overlapping and are under-pinned by common technical issues."

Nanomedicine may be sub-divided into five disciplines including the development of novel therapeutics and drug delivery systems i.e. nanopharmaceuticals. This term has also been defined in the ESF report:

"Nanopharmaceuticals can be developed either as drug delivery systems or biologically active drug products. This sub-discipline was defined as the science and technology of nanometre size scale complex systems, consisting of at least two components, one of which is the active ingredient. In this field the concept of nanoscale was seen to range from 1 to 1000 nm." (ESF, 2005).

"Polymer therapeutics" can be considered one class of nanopharmaceuticals according to this definition. This umbrella term was coined in the mid 1990s (Duncan

et al, 1996) and it describes the field of research encompassing the development of "...polymeric drugs (Donaruma, 1975), polymer-drug conjugates (Duncan, 1992), polymer-protein conjugates (Harris & Chess, 2003), polymeric micelles to which drug is covalently bound (Yokoyama, 1990) and multi-component polyplexes being developed as non-viral vectors (Kabanov, 1998)" (reviewed in Duncan, 2003).

The landmark historical events in this field are illustrated in **Figure 1.3**. Over the past 50 years we have observed increasingly rapid progress in the transfer of polymer therapeutics into routine clinical use. Pioneering events in the field began with the first clinical evaluation of the synthetic polymeric anticancer agent divinylethermaleicanhydride (DIVEMA) in the 1960s (reviewed in Regelson & Parker, 1986), Ringsdorf's vision of the ideal polymer chemistry to effect drug conjugation followed by the concept of the targeted polymer drug-conjugate (Ringsdorf, 1975) and the PEGylated proteins first proposed by Davis and Abuchowski in the 1970s (reviewed in Veronese & Harris, 2008). The "market approval of the first polymer–protein conjugates (PEG–adenosine deaminase, PEG-L-asparaginase and styrene maleic anhydride neocarzinostatin (SMANCS)) in the early 1990s was a landmark step (Fuertges & Abuchowski, 1990). Promising results from clinical trials involving polymer-anticancer-drug conjugates (reviewed in Duncan, 2005) has given further credibility to the field of polymer therapeutics which is now growing exponentially (reviewed in Duncan, 2003).

Polymer-Protein/Peptide Conjugates

In the context of this thesis, the polymer-coiled-coil motif conjugates may be considered a sub-type of polymer-protein conjugates. Polymer-protein conjugates were the first polymer therapeutics to enter the clinic as anti-cancer agents in the 1990s. Less than 20 years on, many polymer-protein conjugates are now used routinely in the clinic as anti-cancer agents, and additionally for an ever-growing range of indications (**Table 1.2**).

The first polymer-protein conjugate to enter the clinic with market approval was Adagen® (PEG-adenosine deaminase) in 1990 for the treatment of severe combined immunodeficiency (SCID) syndrome. Since then many polymer-protein conjugates have been developed and progressed to market with many more at various phases of clinical trial (**Table 1.2**). Shortly after Adagen®, Oncaspar® (PEG-L-asparaginase), was approved by the FDA in 1994, for the treatment of acute lymphoblastic leukaemia

Table 1.2 Polymer-protein conjugates in the clinic or late stage clinical trials.

Polymer-Protein Conjugate	Indication	Phase
Adagen®	SCID Syndrome	Clinic
Neulasta®	Non-Myeloid Malignancies	Clinic
Oncaspar®	Acute Lymphoblastic Leukaemia	Clinic
PEGASYS®	Hepatitis C	Clinic
PEG-INTRON®	Hepatitis C, clinical evaluation in cancer, multiple sclerosis (MS) and HIV/AIDS	Clinic
Somavert®	Acromelagy	Clinic
Zinostatin Stimalamer (SMANCS)	Hepatocellular Carcinoma	Clinic
Macugen™	Age-related macular degeneration	Clinic
Cimzia®	Rheumatoid arthritis and Crohn's disease	Clinic
CDP791	Solid tumours expressing vascular endothelial growth factor receptor-2 (VEGFR-2)	Phase II

(ALL) (reviewed in Graham, 2003).

In Japan, the polymer-protein conjugate SMANCS, was developed by Maeda and colleagues by covalently linking two styrene maleic anhydride (SMA) polymer chains to neocarzinostatin (NCS), an anti-tumour protein (reviewed in Maeda & Konno, 1997). SMANCS was developed for use in patients with advanced liver cancer and administered *via* injection into the hepatic artery. Polymer modification of the NCS protein generated a conjugate that was sufficiently hydrophobic to enable dispersion in the phase contrast agent Lipiodol (Iwai *et al*, 1984, Konno & Maeda, 1987), this made it possible to administer the agent with the aid of X-Ray imaging. With few other effective agents available and the prognosis for primary liver cancer being so poor, the remarkable activity seen with SMANCS resulted in approval being granted in Japan for the treatment of advanced and recurrent hepatocellular carcinoma (reviewed in Abe & Otsuki, 2002). Unlike most other drugs currently in use as anti-cancer agents, SMANCS was used most successfully when administered as a 'patient-individualised therapy' i.e. dosing was adjusted in each patient according to tumour size (area) and further injections only given if the tumour was not seen to regress. Although in concept well ahead of its time, this treatment strategy, coupled with the complex protocol for reconstitution has resulted in failure to meet the regulatory standards required for approval by the FDA and European Medicines Agency (EMEA). Another very significant discovery that was made by Maeda *et al* was that polymer-protein conjugates passively target tumour tissue via the "Enhanced Permeation and Retention" (EPR) effect (Matsumura & Maeda, 1986). Essentially, this effect is due to the vascular tissue in tumours being 'leaky' as a result of rapid, unordered proliferation. Therefore increasing the concentration of conjugate at the target and reducing the potential for dose limiting toxicity.

PEG-interferon followed, with the development of PEGASYS (reviewed in Wang *et al*, 2002) and PEG-Intron (Bukowski *et al*, 2002) as agents for the treatment of Hepatitis. When used in combination with the drug Ribavirin against Hepatitis C, sustained virological response is seen in at least 50 % of patients, as such PEGylated IFN is now the gold standard treatment (reviewed in Cross *et al*, 2008). Both forms of PEG-IFN are now being investigated for the treatment of other diseases and have recently shown great promise in the treatment of stage III melanoma (Eggermont *et al*, 2008). While only a few of the now many polymer-protein conjugates on the market

have been discussed here, it is fair to say that PEG conjugated proteins have been the most successful polymer-protein conjugates to date.

1.3.1 PEGylation

The concept of covalently attaching one or more PEG molecules to, for example, a protein or peptide is now widely referred to as "PEGylation". First described by Davis and Abuchowski in the 1970s (reviewed in Veronese & Harris, 2008), it has proven the most successful technique for the synthesis of polymer-protein conjugates. Today, at least 11 such conjugates (**Table 1.2**) are now either in the clinic or progressing through clinical trials. Thus giving credence to the pharmaceutical applicability of the technique. As such, for preliminary proof of concept studies, PEG with appropriate functionalisation will be used as the polymer to which the coiled-coil motif is conjugated.

What Characteristics make mPEG suitable for Conjugating to Coiled-Coil Motifs?

Whilst many polymers are now used in the design of polymer therapeutics it is necessary to consider the specific physicochemical and biochemical characteristics make only a select few polymers suitable for use in the development of polymer-coiled-coil motifs conjugates. These characteristics relate to solubility, functionality, size, heterogeneity, toxicology, immunogenicity, cost and ease of synthesis. It is pertinent to recognise that the specifications for each of these criteria relate not only to the polymer, but also to the final polymer-peptide conjugate.

PEG has been shown to increase protein solubility and stability as well as reduce potential immunogenicity (reviewed in Harris & Chess, 2003; Pasut *et al*, 2004). PEG is highly soluble in aqueous media at physiological pH (7.4) and temperature (37 °C), and is non-toxic, and non-immunogenic following repeated administration. Furthermore, the biocompatibility, haemocompatibility and immunocompatibility of PEG have been well studied and documented (Rihova & Riha, 1985).

The pharmacokinetic (PK) profile of a protein is improved following PEGylation as a function of reduced renal clearance. PEG is particularly useful here as its hydrodynamic radius is 5-10 times greater than a globular protein of a similar

molecular weight as a result of a highly hydrated structure. The prolonged plasma-half-life results in less frequent dosing and greater convenience to the patient.

One potential caveat, however, is that non-biodegradable polymers such as high molecular weight PEG (> 40,000 g mol^{-1}) which exceed the threshold for renal clearance may accumulate within the body (reviewed in Robinson *et al*, 1990). Should these polymers accumulate within lysosomes then there is a theoretical risk of inducing lysosomal storage disorders (reviewed in Vellodi, 2005; Garnett & Kallinteri, 2006). As such PEG-conjugates are probably best used for diseases that require acute phases of treatment such as cancer rather than long-term chronic infections e.g. arthritis.

Another advantage of PEG is that it is commonly available as a semitelechelic polymer (mPEG), i.e. it has only one reactive functional group. This simplifies the process of synthesising monoPEGylated coiled-coil motif conjugates without the risk of cross-linking occurring. Where this thesis differs from the design of many other (pre-Cimzia®) polymer-protein conjugates is that attachment of mPEG or other polymer to the coiled-coil motif must be *via* either the N or C terminus or an amino acid side chain positioned at one of the termini, and not *via* a random amino acid side chain. Conjugation to the latter would likely disrupt the α-helical structure of the motif and abrogate the ability of the peptide to form a coiled-coil. This is discussed in more detail in Chapter 4.

Previous collaborative research has given some insight into the possibilities of PEGylating coiled-coil motifs (Vandermeulen *et al*, 2003; Vandermeulen *et al*, 2004; Vandermeulen *et al*, 2005). Conjugation *via* the assembly of smaller units using simple chemistries often referred to as 'click chemistry' (Kolb *et al*, 2001) becomes less favourable with large monofunctional polymers such as mPEG > 5,000 g mol^{-1} due to poor kinetics and unacceptably low reaction yields. This is not entirely unexpected as one is trying to react two macromolecules *via* a single reactive group on each. Alternative chemistries and methods of conjugation exist and will be explored in the course of this thesis. An interesting approach is to synthesise the coiled-coil motif from the amine terminus of a 3,000 g mol^{-1} PEG bound by a cleavable linker to a polystyrene resin, or the reverse, whereby mPEG (in excess) is reacted with peptides still attached to the solid-phase support (resin) as conducted by Vandermeulen *et al,* (2005). Another option could be to investigate the use of thiol (R-SH) chemistry to site-specifically conjugate mPEG with the coiled-coil motif peptide via the formation of a thioether linker (Dosio *et al*, 1998). The ideal linker chemistry is one that allows site-specific

conjugation of the PEG chain to the peptide with the resultant bond stable to degradation under physiological conditions and is non-toxic, the pros and cons of the approaches described above are discussed in more detail in Chapter 4.

A Note on the Units Used to Describe Polymers

One of the most important descriptors used for polymers is molecular size. Various physical quantities may be used; most commonly these refer to molecular weight or particle size. The latter is more often used when describing solid micro- or nano-particulate systems. However molecular weight is favoured for polymers since it gives a more precise measure of the composition of the molecule. In the context of this thesis, the terms molecular weight and molar mass may be considered synonymous. The units of molecular weight are commonly expressed as either g mol^{-1} or Daltons (Da); references to molecular weight in biology often use kDa (1,000 Da) when describing proteins or peptides. In polymer science however, it is more common to express molecular weight in g mol^{-1}. Assuming an average isotopic abundance, 1 Da = 1 g mol^{-1}, for consistency the latter will be used throughout this thesis when referring to polymers, peptides or polymer-peptide conjugates. Unlike peptides, proteins and nucleic acids, which have discrete molecular weights, synthetic polymers do not have one unique value, rather it is an average of a distribution. There are many ways in which the average molecular weight can be calculated; the two most commonly used are the number average molecular weight (Mn) and the weight average molecular weight (Mw). Mn is the arithmetic mean and thus represents the total weight of the polymer molecules present, divided by the total number of polymer molecules. It is most often used when describing thermodynamic properties e.g. osmotic pressure where the number of molecules is an important consideration. Mn values are highly sensitive to small molecules in the mixture, whereas Mw, which is a weight average considers the mass of the polymer molecules and therefore gives greater importance to the heavier molecules in the distribution. Therefore, Mw is always greater than Mn. The distribution of polymer molecules will depend upon the manner in which the polymer is prepared and the quality of the synthesis and purification methods used. The molecular weight distribution is expressed in terms of Mn and Mw (Mw/Mn) and is termed the polydispersity index. If Mw/Mn = 1 the polymer is monodisperse, however, for real polymers Mw/Mn is always greater than 1. The amount to which it is greater is a measure of the polydispersity.

1.4 Challenges Associated with the Delivery of Polymer-Coiled-Coil Motif Conjugates

Many of the coiled-coils identified as potential therapeutic targets are of an intracellular location (**Table 1.1**). For this thesis, biological targets of differing cellular localisation were selected (**Figure 1.7**) such that, if intracellular delivery became difficult to realise it would be possible to investigate the biological activity of coiled-coil motifs acting in an extracellular environment. Four protein targets were selected for study and are discussed in more detail in the following section (1.5), three of these targets: E2F1, c-Jun and EbVP35 are of an intracellular location. More specifically, as transcription factors, E2F1 and c-Jun, are predominantly located in the nucleus while EbVP35 has been shown to be located in the cytoplasm following host cell infection by the Ebola virus (Bjorndal *et al*, 2003).

The priority for this thesis was to achieve intracellular delivery, not to determine exactly which mechanisms of uptake were necessarily involved. However, if such information could be acquired in the process, and the mechanisms alluded to then this would obviously be considered advantageous. In order to ascertain whether delivery of the mPEG-coiled-coil motif conjugate to the site of the target protein was achieved an understanding of the barriers to delivery and the main mechanisms of intracellular uptake was deemed important.

Cell Membrane

The cell membrane is a semi-permeable amphipathic-lipid bilayer found in all eukaryotic cells (Alberts *et al* 2002). It is primarily composed of phospholipids, arranged such that the hydrophilic phosphate head groups shield the hydrophobic tails from the aqueous environment by the formation of a continuous bilayer. The abundance of the phosphate head groups at both the extracellular and intracellular membrane results in a highly charged anionic surface. By virtue of their charge, anionic molecules have great difficulty in crossing the membrane (discussed in Chapter 6). Furthermore, the compact structure of lipids, proteins and carbohydrates renders the cell membrane impermeable to most molecules $\geq$ 1,000 g mol^{-1} (reviewed in Bareford & Swaan, 2007). In order for cells to internalise large or highly charged molecules, a process involving invagination of the cell membrane followed by engulfing of the

macromolecule(s) in a lipid membrane vesicle is used. This vesicle, or "endosome" may then be trafficked within the cell.

Endocytosis

The term "endocytosis" is used to broadly describe the many mechanisms by which living cells internalise and traffic macromolecules in the maintenance of homeostasis (**Figure 1.8**). Endocytosis is essential to the healthy function of all cells since it enables the transport of molecules too large or to diffuse through the lipid-bilayer to be sent to various organelles for processing. Xenobiotics, such as polymer therapeutics are known to be endocytosed (Duncan & Kopecek, 1984) using mechanisms similar to those for transferrin (Watts, 1985) or low-density lipoprotein (Anderson *et al*, 1977).

At least six types of encapsulation and internalisation by mammalian cells have been defined and are classified according to their requirements for caveolin, clarithryn, dynamin and lipid rafts (reviewed in Conner & Schmid, 2003). It is important to note that whilst the majority of uptake of a given macromolecule may be *via* one mechanism it cannot be said with any degree of certainty that uptake *via* a minor route is not responsible for the observed biological effect. Whilst elucidation of vesicle composition and encapsulation route would be interesting it is considered to be outside the remit of this thesis. As demonstrated in **Figure 1.8**, the process of endocytic uptake and subsequent trafficking is highly dynamic. As such, it is dangerous to make assertions about particular components without considering the 'big picture' i.e. the whole cell.

Endosomotropic Drug Delivery

Delivery of a macromolecule such as a polymer-coiled-coil motif conjugate from an endosome into the cytosol of a cell constitutes endosomotrophic drug delivery. In the context of this thesis, this is particularly desirable since the peptide coiled-coil motif is likely to be degraded by the many proteolyic enzymes and/or low pH present in lysosomes (Seaman & Luzio, 2001; Luzio *et al*, 2007) (**Figure 1.8**).

Endosomes are the first compartments entered following internalisation at the plasma membrane. The local environment is mildly acidic (pH ~ 6.5) however does not contain proteolytic enzymes (Seaman & Luzio, 2001). The proposed mPEG-coiled-coil motif conjugates are unlikely to escape from endosomes into the cytosol unless the

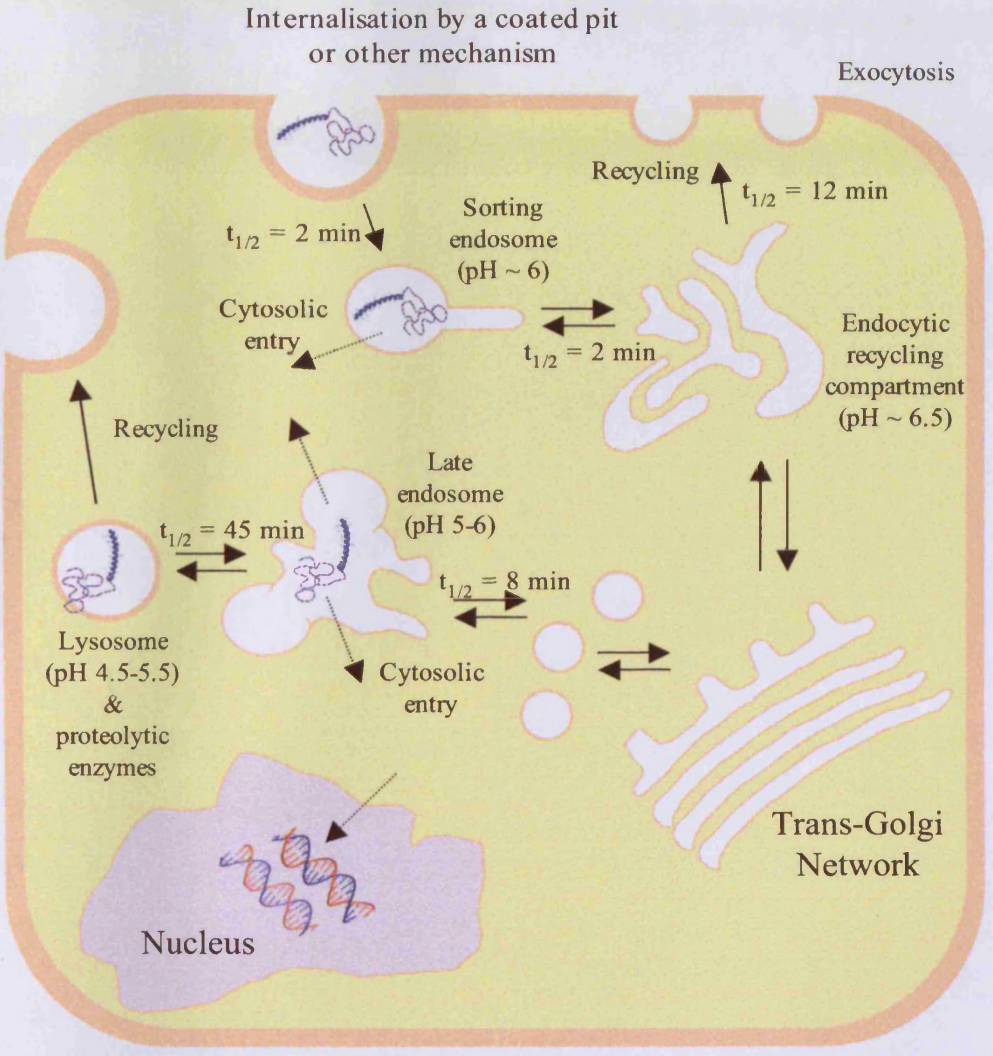

Figure 1.8 An overview of endocytic trafficking in non-polarised mammalian cells. The $t_{1/2}$ values are approximate and are cell-type dependent. Adapted from Maxfield and McGraw, 2004.

peptide coiled-coil motif has an innate endosomolytic feature. Some peptides, e.g. HIV-Tat are able to mediate cytosolic entry by penetrating the cell membrane either directly or during endocytosis (Richard *et al*, 2003; reviewed in Wagstaff & Jans, 2006). It is likely that the large number of positively charged residues (arginine and lysine) in the peptide are responsible for facilitating this process, however the exact mechanisms are not well understood. The use of transfection reagents e.g. cationic peptides and lipids is discussed in more detail in Chapter 6.

1.5 Biological Targets

Many of the proteins reviewed (**Table 1.1**) contained sequences that fulfilled the selection criteria, to test the concept of developing polymer-coiled-coil motifs as novel therapeutics. An important selection criterion was that the protein should be involved in the pathology of a disease with medical significance. As such, proteins involved in the pathogenesis of cancer, in particular breast cancer, were desirable targets.

The E2 factor (E2F) family of transcription factors are fundamental to the control of cell division (Dimova & Dyson, 2005) and function to regulate whether a cell will arrest in G1 or enter S-phase (reviewed in DeGregori, 2002). Furthermore, deregulation of E2F activity has been shown in numerous studies to correlate with human cancers, particularly those with a poor prognosis (Nevins, 2001; Gorgoulis *et al*, 2002; Ebihara *et al*, 2004; Foster *et al*, 2004; Feber *et al*, 2004; Oeggerli *et al*, 2004). Recently, a peptide corresponding to the putative coiled-coil motif of the tumour suppressor protein prohibitin (PHB) has been shown to induce apoptosis possibly *via* a coiled-coil type interaction with E2F1 (Joshi *et al*, 2003). However, since a coiled-coil interaction was inferred rather than shown to exist using either CD or nuclear magnetic resonance (NMR) spectroscopy (see Chapter 3 for discussion) it was deemed necessary to select other target proteins to be sure of testing the hypothesis proposed. It would be too risky to focus this research entirely on PHB/E2F1 only to discover later that the peptide motif identified by Joshi *et al,* (2003) was not active as a coiled-coil.

As such the transcription factor, activator protein-1 composed of the proteins c-Jun and c-Fos was chosen for study (section 1.5.2) (reviewed in Shaulian & Karin, 2002). The crystal structure of c-Jun and c-Fos bound to DNA obtained by Glover and Harrison (1995) demonstrated conclusively, that the active complex was formed *via* a dimeric coiled-coil between the c-Jun and c-Fos proteins. Furthermore numerous

studies have shown the involvement of either c-Jun or c-Fos in breast, amongst many other cancers (Wang *et al*, 2000; Ameyar-Zazoua *et al*, 2005; Lu *et al*, 2005). As transcription factors, both E2F1 and AP-1 are predominantly located in the nucleus, therefore the delivery of polymer-coiled-coil motif conjugates is likely to be a challenge (discussed in section 1.4). Thus, two additional targets were selected on the basis of having different cellular locations.

Many viruses utilise coiled-coil proteins to control key processes fundamental to their pathogenesis. The Ebola virus uses at least two proteins, VP35 (Reid *et al*, 2005) and glycoprotein 2 (GP2) (Watanabe *et al*, 2000) with coiled-coil motifs that are active in the cytosol and at the cell surface/endosomal membrane, respectively. The functions of these proteins are discussed in more detail in sections 1.5.3 and 1.5.4, respectively.

1.5.1 E2F1 and PHB, the Tumour Suppressor Protein

Introduction and Pathophysiology of E2F1/PHB

A therapeutic with the ability to suppress E2F mediated transcription would be a 'blockbuster' of the 21st Century. It would be indicated, not only for numerous cancers but potentially other proliferative disorders e.g. smooth muscle growth in arteriosclerosis (Morishita *et al*, 1995). There is, at present, a huge amount of interest in the E2F family. Coregentech for example, a US biotechnology company is developing decoy oligonucleotides to prevent over-proliferation of vein grafts following surgical implantation.

PHB is protein with potential tumour suppressor activity. It acts by forming a hetero-oligomeric complex with an E2F transcription factor (Joshi *et al*, 2003). There are six members of the E2F family, five of which are transcriptionally active (E2F1-5). PHB has been shown to suppress the activity of all five, active members (Wang *et al*, 1999; Stevaux & Dyson, 2002). Furthermore, the putative coiled-coil motif has also been shown to facilitate homo-dimerisation of PHB, though the biological significance of this has not been determined.

Recently, a synthetic peptide corresponding to the 41 amino acid coiled-coil motif of PHB was shown to suppress E2F1-mediated transcription in TD47 breast cancer cells (Joshi *et al*, 2003). Furthermore, it was also shown to have apoptotic activity in HAEC, MCF-7, WI-38 and TD47 cells (Joshi *et al*, 2003). The authors demonstrated that apoptotic activity involves caspase activation, not a particularly astounding observation since caspases are always activated during apoptosis (Martin &

Green, 1995). A more intellectual question would have been "which caspase?" The answer to this would then allude to the precise mechanism by which the peptide is exerting its effect *in vitro*. Interestingly it is only the synthetic coiled-coil motif that induced apoptosis, whereas full-length PHB induced only growth arrest. Another claim made was that, "it is likely that [the peptide] is affecting the functions of [fos/jun and Bcl2] as well as leading to apoptosis." Although these proteins also interact *via* coiled-coil motifs it is thought unlikely that their peptide is having such non-specific activity, the amino acid sequences that constitute the motifs are all very different.

Molecular Structure of the PHB Protein

PHB is a 272-residue, 29,804 g mol^{-1} protein, with a predicted (PAIRCOIL) coiled-coil motif between amino acids 177 and 217 (inclusive). Up to two mutations have been observed in patients with breast carcinoma, however the coiled-coil motif is conserved as these mutations involve residues numbered 88 and 105 (Sato *et al*, 1992; Sato *et al*, 1993). The minimum sequence required to interact with E2F1 is between amino acids numbered 185 and 214 (inclusive) (Wang *et al*, 1999).

The binding domain in the E2F1 transcription factor was found to be between amino acids numbered 304 and 357 (Wang *et al*, 1999). Interestingly, computational analysis of the whole E2F1 sequence indicates the presence of a possible coiled-coil domain between residues 200-240 (see Chapter 3). However, there is not a significant prediction of a coiled-coil motif between residues 304-357 i.e. the domain by which PHB supposedly interacts. Therefore the primary aim is to determine the nature of the interaction (target hybridisation) between a PHB derived coiled-coil motif and the purported binding domain in the E2F1 protein. Since the shortest PHB sequence required to bind to E2F1 was found to be 30 amino acids it should not be necessary to synthesise the full 41-residue peptide used by Joshi *et al,* (2003).

1.5.2 AP-1 (Jun/Fos) Transcription Factor

Introduction and Pathophysiology of AP-1

The AP-1 transcription factor is ubiquitously expressed in human cells and as one of the first human transcription factors to be described (Angel & Karin, 2001) its oncogenic role has long been known (reviewed in Eferl & Wagner, 2003; Shaulian & Karin, 2002). More recently, it was discovered to play a key role in defining the invasive phenotype of metastatic cancers (Ozanne *et al*, 2007).

The coiled-coil domain of AP-1 was chosen, as a second target to test the hypothesis that "a polymer-coiled-coil motif conjugate could hybridise with a target coiled-coil motif and exert a measurable biological response." The key consideration in selecting the coiled-coil domain of AP-1 as a second target to establish proof of concept, was that the crystal structure of AP-1 had been previously determined (Glover & Harrison, 1995). It was therefore known with certainty (unlike E2F1 - section 1.5.1) that a coiled-coil was not only present but also essential for the function of the transcription factor.

Molecular Structure of AP-1

The AP-1 transcription factor is not a single protein but a dimeric protein complex composed of members of the Jun (c-Jun, JunB and JunD), and Fos (c-Fos, FosB, Fra-1 and Fra-2) families (reviewed in Milde-Langosch, 2005). It is known to regulate many genes that are important mediators of metastasis, apoptosis, invasion, proliferation, differentiation, angiogenesis and hypoxia (**Figure 1.9**). As a result of these apparently opposed functions, it has been described as a "double edged sword in tumourigenesis" (reviewed in Eferl & Wagner, 2003). The specific promoters with which AP-1 binds are dependent upon, among other factors, the composition of the dimer (van Dam & Castellazzi, 2001). This in part explains why AP-1 is associated with such a wide-range of often opposing effects.

AP-1: The c-Jun:c-Fos Heterodimer

The oncogenic c-Jun/c-Fos heterodimer was first identified following the discovery of the viral oncoproteins v-Jun and v-Fos from the Finkel-Biskis-Jinkins osteosarcoma virus and avian sarcoma virus 17, respectively (reviewed in Vogt, 2002). The prefix "c-" denotes the cellular origin of c-Jun and c-Fos, both of which are derived from the proto-oncogenes bearing the same names.

c-Jun and c-Fos are responsible for regulating a large number of target genes with key roles in cancer, including upregulation of genes responsible for proliferation, angiogenesis and invasiveness and downregulation of apoptotic genes (**Table 1.3**). The picture is complicated somewhat however by the observations that FASL (Kasibhatla *et al*, 1998) and BIM (Whitfield *et al*, 2001) (gene products that stimulate apoptosis) are upregulated either by c-Jun, c-Fos or both. These are only two exceptions however,

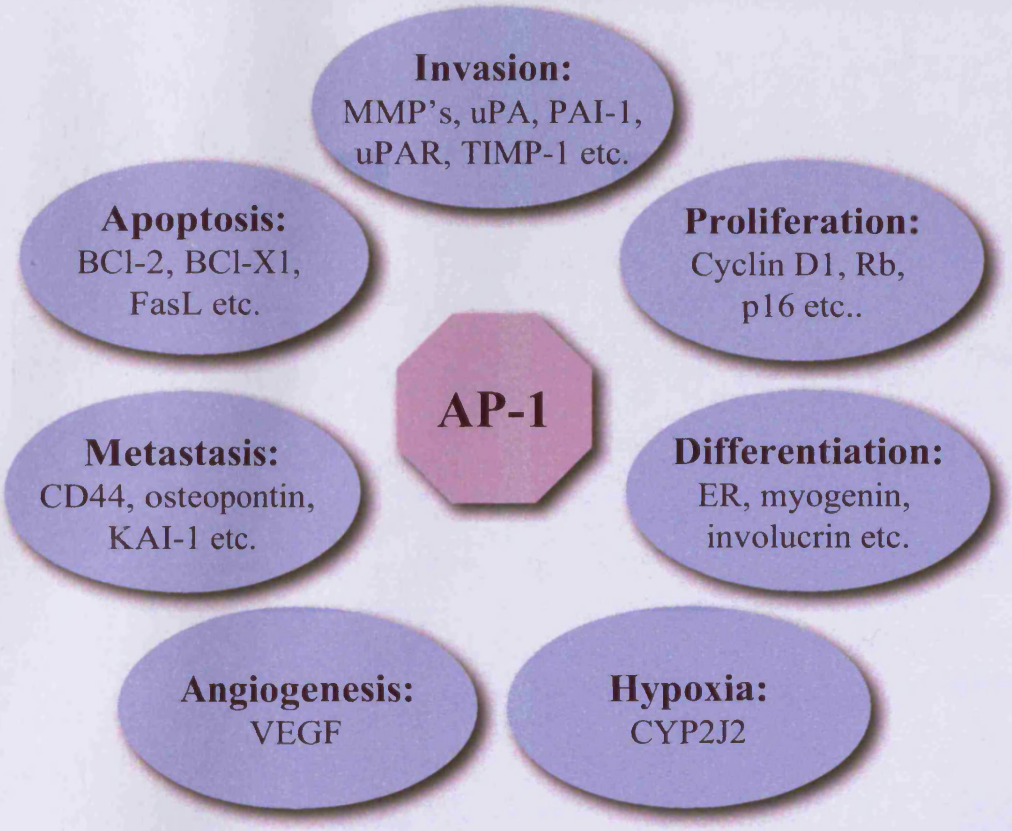

Figure 1.9 AP-1 responsive genes in cancer. Adapted from Milde-Langosch, (2005).

Table 1.3 AP-1 target genes in tumour development and suppression. Adapted from Eferl & Wagner, 2003.

Gene Product	Activity	Main Regulator	Reference(s)
DNMT	DNA Methylation	c-Fos (⇑)	Bakin & Curran, 1999
EGFR	Stimulates proliferation	c-Jun (⇑)	Zenz *et al*, 2003
HB-EGF	Stimulates proliferation	c-Jun (⇑)	Park *et al*, 1999
GM-CSF	Stimulates proliferation	c-Jun (⇑)	Szabowski *et al*, 2000
KGF	Stimulates proliferation	c-Jun (⇑)	Shaulian *et al*, 2000
Cyclin D1	Stimulates proliferation	c-Jun (⇑)	Bakiri *et al*, 2000
WAF-1	Inhibits proliferation	c-Jun (⇓)	Shaulian *et al*, 2000
P53	Inhibits proliferation Stimulates apoptosis	c-Jun (⇓)	Bakiri *et al*, 2000
INK4A	Inhibits proliferation Stimulates apoptosis	c-Jun (⇓)	Passegue & Wagner, 2000
FAS	Stimulates apoptosis	c-Jun (⇓)	Ivanov *et al*, 2001
BCL3	Inhibits apoptosis	c-Jun (⇑)	Rebollo *et al*, 2000
VEGFD	Angiogenesis	c-Fos (⇑)	Marconcini *et al*, 1999
Proliferin	Angiogenesis	c-Jun (⇑)	Toft *et al*, 2001
MMP1	Invasiveness	c-Fos (⇑)	Hu *et al*, 1994
MMP3	Invasiveness	c-Fos (⇑)	Hu *et al*, 1994
CD44	Invasiveness	c-Fos (⇑) c-Jun (⇑)	Lamb *et al*, 1997
Cathepsin L	Invasiveness	c-Fos (⇑)	Hennigan *et al*, 1994
MTS1	Invasiveness	c-Fos (⇑)	Hennigan *et al*, 1994
KRP1	Invasiveness	c-Fos (⇑)	
TSC36/FRP	Invasiveness	c-Fos (⇑)	Hennigan *et al*, 1994
Ezrin	Invasiveness	c-Fos (⇑)	Jooss & Muller, 1995
Tropomyosin 3	Invasiveness	c-Fos (⇑)	Jooss & Muller, 1995
Tropomyoson 5b	Invasiveness	c-Fos (⇑)	Jooss & Muller, 1995

compared with the 23 gene products regulated in an oncogenic manner as indentified in **Table 1.3**.

Molecular Structure of the c-Jun and c-Fos Proteins

Each protein is composed of three distinct domains, an N-terminal transactivating domain, a basic region that binds to a specific promoter in the major groove of a DNA molecule and a C-terminal dimerisation domain (Yao *et al*, 1998). The latter domain is a specific type of coiled-coil motif, known as a leucine zipper due to the predominance of leucine residues at position 'd' of the heptad repeat. The abbreviation bZIP (basic leucine zipper) is commonly used to describe proteins with this characteristic structure.

The c-Jun/c-Fos heterodimeric complex is large; the unprocessed precursor of c-Fos is composed of 380 amino acids (40,695 g mol^{-1}) and c-Jun 331 amino acids (35,676 g mol^{-1}) (www.expasy.org). As discussed in section 1.4, delivery of large therapeutic proteins is potentially challenging, particularly if the target resides in an intracellular location. Therefore the use of (smaller) peptides that could disrupt formation of the AP-1 complex by competitively binding to the coiled-coil domain would make attractive anti-cancer agents.

c-Jun/c-Fos Derived Coiled-Coil Peptides as Potential Therapeutics

Peptides corresponding to the coiled-coil domain would result in therapeutic candidates approximately a 10^{th} of the size of full-length c-Jun or c-Fos proteins. Such peptides have been previously proposed (discussed in Chapter 6) and some have been shown to be cytotoxic in the low μM range when transfected into MCF-7 cells using the cationic lipid Tfx-50™ (Yao *et al*, 1998).

The rationale for choosing to use peptides derived from c-Fos rather than c-Jun is an important one. Only two transcriptionally active dimeric complexes are possible, c-Jun : c-Fos heterodimers (Glover & Harrison, 1995) and c-Jun homodimers (Junius *et al*, 1996); c-Fos does not form homodimeric complexes that mediate transcription (O'Shea *et al*, 1989). Interestingly, overexpression of both c-Jun (Bossy-Wetzel *et al*, 1997) and c-Fos (Lu *et al*, 2005), have been shown to induce apoptosis or have negative effects on cell proliferation. The development of metastases is a key factor in tumour development that generally leads to a poor clinical prognosis (Ramaswamy *et al*, 2003). A hallmark of metastasis is the transformation of tumour cells from an epithelial to

mesenchymal morphology, often referred to as the epithelial-mesenchymal transition (EMT). Whilst c-Jun and c-Fos are both known to induce EMT in mammary epithelial cells, i.e. those responsible for breast carcinoma (Reichmann *et al*, 1992; Fialka *et al*, 1996). Only c-Fos, (not c-Jun) has been shown to induce EMT in cells in collagen gels. This indicates that c-Fos may have a more important role than c-Jun in the later stages of tumour development (Reichmann *et al*, 1992).

Furthermore, experiments were recently conducted to design a Fos peptide with a higher affinity for c-Jun than wild-type c-Fos as a potential therapeutic (Mason *et al*, 2006). A semi-rational design approach was used to generate a library of peptides from which a "winning" peptide was selected. Using CD spectroscopy, the authors showed that the peptide, FosW, had a significantly higher affinity for the model c-Jun peptide than wild-type c-Fos with T_m values of 63 and 16 °C, respectively (Mason *et al*, 2006). The authors of this work noted that there was greater scope for generating an improved Fos peptide (FosW) than there was for a Jun derived peptide (JunW). This is discussed in more detail in Chapter 3.

1.5.3 Ebola Virus VP35 Protein

Introduction and Pathophysiology of EbVP35

The Ebola virus, of which there are four sub-types is a member of the filoviridae family. Three of the four sub-types: Zaire, Sudan and Cote d'Ivoire have been identified as aetiological agents responsible for causing severe haemorrhagic fever (HF) in humans (Bowen *et al*, 1977). The initial symptoms are akin to those associated with any other type of fever: weakness, headache, sore throat etc. However, this is followed by diarrhoea, vomiting, impaired organ (kidney and liver) function, internal and external bleeding. The latter is due to the opening of endothelial tight junctions as a result of excessive cytokine release induced by infected macrophages (Hensley *et al*, 2002; Stroher *et al*, 2001; Villinger *et al*, 1999). Statistics from the WHO indicate that fatality ensues in 50-90 % of cases (**Figure 1.10a**). Of the four sub-types known, Zaire has been associated with the most outbreaks and the highest percentage of fatalities (**Figure 1.10b**). There are at present, no anti-viral treatments or vaccines available.

The exceptional virulence of Ebola is largely mediated by the ability of the virus to down-regulate the immune response of the host. During the course of infection a number of virus-encoded proteins are released, one of these is EbVP35. EbVP35 has a number of functions essential to the pathophysiology of Ebola HF. Initially, research

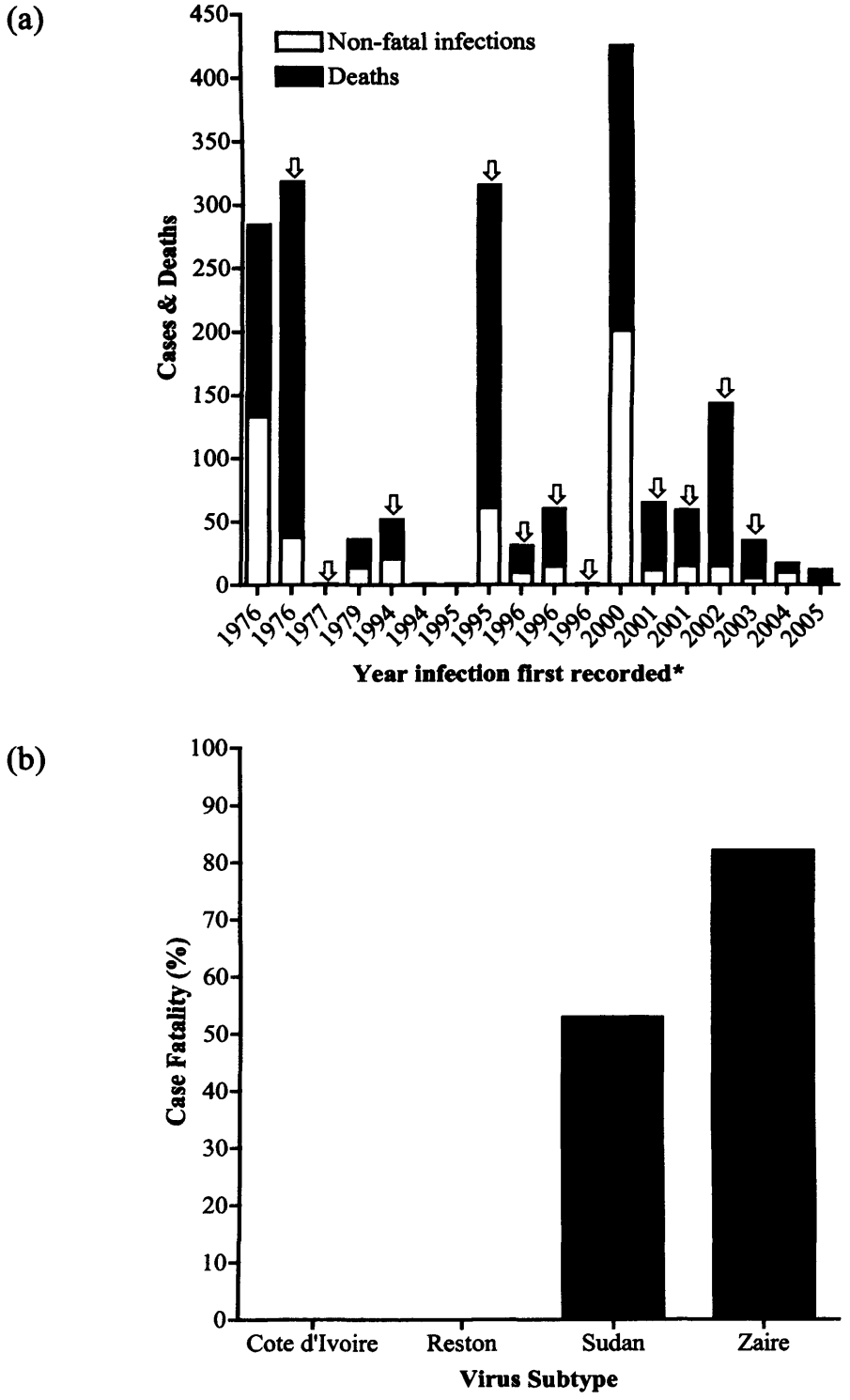

Figure 1.10 Ebola outbreaks since 1976 and fatality rates for each sub-type. Panel (a) shows the number of deaths (black) as a fraction of cases reported each year since records began in 1976. Arrows indicate infections resulting from the Zaire subtype. *Some outbreaks spread into two separate years, in which case the year the outbreak started is indicated. Panel (b) shows a comparison of case fatalities (%) recorded for each of the four known sub-types. Source: WHO, 2008.

demonstrated that VP35 functions as a type I IFN antagonist (Basler *et al*, 2000). More recently however, VP35 has been shown instead to inhibit the intracellular activation of interferon regulatory factor 3 (IRF-3) (Basler *et al*, 2000). IRF-3 is essential for the up-regulation of IFN α/β synthesis in response to viral infection. Thus with the most powerful component of the innate immune response compromised the virus is able to replicate rapidly before the adaptive immune response can counter the infection.

Molecular Structure of Ebola VP35

The Zaire strain of EbVP35 has been sequenced, though not crystallised. Crystallisation is the focus of a current Ph.D. project supervised by Professor E. Sapphire at the Scripps Research Institute, California. EbVP35 is a 340-residue, 37,362 g mol^{-1} protein. The coiled-coil domain is predicted (COILS) to be between amino acids 82-118 (inclusive) (discussed in Chapter 3). Recently the coiled-coil domain has been shown to be essential for EbVP35 to form homo-trimers and possibly higher order oligomers (Reid *et al*, 2005). In the same paper it was demonstrated that the trimeric form is two degrees of magnitude more potent at down-regulating IFN α/β synthesis. Furthermore, it has also been speculated as to whether the coiled-coil may be biologically active with regard to mediating viral RNA synthesis.

The aim is to inhibit or reduce the activity of EbVP35, thereby enabling the host immune system to mount a more effective innate response to viral infection. This is to be achieved by the design and synthesis of a coiled-coil motif with high affinity for the VP35 coiled-coil domain. The proposed action of this synthetic coiled-coil is two-fold: (i) inhibition of IFN down-regulation by blocking EbVP35 oligomerisation and (ii) inhibition of viral RNA synthesis by dimerisation with the EbVP35 coiled-coil. Polymer conjugation may stabilise the binding and additionally, shroud the biologically active C-terminus of the pathogenic protein. If the conjugated polymer abrogates the activity of the peptide then the design will be altered such that the coiled-coil motif is released at the site of action.

1.5.4 Ebola Virus GP2 Protein

Pathophysiology of Ebola GP2 (EbGP2)

An introduction to the Ebola virus and Ebola HF was given in section 1.5.3 above. EbGP2 is thought to be key to fusion of the virus with the host cell membrane and subsequent cytosolic entry (Chan *et al*, 2000; Watanabe *et al*, 2000). The key

advantage of this target is its extracellular location. This makes it a much easier target to access with a polymer-coiled-coil motif therapeutic compared with the intracellular targets discussed in sections 1.5.1-1.5.3.

Molecular Structure of Ebola GP2

GP2 is a component of the Ebola virus GP which protudes as a trimeric spike from the virion surface and is essential for receptor binding, membrane fusion and subsequently cell entry (Takada *et al*, 1997; Wool-Lewis & Bates, 1998). The protein exists in at least three conformational states, one of which, the "trimer-of-hairpins" is thought to form at lowered pH (e.g. in the endosome) and results in driving apposition and fusion of the cell and viral surface membranes (Yang *et al*, 2000; Wahl-Jensen *et al*, 2005). The trimer-of-hairpins structure is a trimeric coiled-coil, formed from the homo-trimerisation of three GP2 proteins with a further three α-helical domains stabilising the structure. This is a very large macromolecular structure as each GP2 subunit is a 676-residue, 74,464 g mol^{-1} protein (www.expasy.org).

In light of the successful development of fusion-inhibitor peptides against HIV-1 (Chan *et al*, 1998), Watanabe *et al*, (2000) proposed the use of peptides to disrupt the formation of the GP2 trimeric coiled-coil complex as a possible therapeutic strategy. Two peptides, GP555 and GP610, corresponding to GP2 amino acid residues 555 to 589 and 610 to 633, respectively were synthesised by Watanabe *et al*, (2000). The first peptide, GP555, was found to be insoluble in all but organic solvents, and precipitated in aqueous tissue media, as such no further experiments could be conducted (Watanabe *et al*, 2000). The second peptide, GP610 however showed promise by reducing the infectivity of an Ebola GP virus mutant in a dose-dependent manner (Watanabe *et al*, 2000). It is proposed that PEGylation of the GP555 peptide will resolve the solubility issue and make testing of the peptide as a potential therapeutic agent possible, furthermore PEGylation of the peptide GP610 may make it more effective as the PEG-chain may also interfere with the viral fusion mechanism.

1.6 The Future, from Laboratory to Clinic

Over the last decade the number of macromolecular drugs and biotechnology products licensed by the US FDA has been steadily increasing. Recently they succeeded small drug molecules in terms of the number of new licences granted per

annum. Furthermore, at the start of this Ph.D. thesis numerous market research reports estimated the worldwide protein therapeutics market to gross over $ 60 billion (2005).

Nonetheless, it remains important that the cost-effectiveness of new treatments is considered. Put simply, the larger the market the more likely a commercial return can be made on the product and therefore make the investment in the technology more appealing. Novel therapeutics for cancer or infectious diseases such as HIV are more likely to be profitable, particularly where they present a risk to the health of populations in developed nations. Therapeutic agents against diseases such as Ebola and other filoviral infections do not have the same potential market size, however they are attractive for development as no effective treatments currently exist, and in the recent political climate there is fear that such organisms could be used for bio-terrorism (Bray, 2003).

Only recently has the pharmaceutical industry started to make steps towards developing in house "biotech" products as opposed to concentrating research funding on small molecules and formulation science. It may be reasoned that until recently the latter have been more costly to research and develop with a greater profitability associated risk. However this approach is short sighted and will enable smaller biotechnology companies with more innovative research programs to steal market share. Pfizer, the largest pharmaceutical company in the world has only recently finished implementing a $4 billion restructuring program that aims to give greater focus to oncology and to incorporate more biotechnology products into its research pipeline.

Almost all polypeptide drugs, until recently, were administered *via* parenteral routes. The formulation of insulin as a dry powder for inhalation and its approval by the US FDA in 2005 marked a significant milestone. However, its withdrawal only a few months later demonstrated the volatility and high risks still associated with the use of cutting-edge drug-delivery technology. Perhaps, in the near future, it will be possible to administer polymer-polypeptide drugs *via* this route, thus increasing their attractiveness further.

1.7 Thesis Aims and Objectives

The global aim of this research was to determine whether it is possible to synthesise bio-responsive polymer therapeutics containing coiled-coil motifs with clinical potential. In order to test the hypothesis outlined on page 1, mPEG-coiled-coil

motif therapeutics will be designed with the potential to interact with one of four protein targets, either E2F1 or c-Jun in cancer pathogenesis, or the viral proteins VP35 or GP2 which are thought to be key to the underlying pathogenesis of Ebola HF. These targets were identified from an extensive literature review (**Table 1.1**) as having pathophysiologies mediated by coiled-coil interactions.

Design and Synthesis of the Coiled-Coil Motifs

First, it was necessary to design, synthesise, purify and characterise peptides for each of the four targets described (Chapter 3). This work was conducted during two visits to EPFL in Switzerland, firstly from February to April 2006 and later followed by a one-month visit in November/December. Since the ultimate goal was to design a novel polymer therapeutic that could be transferred from the laboratory to the clinic certain requirements must be satisfied. Foremost is perhaps the ability to scale-up manufacture. Thus once work has progressed from proof of principle, all syntheses will be planned whilst considering the feasibility of large-scale manufacture. Characterisation must be to stringent pharmaceutical standards. This is more of a challenge with polymer therapeutics as they are large (circa 40-50,000 g mol^{-1}), multi component systems, and as such the heterogeneity is higher than that of small (100-600 g mol^{-1}) drug molecules. Synthesis with minimal heterogeneity is however, highly desirable since it would facilitate the interpretation of biological data and later the process of regulatory approval.

PEGylation of the Coiled-Coil Motifs

In addition to synthesis of the coiled-coil motifs, preliminary experiments were to be conducted to investigate the feasibility of conjugating low molecular weight PEG to the coiled-coil motifs, this work is described at the beginning of Chapter 4. Research pertaining to site-specific PEGylation, purification and subsequent characterisation was conducted at the Welsh School of Pharmacy, Cardiff and constitutes the bulk of data discussed in Chapter 4. In parallel to the synthetic work it was also necessary to develop a "tool-kit" of analytical techniques in particular, though not exclusively including, reverse-phase high-pressure liquid chromatography (RP-HPLC), electrospray ionisation time of flight mass spectrometry (ESI-TOF MS) and matrix-assisted laser desorption/ionisation (MALDI-) TOF MS. As such purity of the coiled-coil motif and subsequent mPEG-conjugates could be assessed following purification with the aim of

obtaining samples of purity ≥ 95 %. For the preparation of all conjugates, mPEG with a low polydispersity index (< 1.1) as determined by size-exclusion chromatography (SEC) will be used.

Biophysical Characterisation

Once prepared and characterised, experiments were to be conducted using NMR and CD spectroscopy to determine whether, in a model physiological environment, the mPEG-coiled-coil motif conjugates could hybridise with their respective targets. Furthermore, to investigate what differences were observed between coiled-coil motif and mPEG-coiled-coil motif target hybridisation. It was envisaged that such studies may require the preparation of recombinant proteins should it not be possible to synthesise the target domains using standard peptide chemistry. This work is detailed in Chapter 5.

Biological Characterisation

Following proof of concept studies with model targets *in vitro* biological characterisation of the mPEG-coiled-coil conjugates was to be an essential component of this thesis. In order to aid interpretation of the proposed cytotoxicity experiments it would be necessary to conduct cellular uptake experiments using fluorescently labelled mPEG-coiled-coil motifs. It has been previously demonstrated that a synthetic, 41 amino acid peptide, corresponding to the coiled-coil motif of the protein PHB may enter cells, in the absence of a carrier molecule (Joshi *et al*, 2003). Therefore it is of interest to see if a similar observation can be made in this study. In the case of c-Fos derived peptides, previous studies have documented the need to use transfection reagents such as the cationic lipid Tfx™-50 (Yao *et al*, 1998). Should biological activity of either conjugate be demonstrated, re-design of the conjugate could be investigated to develop a system that is active without the need for additional transfection reagents. Cytotoxicity experiments using the MCF-7 human breast carcinoma cell line were to be conducted using the MTT assay, and non-specific toxicity assessed with the red blood cell (RBC) lysis assay. This work is detailed in Chapter 6. There are no papers describing the synthesis, or biological behaviour of a synthetic peptide corresponding to the coiled-coil sequence of the Ebola VP35 protein. If mPEG-coiled-coil motif conjugates can be synthesised and characterised to the required standards (detailed in

Chapters 3 and 4) with potential activity against either VP35 or GP2 collaborative studies will be sought.

CHAPTER 2

Materials and General Methods

2.1 MATERIALS AND EQUIPMENT

This section details the materials and equipment used in this thesis. Experimental work was conducted in laboratories in three different countries (UK, Spain and Switzerland). For clarity, information pertaining to the materials has been listed in **Table 2.1** and equipment in **Table 2.2** with sub-headings identifying the laboratory in which the reagents were used. If not listed, standard laboratory grade reagents were used. Double distilled water (ddH_2O) was obtained from either Elga Option 7 or MilliQ purification units. With the exception of N-methylpyrrolidone (NMP), which was distilled prior to use, all reagents were used as received. The competent *E. coli* strains DH5α, TOP10 and BL21 (DE3) used in Cardiff were a kind gift from Dr Simon Richardson while BL21 (DE3) pLysS *E. coli* were obtained from Marc Kelly. Competent BL21-CodonPlus (DE3) *E.coli* for use at CIPF were obtained from Novagen, Barcelona, Spain.

2.2 GENERAL METHODS

This section details the general methods used in these studies. General analytical techniques are provided first (section 2.2.1), followed by chromatography (section 2.2.2), while protocols related to cell culture are provided later (section 2.2.3). Detailed descriptions regarding the application of each of these methods given here are provided in the relevant chapters. Furthermore, since many of the techniques used in this thesis required significant optimisation, the full methods are given in the respective chapters.

2.2.1 General Analytical Techniques

2.2.1.1 Determination of Concentration by UV Spectroscopy

Where possible, sample concentrations were determined by UV spectroscopy. This was of particular importance when determining the concentration of peptides and proteins due to their high propensity to bind H_2O and salts. For bacterial cultures the UV absorbance/optical density (OD) at λ_{600} was measured using UV grade plastic

Table 2.1 Materials used in this study.

Compound	Abbreviation	Cat. No.	Supplier
Materials used at Cardiff University, Cardiff, UK.			
2-mercaptoethanol	n/a	M6250	Sigma-Aldrich, Gillingham, Dorset, UK
Dimethyl sulphoxide ACS spectrophotometric grade	DMSO	154938	Sigma-Aldrich, Gillingham, Dorset, UK
Foetal calf serum	FCS	10106-169	Invitrogen, Inchinnan Business Park, Paisley, UK
HPLC grade trifluoroacetic acid	TFA	91797	Fluka, via Sigma-Aldrich
MCF-7 human breast carcinoma cells	MCF-7	n/a	Tenovus Centre for Cancer Research, Cardiff, UK
Methylthiazolyldiphenyl-tetrazolium bromide	MTT	M5655	Sigma-Aldrich, Gillingham, Dorset, UK
mPEG-amine, Mn = 5,000 g mol^{-1}	mPEG-NH_2	06679-1G	Sigma-Aldrich, Gillingham, Dorset, UK
mPEG-maleimide, Mn = 5,522 g mol^{-1}	mPEG-Mal	ME-050MA	NOF Corporation, Tokyo, Japan
Oregon Green® 488-X, succinimidyl ester *6-isomer*	OGSE488-X	O6185	Invitrogen, Inchinnan Business Park, Paisley, UK
RPMI 1640 Medium (1x) liquid	RPMI 1640	21875-034	Invitrogen, Inchinnan Business Park, Paisley, UK
RPMI 1640 Medium (1x) liquid without Phenol Red	WRPMI 1640	11835-063	Invitrogen, Inchinnan Business Park, Paisley, UK
Sodium Fluoride	NaF	71518	Fluka, *via* Sigma-Aldrich

Table 2.1 Materials used in this study.

Compound	Abbreviation	Cat. No.	Supplier
Tfx™-50 Reagent	Tfx™-50	E1811	Promega, Science Park, Southampton, UK
Trypan Blue solution 0.4 % w/v	-	T8154	Sigma-Aldrich, Gillingham, Dorset, UK
Trypsin-0.53 mM ethylenediaminetetraacetic acid (EDTA) 0.05 % w/v	Trypsin-EDTA	25-300-062	Invitrogen, Inchinnan Business Park, Paisley, UK
Materials used at EPFL, Lausanne, Switzerland.			
1,8-diazabicyclo(5.4.0)undec-7-ene	DBU	33482	Sigma-Aldrich, Buchs SG, SWITZERLAND
2-(6-Chloro-1H-benzotriazole-1-yl)-1,1,3,3-tetramethylaminium hexafluorophosphate	HCTU	RL-1031	Iris Biotech, Marktredwitz, GERMANY
9-fluorenylmethyloxycarbonyl-protected amino acids	Fmoc-amino acids	04-12-1006	NovaBiochem, Läufelfingen, SWITZERLAND
Acetic anhydride	n/a	45830	Sigma-Aldrich, Buchs SG, SWITZERLAND
Anhydrous 1-hydroxybenzotriazole	HOBt	RL-1034	Iris Biotech, Marktredwitz, GERMANY
Dichloromethane	DCM	2630575	SDS, Servion, SWITZERLAND
Diethyl ether	Et_2O	3230104	SDS, Servion, SWITZERLAND
N,N-diisopropylethylamine	DIPEA	387649	Sigma-Aldrich, Buchs SG, SWITZERLAND
N-methylmorpholine	NMM	67869	Sigma-Aldrich, Buchs SG, SWITZERLAND
N-methylpyrrolidone	NMP	n/a	Schweizerhall Chemie AG, Basel, SWITZERLAND

Table 2.1 Materials used in this study.

Compound	Abbreviation	Cat. No.	Supplier
Piperidine	n/a	80640	Sigma-Aldrich, Buchs SG, SWITZERLAND
Rink Amide AM resin (200-400 mesh)	n/a	01-64-0038	NovaBiochem, Läufelfingen, SWITZERLAND
Trifluoroacetic acid (HPLC grade)	TFA	302031	Sigma-Aldrich, Buchs SG, SWITZERLAND
Trifluoroacetic acid (non-HPLC grade)	TFA	91700	Sigma-Aldrich, Buchs SG, SWITZERLAND
Triisopropylsilane	TIPS	92095	Sigma-Aldrich, Buchs SG, SWITZERLAND
Materials used at CIPF, Valencia, Spain.			
^{15}N Labelled ammonium chloride	$^{15}NH_4Cl$	NLM-467-10	Cambridge Isotope Labs, Andover, USA
Acetic acid (glacial)	-	A9967	Sigma-Aldrich, SPAIN
Ammonium chloride	NH_4Cl	168320	Merck, Barcelona, SPAIN
Ammonium persulphate for electrophoresis > 98 %	n/a	A3678-100G	Sigma-Aldrich, SPAIN
Ampicillin	Amp	A9518-25G	Sigma-Aldrich, SPAIN
Bromophenol blue sodium salt	n/a	B6131-25G	Sigma-Aldrich, SPAIN
Calcium chloride	$CaCl_2.2H_2O$	208291	Calbiochem, Barcelona, SPAIN
Chloramphenicol	Cam	C0378-5G	Sigma-Aldrich, SPAIN
Complete EDTA-free protease inhibitor tablets	n/a	11873580001	Roche, Barcelona, SPAIN

Table 2.1 Materials used in this study.

Compound	Abbreviation	Cat. No.	Supplier
Coumassie Brilliant Blue R	n/a	B0149-25G	Sigma-Aldrich, SPAIN
D(+)-Glucose	Glucose	1.08337.100	Merck, Barcelona, SPAIN
DNase I	n/a	1284932	Roche, Barcelona, SPAIN
Glycerol 87 % v/v	n/a	1.04094.100	Merck, Barcelona, SPAIN
Glycine	n/a	1.04201.500	Merck, Barcelona, SPAIN
Imidazole	Imd	12399-500G	Sigma-Aldrich, SPAIN
Isopropyl-beta-D-thiogalactopyranoside	IPTG	15502-10G	Sigma-Aldrich, SPAIN
Lysozyme from hen egg white	Lysozyme	62971	Sigma-Aldrich, SPAIN
MES	n/a	M3671-50G	Sigma-Aldrich, SPAIN
Methanol	MeOH	1.06009.500	Merck, Barcelona, SPAIN
N,N,N',N'-Tetramethylethylenediamine	TEMED	1.07320.100	Merck, Barcelona, SPAIN
SDS-PAGE molecular weight standards (broad range)	n/a	161-0317	Bio-Rad, Barcelona, SPAIN
Sodium dodecyl sulphate	SDS	1.13760.0100	Merck, Barcelona, SPAIN
Sodium fluoride	NaF	71518	Sigma-Aldrich
TALON® metal affinity resin	n/a	635504	BD Biosciences, Madrid, SPAIN
Thiamine hydrochloride	n/a	5871	Merck, Barcelona, SPAIN

Table 2.1 Materials used in this study.

Compound	Abbreviation	Cat. No.	Supplier
Tobacco etch virus protease	TEV protease	n/a	Dr A.K. Schott
Trace elements	n/a	n/a	Prepared by Dr A.K. Schott, CIPF
Trizma base	n/a	T1503-1KG	Sigma-Aldrich
Trizma HCl	n/a	T3253-1KG	Sigma-Aldrich
Tryptone	n/a	1612.00	CONDA, Torrejón de Ardoz-Madrid, SPAIN
ULTRA PURE ProtoGel® 30 % w/v acrylamide: 0.8 % w/v bis-acrylamide (37.5:1)	ProtoGel® (37.5:1)	CSEC8901	Sumilab / Pronadisa, Valencia, SPAIN
Vivaspin 2,000 molecular weight cut-off (MWCO) centrifuge tubes	n/a	VS02H91	Sartorius, Barcelona, SPAIN
Vivaspin 6 10,000 MWCO centrifuge tubes	n/a	VS0602	Sartorius, Barcelona, SPAIN
Yeast extract	n/a	1702.00	CONDA, Torrejón de Ardoz-Madrid, SPAIN

Table 2.2 Equipment used in this study.

Instrument/Equipment	Model	Supplier(s)
Equipment used at Cardiff University, Cardiff, UK.		
Analytical RP-HPLC	Comprised of two PU-980 Intelligent HPLC pumps, a 717 plus autosampler, C18 reverse phase μBondapak column and spectroflow 783 UV detector. Data were acquired using PowerChrom hardware and software (v.2.0.7).	Jasco Ltd, Dunmow, Essex, UK Waters Ltd., Borehamwood, Hertfordshire, UK, Kratos Analytical, Manchester, Lancashire, UK and AD Instruments, Chalgrove, Oxfordshire, UK.
Cell culture cabinets	Bioair and Bioquell Microflow class II laminar flow cabinets	Siziano, Italy and Andover, UK, respectively
CD spectrometer	AVIV model 215 spectrometer. Spectra were acquired using Kaleidagraph software v3.09.	AVIV, Lakewood, New Jersey, USA.
ESI-TOF MS	LCT Premier XE QTOF used in conjunction with a 1525 μL binary HPLC pump and 2777C sample manager. Spectra were acquired and processed using Masslynx™ 4.0 Global Mass Informatics software.	Waters Ltd., Borehamwood, Hertfordshire, UK.
Flow Cytometer	Becton Dickinson FACSCalibur cytometer equipped with an argon laser (488 nm) and emission filter for 550 nm. Data acquisition and analysis were conducted using CELLQuest™ v3.3 software.	Franklin Lakes, USA

Table 2.2 Equipment used in this study.

Instrument/Equipment	Model	Supplier(s)
Fluorescence Plate Reader	FLUOstar OPTIMA fluorescence plate reader.	BMG Labtechnologies GmbH, Offenburg, GERMANY.
Fluorescence Spectrophotomoeter	Amnico-Bowman series 2 luminescence spectrophotometer.	Spectronic Instruments, Leeds, UK
Analytical SEC - Fast Protein Liquid Chromatography (FPLC)	Äkta™ FPLC chromatography system comprising pumps, fixed λ_{280nm} UV detector, conductivity detector and fraction collector (Frac-950). Data was acquired using Unicorn v3.20 software and analysed using FPLC director® v1.10 software.	Amersham Biosciences, Little Chalfont, Buckinghamshire, UK.
Analytical SEC	Aqueous system equipped with a single JASCO HPLC pump and two TSK-gel columns in series (4000 PW followed by 3000 PW) and a guard column (progel PWXL). A differential refractometer (Gilson 153) and a UV spectrometer (UV Severn Analytical SA6504) were connected in series. Data analysis was conducted using PL Caliber Instrument software v7.04.	Polymer Laboratories, Church Stretton, UK.

Table 2.2 Equipment used in this study.

Instrument/Equipment	Model	Supplier(s)
Ion-exchange chromatography	Äkta™prime "one-box" chromatography system comprising pumps, fixed λ_{280nm} UV detector, conductivity detector and fraction collector. The unit was connected to a pre-packed Superdex 75 HR 10/30 column. Data were acquired using PrimeView™ software.	Amersham Biosciences, Little Chalfont, Buckinghamshire, UK.
MALDI-TOF MS	MALDI Micro MX™, Micromass MS technologies. Spectra were acquired and processed using Masslynx™ 4.0 Global Mass Informatics software.	Waters Ltd., Borehamwood, Hertfordshire, UK.
UV plate reader	Sunrise Touchscreen	Tecan, Reading, Berkshire, UK.
UV spectrometer	Cary 1G UV spectrometer, equipped with a Cary temperature controller. All spectra were acquired using Cary WinUV software v2.0.	Varian Ltd., Walton On Thames, Surrey, UK.
Equipment used at EPFL, Lausanne, Switzerland.		
SPPS automated synthesiser	PSW 1100	Chemspeed Technologies AG, Augst, SWITZERLAND
Centrifuge	Biofuge Primo R	Heraeus, Hanau, GERMANY

Table 2.2 Equipment used in this study.

Instrument/Equipment	Model	Supplier(s)
RP-HPLC	Comprised of a Waters 600 automated gradient pump controller module, Waters Prep Degasser, Waters 2487 dual λ absorbance detector and a Waters Fraction Collector with an Atlantis® dC_{18} OBD™ 5 µm, 30 x 150 mm column.	Waters Corporation, Massachusetts, USA
ESI-TOF MS	SSQ 710C mass spectrometer equipped with an ESI source. Data were acquired and processed using ICIS software.	Finnigan MAT, California, USA
UV spectrometer	Cary 1G UV spectrometer, equipped with a Cary temperature controller. All spectra were acquired using Cary WinUV software v2.0.	Varian AG, Steinhausen, SWITZERLAND
CD spectrometer	J-715 CD spectrometer in conjunction with a Jasco PTC-348WI temperature-controlled cell	Jasco GmbH, Groß-Umstadt, GERMANY
Equipment used at CIPF, Valencia, Spain.		
UV spectrometer	Jasco-V-530 spectrometer	Jasco Ltd., Groß-Umstadt, GERMANY
CD spectrometer	Jasco-810 spectrometer with a Peltier temperature controller.	Jasco Ltd., Groß-Umstadt, GERMANY
NMR spectrometer	Bruker Avance Ultrashield Plus 600 MHz spectrometer equipped with a 5 mm single-axis gradient TCI cryoprobe. Data were acquired and processed using Topspin 1.3 software.	Bruker GmbH, Karlsruhe, GERMANY

cuvettes, otherwise all measurements were performed in quartz cuvettes. Mass concentrations were calculated using equation [1] and μmolar concentrations calculated using equation [2]. Molar extinction coefficients used were as follows: tyrosine = 1480 M^{-1} cm^{-1} (280 nm), trptophan = 5540 M^{-1} cm^{-1} (280 nm) (Pace *et al*, 1995) and Oregon Green® succinimidyl ester 488-X (OGSE488-X) = 81,000 M^{-1} cm^{-1} (494 nm).

$$Concentration\ (mg\ mL^{-1}) = \frac{\lambda\ DF\ MW}{l\ \varepsilon} \qquad [1]$$

$$Concentration\ (\mu M) = \frac{\lambda\ DF\ e^{6}}{l\ \varepsilon} \qquad [2]$$

Where λ = absorbance at either 280 or 494 nm, DF = dilution factor, l = path length and ε = molar extinction coefficient, MW = molecular weight.

2.2.1.2 Agarose Gel Electrophoresis

The gel-casting tray was prepared by first cleaning with ddH_2O and then sealed at either end using autoclave tape. Two combs were inserted and the tray was tested for leaks by adding ddH_2O. 0.5x tris-borate-EDTA (TBE) buffer (1 L) was prepared from a 5x TBE stock solution (54 g Tris Base, 27.5 g boric acid, 40 mL of 0.25 M EDTA, up to 1 L with ddH_2O). The agarose gel (2 %) was prepared by adding agarose (2 g) to 0.5x TBE buffer (100 mL) in a conical flask and heating the flask to 100 °C for 1 minute. The solution was left to cool until it reached approximately 60 °C, it was then poured into the gel-casting tray and left to set for 40-50 min. To enable visualisation of the DNA, an aliquot (16 μL) of ethidium bromide (EtBr) solution (10 mg mL^{-1}) was added to 0.5x TBE buffer (800 mL); final EtBr concentration was 0.2 μg mL^{-1}. Once the gel had set, the combs and autoclave tape were removed from the gel and EtBr containing buffer (c.a. 700 mL) was added to the electrophoresis tank; ensuring that the gel was completely covered with buffer solution.

Samples were prepared by adding an aliquot (2 μL) of loading buffer (ddH_2O containing 40 % w/v sucrose and 0.25 % w/v Bromophenol Blue) to each sample (10 μL). DNA ladders were prepared in the same manner and an aliquot (5 μL) of each was

loaded onto the gel. The gel was run at 80 V for 1 h 40 min then imaged using the UV dock (BioRad). Images were exported as .jpeg files.

2.2.1.3 SDS-PAGE

Sodium dodecyl sulphate-polyacrylamide gel electrophoresis (SDS-PAGE) was used extensively in the analysis of recombinant protein expression (Chapter 5). 12 % gels were used in all instances; these were prepared freshly for each experiment. With the exception of ammonium persulphate (10 % w/v), which was prepared fresh on each day of use, solutions A and B were prepared in advance and stored for up to 3 months. Solution A consisted of tris base (1.5 M) containing SDS (0.4 % w/v) in ddH_2O adjusted to pH 8.8, while solution B consisted of tris base (0.5 M) containing SDS (0.4 % w/v) in ddH_2O adjusted to pH 6.8. The set-up and basic operation of the BIO-RAD equipment was conducted as detailed in the manufacturers instructions. Once assembled the casting chambers were filled with ethanol to check for leaks. The quantities of reagents detailed below were sufficient to prepare two gels.

The separating gel was prepared by mixing, ProtoGel®(37.5:1) (3.2 mL), solution A (2 mL), ddH_2O (2.8 mL), ammonium persulphate (40 µL) and TEMED (8 µL) in the order given. The solution was inverted gently several times to ensure mixing of the solutions without introducing any air bubbles. This solution was immediately transferred to the casting chambers, filling up to a line that marked 1-2 mm below the resting point of the sample comb. A thin layer (c.a. 2 mL) of isopropanol was added above the separating gel to prevent oxidation since co-polymerisation of the acrylamide and bis-acrylamide is unable to proceed in an oxidative environment. The polymerisation was left to proceed for approximately 30 min, during which time the stacking gel was prepared.

For the stacking gel, ProtoGel®(37.5:1) (600 µL), solution B (800 µL), ddH_2O (1950 µL), ammonium persulphate (10 µL) and TEMED (10 µL) were combined in the order given and mixed carefully. The isopropanol was removed from the casting chambers and the stacking gel added. A sample comb was immediately added to each chamber, with care taken to ensure that no air bubbles were introduced. Polymerisation of the stacking gel was complete after a further 30-40 min. Once cast, combs were left in place until the gel was required. Best results were obtained using gels prepared freshly on each day of use.

Samples were prepared by adding an aliquot of 5x loading buffer, typically 50 μL, to an aliquot of sample or protein marker solution (200 μL). The 5x loading buffer was prepared in advance and stored at -20 °C in aliquots of 0.5 mL. It was comprised of bromophenol blue (0.2 % w/v), tris HCl 1 M, pH 6.8 (12 % v/v), glycerol (10 % w/v), SDS (2 % w/v), 2-mercaptoethanol (10 % v/v) in ddH_2O. Once mixed with loading buffer, the sample tubes were sealed and heated for 5 min at 100 °C, then frozen for > 1 h at -20 °C, then thawed at room temperature.

Prior to adding the sample solutions to the gel, the assembly was placed into a tank filled with running buffer. This was prepared from a 5x stock solution, which consisted of Tris Base (1.5 % w/v), SDS (0.5 % w/v) glycine (5 % w/v) in ddH_2O. Wells were filled with up to 50 μL of sample solution, while an aliquot (10 μL) of molecular weight marker solution was added generally to the first well. Once all the samples had been added, the unit was connected to a power supply and the gel run for 1 h at 200 V.

To image the gels, they were removed from the glass plates and placed in plastic trays containing a solution of Coumassie Brilliant Blue gel staining solution (150 mL), this comprised of Coumassie Brilliant Blue (0.25 % w/v), glacial acetic acid (10 % v/v), methanol (MeOH) (45 % v/v) and ddH_2O (45 % v/v). After 1 h of gentle agitation, this solution was removed and replaced with a strong de-stain solution (20 % v/v MeOH, 5 % acetic acid in ddH_2O) and again, gently agitated. The de-stain solution was replaced several times until the background became clear and protein bands could be clearly visualised. All gels were scanned and images saved as .tiff files.

2.2.1.4 CD Spectroscopy

Measurements were performed at EPFL, CIPF and in Cardiff; the equipment specifications for each instrument were detailed in section 2.1. In all instances the instruments were previously calibrated with an aqueous solution of (+)-10-camphorsulfonic acid. Samples were prepared in a phosphate buffer derived from the Sorenson method; Na_2HPO_4/NaH_2PO_4 (10 mM, pH 7.4) containing NaF (100 mM) and spectra recorded between 30 min and 3 h after preparation. Concentrations were either determined gravimetrically or by using a UV spectrometer (section 2.2.1.1).

Spectra were acquired in one of two ways; fixed temperature, variable wavelength or fixed wavelength, variable temperature. Fixed temperature scans were performed in either 0.02 or 0.1 cm quartz cuvettes. CD signal was recorded from 260 to

180 nm (dynode voltage permitting). Data acquisition was stopped when the dynode voltage exceeded 500 V. Spectra were acquired using a 1 nm bandwidth, 0.2 nm increments with a recording time of 2 s per point. Fixed wavelength scans were acquired at $\lambda_{222\ nm}$, with a 2 nm bandwidth, temperature increment of 0.5 °C and mean heating rate of approximately 20 °C h^{-1}. Temperature was increased from 4 °C to 95 °C or until the measured ellipticity had reached a stable plateau. All data are shown with the buffer baseline subtracted. Ellipticity was reported as the mean residue ellipticity ([θ]) and calculated as:

$$[\Theta] = [\Theta]_m \left[\frac{1}{10\, l\, c_{Molar}\, n} \right] \qquad [3]$$

Where $[\theta]_m$ = ellipticity measured in millidegrees, n = the number of amide bonds in the main chain of the peptide, c = the total concentration of the sample in mol L^{-1} and l is the optical path length of the cell in centimeters.

2.2.2 General Chromatography Techniques

A range of chromatography methods were employed in this study to both purify and characterise coiled-coil motif peptides and polymer-coiled-coil motif conjugates. The basic principles of the three techniques; reverse-phase, size-exclusion and ion-exchange chromatography that were used in these studies are illustrated in **Figure 2.1**. RP-HPLC was used extensively for the purification and characterisation of peptides and as such its use is detailed in Chapter 3. The use of high-pressure size exclusion and ion-exchange chromatography is detailed in Chapter 4 as both approaches were investigated for the purification and characterisation of the mPEG-coiled-coil conjugates.

Low-pressure size-exclusion chromatography using Sephadex® G-15 and G-25 media was used for the purification and analysis of OG-labelled conjugates described in Chapter 6. A summary of the preparation and use of these columns is given in the following sections.

2.2.2.1 Preparation of Sephadex® G-15 Chromatography Columns

Columns containing Sephadex® G-15 media were necessary for the purification and analysis of OG-labelled peptides, as the molecular weights of the peptides

(a) Reverse-phase (RP) chromatography

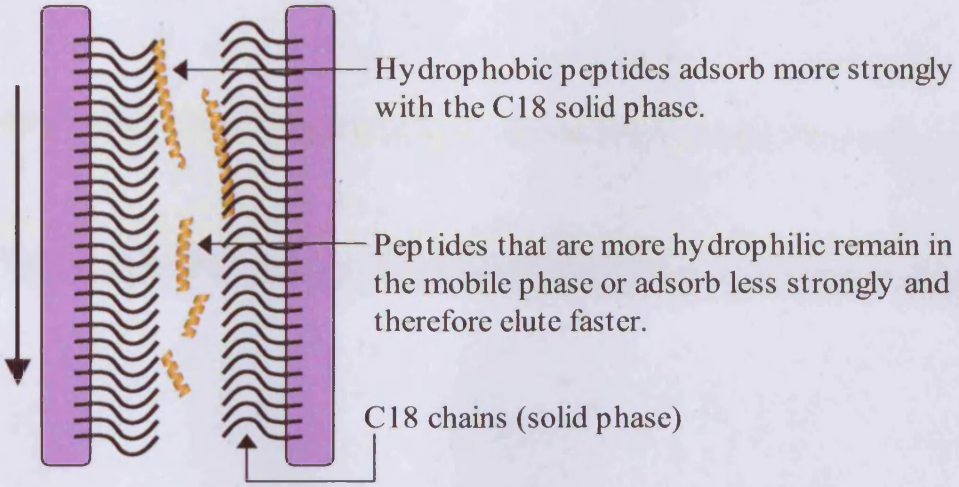

(b) Size-exclusion (SE) chromatography

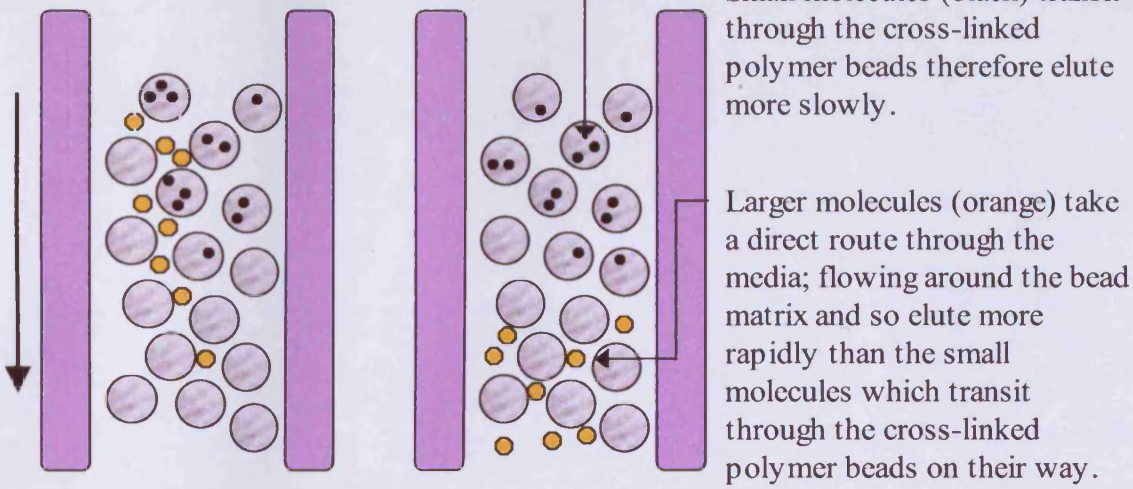

(c) Ion-exchange (cation) chromatography

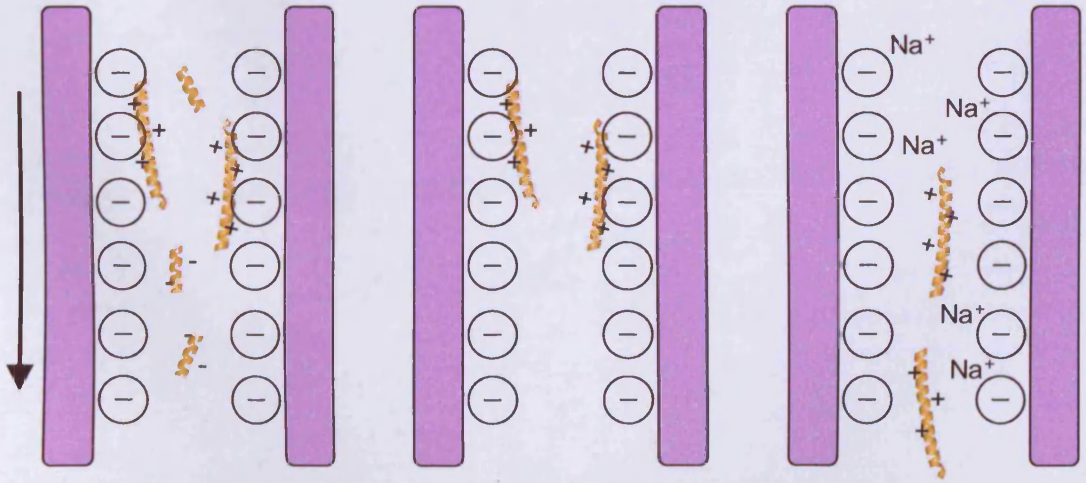

Positively charged molecules adsorb onto the negatively charged solid-phase, while negatively or uncharged molecules are washed off. Elution of the target molecule is then effected by the addition of salt e.g. NaCl.

Figure 2.1 The basic principles of (a) RP, (b) SE and (c) Ion-exchange chromatography. Arrows on left indicate direction of flow through column media.

synthesised in Chapter 3 were below the 5,000 g mol^{-1} cut-off of the commercially available PD-10 columns. Preparation of the columns in accordance with this method made it possible to use them in exactly the same manner as described for the commercially available PD-10 columns (section 2.2.2.2). The quantities of materials detailed here were sufficient to prepare two 8.3 mL settled bed-volume chromatography columns.

Dry Sephadex® G-15 gel (8 g) was weighed into a sterile plastic tube (50 mL). This quantity was calculated on the basis of 1 g of dry gel swelling to a bed volume of between 2.5 and 3.5 mL. Phosphate buffered saline (PBS), pH 7.4 (30 mL) was added and the tube gently inverted 2-3 times to hydrate the gel. The tube was then sealed and incubated for 1 h at 90 °C to allow the gel to swell. During heating, the tube was inverted 5-6 times to ensure even mixing of the beads in the buffer. Once swelled, the suspension was allowed to cool at room temperature for 10 min, following which the supernatant was carefully decanted. PBS, pH 7.4 (8 mL) was added to prepare a 75 % suspension of gel. Filters were inserted into the bottom of empty PD-10 column tubes and gel suspension (11.1 mL/tube) was added. Once settled, wetted top filters were pushed into place and the columns were ready for use.

2.2.2.2 Use of Sephadex G-15 and G-25 Media for the Purification and Analysis of OG-labelled conjugates

Sephadex® G-15 columns were used to purify and characterise OG-labelled peptides, while purification and analysis of mPEG-OG and mPEG-peptide-OG conjugates were conducted using the commercially available PD-10 desalting columns (pre-filled with Sephadex® G-25 media). It was first necessary to ascertain whether the G-15 columns performed in the same manner as the G-25 columns by analysing the elution profile of free (un-reacted OG).

Columns were first equilibrated with PBS, pH 7.4 (25 mL). OGSE488-X (5 mg) was dissolved in MeOH (1 mL) to prepare a stock solution (5 mg mL^{-1}) from which an aliquot (20 μL) was diluted with PBS, pH 7.4 (1980 μL) to prepare a sample solution (2 mL). Aliquots (1 mL) were then added to each column, the first 0.5 ml eluted to waste. Subsequently, aliquots (0.5 mL) of PBS, pH 7.4 were added to each column and the eluting fractions collected (40 fractions in total). A sample (100 μL) of each fraction was transferred to a black 96-well microtitre plate and the fluorescence emission measured using a fluorescence plate reader (FLUOstar OPTIMA) with excitation and

emission filters set at λ_{ex} = 485 nm and λ_{em} = 520 nm, respectively. These filters were chosen as they were closest available to the published $\lambda_{ex\ (max)}$ and $\lambda_{em\ (max)}$ for OGSE (www.invitrogen.com). The elution profiles for OGSE488-X in Sephadex® G-15 and G-25 media are shown in **Figure 2.2**.

Purification of the conjugates prepared in Chapter 6 and analysis of the % free OG content was conducted using this method.

2.2.3 Cell Culture

Cell culture was performed in accordance with the United Kingdom Co-ordinating Committee on Cancer Research (UKCCCR) guidelines (Masters *et al*, 1999). An aseptic environment was maintained within the incubator by spraying all equipment with ethanol 70 % v/v in ddH_2O prior to use. Non-sterile equipment was sterilised either by (i) autoclaving (120 °C, 15 lbm^{-2}, 15 min) e.g. ddH_2O, PBS, glassware and some plastics, (ii) microfiltration (0.2 μm filter) of solutions not suitable for autoclaving or by (iii) UV irradiation (30 min).

2.2.3.1 Defrosting of Cells

Cells were stored under liquid nitrogen in vials containing a suspension (1 mL) of cells. Vials were thawed in a water bath at 37 °C and the suspension was transferred by pipette into a universal containing RPMI 1640 80 % v/v in FCS (9 mL). The suspension was centrifuged at 1000 rpm, 20 °C for 5 min. The supernatant was removed by aspiration and the cells re-suspended in RPMI 1640 95 % v/v in FCS (5 mL), (i.e. complete media). This suspension was then transferred to a 25 cm^2 flask and incubated at 37 °C, 5 % CO_2 for 24 h. After this time the media was aspirated and the cells washed three times with PBS (10 mL) to remove non-viable cells. Fresh media was added and the cells incubated at 37 °C, 5 % CO_2 until 80 % confluency was reached and they could be passaged.

2.2.3.2 Cell Maintenance and Passaging

Cells were passaged at 80 % confluency (approximate determination by light microscopy). The media was removed by aspiration and the cells washed three times with PBS (10 mL). The cells were lifted by incubating with Trypsin-EDTA solution (1.5 mL) at 37 °C, 5 % CO_2 for 3 min. Complete media (8.5 mL) was added, the

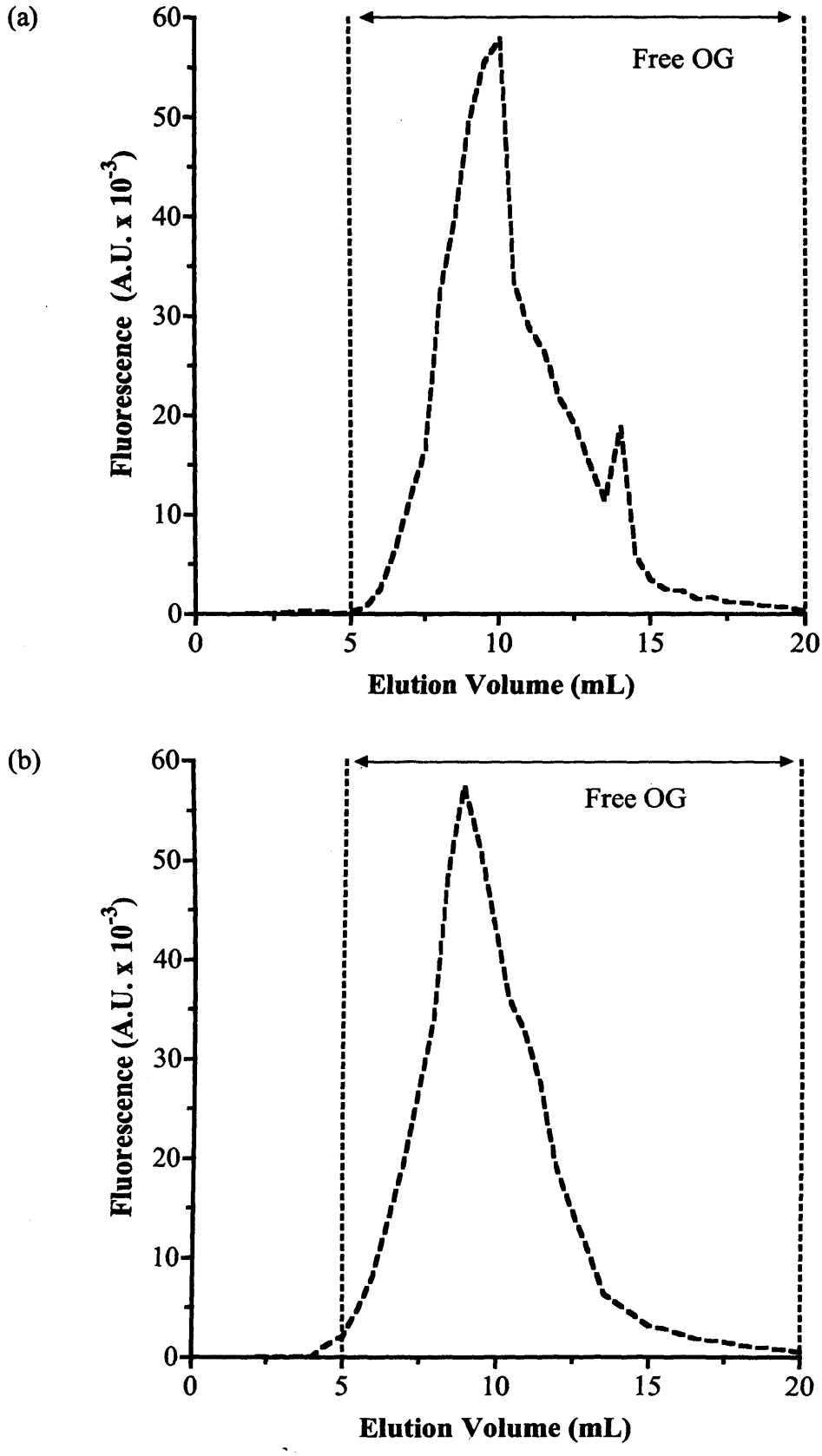

Figure 2.2 Elution profiles for OG from Sephadex® G-15 and G-25 columns. Panel (a) shows the elution of free OG in G-15 media and panel (b) shows the elution profile in G-25 media (pre-packed PD-10 column).

suspension was transferred to a universal and centrifuged at 1000 rpm, 20 °C for 5 min. The supernatant was aspirated and the cells re-suspended in fresh complete media (5 mL). New flasks were prepared by diluting an aliquot (1 mL) of this suspension with compete media. When MCF-7 cells were used for assays, media without phenol red (WRPMI 1640) was used (referred to as clear complete media) as the pH indicator has been shown to have mitogenic activity and as such may interfere with the oestrogen pathway (Devleeschouwer *et al*, 1992).

2.2.3.3 Counting and Seeding Cells

Cell cultures were washed with PBS and re-suspended as described (section 2.2.3.2). To ensure a homogenous suspension of cells the suspension was passed through a 23 G needle under pressure. An aliquot (100 μL) of this suspension was diluted with Trypan Blue 0.2 % w/v in PBS (100 μL). A sample of this solution was placed on a haemocytometer and cells from ten 0.1 mm^3 squares (five from each chamber of the haemocytometer) were counted. Non-viable cells i.e. those stained blue/black with Trypan Blue were not counted. The concentration (cells mL^{-1}) was determined using the following formula:

$$Concentration\ (cells\ mL^{-1}) = Arithmetic\ Mean \times 2 \times e^4 \qquad [4]$$

Where, 2 accounts for the trypan blue dilution and e^4 accounts for the conversion of 0.1 mm^3 to mL. Once determined, the suspension was diluted with clear complete media to obtain the concentration required for the appropriate seeding density used in the assay.

2.2.4 General Biological Assays

Detailed methods for the biological assays used are provided in Chapter 6, however the general methods for two of the techniques used are given here.

2.2.4.1 Quantification of Cell Growth Using the MTT Assay

The MTT assay was used as a method to assess cell growth and viability. Reduction of the soluble MTT reagent in response to mitochondrial respiration generates the insoluble formazan salt (**Figure 2.3**). Cell viability may then be determined by measuring the UV absorbance at $\lambda_{550\,nm}$ (Mosmann, 1983).

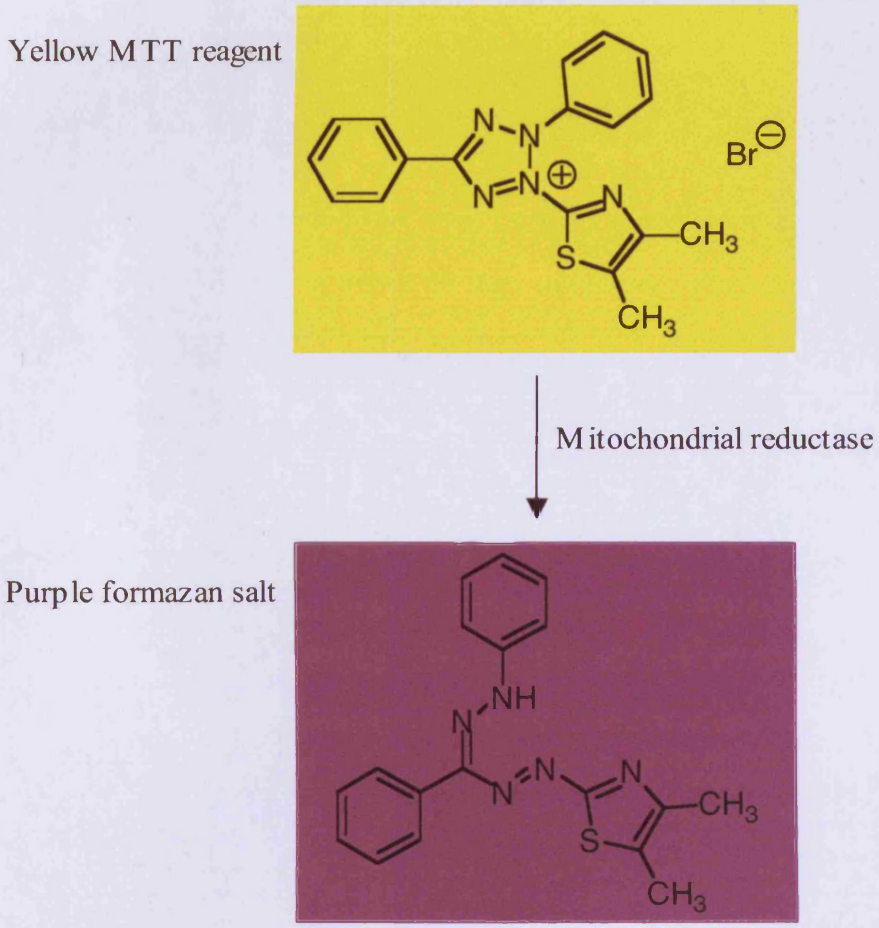

Figure 2.3 Scheme to show the mechanism by which soluble MTT is reduced to form the insoluble formazan salt.

Cells were seeded in a 96 well plate at a density of 40,000 cells mL^{-1} and incubated for 24 h at 37 °C, 5 % CO_2. An aliquot (20 μL) of a sterile, filtered solution of MTT in PBS (5mg mL^{-1}) was added to each of six wells. The plate was then incubated for 5 h at 37 °C, 5 % CO_2. Following this, the media and MTT solution were aspirated and an aliquot (100 μL) of DMSO was added to each of the six wells. After the plate had been incubated for 30 min at 37 °C, 5 % CO_2 the UV absorbance was measured at $\lambda_{550\ nm}$ (Sunrise, Tecan). The DMSO solution was removed by aspiration and PBS (200 μL) was added to each well. The plate was returned to the incubator and the whole procedure repeated every 24 h. The UV absorbance was plotted against time to generate a "growth curve" for the MCF-7 cell line (**Figure 2.4**).

2.2.4.2 Determination of Cytotoxicity by the MTT Assay

Cells were seeded in a 96 well plate at a density of 40,000 cells mL^{-1} using clear complete media and incubated for 24 h at 37 °C, 5 % CO_2. After 72 h, test compounds were prepared at a range of concentrations, typically 0, 0.001 0.01, 0.05, 0.1, 0.5 and 1 mg mL^{-1}, in clear complete media. Aliquots (100 μL) of each in replicates of 6 were added to the respective wells. Plates were then incubated for 67 h, following which an aliquot (20 μL) of a sterile, filtered solution of MTT in PBS (5mg mL^{-1}) was added to each well. The plate was then incubated for a further 5 h at 37 °C, 5 % CO_2. Following this, the media and MTT solution were aspirated and an aliquot (100 μL) of DMSO was added to each of the six wells. After the plate had been incubated for 30 min at 37 °C, 5 % CO_2 the UV absorbance was measured at 550 nm (Sunrise, Tecan). Cell growth as % was determined relative to the control cells i.e. those incubated with only clear complete media.

$$Cell Viability\ (\%) = \frac{\lambda_{550\,nm}\ treated\ cells}{\lambda_{550\,nm}\ untreated\ cells} x\ 100 \qquad [5]$$

2.2.1.3 Use of Flow cytometry to Measure Cellular Uptake of Fluorescent Probes

Flow cytometry was used in Chapter 6 to study the uptake of OG labelled peptides and mPEG-peptide conjugates in MCF-7 cells. Cells were seeded into 6-well (1 mL) plates at a concentration of 5 x 10^5 cells mL^{-1} in clear complete media and incubated for 24 h at 37 °C, 5 % CO_2. Cells were treated with samples using a fixed

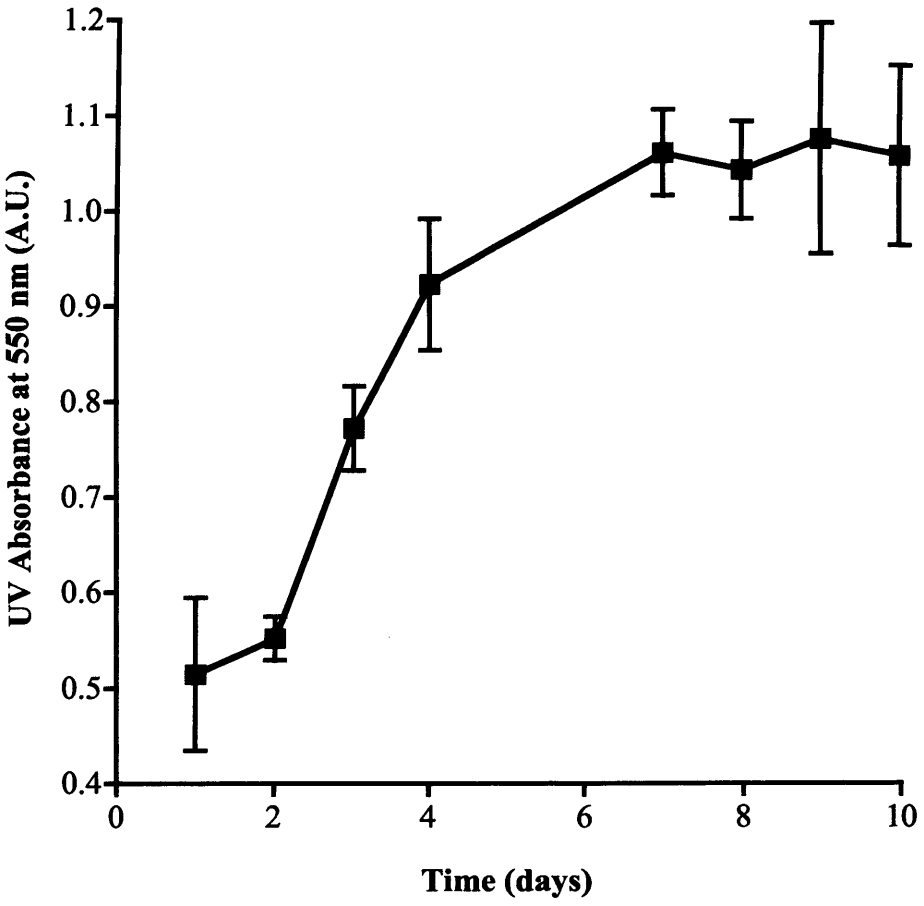

Figure 2.4 Growth curve for the MCF-7 cell line. Cells were seeded at a density of 4 x 10^4 cells mL^{-1}. Data shown represents the arithmetic mean absorbance at 550 nm (n=6) ± SD.

concentration of OGSE488-X (1.5 μg mL^{-1}), optimised in previous studies, and incubated at 37 °C. At the end of the incubation period, the plates were placed on ice and the cells washed with cold (4 °C) PBS, pH 7.4 (1 mL) three times. An aliquot (1 mL) of PBS, pH 7.4 was then added to each well and the adherent cells were scraped from the plate surface and transferred to falcon tubes. The samples were centrifuged at 4 °C for 5 min at 1000 g. Finally, the supernatant was removed and the cells were re-suspended in cold (4 °C) PBS, pH 7.4 (200 μL) and analysed using a Becton Dickinson FACSCalibur cytometer equipped with an argon laser (488 nm) and emission filter for 550 nm.

Data were acquired using 1024 channels with band pass filter FL-1 (530 nm ± 15 nm) and collected with 10,000 cell counts in the gated region per sample and processed using CellQuest™ v3.3 software. The gated region was set to exclude cells that were very small or of a highly granular nature i.e. those that showed in the bottom left of the acquisition dot-plot (**Figure 2.5a**). To remove the cell autofluorescence from acquired data, control cells (cells that had been incubated with only clear complete media) were measured in each experiment.

There are several ways of expressing the fluorescence data acquired in a flow cytometry experiment. The majority of flow cytometers acquire fluorescence data on a logarithmic scale by default such that the entire population distribution of cells with a bright fluorescence signal (e.g. OG) is displayed without some of the points going off scale (**Figure 2.5b**). When acquired on a logarithmic scale the geometric mean (anti-log of the arithmetic mean of log data) is the most appropriate measure of central tendency assuming an approximate Gaussian distribution. The alternative measure is the median, in the past this may have been used for frequently as it was much easier to compute than the geometric mean, however, this is no argument today. The only real advantage is that it is not influenced as much as the geometric mean by values that are far out of the "normal" range, this is probably only of benefit where the distribution of data is heavily skewed or counts pile at one end of the measurement scale. Three methods of interpreting the data were assessed. In the first, the fluorescence of the cell population was estimated using the geometric mean and the second using the median. In these studies little or no difference was seen when the data were processed using either the geometric mean or median.

The third method enabled analysis of only the cells that associated with the fluorescent probe. This was achieved by defining a region that covered 98 % of the

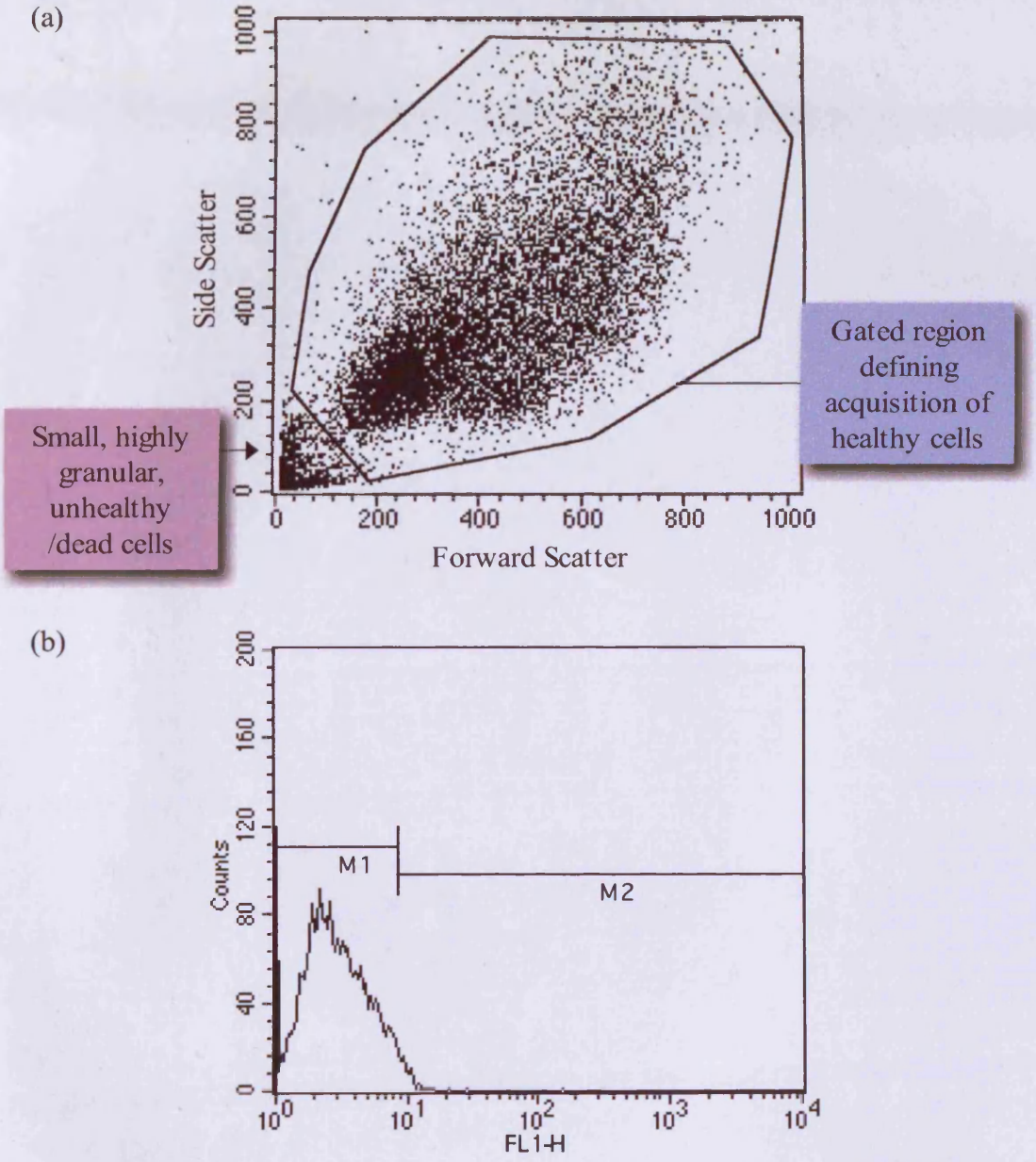

Figure 2.5 Flow cytometry dot-plot and acquisition histogram showing the typical distribution of a control cell population. Panel (a) shows a typical acquisition dot-plot for a control cell sample. Panel (b) shows the corresponding acquisition histogram, where region M1 defines a region of the histogram that includes 98 % of the cells acquired, and M2 designates cells with a higher fluorescence than M1.

control cell population, this was marked M1 (**Figure 2.5b**). The second region (M2) was designated to represent the measured fluorescence greater than M1. Thus as cell associated fluorescence increased so too would the number of events in the M2 region. Measuring only the % of cells in the M2 gate would be too insensitive to differentiate between the populations almost exclusively within the M2 gate. Therefore, the % of cells in the M2 gate was multiplied by the geometric mean to improve the statistical resolving power. All data expressed in this thesis make use of this approach with cell-associated fluorescence reported as defined by equation [6]:

$$\text{Cell Associated Fluorescence} = \frac{\text{M2 Geometric Mean x M2 \% Gated Cells}}{100} \quad [6]$$

2.2.5 Statistics

All data were expressed as mean ± SD (Zaugg, 2003). Minimum statistical significance was set at $p < 0.05$. Where more than two groups of data, grouped by one factor were compared one-way analysis of variance (ANOVA) with a Bonferroni or Tukey post hoc test. The disadvantage of the Bonferroni test is that it is very conservative and it is therefore possible to miss very small, yet real differences. In the analysis of the data presented in Chapter 6 no difference in significance was observed using either post hoc test. Where more than two groups of data, grouped by two factors were compared a two-way ANOVA was conducted and selected pairs of data compared with the Bonferroni test. All statistical calculations were conducted using GraphPad Prism, version 4.0c for Macintosh, 2005.

CHAPTER 3

Coiled-Coil Peptide Design, Synthesis and Characterisation

3.1 Introduction

Following identification of the protein targets (described in Chapter 1, section 1.5), it was first necessary to select and/or design peptide sequences for synthesis. Therefore, the aims of this study were, firstly, to use open-source coiled-coil prediction software to predict the probability of coiled-coil formation for each peptide sequence. Subsequently, it was necessary to synthesise peptides of acceptable purity (≥ 95 %) for use in biological and biophysical studies, and in parallel it was crucial to ensure that the peptides were engineered in such a way that they would be suitable for subsequent PEGylation. Finally, it was necessary to develop techniques for peptide purification and characterisation, namely preparative and analytical RP-HPLC, and ESI-TOF MS. A brief introduction to each of these areas is given in the following sections (3.1.1 to 3.1.4).

3.1.1 Rational Design, Selection and Prediction of Coiled-Coil Motifs

Intellectual, rational design and/or selection of coiled-coil motifs to target the proteins, E2F1 (Joshi *et al*, 2003), AP-1 (Mason *et al*, 2006), EbVP35 (Reid *et al*, 2005) and EbGP2 (Watanabe *et al*, 2000) was an essential first-step for this study. It was vital that coiled-coil motifs could be accurately predicted, as one of the defining features of this thesis was to be the evaluation of polymer-coiled-coil motifs (rather than just polymer-peptides) as potential therapeutic agents. A number of techniques are available that either predict, identify and/or characterise coiled-coil domains in proteins and peptides. These fall into two distinct categories, i.e. computational and biophysical analysis. A summary of the pros and cons of the computational programmes available for use for the prediction of coiled-coils is given in **Table 3.1**. The biophysical techniques used for characterisation are discussed in detail in Chapter 5.

The first coiled-coil prediction programme to be published was "COILS" in the early 1990s (Lupas *et al*, 1991), since then, a number of programs have been developed including "Paircoil" (Berger *et al*, 1995), "LearnCoil-VMF" (Berger & Singh, 1997) "MultiCoil" (Wolf *et al*, 1997) and "Paircoil2" (McDonnell *et al*, 2006), each using differing algorithms and/or protein databases. A caveat of their use however was that the output was predictive and therefore although a good starting point, reliability of the

Table 3.1 A summary of the five computational programmes available to identify and predict coiled-coil motifs in proteins.

Programme	Year of Release	Pros	Cons
COILS	1991	Allows scan for 14, 21 or 28 residues.	Highest frequency of false positives.
Paircoil	1995	Fewer false positives than COILS.	Only identifies dimeric coiled-coils. Superseded by Paircoil2
LearnCoil-VMF	1997	Specifically for viral coiled-coil fusion proteins	False negatives with short sequences
MultiCoil	1997	Distinguishes between dimeric and trimeric coiled-coils.	More false positives than Paircoil/Paircoil2
Paircoil2	2006	Superior performance over all other prediction programs	Limited to parallel coiled-coils.

data could not be assured. Furthermore previous studies had shown that each program gave different predictive outputs for the same protein/peptide sequences. This compounded the difficulty of making accurate and reliable judgments as to the existence of coiled-coils in the protein targets. Thus, for any given sequence a judgment was made following sequence analysis using as many of the programs as possible (four or five depending upon the protein type). LearnCoil-VMF was designed specifically to identify coiled-coil domains in viral membrane fusion proteins, therefore was only used here to assess the sequence of EbGP2. With this exception, the remaining programs (COILS, Paircoil, MultiCoil and Paircoil2) were used to give predictions for all the other proteins. The way that these programmes were used in these studies is described in the methods (section 3.2.1). It is pertinent to note that, AP-1 and EbGP2 were chosen as targets not simply because of their roles in carcinogenesis and Ebola, respectively, but also because the structures of the proteins had been previously solved by X-Ray crystallography (Glover & Harrison, 1995; Weissenhorn *et al*, 1998). This technique is considered by many to be the 'gold-standard' for determining protein structure. Therefore, as a positive control, predictive data was acquired for EbGP2.

Following identification of the protein targets and the peptide sequences that would likely form coiled-coil motifs (using the programs described above), it was necessary to consider the various methods by which the peptides might be synthesised.

3.1.2 Peptide Synthesis

The aim of this thesis was to investigate whether polymer-coiled-coil motif conjugates could be designed as novel therapeutics that might act as molecular switches. Therefore, it was necessary to synthesise the desired coiled-coil motifs for subsequent PEGylation (Chapter 4). However, it was never the intention to spend a lot of time optimising a methodology for peptide synthesis, though it was considered very important to generate peptides of high purity ($\geq$ 95 %) and on a scale appropriate for subsequent experimentation (> 30 mg).

Peptides may be synthesised either biologically using recombinant *E. coli* systems (reviewed in Gräslund *et al*, 2008), or alternatively by a number of different chemical synthesis methods (reviewed in Chan & White, 2000). The most significant advantage offered by chemical synthesis and used in this study was the ability to make

alterations to the primary structure using either natural or synthetic amino acids with relative ease. With a recombinant methodology it would be necessary to prepare a new expression plasmid and optimise the culturing conditions each time one desired a different peptide primary structure. Thereby making it a much slower, and more costly approach. In this chapter chemical peptide synthesis was used exclusively, however it may be noted here that a recombinant approach was used later (Chapter 5), for the preparation of a ^{15}N labelled ([^{15}N]) peptide. A brief history, and an introduction to SPPS as was used in this study is given below.

3.1.2.1 Solid Phase Peptide Synthesis (SPPS)

In 1963, R. B. Merrifield pioneered a new method of for peptide synthesis and described the approach now widely known as SPPS. The following year, synthesis of the ennea-peptide, bradykinin (an endogenous vasodilator) by SPPS (Merrifield, 1964) heralded a breakthrough that triggered a paradigm shift in the peptide synthesis community and enormous interest in this methodology.

In brief, SPPS is a synthetic approach whereby peptides are "grown" on a solid support, typically a polystyrene resin, by the sequential reaction of amino acids with chemically protected amines and side-chain moieties (reviewed in Chan & White, 2000). Amino acids are then sequentially linked *via* reaction of the carboxylic acid (R-COOH) with the exposed amine (R-NH_2) on the polystyrene support. Following the formation of an amide (peptide) bond, the amine-protecting group from the end of the "growing" peptide chain is removed and the next amino acid added. Once the sequence is complete, the peptide is cleaved from the resin and the side-chain protecting groups are removed. The general principle of SPPS is illustrated in **Figure 3.1**.

The Fundamental Components of SPPS

When planning a synthesis using a SPPS approach there is a plethora of apparatus and reagents that one must consider, namely the:

- Solid support (resin)
- Amine protecting chemistry (Boc/Fmoc)
- Amino acid side-chain protecting groups
- Acid-activation chemistry and coupling conditions
- Capping (N-Terminal Acetylation)

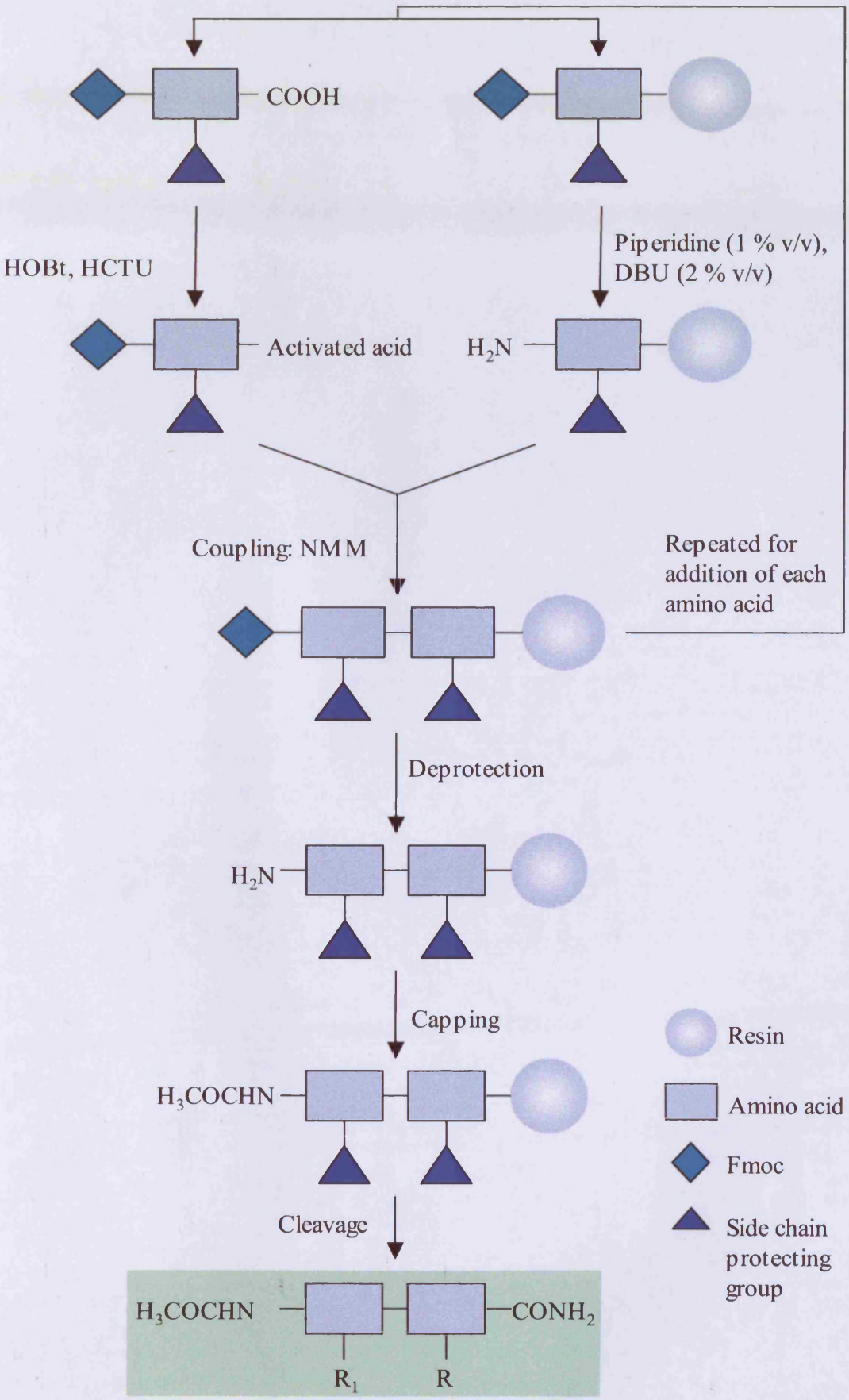

Figure 3.1 The general principles of Fmoc-SPPS. Adapted from Chan & White, (2000).

- Cleavage and side-chain deprotection

Solid Support (Resin)

There are two key factors that must be considered when choosing the solid support: (i) the functionalisation chemistry and (ii) solvent compatibility. The polymer matrix of the trialkoxybenzhydrylamine (Rink Amide AM) resin used throughout this work is composed of copoly(styrene-1 % divinylbenzene) with the Rink Amide linker attached *via* norleucine to aminomethylpolystyrene (**Figure 3.2**) (Rink, 1987). This functionalisation had been previously shown to enable the synthesis of C-terminal amide modified coiled-coil motif peptides (Vandermeulen *et al*, 2003). Furthermore, the study demonstrated the compatibility of the resin with the solvents DCM and NMP. NMP, rather than dimethylformamide (DMF) was used in all syntheses described here due to its superior safety profile.

Amine Protecting Chemistry

In order to ensure that each amino acid being coupled reacts only with the amine of the resin support, or growing peptide chain, rather than uncoupled amino acids it is necessary to use amino acids with a protected amine moiety. There are two commonly used chemistries, t-butoxylcarbonyl (Boc) and Fmoc (**Figure 3.3**). The original, Boc protecting strategy (Merrifield, 1963; Merrifield 1964) required the use of the rather hazardous, liquid hydrogen fluoride for deprotection of the Boc moiety and as such has been largely superceded by Fmoc-SPPS. The Fmoc protecting strategy was first proposed by Carpino in the early 1970s (Carpino & Han, 1972) and utilises basic conditions to effect removal of the Fmoc moiety during the deprotection step. Although probably the most significant development in SPPS since its introduction, it wasn't until the early 1990s when an independent comparison of the Boc and Fmoc methodologies (Fields *et al*, 1993) demonstrated the superiority of the Fmoc approach that Fmoc-SPPS was universally accepted as the preferred method.

Amino Acid Side-Chain Protecting Groups

Side-chain protecting groups are necessary to prevent undesirable side-reactions from occurring during the process of chain elongation in SPPS. Today, many types of protecting groups exist, each with their individual pros and cons. A summary of those available for the amino acids used in this study is given in **Table 3.2**. Previous work

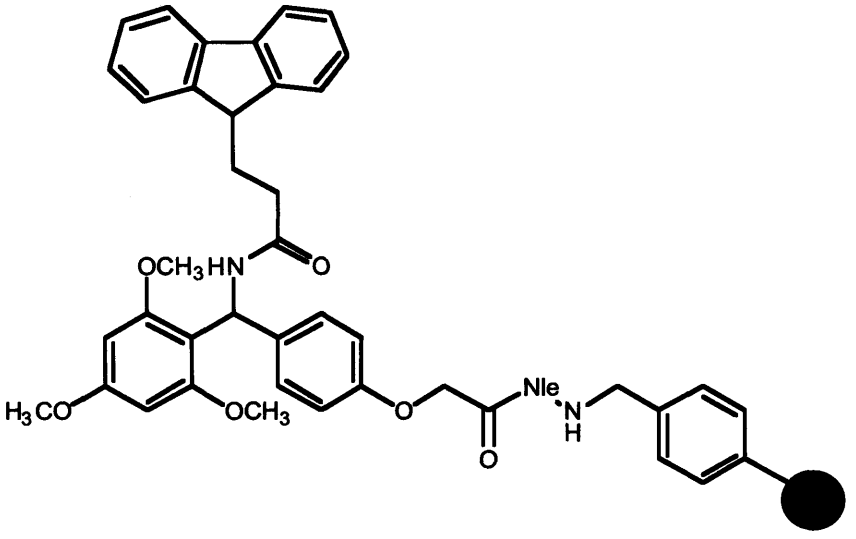

Figure 3.2 The chemical structure of Rink Amide AM Resin.

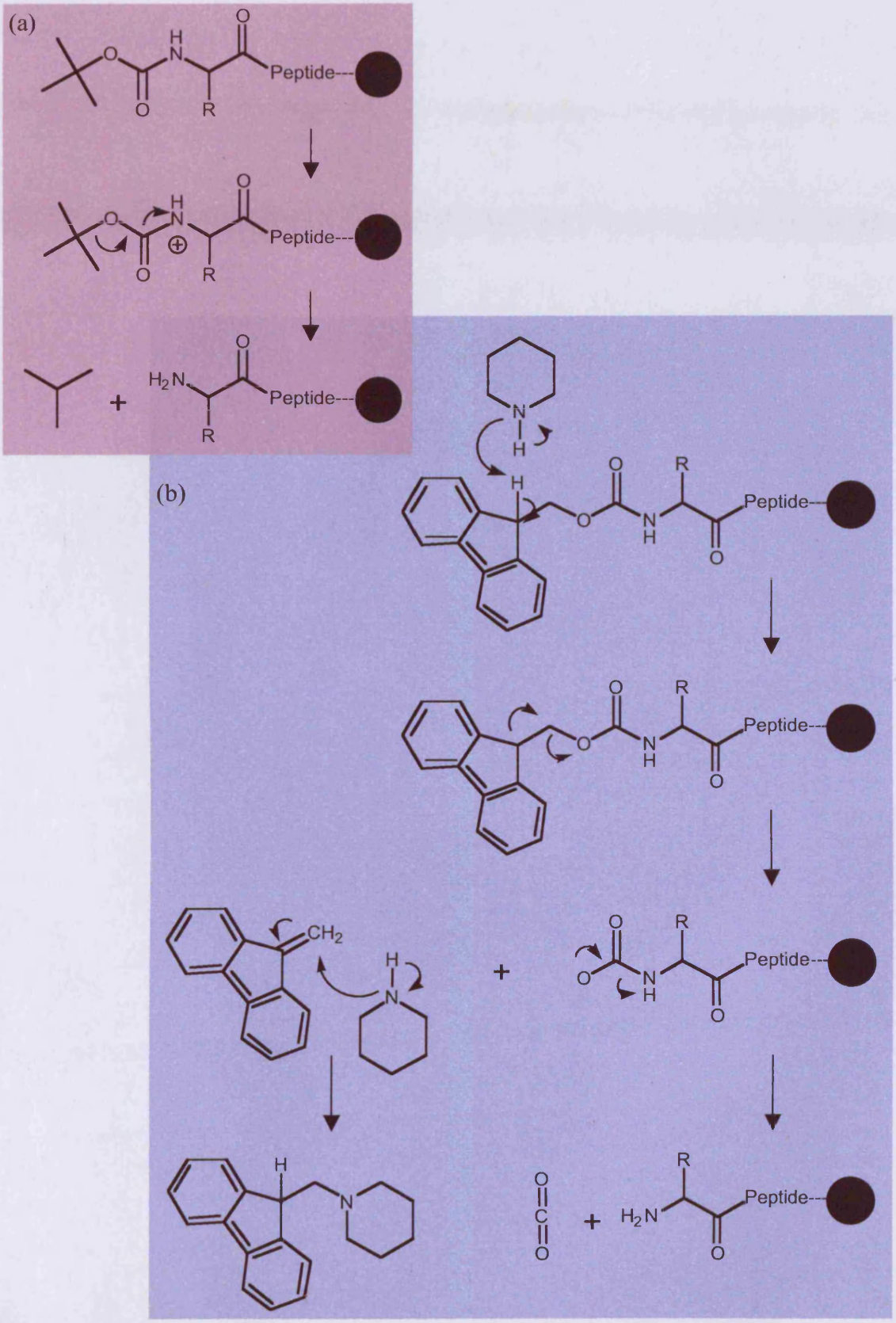

Figure 3.3 Boc and Fmoc protection strategies used in Fmoc-SPPS. Panel (a) shows Boc deprotection and panel (b) shows Fmoc deprotection. Adapted from Jones, (1992).

Table 3.2 A summary of commonly used side-chain protecting groups. The protecting groups highlighted (in bold) were used in this study.

Amino Acid	Side Chain Protecting Group
Alanine	N/A
Arginine	4-Methoxy-2,3,6-trimethylbenzenesulphonyl (Mtr)
	(2,2,4,6,7-Pentamethyldihydrobenzofuran-5-sulfonyl) (Pbf)
	2,2,5,7,8-Pentamethylchroman-6-sulphonyl (Pmc)
Asparagine	**Trityl (Trt)**
Aspartic Acid	***t*-Butoxy (*t*BuO)**
Cysteine	Acetamidomethyl (Acm)
	t-Butyl (*t*Bu)
	t-Butylthio (*t*Buthio)
	Trityl (Trt)
Glutamic Acid	***t*-Butoxy (*t*BuO)**
Glutamine	**Trityl (Trt)**
Glycine	N/A
Histidine	*t*-Butoxymethyl (Bum)
	Trityl (Trt)
	t-butoxycarbonyl (Boc)
Isoleucine	N/A
Leucine	N/A
Lysine	***t*-butoxycarbonyl (Boc)**
	1-(4,4-Dimethyl-2,6-dioxocyclohexylidene3-methylbutyl (Ddiv)
Methionine	N/A
Phenylalanine	N/A
Proline	N/A
Serine	***t*-Butyl (*t*Bu)**
	Trityl (Trt)
Threonine	***t*-Butyl (*t*Bu)**
Tryptophan	***t*-butoxycarbonyl (Boc)**
Tyrosine	***t*-Butyl (*t*Bu)**
Valine	N/A

had identified the optimal protecting chemistries for the synthetic protocol used here (Vandermeulen *et al*, 2003; Vandermeulen *et al*, 2004; Vandermeulen *et al*, 2005).

Acid-Activation Chemistry and Coupling Conditions

In order to effect efficient coupling (of amino acid) to the amine of the peptidyl-resin it is necessary to activate the carboxylic acid group. There are two main categories of activating chemistries in common use: carbodiimides and triazoles (reviewed in Valeur & Bradley, 2009). Carbodiimides have been used longer than the latter and are highly reactive, however as a result of such high reactivity racemisation of the amino acid is common. Triazoles, for example HOBt, as used in this study have become more popular as the active ester they form is less reactive and therefore there is a lower risk of racemisation.

Capping (C-Terminal Amidation and N-Terminal Acetylation)

With a SPPS approach it is possible to synthesise peptides with a variety of C- and N-terminal functionalities. C-terminal amidation was effected as described earlier with the use of Rink Amide AM resin. N-terminal acetylation was performed using acetic anhydride. These modifications were carried out to improve both the biophysical and pharmacokinetic properties of the coiled-coil motif peptides. Since all of the peptide sequences described here have been identified from inner protein domains, charged C- and N-termini would not exist in the native systems. As described in Chapter 1, ionic charges play an important role in the stabilisation or destabilisation of coiled-coils. Amidation and acetylation remove the terminal charges that could have a detrimental effect upon coiled-coil formation and target hybridisation. Furthermore, these modifications have been reported to make peptides more resilient to degradation by endopeptidases and exopeptidases (Landon *et al*, 2004).

Cleavage and Side-Chain Deprotection

Cleavage and deprotection is perhaps the most critical step of peptide synthesis. Rather than one straightforward reaction, the incubation of the peptidyl-resin with a "cleavage cocktail" is a series of competing reactions. Without the appropriate selection of reagents and reaction conditions the peptide may be irreversibly damaged.

There are numerous cleavage and deprotection protocols described in the literature that have been utilised for peptides synthesised with an Fmoc-SPPS strategy (Fields & Noble, 1990; Grant, 1992; Guy & Fields, 1997; Chan & White, 2000). The vast majority of these methods are TFA-based, however, they differ according to concentration, type of nucleophilic reagent (scavenger) and reaction time used. A 'standard' cocktail was used for all reactions in this study (section 3.2.2.3). This was supplemented with ethanedithiol (EDT) to assist in the removal of the Trt protecting group when deprotecting peptides with N-terminal cysteine residues (Chan & White, 2000).

Caveats and Limits of SPPS

Despite widespread use SPPS is not without caveats and limitations. Of particular relevance to this study, is the difficulty in synthesising very long peptides (> 50-residues) due to the effect of accumulated coupling errors on final product yields (discussed in Chan & White, 2000). Furthermore, as the peptide becomes longer the increased number of side-chain protecting groups can adversely affect the solubility thus making subsequent couplings more difficult (Tam & Lu, 1995). Peptides with long stretches of hydrophobic amino acids have the potential to aggregate even as early as the fifth residue (Bedford *et al*, 1992) and/or form beta-sheet structures that can further complicate the synthesis. The size of the resin 'mesh' chosen will govern the space available for the peptides to 'grow' during synthesis. If this is too small the resin will become congested, and a high % of truncation mutants will result.

3.1.3 Engineered Modifications to Wild-Type Peptide Sequences

The use of SPPS in this study afforded the opportunity to introduce new amino acids into the primary structures of the peptides synthesised. Three modifications were of particular importance to this study. Firstly, C-terminal amidation and N-terminal acetylation (discussed previously in section 3.1.2.1), second, the insertion of a UV chromophore to facilitate analysis, and finally addition of an N-terminal cysteine residue to enable site-specific conjugation. All peptides synthesised in this study were prepared with amidated C-termini and acetylated N-termini. Following initial studies with the synthesis of a PHB derived peptide all other peptides were modified so that they contained a UV sensitive chromophore (section 3.1.3.1). Since some of the

peptides synthesised here were to be used to model the coiled-coil binding domains of the target proteins, these were prepared without N-terminal cysteine residues. The peptides that were synthesised as the 'therapeutic' coiled-coil motifs for subsequent PEGylation were prepared with N-terminal cysteine residues (section 3.1.3.2).

3.1.3.1 Insertion of Tyrosine as a UV-Chromophore into Peptide Sequences to Aid Characterisation

Accurate determination of peptide concentration was considered essential, particularly for CD spectroscopy experiments (Chapter 5). A number of techniques can be used, for example, amino acid analysis (AAA), UV spectrometry and colorimetric assays e.g. the bicinchoninic acid (BCA) assay. Gravimetric determination of peptide concentration is widely known to be unreliable. This is largely due to the hygroscopic properties of peptides, however, further error may be introduced due to salt molecule co-ordination with charged amino acid side chains. Previous work by collaborators (Klok *et al*, personal communication) demonstrated that colorimetric assays such as the BCA assay were not sufficiently accurate for CD measurements. AAA can be considered the 'gold standard' technique for the determination of peptide concentration however facilities were not available in either Cardiff or Lausanne.

Thus UV spectroscopy was investigated as a practical alternative. Determination of peptide concentration by UV requires a chromophore with an absorbance wavelength sufficiently red-shifted from that of the peptide bond (c.a. 210-220 nm). The naturally occurring aromatic amino acids, tryptophan (W), tyrosine (Y) and phenylalanine (F) have absorbance maxima at 280, 274 and 257 nm, respectively. If the chain-length of the peptide (and hence number of peptide bonds) is too great the ε of phenylalanine is often too weak and insufficiently red-shifted to allow accurate concentration determinations to be made. Tyrosine has a smaller, less hydrophobic and less immunogenic side-chain than tryptophan, furthermore it's use in synthetic peptides as a chromophore for UV spectroscopic measurements is well documented (Mach *et al*, 1992; Pace *et al*, 1995). In all instances, other than where either tyrosine or tryptophan existed in the native sequence, tyrosine was engineered into the penultimate N-terminal position. Ideally one should choose a solvent exposed position for insertion of the tyrosine residue (Mason *et al*, 2006). Since the peptides were expected to form α-helices and not fold into a globular structure positioning near either the N- or C-termini was considered acceptable.

It was advantageous to insert tyrosine as the penultimate N-terminal residue as a dual wavelength detector could be used to monitor the absorbance at 214 and 274 nm during HPLC purification and analysis. Truncated peptides i.e. those without tyrosine would only show an absorbance at 214 nm, not 274 nm. Furthermore, insertion of tyrosine into the peptide primary sequence would be useful in the characterisation of the mPEG-coiled-coil motif conjugates as it would enable analysis of free and PEG bound peptide using instruments with a fixed wavelength (280 nm) detector (Chapter 4).

3.1.3.2 N-terminal Cysteine Tagging of Peptides for Site-Specific Conjugation

The majority of studies to date, describing protein/peptide conjugates utilise non-specific chemistries to conjugate the protein/peptide to polymers and fluorescent probes of interest (Satchi *et al*, 2001). Since retention of the coiled-coil motif structure is essential for the preservation of biological activity, it was necessary to use a method of site-specifically attaching the polymer (mPEG) to the peptide in these studies. Furthermore, such an approach enables the synthesis of a well-defined therapeutic conjugate, rather than a heterogeneous mixture. Numerous methods of achieving site-specific conjugation have been documented; these are discussed at length in Chapter 4.

In brief, one approach uses the lower pKa of a non-acetylated N-terminal amine (8.9) compared with that of a lysine (K) side-chain (pKa = 10.5) (Selo *et al*, 1996) to facilitate site-specific N-terminal conjugation. However, there is still potential for non-specific attachment to other amines with this method if the pH is not strictly controlled, moreover, reaction times are very long; Vandermeulen *et al*, (2003) found that the PEGylation of coiled-coil motifs using a similar approach required a reaction time of up to 5 days.

An alternative method requires tagging of the protein/peptide with the amino acid cysteine (C). The highly nucleophilic thiol (R-SH) of the cysteine side-chain will react specifically with the unsubstituted C=C double bond of a maleimide for example. At pH 7.0 or lower this reaction is approximately 1000 x as fast as the maleimide-amine reaction due to protonation of the later (Hermanson, 2008). Using this approach, site-specific conjugation with far fewer non-specific reactions is possible in a much shorter time. As such, to facilitate polymer-conjugation peptides were designed with a single cysteine residue at the N-terminus. In principle, it would have been possible to engineer the cysteine residue at the C-terminus, however racemisation is more likely, thus resulting in a product of lower purity (Sieber, 1987; Fujiwara *et al*, 1994).

3.1.4 Post-Synthesis Purification and Characterisation of Peptides

As outlined in section 3.1.2, a high level of purity (≥ 95 %) was desired for all coiled-coil motif peptides synthesised here to facilitate the biophysical structural and binding assays planned with CD and NMR spectroscopy (Chapter 5). Techniques including RP-HPLC and ESI-TOF MS were developed to purify the crude peptides post Fmoc-SPPS, then characterise the 'pure' coiled-coil motif peptide with respect to purity and correct molecular weight.

3.1.4.1 Reverse-Phase High Pressure Liquid Chromatography

RP-HPLC has become the mainstay of peptide purification (reviewed in Mant *et al*, 2007). Most protocols use a linear gradient system (AB) where A = water and B = ACN, each containing TFA as an organic modifier. A preparative system operating under these conditions was used in Lausanne whilst an analytical system was set-up in Cardiff for use in these studies.

Synthetic peptides are usually generated as a TFA salt as a result of its use in HPLC purification. Prior to 1999, little consideration had been given to the potential toxicity of TFA, and as such toxicity may therefore have been wrongly attributed to the peptide studied. TFA toxicity at concentrations of 10^{-8} to 10^{-7} M has since been observed in at least three cell lines; osteoblasts, articular chondrocytes and neonatal mouse calvariae (Cornish *et al*, 1999). The authors suggest that all peptides containing basic residues are converted to a biocompatible salt form e.g. hydrochloride (HCl) prior to use in biological assays. The procedure outlined was used for all peptides containing basic amino acids (section 3.2.5).

3.1.4.2 Electrospray Ionisation Time-of-Flight Mass Spectroscopy

ESI-TOF MS and MALDI-TOF MS have both been widely used in the characterisation of peptides since their inception (reviewed in Zhou & Veenstra, 2008). ESI-TOF MS results in more complicated spectra due to fragmentation of molecules into so called 'molecular ions', however it is a rapid technique that tolerates well the solvent systems used in RP-HLPC. MALDI-TOF (discussed in detail in Chapter 4) often displays a non-fragmented mass, thus making the spectra easier to interpret. However the technique is laborious with regard to sample preparation, and instrument calibration. As such ESI-TOF was utilised predominantly to identify the correct peaks

in the preparative and analytical RP-HPLC chromatograms. Facilities were used both in Lausanne and Cardiff.

3.1.5 Experimental Aims

In summary, the aims of this study were to:

- Identify the regions of the proteins PHB, E2F1, c-Jun, c-Fos, EbGP2 and EbVP35 that are likely to form coiled-coil motifs and in parallel assess and compare the outputs of the five open source coiled-coil prediction programmes reviewed in section 3.1.1.

- Use the information gained from the computational analysis to design peptide sequences that would likely form coiled-coil motifs.

- Synthesise the coiled-coil motif peptides by Fmoc-SPPS on a sufficiently large scale (> 30 mg) to permit further studies, including PEGylation, and for use as controls in biophysical and biological assays.

- Optimise a purification protocol using RP-HPLC for each of the coiled-coil motif peptides to obtain samples of high purity (≥ 95 %).

- Characterise each coiled-coil motif peptide with respect to correct mass using ESI-TOF MS.

Synthesis and RP-HPLC purification of the coiled-coil motif peptides was conducted exclusively at EPFL, Lausanne. Final characterisation, using analytical RP-HPLC and ESI-TOF MS was conducted in Cardiff.

3.2 Methods

The general method for determining peptide concentration using UV-spectroscopy was detailed in Chapter 2 (section 2.2.1.1); all other methods used in this study are described here.

3.2.1 Prediction of Coiled-Coil Motifs Using COILS, Paircoil, LearnCoil-VMF, MultiCoil and Paircoil2

Amino acid sequences for the proteins PHB, E2F-1, c-Fos, c-Jun, EbVP35 and EbGP2 were obtained from the Expert Protein Analysis System (ExPASy) proteomics server of the Swiss Institute of Bioinformatics (www.expasy.org). The amino acid sequences (in one-letter code) were subsequently copied to the input boxes for each of the coiled-coil prediction programs. Each program was operated in accordance with the instructions provided on their respective websites; a brief description of the parameters selected for each of the programs is given in **Table 3.3**. In all instances data was exported and processed using GraphPad Prism v.4.0. Servers were accessed between October 2005 and September 2008.

3.2.2 Synthesis of Peptides by Fmoc-SPPS

All peptides were synthesised by SPPS on Rink Amide AM resin (200-400 mesh, loading 0.71 mmol g^{-1}) using an Fmoc protection strategy with an automated peptide synthesiser (Chemspeed PSW 1100). A MS Excel worksheet was used to facilitate the calculation of reagents for each synthesis, a summary of the calculations is provided in **Tables 3.4** and **3.5** for a typical synthesis. Descriptions and sequences for each of the peptides synthesised are given in the results, since these were obtained with the aid of the computational analysis programmes described above.

3.2.2.1 Distillation of NMP

Peptide synthesis grade NMP was purified in advance by distillation of NMP over calcium hydride (CaH_2). NMP (1.5 L) was added to a glass distillation vessel (3 L) containing CaH_2 (c.a. 50 g). The vessel was placed into an insulated electric heating shell, and a magnetic stirring bar was added to aid agitation. The heating shell was then placed over a magnetic stirrer. A reflux column with a glass condensing tube that led to a glass collection vessel (2 L) was attached to the top of the distillation vessel. A vacuum was applied to the whole system (10 mBar), the stirrer turned on (400 rpm) and the heating shell set to level 1 (100 °C ± 0.5 °C) for 2 h 15 min. Freshly distilled NMP was stored over 4 Å molecular sieves prior to use.

Table 3.3 A summary of the usage parameters and URLs for each of the coiled-coil prediction programmes accessed.

Program Name	Usage Parameters	URL
COILS	Window width: All Matrix: MTIDK Input sequence Format: Plain text	http://www.ch.embnet.org/software/COILS_form.html
Paircoil	Probability cut-off: 0.5 (default)	http://groups.csail.mit.edu/cb/paircoil/cgi-bin/paircoil.cgi
LearnCoil-VMF	Used exclusively for the EbGP2 sequence as it is specific to viral fusion proteins.	http://groups.csail.mit.edu/cb/learncoil-vmf/cgi-bin/vmf.cgi
MultiCoil	Default program options were used.	http://groups.csail.mit.edu/cb/multicoil/cgi-bin/multicoil.cgi
Paircoil2	Minimum search window length: 28 Probability cut-off: 0.5	http://groups.csail.mit.edu/cb/paircoil2/paircoil2.html

Table 3.4 Preparation of amino acid solutions for the parallel synthesis of c-Jun, $FosW_C$ and $EbGP2_{609-630}$. Molecular weights given are those of the side-chain protected amino acids, "frequency" denotes the summed number of each amino acid for the three peptides synthesised in this example.

Amino acid	MW ($g\ mol^{-1}$)	Frequency	Mass to weigh (mg)	Vol. of NMP (mL)
Fmoc-Ala-OH	311.30	15	2984	19.17
Fmoc-Asn(Trt)-OH	596.68	5	1906	6.39
Fmoc-Asp(*t*BuO)-OH	411.45	3	789	3.83
Fmoc-Cys(Trt)-OH	585.68	2	748	2.56
Fmoc-Gln(Trt)-OH	610.68	11	4292	14.06
Fmoc-Glu(*t*BuO)-OH	425.48	14	3806	17.89
Fmoc-Gly-OH	297.31	3	570	3.83
Fmoc-Ile-OH	353.42	5	1129	6.39
Fmoc-Leu-OH	353.40	21	4742	26.84
Fmoc-Met-OH	371.50	1	237	1.28
Fmoc-Lys(Boc)-OH	468.53	7	2096	8.95
Fmoc-Phe-OH	387.40	3	743	3.83
Fmoc-Ser(tBu)-OH	383.40	4	980	5.11
Fmoc-Thr(But)-OH	397.48	7	1778	8.95
Fmoc-Tyr(But)-OH	459.54	3	881	3.83
Fmoc-Val-OH	339.39	2	434	2.56
Fmoc-Arg(Pbf)-OH	648.80	8	3317	10.22

Table 3.5 Preparation of the reaction solutions for the parallel synthesis of c-Jun, $FosW_C$ and $EbGP2_{609-630}$.

Solution	Concentration (M)	Mol. Eq.	Aliquot per AA (μL)	Volume to prepare (mL)
Coupling	0.5	3	639	150
Base	2	6	320	75
Deprotection	n/a	2	1598	450
Capping	0.5	3	1598	10

3.2.2.2 Preparation of Reactants and Automated Fmoc-SPPS Protocol

This method describes a typical synthesis of three peptides (c-Jun, $FosW_C$ and $EbGP2_{609-630}$). Fmoc-protected amino acids were weighed, dissolved in NMP (final concentration 0.5 M), and transferred to glass vials, then sealed with a teflon cap and placed in the peptide synthesiser (**Table 3.4**). Vessels containing the "deprotection solution" (450 mL) (piperidine 1 % v/v, DBU 2 % v/v and HOBt 10 % w/v in NMP), "base solution" (75 mL) (NMM 1.5 M, 6 mol. eq. in NMP), "coupling solution" (150 mL) (HOBt 0.25 M, 1.5 mol. eq., HCTU 0.5 M, 3 mol. eq. in NMP) and "capping solution" (acetic anhydride 0.5 M, 3 mol. eq., HOBt 1.5 % w/v and DIPEA 2.2 % v/v in NMP) were prepared (all in excess) and then placed in the designated wells in the peptide synthesiser (**Table 3.5**). Rink Amide AM resin (150 mg) was weighed into a glass reaction vessel and connected to the peptide synthesiser. This quantity of resin equated to a 0.1 mmol synthesis (resin loading = 0.71 mmol g^{-1}). The instrument was primed and the programmed method started. The mixing of the resin with the various reagents was facilitated by agitation (c.a. 500 rpm).

The first step of the automated programme involved swelling of the resin by the addition of an aliquot (1800 μL) of DCM to each reaction vessel for 20 min. Once complete, two washes with NMP (1800 μL) were conducted (2 min each). The sequential addition of each amino acid was conducted in accordance with the coupling protocol shown in **Table 3.6**. Once the amino acid chain was complete, the termination protocol (**Table 3.7**) was applied to acetylate the N-termini of the resin bound peptides, then wash in preparation for the deprotection step.

3.2.2.3 Resin Cleavage and Removal of Amino Acid Side-Chain Protecting Groups

The reaction vessels containing the peptide-loaded resin were removed from the peptide synthesiser and transferred to a fume cupboard. Peptides without cysteine residues were treated with a cleavage solution (3 mL) of TFA:TIPS:ddH_2O (95:2.5:2.5, v/v) for 3 hours to simultaneously cleave the peptide from the resin and remove all side-chain protecting groups. For peptides containing cysteine residues a cleavage solution (3 mL) containing EDT was used (TFA:TIPS:EDT:ddH_2O, 94:2:2:2, v/v). Agitation was provided to ensure mixing of the solution with the peptide-loaded resin. Once complete, the solution containing the cleaved peptides was transferred to a polypropylene centrifuge tube (50 mL) using a glass syringe fitted with a glass-fritted

Table 3.6 Amino acid coupling protocol for Fmoc-SPPS.

Programmed Step	Reagent/solution	Volume (μL)	Time (min)
Deprotection	Fmoc-deprotection solution	1598	5
Deprotection	Fmoc-deprotection solution	1598	5
Wash	NMP	1800	2
Wash	NMP	1800	2
Aliquot amino acid	Amino acid solution	639	-
Aliquot coupling	Coupling solution	639	-
Aliquot base	Coupling solution	320	-
Wait coupling			30
Wash NMP		1800	2
Aliquot amino acid	Amino acid solution	639	-
Aliquot coupling	Coupling solution	639	-
Aliquot base	Coupling solution	320	-
Wait coupling			25
Wash	NMP	1800	2
Wash	NMP	1800	2

Table 3.7 Termination (N-terminal acetylation) protocol for Fmoc-SPPS.

Programmed Step	Reagent/solution	Volume (μL)	Time (min)
Deprotection	Fmoc-deprotection solution	1598	5
Deprotection	Fmoc-deprotection solution	1598	5
Deprotection	Fmoc-deprotection solution	1598	5
Wash	NMP	1800	2
Capping	Capping solution	1598	15
Wash	NMP	1800	2
Wash	NMP	1850	2
Wash	DCM	1900	4
Wash	DCM	1950	4
Wash	DCM	2000	4
Final wash	DCM	2000	2

filter to exclude the insoluble resin. Crude purification and extraction from the TFA solution was achieved by precipitating the cleaved peptides in cold Et_2O (c.a. 40 mL) and centrifuging for 10 min at 4000 rpm. The supernatant was carefully removed and this process repeated a further two times. After the third precipitation, the peptides were suspended in ddH_2O and lyophilised.

3.2.3 Purification and Analysis of Peptides by RP-HPLC

Post-lyophilisation peptides were purified by preparative RP-HPLC. Peptide solutions were prepared by dissolving the crude peptide lyophilisate in buffer A (ddH_2O containing 0.1 % v/v TFA). Final concentration was typically 5 mg mL^{-1} depending upon solubility of each peptide sample. A linear AB gradient (A = ddH_2O, B = acetonitrile (ACN), both containing 0.1 % v/v TFA) with a flow rate of 20 mL min^{-1} over 25 min and UV absorbance detectors set to 214 and 274 nm was used for the purification of all crude peptide samples. To optimise the gradient for each peptide sample, aliquots (1 mL) of crude peptide in buffer A were injected and the chromatograms analysed using MassLynx v4.0 software. Typically, five runs were required to optimise the gradient conditions; the optimal gradients used for the purification of each peptide are given in the results and discussion (section 3.3.2). Once optimised, larger volumes (5-8 mL) of sample solution were injected and the eluate collected for mass spectral analysis by ESI-TOF MS (section 3.2.4). ACN was evaporated from the eluate under pressure (Büchi Rotavapor®) and the purified samples were lyophilised.

Peptide purity was determined by analytical RP-HPLC using the same protocol described above. Chromatograms were obtained using a gradient of 5-95 % ACN over 25 min, with a flow rate of 1 mL min^{-1} and a sample volume of 50 μL (1 mg mL^{-1}). Data were processed using PowerChrom software v2.0.7 and exported as .xls files.

3.2.4 Characterisation of Peptides by ESI-TOF MS

Characterisation of peptides was performed in two ways. Firstly, peak identification was carried out in Lausanne using an SSQ 710C mass spectrometer in parallel to preparative RP-HPLC experiments to ensure that the eluate corresponding to the full-length coiled-coil motif peptide was collected. A sample (0.5 mL) of eluate was collected from the RP-HPLC and an aliquot (50 μL) injected into the spectrometer. It

should be noted that the solvent was the mobile phase in which the peak eluted from the RP-HPLC system (a mixture of ddH_2O and ACN containing 0.1 % v/v TFA). All spectra were acquired in the positive ion mode in the range of 400 - 2000 m/z; the instrument was pre-calibrated with myoglobin. The electrospray conditions were as follows: capillary voltage, 4.5 kV, source temperature, 200 °C and ESI nebulisation and drying gases were nitrogen. All data were acquired and processed using ICIS software. Final characterisation was performed in Cardiff using a Waters Q-TOF Micro mass spectrometer. Samples were prepared at a concentration of 1 mg mL^{-1} of which an aliquot (20 µL) was injected into the spectrometer by means of an autosampler. All experiments were performed in positive ion mode under the same conditions specified above. All spectra were processed using MassLynx v4.0 software and exported as .xls files. Data are shown as m/z (mass/charge) versus relative abundance (%). z-values were confirmed by measuring the peak cluster ratios. Data are shown as either deconvoluted or raw spectra, the latter was preferable, however earlier data was only collected in the form of deconvoluted spectra.

3.2.5 TFA/HCl Buffer Exchange

Peptides containing basic residues (histidine, lysine and arginine) were converted from the TFA salt to the HCl salt. This method was adapted from that described by Cornish *et al*, (1999). Purified coiled-coil motif peptides (10 µmol) were dissolved in hydrochloric acid (3 mM, 50 µL) and mixed for 1 h at room temperature, after which they were lyophilised. Peptides were then either frozen at - 20 °C for long term storage or diluted to a concentration of 2 mg mL^{-1} and stored in aliquots (1 mL) at - 80 °C for up to 28 days.

3.3 Results & Discussion

This section is divided into two parts, the first (section 3.3.1) describes the identification of the coiled-coil domains in the target proteins using the coiled-coil prediction programmes summarised in **Table 3.3**. The second (3.3.2) discusses the design and/or selection of suitable peptide sequences alongside the synthesis, purification and characterisation of each of the coiled-coil motif peptides by Fmoc-SPPS.

3.3.1 Prediction of Coiled-Coil Motifs in the Proteins E2F1, PHB, EbVP35 and EbGP2 by computational analysis.

For the target protein E2F1, all four programmes predicted the existence of a coiled-coil motif in the same region, albeit with differing degrees of probability (**Figure 3.4**). Assuming a 0.5 probability cut-off, all scanning windows using the COILS programme predicted a coiled-coil motif between residues 201 and 226, inclusive. The probability scores obtained with Paircoil, Multicoil and Paircoil2 are much lower however all agree on a similar region, ranging between residues 199 and 240. None of the programmes predicted the existence of a coiled-coil motif between residues 304 and 357 i.e. the domain that Wang *et al*, (1999) identified as the binding site for PHB.

Similarly, for PHB all four programmes predicted the existence of a coiled-coil motif in the same region (**Figure 3.5**). Again, COILS gave the highest score of the four programmes with a coiled-coil motif predicted between residues 177 and 216 using either a 21 or 28-residue window. Use of the 14-residue window skewed the predictive output towards the lower numbered residues in the same frame, with the highest prediction between residues 184 and 197. It should be noted that Lupas *et al*, (1991) recommend that the 14-residue window should only be used in the analysis of known coiled-coil domains, not for speculative predictions. Paircoil predicted a coiled-coil motif with a high probability score (> 0.8) between residues 181 and 210, while the programmes Multicoil and Paircoil2 predicted a coiled-coil motif in a similar region albeit with lower probability scores (< 0.5).

As seen for the previous two proteins (E2F1 and PHB) COILS gave the highest probability score for the existence of a coiled-coil motif in Zaire EbVP35 (**Figure 3.6**). Predictions varied in probability score depending upon the size of window used. Use of 14, 21 and 28-residue windows predicted a coiled-coil motif between residues 103-119, 96-116, and 88-116, respectively. This was slightly different to the 82-118-residue region quoted by Reid *et al*, (2005). A similar pattern to the COILS prediction was seen in the predictive outputs of Paircoil, Multicoil and Paircoil2, with all programmes agreeing upon the same region as COILS but with low probability scores of 0.28, 0.11 and 0.42, respectively.

The proteins c-Jun, c-Fos and EbGP2 have been shown in previous studies using X-Ray crystallography to contain coiled-coil motifs (Chapter 1, section 1.5). However, using the EbGP2 sequence as an example, a comparison of the predictive outputs for

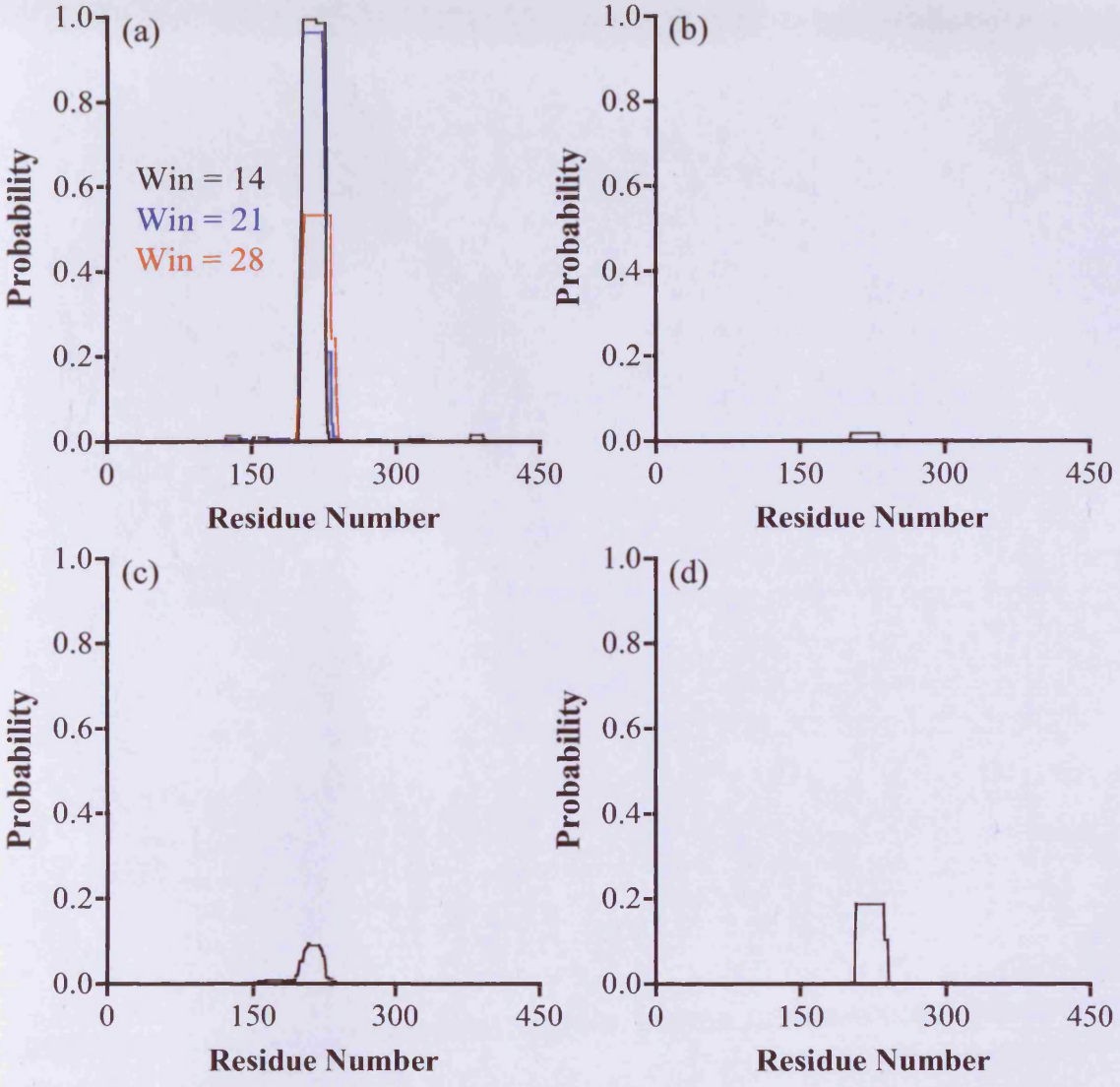

Figure 3.4 Coiled-coil prediction for the 437-residue target protein E2F1. Panels a-d show a comparison of the predictive outputs for each of the four programmes (a) COILS, (b) Paircoil, (c) MultiCoil and (d) Paircoil2, respectively, using the human E2F1 sequence (Expasy primary accession no. Q01094).

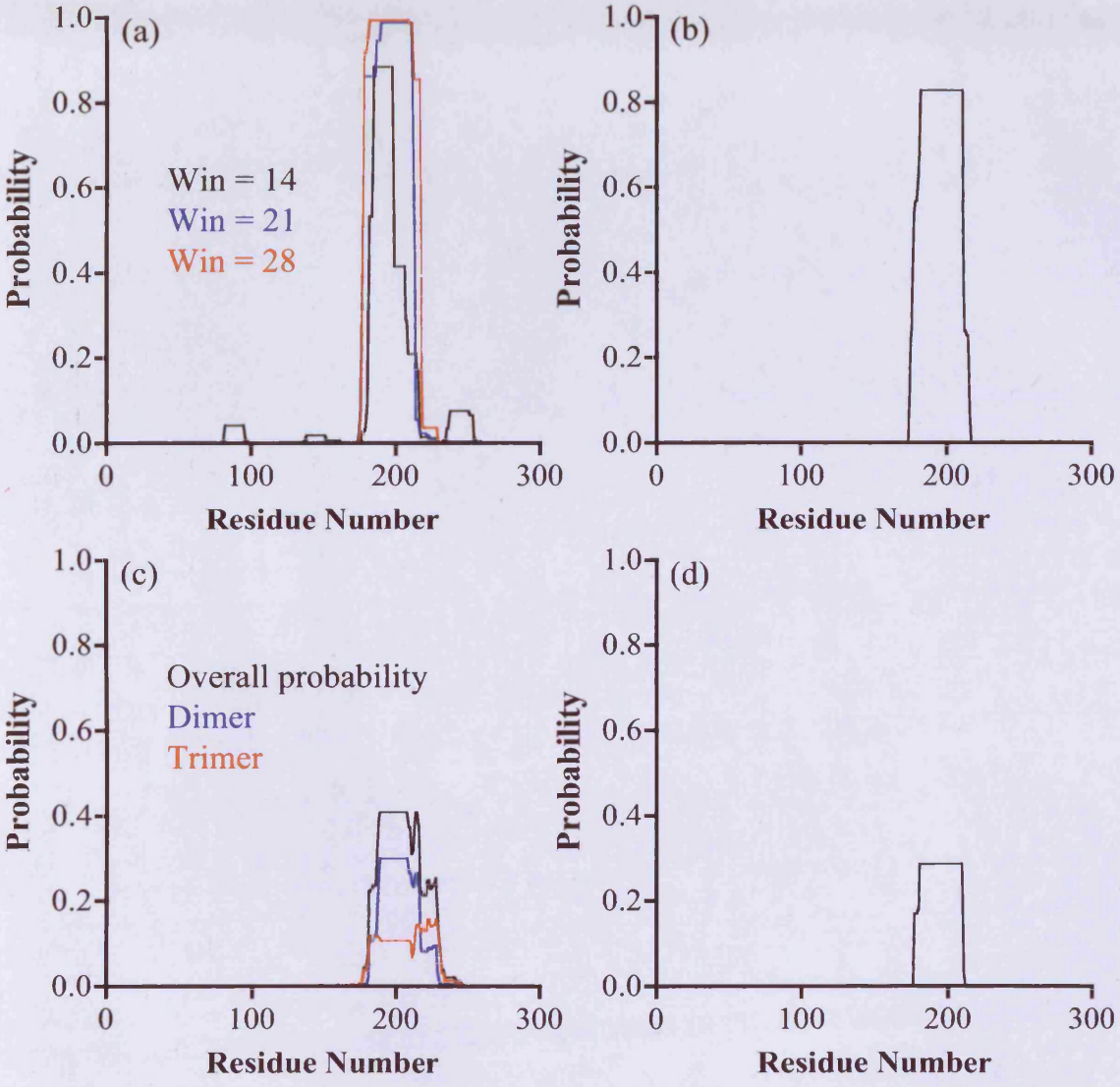

Figure 3.5 Coiled-coil prediction for the 272-residue protein PHB. Panels a-d show a comparison of the predictive outputs for each of the four programmes (a) COILS, (b) Paircoil, (c) MultiCoil and (d) Paircoil2, respectively, using the human PHB sequence (Expasy primary accession no. P35232).

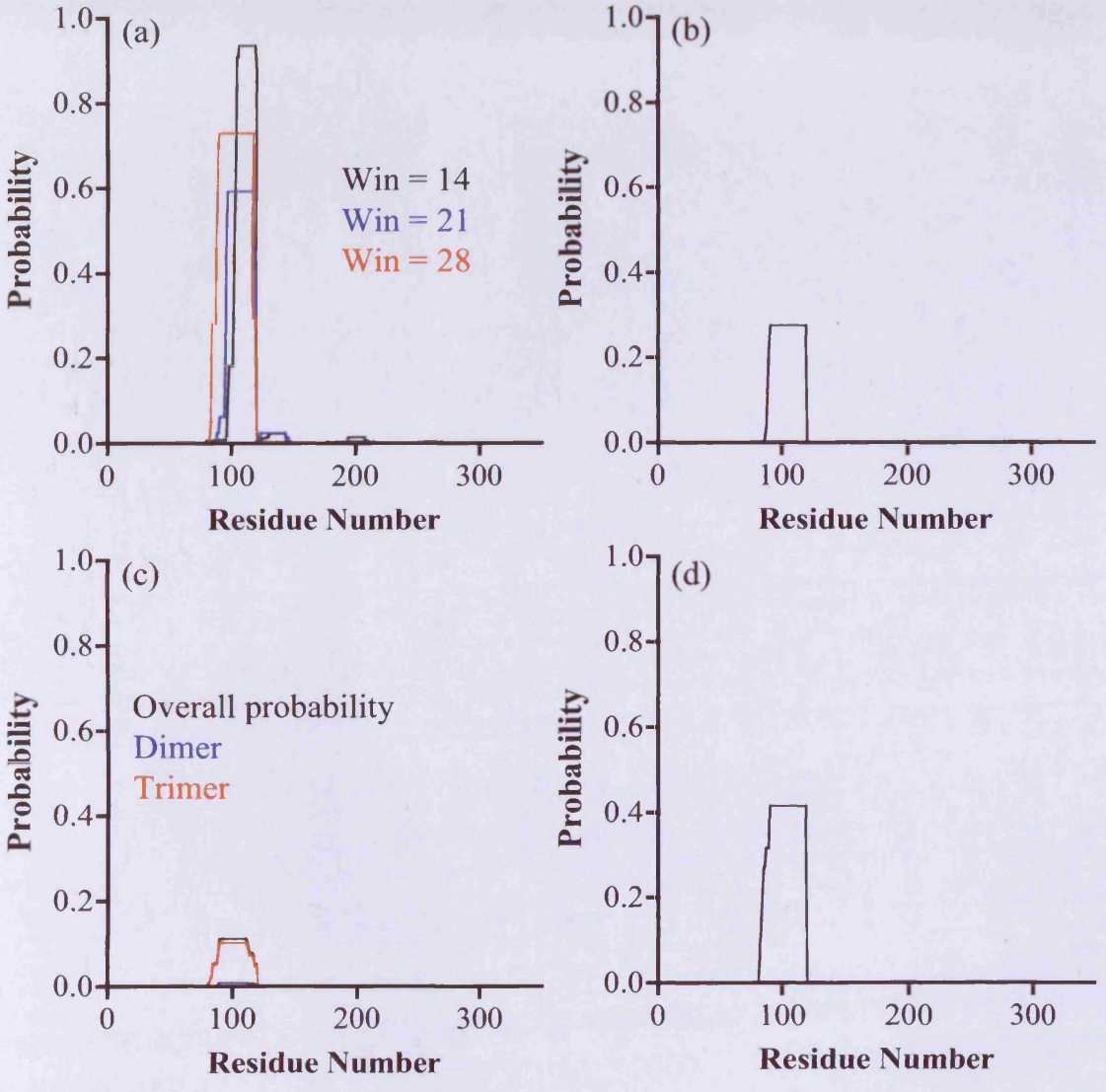

Figure 3.6 Coiled-coil prediction for the 340-residue protein EbVP35. Panels a-d show a comparison of the predictive outputs for each of the four programmes (a) COILS, (b) Paircoil, (c) MultiCoil and (d) Paircoil2, respectively, using the Zaire Ebola VP35 sequence (Expasy primary accession no. Q05127).

each of the five programmes was conducted to illustrate the marked differences seen for each programme (**Figure 3.7**). Of the five programmes used to predict of coiled-coil motifs in Zaire EbGP2, two (Paircoil and Paircoil2) gave a zero probability score for the entire sequence. COILS predicted coiled-coil motifs in two regions using a 14-residue window, the first was between residues 291 and 304 and had a high probability score (> 0.8), the second, between residues 556 and 570 had a much lower score (0.1). Scanning the sequence using the larger windows (21 or 28) failed to predict any coiled-coil motif regions. The programme LearnCoil-VMF, developed specifically for viral fusion proteins predicted (probability > 0.97) that residues 555 to 596 would form a coiled-coil motif. A similar prediction was made by MultiCoil but with a much lower probability score (0.043).

In summary, consensus sequences were identified as "likely to contain" coiled-coil motifs using the predictions given by computational analysis in conjunction with published data, detailed descriptions are provided in the following section.

3.3.2 Design and Synthesis of Coiled-Coil Motif Peptides

For ease of reference, the sequences for all of the peptides designed and subsequently synthesised by Fmoc-SPPS in this study are summarised in **Table 3.8**.

3.3.2.1 Design and Synthesis of PHB and E2F1 Derived Peptides

Design of peptides corresponding to the binding domain of the E2F1 protein and the putative coiled-coil domain of PHB utilised information gleaned from two studies by Wang *et al*, (1999 & 2002) and a later study by Joshi *et al*, (2003). In the first study, Wang *et al*, (1999) demonstrated that a region in the PHB protein between residues 185 and 214 was essential for binding to E2F1 and mediating the tumour suppressor activity of PHB. The second study identified a 54-residue region within the E2F1 protein with which PHB hybridised (Wang *et al*, 2002). This region was between residues 304 and 357, interestingly the computational analyses shown in **Figure 3.4** failed to predict a coiled-coil in this region. The study by Joshi *et al*, (2003) used a computational analysis (Paircoil) to assert that the PHB domain which hybridised with E2F1 formed a coiled-coil domain, however provided no further biophysical evidence with either CD or NMR spectroscopy. At this point it is important to note that neither protein has been crystallised in the regions of interest here. Two possibilities exist, first that PHB hybridises with E2F1 *via* the formation of a coiled-coil as depicted in **Figure 3.8a**.

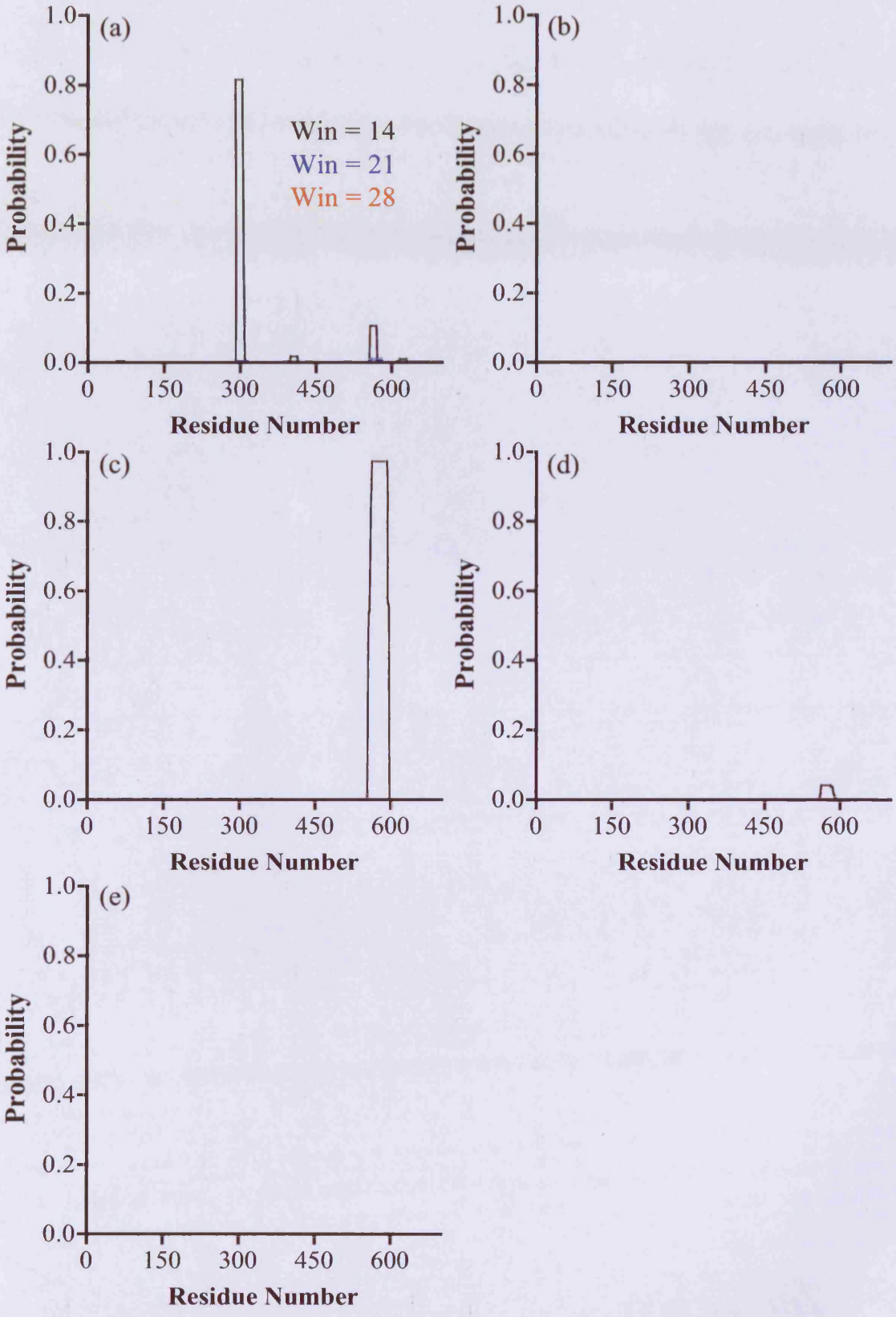

Figure 3.7 Coiled-coil prediction for the 676-residue protein EbGP2. Panels a-d show a comparison of the predictive outputs for each of the five programmes (a) COILS, (b) Paircoil, (c) LearnCoil-VMF (d) Multicoil and (e) Paircoil2, respectively, using the Zaire Ebola GP2 sequence (Expasy primary accession no. Q05320).

Table 3.8 Summary of amino acid sequences for the peptides synthesised in this study.

Peptide	Sequence abcdefgabcdefgabcdefgabcdefgabcdef	Length (residues)	Molecular Weight[#] (g mol^{-1})
E2F1 and PHB derived peptides			
$Phb_{185-214}$	**A**K**Q**V**A**Q**Q**E**A**E**R**A**R**F**V**V**E**K**A**E**Q**Q**K**K**A**A**I**I**S**A**	30	3367.83
$Phb_{Y185-214}$	**Y**A**K**Q**V**A**Q**Q**E**A**E**R**A**R**F**V**V**E**K**A**E**Q**Q**K**K**A**A**I**I**S**A**	31	3531.01
$Phb_{CY185-214}$	C**Y**A**K**Q**V**A**Q**Q**E**A**E**R**A**R**F**V**V**E**K**A**E**Q**Q**K**K**A**A**I**I**S**A**	32	3634.15
E2F1a[†]	**Y**P**G**K**T**P**S**Q**E**V**T**S**E**E**E**N**R**A**	18	2063.15
E2F1b[†]	**Y**L**T**T**D**P**S**Q**S**L**L**S**L**E**Q**E**G**G**	18	1979.11
c-Jun and c-Fos derived peptides			
c-Jun[†]	**A**S**I**A**R**L**E**E**K**V**K**T**L**K**A**Q**N**Y**E**L**A**S**T**A**N**M**L**R**E**Q**V**A**Q**L**G**A**	36	3987.57
$FosW_C$	C**A**S**L**D**E**L**Q**A**E**I**E**Q**L**E**E**R**N**Y**A**L**R**K**E**I**E**D**L**Q**K**Q**L**E**K**L**G**A**	37	4358.87

[†] Peptides that represent target domains for use in *in-vitro* binding assays.

[#] Theoretical molecular weight based upon the average isotopic abundance of naturally occurring elements.

N.B. Apolar residues in positions "a" and "d" are shown in bold type font.

Table 3.8 Summary of amino acid sequences for the peptides synthesised in this study.

Peptide	Sequence	Length	Molecular Weight[#]
	abcdefgabcdefgabcdefgabcdefgabcdefgab	(residues)	(g mol^{-1})
EbVP35 derived peptides			
$EbVP35_{82\text{-}119}$	**SFEEVVQTLASLATVVQQQTIASESLEQRITSLENGLK**	38	4189.66
$EbVP35_{CY88\text{-}119}$	**CYQTLASLATVVQQQTIASESLEQRITSLENGLK**	34	3697.18
EbGP2 derived peptides			
	abcdefg abcdefgabcdefgabcdefgabcdef		
$EbGP2_{609\text{-}630}$*	**CIEPHDWTKNITDKIDQIIHDF**	22	2723.04
$EbGP2_{CY557\text{-}589}$	**CYGLRQLANETTQALQLFLRATTELRTFSILNRKA**	35	4082.72
$EbGP2_{CY557\text{-}595}$	**CYGLRQLANETTQALQLFLRATTELRTFSILNRKAIDFLLQ**	41	4812.59
$EbGP2_{CY566\text{-}589}$	**CYTQALQLFLRATTELRTFSILNRKA**	26	3099.63

[#] Theoretical molecular weight based upon the average isotopic abundance of naturally occurring elements.

N.B. Apolar residues in positions "a" and "d" are shown in bold type font (*heptad positions are not assigned for peptide $EbGP2_{609\text{-}630}$ as is an α-helix, not strictly a coiled-coil motif).

(a)

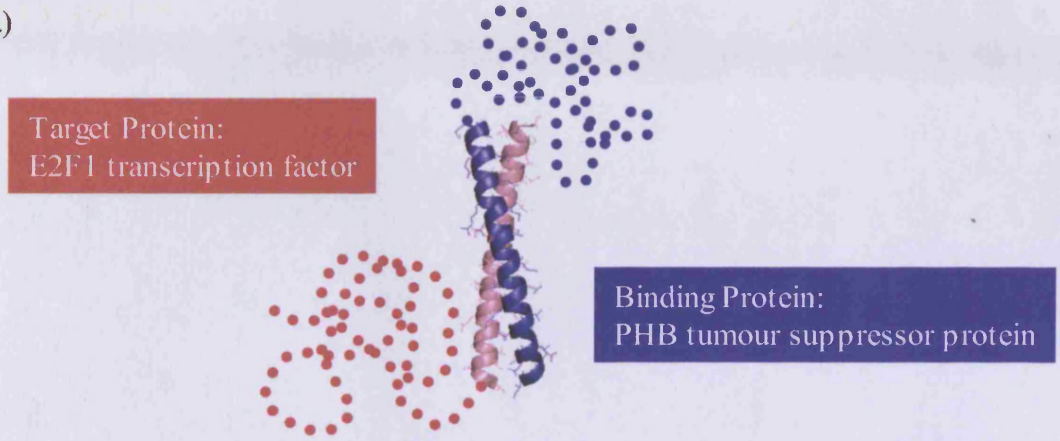

The two proteins are known to interact *via* residues 304-357 (Wang *et al*, 2002) in the E2F1 protein and residues 185-214 (Wang *et al*, 1999) in the PHB protein. However whether the interaction is *via* the formation of a coiled-coil is not known.

(b) Design of peptides to model the E2F1 binding domain

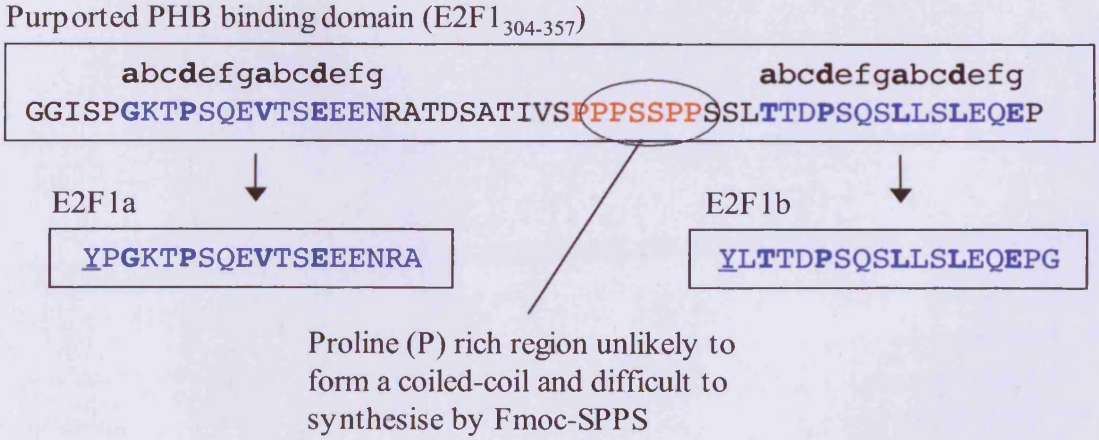

Figure 3.8 Design of E2F1 and PHB-derived peptides for synthesis by Fmoc-SPPS. Panel (a) shows an illustration of possible E2F1:PHB hybridisation. Panel (b) shows the sequence of the E2F1 binding domain and the peptides E2F1a and E2F1b chosen for synthesis. Underlined residues indicate tyrosine tags.

Second, that the two proteins hybridise *via* an alternative 3D structure and it is co-incidental that the PHB has a predicted coiled-coil domain in the same region. Indeed, Joshi *et al*, (2003) have shown that the PHB coiled-coil domain may mediate homo-dimerisation, thus one could speculate that the coiled-coil domain is responsible for holding PHB in an inactive dimeric state that cannot bind to E2F1. Nonetheless in an effort to deepen the understanding of the E2F1 : PHB interaction peptides were designed for synthesis by Fmoc-SPPS. The design and synthesis of peptides in this section can be divided into two sub-sections, first synthesis of peptides corresponding to the coiled-coil domain of PHB (to be used as "therapeutic" coiled-coil motifs), and second, synthesis of "target" peptides to represent the binding domain in the target protein E2F1.

Synthesis of "Therapeutic" Peptides Derived from the PHB Coiled-Coil Domain: $Phb_{185-214}$, $Phb_{Y185-214}$ and $Phb_{CY185-214}$

As the whole region purported necessary for hybridisation with E2F1 (Wang *et al*, 1999) was 30-residues in length it was possible to design the complete region for synthesis. The peptide, $Phb_{185-214}$ was shorter than the 41-residue peptide described by Joshi *et al*, (2003), however, it was not seen necessary to include the extra residues and make the synthesis more challenging by virtue of it being a longer peptide. Moreover, upon closer inspection Joshi *et al*, (2003) do not actually give the exact peptide sequence that they used in the study, rather they note that a 41-residue peptide was derived from the 177-217 region.

A single batch (0.1 mmol) of the peptide $Phb_{185-214}$ was synthesised. The crude peptide was visualised upon precipitation in cold diethyl ether, found to be soluble in ddH_2O and lyophilised. When dry, the crude yield was 330 mg (92 %) and the peptide had the appearance of a white, "fluffy" powder that was easily soluble. As the only aromatic residue in the peptide $Phb_{185-214}$ was phenylalanine the second detector on the preparative RP-HPLC was set to 257 nm. Multiple peaks were observed in both chromatograms (**Figure 3.9a**), however subsequent analysis by ESI-TOF MS confirmed that peak 1 matched the theoretical molecular weight of full-length $Phb_{185-214}$ peptide (data not shown). A gradient of 25-35 % ACN was found to be optimal for purification by RP-HPLC. Analysis using the same RP-HPLC set-up showed a single predominant peak (**Figure 3.9b**). Analysis of the purified peptide by ESI-TOF MS confirmed the

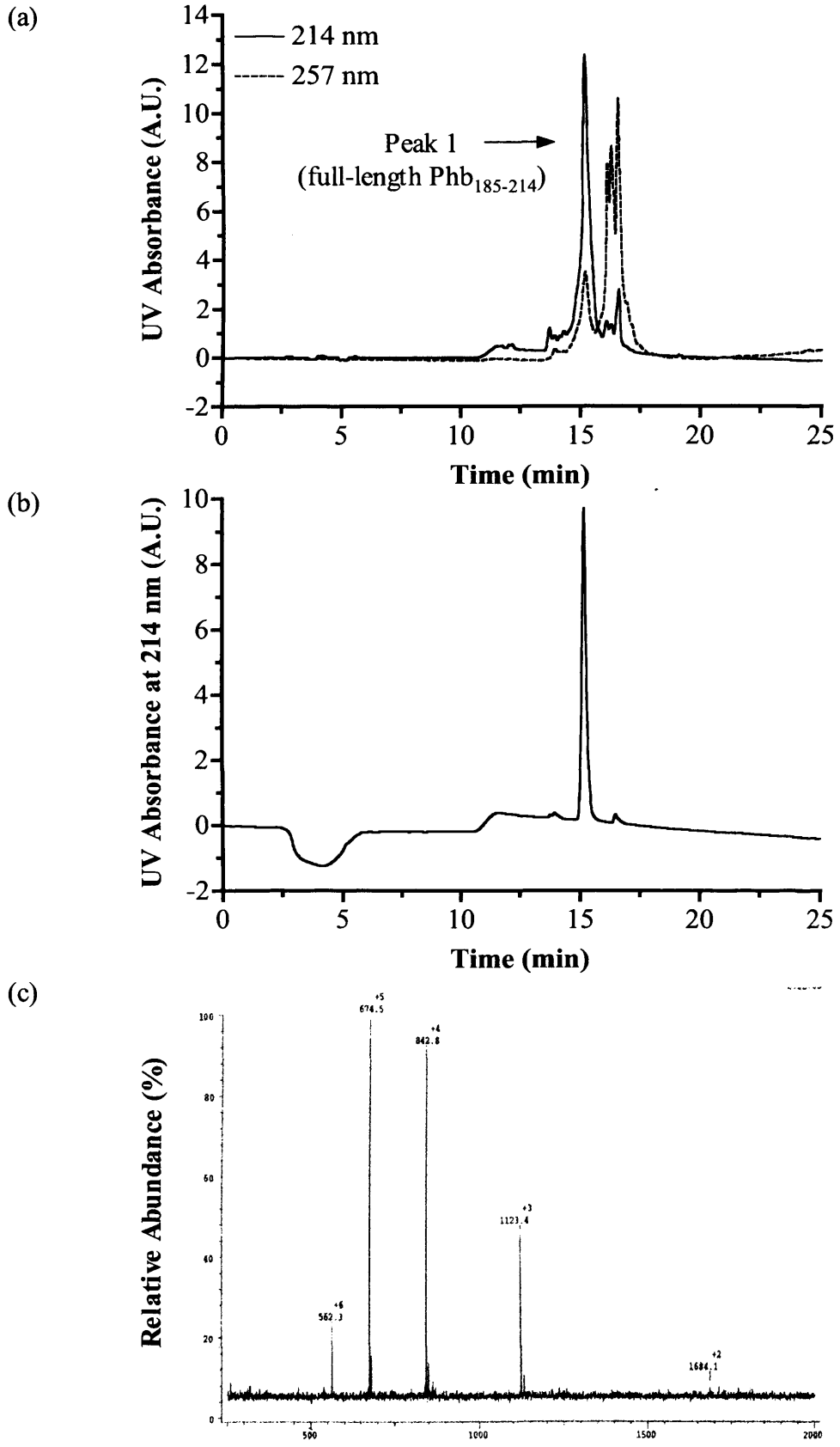

Figure 3.9 Purification and characterisation of $Phb_{185-214}$. Panels (a) and (b) show RP-HPLC chromatograms of crude peptide and pure $Phb_{185-214}$ (post-purification), respectively. Panel (c) ESI-TOF MS spectrum of pure $Phb_{185-214}$.

theoretical molecular weight of 3367.83 g mol^{-1} expected for full-length $Phb_{185-214}$ peptide (**Figure 3.9c**). Purity was > 95 % and the final yield was 75 mg (21 %).

It was originally anticipated that it would be possible to use the UV-chromophore of the phenylalanine residue to determine the concentration of the peptide using UV spectroscopy (section 2.2.1.1). However, the weak intensity of the UV absorbance at 257 nm provided by the single phenylalanine residue relative to that of the 29-peptide bonds which absorb at 214 nm made it impossible to make an accurate determination of concentration (data not shown). Thus, a tyrosine residue was introduced at the N-terminus of the peptide sequence yielding $Phb_{Y185-214}$. The crude peptide was freely soluble in ddH_2O and when dry the yield determined to be 345 mg (92 %). Its physical appearance was indistinguishable from $Phb_{185-214}$. Only one well-resolved peak was observed in the overlaid RP-HPLC chromatograms (**Figure 3.10a**). However the irregular baseline (in particular at 214 nm) indicated the presence of numerous truncated peptides. ESI-TOF MS confirmed that the predominant peak represented full-length $Phb_{Y185-214}$ (data not shown). The optimal purification gradient was found to be 26-31 % ACN. The single peak observed in the analytical RP-HPLC chromatogram demonstrated that the peptide was > 95 % pure (**Figure 3.10b**). The later elution time compared with that seen for $Phb_{185-214}$ was likely due to the hydrophobic nature of the tyrosine residue. Deconvolution of the three peaks seen in the ESI-TOF mass spectrum confirmed that the purified sample was of the correct theoretical molecular weight (3531.01 g mol^{-1}) (**Figure 3.10c**). The final yield was 82 mg (22 %).

The third PHB derived peptide, $Phb_{CY185-214}$ was designed with the addition of a cysteine residue at the N-terminus to facilitate thiol directed PEGylation (Chapter 4). A successful synthesis was conducted on the same scale as the previous PHB derived peptides and in physical appearance the peptide $Phb_{CY185-214}$ was indistinguishable. The crude yield was determined to be 375 mg (97 %). Upon analysis by RP-HPLC two peaks were identified with retention times of 12.72 and 13.02 min, respectively (**Figure 3.11a**). These were present in both chromatograms (214 and 274 nm), however the chromatogram obtained from the 214 nm detector showed the presence of a many other contaminants, likely truncated peptides. ESI-TOF MS confirmed that peak 1 represented full-length $Phb_{CY185-214}$ (data not shown). The optimal purification gradient was found to be 27-37 % ACN. Post-purification a single peak was observed in the analytical RP-HPLC chromatogram and demonstrated that the peptide was > 95 % pure

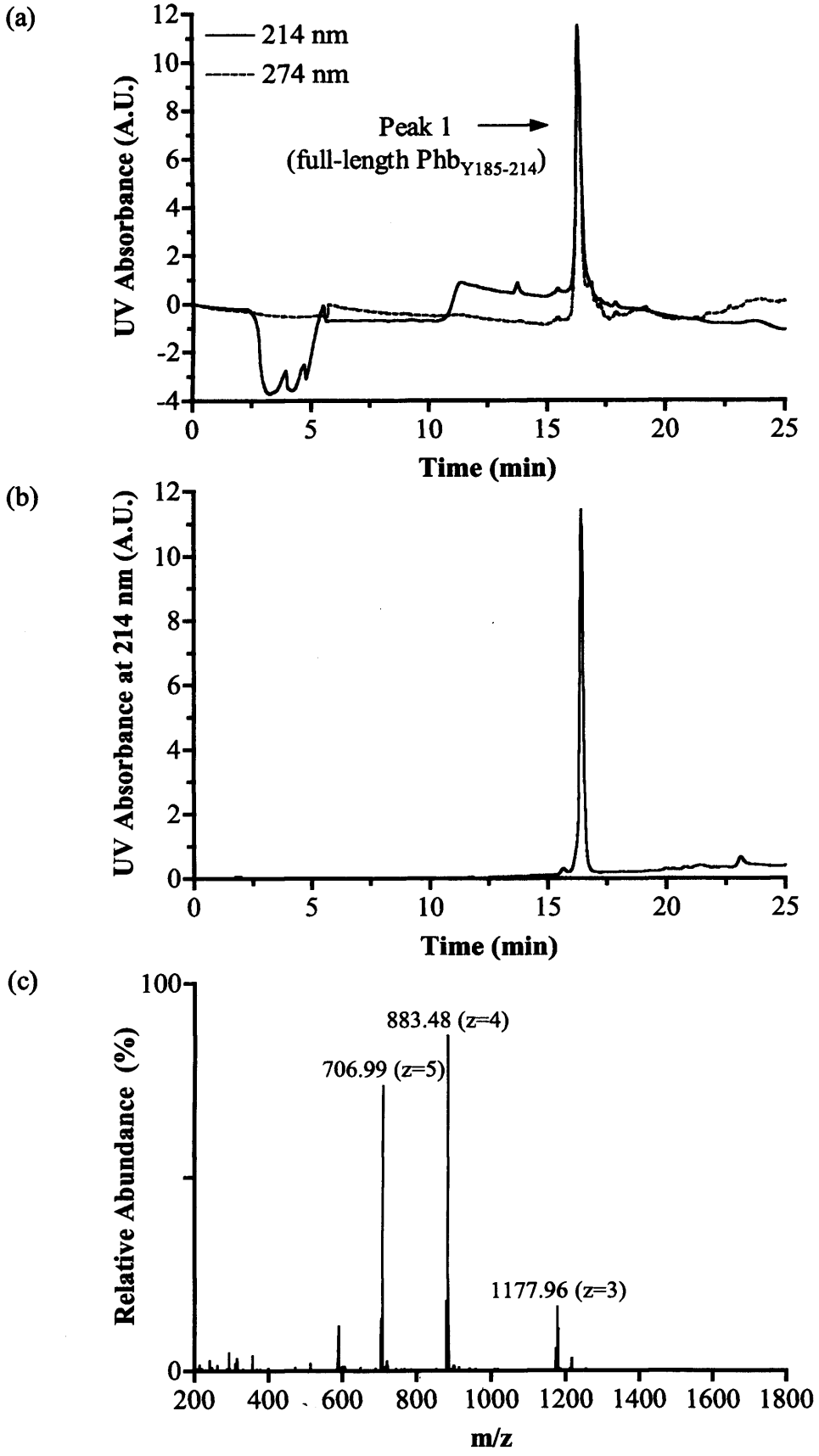

Figure 3.10 Purification and characterisation of Phb$_{Y185-214}$. Panels (a) and (b) show RP-HPLC chromatograms of crude peptide and pure Phb$_{Y185-214}$ (post-purification), respectively. Panel (c) ESI-TOF MS spectrum of pure Phb$_{Y185-214}$.

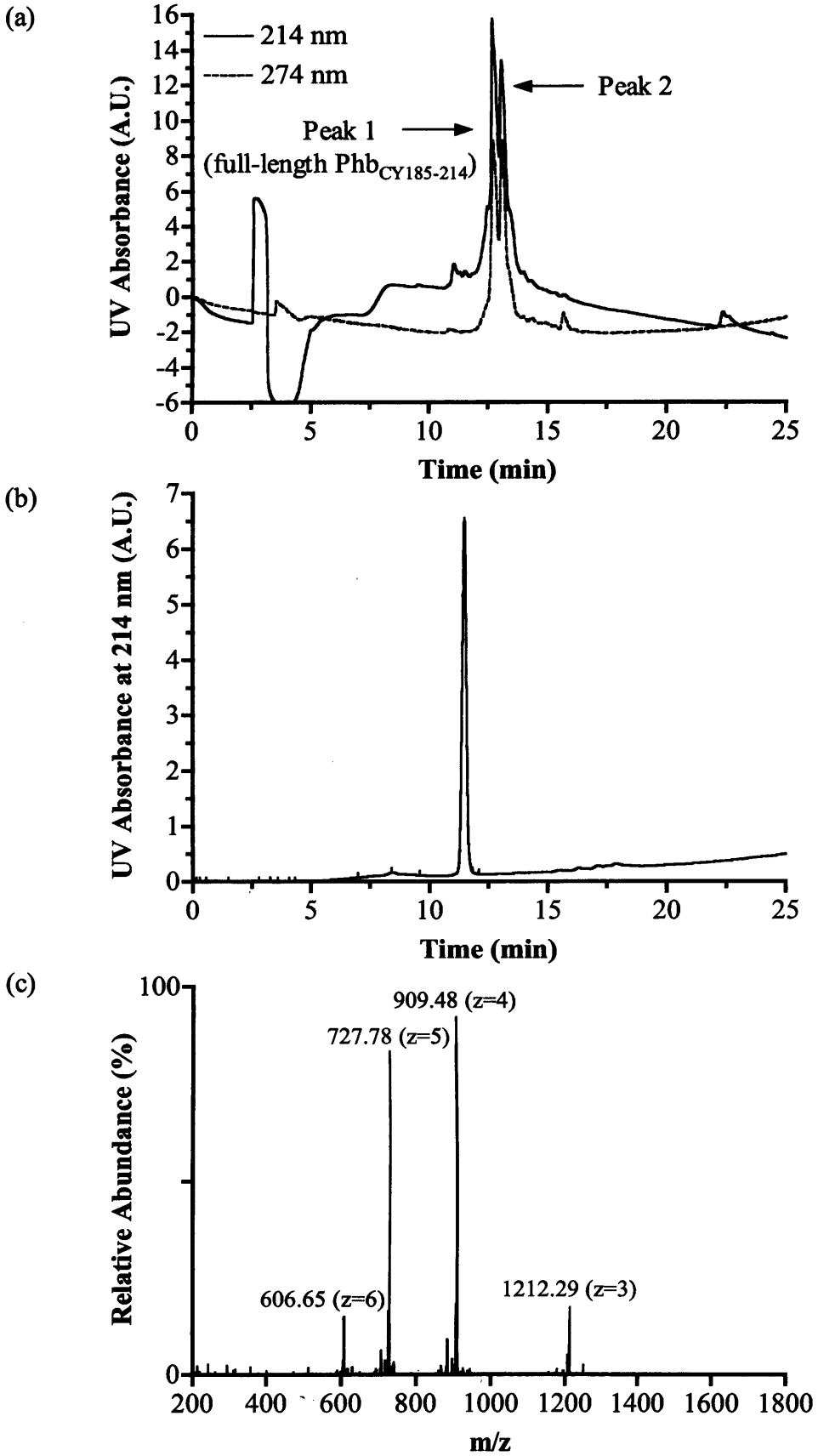

Figure 3.11 Purification and characterisation of Phb$_{CY185-214}$. Panels (a) and (b) show RP-HPLC chromatograms of crude peptide and pure Phb$_{CY185-214}$ (post-purification), respectively. Panel (c) ESI-TOF MS spectrum of pure Phb$_{CY185-214}$.

(**Figure 3.11b**). The rising baseline, although not seen before is fairly typical of a ddH_2O:ACN gradient, since ACN often has a higher UV absorbance than ddH_2O at 214 nm. Deconvolution of the four peaks seen in the ESI-TOF mass spectrum confirmed that the purified sample was of the correct theoretical molecular weight (3634.15 g mol^{-1}) (**Figure 3.11c**). The final yield was 35 mg (9 %).

Synthesis of "Target" Peptides Derived from the E2F1 Binding Domain: E2F1a and E2F1b

The peptide sequence for the E2F1 binding domain ($E2F1_{304-357}$) is shown in **Figure 3.8b**. Whilst COILS failed to predict a coiled-coil domain in this region, the programme did assign possible heptad repeat sequences in two sub-regions with each comprising two heptads. These formed the basis of the peptides E2F1a and E2F1b selected for synthesis. Tyrosine residues were added to the N-termini of both sequences to facilitate analysis as described in section 3.1.3.1. Two glycine residues were added to the C-terminus of the E2F1b peptide sequence since proline easily cyclizes to form a diketopiperazine if it is first residue coupled to the solid phase resin (Chan & White, 2000). Ideally it would have been possible to synthesise this entire region by Fmoc-SPPS, however at 54-residues it was considered too long; moreover the sequence contained a 7-residue region which contained five proline residues. Such a sequence would be very challenging to synthesise (Klok *et al*, personal communication). Furthermore it is well documented that proline residues can disrupt coiled-coil formation (Chang *et al*, 1999). Indeed, it was of concern that the occurrence of proline residues within the heptad repeat sequences might indicate that the COILS predictions were incorrect. However the only way to answer such speculations was to synthesise the peptides.

The first attempt at synthesising peptides E2F1a and E2F1b yielded peptides that did not correspond to their theoretical molecular weights when analysed by ESI-TOF MS (data not shown). A second attempt at the synthesis of each peptide failed due to an unknown error in the programming of the automated peptide synthesiser. A third attempt at the synthesis was successfully conducted on a smaller scale (0.05 mmol).

E2F1a was soluble in ddH_2O with the aid of vigorous agitation, post-lyophilisation, the crude yield was 120 mg (82 %). Analysis of the crude peptide showed the presence of multiple peaks in both chromatograms (**Figure 3.12a**). The first peak in the second cluster was identified as full-length E2F1a using ESI-TOF MS (data

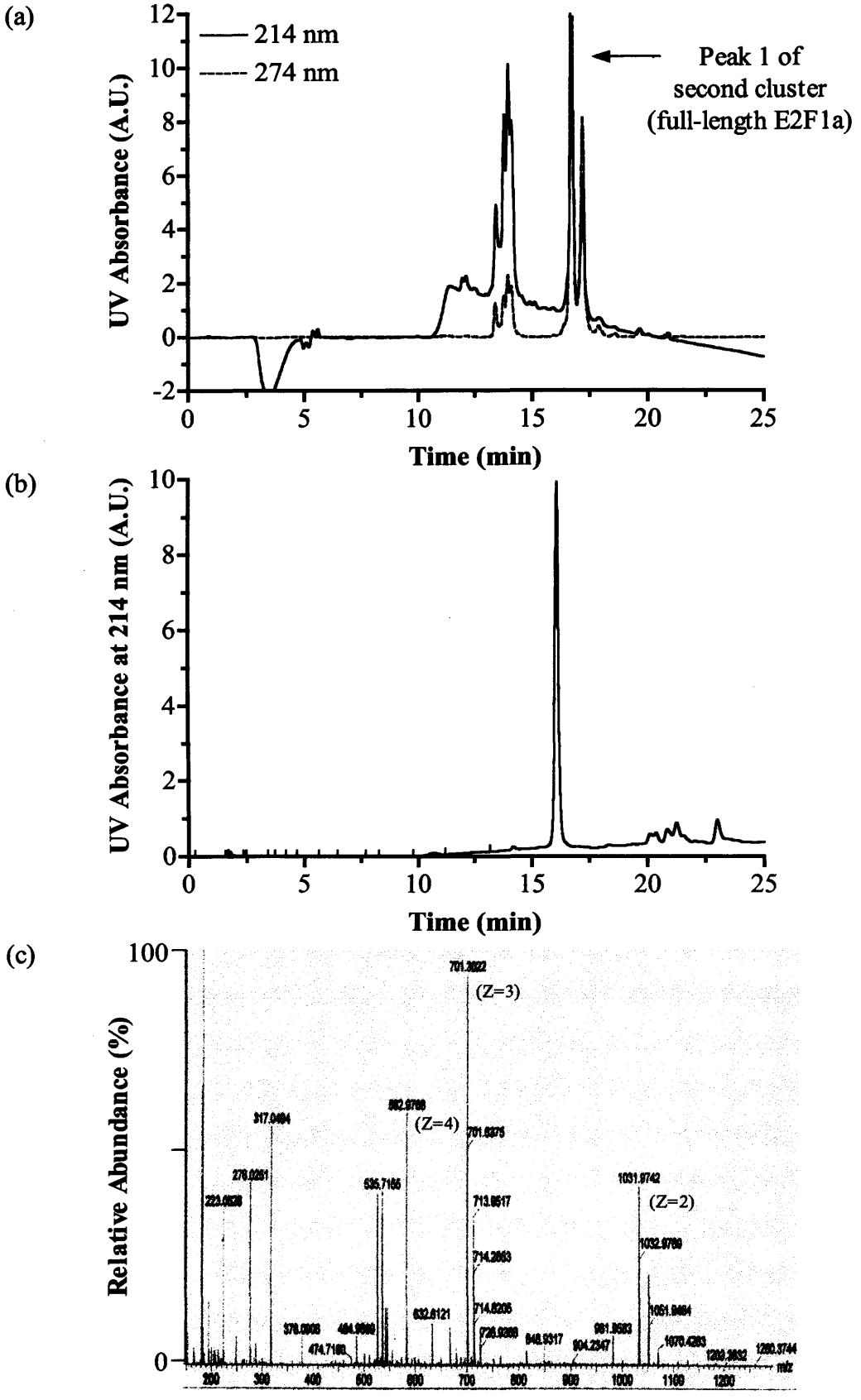

Figure 3.12 Purification and characterisation of E2F1a. Panels (a) and (b) show RP-HPLC chromatograms of crude peptide and pure E2F1a (post-purification), respectively. Panel (c) ESI-TOF MS spectrum of pure E2F1a.

not shown). An isocratic gradient of 18 % ACN was found to be optimal for purification. Purity was determined to be > 95 % as judged by the analytical RP-HPLC chromatogram (**Figure 3.12b**). Interestingly, a number of smaller peaks eluted between 20 and 25 min that were not seen in the original RP-HPLC chromatograms. Deconvolution of the three main peaks seen in the ESI-TOF mass spectrum (annotated z = 2, 3 and 4) confirmed that the purified sample was of the correct theoretical molecular weight (2063.15 g mol^{-1}) (**Figure 3.12c**). The final yield was 20 mg (14 %).

E2F1b was only soluble in ddH_2O with the aid of vigorous agitation; post-lyophilisation the crude yield was 115 mg (82 %). When the sample was prepared in ddH_2O containing 0.1 % TFA for injection into the RP-HPLC sediment was observed to form, indicating that some of the crude peptide was insoluble in the injection buffer. In this instance the crude peptide was of higher purity than seen for E2F1a as judged by the singular peak in the RP-HPLC chromatogram (**Figure 3.13a**). The raised baseline (between 8 and 13 min) seen in the chromatogram for the 214 nm detector suggested the presence of truncated peptides that lacked the N-terminal tyrosine residue of full-length E2F1b. The singular peak was identified as full-length E2F1b using ESI-TOF MS (data not shown). An 18-30 % ACN gradient was found to be optimal for purification. Purity was determined to be > 95 % as judged by the analytical RP-HPLC chromatogram (**Figure 3.13b**). Deconvolution of the single peak seen in the ESI-TOF mass spectrum confirmed that the purified sample was of the correct theoretical molecular weight (1979.11 g mol^{-1}) (**Figure 3.13c**). The final yield was 11 mg (8 %).

3.3.2.2 Design/Selection and Synthesis of c-Jun and c-Fos Derived Peptides

As discussed in Chapter 1 (section 1.5.2) a coiled-coil domain that drives the heterodimerisation of c-Jun and c-Fos proteins has been shown to exist using X-Ray crystallography (Glover & Harrison, 1995). The structure of the bZIP coiled-coil region is shown in **Figure 3.14a**. As such it was not necessary to perform a computational analysis of the sequence to predict possible coiled-coil domains. Mason *et al*, (2006) developed a synthetic mutant of c-Fos (FosW) that had a higher affinity for the bZIP coiled-coil domain of the c-Jun protein as a potential therapeutic agent. This sequence was used here (**Table 3.8**), but with further engineering to introduce an N-terminal cysteine residue ($FosW_C$) for site-specific PEGylation and removal of the C-terminal proline to aid large-scale synthesis (**Figure 3.14b**). The c-Jun sequence was also modified to remove the C-terminal proline (**Table 3.8**). The tyrosine residues that had

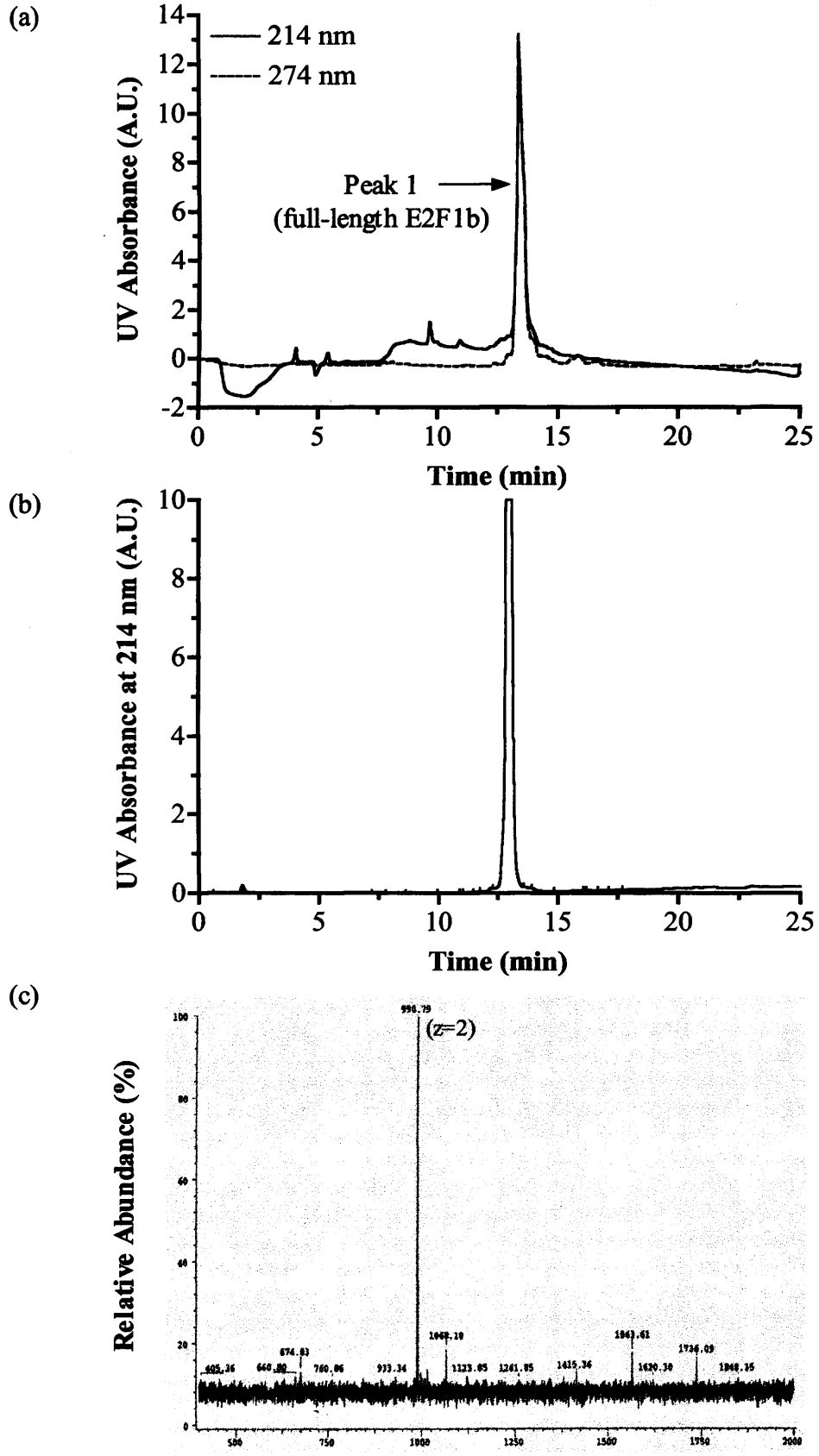

Figure 3.13 Purification and characterisation of E2F1b. Panels (a) and (b) show RP-HPLC chromatograms of crude peptide and pure E2F1b (post-purification), respectively. Panel (c) ESI-TOF MS spectrum of pure E2F1b.

(a) AP-1 (c-Jun:c-Fos) transcription factor complex bound to DNA

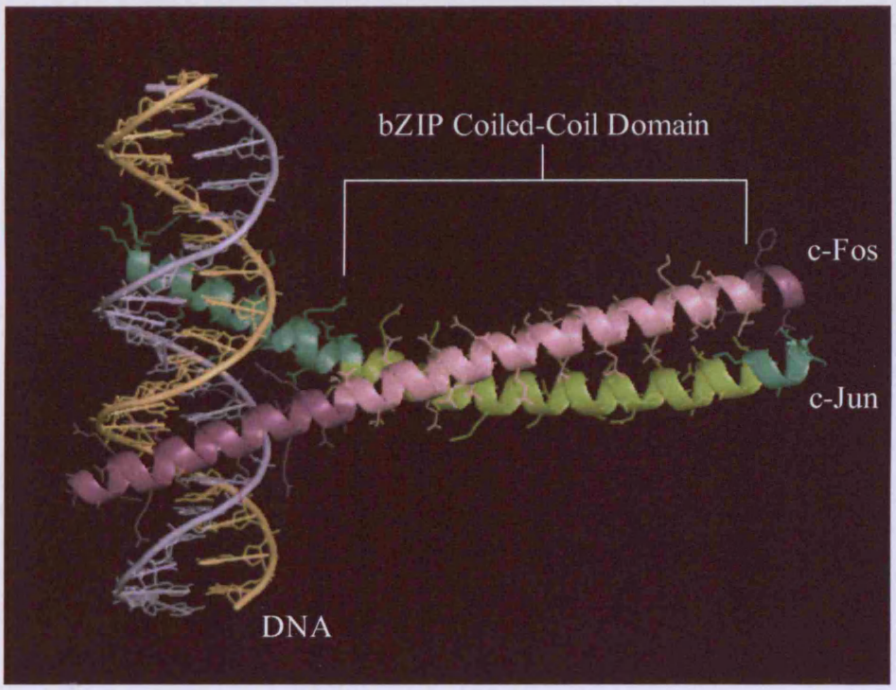

(b) Structures of $FosW_C$ and c-Jun peptides derived from the bZIP coiled-coil of AP-1. Modifications made to the structure of $FosW_C$ by Mason *et al*, (2006) are shown in red, those made to c-Jun are shown in white.

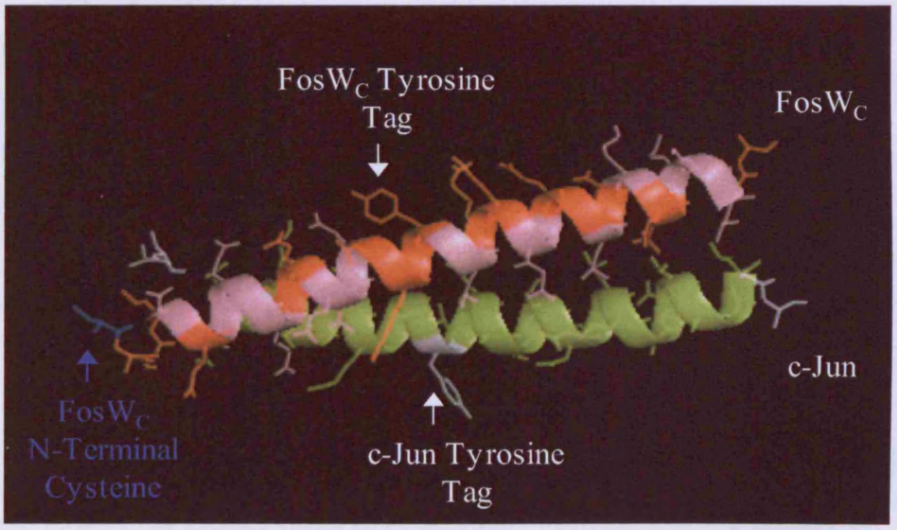

Figure 3.14 Structures of c-Jun:c-Fos and c-Jun:FoW$_C$ coiled-coil complexes. Panel (a) shows the crystal structure of the c-Jun and c-Fos heterodimer bound to DNA. Panel (b) shows the structures of the modified $FosW_C$ and c-Jun peptides synthesised in this study. The protein structure file was obtained from the PDB, DOI:10.2210/pdb1fos/pdb, editing and rendering was conducted using MacPyMOL.

been engineered into both peptides by Mason *et al*, (2006) to allow quantitation by UV spectroscopy are identified in **Figure 3.14b**. As the structure clearly shows, both tyrosine residues were positioned in solvent exposed "b3" positions away from the hydrophobic seam where they might interfere with coiled-coil driven hybridisation.

A single batch (0.1 mmol) of the peptide c-Jun, to be used for target hybridisation studies, was successfully synthesised. Precipitation in cold ether showed the presence of ample crude peptide in the form of a white semi-solid suspension. Subsequent lyophilisation generated a dry white, "fluffy" crude peptide powder (435 mg) that was easily soluble. This equated to a crude yield > 100 % suggesting that the powder was either not fully dry, or comprised some peptides that had not been completely deprotected. Upon analysis by RP-HPLC two peaks were identified with retention times of 14.02 and 14.32 min, respectively (**Figure 3.15a**). The chromatograms obtained at 214 and 274 nm were almost super-imposable between 12.80 and 15.13 min indicating that the peptide(s) eluting in this range all contained the tyrosine chromophore. Unfortunately in this instance, since the tyrosine residue was positioned in position "b" of the third heptad (b3) and not at the N-terminus it was not possible to confirm with the RP-HPLC chromatogram that the peptides eluting within this range corresponded to full-length c-Jun. Analysis by ESI-TOF MS (data not shown) demonstrated that peak 1 corresponded to the theoretical molecular weight (3987.57 g mol^{-1}) of full-length c-Jun. A gradient of 30-45 % ACN was found to be optimal for purification and once dried the yield of pure peptide was determined to be 91 mg (21 %). Analysis of the purified peptide by RP-HPLC showed a single peak eluting at 13.53 min, suggesting a purity of > 95 % (**Figure 3.15b**). Analysis by ESI-TOF MS confirmed that the purified sample of c-Jun peptide was of the correct molecular weight (**Figure 3.15c**). The three peaks observed in the mass spectrum all corresponded to full-length c-Jun peptide.

Two successful syntheses of $FosW_C$ were conducted, each on the same scale as for c-Jun (0.1 mmol). Precipitation in cold ether yielded a white semi-solid suspension of crude peptide that was easily solubilised in ddH_2O prior to lyophilising. The total crude yield of white, "fluffy" powder was determined to be 879 mg (95 %). As for c-Jun, two predominant peaks were observed in the preparative RP-HPLC chromatograms (**Figure 3.16a**). Analysis of the HPLC eluate by ESI-TOF MS (data not shown) confirmed that the first of these (peak 1) corresponded to full-length $FosW_C$ with a molecular weight of 4358.87 g mol^{-1}. The optimum gradient for purification of full-

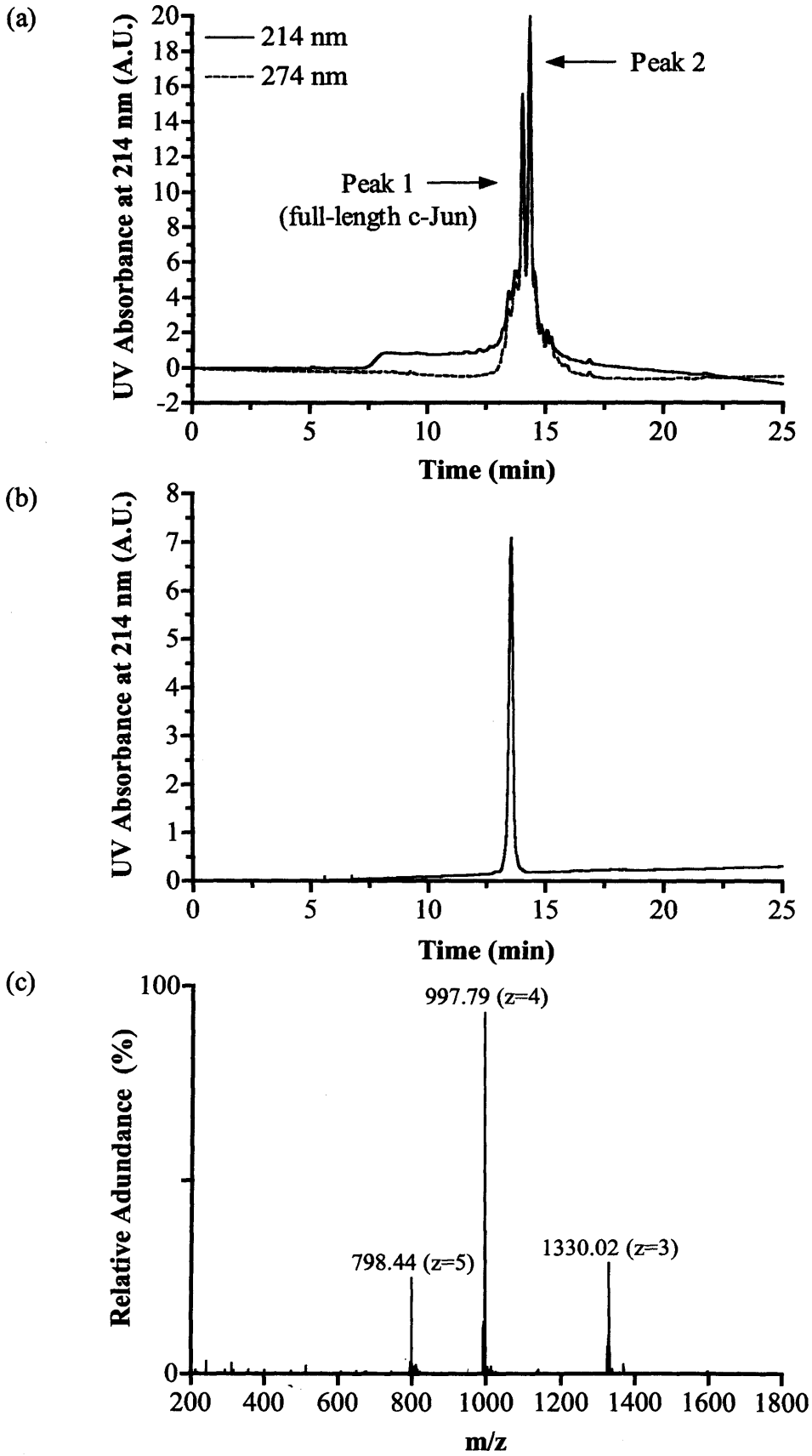

Figure 3.15 Purification and characterisation of c-Jun. Panels (a) and (b) show RP-HPLC chromatograms of crude peptide and pure c-Jun (post-purification), respectively. Panel (c) ESI-TOF MS spectrum of pure c-Jun.

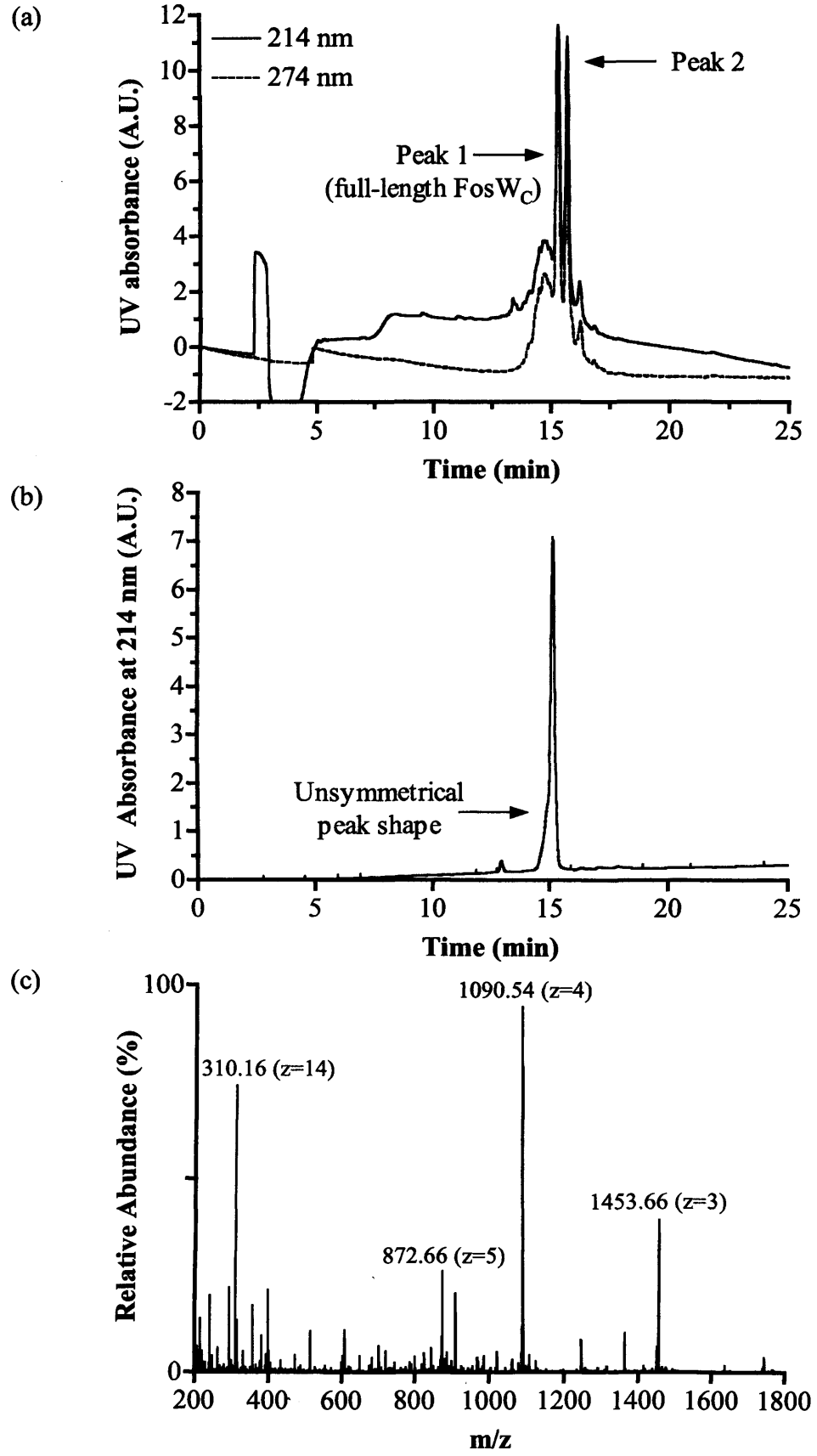

Figure 3.16 Purification and characterisation of FosW$_C$. Panels (a) and (b) show RP-HPLC chromatograms of crude peptide and pure FosW$_C$ (post-purification), respectively. Panel (c) ESI-TOF MS spectrum of pure FosW$_C$.

length $FosW_C$ using RP-HPLC was 38-55 % ACN. A single peak was observed in the analytical RP-HPLC chromatogram (**Figure 3.16b**). However the peak shape was not quite symmetrical at the base, suggesting the possibility of a very small degree of truncated peptide contamination. No disulphide bonded $FosW_C$ was visible in the chromatogram. Deconvolution of the four predominant peaks shown in the ESI-TOF mass spectrum confirmed that the purified sample of $FosW_C$ peptide was of correct mass (**Figure 3.16c**). However, in this instance the mass spectrum showed the presence of a number of other small peaks (< 20 % relative abundance), this indicated that there might have been compounds of differing molecular weight present in the sample. Nonetheless, the purified sample of $FosW_C$ was likely to be > 95 % as judged by the analytical RP-HPLC chromatogram. The final yield of purified $FosW_C$ peptide was 192 mg; at 22 % the reaction efficiency was similar to that seen for c-Jun.

3.3.2.3 Design and Synthesis of EbVP35 Derived Peptides

As discussed in Chapter 1 (section 1.5.3), the EbVP35 protein found in the Zaire strain of the Ebola virus has been sequenced, however at the time of writing, a crystal structure had not been published. Reid *et al*, (2005) were the first to suggest that the EbVP35 protein possessed a putative coiled-coil domain that was essential to the biological activity of the protein. This assertion by Reid *et al*, (2005) was based upon a computational analysis of the EbVP35 sequence using COILS. As shown in **Figure 3.6** (and discussed in section 3.3.1) three other computational analysis programmes agreed with this prediction, albeit with varying probability outputs. Reid *et al*, (2005) also demonstrated that the EbVP35 protein formed homo-oligomers, most likely homo-trimers, and then subsequently proved that the coiled-coil domain (**Figure 3.17a**) was essential for their formation. Furthermore, the trimeric form of the EbVP35 protein was found to be 100-fold more active than the monomeric form at downregulating IRF-3 (Reid *et al*, 2005). In this study, two peptide variants ($EbVP35_{82\text{-}119}$ and $EbVP35_{CY88\text{-}119}$) corresponding to the coiled-coil domain were designed (**Figure 3.17a**). The first peptide $EbVP35_{82\text{-}119}$ corresponded to the full coiled-coil domain described by Reid *et al*, (2005) with an additional lysine residue from the native EbVP35 sequence to improve solubility at the C-terminus.

The crude peptide obtained from the synthesis of $EbVP35_{82\text{-}119}$ was seen to precipitate in cold ether as for all the previous peptides. However it did not appear to be soluble in ddH_2O when diluted in preparation for lyophilisation. Furthermore, the

(a) Design of EbVP35 derived coiled-coil motif peptides

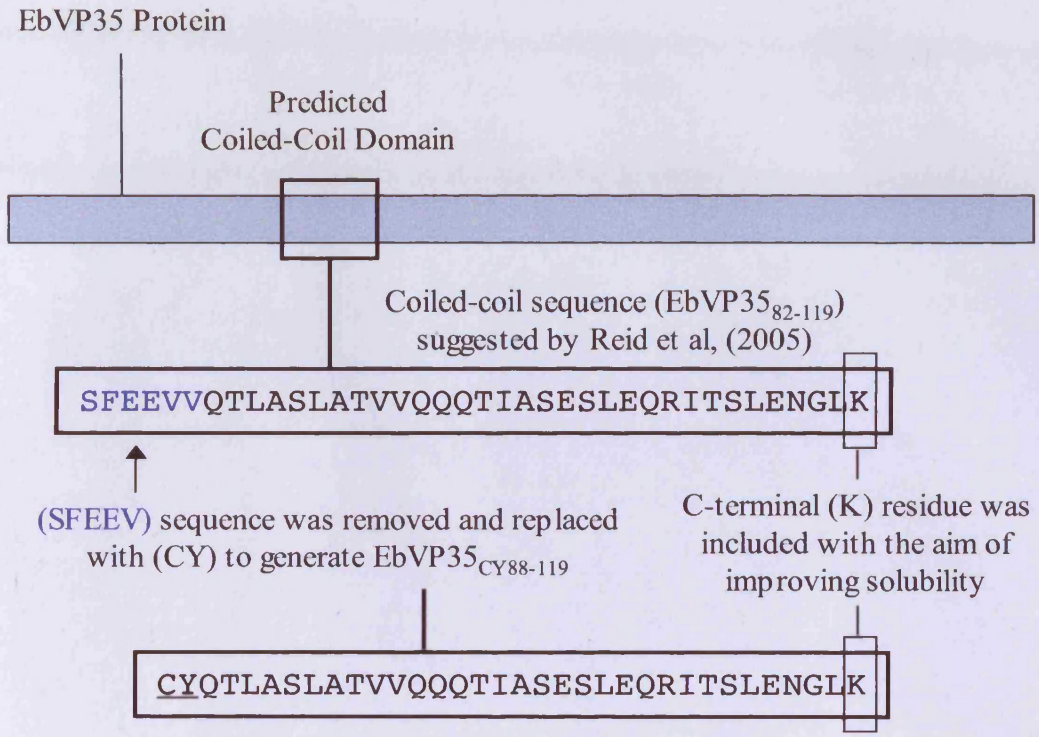

(a) Hydrophilicity plots for (i) EbVP35$_{82-119}$ and (ii) EbVP35$_{88-119}$. Green and red bars represent hydrophilic and hydrophobic residues, respectively.

(i) EbVP35$_{82-119}$

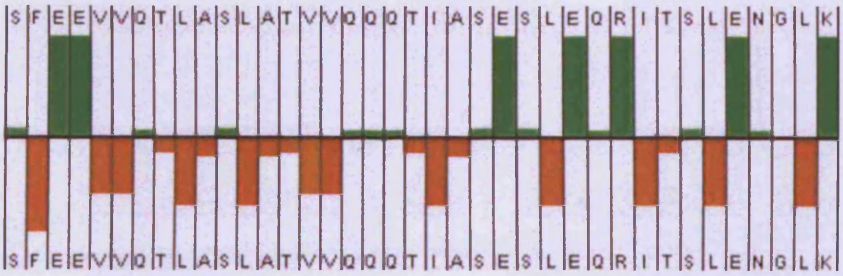

(ii) EbVP35$_{88-119}$

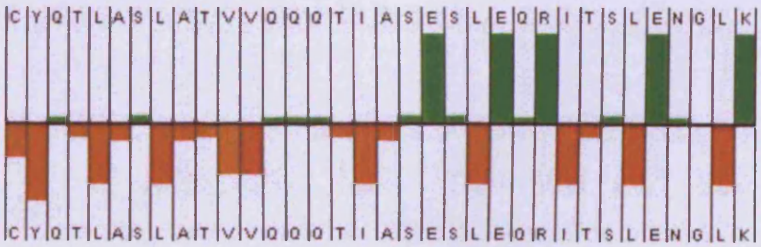

Figure 3.17 Design of the EbVP35 derived peptides EbVP35$_{82-119}$ and EbVP35$_{88-119}$. Panel (a) shows a schematic of the EbVP35 sequence and sequences of the putative coiled-coil motif peptides. Panel (b) shows hydrophilicity plots for each peptide calculated using the Innovagen peptide property calculator.

sample (post-lyophilisation) had an entirely different appearance to the other peptides synthesised. It had dried into a hard, crystalline powder that could only be solubilised in 100 % TFA. Attempts at solubilising the peptide in a range of solvents including DCM, ddH_2O (± 0.1 % TFA), ACN (± 0.1 % TFA), ACN (50 % in ddH_2O ± 0.1 % TFA) MeOH, Ethanol (EtOH) and NMP were made to no avail. Further attempts at solubilisation were conducted by first preparing a solution of crude peptide in TFA followed by dilution with each of the above solvents also failed. As the peptides could not be solubilised in a solvent compatible with ESI-TOF MS, MALDI-TOF MS or RP-HPLC, the crude peptide could not be characterised. This was surprising since there was a fairly equal balance between hydrophilic and hydrophobic residues in the structure as seen by the hydrophilicity plot (**Figure 3.17b**).

The second peptide $EbVP35_{CY88-119}$ was synthesised however the same problems were encountered. Whilst the hydrophobicity of this peptide was higher than the $EbVP35_{82-119}$ due to the addition of the cysteine and tyrosine residues at the N-terminus the hyrdophilicity plot estimated the ratio of hydrophilic amino acids to be 44 % of the total (**Figure 3.17b**). This was not thought to be too low to result in such poor solubility. It was postulated that either peptide might have been insufficiently deprotected and that the hydrophobic protecting groups were responsible for the poor solubility. Both peptides were incubated with the cleavage cocktail for a second time, then precipitated in ether and lyophilised. However no improvement in solubility was seen and so no further characterisation could be conducted.

3.3.2.4 Design and Synthesis of EbGP2 Derived Peptides

Unlike EbVP35, a crystal structure had been determined for the Zaire strain of the Ebola GP2 protein (Weissenhorn *et al*, 1998). The homo-trimerisation of GP2 is driven by the N-terminal α-helix in each protein that subsequently forms a central homo-trimeric coiled-coil (**Figure 3.18a**) (Weissenhorn *et al*, 1998). While the C-terminal α-helix does not form a coiled-coil, it packs against the trimeric coiled-coil further stabilising the structure.

A C-terminal peptide ($EbGP2_{609-630}$) was designed first (**Figure 3.18b**) and was very similar to the peptide GP610 synthesised by Watanabe *et al*, (2000). However the extra three C-terminal residues included in the GP610 sequence that are not in the crystal structure were not included in the $EbGP2_{609-630}$ sequence synthesised here.

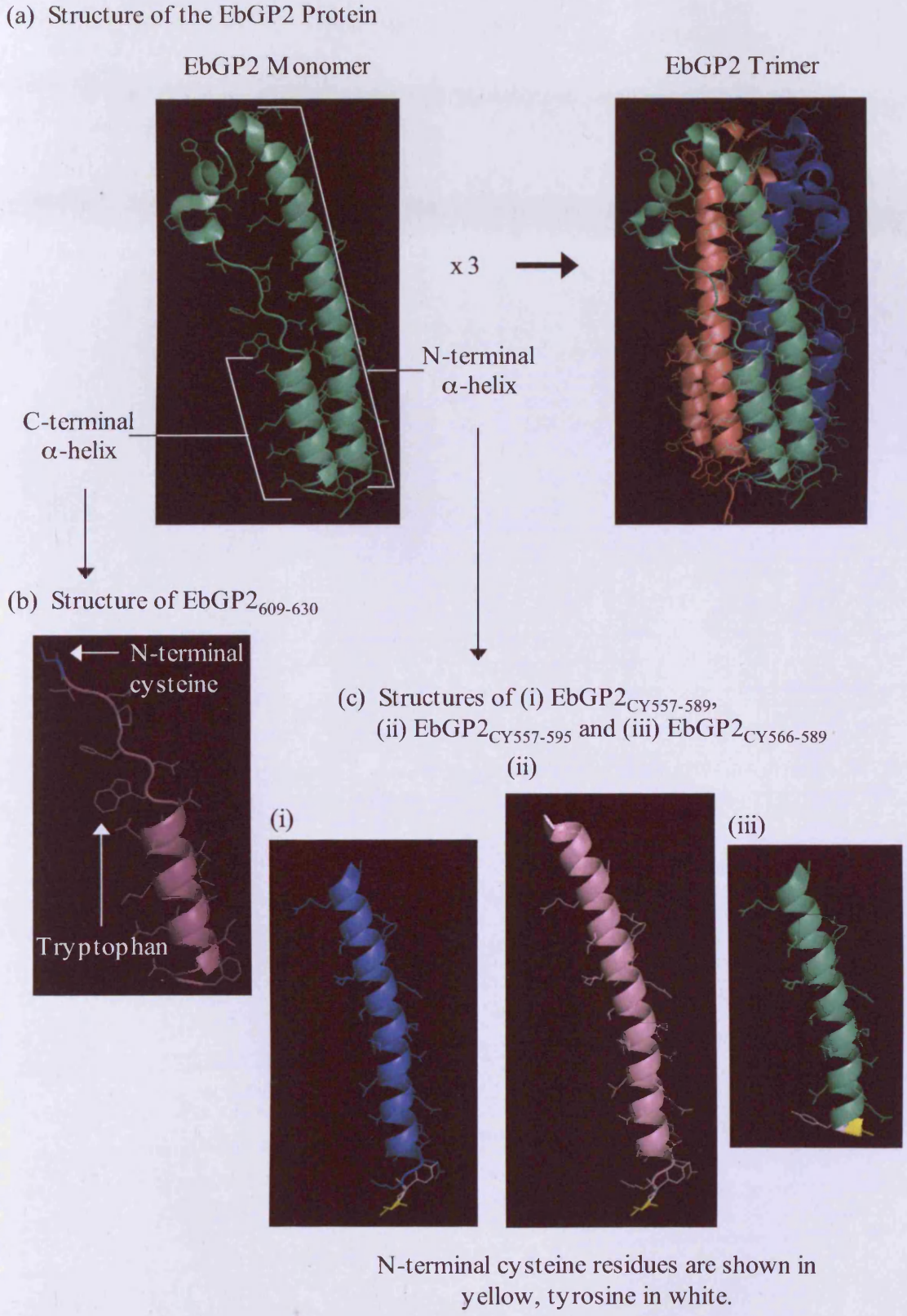

Figure 3.18 Design of EbGP2 derived peptides. Panel (a) shows the structure of the EbGP2 protein, as a monomer and the coiled-coil driven homotrimer. Panel (b) shows the structures of the four peptides synthesised in this study. Protein structure files were obtained from the PDB, DOI:10.2210/pdb2ebo/pdb, editing and rendering was conducted using MacPyMOL.

Furthermore, to facilitate thiol-directed PEGylation a single cysteine residue was introduced at the N-terminus of the peptide.

Post-synthesis, precipitation in cold ether yielded a white semi-solid suspension of crude peptide that was easily solubilised in ddH_2O prior to lyophilisation. When dry, the crude peptide had the appearance of a white, "fluffy" powder and the mass was determined to be 332 mg (114 %). This suggested that the peptide was very hygroscopic and had adsorbed ddH_2O preventing its loss on drying. Analysis of the crude peptide using the preparative RP-HPLC set-up showed the presence of multiple peaks in the 214 nm chromatogram (**Figure 3.19a**). When the chromatogram obtained using the 280 nm detector was overlaid, it was clear that peak 1 was most likely to be full-length $EbGP2_{609\text{-}630}$. Peaks 2, 3 and 4 did not show at 280 nm, this suggested that they lacked the tryptophan residue responsible for absorbing UV light at the higher wavelength. Analysis of the HPLC eluate by ESI-TOF MS (data not shown) confirmed that peak 1 corresponded to full-length $EbGP2_{609\text{-}630}$ with a molecular weight of 2723.04 g mol^{-1}. Purification was optimised and conducted using a 40-55 % ACN gradient. Analysis of the purified peptide showed a single peak in the analytical RP-HPLC chromatogram confirming purity > 95 % (**Figure 3.19b**). Deconvolution of the three peaks shown in the ESI-TOF mass spectrum confirmed that the purified sample of $EbGP2_{609\text{-}630}$ peptide was of correct mass (**Figure 3.19c**). The final yield of purified $EbGP2_{609\text{-}630}$ peptide was 128 mg; at 44 % the reaction efficiency was more than double that seen for the other peptides synthesised in this study.

Three N-terminal peptides were designed (**Figure 3.18c**). The first ($EbGP_{CY557\text{-}589}$) used the same sequence as the GP555 peptide prepared by Watanabe *et al*, (2000) with two amendments to the N-terminal residues. The N-terminal isoleucine residue was replaced by cysteine and the penultimate cysteine residue was replaced by tyrosine. However, post-synthesis the crude peptide was found to be insoluble in ddH_2O when the sample was prepared for lyophilisation, nonetheless the insoluble suspension was lyophilised. Once dry the crude peptide was found to be equally insoluble in all except TFA. It had the physical appearance of a hard, crystalline solid, very similar to the insoluble EbVP35 peptides described above (section 3.3.2.3). As $EbGP_{CY557\text{-}589}$ could not be solubilised in a solvent compatible with ESI-TOF MS, MALDI-TOF MS or RP-HPLC, the crude peptide could not be characterised.

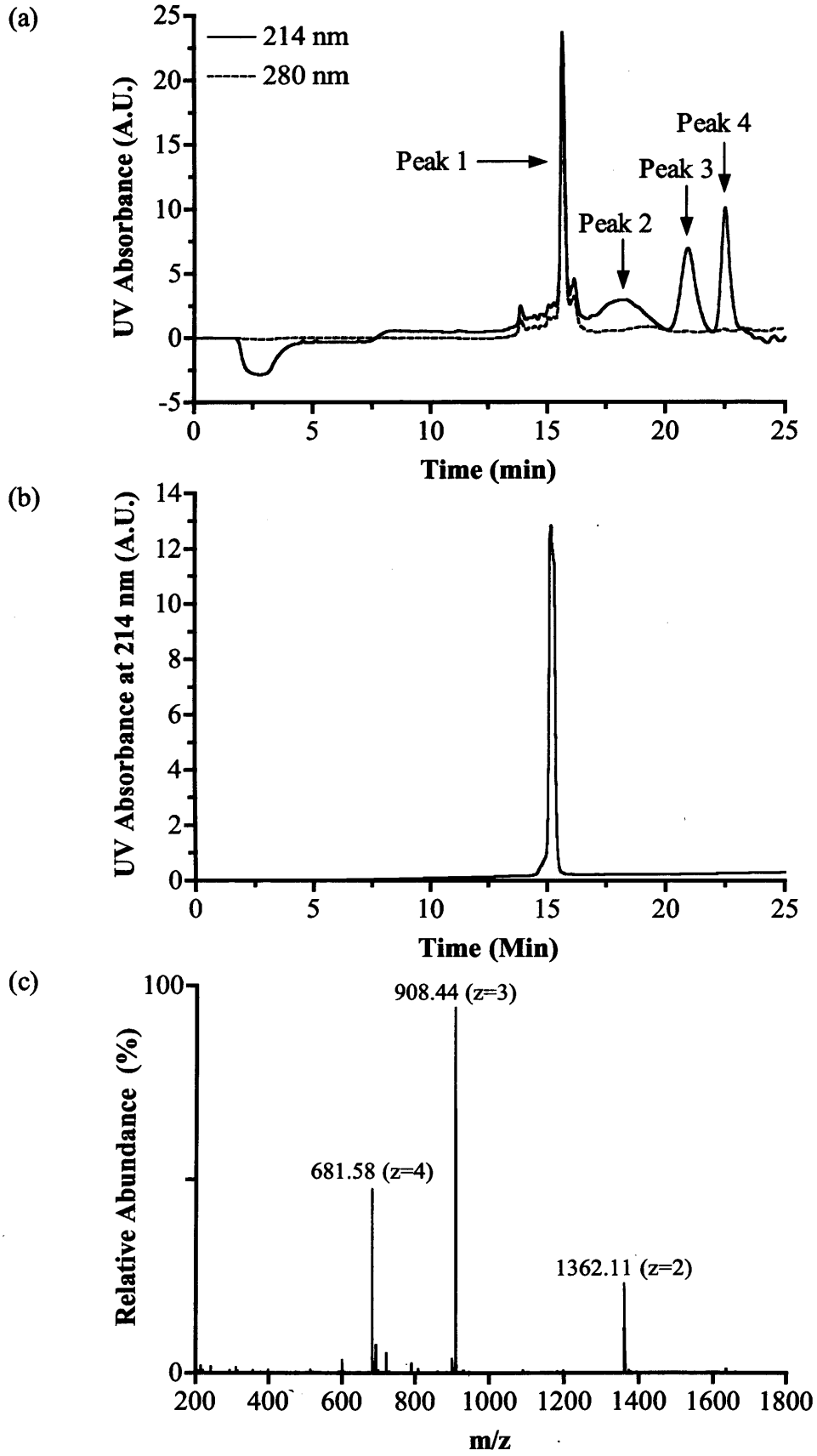

Figure 3.19 Purification and characterisation of EbGP2$_{609-630}$. Panels (a) and (b) show RP-HPLC chromatograms of crude peptide and pure EbGP2$_{609-630}$ (post-purification), respectively. Panel (c) ESI-TOF MS spectrum of pure EbGP2$_{609-630}$.

The second peptide ($EbGP_{CY557-595}$) included an additional six residues at the C-terminus. Synthesis of a second N-terminal α-helical peptide ($EbGP2_{CY557-595}$) was attempted, this derivative was slightly longer and comprised an additional 6-residues from the fifth heptad at the C-terminus of the peptide. However, the crude product again could not be solubilised and hence characterisation was not possible.

In an effort to generate a soluble peptide, a third peptide ($EbGP_{CY566-589}$) that was shorter than the previous two and comprised only three heptads was designed (**Figure 3.18**). As with the other peptides, cysteine and tyrosine residues were added to the N-terminus. After vigorous shaking (1-2 h), it was possible to dissolve the crude peptide in ddH_2O containing 0.1 % TFA. Analysis using the preparative RP-HPLC set-up showed the presence of multiple peaks in the 214 nm chromatogram (**Figure 3.20a**). Peak 1 was identified as corresponding to full-length $EbGP_{CY566-589}$ using ESI-TOF MS (data not shown). After removal of ACN and subsequent lyophilisation the purified peptide was dissolved in ddH_2O containing 0.1 % TFA, however, as solution was slightly cloudy it was decided against injecting the sample into the analytical RP-HPLC. ESI-TOF MS confirmed the expected molecular weight of 3099.63 g mol^{-1} (**Figure 3.20b**). The yield of purified peptide was 35 mg, (8 %). Assuming that the purification was as effective as with earlier peptides, the purity was estimated to be > 95 %.

3.3.3 General Challenges in the Identification of Coiled-Coil Domains

Accurate prediction and identification of coiled-coil domains was a key objective of this study. Comparisons of the predictions made by the computational analysis programmes demonstrated that the outputs vary greatly according to which programme is used. It was therefore surprising that the studies published by Joshi *et al*, (2003) and Reid *et al*, (2005) each presented the data obtained from only one programme, Paircoil and COILS, respectively. There remains an inherent risk of overstating the probability of a coiled-coil by taking this approach. Computational analysis is essentially a predictive tool and thus a good starting point. However the predictions should ideally be supported by biophysical studies such as those outlined in **Table 3.9**. As discussed in section 3.1.1, X-Ray crystallography is the gold-standard technique for determining the structures of large protein complexes, though advances in the use of 2D NMR spectroscopy make this a very good alternative (reviewed in Chapter 5, section 5.1.2.2).

(a)

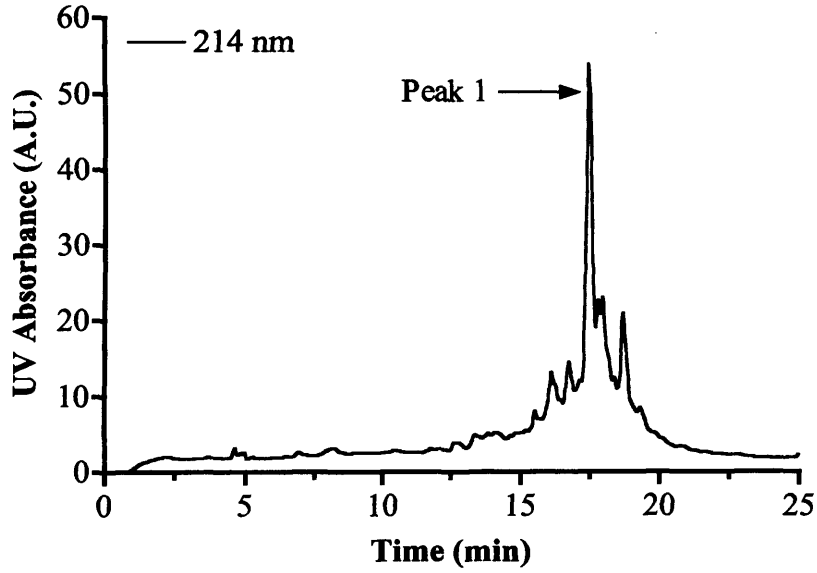

(b)

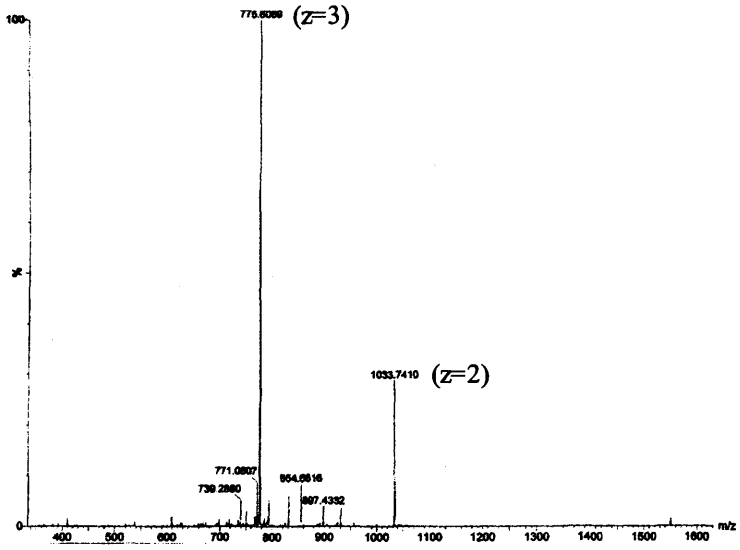

Figure 3.20 Purification and characterisation of EbGP2$_{CY556-589}$. Panel (a) shows the RP-HPLC chromatogram of crude peptide and panel (c) shows the ESI-TOF MS spectrum of pure EbGP2$_{CY566-589}$.

Table 3.9 Pros and cons of the biophysical techniques used to identify and characterise coiled-coil motifs.

Technique	Pros	Cons	Reference
CD spectroscopy	Relatively simple to use. Instant data, i.e. complex interpretation is not necessary for a "look see" type experiment.	Infers a coiled-coil as a result of ratio between minima at 208 and 222 nm.	Vandermeulen *et al*, 2004
Fourier Transform-Infra Red (FT-IR) spectroscopy	Direct spectrographic detection.	Measurements may require the instrument to be nitrogen cooled. Samples must be prepared in D_2O. Complex interpretation of data.	Heimburg *et al*, 1996
Fluorescence spectroscopy	Possible to determine whether coiled-coil is parallel or anti-parallel.	Each complementary alpha helix must be synthesised and dye-labelled.	Daugherty, 1999
X-Ray crystallography	Gold standard.	Shows only one conformational state. Complex and very time consuming.	Weissenhorn *et al*, 1998
NMR spectroscopy	Detailed data gives exact 3D structure of solution conformation.	Data can be very complex to interpret, particularly for large proteins.	Dames *et al*, 1998

3.3.4 Challenges in the Preparation of Synthetic Peptides

Previous basic research studies designed a novel library of LAEIEAK based coiled-coil sequences that were used to synthesise PEG-*b*-peptide hybrid block co-polymers with self-assembly properties (Vandermeulen et al, 2003; Vandermeulen et al, 2005). These studies demonstrated that the PEGylated coiled-coil conjugates retained their ability to form coiled-coils. However, CD spectroscopy and other techniques showed that self-organisation could be described as a two-state equilibrium between discrete monomers and dimeric coiled-coil aggregates.

The aim of this study was to identify novel coiled-coil sequences from the literature that would have real potential for further development as a new sub-category of polymer-therapeutics. Then make synthetic modifications to the primary peptide sequence to facilitate PEGylation. It was considered essential to select/design peptides that would preferentially form discreet hetero-oligomers with the target domains. Coiled-coil motif peptides that form homo-oligomers may not readily interact with the target domain and so may be less effective therapeutic agents.

The synthesis of the PHB derived peptides was a fairly straightforward process. All the sequences designed were easily solubilised, a characteristic that facilitated purification and later analysis. The observation that the UV absorbance of the single phenylalanine residue was too weak relative to the strong absorbance of the peptide bond resulted in all subsequent peptides being tagged at the N-terminus with a tyrosine residue if one was not already present in the structure. The only exception was $EbGP2_{609\text{-}630}$ as the peptide already contained the aromatic residue tryptophan. From a biological perspective the incorporation of tyrosine or tryptophan may not be ideal due to the potentially increased immunogenicity (Sela *et al*, 1962). However, the advantages conferred i.e. the ability to accurately determine mass/concentration outweighed this potential disadvantage. Preliminary investigations revealed that gravimetric determinations of mass were overestimating the true quantity of peptide by up to 50 %. Thus if solutions were prepared, the actual concentration of peptide may have been much less than expected. This should be considered a caveat to those working with small proteins and peptides if using gravimetric methods of sample preparation.

The E2F1 derived peptides, E2F1a and E2F1b were more challenging to prepare. Significant amounts of both peptides precipitated out of solution prior to purification, this is perhaps why the % yields were markedly lower than those seen for other peptides in this study.

The purity of the peptides c-Jun and $FosW_C$ was comparable the synthesis of the similar peptides c-Jun and FosW prepared by Mason *et al*, (2006). No mention of synthesis scale was made in the study; however judging by the size of the RP-HPLC column used and the flow rate applied it is likely that it was much smaller than the 0.1 mmol scale used here. The large-scale synthesis of $FosW_C$ was particularly important since it was needed for PEGylation (Chapter 4).

Disappointingly it was not possible to synthesise a soluble EbVP35 peptide. As none have been described to date in the literature, this would have been a very interesting coiled-coil motif peptide to study. It may still yet be possible to prepare a soluble EbVP35 peptide if a semi-rational design approach is taken to thoroughly optimise the sequence as performed by Mason et al, (2006) in the preparation of FosW.

Synthesis of $EbGP2_{609\text{-}630}$ was achieved with relative ease and very high yield (44 %). Furthermore, since the sequence already contained both an N-terminal cysteine and mid-sequence tryptophan residue it was not necessary to engineer either of these into the peptide. All concentration determinations for subsequent studies could then be made using the molar extinction coefficient of tryptophan. Other methods such as chemo-selective ligation (reviewed in Tam *et al*, 2001) were considered an alternative synthesis method for $EbGP2_{CY\text{-}557\text{-}595}$ due to the high potential for inter-chain H-bonding. However since the shorter $EbGP2_{CY\text{-}566\text{-}589}$ peptide was found to be soluble this approach was deemed unnecessary.

Notes on Interpretation of ESI-TOF mass spectra and RP-HPLC chromatograms

Differences in the clarity of the ESI-TOF mass spectra should not be viewed as an indication of purity since some compounds will ionise easier than others. As such, the technique should only be used to determine whether the peptide is of the correct molecular weight as used here.

Discrepancies were seen in the elution times for many of the peptides when comparing the preparative and analytical chromatograms. In most cases these were relatively small and may be explained by the differing proportions of the C-18 columns used. Ideally, an analytical Atlantis™ column (matching the Atlantis™ preparative

column) would have been used to perform the final characterisation, however such a column was not available.

3.3.5 Conclusions

It has been possible to synthesise the desired peptides for each of the cancer models to be studied. The analytical data demonstrate that despite the long length of many of the peptides, synthesis was possible by a standard chain elongation methodology (reviewed in Chan & White, 2000). Target peptides (E2F1a, E2F1b and c-Jun) required to study the E2F1 : PHB and c-Jun:FosW_C interactions were synthesised and purified (> 95 %) in sufficient quantities to permit characterisation by CD and NMR spectroscopy (Chapter 5). Moreover, sufficient $Phb_{CY185\text{-}214}$ and FosW_C were prepared for PEGylation (Chapter 4). A summary of the characterisation data for each peptide synthesised is provided in **Table 3.10**.

It was not possible to synthesise a soluble EbVP35 peptide, however it may be possible to conjugate the crude peptides to polymers to confer solubility then use size exclusion chromatography to remove the lower molecular weight peptide contaminants. This will be investigated in Chapter 4.

Successful synthesis of a C-terminal α-helical peptide ($EbGP2_{609\text{-}630}$) and a coiled-coil motif peptide ($EbGP_{CY566\text{-}589}$) will enable PEGylated conjugates to be prepared in Chapter 4 as the first polymer-therapeutic viral fusion inhibitors.

Table 3.10 Summary of synthesis data for each of the peptides prepared in this study.

Peptide	Batch No.	Crude Yield		RP-HPLC Gradient	Pure Yield		Length	Molecular weight[#]
		mg	%	% ACN	mg	%	(residues)	g mol^{-1}
E2F1 and PHB derived peptides								
$Phb_{185-214}$	01	330	92	25-35	75	21	30	3367.83
$Phb_{Y185-214}$	01	345	92	26-31	82	22	31	3531.01
$Phb_{CY185-214}$	01	375	97	27-37	35	9	32	3634.15
E2F1a	03	120	82	18[†]	20	14	18	2063.15
E2F1b	03	115	82	18-30	11	8	18	1979.11
c-Jun and c-Fos derived peptides								
c-Jun	01	435	99	30-45	91	21	36	3987.57
$FosW_C$	01	879	92	38-55	192	22	37	4358.87

[†] Isocratic gradient.

[#] Theoretical value confirmed by ESI-MS

Table 3.10 Summary of synthesis data for each of the peptides prepared in this study.

Peptide	Batch No.	Crude Yield		RP-HPLC Gradient	Pure Yield		Length	Molecular weight[#]
		mg	%	% ACN	mg	%	(residues)	g mol^{-1}
EbVP35 derived peptides								
$EbVP35_{82\text{-}119}$	01	434	97	Insoluble	n/a	n/a	38	4189.66
$EbVP35_{CY88\text{-}119}$	01	419	107	Insoluble	n/a	n/a	34	3697.18
EbGP2 derived peptides								
$EbGP2_{609\text{-}630}$	01	332	114	40-55	128	44	22	2723.04
$EbGP2_{CY557\text{-}589}$	01	358	85	Insoluble	n/a	n/a	35	4082.72
$EbGP2_{CY557\text{-}595}$	01	457	89	Insoluble	n/a/	n/a	41	4812.59
$EbGP2_{CY566\text{-}589}$	01	412	94	40-60	35	8	26	3099.63

[#] Theoretical value confirmed by ESI-MS

CHAPTER 4
Site-Specific PEGylation

4.1 Introduction

In parallel to the design and synthesis of the coiled-coil peptides described in the previous chapter, it was necessary to develop a methodology for site-specific PEGylation and subsequently purification and characterisation of the final mPEG-coiled-coil motif conjugates. To aid the selection of appropriate methods, each of these areas was reviewed and summarised in sections 4.11 to 4.14.

The overall rationale for using PEG as a model polymer in these studies (from both a biological and chemical perspective) was discussed in Chapter 1. Current state of the art PEGylation chemistry permits the synthesis of polymers with very low polydispersity (c.a. 1.01), low diol content and molecular weights in the range of 100 to 60,000 g mol^{-1}. Other advantages include the ability to engineer physiologically stable or cleavage linkers, using either mono or homo/hetero bifunctional PEG molecules of pharmaceutical grade. Finally, a key advantage is the availability of a wide range of reactive chemistries, some of which permit site-specifc, rather than random conjugation of PEG. For a more detailed background, these features have been discussed in a number of excellent reviews, including those by Roberts *et al*, 2002; Harris & Chess, 2003; Veronese & Harris, 2008. A brief discussion of the developments that have led to the advanced PEGylation chemistry available today is given below.

4.1.1 The Chemistry of PEGylation

Covalent attachment of PEG to a peptide, protein or small drug molecule requires the PEG chain to be activated at either one or both termini. With more than 30 years of research devoted to this field it is now possible to obtain PEG commercially with almost any type of end group functionalisation desired. An increasing number of companies now exist that offer a wide range of functionalised PEG molecules for example, Nektar (www.nektar.com) and NOF (www.peg-drug.com).

Peptides and proteins possess N- and C-terminal amines and carboxylic acids and a number of reactive side chain groups including R-NH_2 (arginine and lysine), R-COOH (aspartic acid and glutamic acid) and R-SH (cysteine), which may be exploited

for the purpose of conjugating PEG (reviewed in Roberts *et al*, 2002). A summary of the PEG derivatives used in each of the FDA approved PEG-protein/drug conjugates is given in **Table 4.1**. Early PEGylation chemistry utilised the amine reactive succinimidyl carbonate group for conjugation (Abuchowski *et al*, 1984), for example, in the preparation of the FDA approved conjugates Adagen®, Oncaspar®, PEG-INTRON® and Somavert® (**Table 4.1**). Succinimidyl carbonates were used as they reacted preferentially with the R-NH_2 side-chain of lysine residues to form carbamate linkers. However carbamate linkers have also been shown to result from reactions with the side-chains of histidine and tyrosine residues (Zalipsky *et al*, 1992; Miron *et al*, 1993). Therefore, the resultant conjugates are heterogenous mixtures, with mPEG chains potentially attached at a range of different sites. Furthermore, all of these early mPEG-protein conjugates were developed using mPEGs of low molecular weight (< 12,000 g mol^{-1}).

Second generation PEGylation chemistry sought to improve product heterogeneity by using mPEGs with site-specific reactive chemistries and a low-diol content (to reduce the potential for protein/peptide cross-linking). Furthermore, these efforts were conducted using mPEGs of higher molecular weight (c.a. 20,000 g mol^{-1}). The first FDA approved conjugate to utilise a method of site-specific conjugation was Neulasta® in 2002 (**Table 4.1**). This conjugate was synthesised using a 20,000 g mol^{-1} aldehyde-activated mPEG to effect N-terminal PEGylation. Selectivity of the conjugation reaction was achieved by virtue of the lower pK_a of the N-terminal α-amine relative to that of the other side-chain nucleophiles (Kinstler *et al*, 1996). However, whilst conjugate homogeneity was improved using this approach, near complete selectivity of the reaction was not possible using this chemistry.

The first commercially available product to be prepared using site-specific chemistry that generated a single species was the mPEG-aptamer conjugate Macugen®. In this case, site-specific PEGylation at the 5' end of the aptamer was achieved using an N-hydroxysuccinimide (NHS) activated mPEG derivative. Furthermore, this was the first time a branched PEG, consisting of two 20,000 g mol^{-1} mPEG chains was used for conjugation. Whilst this approach demonstrated the site-specific conjugation of mPEG-NHS to an aptamer, synthesis of the mPEG-interferon conjugate, PEGASYS, showed that it was not possible to use the same mPEG derivative to site-specifically PEGylate

Table 4.1 Summary of PEG characteristics used in the synthesis of the eight FDA approved PEG-protein conjugates.

FDA Approval (Year)	Drug Trade Name	PEG MW (g mol^{-1})	PEG Functionalisation	Site of Conjugation	Number of PEG chains	Reference
1990	Adagen®	5,000	mPEG-succinimidyl carbonate 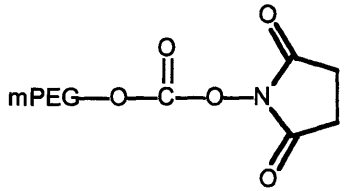	Random	11 to 17	Reviewed in Pasut & Veronese, 2007
1994	Oncaspar®	5,000	mPEG-succinimidyl carbonate	Random	Several	Reviewed in Pasut *et al*, 2008
2001	PEG-INTRON®	12,000	mPEG-succinimidyl carbonate	Random	1	Wang *et al*, 2002
2002	PEGASYS®	40,000	mPEG2-NHS 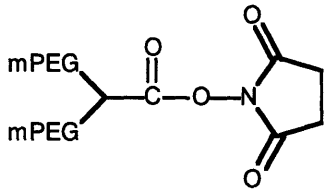	Random amine	1	Rajender Reddy *et al*, 2002
2002	Neulasta®	20,000	mPEG-aldehyde 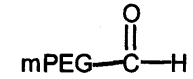	N-terminus	1	Nektar (www.nektar.com)

Table 4.1 Summary of PEG characteristics used in the synthesis of the eight FDA approved PEG-protein conjugates.

FDA Approval (Year)	Drug Trade Name	PEG MW (g mol^{-1})	PEG Functionalisation	Site of Conjugation	Number of PEG chains	Reference
2003	Somavert®	5,000	mPEG-SPA (succinimidyl-propionate) 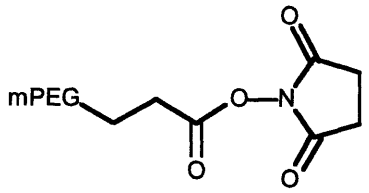	Random amine	4-5	Parkinson *et al*, 2003
2004	Macugen®	40,000	mPEG2-NHS 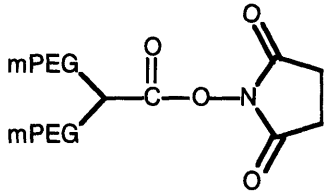	5' of aptamer	1	Nektar (www.nektar.com)
2008	Cimzia®	40,000	mPEG-MAL 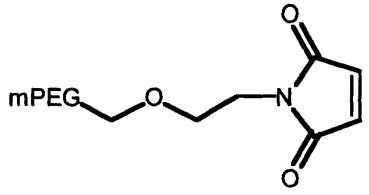	Thiol	1	Chapman *et al*, 1999

peptides or proteins with the same reagent as the NHS group can react with many different side-chain nucleophiles (Hermanson, 2008).

Of the amino acids mentioned above that have potentially reactive side-chain groups, the thiol of cysteine is the strongest nucleophile. Therefore, thiol-directed PEGylation has the greatest potential to yield, well-defined (single-product) mPEG-peptide conjugates. Towards this end, mPEG functionalised with iodoacetamide, maleimide, orthopyridyl and vinylsulphone chemistries were developed with each having particular pros and cons (Goodson & Katre, 1990; Kogan, 1992; Woghiren *et al*, 1993; Morpurgo *et al*, 1996). While progress had been made in the development of mPEG derivatives, until recently, the major limitation of mPEG-conjugation *via* the cysteine thiol was that the protein or peptide of interest needed to have an accessible cysteine residue not involved in an intra-molecular disulphide bond. Since few naturally occurring proteins/peptides have free thiols, molecular biology is now being used to circumvent this problem by introducing cysteine residues into recombinant proteins to facilitate site-specific conjugation (Doherty *et al*, 2005). With peptides, it is possible to introduce cysteine residues either using the same recombinant approach or by Fmoc-SPPS as described in Chapter 3. An alternative, rather elegant approach described by Balan *et al* in 2007 involves the attachment of a mPEG chain across a native disulphide bond. This method first requires reduction of the native disulphide bond, followed by bis-alkylation with a three-carbon bridge linker to which mPEG is attached.

The only marketed product to use site-specific, thiol, chemistry for PEGylation is the mPEG-anti-TNF Fab conjugate Cimzia®, which was approved by the FDA in April 2008 for the treatment of Crohn's disease. In this instance, a single 40,000 g mol^{-1} maleimide activated mPEG was conjugated to a cysteine residue engineered into the antibody fragment. The mPEG-MAL derivative is highly reactive towards the nucleophilic thiol and at pH < 8, the reaction is reported to be approximately 1000 fold faster than seen with an α-amine nucleophile (Hermanson, 2008), as such conjugation is highly efficient and yields a homogenous product.

4.1.1.1 Importance of Site-Specific Conjugation

Over the years there has been a clear trend towards the use of site-specific PEGylation, and products like Cimzia® are now a benchmark standard for future conjugates entering the clinic. As discussed in Chapter 1, it was considered very

important here to synthesise mPEG-coiled-coil motif conjugates site-specifically to ensure a well-defined 1:1 structure. Furthermore, it was envisaged that random and/or multi-site conjugation would likely disrupt the ability of the coiled-coil motif to fold and thus interact with the target domain. For a typical peptide it would be possible to effect conjugation *via* a range of amino acid side-chains or *via* the N and C-termini. However, C-terminal amidation and N-terminal acetylation of the coiled-coil motifs prepared in Chapter 3 had removed the charged termini and therefore left only the amino acid side chains as possible PEGylation sites (**Figure 4.1**). For this reason, a review of the possible synthetic strategies that would enable site-specific conjugation of mPEG to the coiled-coil motif was conducted; the two approaches used in this study are discussed below.

4.1.1.2 Solid and Solution Phase Methodologies for Site-Specific PEGylation

Before describing the two site-specific conjugation approaches considered in this study it is important to appreciate that the position of the PEG acronym in the naming of the conjugates indicates the site of PEGylation. Peptide sequences, by convention are written from N to C (since this is the direction of ribsosomal synthesis) and as such the PEG acronym was placed at the start (prefix) to indicate N-terminal conjugation or at the end (suffix) to indicate C-terminal conjugation. For example, PEG-(peptide) indicates N-terminal PEGylation, whereas (peptide)-PEG indicates C-terminal PEGylation. Furthermore, it should be noted that it was not possible to use mPEG for the synthesis of the conjugates using the solid-phase approach detailed below, instead the free PEG had a hydroxyl functionality and as such (m) is omitted from the acronym where appropriate.

In the first approach, the coiled-coil motif could be synthesised directly on a PEG modified resin using the same Fmoc-SPPS chemistry described in Chapter 3. This methodology is a solid-phase approach and is illustrated in **Figure 4.2**; it offers the advantage that preparation of the conjugates can be obtained in a single synthesis step. Use of a PEG modified resin such as TentaGel™ PAP (PEG-attached-products) (**Figure 4.2**) would make it possible to prepare C-terminal coiled-coil motif-PEG conjugates (Rösler *et al*, 2003). Alternatively, N-terminal PEG-coiled-coil motif conjugates can be prepared by synthesising the peptides using Fmoc-SPPS and subsequently reacting PEG with the N-terminus of the peptide chains prior to acid cleavage (Vandermeulen *et al*, 2003). The main disadvantage of this solid phase approach is that the conjugates

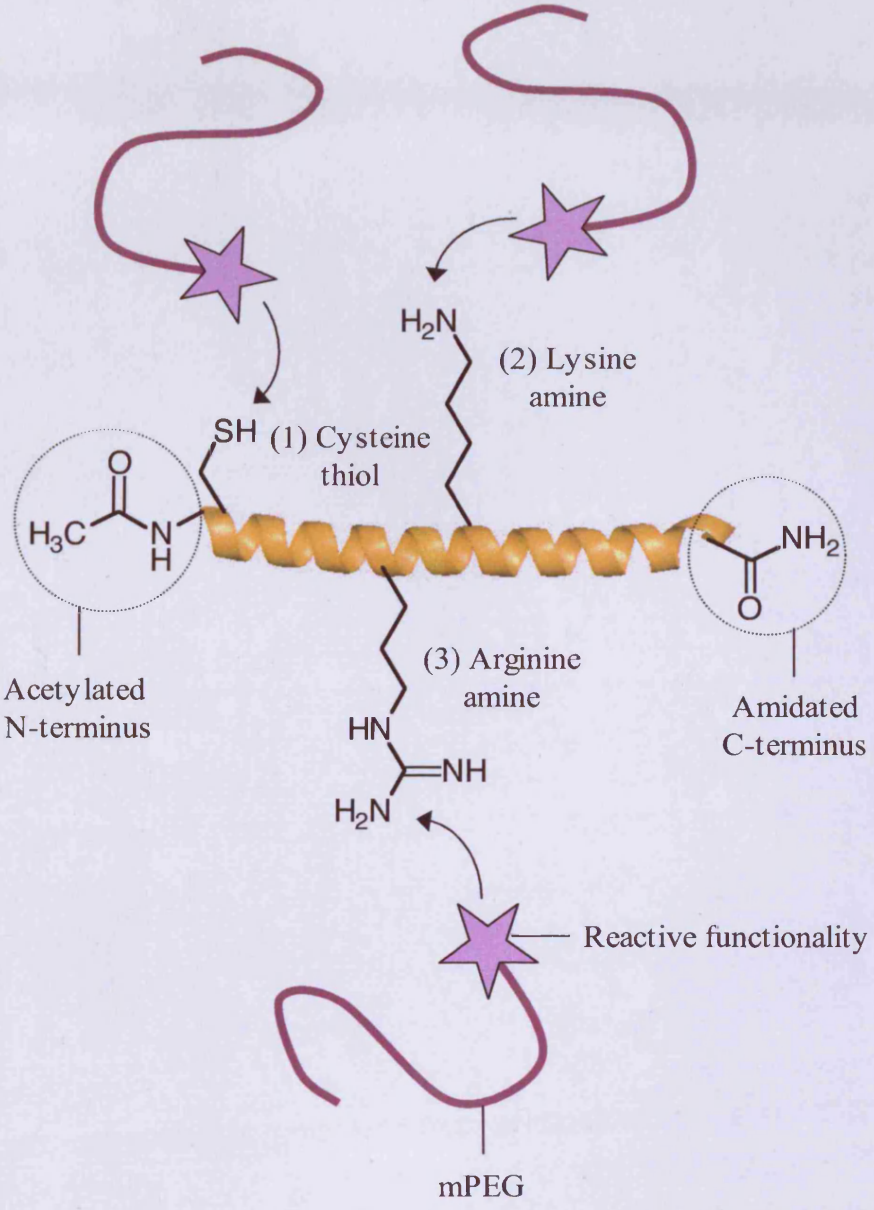

Figure 4.1 Theoretical coiled-coil motif PEGylation sites. Cartoon to illustrate the possible sites of polymer conjugation to a coiled-coil motif, (1) cysteine thiol, (2) lysine amine and (3) arginine amine. N-terminal acetylation and C-terminal amidation preclude these as possible conjugation sites.

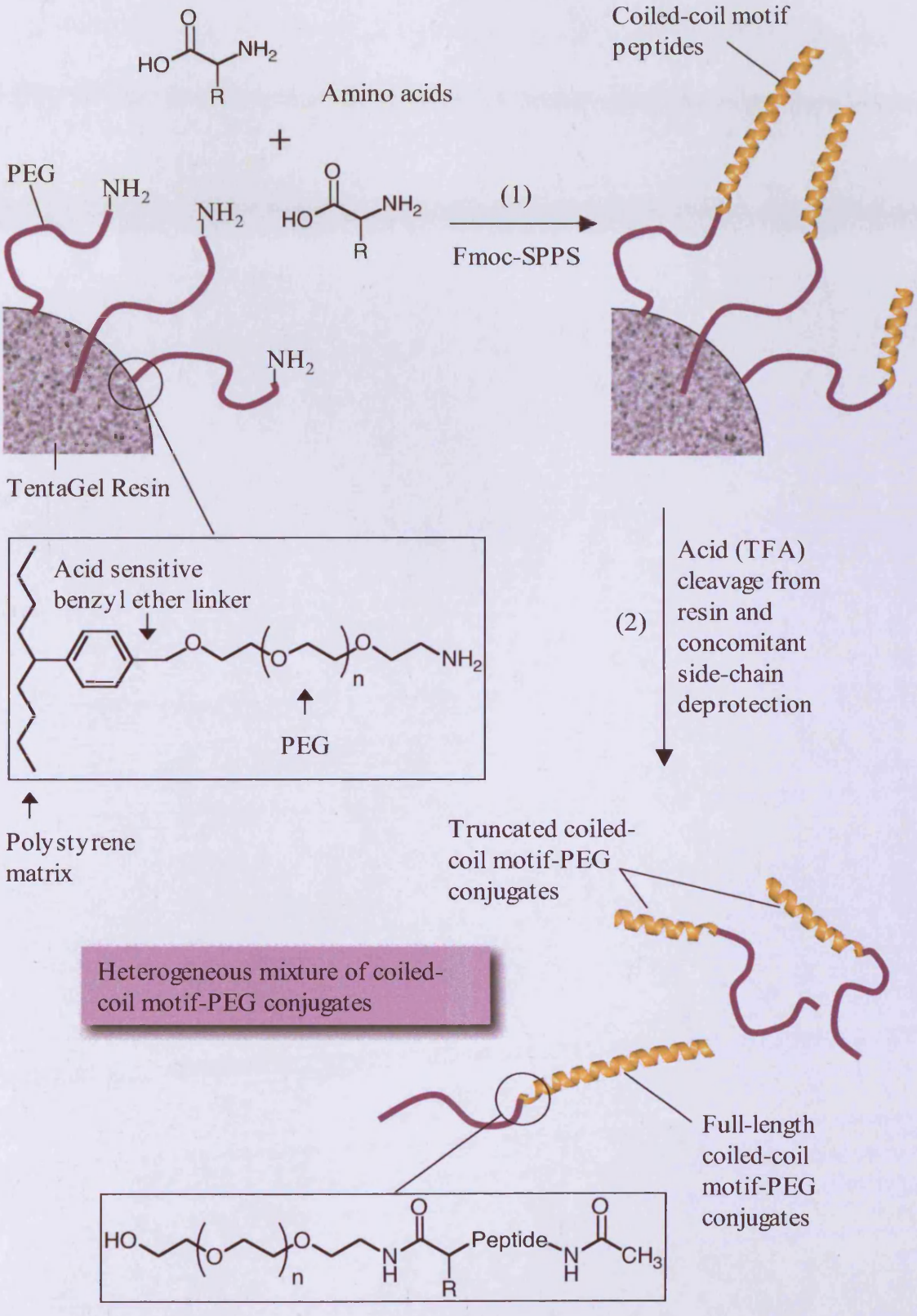

Figure 4.2 Two-step solid phase methodology for the synthesis of C-terminal coiled-coil motif-PEG conjugates.

prepared would likely be a heterogeneous mixture, containing peptides of different lengths due to inefficient coupling of amino acids inherent in SPPS. As such a purification method with the ability to resolve each different conjugate would need to be developed.

A second approach allows solution-phase conjugation. This is a two-step process whereby peptides would be first synthesised by SPPS, cleaved from the resin, purified and characterised then subsequently PEGylated (**Figure 4.3**). This has the main advantage that the peptides used for conjugation have much greater purity, typically > 95 %, thus yielding very well defined single-product conjugates. Furthermore, all of the PEG conjugates that have already received FDA approval were synthesised using this solution phase approach. As discussed in Chapter 3, the coiled-coil motif peptides developed here were synthesised with engineered N-terminal cysteine residues. This enabled the use of thiol-reactive mPEG derivatives to effect site-specific PEGylation. The mPEG-MAL derivative used to prepare Cimzia® was used in this study, though an mPEG of a lower molecular weight (c.a. 5,000 g mol^{-1}) was used. A nucleophilic addition reaction allows the thiol to react stoichiometrically with the δ^{+ve} carbon atom of the maleimide to yield a stable thioether linked conjugate (**Figure 4.4**). In these studies, the protocol used for solution-phase conjugation was adapted from a method described previously to conjugate mPEG-MAL to cysteine terminated poly(lysine) peptides (Chen *et al*, 2004). However, it was necessary to optimise the reaction conditions for the coiled-coil motifs and mPEG-MAL used here. This was achieved with the aid of a colorimetric assay to qualitatively determine the disappearance of free thiol with time.

4.1.1.3 Ellman's Assay for Free Thiols

The colorimetric assay commonly known as "Ellman's assay for free thiols" was originally designed to determine tissue R-SH concentrations (Ellman, 1959), however it has subsequently been used to analyse the R-SH concentration of proteins and peptides (Bulaj *et al*, 1998). Ellman's reagent (5,5'-dithiobis(2-nitrobenzoic acid) - DTNB) was designed to react in a stoichiometric manner with free R-SH to yield a 3-carboxylato-4-nitrothiophenolate anion with a UV-absorption maximum at 412 nm (**Figure 4.5**). Therefore it was postulated that a decrease in the optical density at this wavelength could be used here to measure the R-SH/MAL PEGylation. Once conjugates were prepared it was then necessary to consider the potential methods for purification.

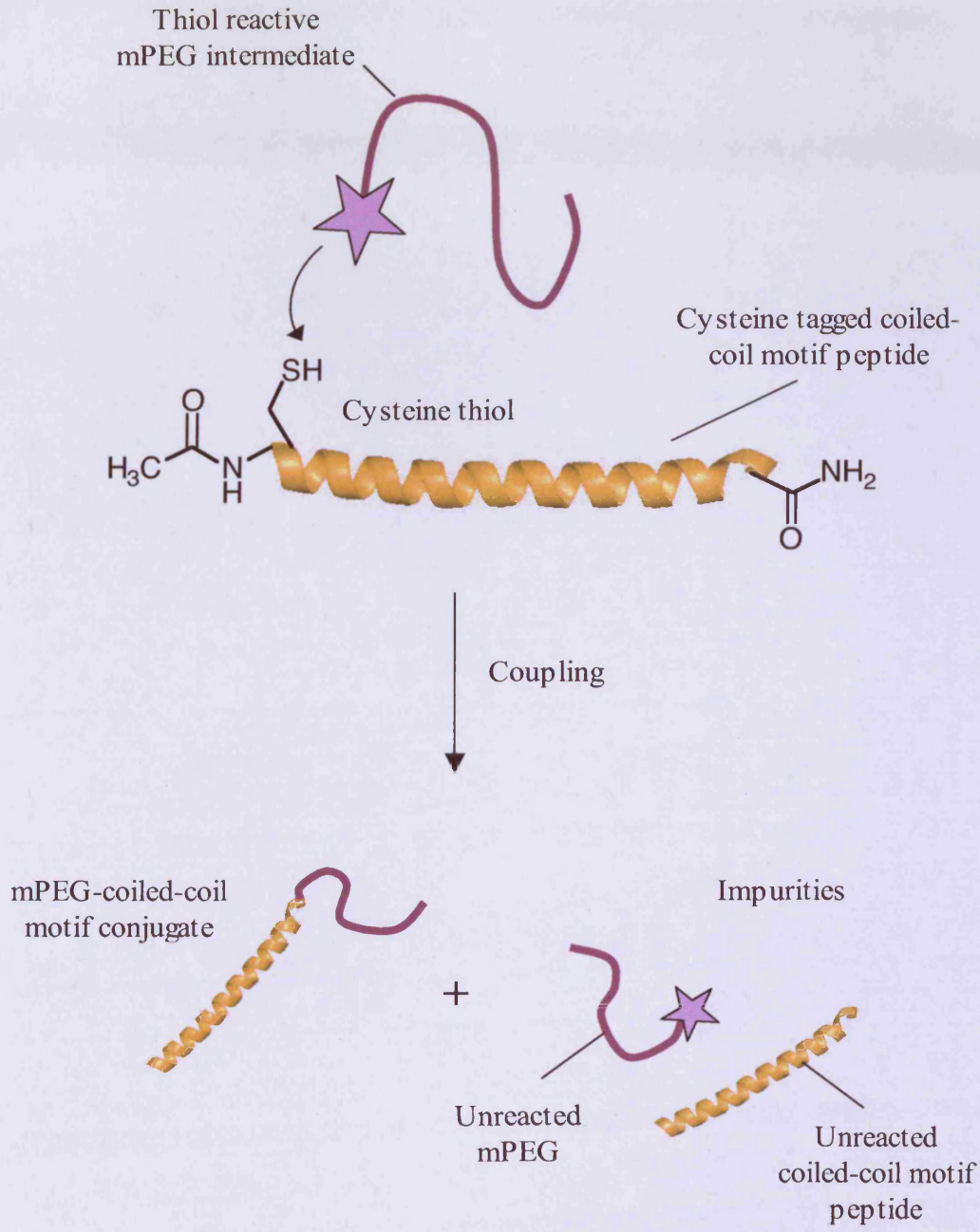

Figure 4.3 Proposed solution phase methodology for site-specific thiol-directed PEGylation.

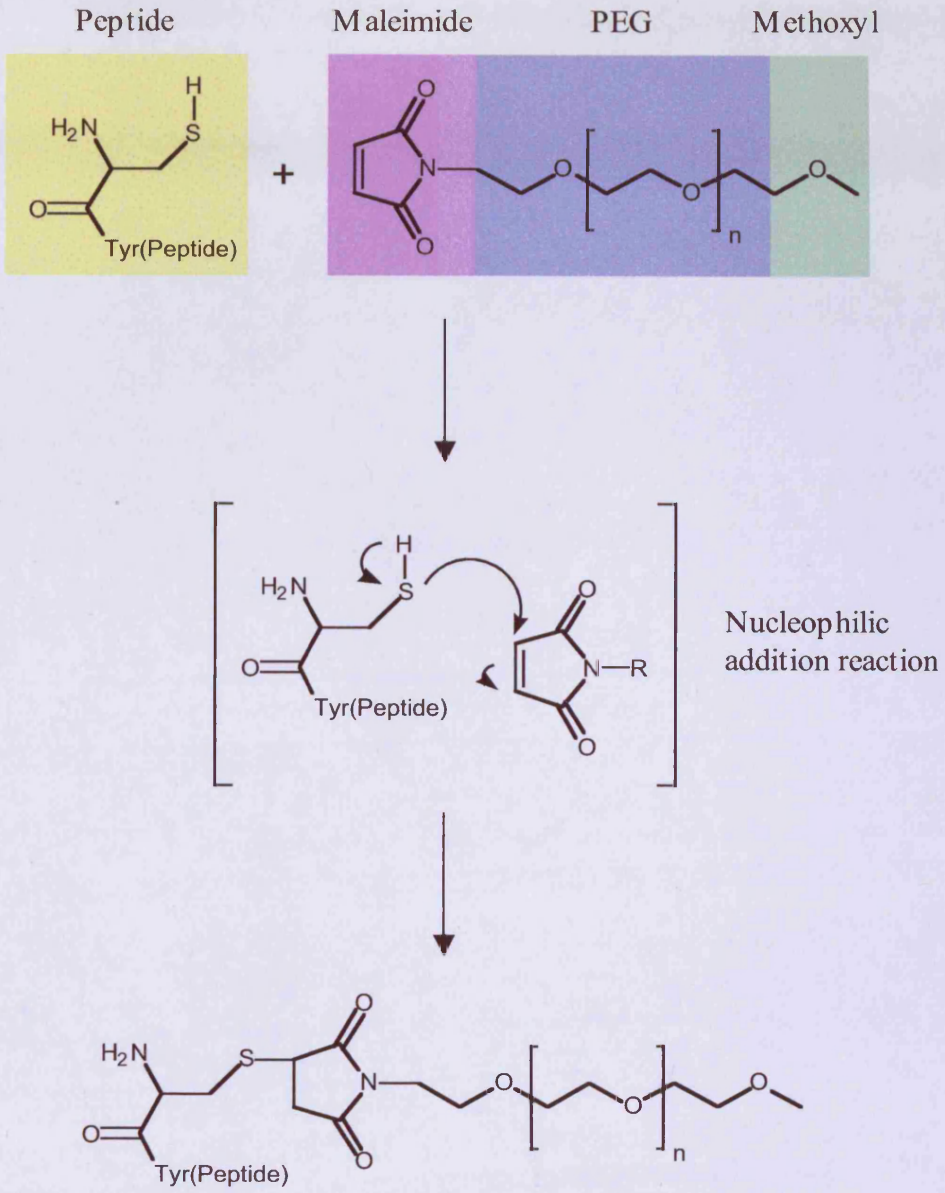

Figure 4.4 Thiol directed conjugation shown with mPEG-maleimide.

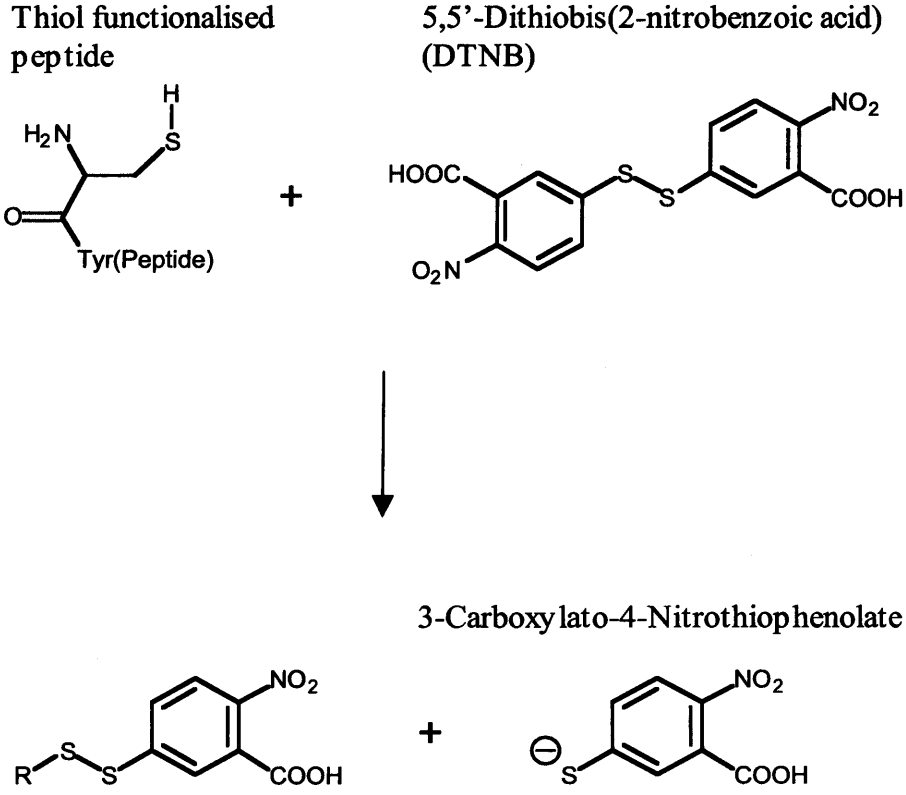

Figure 4.5 Reaction of Ellman's reagent with R-SH. Adapted from Ellman, (1959).

4.1.2 Assessment of the Methods for Conjugate Purification

The purification of PEG-peptide conjugates poses a number of challenges. For the solution-phase conjugate synthesis, it is necessary to resolve the product (i.e. mono-PEGylated-coiled-coil motif peptide) from both unreacted PEG and the free peptide. In the case of conjugate synthesis by the solid phase methodology, it was necessary to consider a method capable of resolving the desired product from any PEG-conjugated truncated peptides.

The three most commonly used methods of purifying polymer-peptide and polymer-protein conjugates are RP, SE and ion-exchange chromatography; the principles of each technique were discussed in Chapter 2 (**Figure 2.1**). Each of these approaches was investigated here with the aim of establishing a methodology that could be used to purify, and characterise with respect to purity, any of the mPEG-coiled-coil motif conjugates synthesised in this study.

4.1.3 Use of MALDI-TOF MS for mPEG-Coiled-Coil Motif Conjugate Characterisation

MALDI-TOF MS is one of the most important techniques used in polymer characterisation (reviewed in Hanton, 2001) and is frequently used to determine end-group functionality, absolute molecular weight and polydispersity (reviewed in Weidner *et al*, 1998; Nielen, 1999; Hanton, 2001). However, since different chain-lengths of polymer are likely to ionise with more or less ease, one must be extremely careful not to overstate the reliability of data pertaining to the polydispersity of the sample. For the same reason (and as for ESI-TOF MS discussed in Chapter 3) it is also inappropriate to attempt to quantify the acquired spectra and make assertions regarding the purity of the sample.

To conduct a MALDI-TOF analysis, the sample is first crystallised on a stainless steel plate (**Figure 4.6a**). Once loaded, effective ionisation of the sample matrix (**Figure 4.6b**) is key to the success of the experiment. The instrumentation used in this study enabled spectra to be acquired using either a reflectron or linear detector (**Figure 4.6c**). In theory the reflectron detector generates spectra of a higher resolution due to improved separation afforded by the electrostatic mirror. Nevertheless the technique is limited to analysis of samples with a molecular weight of $\leq$ 8,000 g mol^{-1}. A linear mode detector is capable of analysing samples of much higher molecular

(a) MALDI-TOF sample plate schematic

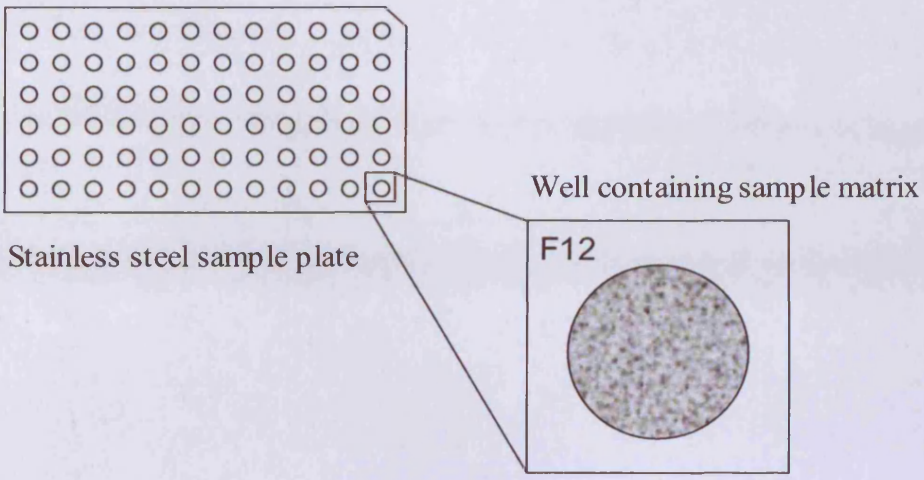

(b) Ionisation of sample matrix

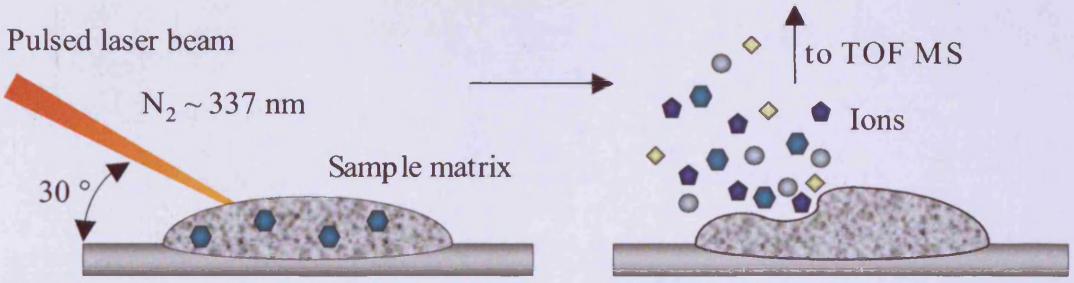

(c) Instrumentation schematic depicting ion flight in linear and reflectron modes

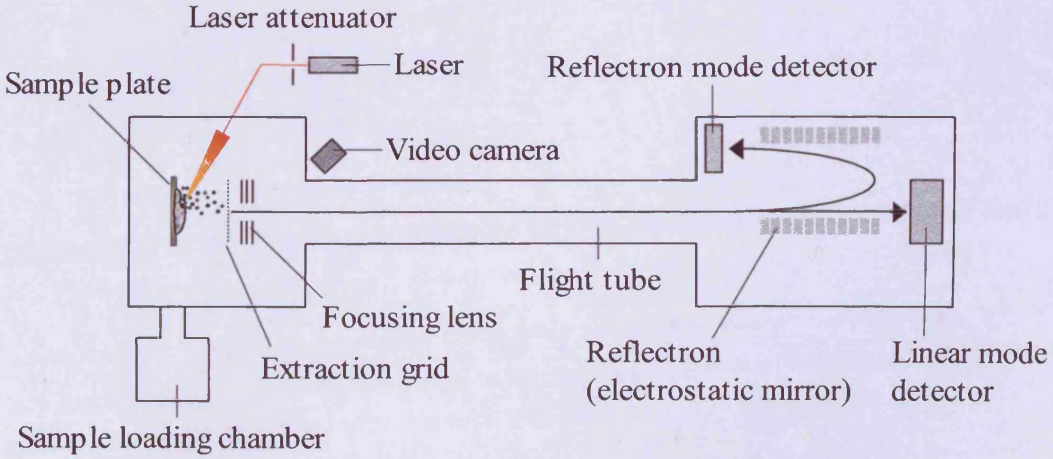

Figure 4.6 Characterisation by MALDI-TOF MS. Panel (a) shows the stainless steel plate upon which the samples were prepared. Panel (b) shows the ionisation of the crystalline sample matrix. Panel (c) shows a schematic of the MALDI-TOF MS equipment.

weight (theoretically up to 500,000 g mol^{-1}). Both modes were used in the course of this study.

The most challenging aspect of MALDI-TOF analysis is sample preparation. Of the numerous preparation methods that have been described in the literature (reviewed in Murgasova & Hercules, 2002; Pasch & Schrepp, 2003), the "dried droplet" and "thin layer" approaches are perhaps the most common. The dried droplet method requires pre-mixing of three solutions, typically analyte, salt and matrix. This mixture is then spotted onto the MALDI plate (**Figure 4.6a**) and dried under an air current (Chaudhary *et al*, 1996; Whittal *et al*, 1997; Rashidzadeh *et al*, 2000; McEwen & Peacock, 2002). The thin layer technique requires each of the solutions to be spotted onto the MALDI-plate separately and dried before application of the next layer. This approach has been widely used in the analysis of peptides and proteins (Dai *et al*, 1999; Garcia *et al*, 2002; Miliotis *et al*, 2002) as well as synthetic polymers (Linnemayr *et al*, 1998; Meier & Schubert, 2003). Meier and Schubert (2003) were the first to optimise a specific protocol for the analysis of PEGs up to 35,000 g mol^{-1}.

The thorough optimisation of the multi-layer technique described by Meier and Schubert (2003) formed the basis of the characterisation of the mPEG-coiled-coil motif conjugates described here. Meier and Schubert (2003) investigated and compared numerous combinations of analyte, salt and matrix and their order of application to the MALDI plate, with respect to "relative signal intensity" and "signal to noise ratio". Meier and Schubert (2003) demonstrated that:

"...the order of spotting the three layers (matrix, sample and doping salt) greatly influenced the quality of the obtained MALDI spectra"

They concluded that optimum order of application to the MALDI plate was first the matrix, then salt and finally PEG solution (Meier and Schubert, 2003). In particular, when using a matrix of dithranol saturated in chloroform ($CHCl_3$), a saturated salt solution of sodium iodide (NaI) in acetone and PEG dissolved in DCM (25 mg mL^{-1}) the relative signal intensity was twice that of the "dried droplet" preparation and the signal to noise ratio was markedly improved (Meier and Schubert, 2003). This methodology was a significant advance (compared with previously reviewed protocols Nielen, 1999; Hanton, 2001) since it enabled the acquisition of MALDI-TOF spectra for PEG up to 35,000 g mol^{-1}.

4.1.4 Use of 2D DOSY for mPEG-Coiled-Coil Motif Conjugate Characterisation

2D diffusion ordered spectroscopy (DOSY) is an NMR diffusion experiment that provides a method of separating compounds according to their differing diffusion coefficients. As the diffusion coefficient is proportional to the molecular size/hydrodynamic radius of the molecule (Barjat *et al*, 1995), this technique may be considered akin to chromatographic separation. However, unlike the techniques discussed in section 4.1.2, it is possible to conduct the DOSY analysis in almost any solvent and without need for the time-consuming optimisation of a chromatographic method. Moreover, it avoids the need for complex, and often empirical, sample preparation associated with characterisation by MALDI-TOF MS. The use of DOSY analysis for the characterisation of polymer therapeutics was first demonstrated with the model conjugate dextrin-trypsin (Duncan *et al*, 2008).

4.1.5 Experimental Aims

In summary, the specific aims for this study were to:

- To establish a methodology for the site-specific mono-PEGylation of the desired coiled-coil motif peptide sequences.

- To determine an optimal time for the solution phase reaction of mPEG-MAL with cysteine tagged coiled-coil motif-peptides using Ellman's assay to measure the disappearance of free thiols.

- To identify the optimal chromatographic technique to allow isolation of the synthesised conjugates to an acceptable level of purity ($\geq$ 95 %). In particular, to develop a method that would enable the removal of both unreacted mPEG and coiled-coil motif peptide.

- To develop and optimise a methodology for the characterisation of mPEG-coiled-coil motif conjugates by MALDI-TOF MS.

- To investigate the use of 2D DOSY for the characterisation of mPEG-coiled-coil motif conjugates.

4.2 Methods

The general methods, including UV spectroscopy (section 2.2.1.1), RP-HPLC (section 2.2.2) and SEC (section 2.2.2) used in this study are detailed in Chapter 2. For ease of navigation, an overview of the experiments conducted in this study is provided **(Figure 4.7)**

4.2.1 Synthesis of $Phb_{Y185-214}$-PEG and $EbVP35_{Y88-119}$-PEG Using Solid-Phase C-terminal PEGylation with TentaGel PAP Resin

Early studies investigated the potential of using a TentaGel resin to prepare the C-terminal conjugates $Phb_{Y185-214}$-PEG and $EbVP35_{Y88-119}$-PEG **(Figure 4.2)**.

The protocol used to prepare the conjugates was very similar to the one detailed in Chapter 3 (section 3.2.2) for the synthesis of peptides by Fmoc-SPPS. Instead of Rink Amide AM resin, TentaGel PAP resin (200 mg, PEG-NH_2 loading 0.24 mmol g^{-1}) was used as the solid phase. The resin was first swelled with DCM (1.5 mL), then the automated peptide synthesis protocol described in Chapter 3 (section 3.2.2.2) was used to synthesise $Phb_{Y185-214}$ and $EbVP35_{Y88-119}$ from the PEG-NH_2 of the TentaGel PAP resin. Acetylation of the N-terminal α-amines was conducted as previously described (section 3.2.2.2). Cleavage of the $Phb_{Y185-214}$-PEG and $EbVP35_{Y88-119}$-PEG conjugates from the resin and concomitantly side-chain deprotection were effected using cleavage cocktail "A" which consisted of TFA:TIPS:ddH_2O 96:2:2 v/v (3 mL). Each reaction was left to proceed for 3 h with vigorous agitation. The reaction mixtures were then transferred to glass round-bottomed flasks containing cold (-20 °C) Et_2O (c.a. 50 mL) using a fritted glass pipette to ensure the TentaGel PAP resin was left behind. The flasks were stored at -20 °C overnight (16 h) to allow the conjugates to precipitate. The supernatant was decanted and the precipitate washed two times with cold Et_2O after which the conjugates were suspended in ddH_2O and lyophilised. The lyophilisate was dissolved in ddH_2O containing 0.1 % v/v TFA and purification by RP-HPLC (as described for peptides in Chapter 3, section 3.2.3) was investigated.

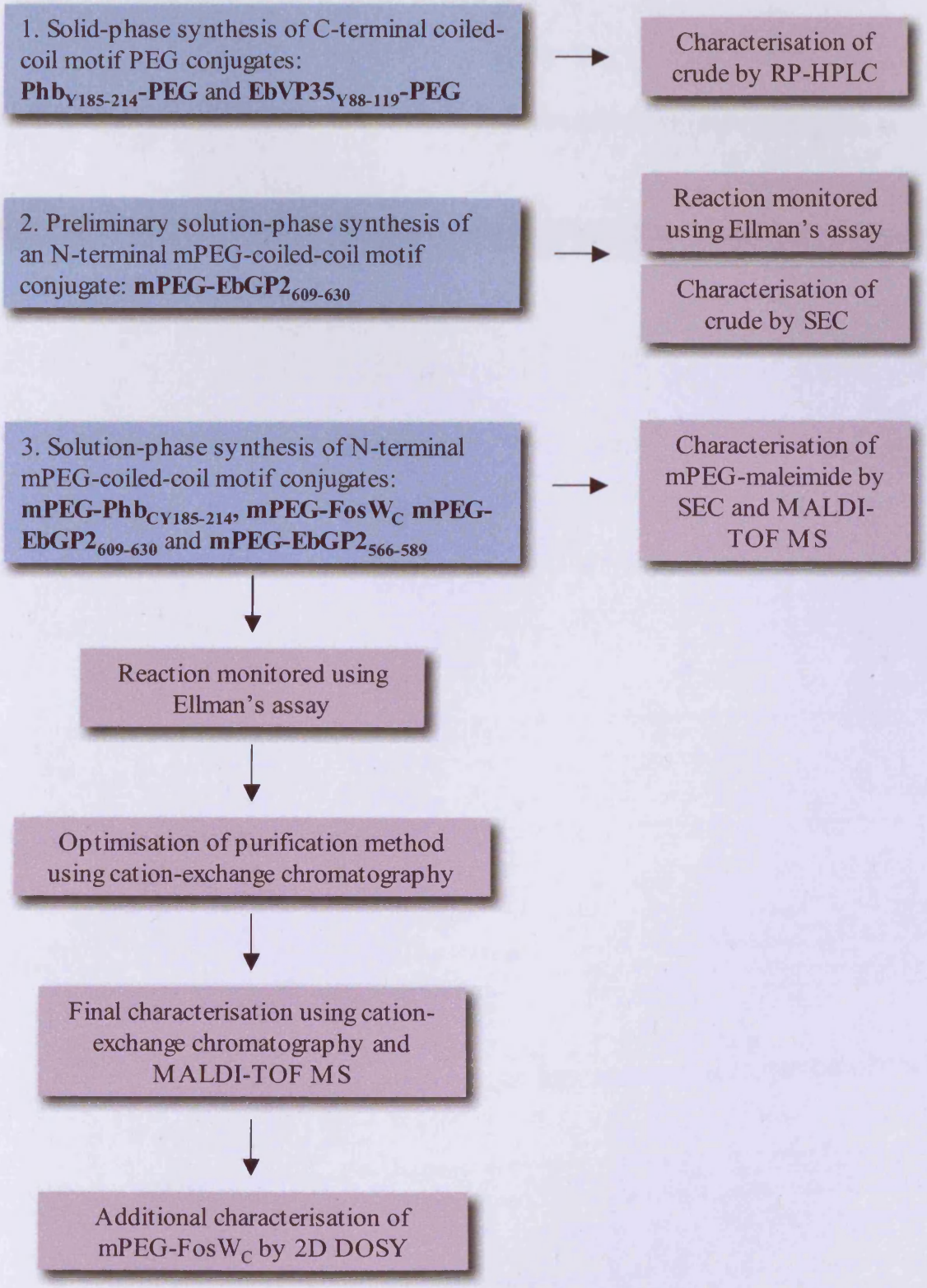

Figure 4.7 Overview of the experiments conducted in this study.

4.2.2 Synthesis of mPEG-Phb$_{CY185-214}$, mPEG-FosW$_C$, mPEG-EbGP2$_{609-630}$ and mPEG-EbGP2$_{CY566-589}$ Using Solution-Phase Thiol-Directed PEGylation

The second method of synthesising mPEG-coiled-coil motif conjugates employed a solution phase approach as illustrated in **Figure 4.3**. Whilst reactant quantities were varied, the ratios of each remained the same for each conjugation reaction. A summary of the quantities of each reactant is given for each synthesis in **Table 4.2**, whilst a typical method is described below.

Conjugates were prepared by reacting mPEG-MAL (Mn 5,520 g mol^{-1}, Mw/Mn 1.1) with peptide at a 1.5:1 molar ratio in phosphate buffer (10 mM, pH 7.0) for 2 h. Typically, peptide (3.7 μmol) was dissolved in 0.1 % v/v TFA (0.4 mL) and added to mPEG-MAL (5.5 μmol) dissolved in degassed phosphate buffer (1.6 mL) (adapted from Chen *et al*, 2004). Progress of the reaction was monitored using Ellman's (DTNB) reagent for free thiols as described below (section 4.2.3).

In a control study with mPEG-MAL and EbGP2$_{609-630}$, aliquots (25 μL) were taken at time points of 2 min, 1 h and 3 h and immediately frozen in liquid N_2 (- 196 °C). The study demonstrated that there was little change in the reaction after 1 h (see results) therefore, for all the other PEGylation reactions aliquots (25 μL) were taken at time points of 2 min and 2 h. At the end of the reaction the mixture was frozen in liquid N_2 and lyophilised prior to analysis and purification.

4.2.3 Ellman's Assay for Free Thiols

A stock solution of DTNB reagent consisting of sodium acetate (NaAc) (50 mM) and DTNB (2 mM) in ddH_2O was first prepared. Typically 5 mL of reagent was freshly prepared for each analysis. All samples were prepared directly in a quartz cuvette (1 cm pathlength) and mixed thoroughly as follows.

An aliquot (50 μL) of DTNB reagent was mixed with Tris buffer pH 8, 1 M (100 μL) and ddH_2O (840 μL) followed by the addition of sample (10 μL). After 5 min equilibration time, measurements of UV absorbance were made across a wavelength range of 600 to 200 nm for the trial synthesis of EbGP2$_{609-630}$, for subsequent reactions readings were acquired at 412 nm. All measurements were performed in duplicate, hence 25 μL of sample was collected at each time point during the PEG-MAL/thiol-peptide conjugation reaction as described above in section 4.2.2. Spectra were also recorded for each of the starting materials (peptide and mPEG-MAL) as positive and

Table 4.2 Summary of reactants and solvents used in the solution-phase synthesis of the four conjugates listed.

Conjugate name	Peptide			mPEG-maleimide		
	Mass (mg)	μMoles	0.1 % TFA (mL)	Mass (mg)	μMoles	Phosphate buffer, pH 7.0 (mL)
mPEG-EbGP2$_{609\text{-}630}$	50	18	1.0	152	28	4.0
mPEG-FosW$_C$	80	18	1.6	152	28	6.4
mPEG-Phb$_{CY185\text{-}214}$	25	7	0.5	56	10	2.0
mPEG-EbGP2$_{CY566\text{-}589}$	30	10	0.6	120	15	2.4

negative controls, respectively.

4.2.4 Purification of mPEG-Coiled-Coil Motif Conjugates by Cation-Exchange Chromatography

Cation-exchange chromatography was developed and optimised for each of the conjugates synthesised by varying the composition and pH of the elution buffers used (see results, section 4.3.2.3, **Table 4.3**). These changes were necessary since the iso-electric point of each of the peptides was different. Iso-electric points were calculated using the Innovagen peptide property calculator (http://www.innovagen.se/custom-peptide-synthesis/peptide-property-calculator/peptide-property-calculator.asp) (see results, section 4.3.2.3, **Table 4.3**).

The HPLC system was comprised of an ÄktaPrime™ unit equipped with a fixed wavelength detector (280 nm) and a pre-packed MacroCap SP cation-exchange column (5 mL). All solvent solutions were filtered (0.2 μm filter) then degassed (bath sonication) for 30 min prior to use. During storage the system was equilibrated with a solution of 20 % EtOH in ddH_2O. The unit was primed prior to each use by washing (flow rate = 5 mL min^{-1}) with 10 column volumes (50 mL) of ddH_2O, then 5 column volumes of buffer A (25 mL), 5 column volumes (25 mL) of buffer B, and finally 5 column volumes of A:B (50:50, 25 mL). A programmed method (running time = 15 min, 75 mL) was developed using a linear AB gradient (flow rate = 5 mL min^{-1}) to resolve each of the species in the crude reaction mixture (see **Figure 4.8**). Using this method it was expected that the unreacted mPEG-MAL would elute as the sample was injected onto the column and during wash phase 1. mPEG-coiled-coil motif conjugates were expected to elute as the % of buffer B was increased i.e. during phase (d) (see **Figure 4.8**). Before injection of the crude reaction mixture a blank run was conducted to ensure a stable baseline.

Prior to injection, the lyophilised samples of crude reaction mixture (see above, section 4.2.2) were first reconstituted in buffer A. A partial filling method of sample injection was used whereby buffer A (25 mL) was used to purge the injection loop (total volume 5 mL), followed by injection of sample, typically 2.5 mL. Fractions (1 mL) of eluate were collected and those corresponding to peaks of interest were collated and lyophilised to reduce the sample volume. Each sample of lyophilisate was desalted by centrifugation using a Centriprep YM-3 tube and spun for 45 min at 3,000 g. The supernatant was washed with ddH_2O and centrifuged a second time. This process of

Table 4.3 Summary of buffers required for purification, yield and molecular weights for the four conjugates synthesised.

Conjugate name	Iso-electric point	Buffer for cation-exchange chromatography			Yield		Estimated molecular weight[†]		Molecular weight by MALDI-TOF MS
		Salt	pH	Molarity	%	mg	Mn (g mol^{-1})	Mw (g mol^{-1})	m/z (±100)
mPEG-EbGP2$_{609\text{-}630}$	4.5	Citrate	3.2	20 mM	39	59	8,245	8,411	8,265
mPEG-FosW$_C$	4.2	Citrate	3.2	20 mM	38	68	9,881	10,047	9,890
mPEG-Phb$_{CY185\text{-}214}$	10.2	Phosphate	6.2	10 mM	52	30	9,156	9,322	~ 3,000 and ~5,900
mPEG-EbGP2$_{CY566\text{-}589}$	12.1	Phosphate	7.0	10 mM	29	24[#]	8,622	8,788	~ 3,000 and ~5,900

[†]Summed molecular weight of mPEG-maleimide (Mn = 5,520 g mol^{-1} and Mw = 5,688 g mol^{-1}) and respective peptide (Chapter 3, **Table 3.8**).

[#]Peak 1 fraction = 7 mg, peak 2 = 17 mg.

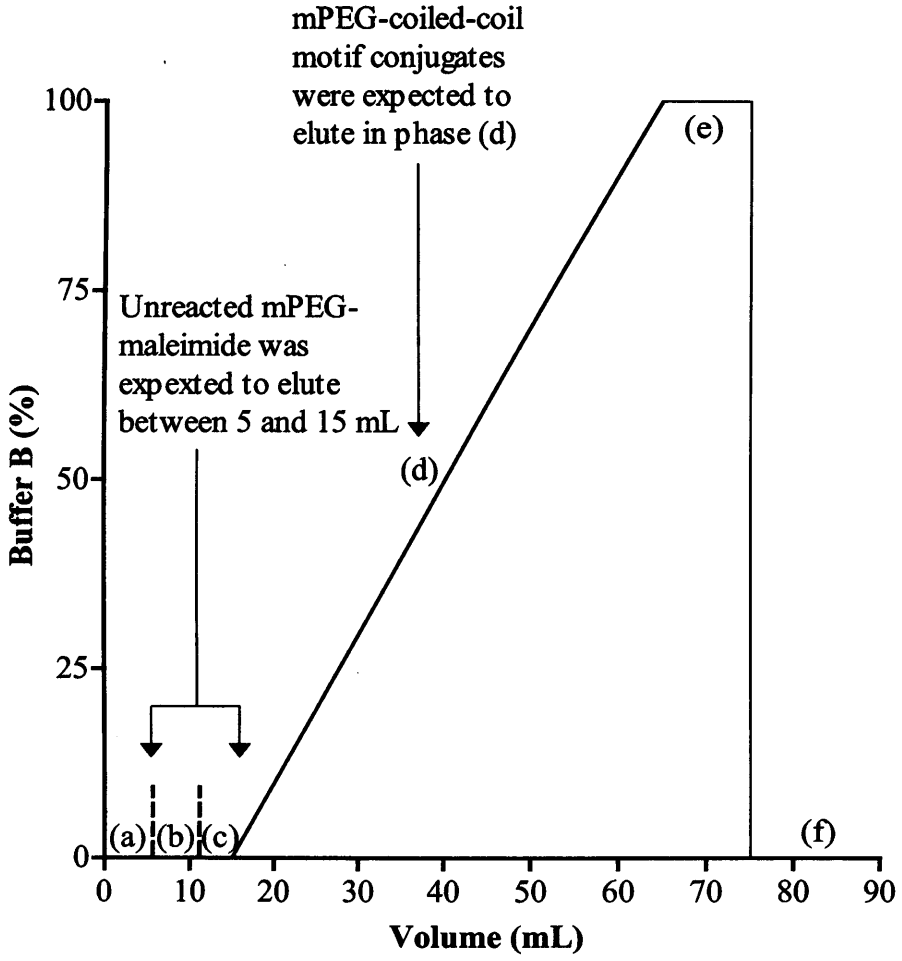

Figure 4.8 Gradient elution method used for cation-exchange chromatography purification and analysis of the mPEG-coiled-coil motif conjugates. The schematic illustrates each phase of the programmed method: (a) equilibration volume, (b) sample injection volume, (c) wash phase 1, (d) gradient elution 0-100 % B, (e) wash phase 2, and (f) re-equilibration.

washing and centrifugation was repeated a third time. The peptide concentration of the final product was determined by UV spectroscopy as described in Chapter 2 (section 2.2.1.1). Aliquots of each conjugate were stored at -80 °C.

4.2.5 MALDI-TOF MS Characterisation of mPEG-Coiled-Coil Motif Conjugates

Preliminary studies assessed both the "dried droplet" and thin layer methods of sample preparation, each approach was investigated using a range of different matricies, salts and solvents; a summary is provided in the results (section 4.3.2.3, **Table 4.4**). The optimised sample preparation method used in this study is described as follows.

Stock solutions (5 mL) of dithranol saturated (10 mg mL^{-1}) in $CHCl_3$ (matrix), and NaI (2 mg mL^{-1}) dissolved in ACN:ddH_2O (50:50) (salt) were first prepared. mPEG-MAL and/or conjugate solutions were freshly prepared by dissolving the sample (1 mg) in DCM (40 µL) to give a final concentration of 25 mg mL^{-1}. Aliquots (1 µL) of each solution were then applied to the MALDI plate and dried under an air current (approx. 1 min) before application of the next layer. The spotting order of the respective layers was first matrix then salt and finally sample. Data were acquired once the vacuum pressure had equilibrated to approximately 2 $x10^{-6}$. Spectra were acquired using the following input values: laser power = 250, pulse = 1400, detector = 2749 (max) and suppression = 1000. Data were exported as .xls files and processed using GraphPad Prism v4.0.

4.2.6 Characterisation of mPEG-FosW$_C$ Using 2D Diffusion-Ordered NMR Spectroscopy (DOSY)

Samples (500 µL) were prepared at a peptide concentration of 75 µM in NaH_2PO_4/Na_2HPO_4 (10 mM) containing NaF (100 mM) in ddH_2O containing D_2O (5 % v/v). Proton NMR spectra were acquired with 16 K complex points and a spectral width of 8.4 kHz. The total number of scans was 256, with a repetition delay of 1.5 s. A WATERGATE scheme was used to suppress the water signal. DOSY was performed with a stimulated echo sequence using bipolar gradient pulses (Brand *et al*, 2005) and with a WATERGATE scheme to suppress the water signal. The lengths of pulses and delays were held constant, and 20 spectra of 64 scans each were acquired with the strength of the diffusion gradient varying between 5 and 100 %. The lengths of the diffusion gradient and the stimulated echo were optimized for each sample. Typical

Table 4.4 Summary of attempts to acquire MALDI-TOF spectra of mPEG-coiled-coil motif conjugates

Matrix	Matrix solvent	Salt	Salt solvent	Analyte solvent and [analyte]	Method(s) of preparation	Spectra successfully acquired
α-Cyano-4-hydroxycinnamic acid (10 mg mL^{-1})	ddH_2O:ACN (1:1)	± silver trifluoroacetate (2 mg mL^{-1})	ddH_2O:ACN (1:1)	ddH_2O:ACN (1:1) (5 mg mL^{-1})	Thin layer and dried droplet	✘
Dithranol (10 mg mL^{-1})	$CHCl_3$	NaI (2 mg mL^{-1})	Acetone	DCM (25 mg mL^{-1})	Thin layer and dried droplet	✘
Dithranol (10 mg mL^{-1})	$CHCl_3$	NaI (2 mg mL^{-1})	ddH_2O:ACN (1:1)	DCM (25 mg mL^{-1})	Thin layer in specific order	✓
Dithranol (10 mg mL^{-1})	$CHCl_3$	NaI (2 mg mL^{-1})	ddH_2O:ACN (1:1)	DCM (25 mg mL^{-1})	Dried droplet	✘
DHB (10 mg mL^{-1})	DCM	-	n/a	THF (5 mg mL^{-1})	Thin layer and dried droplet	✘
DHB (10 mg mL^{-1})	DCM:THF	-	n/a	DCM:THF (5 mg mL^{-1})	Thin layer and dried droplet	✘
DHB (10 mg mL^{-1})	ddH_2O:EtOH (9:1)	± NaCl (2 mg mL^{-1})	ddH_2O	ddH_2O (5 mg mL^{-1})	Thin layer and dried droplet	✘

values were (δ) 4–5 ms and (Δ) 60–110 ms. Processing and analysis of the data were performed with the DOSY protocol included in the Topspin 1.3 software package.

4.3 Results

4.3.1 Preparation of C-terminal PEG Conjugates: $Phb_{Y185-214}$-PEG and $EbVP35_{Y88-119}$-PEG

It was not possible to solubilise the crude product from the synthesis of $EbVP35_{Y88-119}$-PEG. After precipitation in cold Et_2O it formed a very sticky off-white substance that could only be solubilsed with the addition of 100 % TFA. As for the attempted synthesis of the $EbVP35_{CY88-119}$ peptide it was not possible to characterise the crude product any further.

The crude product obtained from the synthesis of $Phb_{Y185-214}$-PEG was easily soluble in ddH_2O containing 0.1 % TFA and so initial characterisation was conducted using RP-HPLC. The RP-HPLC chromatograms obtained (**Figure 4.9**) following injection of the $Phb_{Y185-214}$-PEG crude reaction mixture (2 mL, 5 mg mL^{-1}) showed the presence of multiple peaks in the UV absorbance traces at 214, 274 and 257 nm. Post-initialisation (0-5 min) the first peaks eluted at 13.6 and 14.9 min, absorbing strongly at 214 nm, while lacking any absorbance at 257 and 274 nm. This suggested that these poorly resolved peaks corresponded to truncated peptide-PEG conjugates where the peptides were ≤ 14 residues in length (phenylalanine was positioned at residue 15). The largest peak in the trace at 257 nm eluted at 15.24 min, the low absorbance at 214 nm suggested this was a truncated peptide ≥ 15-residues, present in very small amounts relative to the other truncations. The peak with greatest intensity in the 214nm was next too elute (16.10 min), it is likely that this was again a truncated peptide ≥ 15-residues, it was not full-length since the absorbance of at 274 nm attributable to the N-terminal tyrosine was very low.

The peak that most likely corresponded to the full-length peptide-conjugate eluted at 22.89 min. A strong signal was detected at 274 nm (N-terminal tyrosine residue), this corresponded with a poorly resolved peak at 214 nm. However, no signal was detected in the 257 nm trace suggesting the possibility that phenylalanine was not present. The baseline continued to rise at 274 nm until the end of the run. Subsequent efforts to obtain a clean baseline trace by repeating the run without injecting any sample

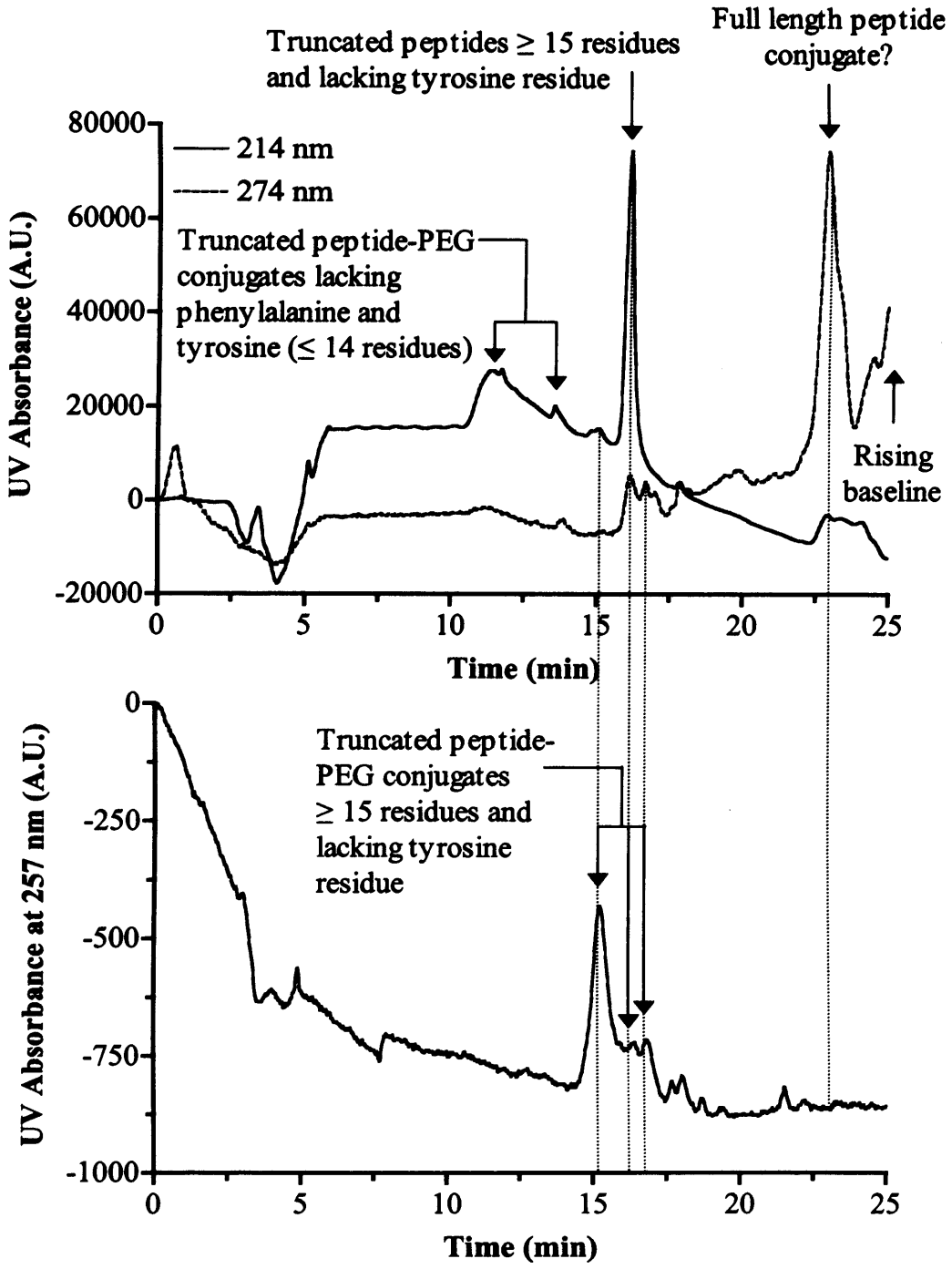

Figure 4.9 Characterisation of crude Phb-PEG by semi-preparative RP-HPLC. Panel (a) shows the absorbance at 274 and 214 nm. Panel (b) shows the absorbance of a second sample at 257 nm. Atlantis® dC_{18} OBD™ 5 µm, 30 x 150 mm column.

showed the presence of multiple peaks at 214 and 257 nm. This indicated that peptide-PEG conjugates were "adsorbing" or getting trapped in the column matrix and it took several attempts using high % ACN washes to clean the column. In light of these observations RP-HPLC was not used again in this study to purify PEGylated peptides for fear of damaging the columns used. Furthermore the study highlighted the difficulties in resolving truncated peptide-PEG conjugates that had high affinity for the C18 media of the RP column. Subsequent studies detailed here describe solution-phase synthesis of the mPEG-coiled-coil motif conjugates followed by the evaluation of size-exclusion and ion-exchange chromatography as alternative purification methods.

4.3.2 Preparation of N-terminal mPEG-Coiled-Coil Motif Conjugates Using mPEG-MAL

4.3.2.1 Characterisation of mPEG-MAL by SEC and MALDI-TOF MS

Prior to conjugation to each of the respective coiled-coil motif peptides it was necessary to characterise the commercial mPEG-MAL obtained with respect to molecular weight and purity. Using SEC, the mPEG-MAL obtained from NOF and Fluka eluted at approximately 17.6 and 17.7 mL, respectively (**Figure 4.10**). The Fluka product showed the presence of an additional broad, higher molecular weight "shoulder" (14.3-16.7 mL) and a second peak at 19.8 mL of much lower intensity, compared to the NOF product, which had a much cleaner trace. The latter showed good peak symmetry with no "shoulders" or other peaks in the chromatogram.

In these studies the Fluka product was only used in an early trial synthesis of mPEG-EbGP2$_{609\text{-}630}$. All other conjugates were prepared using the NOF mPEG-MAL due to its greater purity. Prior to the synthesis of these conjugates, further characterisation of the NOF mPEG-MAL was conducted using MALDI-TOF MS (**Figure 4.11**). Spectra were acquired in both reflectron (**Figure 4.11a**) and linear mode (**Figure 4.11b**) (data shown for m/z values of 4250 to 7250). No other peaks were detected between 1,000-10,000 m/z. The Gaussian distributions in both spectra were in good agreement, showed similar resolutions and signal to noise ratios, and as expected the interval between each peak corresponded an m/z of 44 (molecular weight of the PEG monomer). Moreover, assuming that z=1, the peaks of each Gaussian distribution were in excellent agreement with the Mw of 5688 g mol^{-1} (Mn = 5522 g mol^{-1}) determined by SEC (provided by NOF).

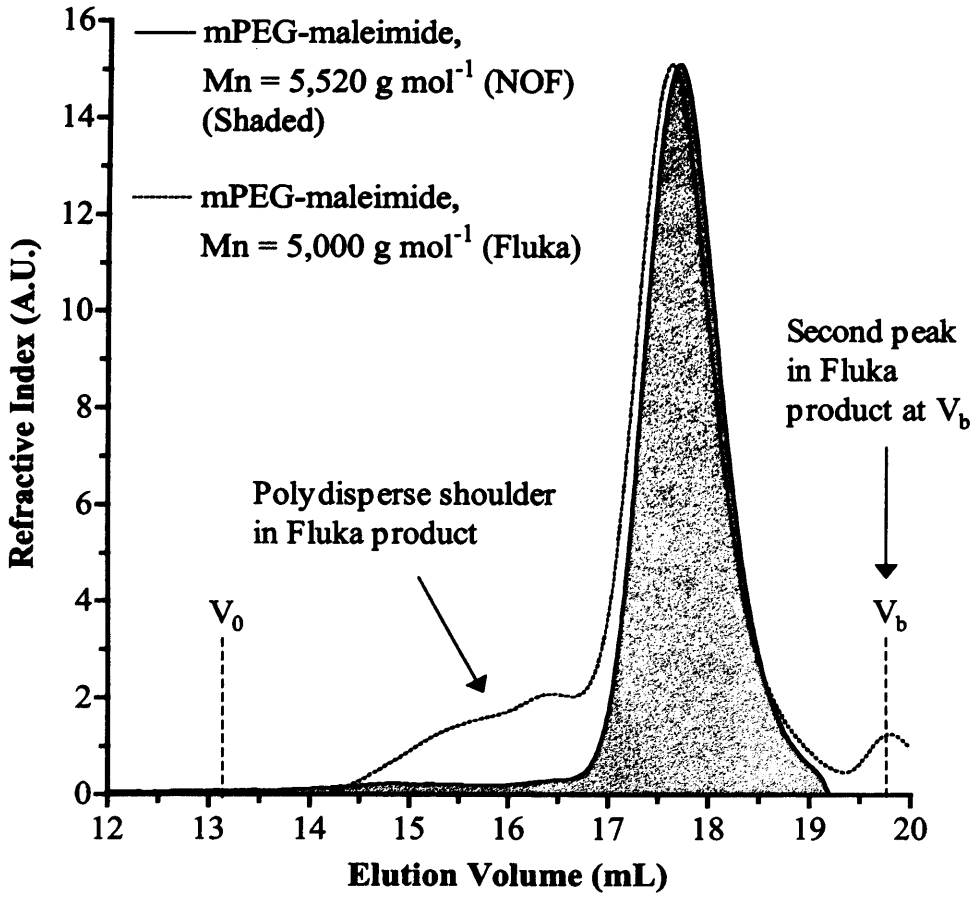

Figure 4.10 SEC characterisation of the NOF and Fluka mPEG-maleimide intermediates. Chromatogram was obtained using two TSK-gel SEC columns (G4000 and G3000 PWXL) in series. V_0 and V_b were 13.2 and 19.8 mL, respectively, mobile phase = PBS, pH 7.4 and flow rate = 1 mL min^{-1}.

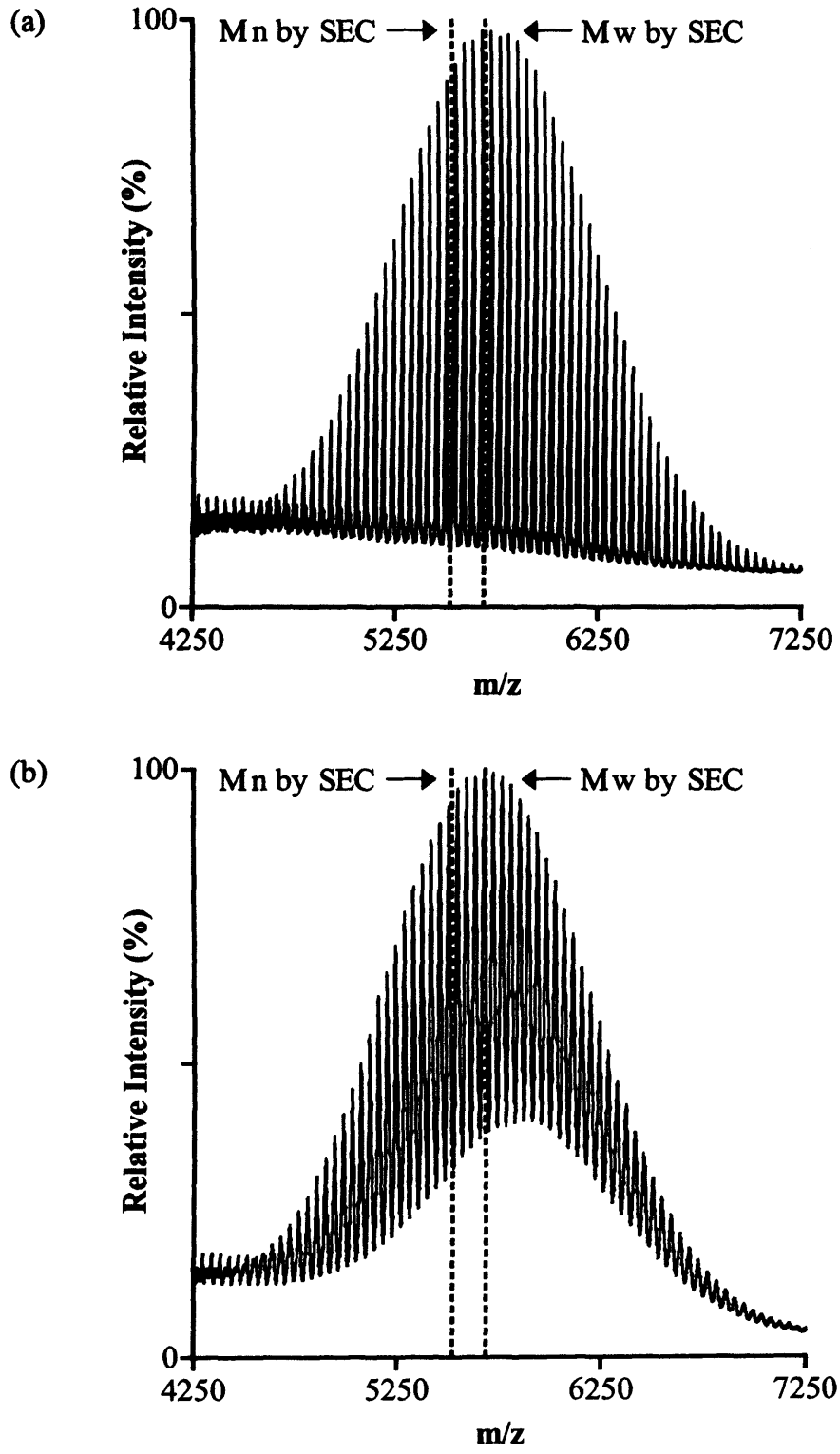

Figure 4.11 Characterisation by MALDI-TOF of the NOF mPEG-maleimide intermediate. Panel (a) reflectron mode, panel (b) linear mode. Dotted lines represent the Mn and Mw values of 5522 and 5688 g mol^{-1}, respectively, provided by NOF (determined by SEC).

4.3.2.2 Optimisation of Solution-Phase Synthesis Using mPEG- EbGP2$_{609-630}$

A preliminary synthesis of the mPEG-EbGP2$_{609-630}$ conjugate was conducted on a small scale to define the analytical techniques that could be used to (i) monitor progress of the reaction, (ii) identify the product(s) and (iii) confirm the product purity.

The UV spectrum for the EbGP2$_{609-630}$ peptide (positive) control showed a peak at 412 nm, which indicated the presence of free (reduced) R-SH (**Figure 4.12**). No signal was seen for the mPEG-MAL (negative) control, demonstrating that it did not interfere with the reduction of DTNB to the carboxylato-4-nitrothiophenolate anion. At t=2 min, an 83 % reduction was seen in the UV absorbance at 412 nm for the reaction mixture, there was only a very small further decreases at t=1 h (86 %) and t=3 h (91 %). This indicated that the nucleophilic addition reaction between mPEG-MAL and EbGP2$_{609-630}$ was almost complete after as little as 2 min. It was decided to use a reaction time of 2 h for all further reactions to allow for possible peptide-peptide variability.

SEC chromatograms of mPEG-MAL (Fluka) and the putative mPEG-EbGP2$_{609-630}$ conjugate (crude reaction mixture) showed similar profiles with only small differences in their elution volumes (**Figure 4.13**). However, the peak for the reaction mixture was broader, suggesting a more heterogeneous mixture as was expected.

The third observation was that the chromatograms showed marked differences in the relative intensities of the two peaks eluting at 19.83 mL and 21.10 mL. The bed volume (V_b) of the TSK-gel columns (G4000 PWXL and G3000 PWXL in series) was previously determined to be 19.8 mL, therefore it is difficult to speculate as to the exact identity of these peaks. They are either low molecular weight contaminants, present in the original mPEG-MAL product (since they appear in both traces) or artefacts resulting from dissolved gasses in the sample. The latter is perhaps more likely as similar peaks have been observed in previous chromatograms during the characterisation of entirely different samples. Nonetheless, the chromatograms suggest that either, (i) the synthesis of the conjugate mPEG-EbGP2$_{609-630}$ was not successful or, (ii) the resolution of the column set-up is not sufficient to distinguish mPEG-MAL from mPEG-EbGP2$_{609-630}$. Free peptide was too small to be characterised using this system.

When an alternative SEC column (Superdex HR 10/30) with a separation range of 3,000 to 70,000 g mol^{-1} (determined for globular proteins) was used, the mPEG-MAL intermediate displayed four peaks eluting at 7.5, 10.7, 13.1 and 19.4 mL (**Figure**

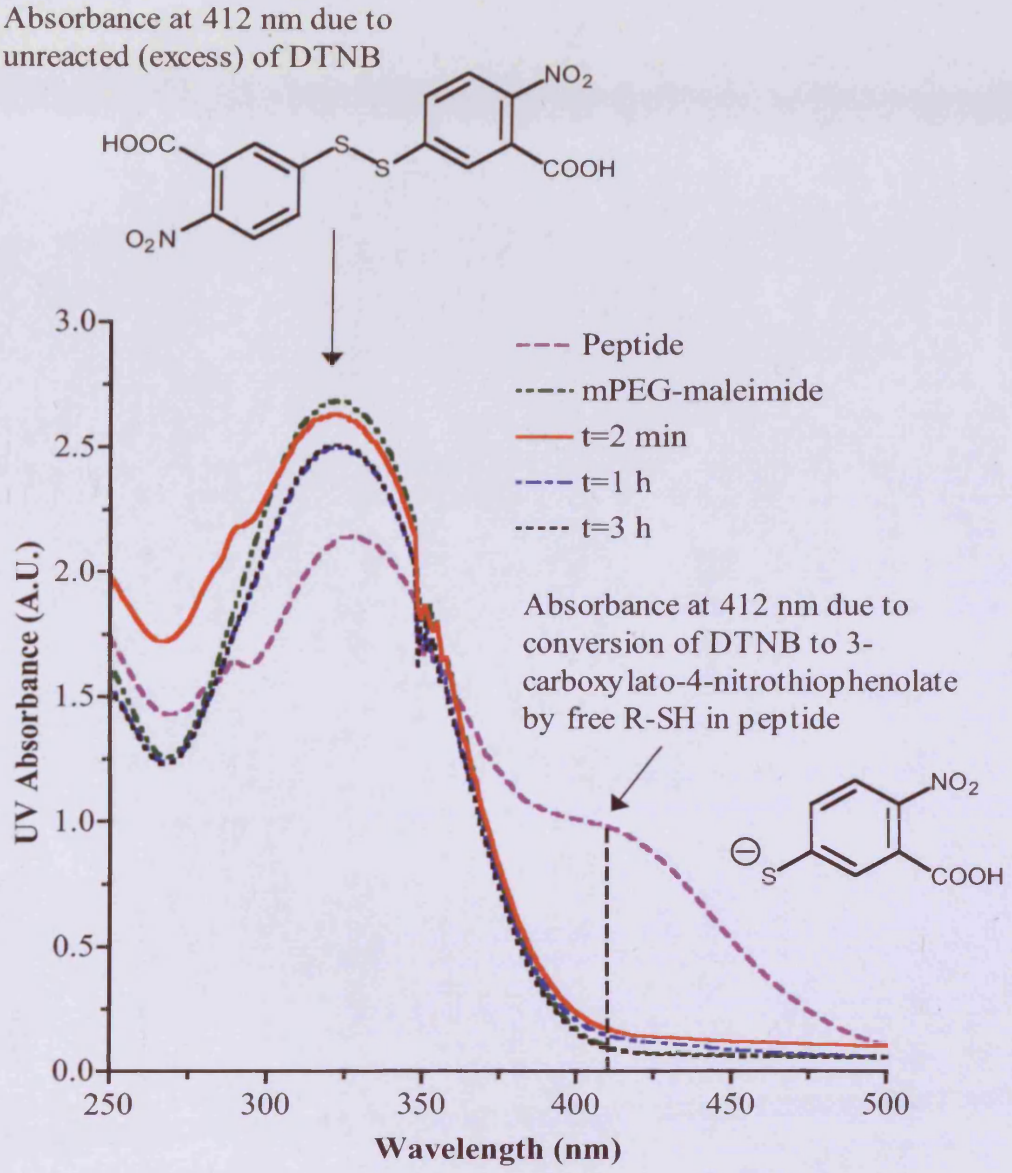

Figure 4.12 Rate of PEGylation of EbGP2$_{609-630}$ monitored by Ellman's assay.

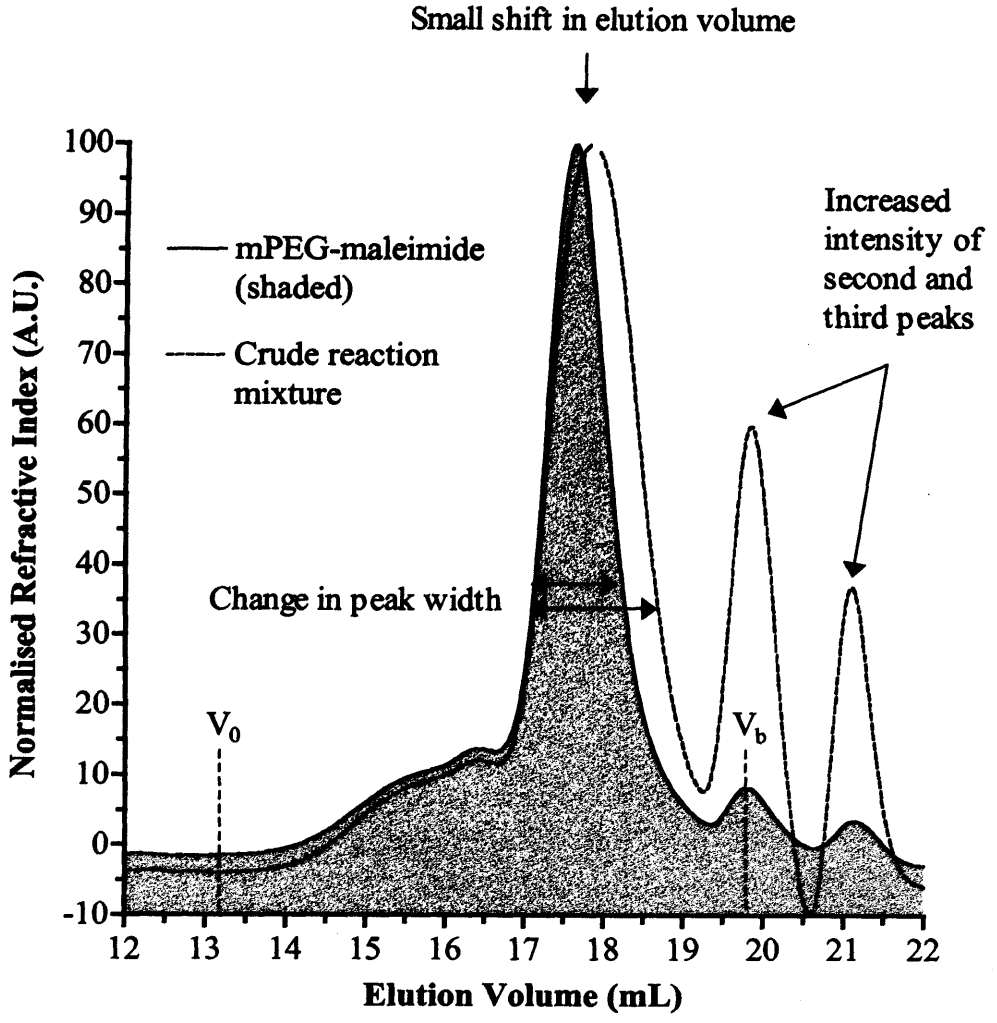

Figure 4.13 SEC (TSK-gel columns) characterisation of crude mPEG-EbGP2$_{609-630}$. Chromatogram was obtained using two TSK-gel SEC columns (G4000 and G3000 PWXL) in series. V_0 and V_b were 13.2 and 19.8 mL, respectively, mobile phase = PBS, pH 7.4 and flow rate = 1 mL min^{-1}.

4.14). The $EbGP2_{609\text{-}630}$ peptide produced a single peak at 15.7 mL and this was well resolved from all of the mPEG-MAL peaks. When the crude reaction mixture was analysed on this system it also showed four peaks (with very similar elution times) to those observed for the mPEG-MAL sample. However, almost no signal was observed at 15.7 mL (peak for free peptide) in the crude reaction mixture. This suggested that there was no free peptide left and so gave the first indication that the PEGylation reaction had been successful. Nonetheless, it was difficult to discern which peak corresponded to the conjugate as no new peaks (only different relative intensities) were seen in the reaction mixture compared with the mPEG-MAL intermediate.

Given these results, no further analyses were conducted using the reaction mixture from this preliminary synthesis due to the impure nature of the mPEG-MAL (Fluka) used for conjugation. A second batch of mPEG-$EbGP2_{609\text{-}630}$ and the synthesis of all the other conjugates (mPEG-$Phb_{CY185\text{-}214}$, mPEG-$FosW_C$ and mPEG-$EbGP2_{566\text{-}589}$) were conducted using the higher purity mPEG-MAL obtained from NOF.

4.3.2.3 Solution-Phase Synthesis of mPEG-$Phb_{CY185\text{-}214}$, mPEG-$FosW_C$ mPEG-$EbGP2_{609\text{-}630}$ and mPEG-$EbGP2_{566\text{-}589}$

In each instance, upon addition of the acidic peptide solution to the solution of mPEG-MAL in phosphate buffer the solution rapidly changed from slightly turbid to almost clear within a matter of seconds. If these observations indicated with progression of the nucleophilic addition reaction, they would corroborate the measurements of thiol content (Ellman's assay) and so suggest the very rapid PEGylation of the coiled-coil motifs.

Optimisation of Cation-Exchange Chromatography for Purification of the Crude Reaction Mixtures

Due to the difficulties explained above (section 4.3.2.2) with SEC, an alternative approach using cation-exchange chromatography was developed to characterise the putative mPEG-coiled-coil motif conjugates.

The blank injection run conducted before sample injection showed the stable baseline of the UV (280 nm) detector and increase in conductivity (**Figure 4.15a**). There was a small lag between the increase in % of buffer B and the measured conductivity; this was typical of runs with this method. mPEG-MAL was shown to elute as a single peak in the wash phase of the method (c.a. 7 mL), with no adsorption to

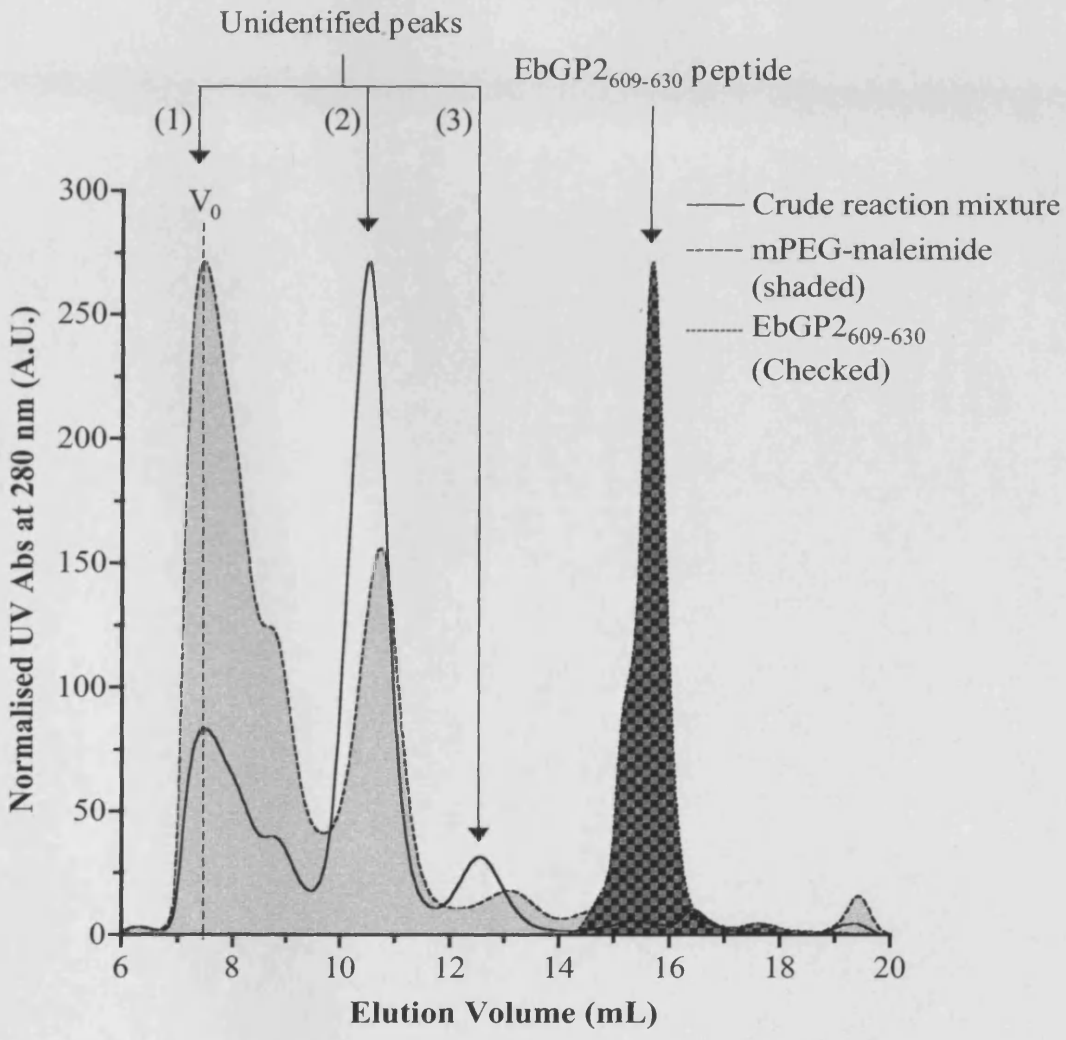

Figure 4.14 SEC (Superdex HR 10/30 column) characterisation of crude mPEG-EbGP2$_{609-630}$. V_0 and V_b were 7.5 and 24.0 mL, respectively, mobile phase = PBS, pH 7.4 and flow rate = 1 mL min^{-1}.

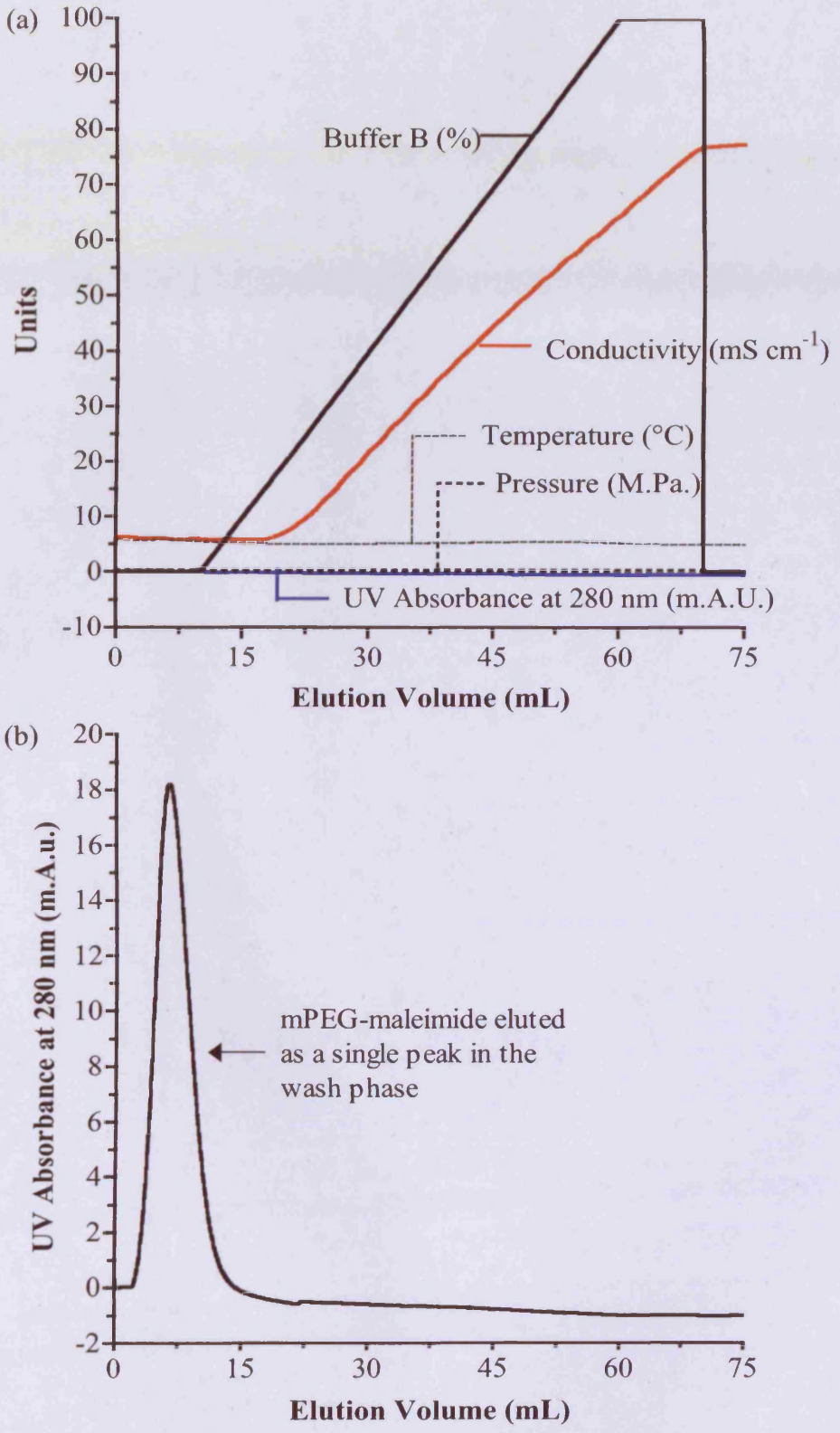

Figure 4.15 Optimisation of conditions for cation-exchange chromatography characterisation. Panel (a) shows a typical "blank" injection (buffer A) profile. Panel (b) shows the elution profile of mPEG-maleimide (citrate buffer, 200 mM, pH 3.2)

the column media (**Figure 4.15b**). This example shows the elution using a 200 mM citrate buffer, however, no change in the elution profile of mPEG-MAL was observed for any of the buffers (or molarities) used in this study.

Synthesis and Characterisation of mPEG-EBGP2$_{609-630}$

Analysis by Ellman's assay showed that the % free thiol in the reaction mixture had decreased by 94 % after 2 h, in line with the observation made for the previous trial syntheis of mPEG-EbGP2$_{609-630}$. The iso-electric point of the peptide EbGP2$_{609-630}$ was estimated to be 4.5, therefore a citrate buffer (pH 3.2) was used for purification and analysis (**Table 4.3**). First studies were conducted to characterise the elution profile of the free peptide EbGP2$_{609-630}$ to ensure that it would bind to the column and elute in the gradient phase. Very little binding was seen when a 200 mM buffer was used (**Figure 4.16a**), this indicated that the ionic strength of the mobile phase was too high. The chromatogram obtained using a 50 mM buffer showed that the amount of peptide binding to the column and eluting in the gradient phase increased with a corresponding decrease in the area of the peak in the wash phase (**Figure 4.16b**). Optimal conditions were found using a 20 mM citrate buffer (**Table 4.3**) with less than 5 % of the peptide eluting in the wash phase (**Figure 4.16c**). Some of this peptide may have been truncated peptide lacking the charged residues necessary for binding to the column.

A typical elution profile of the crude reaction mixture is shown in **Figure 4.17** along with an overlaid chromatogram obtained from injection of the EbGP2$_{609-630}$ peptide alone. The crude reaction mixture showed three peaks: P1 (7.6 mL), P2 (25.7 mL) and P3 (34.6 mL). P1 eluted in the wash phase whereas P2 and P3 eluted with increasing NaCl concentration as shown by the measure of conductivity (red). P3 eluted at the same volume as the EbGP2$_{609-630}$ peptide, suggesting that this was a small amount of unreacted EbGP2$_{609-630}$ peptide present in the reaction mixture. mPEG-MAL was previously shown to elute in the wash phase. Therefore, as only three species were predicted (**Figure 4.2**) to be present in the crude reaction mixture, it was likely that P2 represented the mPEG-EbGP2$_{609-630}$ conjugate. Fractions corresponding to P2 were collected, desalted and the concentration determined by UV spectroscopy such that the mass and % yields could be calculated (**Table 4.3**).

The purity of the mPEG-EBGP2$_{609-630}$ conjugate isolated in this way was assessed using the same method of cation-exchange chromatograpy and a single peak was observed with an elution volume of 25.3 mL (**Figure 4.18a**). The molecular

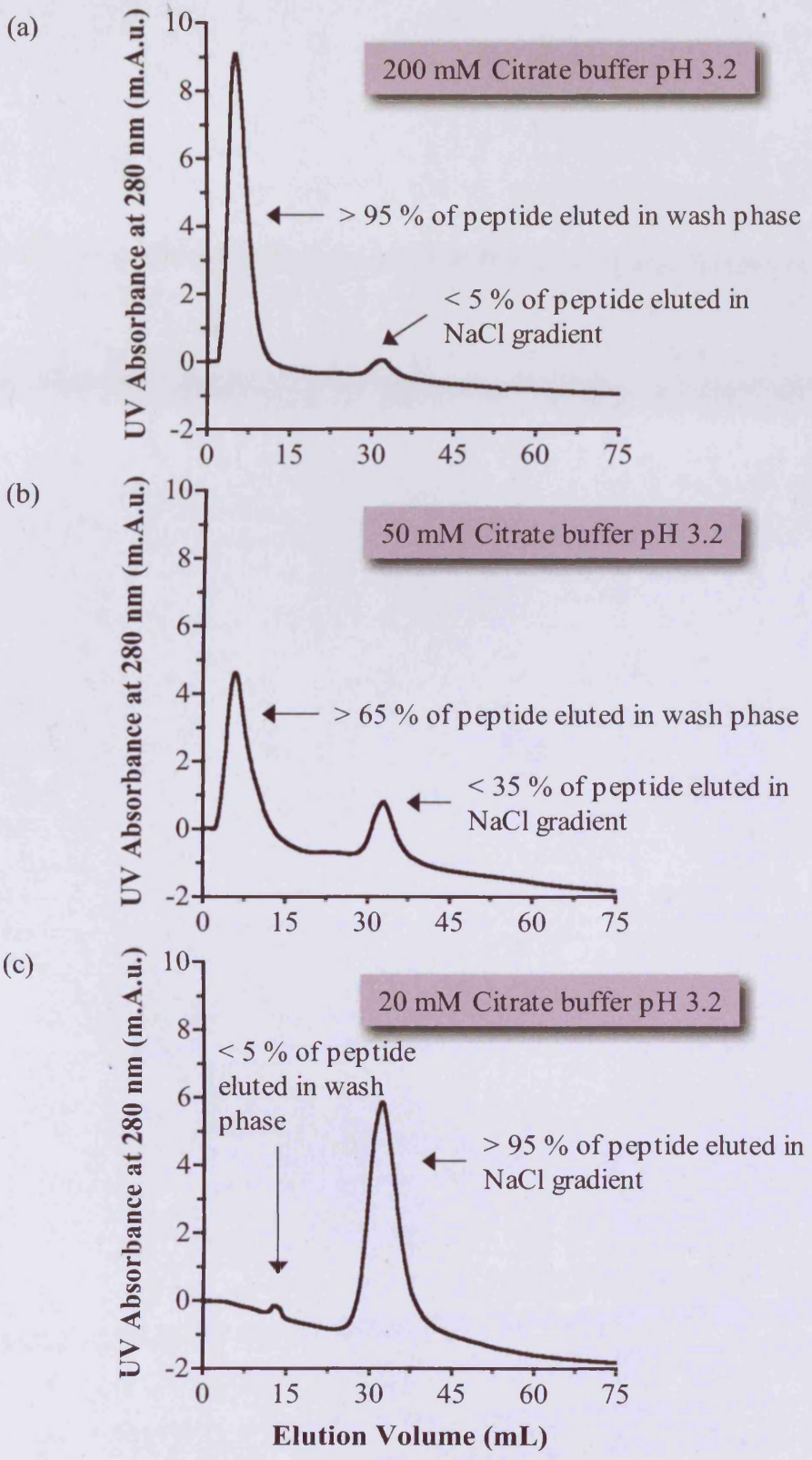

Figure 4.16 Characterisation by cation-exchange chromatography of the peptide EbGP2$_{609-630}$ with decreasing buffer molarity.

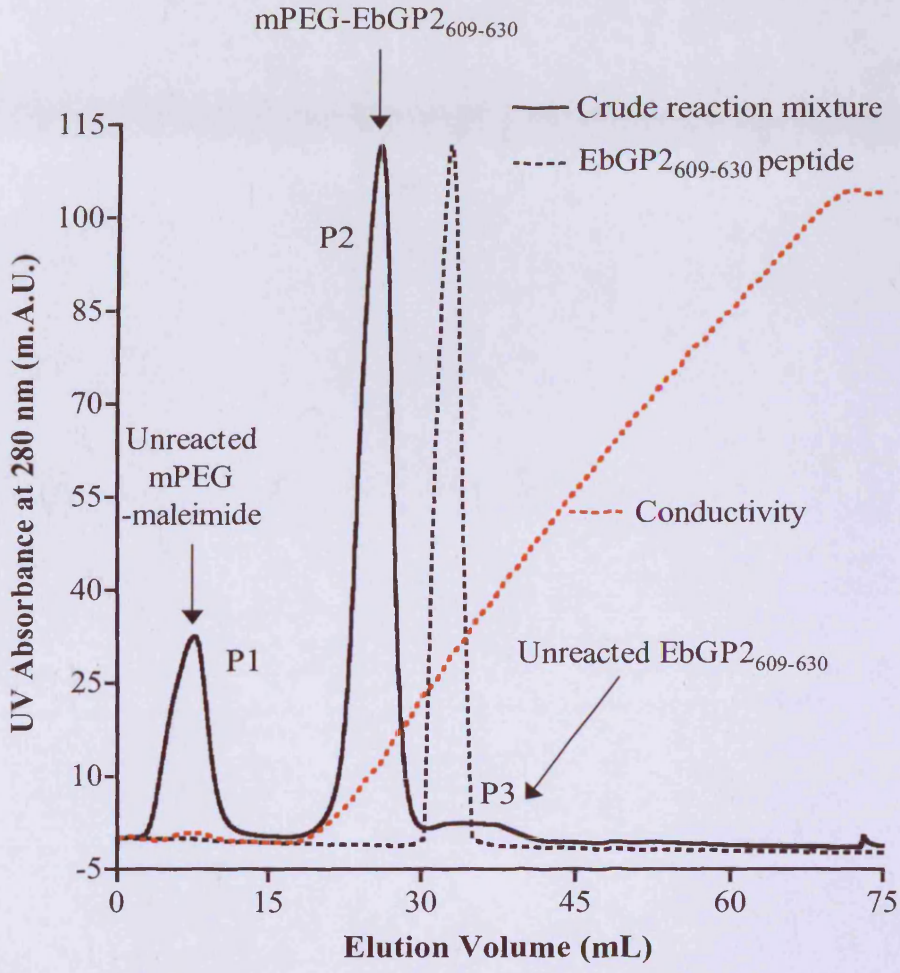

Figure 4.17 Purification of mPEG-EbGP2$_{609-630}$ by cation-exchange chromatography (MacroCap SP). Solid line shows the typical elution profile of the crude reaction mixture. Dashed line shows the overlaid elution profile of the RP-HPLC pure EbGP2$_{609-630}$ peptide. Conductivity (mS cm^{-1}) as a measure of increasing NaCl is shown in red (dotted line).

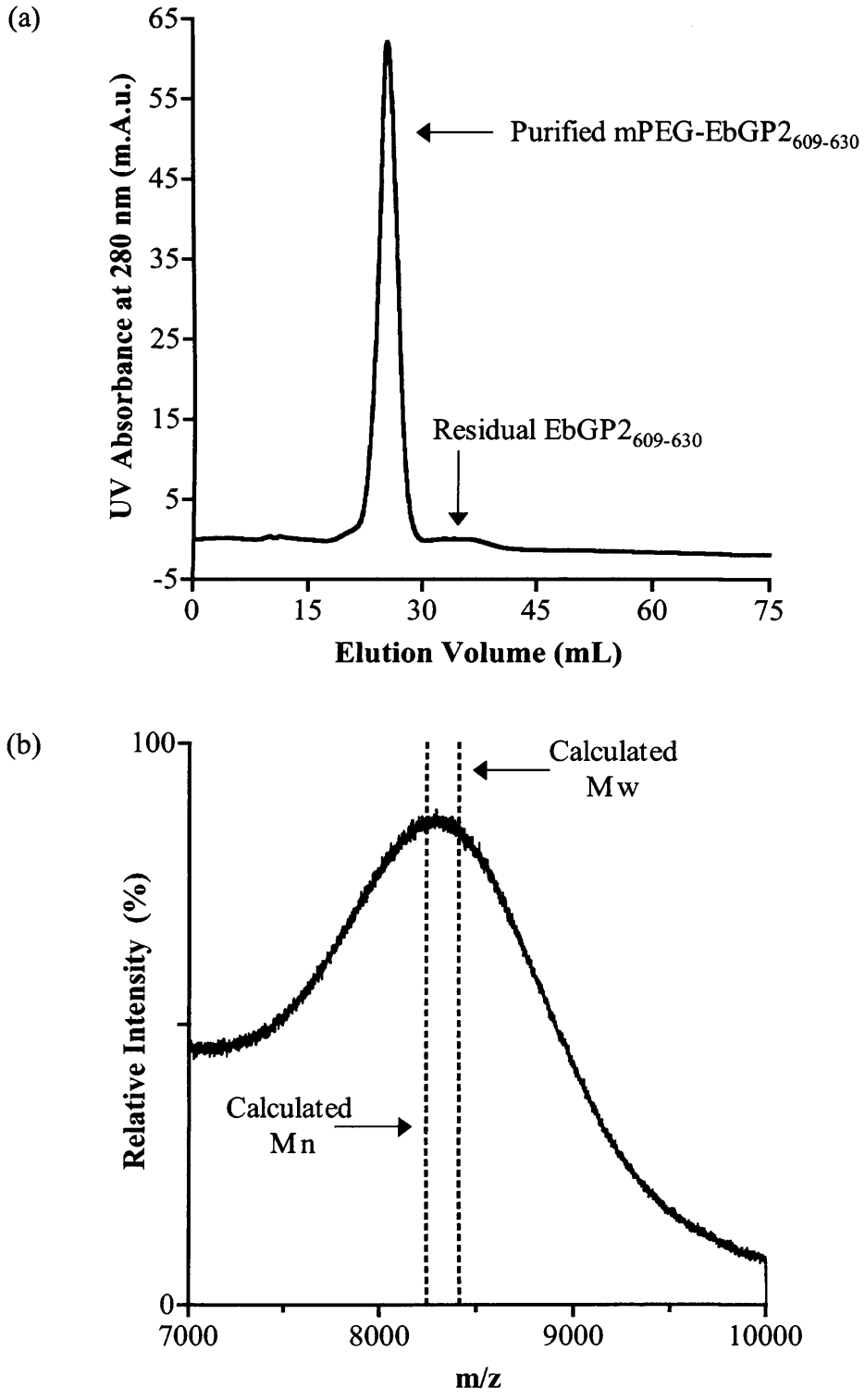

Figure 4.18 Characterisation of purified mPEG-EbGP2$_{609-630}$ by cation-exchange chromatography and MALDI-TOF MS. Panel (a) shows the analysis of purified and desalted mPEG-EbGP2$_{609-630}$ by cation-exchange chromatography (MacroCap SP). Panel (b) shows the MALDI-TOF mass spectrum acquired for the same sample, the dotted lines show the expected Mw and Mn of the mPEG-EbGP2$_{609-630}$ conjugate.

weight of this peak was determined using MALDI-TOF MS (**Figure 4.18b**). The mass spectrum showed a peak that was in good agreement with the theoretical Mn and Mw (8,245 g mol^{-1} and 8,411 g mol^{-1}, respectively - represented by the dotted lines) calculated for the conjugate. It took a considerable effort to optimise the sample preparation parameters for the acquisition of the MALDI-TOF mass spectrum as many approaches failed (**Figure 4.18b**). The matricies, salts and solvents along with the methods of preparation that were investigated during the course of this study are summarised in **Table 4.4**.

Synthesis and Characterisation of mPEG-FosW_C

Analysis by Ellman's assay showed that the % free thiol in the reaction mixture had decreased by 92 % after 2 h. This was comparable to that seen for the previous reactions. The same cation-exchange chromatography protocol was used for purification, and since the iso-electric point of the FosW_C peptide was estimated to be 4.2 the same citrate buffer (20 mM, pH 3.2) was used as the mobile phase (**Table 4.3**). A typical elution profile of the crude reaction mixture is shown in **Figure 4.19** along with an overlaid chromatogram obtained from injection of the FosW_C peptide alone. The crude reaction mixture displayed three peaks: P1 (5.6 mL), P2 (32.9 mL) and P3 (54.6 mL). P1 eluted in the wash phase whereas P2 and P3 elute with increasing NaCl concentration as shown by the measure of conductivity (red). The elution volume of P3 (54.6 mL) corresponded reasonably well with the single peak of the RP-HPLC pure FosW_C peptide (51.1 mL). This suggested that P3 was unreacted FosW_C peptide and P1 as discussed above (section 4.3.2.3) was unreacted mPEG-MAL. P2, which had a broad elution profile with two shoulders, one before the main peak at 28.2 mL and the second at 38.2 mL was assumed to be the mPEG-FosW_C conjugate. As before, fractions corresponding to P2 were collected, desalted and the concentration determined by UV spectroscopy such that the mass and % yields could be calculated (**Table 4.3**).

The purity of the mPEG-FosW_C conjugate isolated in this way was assessed using the same method of cation-exchange chromatograpy and a single peak was observed with an elution volume of 32.7 mL (**Figure 4.20a**). Characterisation by MALDI-TOF MS (**Figure 4.20b**) confirmed that this peak was of the correct expected mass as the spectrum showed a peak that was in good agreement with the theoretical Mn and Mw (9,881 g mol^{-1} and 10,047 g mol^{-1}, respectively - represented by the dotted lines) for the conjugate.

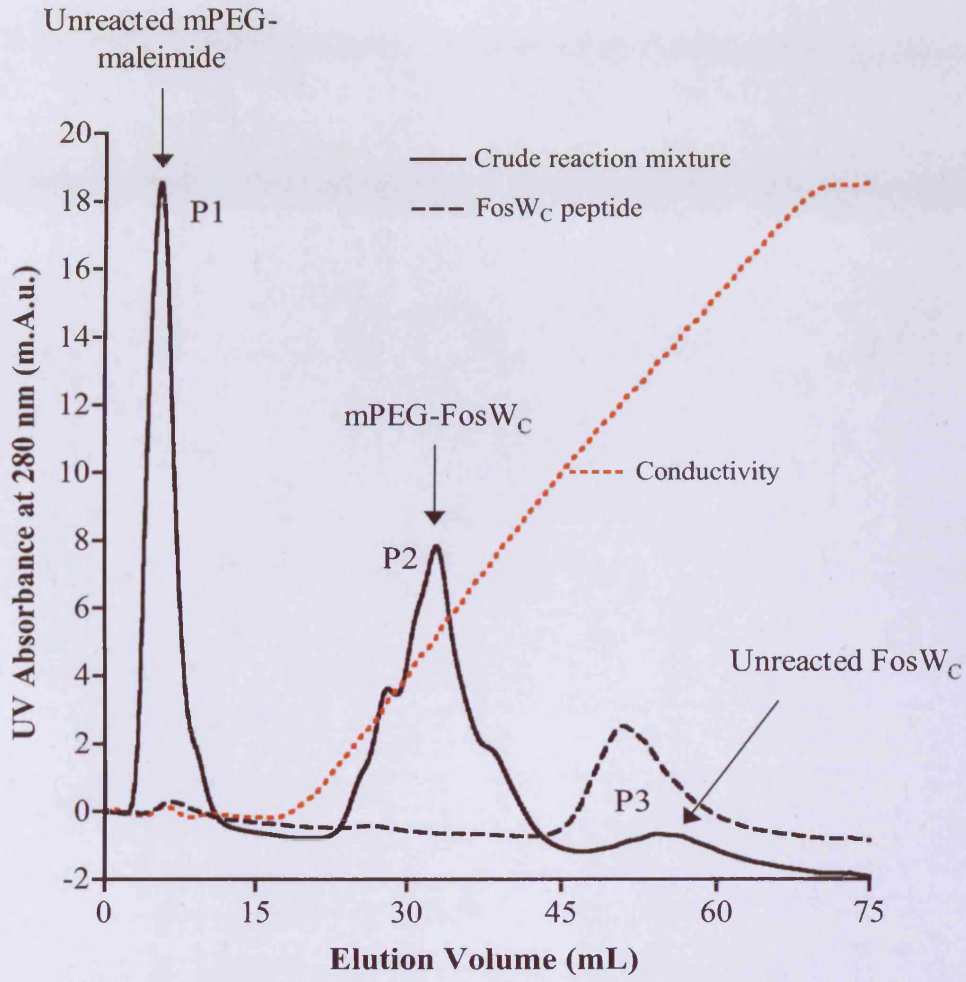

Figure 4.19 Purification of mPEG-FosW$_C$ by cation-exchange chromatography (MacroCap SP). Solid line shows the typical elution profile of the crude reaction mixture. Dashed line shows the overlaid elution profile of the RP-HPLC pure FosW$_C$ peptide. Conductivity (mS cm^{-1}) as a measure of increasing NaCl is shown in red (dotted line).

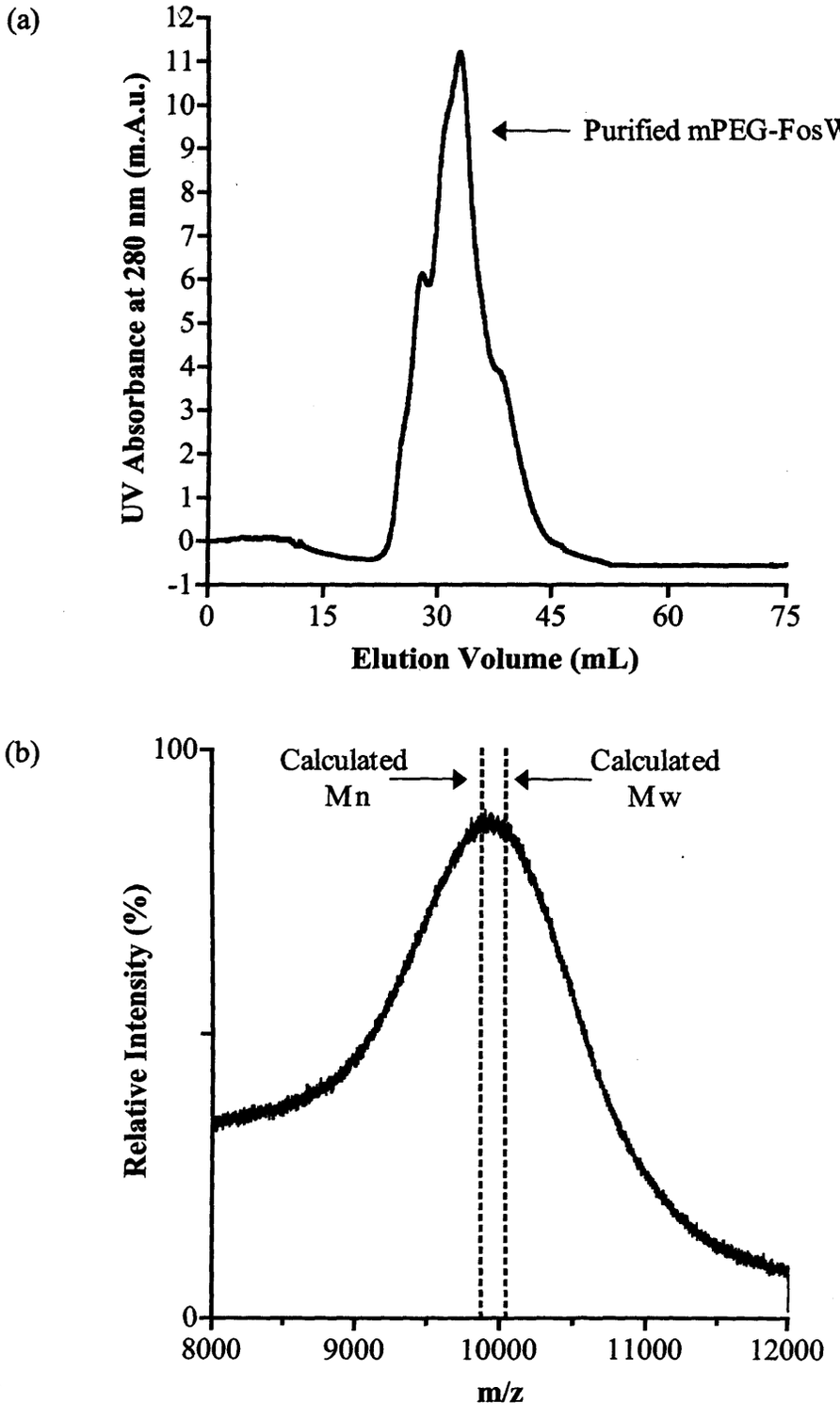

Figure 4.20 Characterisation of purified mPEG-FosW$_C$ by cation-exchange chromatography and MALDI-TOF MS. Panel (a) shows the analysis of purified and desalted mPEG-FosW$_C$ by cation exchange chromatography (MacroCap SP). Panel (b) shows the MALDI-TOF mass spectrum acquired for the same sample, the dotted lines show the expected Mw and Mn of the mPEG-FosW$_C$ conjugate.

Further characterisation by 2D DOSY showed that the mPEG-FosW_C conjugate had a higher diffusion coefficient than either mPEG-MAL or FosW_C peptide (**Figure 4.21**). This confirmed that the conjugate had a larger molecular size/hydrodynamic volume. Furthermore, no free mPEG-MAL or FosW_C peptide was detected in the mPEG-FosW_C conjugate sample, corroborating the assessment of purity made by cation-exchange chromatography. The DOSY analysis also showed the presence of a small, low molecular weight contaminant (2.3 and 2.4 ppm on F1 axis) in the purified mPEG-FosW_C conjugate sample. This is likely to be citric acid, which suggested that the desalting protocol used post-purification could be improved.

Synthesis and Characterisation of mPEG-Phb$_{CY185-214}$

Analysis by Ellman's assay showed that the % free thiol in the reaction mixture had decreased by 97 % after 2 h, this was a slightly bigger decrease than seen previously. The same cation-exchange chromatography protocol was used as for the purification of the previous conjugates, with one alteration. Since the iso-electric point of the Phb$_{CY185-214}$ peptide was estimated to be 10.2, a phosphate buffer pH 6.2 was used as the mobile phase (**Table 4.3**). Initially a 50 mM buffer was used, however the chromatogram showed only a single peak in the wash phase, this indicated that the putative conjugate did not bind to the column media (data not shown) and as such, the molarity of the buffer was reduced to 10 mM. The typical chromatogram obtained for a sample of the crude reaction mixture showed two peaks: P1 (5.1 mL) and P2 (18.8 mL) (**Figure 4.22**). RP-HPLC pure Phb$_{CY185-214}$ peptide eluted as a single peak at 27.7 mL, therefore, P2 was assumed to represent the mPEG-Phb$_{CY185-214}$ conjugate. There was no sign of unreacted Phb$_{CY185-214}$ peptide in the crude reaction mixture. Fractions corresponding to P2 were collected, desalted and the concentration determined by UV spectroscopy such that the mass and % yield could be calculated (**Table 4.3**).

The purity of the mPEG-Phb$_{CY185-214}$ conjugate isolated in this way was assessed using the same method of cation-exchange chromatograpy and a single peak was observed with an elution volume of 22.4 mL (**Figure 4.23a**). Characterisation by MALDI-TOF MS (**Figure 4.23b**) failed to confirm the estimated molecular weight for the conjugate (Mn= 9,156 g mol^{-1}, Mw = 9,322 g mol^{-1}). Instead the mass spectrum showed two peaks corresponding to molecular weights of approximately 3,000 g mol^{-1} and 5,900 g mol^{-1} (assuming that z=1).

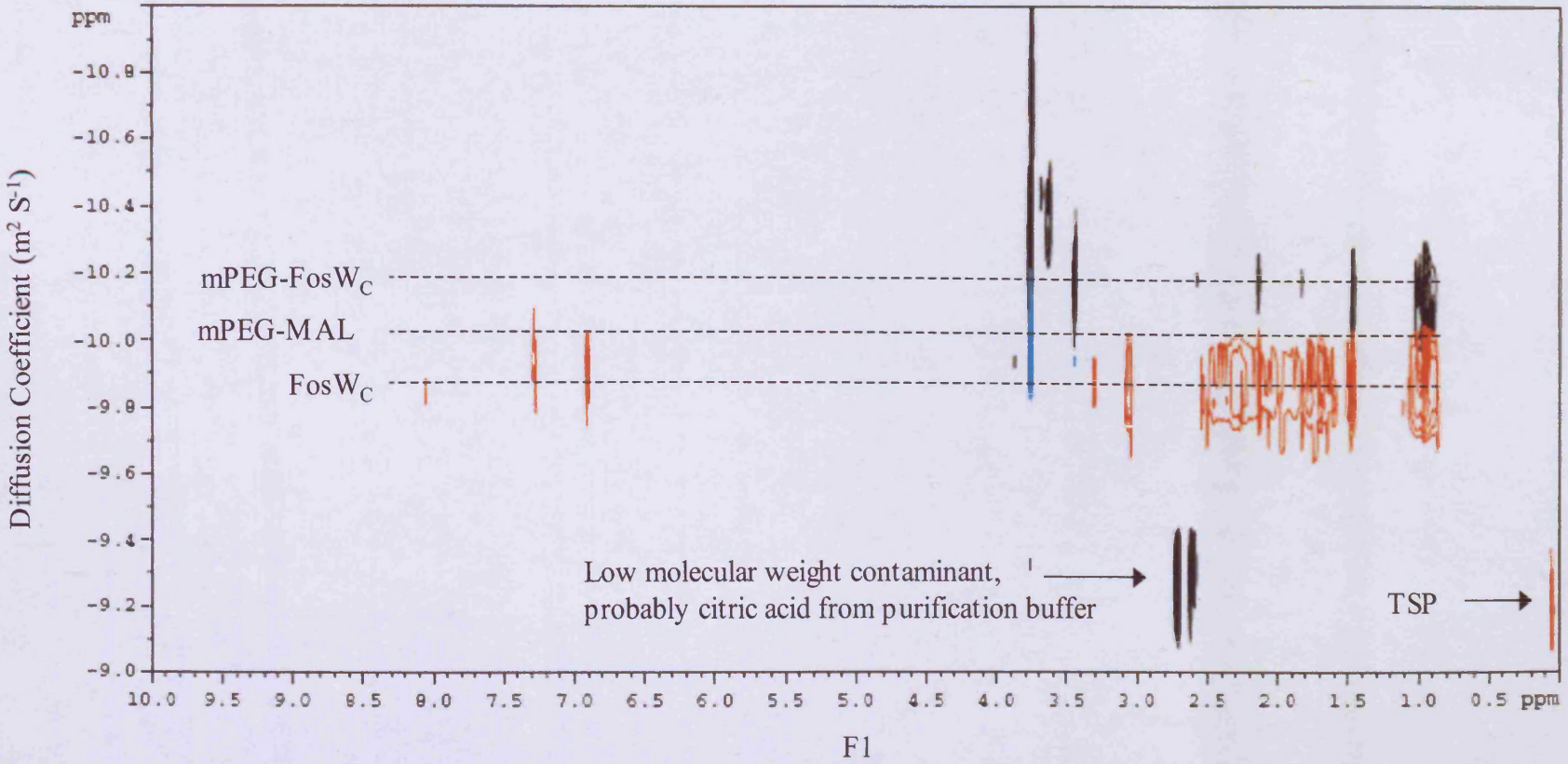

Figure 4.21 Characterisation of mPEG-FosW$_C$ by 2D DOSY. An overlay of three spectra is shown: FosW$_C$ peptide (red), mPEG-FosW$_C$ (black) and mPEG-MAL (cyan). TSP was included as an internal standard. Individual spectra showed no overlapping signals, thus confirming that unreacted mPEG-MAL and FosW$_C$ had been successfully removed from the mPEG-FosW$_C$ sample by ion-exchange chromatography.

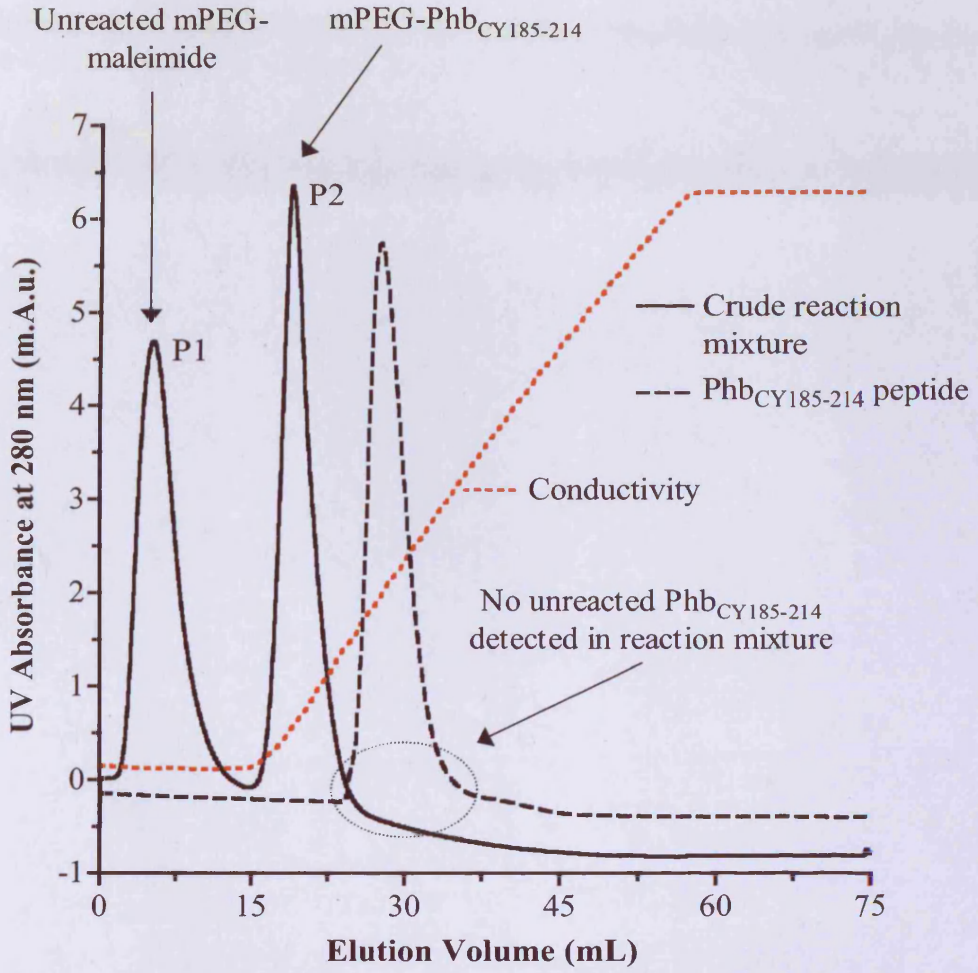

Figure 4.22 Purification of mPEG-Phb$_{CY185-214}$ by cation-exchange chromatography (MacroCap SP). Solid line shows the typical elution profile of the crude reaction mixture. Dashed line shows the overlaid elution profile of the RP-HPLC pure Phb$_{CY185-214}$ peptide. Conductivity (mS cm^{-1}) as a measure of increasing NaCl is shown in red (dotted line).

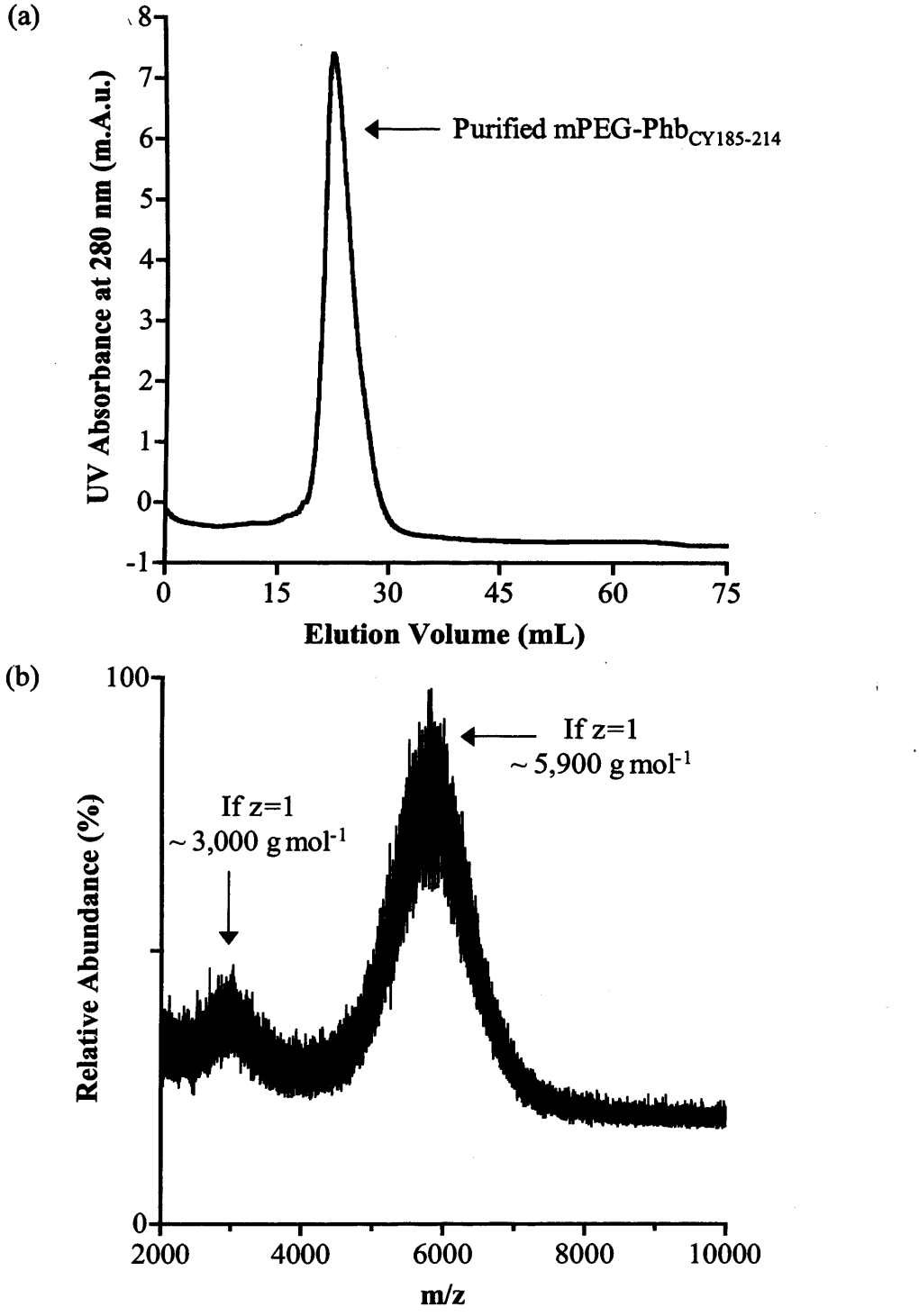

Figure 4.23 Characterisation of mPEG-Phb$_{CY185-214}$ by cation-exchange chromatography and MALDI-TOF MS. Panel (a) shows the analysis of purified and desalted mPEG-Phb$_{CY185-214}$ by cation exchange chromatography (MacroCap SP). Panel (b) shows the MALDI-TOF mass spectrum acquired for the same sample.

Synthesis and Characterisation of mPEG-EbGP2$_{CY566-589}$

Analysis by Ellman's assay showed that the % of free thiol in the reaction mixture had decreased by 83 % after 2 h, slightly less than seen for previous reactions. A further aliquot was assayed at 2.5 h, this showed a decrease of 84 % which was not significantly different to the measurement at 2 h, therefore the reaction was stopped.

A similar cation-exchange chromatography protocol was used as for the purification of the previous conjugates. As the iso-electric point of the Phb$_{CY185-214}$ peptide was calculated to be 12.1, a phosphate buffer (10 mM), pH 7.4 was used for purification and analysis (**Table 4.3**). Normally, a buffer of only 1-2 units below the iso-electric point is used, however, there was concern that a basic buffer may lead to degradation of the peptide. A typical elution profile of the crude reaction mixture is shown in **Figure 4.24**. The EbGP2$_{CY566-589}$ peptide eluted as a single peak in the wash phase and there was not sufficient peptide available to conduct further studies to optimise the conditions (data not shown). The first peak to elute indicated the presence of two separate compounds as two "spikes" were observed. This suggested that any unreacted EbGP2$_{CY566-589}$ peptide eluted along with mPEG-MAL in the wash phase. Two poorly resolved peaks eluted at 24.2 and 34.6 mL as the NaCl gradient was applied. In light of previous observations it would seem probable that one or more of these peaks corresponded the mPEG-EbGP2$_{CY566-589}$ conjugate. Fractions corresponding to each peak were collected, lyophilised, and desalted using a PD-10 column (secion 2.2.2.2). Two fractions (> 5,000 g mol^{-1} and < 5,000 g mol^{-1}) were collected for each peak and lyophilised before analysing by MALDI-TOF MS. Mass and % yields are shown in **Table 4.3**. MALDI-TOF analysis of the low molecular weight fractions did not show any peaks between 1,000 and 10,000 m/z (data not shown). Subsequent analysis of the higher molecular weight fractions failed to confirm the estimated molecular weight of the mPEG-EbGP2$_{CY566-589}$ conjugate (Mn= 8,622 g mol^{-1}, Mw = 8,788 g mol^{-1}). However, for both samples the mass spectrum showed the same two peaks corresponding to molecular weights of approximately 3,000 g mol^{-1} and 5,900 g mol^{-1} (assuming that z=1) (**Figure 4.25**). These values are very similar to the calculated molecular weights for the EbGP2$_{CY566-589}$ peptide and mPEG-MAL, however the resolution of the peaks is very different to that which would be expected either for a mono-disperse peptide or for unreacted mPEG-MAL.

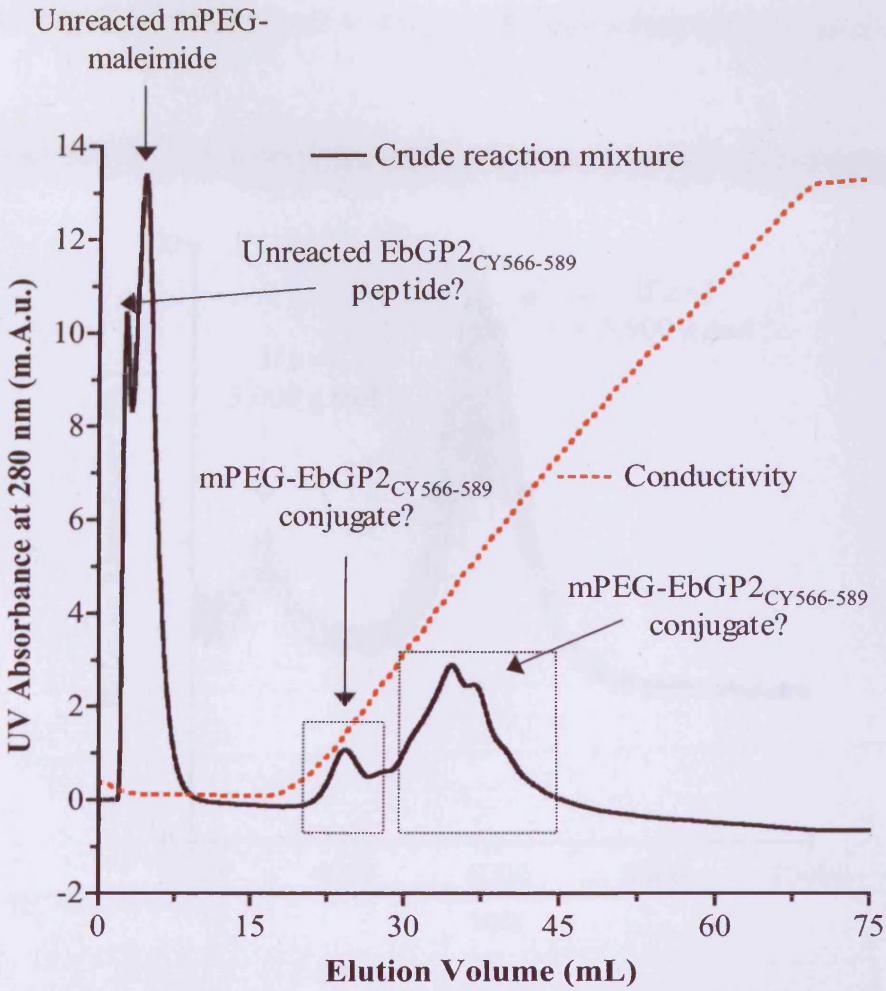

Figure 4.24 Purification of mPEG-EbGP2$_{CY566-589}$ by cation-exchange chromatography (MacroCap SP). Solid line shows the typical elution profile of the crude reaction mixture. Conductivity (mS cm^{-1}) as a measure of increasing NaCl is shown in red.

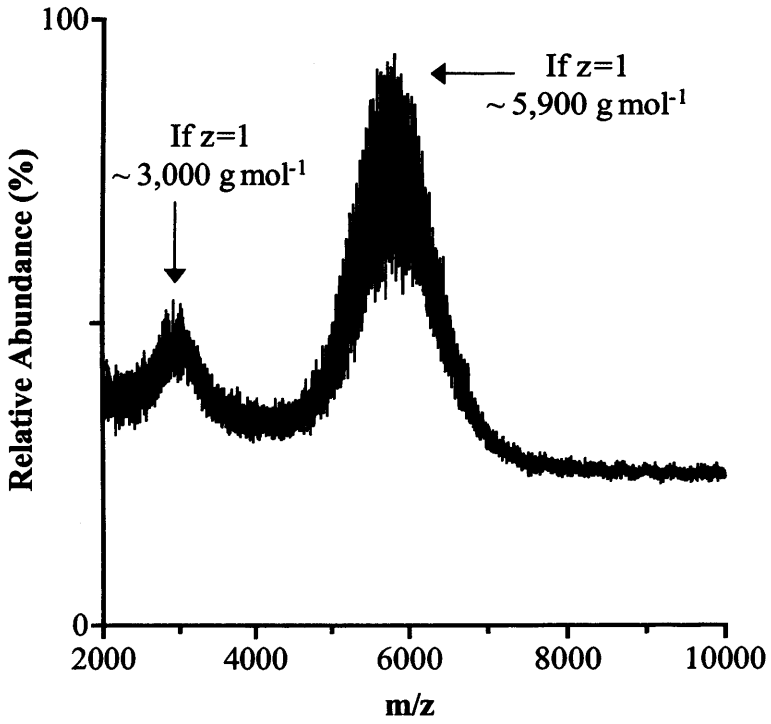

Figure 4.25 Characterisation of mPEG-EbGP2$_{CY566-589}$ by MALDI-TOF MS.

4.4 Discussion

4.4.1 Comparison of the Relative Merits of the Synthetic Methods Used

PEGylation by solid-phase synthesis was first investigated using a TentaGel PAP resin as the solid support. Peptides were "grown" from the NH_2 terminated PEG chains using an Fmoc-SPPS chain elongation approach as first described by Fields & Noble, (1990) and more recently by Rösler *et al*, (2003). This approach did not improve the solubility of the $EbVP35_{CY88-119}$ peptide (discussed in Chapter 3, section 3.3.2.3) however it did generate a water-soluble $Phb_{CY185-214}$-PEG conjugate.

One of the main concerns with this synthetic approach was that the removal of PEGylated truncation peptides or unreacted PEG by RP-HPLC would be an insurmountable challenge in the time available. Whilst ideal for the preparative-scale purification of the coiled-coil motif peptides (Chapter 3), the RP-HPLC column (Atlantis® dC_{18} OBD™ 5 μm, 30 x 150 mm) was not optimal for the purification of the C-terminal PEG-conjugates. Fundamentally, it did not provide sufficient resolving power at high ACN concentrations, nor was the pore size large enough to prevent clogging of the sample within the column. These issues were only fully realised during attempts at purify the $Phb_{CY185-214}$-PEG conjugate.

As outlined in Chapter 1 one of the goals of this study was to develop methods that could be easily adapted for the preparation of conjugates for clinical study in the longer-term. The PEG-conjugates that have recently received FDA approval (see **Table 4.1**) have all used higher molecular weight PEGs (20,000 to 40,000 g mol^{-1}), therefore it was important that the synthetic approach developed here could be adapted accordingly. The molecular weight of the PEG grafted onto the commercially available TentaGel PAP resin is approximately 2,000 to 3,000 g mol^{-1} (www.rapp-polymere.com). The possibility of modifying the TentaGel PAP resin with a higher molecular weight PEG existed, however this is capped at 10,000 g mol^{-1}; any higher and there would be insufficient room within the polystyrene matrix to permit efficient synthesis of peptides from the NH_2 termini of the PEG chains (personal communication from Dr Rapp, Rapp-Polymere).

In light of these early results it was decided to abandon the solid-phase approach for the preparation of peptide-PEG conjugates and focus on the development of a

solution-phase methodology. Towards this end, it was first necessary to characterise the mPEG-MAL used for synthesis and develop a "tool-kit" of analytical techniques.

*4.4.1.1 Quality of the mPEG-*MAL *intermediate and the Challenges of Solution-Phase Synthesis*

Characterisation of the first trial synthesis of mPEG-EbGP2$_{609\text{-}630}$ (which used the Fluka mPEG-MAL) was hampered by the impure nature of the product. As a result of the multiple peaks detected in the SEC chromatograms of the crude reaction material it was impossible to discern whether or not the solution-phase PEGylation was successful. SEC chromatography of the raw material (mPEG-MAL) clearly demonstrated the greater purity of the NOF product over that from Fluka (**Figure 4.9**). Furthermore, the data obtained for the NOF mPEG-MAL correlated well with the certificate of analysis provided by the supplier stating the sample to be of superior purity with a polydispersity of 1.03 and Mn of 5,522 g mol^{-1}.

The solution-phase synthesis of the conjugates described in this study was adapted from a method described by Chen *et al*, 2004 for the synthesis of PEGylated poly-lysine conjugates. One of the main differences between the approach used here and the one adopted by Chen *et al*, (2004) was that the coiled-coil motif peptides were not treated with a reducing agent prior to synthesis. Such treatment was not considered necessary since it was unlikely that disulphide bonds would have had the opportunity to form post-synthesis; the environment in which they were prepared and stored was acidic, very cold (- 80 °C) and devoid of oxygen by virtue of degassing all the solvents used. Furthermore, if either dithiolthreitol (DTT) or tris(2-carboxyethyl)phosphine hydrochloride (TCEP) were used as reducing agents they would have required removal prior to addition of mPEG-MAL since studies have shown that either agent can competitively react with maleimide derivatives (Shafer *et al*, 2000).

In order to assess the progress of the nucleophilic addition reaction between the cysteine thiol and the mPEG-MAL intermediate it was necessary to develop a suitable analytical method. Three possibilities existed: (i) to monitor appearance of the conjugate, (ii) to monitor disappearance of the maleimide moiety and (iii) to monitor disappearance of the thiol moiety. Use of Ellman's reagent to measure the latter (Ellman, 1959) proved a very useful approach. The assay suggested that the reaction

proceeded very quickly (> 80 % complete in 2 min), this was surprising, however, a recent study by Tom *et al*, (2007) in which mPEG-MAL was conjugated to 28-38-residue peptides supported this observation. Furthermore, as the assay demonstrated that the thiol concentration decreased following PEGylation, one may assume that site-specific (thiol-directed) conjugation was successfully effected.

It is important to note here, that while Ellman's reagent was not used in this study to quantify the concentration of thiols present (merely to provide a qualitative comparison) the extinction coefficient of 1360 at 412 nm published in the original reference (Ellman, 1959), was found to be an underestimate (Collier, 1973); the currently accepted value is 1414.

4.4.2 Challenges of characterising mPEG-coiled-coil conjugates

While Ellman's assay gave an indirect indication that the PEGylation reaction was successful, philosophically it was more desirable to use an additional method that could confirm the existence of an mPEG-coiled-coil conjugate rather than the disappearance of a reactive moiety.

RP-HPLC and SEC

As discussed in section 4.4.1 characterisation by RP-HPLC was not possible with the column available (Atlantis® dC_{18} OBD™ 5 µm, 30 x 150 mm). SEC was also assessed towards characterising the putative conjugate mPEG-EbGP2$_{609\text{-}630}$. However, neither of the columns used in this study were able to resolve mPEG-MAL from the mPEG-coiled-coil motif conjugate. It has been reported that PEGs typically appear between five and ten times larger than proteins of similar molecular weight due to their capacity to bind large quantities of water molecules (reviewed in Roberts *et al*, 2002). Thus, one may conclude that coupling of the coiled-coil motif peptide to the PEG intermediate did not increase the hydrodynamic volume relative to that of mPEG-MAL alone. SEC using the Superdex HR 10/30 column did however show that no peptide was present in the crude reaction mixture of the trial synthesis; this again gave an indirect indication that the reaction was successful.

Cation-exchange chromatography

This approach made it possible to separate the three predicted species in the crude reaction mixture: unreacted mPEG-MAL, peptide and the desired conjugate. Thereby, giving the first direct indicator that the PEGylation reaction was successful.

While it was expected that mPEG-MAL would elute in the wash phase, resolving the conjugate from unreacted peptide was an unexpected benefit of this technique. Since the iso-electric point of the peptide had not been altered by conjugation (as it would if amine-directed conjugation had been effected) the affinity of both species for the cation-exchange media was predicted to remain the same. It may be concluded that the PEG chain had a steric effect and thereby reduced the binding affinity of the peptide with the column media.

In this study, cation-exchange chromatography was particularly useful since with minor alterations to the protocol used (typically buffer composition, pH and molarity), it proved to be adaptable for the purification and analysis of all of the conjugates prepared. The mPEG-EbGP2$_{609\text{-}630}$ peptide was the simplest to work with since the peptide contained a tryptophan residue rather than tyrosine as the UV-chromophore. The extinction coefficient of tryptophan is approximately 3.5 times that of tyrosine, therefore detection with the fixed wavelength 280 nm detector was much easier. Of the four conjugates prepared in this study, mPEG-EbGP2$_{CY566\text{-}589}$ was the most difficult. At least two poorly resolved peaks were detected where the conjugate was expected to elute. As a homo-trimeric coiled-coil motif, one possible explanation is that the peaks represent differing oligomeric states. This suggestion is supported by previous studies (Vandermeulen *et al*, unpublished data - personal communication) with PEGylated homo-oligomeric coiled-coil motifs that showed multiple peaks in SEC chomatograms.

MALDI-TOF MS

With a minor modification to the optimised spotting protocol adapted from the method described by Meier and Schubert, (2003) it was possible to confirm the expected molecular weights of mPEG-EbGP2$_{609\text{-}630}$ and mPEG-FosW$_C$. The indisputable advantage of characterisation by MALDI-TOF MS is that it cannot give a "false positive" result. Therefore, the existence of the peaks in the expected mass-range was conclusive proof that mono-PEGylated conjugates had been successfully synthesised. However MALDI-TOF can, and often does give a "false-negative" result

if the method of sample preparation does not permit ionisation of the conjugate. It is likely (in light of the cation-exchange chromatography data) that this was the case for the conjugates mPEG-$Phb_{CY185-214}$ and mPEG-$EbGP2_{CY566-589}$. Further optimisation of the sample preparation method is required to enable MALDI-TOF spectra to be acquired. Recent advances in MALDI-TOF MS have even shown that it is possible to identify (or confirm) the site of PEGylation using a modified "reflector in-source decay analysis" approach (Yoo *et al*, 2009). A "crystal seed" method was used in conjunction was sinapinic acid or DHB as the matrix; it is possible that this approach could be successfully used to characterise either mPEG-$Phb_{CY185-214}$ or mPEG-$EbGP2_{CY566-589}$. However, the caveat is that since the peptide sequences here are entirely different to those used in the above study the successful acquisition of spectra cannot be guaranteed.

DOSY

Characterisation by 2D DOSY was only conducted for mPEG-$FosW_C$ conjugate as it was the only conjugate taken to CIPF in Valencia for the 2D NMR target hybridisation studies detailed in Chapter 5. The 2D DOSY spectrum is shown here as it supports the other characterisation data. It has a greater resolving power that the SEC approaches described earlier as it demonstrated that the conjugate had a greater molecular size/hydrodynamic volume than either mPEG-MAL or $FosW_C$ as would be expected. The ease with which the spectra were acquired, and lack or requirement for complex sample preparation makes 2D DOSY the analytical technique of choice. It is probable that a calibration curve could be constructed that would enable the molecular weight of mPEG-coiled coil conjugates to be estimated by 2D DOSY, however, MALDI-TOF MS remains the better approach for determining absolute molecular weight (provided the sample can be ionised effectively).

4.4.3 Conclusions

Conjugation of peptides to mPEG-MAL using the solution-phase MAL/thiol reaction enabled site-specific conjugation. This was particularly important to avoid disrupting the alpha-helical structure of the coiled-coil motif. Often it is difficult to remove free polymer as well as free peptide from such conjugates. However, a method optimised from that described by Chen *et al* (2004) made it possible here to prepare samples of very high purity (> 95 %) and suitable for further study by NMR and CD spectroscopy (Chapter 5) and biological assessment (Chapter 6).

CHAPTER 5

Investigation of mPEG-Coiled-Coil Motif Target Hybridisation Using Phb : E2F1 and c-Jun : $FosW_C$ as Models: Preparation of Recombinant Targets and Development of Analytical Techniques

5.1 Introduction

The primary aim of this study was to investigate whether PEGylated-coiled-coil motifs would indeed be able to hybridise with their respective targets *via* the formation of heterodimeric coiled-coils in preference to homodimers, which would have no use as polymer therapeutics. The transcription factors E2F1 and c-Jun were chosen as targets to test this hypothesis.

Putative Phb:E2F1 Coiled-Coil Interaction

As discussed in Chapter 1 (section 1.5.1), Wang *et al*, (1999) first demonstrated that the tumour suppressor protein PHB suppressed the activity of the transcription factor E2F1. Joshi *et al*, (2003) subsequently made the assertion that the PHB : E2F1 interaction was mediated by a putative coiled-coil domain in the PHB protein (illustrated in **Figure 3.8**). Moreover, it was also shown that a peptide corresponding to the PHB coiled-coil domain was able to suppress E2F1 mediated transcription (Joshi *et al*, 2003).

These studies sought to investigate whether the PHB derived coiled-coil motif peptides ($Phb_{X185-214}$) prepared in Chapter 3 could indeed hybridise with the E2F1 target protein *via* the formation of a coiled-coil. If so, to see whether PEGylation of $Phb_{CY185-214}$ (Chapter 4) would affect this hybridisation. First studies were conducted using CD spectroscopy to investigate the interaction of the coiled-coil motif peptides ($Phb_{185-214}$ and $Phb_{Y185-214}$) with peptides (E2F1a and E2F1b), which were designed to model the E2F1 target hybridisation domain (**Figure 5.1a**). The ideal approach to assess the mechanism of target hybridisation was to try to use full-length E2F1 protein, rather than the E2F1 derived peptides used in the early studies. Towards this end, experiments were conducted with the aim of expressing recombinant human (rh) E2F1 protein in sufficient quantities to allow characterisation of the Phb : E2F1 interaction using CD or NMR spectroscopy (**Figure 5.1b**).

c-Jun:$FosW_C$ Coiled-Coil Interaction

Since there was doubt over whether the Phb : E2F1 interaction was mediated by the formation of a coiled-coil, it was considered important to study a second target, hence c-Jun was chosen. As discussed in Chapter 1 (section 1.5.2), c-Jun constitutes

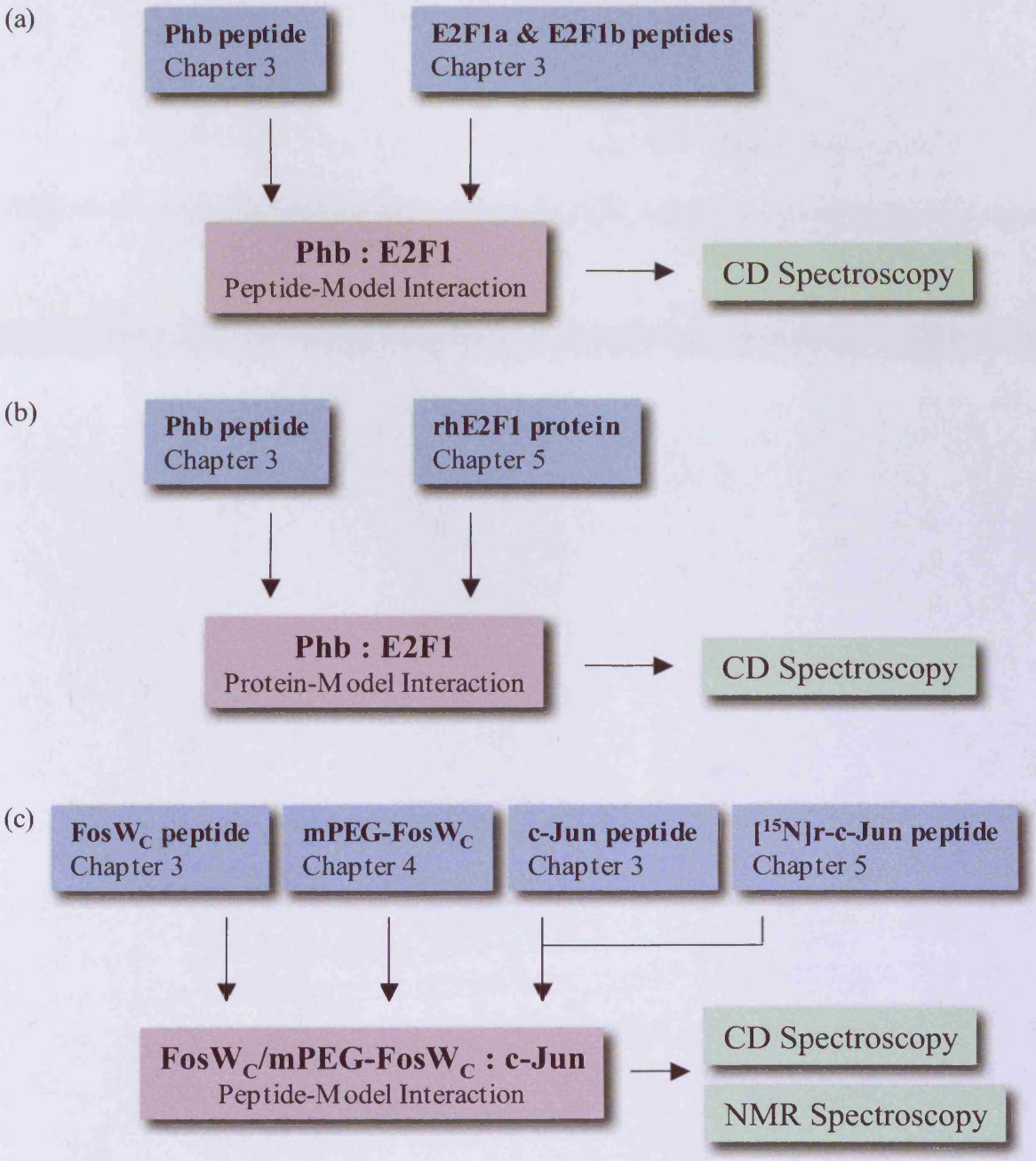

Figure 5.1 Schematic overview of the three target hybridisation studies conducted.

one half of the heterodimeric and oncogenic AP-1 transcription factor (reviewed in Eferl & Wagner, 2003; Shaulian & Karin 2002). The heterodimeric coiled-coil that drives the hybridisation of c-Jun and c-Fos (**Figure 3.14a**) has been shown to exist using X-Ray crystallography (Glover & Harrison, 1995). FosW, a synthetic mutant of c-Fos was designed as a potential therapeutic with a higher affinity for the bZIP domain of c-Jun than native c-Fos (Mason *et al*, 2006). In this study, using the FosW_C peptide prepared in Chapter 3 and the mPEG-FosW_C conjugate (Chapter 4) the interaction with the coiled-coil domain of c-Jun was studied (**Figure 5.1c**). It was first necessary to consider the analytical techniques that might be used to confirm target hybridisation. NMR and CD spectroscopy were deemed to offer a more definitive approach than other methods such as native PAGE. While it was possible to conduct CD spectroscopy experiments using the c-Jun peptide synthesised in Chapter 3, to enable sophisticated characterisation by 2D ^{1}H, ^{15}N-Heteronuclear Single Quantum Coherence (HSQC) NMR spectroscopy it was necessary to synthesise a ^{15}N-labelled c-Jun peptide ([^{15}N]r-c-Jun) using a recombinant approach.

This peptide could theoretically have been prepared using Fmoc-SPPS (Chapter 3), however, Fmoc protected [^{15}N]amino acids typically cost in excess of $300-1000 per g (Cambridge Isotope Laboratories, Inc. 2008). This made the prospect of preparing the [^{15}N]c-Jun peptide by Fmoc-SPPS a very expensive venture. With a recombinant approach, it is necessary to enrich the growth media with a single ^{15}N source such as [^{15}N]H_4Cl; available for as little as $40 per g (Cambridge Isotope Laboratories, Inc. 2008). As such, a recombinant expression system was chosen to generate [^{15}N]r-c-Jun.

The background and issues that were considered before choosing the methods used for the preparation of rhE2F1 and [^{15}N]r-c-Jun, and subsequently analysis of target hybridisation by NMR and CD spectroscopy are summarised below (sections 5.1.1 and 5.1.2, respectively).

5.1.1 Development of a Method for Recombinant Expression and Purification of Targets rhE2F1 and r-c-Jun/[^{15}N]r-c-Jun

The general steps involved in the recombinant expression of a protein or peptide as summarised in **Figure 5.2**. For a comprehensive assessment of protein production and purification the reader is referred to a recent review article by Gräslund *et al*, (2008).

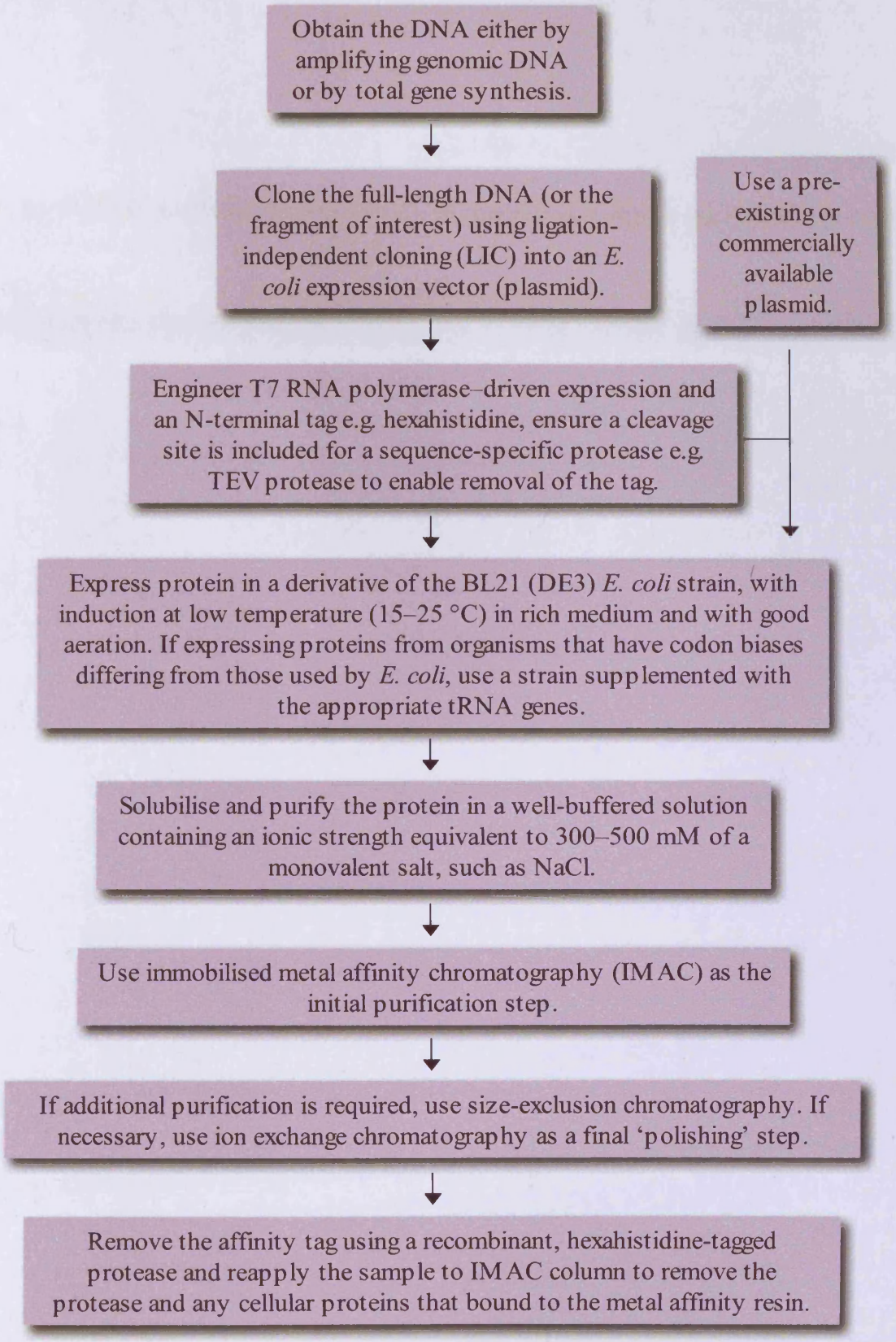

Figure 5.2 The consensus protocol for recombinant protein expression and purification, recommended by Gräslund *et al*, (2008).

Before continuing, it may be helpful to clarify the nomenclature used in this study. The prefix "r" is used following standard convention to denote a recombinant peptide/protein. This is followed by the letter "h" if the source of the DNA used to translate the peptide/protein is human, hence rhE2F1. In relation to r-c-Jun, the letter "h" is intentionally omitted due to the structural alterations that were made to the peptide sequence, first by Mason *et al*, (2006), and subsequently in the course of this study.

Plasmid Assembly/Acquisition, Purification and Characterisation

The starting point for the expression of any protein or peptide involves either the assembly of a plasmid encoding the appropriate DNA sequence or, the acquisition of an existing plasmid i.e. one that has been prepared previously. For this study, a plasmid encoding the rhE2F1 protein (pGEX-KG-(GST)-E2F1) was a kind gift from Professor N. La Thangue (CRUK) (Bandara *et al*, 1993; Girling *et al*, 1993), while the plasmid encoding r-c-Jun (pET15B-cytb5-ENLYFQGT-r-c-Jun) was custom designed and characterised by Dr A.K. Schott (CIPF).

The pET15B-cytb5-ENLYFQGT-r-c-Jun plasmid was prepared in advance in sufficient quantities for use in this study, however, in the case of the pGEX-KG-(GST)-E2F1 plasmid it was first necessary to amplify the stock solution to ensure enough material for characterisation and subsequent optimisation of expression. This is now a fairly straightforward laboratory technique for which there are many commercially available kits (e.g. Qiagen) depending upon the yield of plasmid desired.

Characterisation of the pGEX-KG-(GST)-E2F1 plasmid and verification of the DNA sequence along with the ATG start and TGA stop codons was crucial prior to attempting expression since this data was not in existence (La Thangue - personal comminucation). This work was conducted under the tutelage of Dr S. Richardson. A quick assessment of purity to determine the extent of protein contamination is typically made by determining the ratio of UV absorbance of the sample at 260 nm to that at 280 nm (Glasel, 1995). The basis of this analysis rests on the Beer-Lambert Law (as defined in Chapter 2, Section 2.2.1.1). DNA absorbs UV radiation strongest at 260 nm, with weaker absorption at 280 nm, for a protein or peptide with one or more aromatic residues the inverse is true. Therefore, pure nucleic acid samples typically have an A_{260}:A_{280} ratio of 2.0, while pure protein samples would be 0.57. Thus, for samples that contain a mixture of protein and DNA the ratio is influenced by the UV absorbance

spectra of both macromolecules and so reads somewhere between 0.57 and 2.0. The generally accepted benchmark for purity is an A_{260}:A_{280} ratio of between 1.8 and 2.0 (reviewed in Middaugh *et al*, 1998).

Further plasmid characterisation can be conducted using either agarose gel electrophoresis (Helling *et al*, 1974) to determine its size (number of base pairs), or ideally automated DNA sequencing to confirm the nucleotide sequence (reviewed in França *et al*, 2002). The former is generally only valuable if the vector map is known so that a restriction digest may be performed. Electrophoresis of "uncut" plasmid DNA is often of limited value (as shown later in this study) due to the propensity of the DNA molecules to super-coil, hence making accurate determinations of size impossible (reviewed in Middaugh *et al*, 1998). The best approach is to sequence the plasmid using either commercially available or custom primers (oligonucleotides) followed by amplification in the presence of dye with the polymerase chain reaction (PCR) (reviewed in França *et al*, 2002).

Choice of Expression Organism/Strain and Optimisation of Expression

Once characterised, it was important to consider the strain of bacteria (or other organism) in which to express the plasmid. For most peptides and proteins, *Escherichia coli* (*E. coli*) has proven a suitable expression host (Peti & Page, 2007) and is the recommended starting point for the recombinant expression of any protein (reviewed in Gräslund *et al*, 2008).

Prior to commencing this study the expression of the r-c-Jun peptide was found to be optimal in BL21-CodonPlus (DE3) strain of *E. coli* (Dr A.K. Schott, personal communication). Similarly, expression of the rhE2F1 protein was previously demonstrated in the BL21 (DE3) *E. coli* strain (Dr K. Luoto, personal communication). The BL21 (DE3) strain is often ideal for high-level protein production as it has the advantage of being deficient in *lon* and *ompT* proteases (Studier *et al*, 1990). Moreover the designation "DE3" indicates that it is compatible with the T7 *lacO* promoter system and is therefore suitable for induction with IPTG (Studier *et al*, 1990). The "CodonPlus" strain of BL21 *E. coli* designed by Stratagene has the added advantage of containing extra copies of tRNA genes normally rare in *E. coli* but sometimes required for the biosynthesis of proteins originating from other organisms (www.stratagene.com). Optimisation of culturing conditions such as media

composition, incubation temperature, induction time etc. was determined for each protein expression system during the course of this study.

Lysis and Purification

Once an optimal level of expression has been confirmed, typically by denaturing SDS-PAGE analysis with Coumassie Blue staining (Bradford, 1976), the *E. coli* host needs to be lysed (as neither r-c-Jun nor rhE2F1 are thought to be secreted). The most efficient methods use mechanical forces in the form of probe sonication or the use of a French press (reviewed in Gräslund *et al*, 2008). Other methods, such as enzymatic degradation of the bacterial cell wall using lysozyme followed by osmotic shock are often less efficient without the use of detergents. Due to the nature of this study, it was essential that detergents were not used in the preparation of either rhE2F1 or r-c-Jun as they can dramatically affect the 3D structure of the protein/peptide and are very difficult to remove (Dr S. Richardson, personal communication).

To purify the over-expressed protein/peptide from the crude cell lysate a number of different tags have been developed, of which glutathione s-transferase (GST) and hexahistadine tags are probably the most common. They are usually encoded in the vector so that the tag is either immediately 5' or 3' of the protein/peptide DNA sequence. When over-expressed the fusion protein can then be isolated from the crude lysate using affinity chromatography. After purification the tag can be site-specifically cleaved using a protease such as TEV to yield the desired protein/peptide (Carrington & Dougherty, 1988). Upon comparison of most of the available affinity tags, not one has been shown to be consistently superior in the preparation of soluble and active recombinant proteins/peptides (Arnau *et al*, 2006).

In this study, rhE2F1 was expressed as a glutathione-s-transferase (GST) fusion protein whereas an alternative tag, (derived from cytochrome b_5 - cytb5) in combination with a hexahistidine domain was engineered into the r-c-Jun expression plasmid. Use of the highly soluble, heme-binding domain of cytb5 as a tag, was first described in a pioneering study by Mitra *et al*, (2005). The authors noted that, "very few proteins possess the dual characteristics of high expression and high solubility that would qualify them to be "good hosts" for fusion protein systems" (Mitra *et al*, 2005). Cytb5 has both of these key characteristics and significantly has the added advantage that it is a coloured protein. The distinct red/orange colour would make it possible to visually

check the efficiency of each step in the expression protocol without having to rely solely on denaturing SDS-PAGE and/or western blotting techniques.

5.1.2 Analytical Techniques Used to Study Target Hybridisation

5.1.2.1 CD Spectroscopy

CD spectroscopy was used in several studies to investigate coiled-coil motif and mPEG-coiled-coil motif target hybridisation. CD spectroscopy is an excellent tool for the analysis of peptide and protein structure as the shape of the far-UV CD spectrum can be correlated with different types of secondary structure. Typical spectra for peptides, including an α-helix, a β-sheet, an aperiodic/random coil, a β-turn-1 and a β-turn-2 are shown in **Figure 5.3** (Perczel *et al*, 1991). The α-helix is of particular importance here as it is a constituent of the coiled-coil, and as discussed in Chapter 1 (section 1.2) a "coiled-coil motif" is defined in this thesis an α-helical peptide with the propensity to form a coiled-coil. α-Helicies are characterised by a spectrum with two distinct minima at approximately 208 and 222 nm and a sharp peak at 195 nm approximately twice the intensity of the minimum at 208 nm (Greenfield, 2006) (**Figure 5.3**). From the analysis of many protein and peptide structures it has been shown that a coiled-coil is probable when the ratio of the two minima (same $[\theta]_{208}$: $[\theta]_{222}$) is ≥ 1 (Lau *et al*, 1984). However, CD spectroscopy does not give the residue-specific resolution of data that can be obtained by NMR spectroscopy. Furthermore, it is not possible with CD spectroscopy to accurately detect a switch between a homooligomeric and heterooligomeric state. Since many peptides/proteins with a propensity to form a coiled-coil may also homooligomerise it was considered important to also study target hybridisation using 2D NMR techniques that can differentiate between homo and hetero-oligomerisation. A brief introduction to the NMR spectroscopy experiments used here is given below.

5.1.2.2 2D ^{1}H, ^{15}N-HSQC and ^{1}H-NMR Spectroscopy

NMR spectroscopy is probably the most powerful tool with which to study 3D structure and the interactions of macromolecules in solution, unlike X-Ray crystallography where characterisation is conducted in a crystalline state (reviewed in Zuiderweg, 2002). The method is particularly attractive as it is possible to adjust a wide range of solution conditions such as temperature, pH, buffer composition and salt

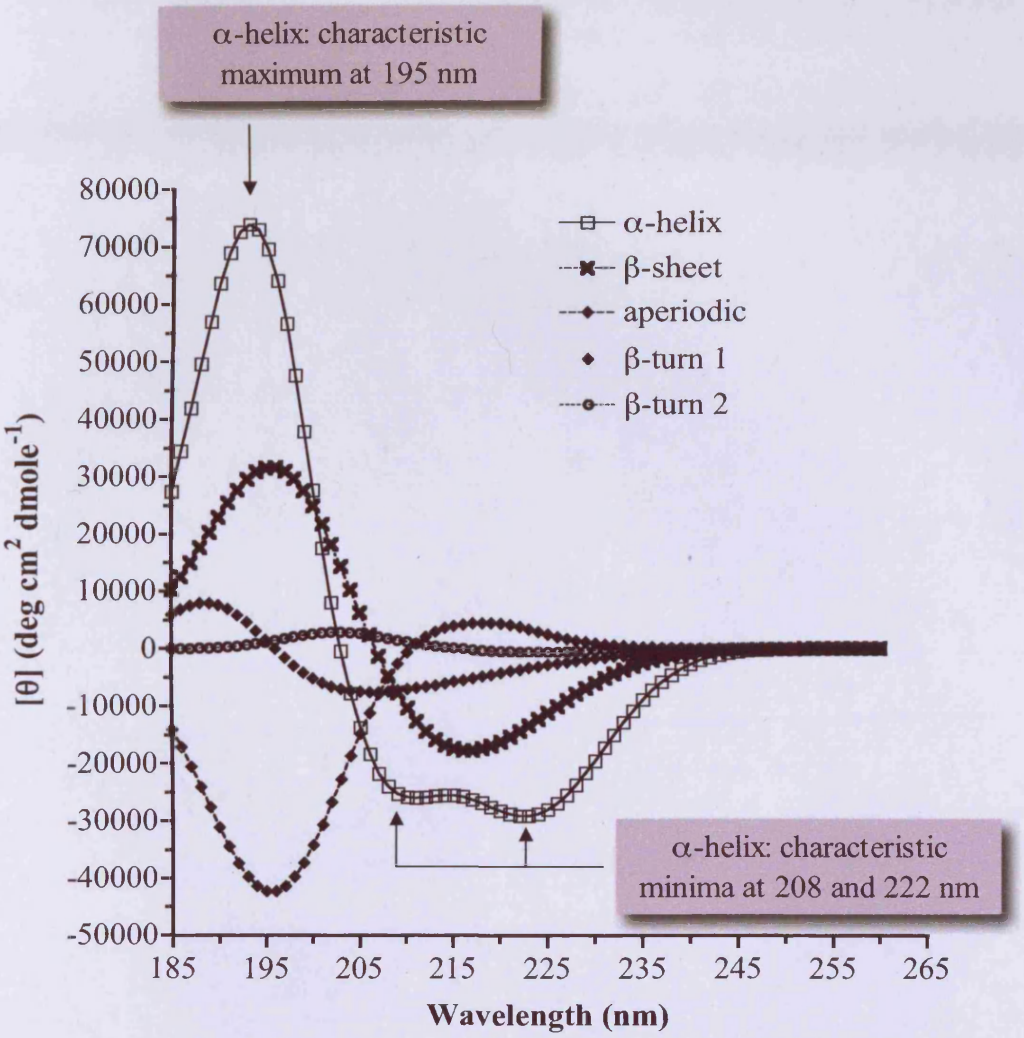

Figure 5.3 Characteristic CD spectra of common peptide structures. Spectra adapted from Perczel *et al*, (1991).

concentration in order to model a physiological environment. Conversely, one may also adjust the conditions to investigate denaturation and/or degradation of the protein/peptide.

Two different types of NMR spectroscopy were conducted to study the interaction of $FosW_C$ and mPEG-$FosW_C$ with [^{15}N]r-c-Jun, these were 2D ^{1}H, ^{15}N-HSQC and ^{1}H-NMR. The usefulness of the latter is limited in the analysis of peptide and proteins as there are many overlapping peaks in the 1D ^{1}H-NMR spectrum (**Figure 5.4a**). The 2D HSQC experiment, first described by Bodenhausen & Rubenin, (1980) however is able to resolve a peak for each unique proton that is attached to a heteronucleus (a nucleus other than a proton) (**Figure 5.4b**). In this study the only heteronucleus used was ^{15}N, in the form of isotopically labelled [^{15}N]r-c-Jun peptide. Previous studies have shown that when a peptide/protein is structured, for example, an α-helix or coiled-coil the peaks in the 2D HSQC spectrum are usually well dispersed and it is possible to resolve each individual peak (Takeuchi & Wagner, 2006). If however, the peptide is largely unstructured only a limited number of backbone ^{1}H-^{15}N correlations with a very low dispersion will be distinguishable as most of the signals from the NH groups will be lost due to exchange with the water. For the [^{15}N]r-c-Jun peptide, each amino acid residue (with the exception of proline) has an amide proton that is attached to the ^{15}N heteronucleus. When folded, one cross peak per backbone NH (i.e. per amino acid), minus the number of proline residues in the sequence, plus two extra cross peaks per glutamine/asparagine residue (from the NH_2 side chain) would be expected. Therefore if changes in structure occur following target hybridisation one would expect to observe a change in the number of resolvable peaks; an increase would suggest more structure, the converse, less (reviewed in Otting & Wüthrich, 1990). To the best of our knowledge this is the first time that this technique has been proposed to study the target hybridisation of PEGylated coiled-coil motfis.

5.1.3 Experimental Aims

The specific aims for this study can be divided into three sections and summarised as follows:

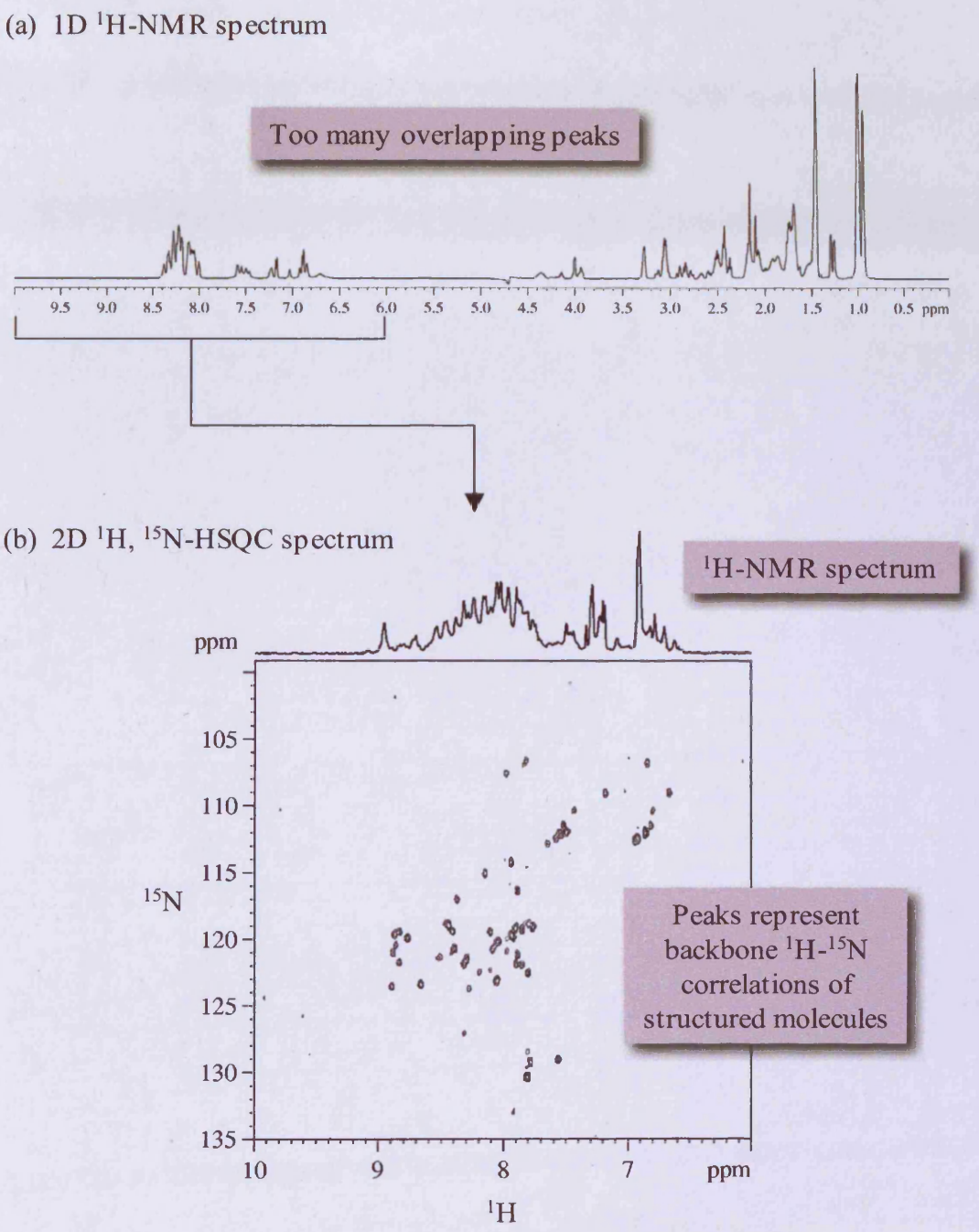

Figure 5.4 Typical 1D ^{1}H-NMR and 2D ^{1}H, ^{15}N-HSQC spectra for a 36-residue peptide.

Recombinant preparation of the rhE2F1 protein

- To characterise the pGEX-KG-(GST)-E2F1 plasmid obtained for the expression of the rhE2F1 protein.
- Amplify the pGEX-KG-(GST)-E2F1 plasmid stock.
- Identify an appropriate host organism and optimise the culturing conditions for expression of rhE2F1 protein.
- Express and purify sufficient rhE2F1 protein (> 3 mg) to enable analysis by CD spectroscopy.
- Characterise the rhE2F1 protein by MALDI-TOF MS.

Recombinant preparation of the r-c-Jun and [^{15}N]r-c-Jun peptides

- Optimise the expression protocol for r-c-Jun in "normal" M9 media.
- Express and purify sufficient [^{15}N]r-c-Jun (> 3 mg) to enable analysis by 2D ^{15}N, ^{1}H-HSQC spectroscopy.
- Characterise the r-c-Jun and [^{15}N]r-c-Jun peptides by MALDI-TOF MS.

Characterisation of the Phb:E2F1 Interaction Using CD Spectroscopy

- To determine whether the putative coiled-coil motif peptide $Phb_{185-214}$ interacted with the peptides E2F1a and E2F1b *via* the formation of a coiled-coil.
- To determine whether the putative coiled-coil motif peptide $Phb_{185-214}$ interacted with the protein rhE2F1 *via* the formation of a coiled-coil.

Characterisation of the c-Jun:$FosW_C$ Interaction Using CD Spectroscopy ^{1}H-NMR and 2D ^{15}N, ^{1}H-HSQC spectroscopy

- To use 2D ^{15}N, ^{1}H-HSQC spectroscopy to characterise the coiled-coil driven target hybridisation of $FosW_C$ with c-Jun.
- To use 2D ^{15}N, ^{1}H-HSQC spectroscopy to determine whether the presence of N-terminal mPEG affected coiled-coil driven target hybridisation between mPEG-$FosW_C$ and c-Jun.
- To use 2D ^{15}N, ^{1}H-HSQC spectroscopy to investigate what effect the ratio of mPEG-$FosW_C$ and $FosW_C$: [^{15}N]r-c-Jun had on hybridisation.
- To use CD spectroscopy to confirm that the target hybridisation interaction observed was *via* the formation of a coiled-coil and not non-specific aggregation.

- To determine by thermal denaturation whether there was a qualitative difference in the strength of binding between mPEG-$FosW_C$ and $FosW_C$ with c-Jun and compare with changes observed in the ^{1}H-NMR spectra acquired over a similar temperature range.

5.2 Methods

The peptides E2F1a, E2F1b, $Phb_{185-214}$, $Phb_{Y185-214}$, c-Jun and $FosW_C$ were prepared for this study as described in Chapter 3. The mPEG-$Phb_{CY185-214}$ and mPEG-$FosW_C$ conjugates were prepared as described in Chapter 4. The recombinant methods developed for the preparation of rhE2F-1 and r-c-Jun and [^{15}N]r-c-Jun are described in detail below. The general methods used for UV spectroscopy (Section 2.2.1.1), Agarose Gel Electrophoresis (Section 2.2.1.2), SDS-PAGE (Section 2.2.1.3) CD spectroscopy (Section 2.2.1.4), are all given in Chapter 2.

5.2.1 Expression of rhE2F1

A plasmid purportedly encoding rhE2F1 was obtained from Professor N. La Thangue (CRUK). However, no characterisation data were available for this plasmid. In order to characterise the pGEX-KG-(GST)-E2F1 plasmid (by agarose gel electrophoresis and/or automated DNA sequencing), it was first necessary to amplify the aliquot provided to generate a stock of plasmid.

5.2.1.1 Transformation of DH5α and TOP10 E. coli with pGEX-KG-(GST)-E2F1 and Plasmid Purification

The pGEX-KG-(GST)-E2F1 plasmid was transformed into *E. coli* strains DH5α and TOP10 affording two recombinant strains as follows. For each strain, competent *E.coli* (100 ng μL^{-1}, 50 μL) were thawed on ice, an aliquot (1 μL) of pGEX-KG-(GST)-E2F1 added and then left on ice for a further 30 min. Transformation was achieved by heat shocking at 42 °C for 30 sec, followed by cooling on ice for 5 min. An aliquot (450 μL) of SOC media was added and the freshly transformed bacteria were left to propagate at 37 °C for 1 h (orbital shaker - 180-220 rpm).

Pre-cultures were prepared by inoculating Luria Broth (LB) media (yeast extract 0.5 % w/v, tryptone 1 % w/v and NaCl 1 % w/v in ddH_2O) (10 mL) containing Amp (100 μg mL^{-1}) and with an aliquot (100 μL) of freshly transformed bacteria. The

culture was incubated at 37 °C overnight (orbital shaker - 180-220 rpm). Simultaneously, an agar plate was inoculated with an aliquot (50 µL) of freshly transformed bacteria in the presence of Amp. The following day, a culture (500 mL) of each strain was prepared by inoculating LB media with the pre-culture (10 mL). Each culture was incubated at 37 °C for 5 h in an orbital shaker (180-220 rpm) until an OD at λ_{600nm} of approximately 0.6 was reached. The cultures (500 mL) were transferred to four large centrifuge tubes (ca. 250 mL) and spun at 3,500 g, 4 °C for 15 min. Extraction and purification of plasmid DNA was conducted using a Qiagen EndoFree Plasmid Mega Kit, which was used in accordance with the manufacturers instructions. Following amplification of the plasmid stock in TOP10 and DH5α *E.coli* samples were analysed with respect to purity and concentration using UV spectroscopy to determine the A_{260} : A_{280} ratio (section 2.2.1.1) and agarose gel electrophoresis (section 2.2.1.2).

5.2.1.2 Sequencing of the pGEX-KG-(GST)-E2F1 Plasmid

Since full sequence data was not available it was necessary to draw a plan to sequence the insert in the pGEX-KG plasmid and aid design of the appropriate primers. The multiple cloning site (MCS) into which the E2F1 gene was most likely engineered is shown in the pGEX-KG vector map (**Figure 5.5a**) and a schematic of the vector containing the E2F1 gene is shown in **Figure 5.5b**. It was envisaged that a minimum of six primers would be needed to sequence the unknown region (blue). The primers pGEX 5' F and pGEX 3' R read from the known vector sequence (pGEX-KG) so their sequences were available from Addgene (http://www.addgene.org/pgvec1?f=c&cmd=showvecinfo&vectorid=5100) and subsequently ordered from Invitrogen™. However, custom sequences were designed using the OligoPerfect™ Designer software (accessible online *via* the Invitrogen™ website: http://tools.invitrogen.com/content.cfm?pageid=9716) for each of the remaining primers (2F, 3R, 4F and 5R). This software required several inputs.

In step 1, "sequencing" was selected in the application field and the human E2F1 nucleotide sequence entered into the target sequence field in text format. In step 2, the following parameters were selected for design of the forward reading primers 2F and 4F:

Primer size (bases):	Min 16	Opt 20	Max 26
Primer Tm (°C):	Min 50	Opt 60	Max 75

(a)

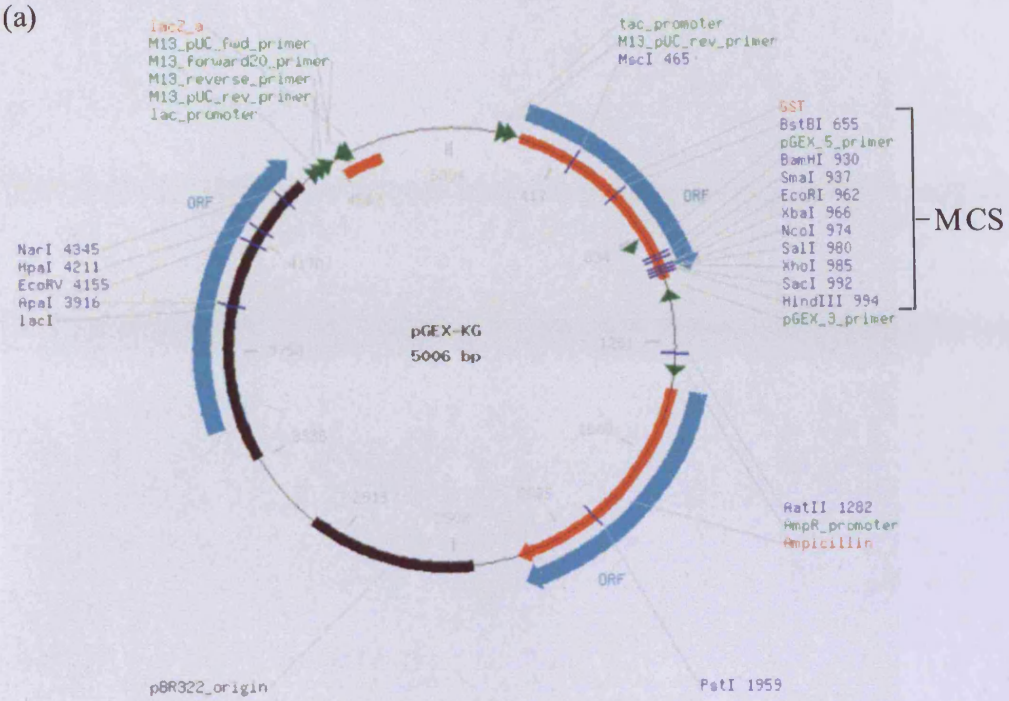

(b)

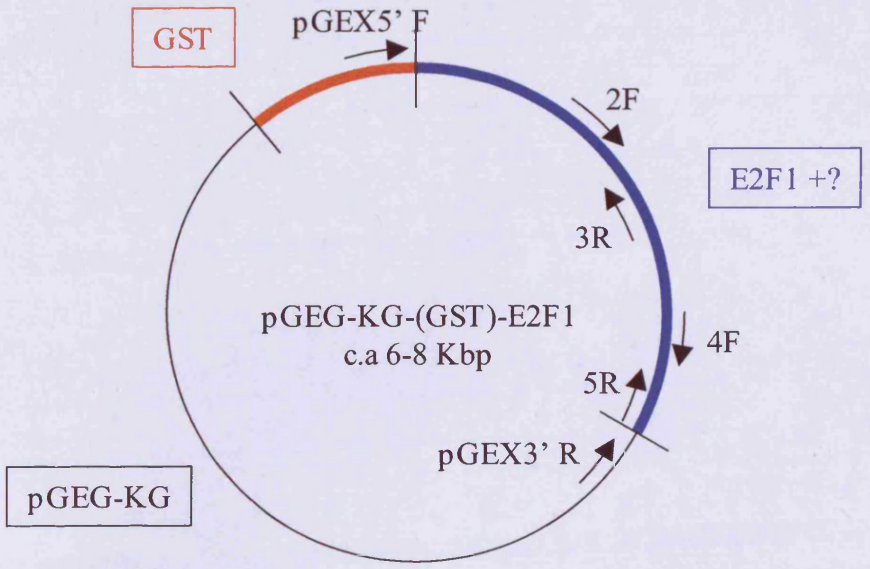

Figure 5.5 pGEX-KG vector map and schematic of pGEX-KG-(GST)-E2F1 sequencing strategy. Panel (a) shows the pGEX-KG vector map (www.addgene.com) and MCS within which the E2F1 gene was purportedly engineered (3' of the GST reading frame). Panel (b) shows a schematic of the vector with the E2F1 gene insert. The approximate positions of the primers designed or selected to sequence the unknown region (blue) are shown along with their direction of reading, also indicated by the final letter in the ID of each primer, "F" for forward (clockwise) and "R" for reverse (anti-clockwise).

Primer %GC:	Min 20	Opt 50	Max 80
Sequencing Region:	From 1 bp	To 1314 bp	
Primer Position:	Lead 0 bp	Spacing 400-500 bp	
Experimental Conditions:	Salt conc. 50mM	Primer conc. 50 nM	

The number three was entered in the field designated "Maximum number of Primers per Sequencing Subregion to return". The reverse read primers (3R(1°), 3R(2°) and 5R) were designed by checking the "sequence complimentary strand" box. Finally, in step 3 the primers identified by the software that corresponded to approximate positions as defined in the sequencing plan (**Figure 5.5b**) were chosen. Sequences that were generated by the software yet, had more than 3 'C's or 'G's at the 3' end were discarded. In step 4, no 5' or 3' modifications were selected, the purity level chosen was "desalted" and the scale of synthesis was set at 25 nmole. For clarity the sequences, IDs and other data relating to each of the primers is provided in **Table 5.1**.

PCR and Automated DNA Sequencing

Stock solutions (100 pmol μL^{-1}) of each primer were prepared in nuclease free ddH_2O and stored at -20 °C. Prior to use, each primer stock solution was diluted (1/100) to 1 pmol μL^{-1}. Working on ice (4 °C), to each reaction tube, primer (5 µL), "BigDye ready reaction premix" (4 µL), "BigDye sequencing buffer" (2 µL), pGEX-KG-(GST)-E2F1 plasmid (500 ng) and nuclease free ddH_2O were added in the order stated. Each tube was placed in a thermal cycler and the following reaction conditions used for 30 cycles:

1.	Denature	96 °C	30 sec
2.	Anneal	50 °C	15 sec
3.	Polymerise	60 °C	4 min

After completion of the PCR reaction the tubes were removed from the heating block, the top 4 mm of each tube cut-off and placed upside down in 1.5 mL Eppendorf tubes. The PCR reaction mixture was transferred to the Eppendorf tube by centrifugation at 14,000 rpm for 10 s at 4 °C. The empty PCR reaction tubes were discarded and an aliquot (90 µL) of 70 % isopropanol was added to each tube for 15 min. PCR product was precipitated by centrifugation (14,000 rpm for 30 min at 4°C).

Table 5.1 Characteristics of the primers used to determine the sequence of the E2F1 ORF.

Primer ID	Direction	Sequence	Annealing Region	No. of Bases	GC Content (%)	Tm (°C)
pGEX5' F	Forward	GGGCTGGCAAGCCACGTTTGGTG	869-891 (vector)	23	65.2	*
2F	Forward	CTATGACATCACCAACGTCC	501-520 (E2F1)	20	50.0	56.3
3R(1°)	Reverse	GGGTCTCAGGAGGGGCTTT	814-796 (E2F1)	19	63.2	62.8
3R(2°)	Reverse	GCAGGCGCAGCTGCGTAGTAC	700-680 (E2F1)	21	66.7	70.0
4F	Forward	AGCCTTTCCCCACCCCAC	1201-1218 (E2F1)	18	66.7	64.5
5R	Reverse	TCAGAAATCCAGGGGGGT	1314-1297 (E2F1)	18	55.6	60.3
pGEX3' R	Reverse	CCGGGAGCTGCATGTGTCAGAGG	1078-1056 (vector)	23	65.2	*

* Data not available as these primers were not designed using the Invitrogen™ OligoPerfect™ software.

The supernatant was removed and the PCR product washed twice with 180 μL of 70 % isopropanol. Once dry, the tubes were sealed and stored at -20 °C, sequence analysis was conducted within 48 h. Automated DNA sequence analysis was conducted Mr Barrie Francis (Central Biotechnology Services, Henry Wellcome Research Institute, Cardiff University) with an ABI Prism 3130xl Genetic Analyser, all data were exported as .ab1 files.

5.2.1.3 Sequence Analysis and In Silico Construction of the pGEX-KG-(GST)-E2F1 Plasmid Map

Sequencing files were provisionally reviewed using the software 4peaks (v1.7.2). However, for more advanced processing e.g. alignment of the respective sequences and construction of a complete plasmid map, the software Geneious (v3.5.5 with "Pro" functions) was used. Creation of the complete plasmid map is described in the results (section 5.3.1.1). The full consensus sequence was exported in FASTA format and annotated accordingly.

5.2.1.4 Mini-Induction to Test Expression of rhE2F1

Expression of the rhE2F1 protein was assessed in the the same *E.coli* strains (DH5α and TOP10) used to amplify the pGEX-KG-(GST)-E2F1 and later in the *E. coli* strains BL21 (DE3) and BL21 (DE3) pLysS.

The pGEX-KG-(GST)-E2F1 plasmid was transformed into each strain as described above (section 5.2.1.1). Starter-cultures were prepared by inoculating SOC media (10 mL) with an aliquot (50 μL) of freshly transformed bacteria. DH5α and TOP10 strains were incubated in the presence of Amp (100 μg mL^{-1}) while BL21 (DE3) and BL21 (DE3) pLysS strains were incubated with both Amp (100 μg mL^{-1}) and Cam (25 μg mL^{-1}). The culture was incubated at 37 °C for 4 h (orbital shaker), then agar plates containing the appropriate antibiotics inoculated with an aliquot (50 μL) of culture and incubated overnight at 37 °C. A single colony from each plate was selected and used to innoculate a mini-culture of LB media (10 mL). Each culture was incubated at 37 °C for 5 h in an orbital shaker (180-220 rpm) until an OD at λ_{600nm} of approximately 0.6 was reached expression induced with IPTG (0.5 mM final concentration). Following a post-induction time of 4 h, cultures were removed from the incubator, centrifuged (3,500 g, 10 min) and the supernatant removed. The pellet was

lysed and solubilised by the addition of an aliquot (100 μL) of gel loading buffer and analysis conducted using denaturing SDS-PAGE (Chapter 2, section 2.2.1.3).

Further optimisation of the expression conditions was conducted using the BL21 (DE3) pLysS strain. In these studies, 24 mini-cultures (four for each OD) were prepared as described above and incubated until ODs of 0.2, 0.3, 0.4, 0.5, 0.6, 0.7 were measured. For each OD, two cultures were induced with IPTG (0.5 mM final concentration) and two were used as controls. Two cultures for each OD (± IPTG) were incubated for a post-induction time of 4 h at 37 °C, and two cultures for each OD (± IPTG) incubated overnight (~ 16 h) at 20 °C. Following incubation, cultures were prepared for analysis by denaturing SDS-PAGE as described above.

As a mechanical method (e.g. probe sonicator or French press) of lysing the bacteria was unavailable at the Welsh School of Pharmacy it was not possible to conduct further studies and express sufficient quantities (> 3 mg) of rhE2F1 protein in Cardiff. Coupled with the lack of evidence for a coiled-coil mediated interaction between $Phb_{Y185-214}$ and E2F1 (see results section 5.3.3.1) further studies focused on expression of r-c-Jun and [^{15}N]r-c-Jun towards investigating target hybridisation in the second cancer model, c-Jun : $FosW_C$. The methods detailed below (section 5.2.2) were developed during a four-week visit to CIPF, Valencia.

5.2.2 Expression of r-c-Jun and [^{15}N]r-c-Jun

For ease of reference, an illustration of the steps taken to prepare r-c-Jun and [^{15}N]r-c-Jun is shown in **Figure 5.6**.

5.2.2.1 Assembly and Characterisation of the cytb5-r-c-Jun Plasmid

The pET15B-cytb5-ENLYFQGT-r-c-Jun plasmid was prepared by Dr A.K. Schott for use in this study, however a brief description of the method used is given below.

pET15B-cytb5-ENLYFQGT-r-c-Jun was assembled by conventional cloning using an in house modified version of the commercially pET15b plasmid containing, between the restriction sites NdeI and BamHI an N-terminal fusion-tag from the codon optimised sequence of rat cytb5 followed by a TEV protease recognition site ENLYFQ-KpnI (adapted from Mitra *et al*, 2005). The c-Jun fragment was obtained by gene synthesis (Itakura *et al*, 1977; Echt *et al*, 2004) using the partially complementary oligonucleotides c-Jun_forward (5′ ataata*ggtacc*gcctctatcgcgcgtctggaggagaaggtgaaaacgt

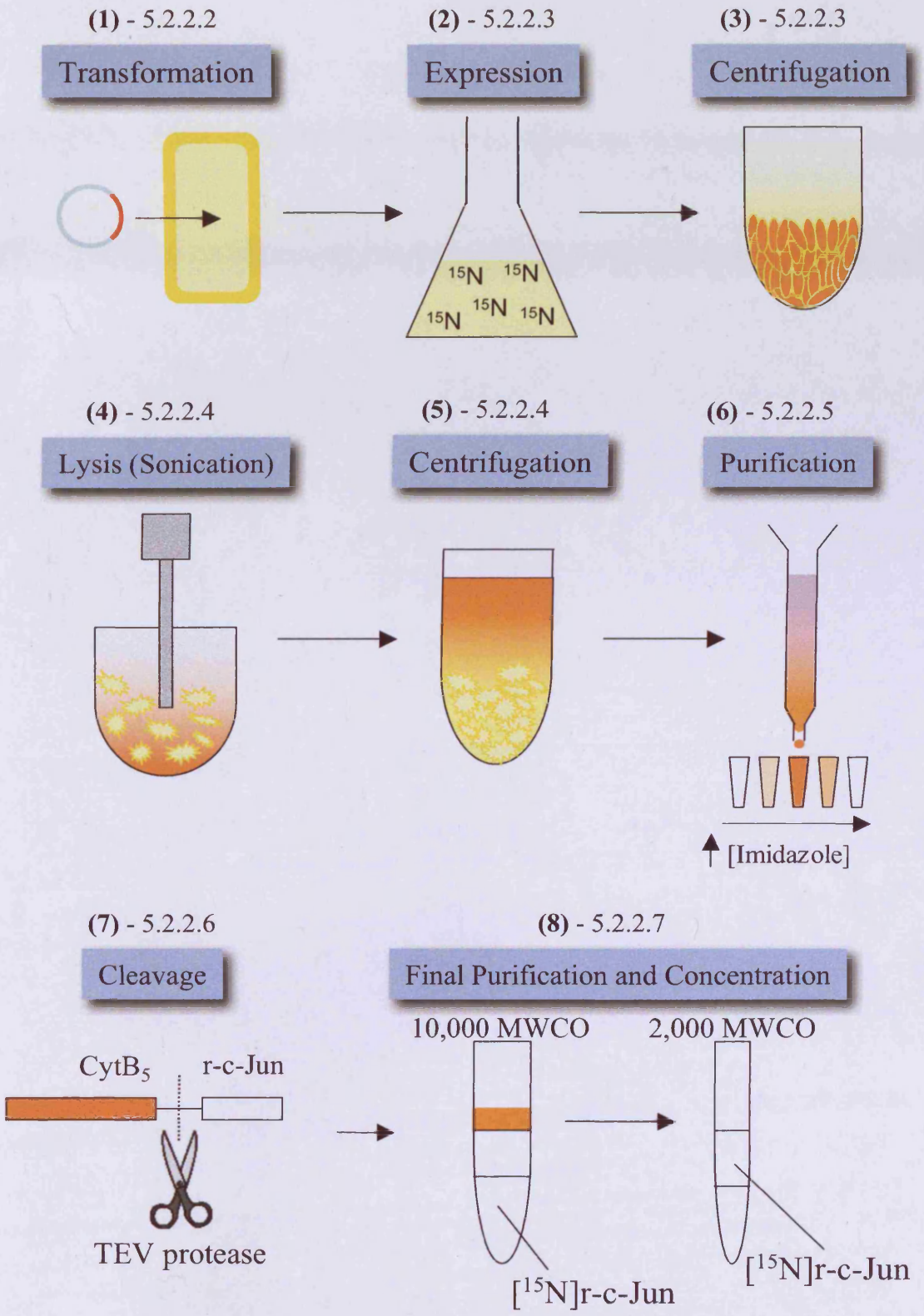

Figure 5.6 Illustration of the recombinant method used to express peptides r-c-Jun and [^{15}N]r-c-Jun. Sections in which each method is detailed are annotated.

taaaagcccaaaactatgaattagcgtc 3′), and c-Jun_reverse (5` tattatggatccttacgcacctaattgggc aacctgctcacgcagcatattggcggtagacgctaattcatagttttgggctt 3`), which were annealed and treated with DNA polymerase. The resulting 138 bp segment was amplified by PCR, purified with a gel extraction kit, restricted with the endonucleases KpnI and BamHI, and ligated into the pET15b-cytb5 plasmid, which had been treated with the same restriction endonucleases. Sequencing of clone no. 5 (pET15B-cytb5-ENLYFQGT-r-c-Jun-5) confirmed the expected sequence; the TEV protease cleavage site, the His tag, and the start and stop codons.

5.2.2.2 Transformation of BL21-CodonPlus (DE3) with the pET15B-cytb5-ENLYFQGT-r-c-Jun-5 Plasmid

The pET15B-cytb5-ENLYFQGT-r-c-Jun-5 plasmid was transformed into *E. coli* strain BL21-CodonPlus (DE3) affording the recombinant strain BL21-CodonPlus (DE3)-pET15B-cytb5-ENLYFQGT-r-c-Jun-5 as follows. Competent BL21-CodonPlus (DE3) *E.coli* (100 ng μL^{-1}, 50 µL) were thawed on ice, an aliquot (1 µL) of pET15B-cytb5-ENLYFQGT-r-c-Jun-5 added and left on ice for a further 30 min. Transformation was achieved by heat shocking at 42 °C for 45 sec, followed by cooling on ice for 2 min. An aliquot (450 µL) of LB media was added and the freshly transformed bacteria were left to propagate at 37 °C for 1 h (orbital shaker -180 rpm).

5.2.2.3 Expression of cytb5-c-Jun in BL21-CodonPlus (DE3) E. coli

This protocol details the methodology used initially for the expression of r-c-Jun. Alterations made when scaling the expression to 2 L (i.e. four 500 mL cultures) in the presence of ^{15}N containing media are described under a separate italicised heading in each section. Unless otherwise stated "an aliquot (x mL) was taken for analysis..." should be understood to indicate that the sample was analysed by SDS-PAGE electrophoresis as described in Chapter 2 (Section 2.2.1.3).

A pre-culture was prepared by inoculating LB media (25 mL) containing Amp (100 µg mL^{-1}) and chloramphenicol (Cam) (25 µg mL^{-1}) with an aliquot (50 µL) of freshly transformed bacteria. The culture was incubated at 37 °C overnight (orbital shaker). Simultaneously, an agar plate was inoculated with an aliquot (50 µL) of freshly transformed bacteria in the presence of Amp and Cam.

The following day, the pre-culture was centrifuged (3500 g, 10 min) and the media removed. A culture (500 mL) was prepared by inoculating M9 media with the re-suspended pellet of pre-culture. The culture was incubated at 37 °C for 5 h in an orbital shaker until an OD at λ_{600nm} of approximately 0.6 was reached. After 5 h, aliquots of glucose (20 % w/v, 5 mL) and IPTG (1M, 250 µL) were added. Following a post-induction time of 4.5 h cultures were removed from the incubator and stored at 4 °C overnight. The next day, an aliquot (1 mL) was taken, diluted 1:10 with ddH_2O and the OD at λ_{600nm} measured. The remaining volume (900 µL) was centrifuged, the pellet re-suspended in ddH_2O and an aliquot (20 µL) taken for analysis. The culture (500 mL) was transferred to a large centrifuge tube (ca. 1 L) and spun at 3500 g, 4 °C for 15 min. The pellet was transferred to a small centrifuge tube (50 mL) and spun at 6000 g, 4 °C for 5 min, weighed, then placed at - 20 °C and left for 1 h.

Expression of [^{15}N]cytb5-c-Jun in BL21-CodonPlus (DE3) E. coli

Four cultures: A, B, C and D (500 mL each) were prepared and each inoculated with pre-culture (25 mL). Culture media (M9) was freshly prepared containing [^{15}N], provided in the form of [^{15}N]H_4Cl.

5.2.2.4 Lysis of BL21-CodonPlus (DE3) E. coli by Probe Sonication

Lysis buffer was freshly prepared, cooled to 4 °C and used to re-suspend the frozen bacterial pellet (approx. 10 mL buffer to 1 g pellet). The suspension was vortexed to obtain a homogenous mixture and left on ice (4 °C) for 30 min. The mixture was transferred to a sterile glass beaker (on ice) and the bacteria lysed by probe sonication, using 6 x 30 sec pulses with 30 sec intervals. An aliquot (500 µL) of the lysate was taken for analysis. The remaining lysate was centrifuged at 10,000 g, 4 °C for 30 min. The supernatant was removed from the pellet and both were stored on ice (4 °C). Aliquots (20 µL) of each were collected for analysis.

Lysis of BL21-CodonPlus (DE3) E. coli by Probe Sonication

Lysis buffer (60 mL, total volume) was used to re-suspend the frozen pellets (each weighed approximately 2.3 g). Lysis by probe sonication utilised 8 x 30 sec pulses with 30 sec intervals. An aliquot (500 µL) was taken for analysis. Following centrifugation of the lysate, the pellet was still pink in colour. Therefore a second round

of sonication (6 x 30 sec pulses with 30 sec intervals) was performed. An aliquot (500 μL) of the lysate was taken for analysis.

5.2.2.5 Purification of cytb5-r-c-Jun from Crude Lysate

Purification was achieved by affinity chromatography using TALON® metal affinity resin. The bed volume was calculated on the basis that the fusion protein content of the crude lysate was 60-70 % (protein concentration approximated from the OD at λ_{280nm}). The binding capacity of the resin used was published to be 20 mg protein mL^{-1}. TALON® media was applied to the column as a 50 % w/v slurry stored in 20 % v/v EtOH in ddH_2O. The media was washed with five-column volume of ddH_2O followed by five-column volumes of freshly prepared Tris HCl buffer, pH 8.0, 20 mM. Crude lysate supernatant was applied to the media and recycled twice. Proteins and other cellular debris were removed by washing with ten column volumes of Tris HCl buffer, pH 8.0, 20 mM containing imidazole, 5 mM. Stepwise elution with increasing imidazole concentrations was as follows:

- 2 mL imidazole 50 mM
- 2 mL imidazole 250 mM
- 3 mL imidazole 500 mM
- 2 mL imidazole 1000 mM

Fractions (1 mL) were collected for analysis. The column was cleaned by washing with two-column volumes of Tris HCl buffer, pH 8.0, 20 mM containing imidazole, 1000 mM. Followed by five-column volumes of ddH_2O, five-column volumes of MES buffer, pH 5.0, 20 mM, five-column volumes of ddH_2O and two-column volumes of 20 % v/v EtOH in ddH_2O. The column was sealed and the media stored at 4 °C for future use.

Purification of [^{15}N]cytb5r-c-Jun from Crude Lysate

A bed volume of 6 mL was used (12 mL 50 % w/v slurry) due to the larger scale of the preparation. The media was equilibrated as described, transferred to a polypropylene container (ca. 250 mL) and incubated with the crude lysate supernatant at 4 °C for 30 min, agitating every 5-10 min. The media and lysate suspension were transferred back to the purification column and washed with five-column volumes (30

mL) of Tris HCl buffer containing imidazole, 10 mM. Stepwise elution with increasing imidazole concentrations was performed as follows:

- 30 mL imidazole 50 mM
- 6 mL imidazole 250 mM
- 9 mL imidazole 500 mM
- 6 mL imidazole 1000 mM

Fractions were collected corresponding to each imidazole concentraion and aliquots (20 μL) taken for analysis. The column was washed with three-column volumes of Tris HCl buffer containing imidazole, 1000 mM and the original cleaning protocol followed to regenerate the TALON® media.

5.2.2.6 Cleavage of cytb5-r-c-Jun Using TEV Protease

Following analysis of the eluted fractions by SDS-PAGE electrophoresis, TEV protease (3.79 mg mL^{-1}, 50 μL) was added the fraction (1 mL) containing the desired fusion protein in highest purity and the solution incubated at 4 °C. Aliquots (20 μL) were taken at 2.5 h, 16 h and 60 h for analysis, after 16 h, a further aliquot (50 μL) of TEV protease was added.

Cleavage of [^{15}N]CytB$_5$r-c-Jun Using TEV Protease

The protein content of the pooled fractions (imidazole concentration of 50, 250 and 500 mM) was estimated to be *circa* 40 mg therefore TEV protease (250 μL) was added and the cleavage reaction allowed to proceed overnight (16 h) at 4 °C. An aliquot (20 μL) was taken for analysis and a further aliquot of TEV protease (100 μL) added for a further 3 h.

5.2.2.7 Final Purification and Concentration of r-c-Jun

TEV protease, cytb5 and other contaminating proteins remaining from TALON® purification were removed using a Vivaspin 10 kDa MWCO centrifuge tube. Prior to sample addition the membrane was washed with ddH_2O was centrifuged at 4000 g, 4 °C for 10 min. The membrane was washed again with ddH_2O and the centrifugation repeated once, thus ensuring removal of residual glycerol/Na azide. The TEV protease cleavage solution was added to the primed tube and spun at the same conditions. The

membrane was washed with ddH_2O and centrifuged a final time. An aliquot (20 μL) of the high molecular weight fraction was taken for analysis. The elutates were pooled and concentrated using a Vivaspin 2 kDa MWCO centrifuge tube. As before, the tube was first primed by washing twice and centrifuging with ddH_2O. Once a volume of approximately 100 μL was obtained the sample was washed twice with ddH_2O, the OD of both the high Mw fraction and eluate was measured and samples taken for analysis by SDS-PAGE electrophoresis and MALDI-TOF mass spectroscopy.

Final Purification and Concentration of [^{15}N]r-c-Jun

Centrifugation using Vivaspin 10 kDa MWCO tubes was performed at 12 °C to reduce the likelihood of c-Jun homo-dimerising (c.f. 4 °C). Concentration was achieved using two Vivaspin 2 kDa MWCO centrifugation tubes (8000 g, 4 °C for 11 min). This process was repeated until the final volume was reduced to *circa* 600 μL. The retentate was freeze dried, weighed and stored at -20 °C.

5.2.3 Characterisation of r-c-Jun and [^{15}N]r-c-Jun Peptides by MALDI-TOF MS

MALDI-TOF MS was conducted to verify the mass of each peptide. In earlier studies (Chapter 3), MS of peptides was conducted using ESI-TOF MS, however, this study was conducted at CIPF and MALDI-TOF was the only MS technique available. The MS suite was operated as a technician led service and therefore samples were simply sent as a dry lyophilisate for analysis and data were received as .xls files.

5.2.4 Preparation of Samples for Target Hybridisation Studies by CD and NMR Spectroscopy

All samples were prepared for either CD or NMR experiments in the same buffers. Dry lyophilisate (peptide or conjugate) was dissolved in a phosphate buffer comprising of NaH_2PO_4/Na_2HPO_4 (10 mM) containing NaF (100 mM) in ddH_2O. Concentrations were then determined by UV spectroscopy as described in Chapter 2 (Section 2.2.1.1).

5.2.4.1 Characterisation by CD Spectroscopy

The general method is described in Chapter 2 (section 2.2.1.4).

$Phb_{185-214}$, $Phb_{Y185-214}$, E2F1a and E2F1b

Initial CD experiments were conducted at EPFL with peptides $Phb_{185-214}$, $Phb_{Y185-214}$, E2F1a and E2F1b and used a total peptide concentration of 80 μM. The concentration of $Phb_{185-214}$ was determined gravimetrically while the UV spectroscopy (section 2.2.1.1) was used to determine the concentration of all other peptides in this study. Thermal denaturation spectra were acquired in temperature steps of 5 °C over a range of 5-95 °C.

c-Jun, [^{15}N]r-c-Jun, $FosW_C$, mPEG-$FosW_C$ and mPEG-MAL

Characterisation of the peptides c-Jun, [^{15}N]r-c-Jun was conducted at CIPF, all further studies were conducted in Cardiff. The temperatures used and cuvette pathlength are all detailed in the figure legends (see results section 5.3.3.2). One experiment was conducted using a tandem cell: a quartz cuvette with a two chambers separated by a thin screen of quartz. This made it possible to acquire a far UV CD spectrum pre-mixing, followed by the acquisition of a spectrum by post-mixing without introducing any error by pipetting.

5.2.4.2 Characterisation by 1D, ^{1}H-NMR and 2D ^{1}H, ^{15}N-HSQC Spectroscopy

Samples solutions (1 mL) were prepared as described above (section 5.2.4) however, with the addition of D_2O (5 % v/v) and an aliquot (30 μM ~ final concentration) of the internal standard 2,2,3,3-tetradeutero-3-trimethylsilylpropionic acid (TSP). Measurements were conducted using quartz NMR tubes filled with 500 μL of sample solution. All spectra were recorded using peptide concentrations of 75 μM as used in the latter CD studies (section 5.2.4.1) and unless otherwise noted all experiments were conducted at 37 °C and pH 7.4 to model the physiological environment. All data were processed using the program Topspin 1.3.

Acquisition of 1D ^{1}H-NMR Spectra of c-Jun, $FosW_C$ and mPEG-$FosW_C$

^{1}H-NMR spectra were acquired with 16 K complex points and a spectral width of 8.4 kHz. The total number of scans was 256, with a repetition delay of 1.5 s. A WATERGATE scheme was used to suppress the water signal.

Acquisition of 2D ^{1}H, ^{15}N-HSQC Spectra of [^{15}N]r-c-Jun, $FosW_C$: [^{15}N]r-c-Jun and mPEG-$FosW_C$: [^{15}N]r-c-Jun

2D, ^{1}H, ^{15}N-HSQC heteronuclear experiments were acquired with spectral widths of 8 kHz (^{1}H dimension) and 2.2 kHz (^{15}N dimension), 40 scans and a repetition delay of 1s. All measurements were first conducted using [^{15}N]r-c-Jun (75 μM) then then an aliquot of either $FosW_C$ or mPEG-$FosW_C$ added and the concentration of each peptide adjusted to 75 μM.

5.3 Results

Early CD studies with Phb and target peptides E2F1a and E2F1b were conducted at EPFL, Lausanne. The characterisation of the pGEX-KG-(GST)-E2F1 plasmid and expression of rhE2F1 and detailed CD studies with c-Jun, $FosW_C$ and mPEG-$FosW_C$ were conducted in Cardiff, while expression and characterisation of r-c-Jun/[^{15}N]r-c-Jun, first CD studies and detailed analyses by 1D, ^{1}H-NMR and 2D ^{1}H, ^{15}N-HSQC spectroscopy were conducted during a visit to the structural biology laboratory at CIPF in Valencia, Spain.

5.3.1 Preparation and Characterisation of rhE2F1 and r-c-Jun

5.3.1.1 Characterisation of the pGEX-KG-(GST)-E2F1 Plasmid and Expression of rhE2F1 Protein

For ease of reference, a summary of the experiments conducted in this section is shown in **Figure 5.7**.

The A_{260} : A_{280} ratios were 1.88 and 1.63 for TOP10 and DH5α respectively. This indicated that the sample obtained from the TOP10 *E.coli* was of superior purity (less protein contamination). Furthermore, significantly more plasmid was obtained using this strain, with a yield of 761 μg compared with 272 μg of lower purity plasmid obtained from the DH5α strain.

Characterisation of "uncut" plasmid by agarose gel electrophoresis showed two bands > 10 Kb in the TOP10 *E.coli* samples and a single band > 10 Kb for the DH5α samples (**Figure 5.8**). As the plasmid was expected to be approximately 6-8 Kb, the data suggested that the DNA was running as non-covalent, intermolecular multimers. Smearing was seen in both lanes (0.2 μg and 0.5 μg) for the DH5α derived plasmid suggesting the presence of protein contamination, however, none was seen for the

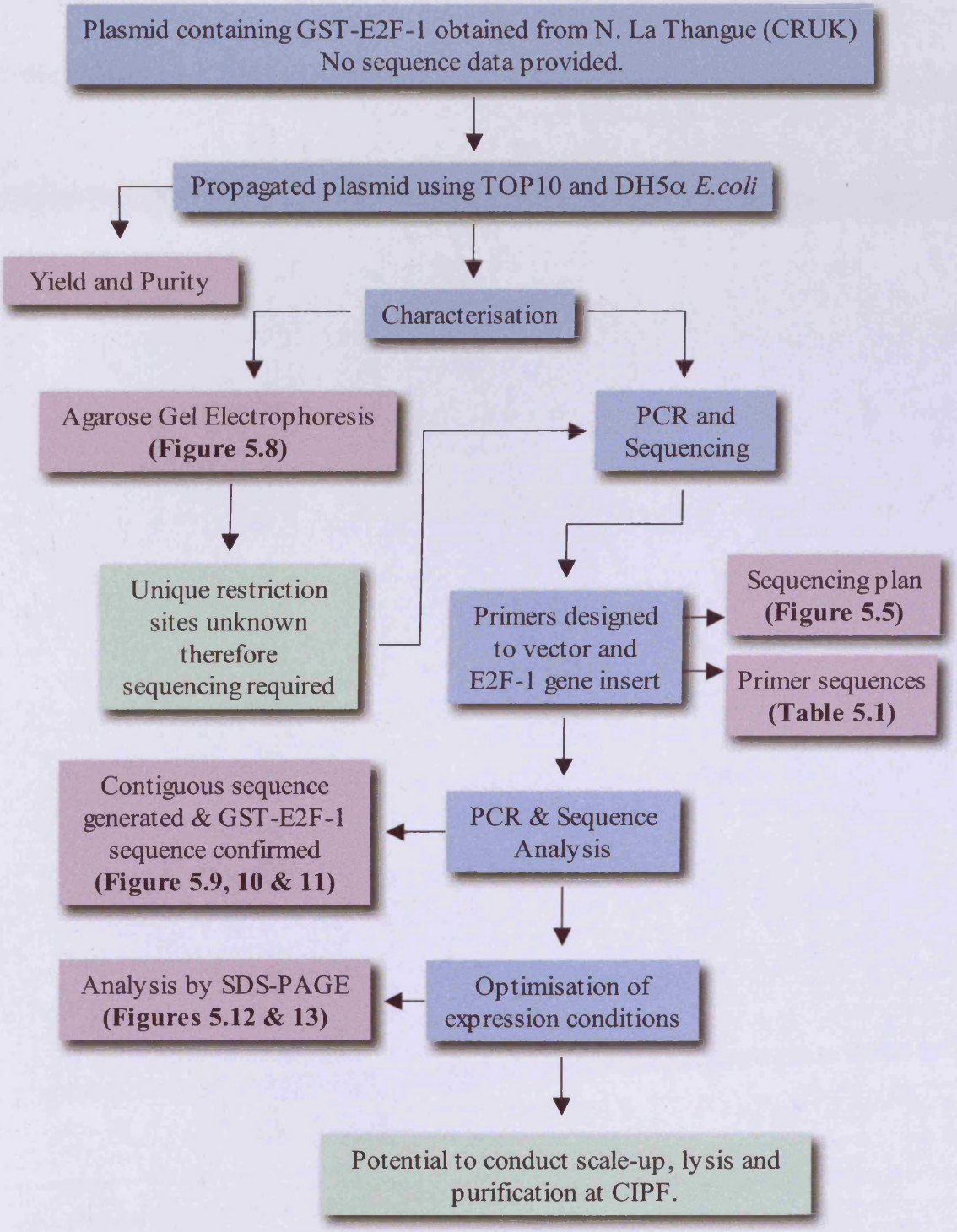

Figure 5.7 Summary of the experiments conducted towards recombinant expression of the rhE2F1 target protein.

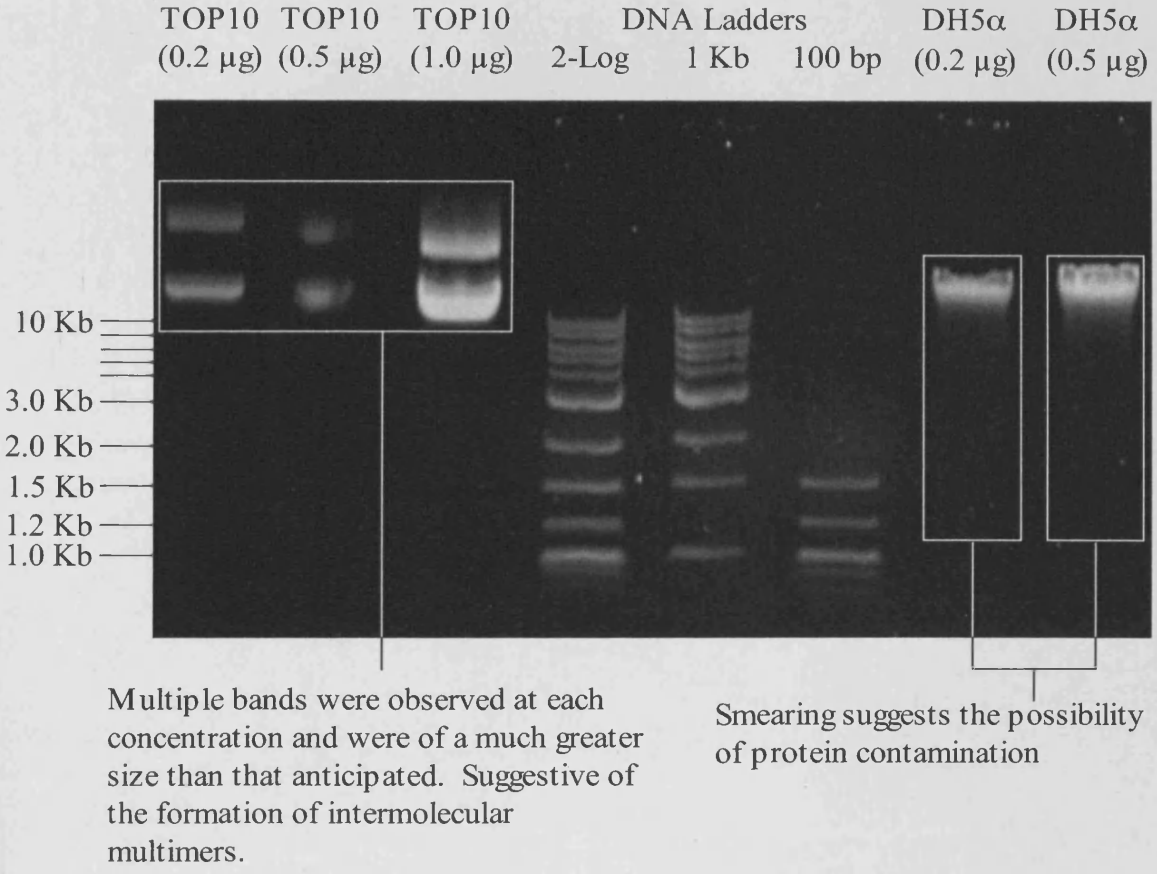

Figure 5.8 Characterisation by agarose gel electrophoresis of the pGEX-KG-E2F1 plasmid. Plasmid was obtained following amplification in two *E.coli* strains (TOP10 and DH5α).

TOP10 derived plasmid. These observations supported the quantitative assessment of purity given by the ratio of A_{260}/A_{280}.

Sequencing of the pGEX-KG-(GST)-E2F1 Plasmid

Preliminary experiments using 50 ng of template (plasmid) and 3 pmol of primer per reaction yielded very low levels of PCR product such that the signal was hardly distinguishable from the noise in the electropherogram (data not shown), as such the quantity of plasmid template used was increased ten-fold (500 ng) and quantity of primer increased to 5 pmol per reaction. The only primer to fail to generate a PCR product on the second attempt was primer 3R(1°), as such a second primer was designed (3R(2°)) rather than attempt to optimise the myriad of possible conditions in the PCR. The reaction with the new primer was successful as judged by the electropherogram (data not shown).

The linear illustration of contiguous sequence shows the successful alignment and overlap of each piece of sequence data provided by the respective primers (**Figure 5.9**). A more detailed representation of the sequence assembly shows the substantial degree of overlay (> 150 bases) between primer/primer or primer/plasmid sequence (**Figure 5.10**). In panel (c) primer 5R did not confer any significant additional sequence data not provided by the other three primers. The single discrepancy identified by the break in the green bar of panel (c) is the result of disagreement between the sequence data provided by primers pGEX3'R and 4F, and the vector sequence. It is most likely that the sequencing data has misread and entered an extra base, in this instance "A" since the sequences otherwise agree with the vector sequence. It is not of great significance since this discrepancy is after the TGA stop codon encoding rhE2F1.

The full consensus sequence showed that the sequence is 100 % homologous with the sequence for Human E2F-1 and the start (ATG) and stop (TGA) codons are both present (**Figure 5.11**). Furthermore, it was possible to identify the likely cut sites used to first assemble the plasmid. The single cut, restriction enzymes that would have probably been used are identified in bold font as SmaI (5' of the E2F1 DNA) and XhoI (3' of the E2F1 DNA).

Expression of rhE2F1 Protein

No bands corresponding to over-expression of GST-rhE2F1 protein were observed following analysis of DH5α, TOP10 and BL21 (DE3) *E. coli* crude lysate by

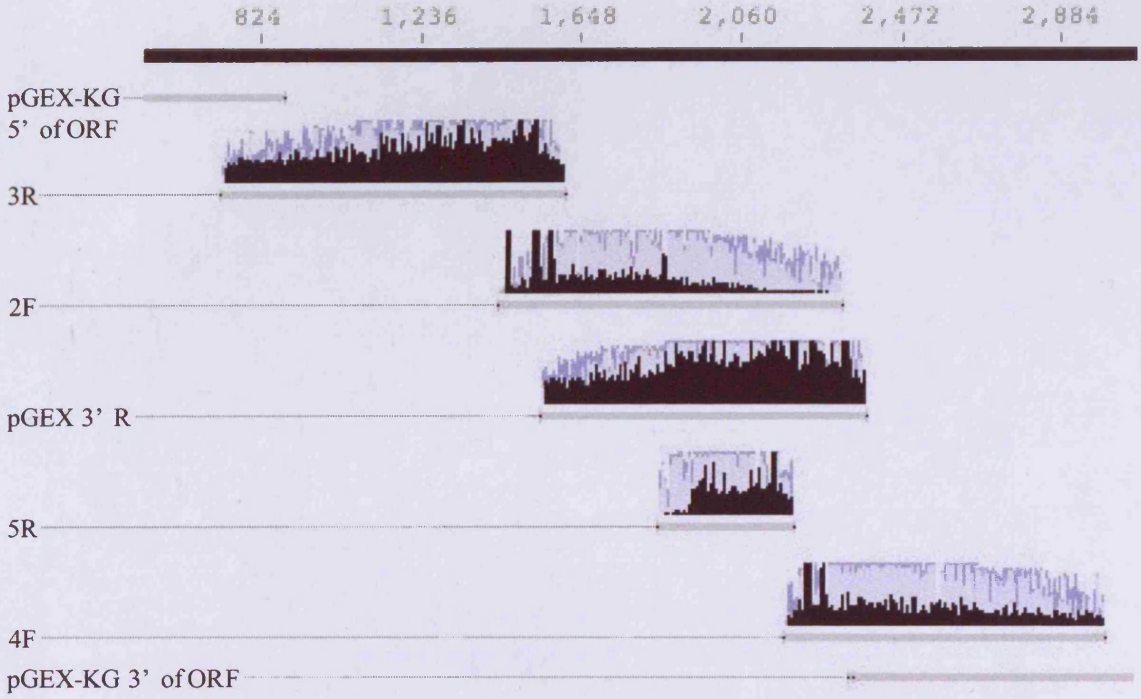

Figure 5.9 Linear alignment of the contiguous pGEX-KG-(GST)-E2F1 plasmid sequence. Sequences are shown as grey bars and represent their actual alignment. The chromatograms, in black show the signal intensity for each of the sequenced bases. Assembly was performed using Geneious software version 3.5.5.

(a) Overlay of 3R primer sequence with the vector 5' of the ORF.

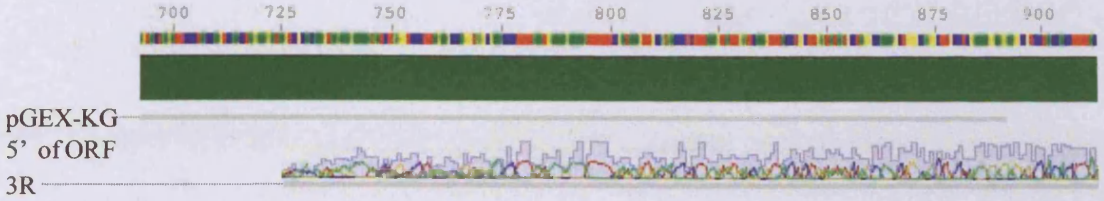

(b) Overlay of the 3R, 2F and pGEX 3' R primer sequences in the centre of the E2F-1/unknown sequence region

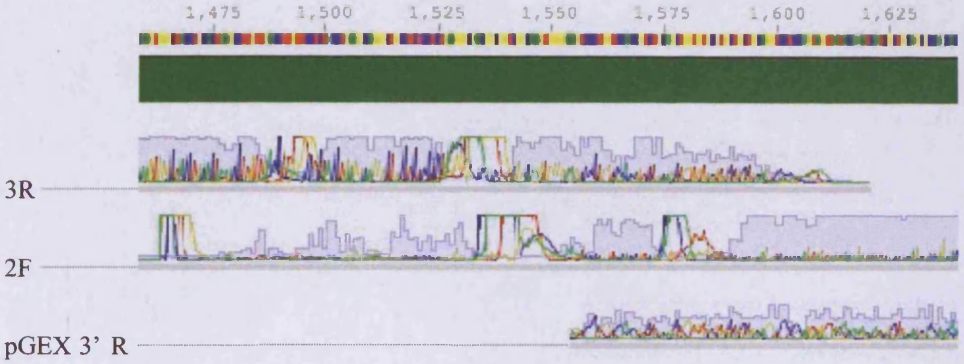

(c) Overlay of the 2F, pGEX 3' R, 5R and 4F primer sequences with the vector 3' of the E2F-1/unknown sequence region.

Figure 5.10 Magnified alignment of the contiguous pGEX-KG-(GST)-E2F1 plasmid sequence. Panels a, b and c show in greater detail the alignment of the primer derived sequences and vector pGEX-KG. Solid green bars represent 100 % homology between the overlaid sequences. The colours used in the chromatograms and consensus sequence bar represent the bases A (red), C (blue), G (gold) and T (green).

>pGEX-KG-E2F-1 Consensus Sequence 1-6365bp
ACGTTATCGACTGCACGGTGCACCAATGCTTCTGGCGTCAGGCAGCCATCGGAAGCTGTGGTATGGCTGTGCAGGTCGTAAATCACTGCATAATTC
GTGTCGCTCAAGGCGCACTCCCGTTCTGGATAATGTTTTTTGCGCCGACATCATAACGGTTCTGGCAAATATTCTGAAATGAGCTGTTGACAATTA
ATCATCGGCTCGTATAATGTGTGGAATTGTGAGCGGATAACAATTTCACACAGGAAACAGTATTCATGTCCCCTATACTAGGTTATTGGAAAATTA
AGGGCCTTGTGCAACCCACTCGACTTCTTTTGGAATATCTTGAAGAAAAATATGAAGAGCATTTGTATGAGCGCGATGAAGGTGATAAATGGCGAA
ACAAAAAGTTTGAATTGGGTTTGGAGTTTCCCAATCTTCCTTATTATATTGATGGTGATGTTAAATTAACACAGTCTATGGCCATCATACGTTATA
TAGCTGACAAGCACAACATGTTGGGTGGTTGTCCAAAAGAGCGTGCAGAGATTTCAATGCTTGAAGGAGCGGTTTTGGATATTAGATACGGTGTTT
CGAGAATTGCATATAGTAAAGACTTTGAAACTCTCAAAGTTGATTTTCTTAGCAAGCTACCTGAAATGCTGAAAATGTTCGAAGATCGTTTATGTC
ATAAAACATATTTAAATGGTGATCATGTAACCCATCCTGACTTCATGTTGTATGACGCTCTTGATGTTGTTTTATACATGGACCCAATGTGCCTGG
ATGCGTTCCCAAAATTAGTTTGTTTTAAAAAACGTATTGAAGCTATCCCACAAATTGATAAGTACTTGAAATCCAGCAAGTATATAGCATGGCCTT
TGCA<pGEX5'>GGGCTGGCAAGCCACGTTTGGTGGTGGCGACCATCCTCCAAAATCGGATCTGGTTCCGCGTGGATC<SmaI>CCAT[redacted]GCCTT
GGCCGGGGCCCCTGCGGGCGGCCCATGCGCGCCGGCGCTGGAGGCCCTGCTCGGGGCCGGCGCGCTGCGGCTGCTCGACTCCTCGCAGATCGTCAT
CATCTCCGCCGCGCAGGACGCCAGCGCCCCGCCGGCTCCCACCGGCCCCGCGGCGCCCGCCGCCGGCCCCTGCGACCCTGACCTGCTGCTCTTCGC
CACACCGCAGGCGCCCCGGCCCACACCCAGTGCGCCGCGGCCCGCGCTCGGCCGCCCGCCGGTGAAGCGGAGGCTGGACCTGGAAACTGACCATCA
GTACCTGGCCGAGAGCAGTGGGCCAGCTCGGGGCAGAGGCCGCCATCCAGGAAAAGGTGTGAAATCCCCGGGGGAGAAGTCACGCTATGAGACCTC
ACTGAATCTGACCACCAAGCGCTTCCTGGAGCTGCTGAGCCACTCGGCTGACGGTGTCGTCGACCTGAACTGGGCTGCCGAGGTGCTGAAGGTGCA
GAAGCGGCGCAT<2F>CTATGACATCACCAACGTCCTTGAGGGCATCCAGCTCATTGCCAAGAAGTCCAAGAACCACATCCAGTGGCTGGGCAGCC
ACACCACAGTGGGCGTCGGCGGACGGCTTGAGGGGTTGACCCAGGACCTCCGACAGCTGCAGGAGAGCGAGCAGCAGCTGGACCACCTGATGAATA
TCT<3R(2°)>GTACTACGCAGCTGCGCCTGCTCTCCGAGGACACTGACAGCCAGCGCCTGGCCTACGTGACGTGTCAGGACCTTCGTAGCATTGC
AGACCCTGCAGAGCAGATGGTTATGGTGATC<3R(1°)>AAAGCCCCTCCTGAGACCCAGCTCCAAGCCGTGGACTCTTCGGAGAACTTTCAGATC
TCCCTTAAGAGCAAACAAGGCCCGATCGATGTTTTCCTGTGCCCTGAGGAGACCGTAGGTGGGATCAGCCCTGGGAAGACCCCATCCCAGGAGGTC
ACTTCTGAGGAGGAGAACAGGGCCACTGACTCTGCCACCATAGTGTCACCACCACCATCATCTCCCCCCTCATCCCTCACCACAGATCCCAGCCAG
TCTCTACTCAGCCTGGAGCAAGAACCGCTGTTGTCCCGGATGGGCAGCCTGCGGGCTCCCGTGGACGAGGACCGCCTGTCCCCGCTGGTGGCGGCC
GACTCGCTCCTGGAGCATGTGCGGGAGGACTTCTCCGGCCTCCTCCCTGAGGAGTTCATC<4F>AGCCTTTCCCCACCCCACGAGGCCCTCGACTA
CCACTTCGGCCTCGAGGAGGGCGAGGGCATCAGAGACCTCTTCGACTGTGACTTTGGGGACCTC<5R>ACCCCCCTGGATTTC[redacted]CAGGATGCAT
GAATTCTGCAGATATCCATCACACTGGCGGCCG<XhoI>CTCGAGCATGCATCTAGAGGGCCCTATTCTATAGTGTCACCTAAATGCTAGAGCTCA
AGCTTAATTCATCGTGACTGACTGACGATCTGCCTCGCGCGTTTCGGTGATGACGGTGAAAA<pGEX3'>CCTCTGACACATGCAGCTCCCGGAGA
CGGTCACAGCTTGTCTGTAAGCGGATGCCGGGAGCAGACAAGCCCGTCAGGGCGCGTCAGCGGGTGTTGGCGGGTGTCGGGGCGCAGCCATGACCC
AGTCACGTAGCGATAGCGGAGTGTATAATTCTTGAAGACGAAAGGGCCTCGTGATACGCCTATTTTTATAGGTTAATGTCATGATAATAATGGTTT
CTTAGACGTCAGGTGGCACTTTTCGGGGAAATGTGCGCGGAACCCCTATTTGTTTATTTTTCTAAATACATTCAAATATGTATCCGCTCATGAGAC
AATAACCCTGATAAATGCTTCAATAATATTGAAAAAGGAAGAGTATGAGTATTCAACATTTCCGTGTCGCCCTTATTCCCTTTTTTGCGGCATTTT
GCCTTCCTGTTTTTGCTCACCCAGAAACGCTGGTGAAAGTAAAAGATGCTGAAGATCAGTTGGGTGCACGAGTGGGTTACATCGAACTGGATCTCA
ACAGCGGTAAGATCCTTGAGAGTTTTCGCCCCGAAGAACGTTTTCCAATGATGAGCACTTTTAAAGTTCTGCTATGTGGCGCGGTATTATCCCGTG
TTGACGCCGGGCAAGAGCAACTCGGTCGCCGCATACACTATTCTCAGAATGACTTGGTTGAGTACTCACCAGTCACAGAAAAGCATCTTACGGATG
GCATGACAGTAAGAGAATTATGCAGTGCTGCCATAACCATGAGTGATAACACTGCGGCCAACTTACTTCTGACAACGATCGGAGGACCGAAGGAGC
TAACCGCTTTTTTGCACAACATGGGGGATCATGTAACTCGCCTTGATCGTTGGGAACCGGAGCTGAATGAAGCCATACCAAACGACGAGCGTGACA
CCACGATGCCTGCAGCAATGGCAACAACGTTGCGCAAACTATTAACTGGCGAACTACTTACTCTAGCTTCCCGGCAACAATTAATAGACTGGATGG
AGGCGGATAAAGTTGCAGGACCACTTCTGCGCTCGGCCCTTCCGGCTGGCTGGTTTATTGCTGATAAATCTGGAGCCGGTGAGCGTGGGTCTCGCG
GTATCATTGCAGCACTGGGGCCAGATGGTAAGCCCTCCCGTATCGTAGTTATCTACACGACGGGGAGTCAGGCAACTATGGATGAACGAAATAGAC
AGATCGCTGAGATAGGTGCCTCACTGATTAAGCATTGGTAACTGTCAGACCAAGTTTACTCATATATACTTTAGATTGATTTAAAACTTCATTTTT
AATTTAAAAGGATCTAGGTGAAGATCCTTTTTGATAATCTCATGACCAAAATCCCTTAACGTGAGTTTTCGTTCCACTGAGCGTCAGACCCCGTAG
AAAAGATCAAAGGATCTTCTTGAGATCCTTTTTTTCTGCGCGTAATCTGCTGCTTGCAAACAAAAAAACCACCGCTACCAGCGGTGGTTTGTTTGC
CGGATCAAGAGCTACCAACTCTTTTTCCGAAGGTAACTGGCTTCAGCAGAGCGCAGATACCAAATACTGTCCTTCTAGTGTAGCCGTAGTTAGGCC
ACCACTTCAAGAACTCTGTAGCACCGCCTACATACCTCGCTCTGCTAATCCTGTTACCAGTGGCTGCTGCCAGTGGCGATAAGTCGTGTCTTACCG
GGTTGGACTCAAGACGATAGTTACCGGATAAGGCGCAGCGGTCGGGCTGAACGGGGGGTTCGTGCACACAGCCCAGCTTGGAGCGAACGACCTACA
CCGAACTGAGATACCTACAGCGTGAGCTATGAGAAAGCGCCACGCTTCCCGAAGGGAGAAAGGCGGACAGGTATCCGGTAAGCGGCAGGGTCGGAA
CAGGAGAGCGCACGAGGGAGCTTCCAGGGGGAAACGCCTGGTATCTTTATAGTCCTGTCGGGTTTCGCCACCTCTGACTTGAGCGTCGATTTTTGT
GATGCTCGTCAGGGGGGCGGAGCCTATGGAAAAACGCCAGCAACGCGGCCTTTTTACGGTTCCTGGCCTTTTGCTGGCCTTTTGCTCACATGTTCT
TTCCTGCGTTATCCCCTGATTCTGTGGATAACCGTATTACCGCCTTTGAGTGAGCTGATACCGCTCGCCGCAGCCGAACGACCGAGCGCAGCGAGT
CAGTGAGCGAGGAAGCGGAAGAGCGCCTGATGCGGTATTTTCTCCTTACGCATCTGTGCGGTATTTCACACCGCATAAATTCCGACACCATCGAAT
GGTGCAAAACCTTTCGCGGTATGGCATGATAGCGCCCGGAAGAGAGTCAATTCAGGGTGGTGAATGTGAAACCAGTAACGTTATACGATGTCGCAG
AGTATGCCGGTGTCTCTTATCAGACCGTTTCCCGCGTGGTGAACCAGGCCAGCCACGTTTCTGCGAAAACGCGGGAAAAAGTGGAAGCGGCGATGG
CGGAGCTGAATTACATTCCCAACCGCGTGGCACAACAACTGGCGGGCAAACAGTCGTTGCTGATTGGCGTTGCCACCTCCAGTCTGGCCCTGCACG
CGCCGTCGCAAATTGTCGCGGCGATTAAATCTCGCGCCGATCAACTGGGTGCCAGCGTGGTGGTGTCGATGGTAGAACGAAGCGGCGTCGAAGCCT
GTAAAGCGGCGGTGCACAATCTTCTCGCGCAACGCGTCAGTGGGCTGATCATTAACTATCCGCTGGATGACCAGGATGCCATTGCTGTGGAAGCTG
CCTGCACTAATGTTCCGGCGTTATTTCTTGATGTCTCTGACCAGACACCCATCAACAGTATTATTTTCTCCCATGAAGACGGTACGCGACTGGGCG
TGGAGCATCTGGTCGCATTGGGTCACCAGCAAATCGCGCTGTTAGCGGGCCCATTAAGTTCTGTCTCGGCGCGTCTGCGTCTGGCTGGCTGGCATA
AATATCTCACTCGCAATCAAATTCAGCCGATAGCGGAACGGGAAGGCGACTGGAGTGCCATGTCCGGTTTTCAACAAACCATGCAAATGCTGAATG

Legend:

Black - Vector (pGEX-KG). Red - GST sequence.
Blue - E2F-1. Pink - Named primer annealing regions

Black highlighted regions show the correct start and end codons.

SmaI and **XhoI** are the likely cut-sites used to insert the E2F1 gene during the original synthesis

A (bold and underlined) represents the single discrepancy resulting from alignment of the primer derived sequencing data and the vector sequence.

Figure 5.11 Consensus sequence for the pGEX-KG-(GST)-E2F1 plasmid in FASTA format.

denaturing SDS-PAGE (data not shown). However, successful over-expression was observed using the BL21 (DE3) pLysS *E. coli* strain irrespective of the OD at which induction took place (**Figure 5.12**). The band corresponded to a higher molecular weight than expected, however, this is likely due to dimerisation of the fusion protein driven by the GST tag. When the cultures were incubated at 20 °C (rather than 37 °C) post-induction, over-expression of GST-rhE2F1 was hardly detectable (**Figure 5.13**). Strongest bands correlating to over-expressed rhE2F1were seen at ODs of 0.2-0.4, however at higher ODs no over-expression was detected.

5.3.1.2 Expression and Characterisation of r-c-Jun and [^{15}N]r-c-Jun Peptides

The plasmid encoding r-c-Jun was previously prepared and characterised by Dr A.K. Schott (CIPF) so that this project could start with optimisation of the expression and purification protocols. For ease of reference, the experimental approach is summarised in **Figure 3.14**.

Optimisation of Expression and Purification of r-c-Jun peptide

Successful lysis by probe sonication was confirmed by the detection of cytb5-c-Jun fusion protein in the post-sonication supernatant (lane 1), however, the fusion protein was also detected in the pellet post-sonication (lane 2) (**Figure 5.15a**). Purification with TALON® metal affinity media using a stepwise elution protocol (lanes 3-11) showed that cytb5-r-c-Jun fusion protein and cytb5 begin to elute at an imidazole concentration of 250 mM with the most intense bands observed in the first 500 mM fraction (**Figure 5.15a**). The time required for cleavage by the TEV protease was investigated at three time points; at 2.5 h a strong band for the fusion protein was detected, while almost no fusion protein was detected after 16 h and complete conversion to cytb5 and r-c-Jun was seen in 60 h (**Figure 5.15b**). Post centrifugation, a sample (lane 1) from the upper fraction (retentate) showed a single band that corresponded approximately to the expected molecular weight for r-c-Jun (**Figure 5.15c**). No bands were visible for the lower fraction (eluate) in lane 2 (**Figure 5.15c**).

Expression and Purification of [^{15}N]r-c-Jun

The expression levels in all four cultures (A-D, lanes 1-4) were consistent (**Figure 5.16a**). Similarly to the optimisation study described above, soluble [^{15}N]cytb5-r-c-Jun fusion protein was detected in the post-sonication supernatant (lane

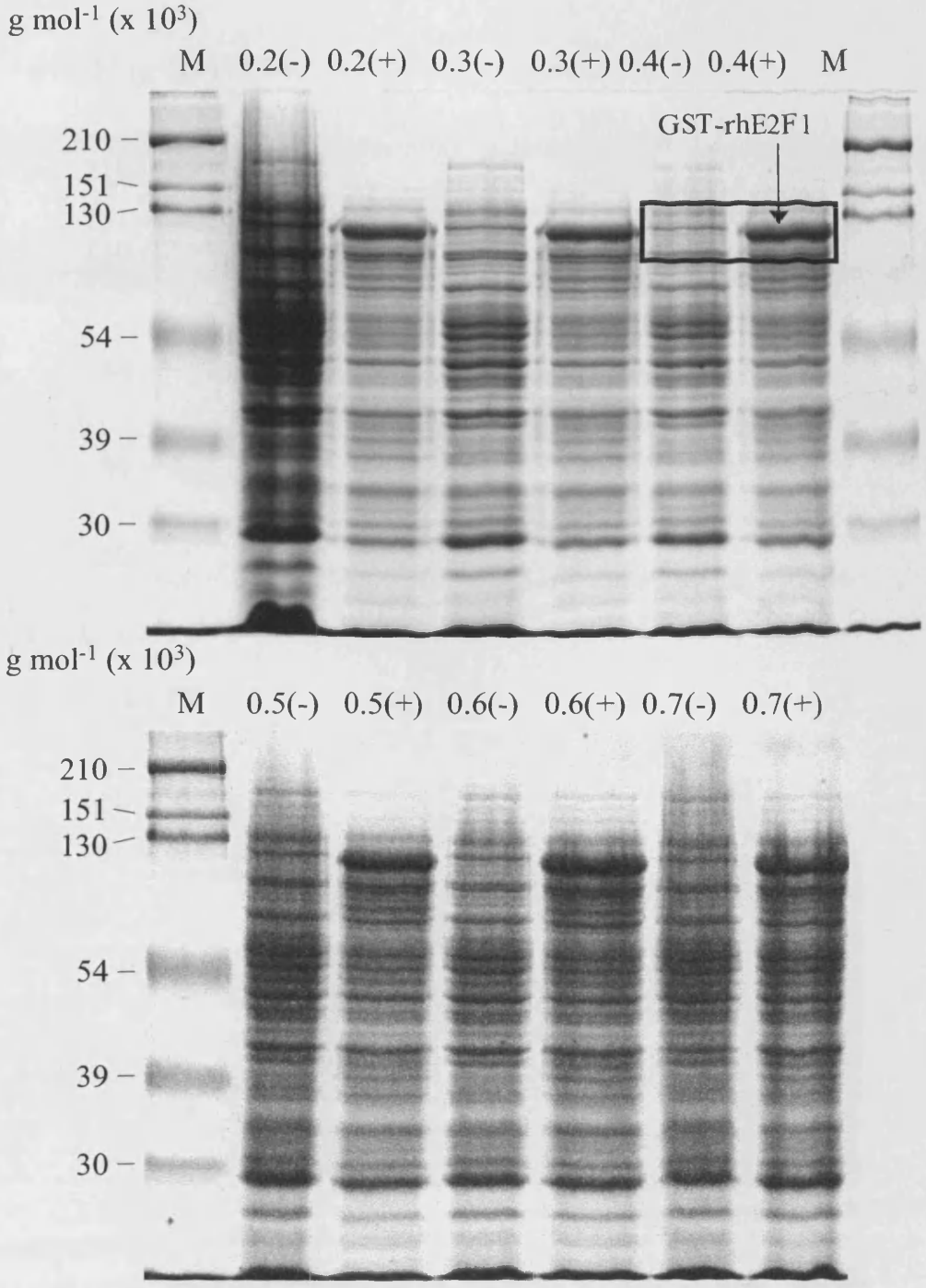

Figure 5.12 SDS-PAGE characterisation of rhE2F1 expression in BL21 (DE3) pLysS *E. coli*. Post-induction cultures were incubated at 37 °C for 4 h. M = marker, -/+ indicates whether where sample was induced with IPTG (0.5 mM). Numbers on left of figure represent approximate molecular weight of the standards used. The darker band seen only in (+) lanes indicated over-expression of the fusion protein GST-rhE2F1.

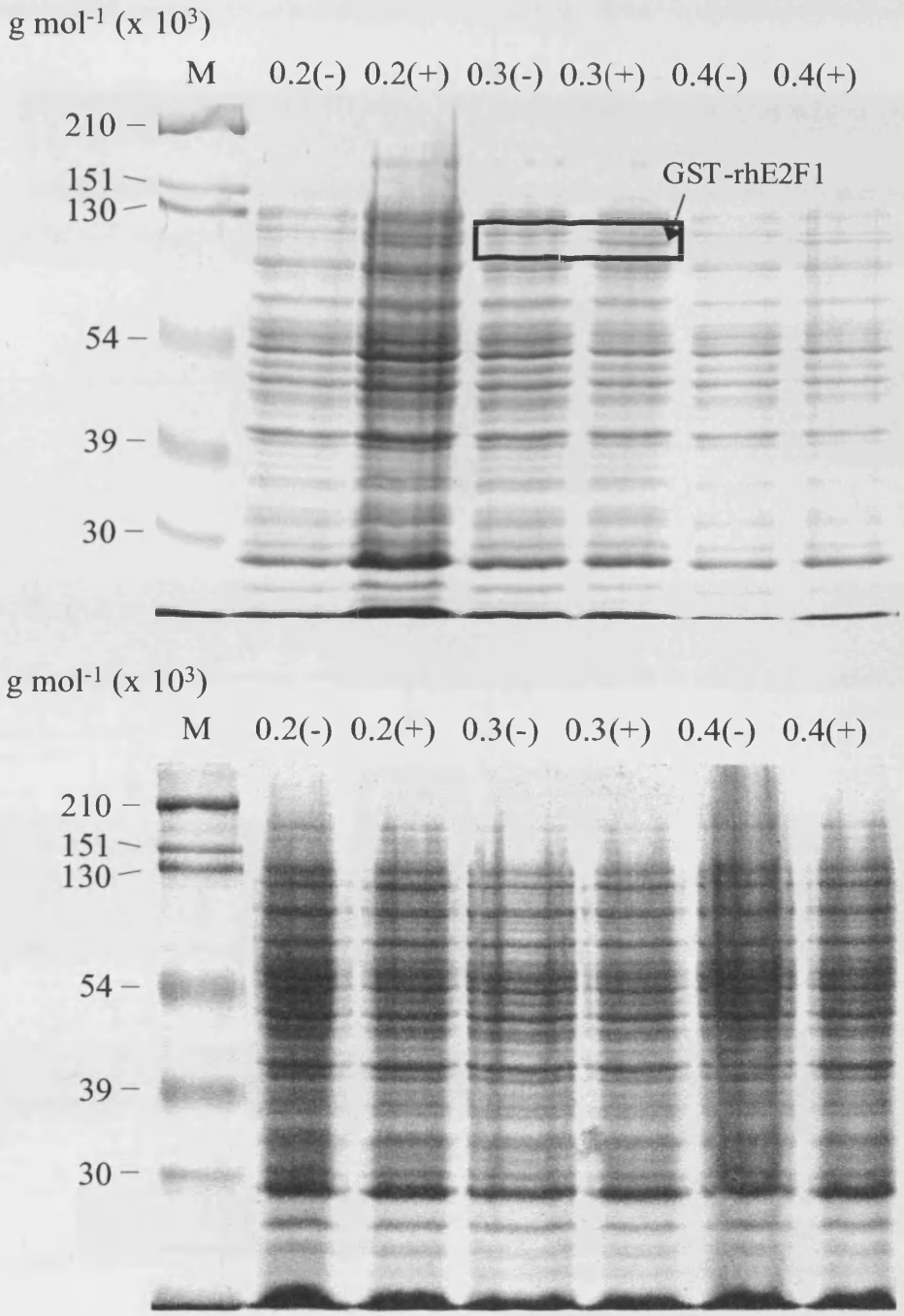

Figure 5.13 SDS-PAGE characterisation of rhE2F1 expression in BL21 (DE3) pLysS *E. coli*. Post-induction temperature was 20 °C incubation overnight (~ 16 h). M = marker, -/+ indicate whether where sample was taken pre/post induction with IPTG (0.5 mM). Numbers on left of figure represent approximate molecular weight of the standards used. Faint additional band in (+) lanes at ODs of 0.2, 0.3 and 0.4 suggests low expression of GST-rhE2F1.

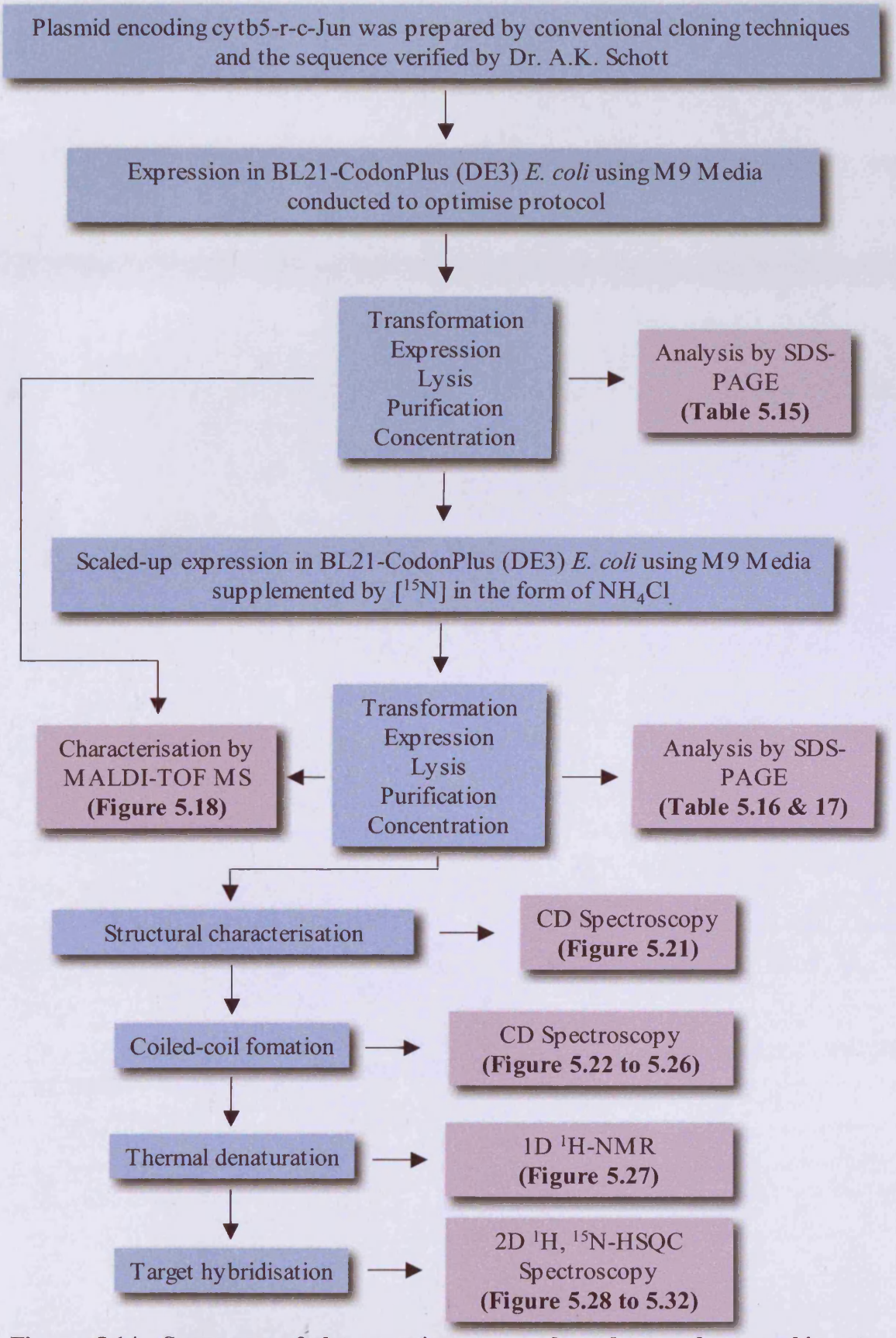

Figure 5.14 Summary of the experiments conducted towards recombinant expression of the [^{15}N]r-c-Jun target peptide and analysis of target hybridisation with $FosW_C$/mPEG-$FosW_C$.

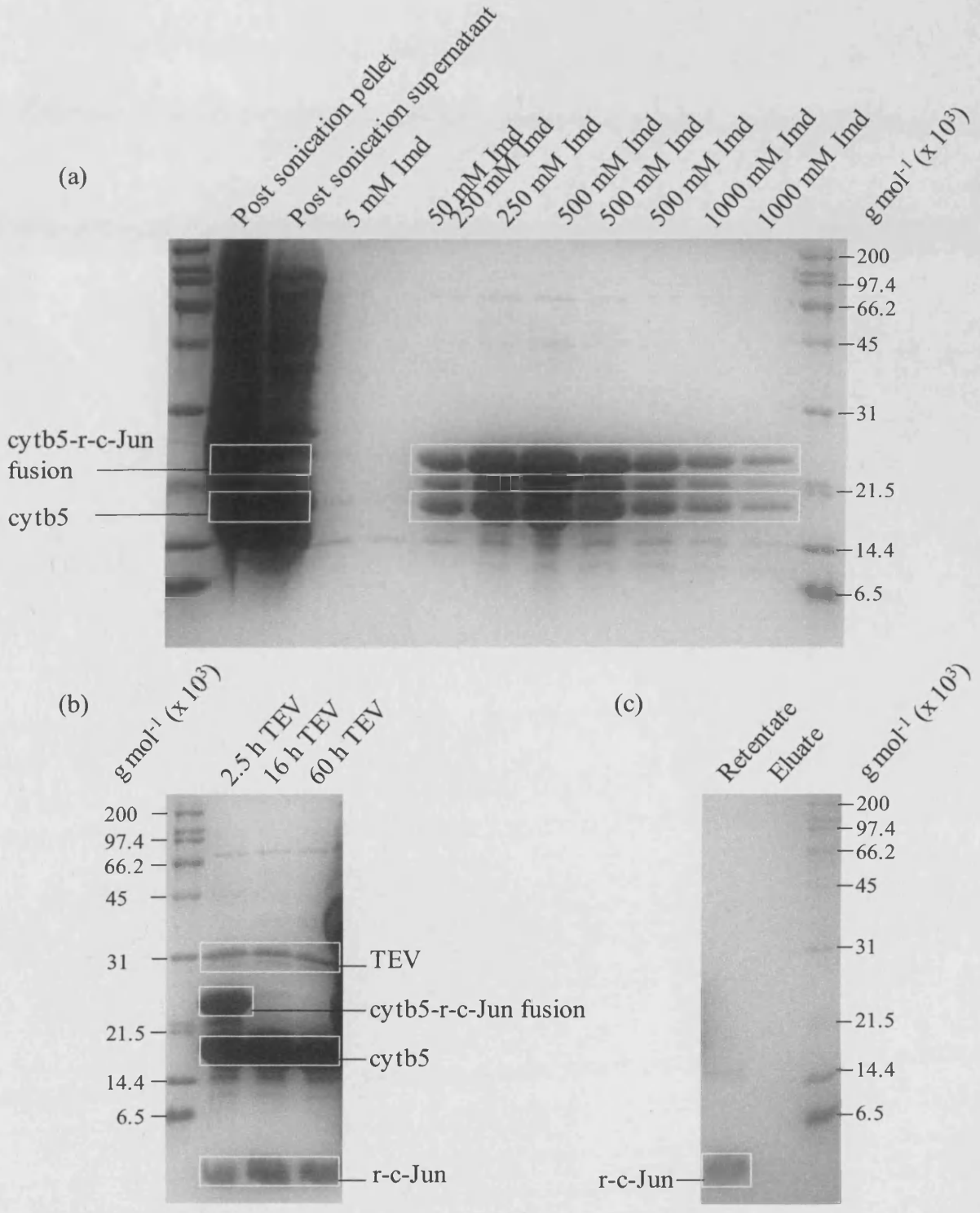

Figure 5.15 SDS-PAGE analysis of the expression of r-c-Jun in BL21-CodonPlus (DE3) *E.coli*. Panel (a) shows the analysis post lysis and during purification, panel (b) shows optimisation of the TEV cleavage reaction, panel (c) shows pure r-c-Jun post-purification and concentration.

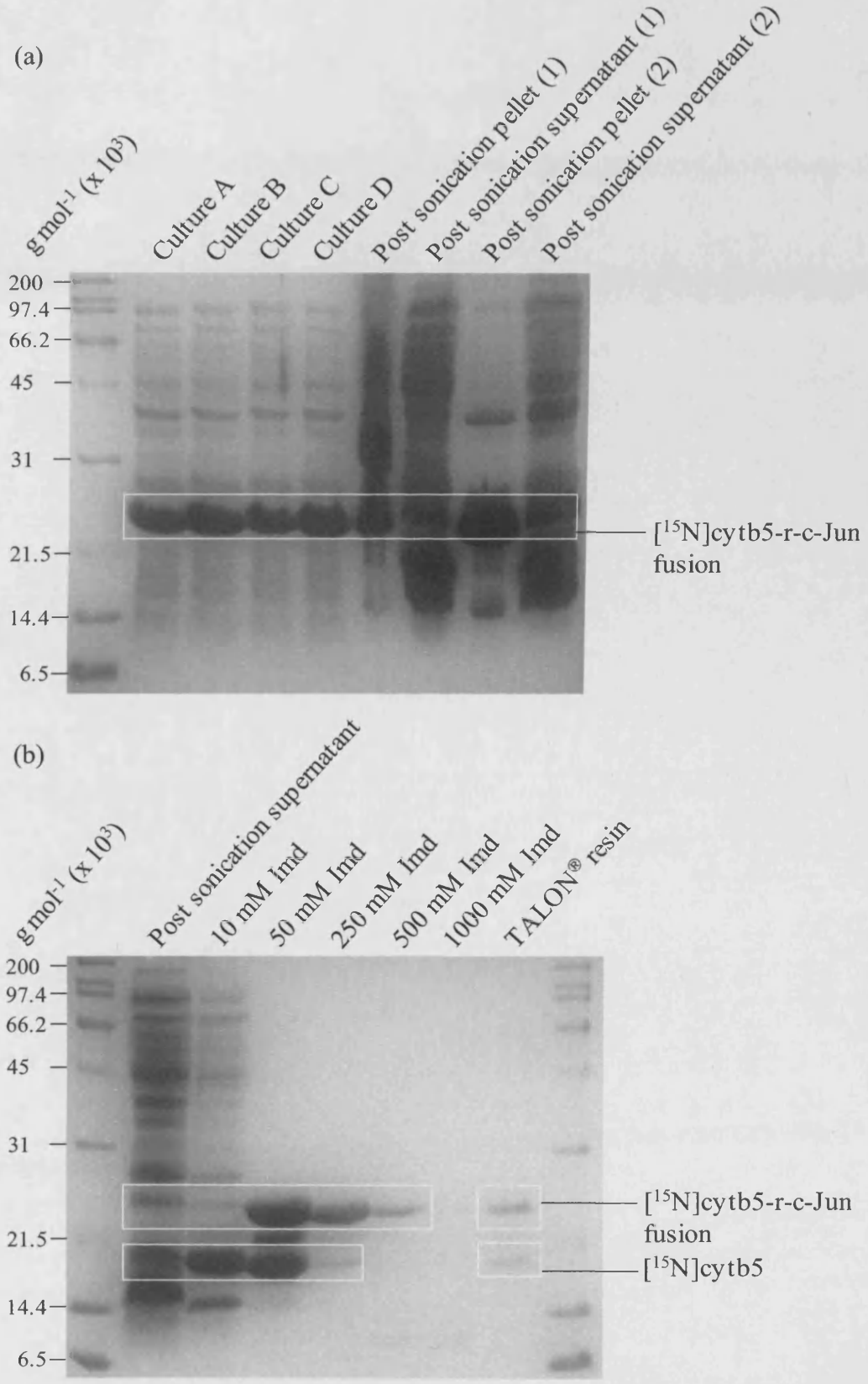

Figure 5.16 SDS-PAGE analysis of the expression of [^{15}N]r-c-Jun in BL21-CodonPlus (DE3) *E.coli*. Panel (a) shows expression levels in each culture followed by analysis of the sonication method. Panel (b) shows the analysis of the purified fractions.

6, **Figure 5.16a**). However, fusion protein remained in the pellet, even after a second lysis step was performed, suggesting that the protocol could be further optimised (lanes 7 and 8, **Figure 5.16a**). The majority of undesired proteins were removed with the 10 mM imidazole wash (lane 2, **Figure 5.16b**), and the fusion protein then eluted over a broad range i.e. 50 to 500 mM imidazole (lanes 3-5, **Figure 5.16b**). Despite washing with 1000 mM imidazole a small amount of protein remained bound to the resin (lanes 6 and 7, **Figure 5.16b**). Cleavage by TEV protease was monitored following an overnight reaction of approximately 16 h (lane 1, **Figure 5.17**). This lane ran slightly slower on the gel compared with lanes 2-4. Additionally, unlike in **Figure 5.15b** cleaved [^{15}N]r-c-Jun was not detected. However, a band corresponding to that expected for [^{15}N]r-c-Jun peptide was detected following removal of the higher molecular weight proteins and subsequent concentration (lane 2, **Figure 5.17**). Purity was assessed to be > 90 % with less than 10 % [^{15}N]cytb5 remaining as a contaminant. Analysis of the insoluble retentate (lane 3, **Figure 5.17**) showed that it was composed of a mixture of [^{15}N]cytb5-c-Jun, [^{15}N]cytb5 and [^{15}N]r-c-Jun. In agreement with the earlier study, no staining was observed for the eluate sample (lane 4, **Figure 5.17**).

Characterisation of r-c-Jun and [^{15}N]r-c-Jun by MALDI-TOF MS

Characterisation by MALDI-TOF MS confirmed the expected molecular weights for both peptides, r-c-Jun (**Figure 5.18a**) and [^{15}N]r-c-Jun (**Figure 5.18b**). The peaks $(M+H)^+$ are in good agreement with the theoretical values of 4104.68 and 4156.30 g mol^{-1} respectively. The inset spectra confirm that each of the m/z peaks observed corresponds to full-length peptide as the distance measured between each peak in the cluster is approximately equal to 1.0.

5.3.3 Target Hybridisation Studies

5.3.3.1 Preliminary Characterisation by CD Spectroscopy of the Interaction Between Phb and E2F1 Peptides E2F1a and E2F1b

When the $Phb_{185\text{-}214}$ peptide was characterised by CD spectroscopy over a temperature range of 5 to 95 °C a clear α-helical structure was observed at 5 °C as judged by the minima at 205 and 222 nm (**Figure 5.19a**). However, as the temperature was increased, a loss of secondary structure with a transition to a random coil was observed above 20 °C. The tyrosine tagged peptide, $Phb_{Y185\text{-}214}$ produced spectra

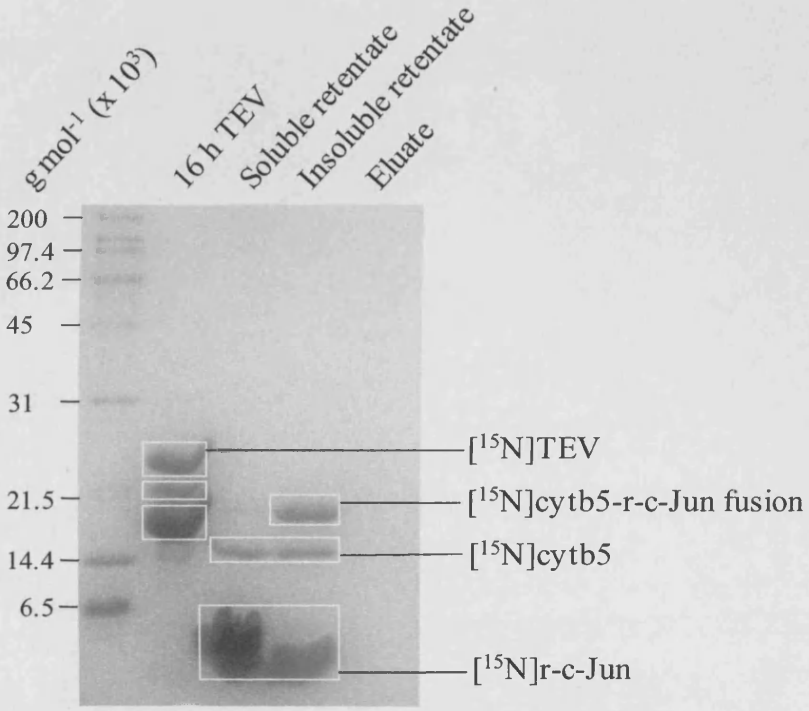

Figure 5.17 SDS-PAGE analysis of the TEV cleavage and final purification of [^{15}N]r-c-Jun.

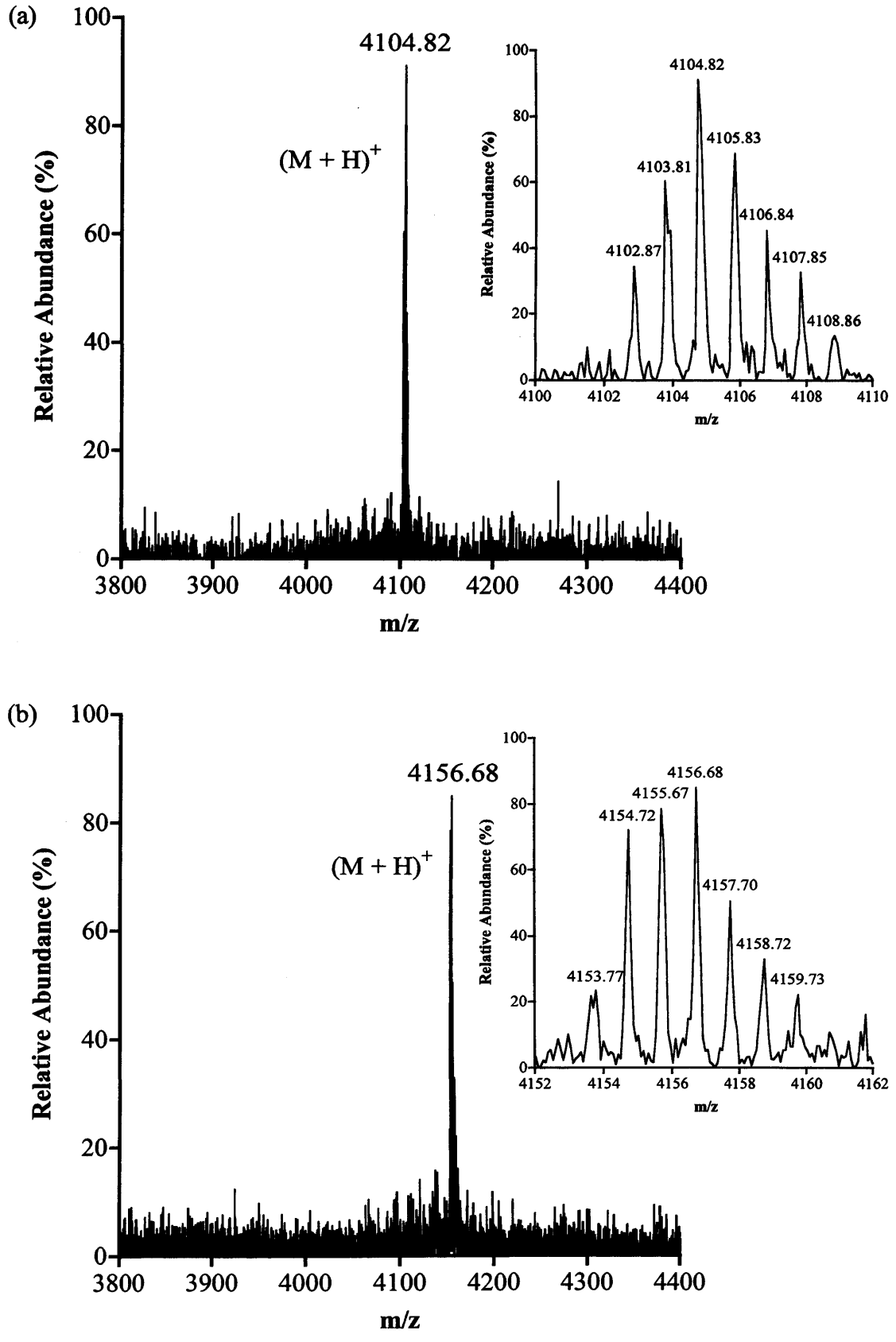

Figure 5.18 MALDI-TOF MS characterisation of peptdes r-c-Jun and [^{15}N]r-c-Jun. Panel (a) shows r-c-Jun, panel (b) shows [^{15}N]r-c-Jun. Inset panels show a magnification of the main peak.

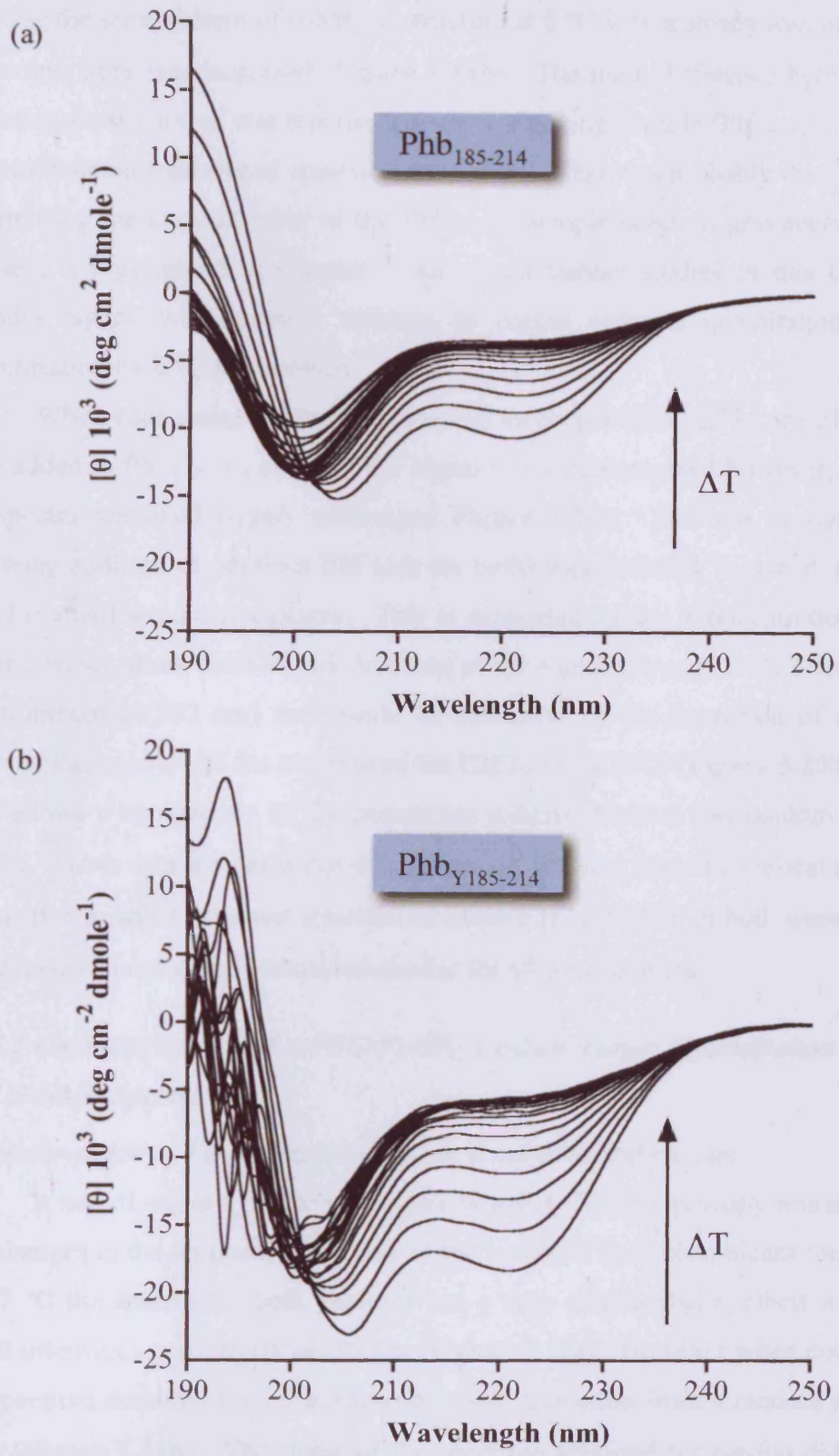

Figure 5.19 Analysis of $Phb_{185-214}$ and $Phb_{Y185-214}$ thermal denaturation by CD spectroscopy. Samples were prepared such that the total peptide concentration was 80 μM.

showing the same pattern of α-helical structure at 5 °C with a steady loss of structure as the temperature was increased (**Figure 5.19b**). The main difference between the two sets of spectra acquired was that the tyrosine containing peptide ($Phb_{Y185-214}$) showed an increased signal intensity of approximately 50 %. This was probably due to an error in determining the concentration of the $Phb_{185-214}$ sample solution gravimetrically. This problem is highlighted in Chapter 3 and so all further studies in this Chapter used peptides tagged with tyrosine residues to enable accurate quantitation of peptide concentration by UV spectroscopy.

When equi-molar amounts of potential target peptides E2F1a or E2F1b (or both) were added to $Phb_{Y185-214}$ at 37 °C the signal intensity decreased however, the shape of the spectra remained largely unchanged **Figure 5.20a**. The loss in signal intensity following addition of peptides E2F1a/b (or both) was probably in part due to dilution, but also small structural changes. This is supported by the "concentration corrected" spectra, which show there is little increase in the signal intensity at 222 nm (relative to the minimum at 202 nm) that would be indicative of the formation of a coiled-coil between $Phb_{Y185-214}$ and the target peptides E2F1a and E2F1b (**Figure 5.20b**). The inset table shows a comparison of the percentage α-helix, β-sheet and random coil in each sample. These data indicated that there was a progressive loss of α-helical structure and a transition towards a β-sheet structure as either E2F1a, E2F1b or both were added. The percentage of random coil remained similar for all four samples.

5.3.3.2 Characterisation of mPEG-$FosW_C$: c-Jun Target Hybridisation by CD and 1D, ^{1}H-NMR Spectroscopy

Characterisation of Target Peptides - c-Jun (synthetic) and r-c-Jun

It was of interest first to investigate whether CD spectroscopy was able to detect any changes in the secondary structure of the synthetic and recombinant forms of c-Jun. At 37 °C the spectra for both peptides had a very similar shape, albeit with differing signal intensities particularly at 197 nm (**Figure 5.21a**). However when cooled to 4 °C, the spectrum acquired for c-Jun showed a clear transition from a random coil to an α-helix (**Figure 5.21b**). The shape of the spectrum acquired for r-c-Jun did not change following cooling, however the intensity of the signal was stronger as one might expect due to stabilisation of the structure. Synthetic c-Jun peptide was used for all further CD studies.

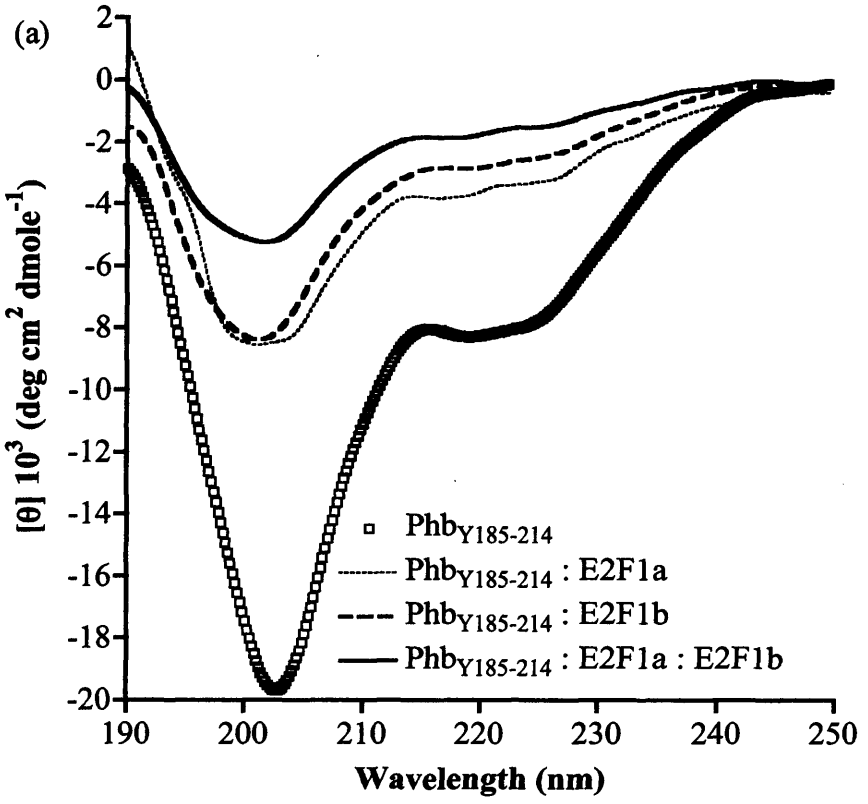

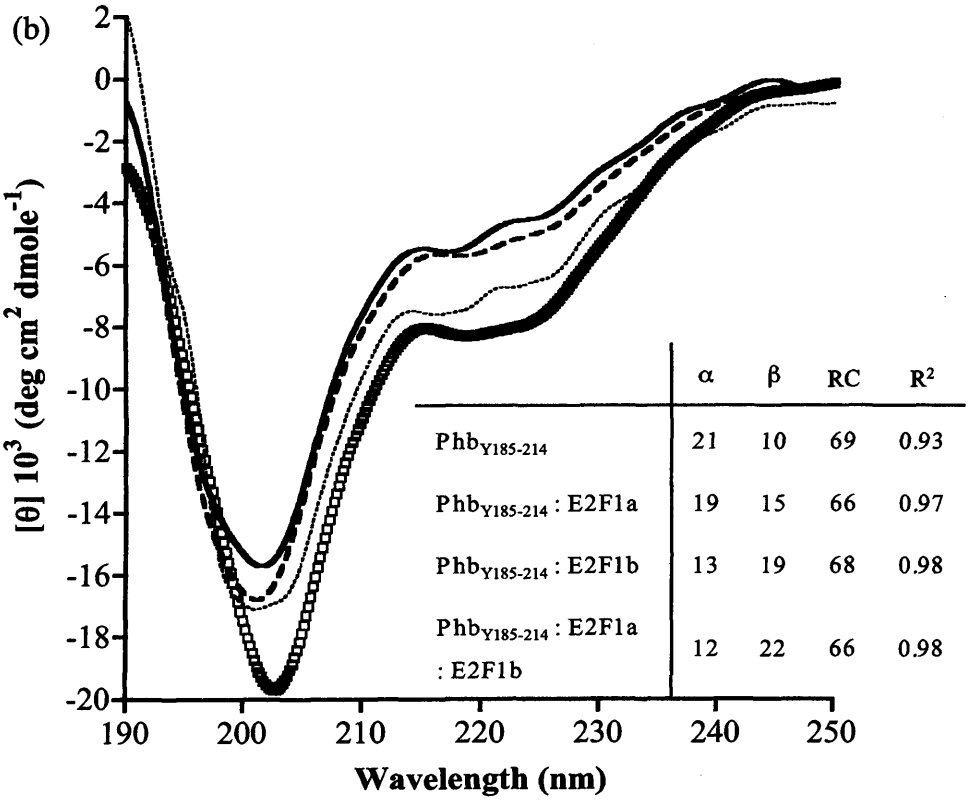

	α	β	RC	R^2
$Phb_{Y185-214}$	21	10	69	0.93
$Phb_{Y185-214}$: E2F1a	19	15	66	0.97
$Phb_{Y185-214}$: E2F1b	13	19	68	0.98
$Phb_{Y185-214}$: E2F1a : E2F1b	12	22	66	0.98

Figure 5.20 Characterisation of the interaction between $Phb_{Y185-214}$ and target peptides E2F1a and E2F1b using CD spectroscopy. Panel (a) shows the CD spectra expressed as a total peptide concentration of 80 μM. Panel (b) shows the data corrected to a $Phb_{Y185-214}$ concentration of 80 μM. The percentage α-helix, β-sheet and random coil was estimated using the programme PEPFIT (Reed *et al*, 1997) and adapted for use in MS Excel by Amon *et al*, 2008.

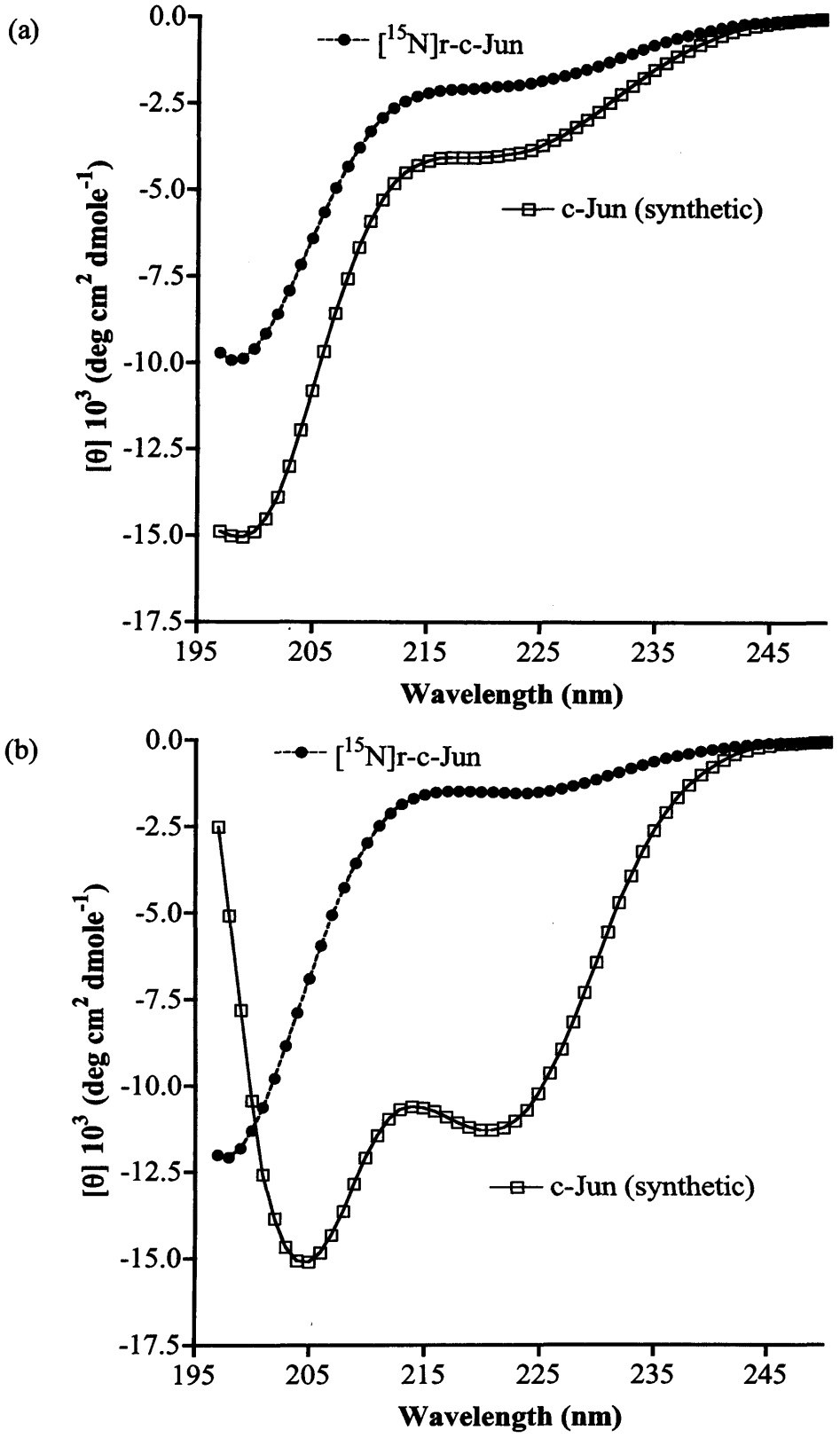

Figure 5.21 Characterisation of [^{15}N]r-c-Jun and synthetic c-Jun at 37 °C and 4 °C using CD spectroscopy. Panel (a) shows spectra at 37 °C, panel (b) shows spectra at 4 °C, peptide concentration was 75 μM.

Characterisation of mPEG-MAL

It was first necessary to ensure that mPEG-MAL had no structure in the far-UV range that might interfere with the acquisition of spectra for mPEG-$FosW_C$. These earlier experiments used lower concentrations of mPEG-MAL and mPEG-$FosW_C$ than those used later to compare with the HSQC studies, nonetheless, they demonstrated that mPEG-MAL had no observable structure as judged by its far UV CD spectrum between 185 and 260 nm (**Figure 5.22**).

Characterisation of $FosW_C$ and mPEG-$FosW_C$: c-Jun Target Hybridisation

The far UV CD spectra acquired with c-Jun and mPEG-$FosW_C$ using the tandem cell showed that the $[\theta]_{208}/[\theta]_{222}$ ratio increased post mixing, indicative of the formation of a coiled-coil (**Figure 5.23**). The ability to mix by simply inverting the cell removed the risk of contributing error to the measurement as a result of pipetting, however the disadvantage was that a maximum concentration of 7.5 μM could be used due to the long (10 mm) pathlength of the cuvette. A concentration of 75 μM of each peptide was desired so that the data could be compared directly with the ^{1}H, ^{15}N-HSQC data and the CD data published by Mason *et al* (2006). Therefore no further measurements were used using the tandem cell.

Far UV CD spectra measured in a 0.2 mm quartz cuvette for the c-Jun : $FosW_C$ and the c-Jun : mPEG-$FosW_C$ complexes at 37 °C demonstrated a high degree of α-helical structure with the characteristic bands at 192, 208 and 222 nm (**Figure 5.24**). Moreover, the $[\theta]_{208}/[\theta]_{222}$ ratio was indicative of the formation of a coiled-coil for both complexes. The narrow pathlength of this cuvette made it possible to acquire spectra as low as 180 nm, however it was not possible to use this cuvette for thermal denaturation experiments. Therefore measurements were repeated in a 1 mm cuvette (suitable for heating) for comparison. The far UV CD spectra shown in **Figure 5.24b** are almost identical to those in **Figure 5.24a** within the recorded range.

Studies on Thermal Stability Using CD and 1D, ^{1}H-NMR Spectroscopy

Thermal stability was investigated for both the c-Jun : $FosW_C$ and the c-Jun : mPEG-$FosW_C$ complexes. Upon heating a T_m value of 70.1 °C was determined for the c-Jun : $FosW_C$ complex (**Figure 5.25a**) whereas a value of 45.5 °C was determined for the c-Jun : mPEG-$FosW_C$ complex (**Figure 5.25b**). Both samples showed a cooperative transition from the folded to unfolded state, but whereas c-Jun : $FosW_C$ exhibited > 90

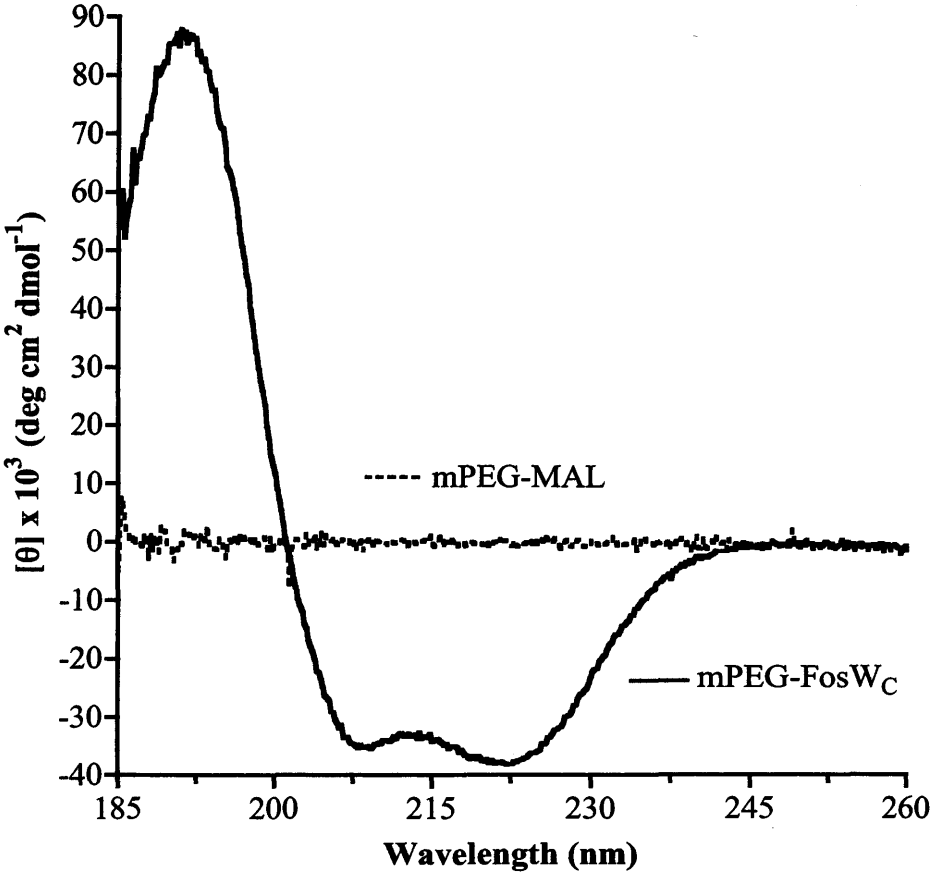

Figure 5.22 Characterisation of mPEG-maleimide and mPEG-$FosW_C$ by CD spectroscopy. Spectra were acquired at 4 °C in a 1 mm pathlength quartz cuvette, peptide/polymer concentration was 15 μM.

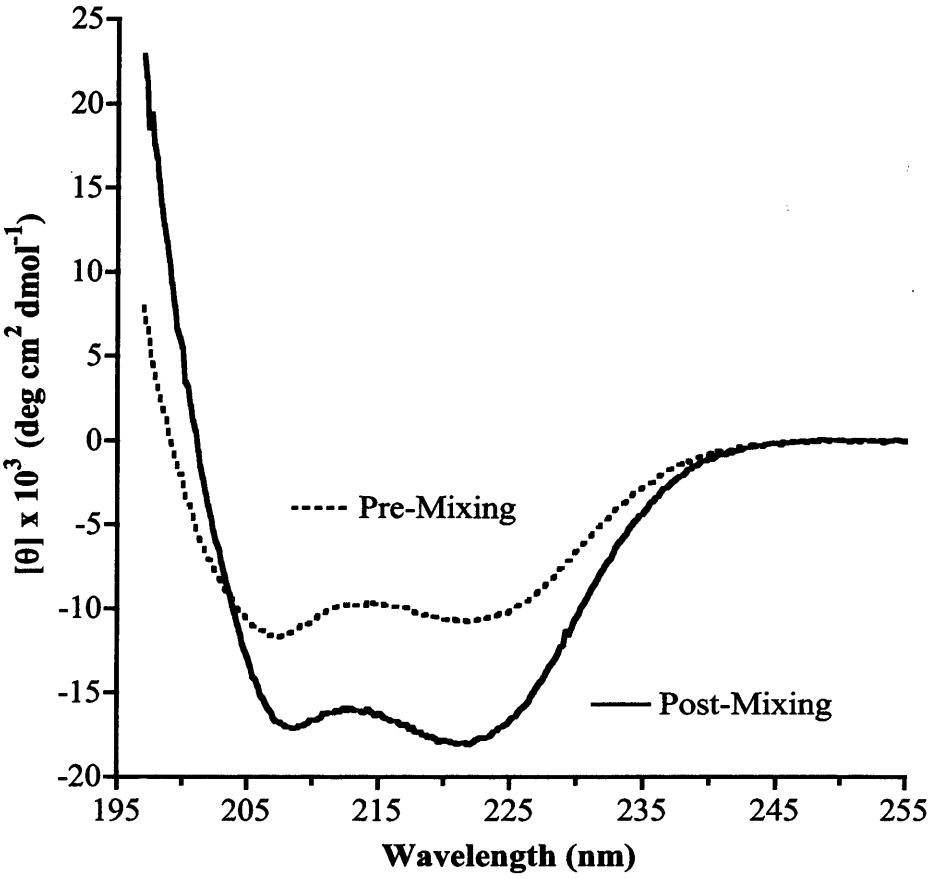

Figure 5.23 Characterisation of c-Jun : mPEG-$FosW_C$ by CD spectroscopy using a "Tandem Cell". Spectra were acquired at 37 °C in a 10 mm pathlength quartz cuvette, concentration of each peptide was 7.5 μM.

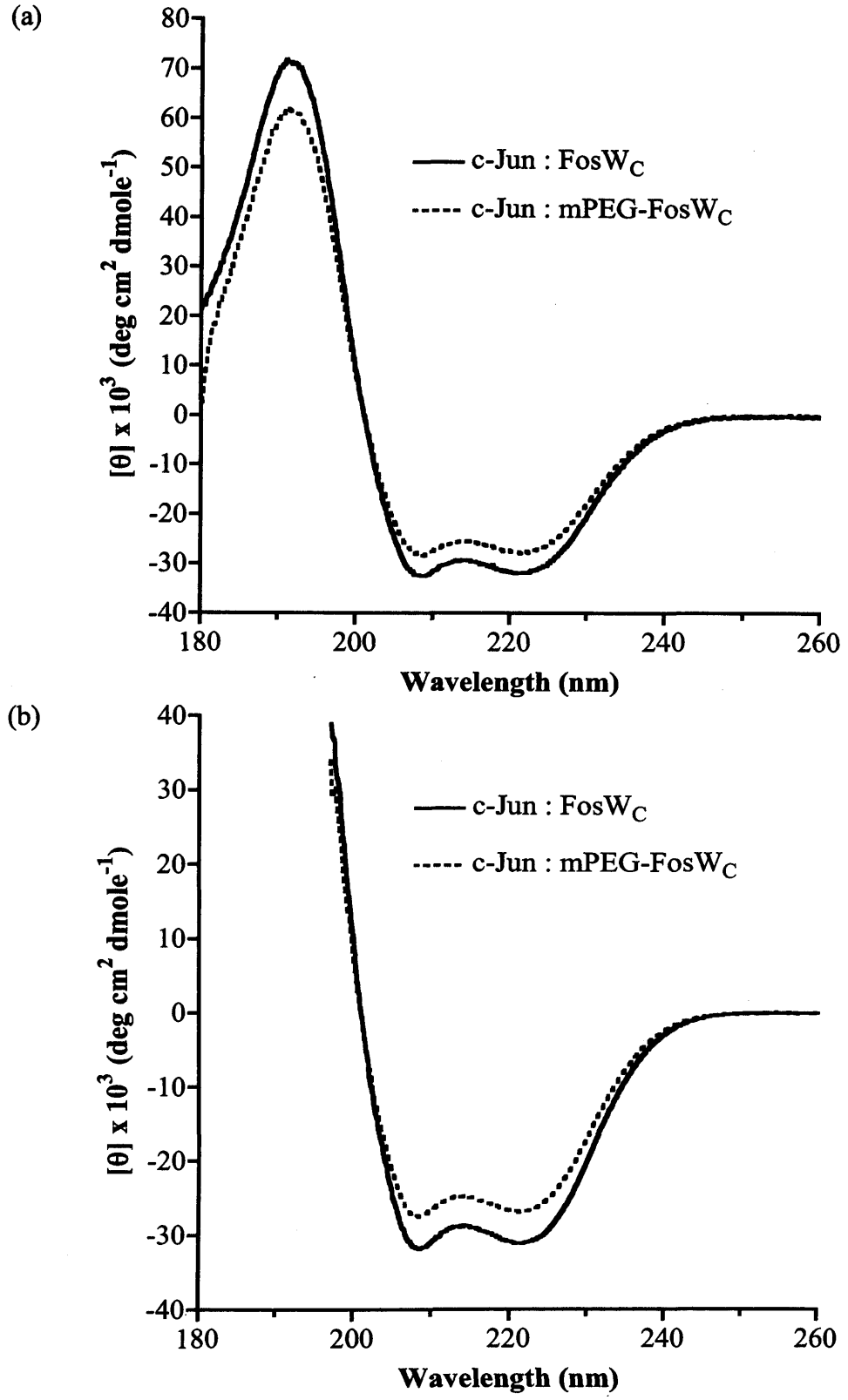

Figure 5.24 Characterisation of c-Jun : $FosW_C$ and c-Jun : mPEG-$FosW_C$ by CD spectroscopy. Panel (a) shows data acquired using a 0.2 mm pathlength quartz cuvette whilst panel (b) shows data acquired using a 1 mm pathlength quartz cuvette. All spectra recorded were acquired at 37 °C, peptide concentration 75 μM.

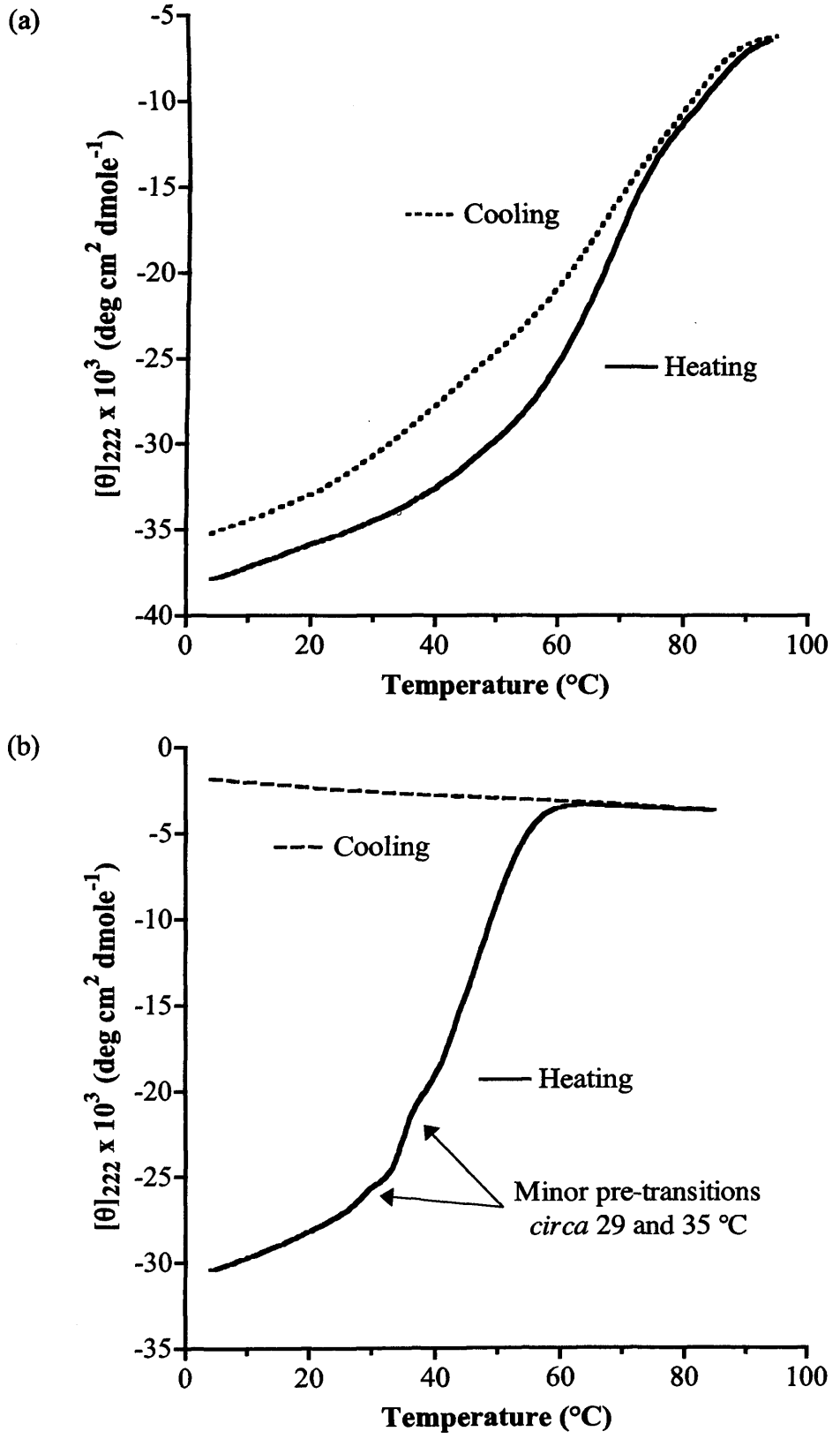

Figure 5.25 Analysis of the thermal denaturation of c-Jun : $FosW_C$ and c-Jun : mPEG-$FosW_C$ complexes by CD spectroscopy. Panel (a) shows c-Jun : $FosW_C$ complex, panel (b) shows c-Jun : mPEG-$FosW_C$ complex. Spectra were acquired using a 1 mm pathlength quartz cuvette, peptide concentration 75 μM.

% recovery of its initial signal upon cooling, the PEGylated complex remained irreversibly denatured. Furthermore the c-Jun : mPEG-$FosW_C$ denaturation curve displayed minor pre-transitions at *circa* 29 and 35 °C. Spectra of renatured c-Jun : $FosW_C$ show the same $[\theta]_{208}/[\theta]_{222}$ ratio as the original material (**Figure 5.26a**), whereas spectra of the c-Jun : mPEG-$FosW_C$ complex exhibited a minimum at 198 nm typical for a denatured protein (**Figure 5.26b**).

^{1}H-NMR spectra acquired from 4 to 49 °C for synthetic c-Jun, $FosW_C$ and mPEG-$FosW_C$ show marked differences as a result of temperature variation, particularly in the NH and aromatic region from 6.5 to 9.0 ppm (**Figure 5.27**). For c-Jun, the spectra show near complete loss of signal from the NH region above 24 °C, indicative of denaturation (**Figure 5.27a**). The spectra acquired for $FosW_C$ show fewer changes in peak intensity up to 37 °C (**Figure 5.27b**). At 49 °C a considerable number of peaks disappeared, intensities reduced and peak shape changed more markedly, indicating denaturation of the peptide. The spectra obtained for mPEG-$FosW_C$ showed a very similar pattern as seen for $FosW_C$ and denaturation appeared to occur at a similar temperature (**Figure 5.27c**).

5.3.3.3 Characterisation of mPEG-$FosW_C$: c-Jun Target Hybridisation Using 2D ^{1}H, ^{15}N-HSQC Spectroscopy

2D ^{1}H, ^{15}N-HSQC spectra of isotopically labelled [^{15}N]r-c-Jun peptide were obtained at 37 °C, pH 7.4 and the spectra showed a limited number of backbone ^{1}H-^{15}N correlations (6.7-8.3 ppm), with a very low dispersion (**Figure 5.28a**). This was an indication of a disordered (unstructured) peptide, as most of the signals from the NH groups were lost due to exchange with the water. It was observed that acidification of the sample resulted in an increase in the number of peaks (backbone ^{1}H-^{15}N correlations) in the spectrum, suggesting increased structure (data not shown).

Addition of equimolar amounts of the unlabelled peptide $FosW_C$ to [^{15}N]r-c-Jun produced a dramatic change in the spectrum, as a significant number of cross peaks not present on the spectrum of [^{15}N]r-c-Jun alone (**Figure 5.28a**) were observed (**Figure 5.28b**). As $FosW_C$ was unlabelled, no signals could originate from this peptide in the HSQC spectrum, therefore the new peaks belonged to [^{15}N]r-c-Jun and were a consequence of structural changes having occurred to this peptide. The increase in the

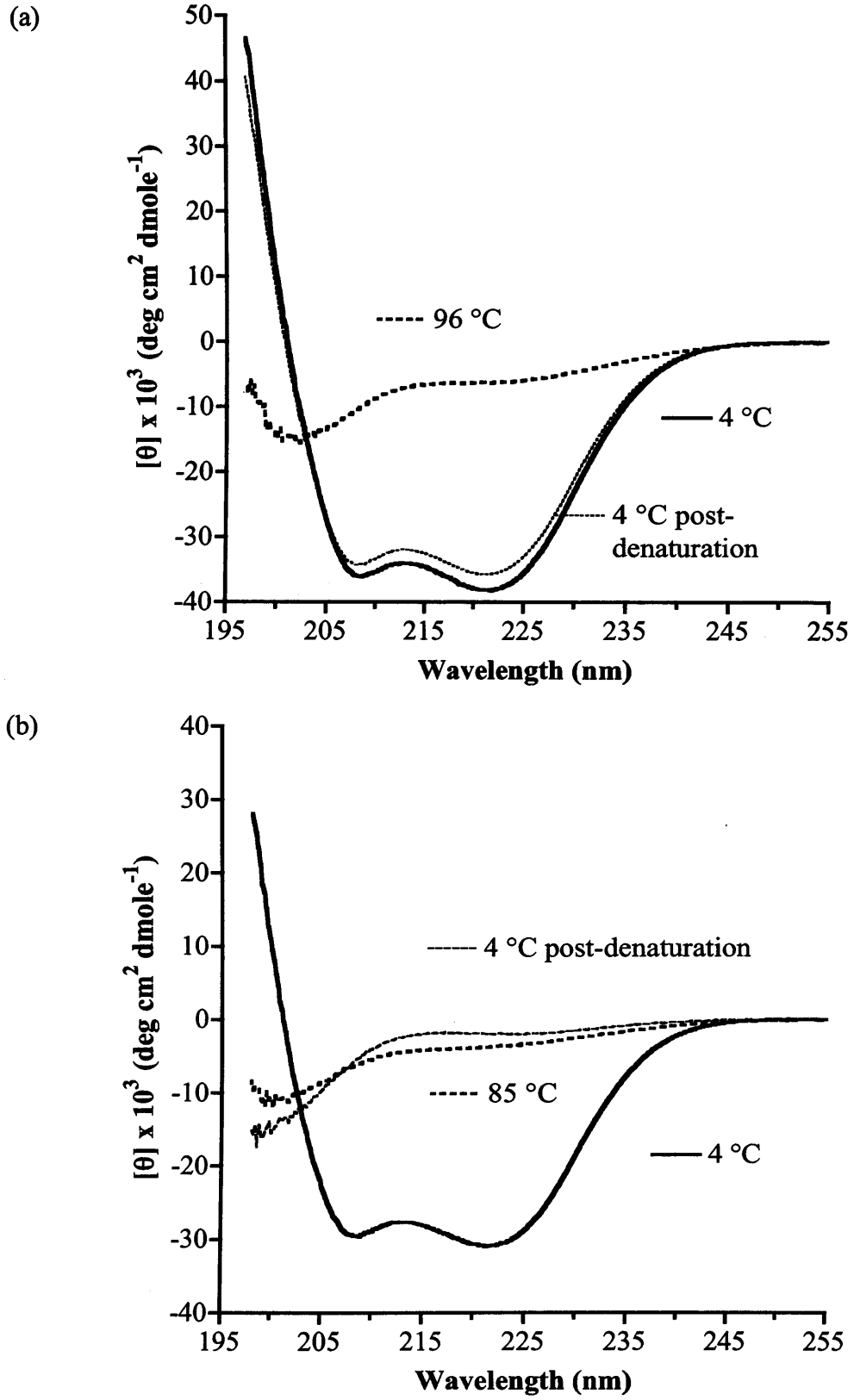

Figure 5.26 Characterisation of c-Jun : $FosW_C$ and c-Jun:mPEG-$FosW_C$ complexes before and after thermal denaturation and after renaturation (cooling) using CD spectroscopy. Panel (a) shows c-Jun : $FosW_C$ complex, panel (b) shows c-Jun : mPEG-$FosW_C$ complex. Spectra were acquired using a 1 mm pathlength quartz cuvette, peptide concentration 75 μM.

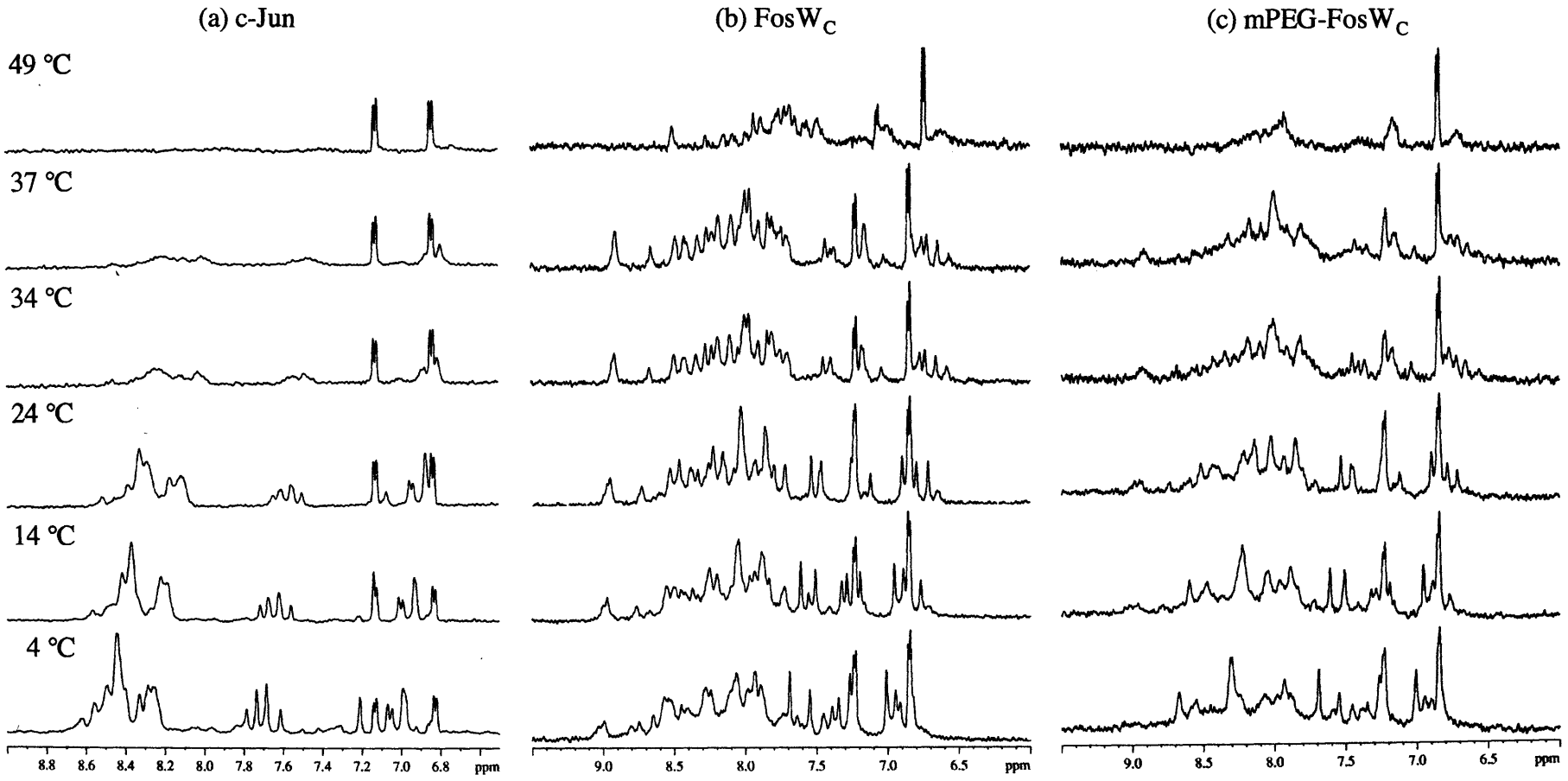

Figure 5.27 . Characterisation of the thermal denaturation of c-Jun (synthetic), FosW$_C$ and mPEG-FosW$_C$ using 1D ^{1}H-NMR spectroscopy. Samples were prepared at a peptide concentration of 75 μM.

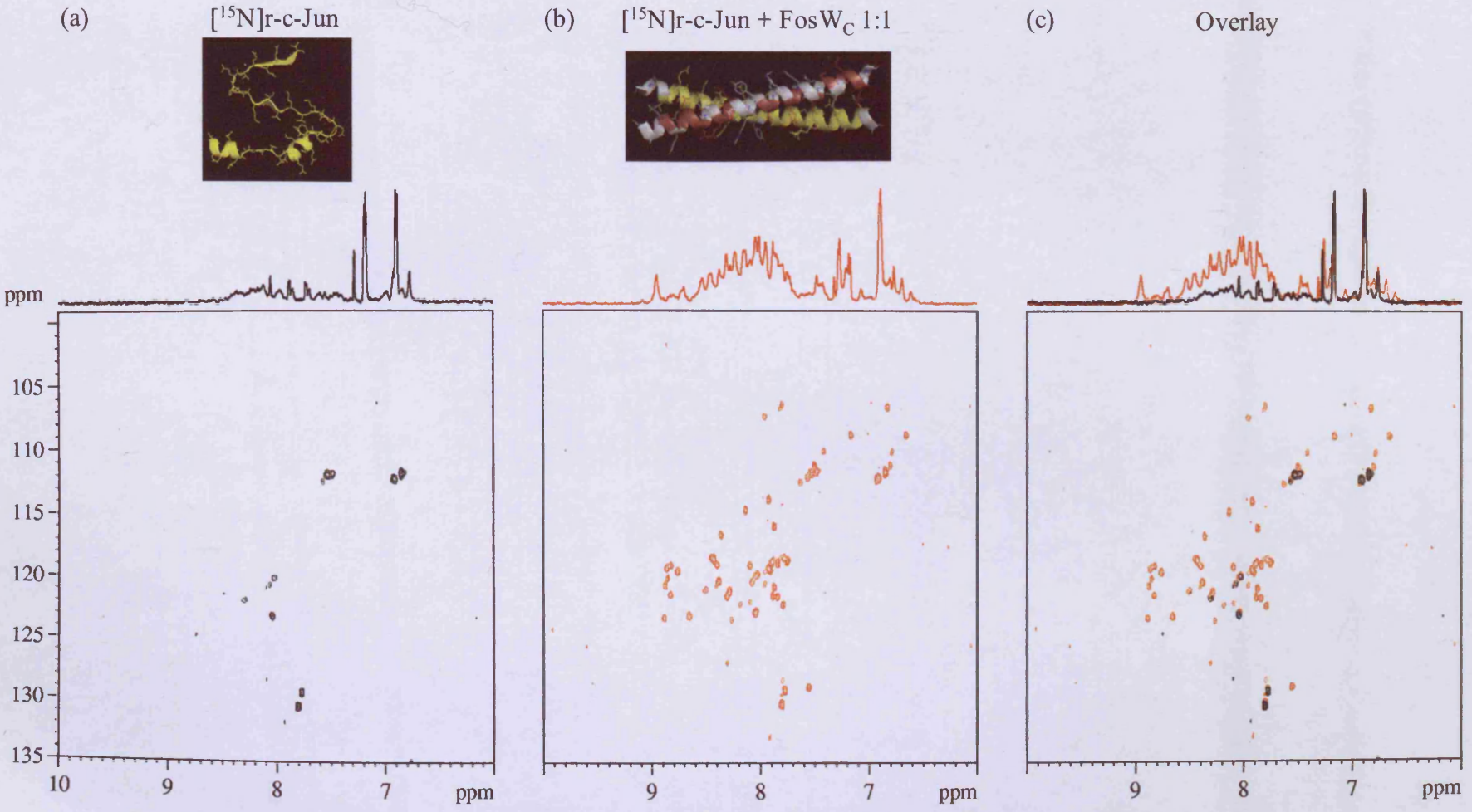

Figure 5.28 2D ^{1}H, ^{15}N HSQC characterisation of the [^{15}N]r-c-Jun : FosW$_C$ (1:1) coiled-coil complex. Panel (a) shows [^{15}N]r-c-Jun, panel (b) shows [^{15}N]r-c-Jun + unlabelled FosW$_C$ (1:1) and panel (c) shows the spectra overlaid. Samples were prepared at peptide concentrations of 75 μM.

number of signals was indicative of a transition from the unordered structure on its own, to the formation of a structured combination of [^{15}N]r-c-Jun and $FosW_C$. The overlaid spectra (**Figure 5.28c**) showed that there were no chemical shifts for the peaks in the 2D spectrum. A 2D nuclear Overhauser effect spectroscopy (NOESY) spectrum of [^{15}N]r-c-Jun : $FosW_C$ acquired by Dr R. Carbajo showed characteristic NH-NH NOE peaks which were indicative of an alpha-helical structure (data not shown).

When mPEG-$FosW_C$ was added to the [^{15}N]r-c-Jun peptide at a 1:1 ratio the number of peaks (backbone ^{1}H-^{15}N correlations) observed increased significantly (**Figure 5.29b**). As before, the overlaid spectra (**Figure 5.29c**) showed that there were no chemical shifts for the peaks in the 2D spectrum suggesting that the small amount of ordered structure seen for [^{15}N]r-c-Jun peptide alone (**Figure 5.29a**) was not altered in form, rather the remaining residues in the [^{15}N]r-c-Jun peptide became structured through interaction with mPEG-$FosW_C$.

Both target hybridisation spectra for [^{15}N]r-c-Jun : FosWc and [^{15}N]r-c-Jun : mPEG-$FosW_C$ were overlaid **(Figure 5.30)** to determine whether any differences were detected between the addition of $FosW_C$ and addition of mPEG-$FosW_C$. The pattern observed was almost identical, therefore, it could be concluded that the hybridisation of the peptides produced the same type of structural motif.

Further experiments investigated the effect of increasing the ratio of [^{15}N]r-c-Jun to $FosW_C$/mPEG-$FosW_C$ from 1:1 (**Figure 5.31/32a**) to 1:2 (**Figure 5.31/32b**), in order to check whether homodimerisation of the $FosW_C$ peptides was preferred over heterodimerisation with [^{15}N]r-c-Jun. When overlaid (**Figure 5.31/32c**), no changes in the chemical shifts of the signals were detected. Furthermore, the volumes of the peaks were compared for both ratios and found to be the same. This indicated that heterodimeric hybridisation was saturated at a 1:1 ratio, i.e. at the 1:2 ratio no further increase in signal intensity was observed because all the [^{15}N]r-c-Jun molecules existed as heterodimeric complexes. This data strongly supports the statement that the heterodimeric state is more favourable than the possible homodimeric states under model physiological conditions.

5.4 Discussion

This Chapter set out to investigate whether the mPEG-coiled-coil motifs could interact with their targets in a similar manner to which the free coiled-coil motif

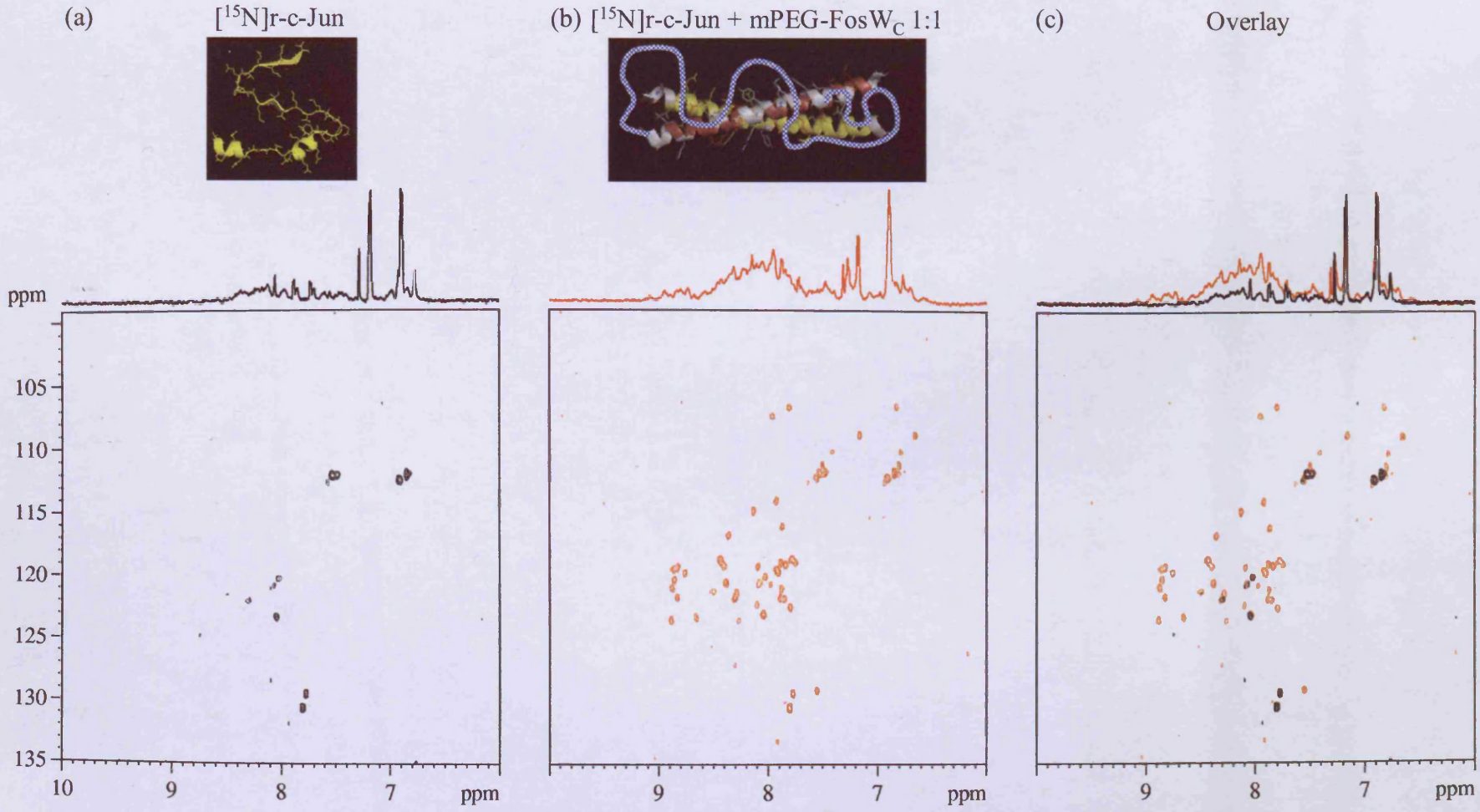

Figure 5.29 2D ^{1}H, ^{15}N HSQC characterisation of the [^{15}N]r-c-Jun : mPEG-FosW$_C$ (1:1) coiled-coil complex. Panel (a) shows [^{15}N]r-c-Jun, panel (b) shows [^{15}N]r-c-Jun + unlabelled mPEG-FosW$_C$ (1:1) and panel (c) shows the overlaid spectra. Samples were prepared at peptide concentrations of 75 μM.

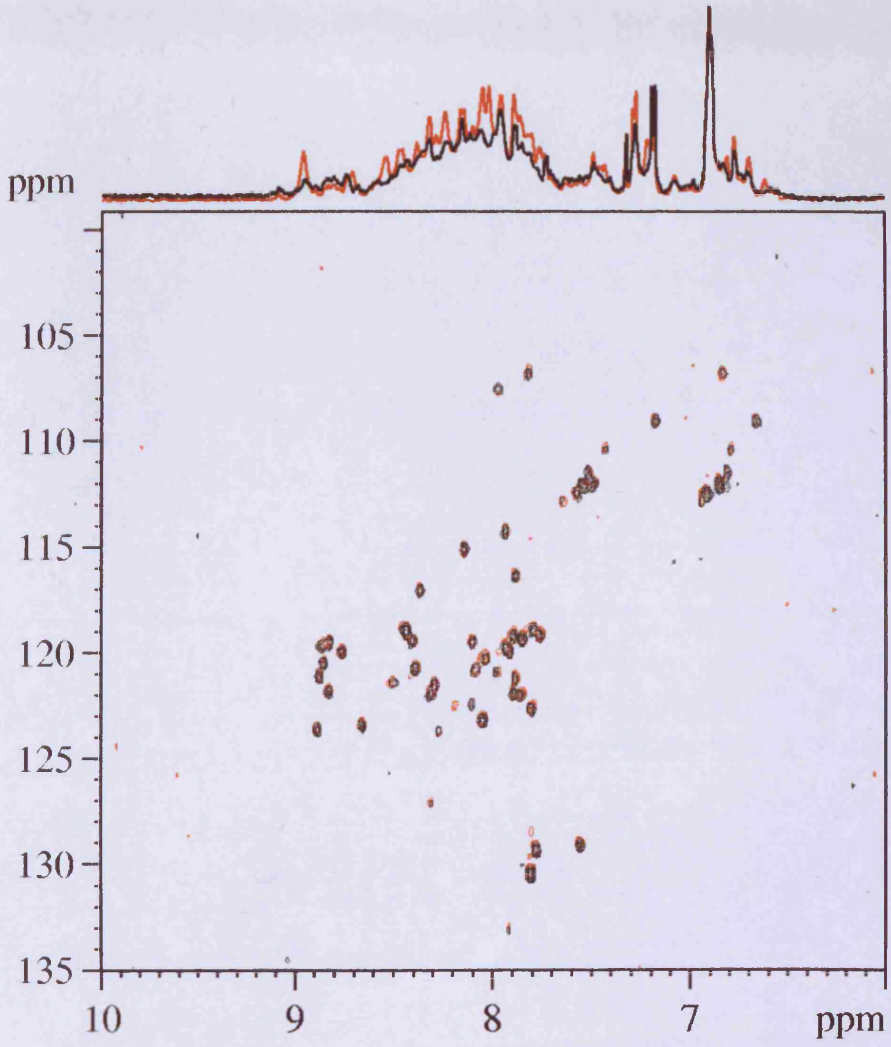

Figure 5.30 2D ^{1}H, ^{15}N HSQC characterisation of the [^{15}N]r-c-Jun : $FosW_C$ (1:1) and [^{15}N]r-c-Jun : mPEG-$FosW_C$ (1:1) coiled-coil complexes. [^{15}N]r-c-Jun : $FosW_C$ (1:1) is shown in red and [^{15}N]r-c-Jun : mPEG-$FosW_C$ (1:1) is shown in black. Each sample was prepared at a peptide concentration of 75 μM.

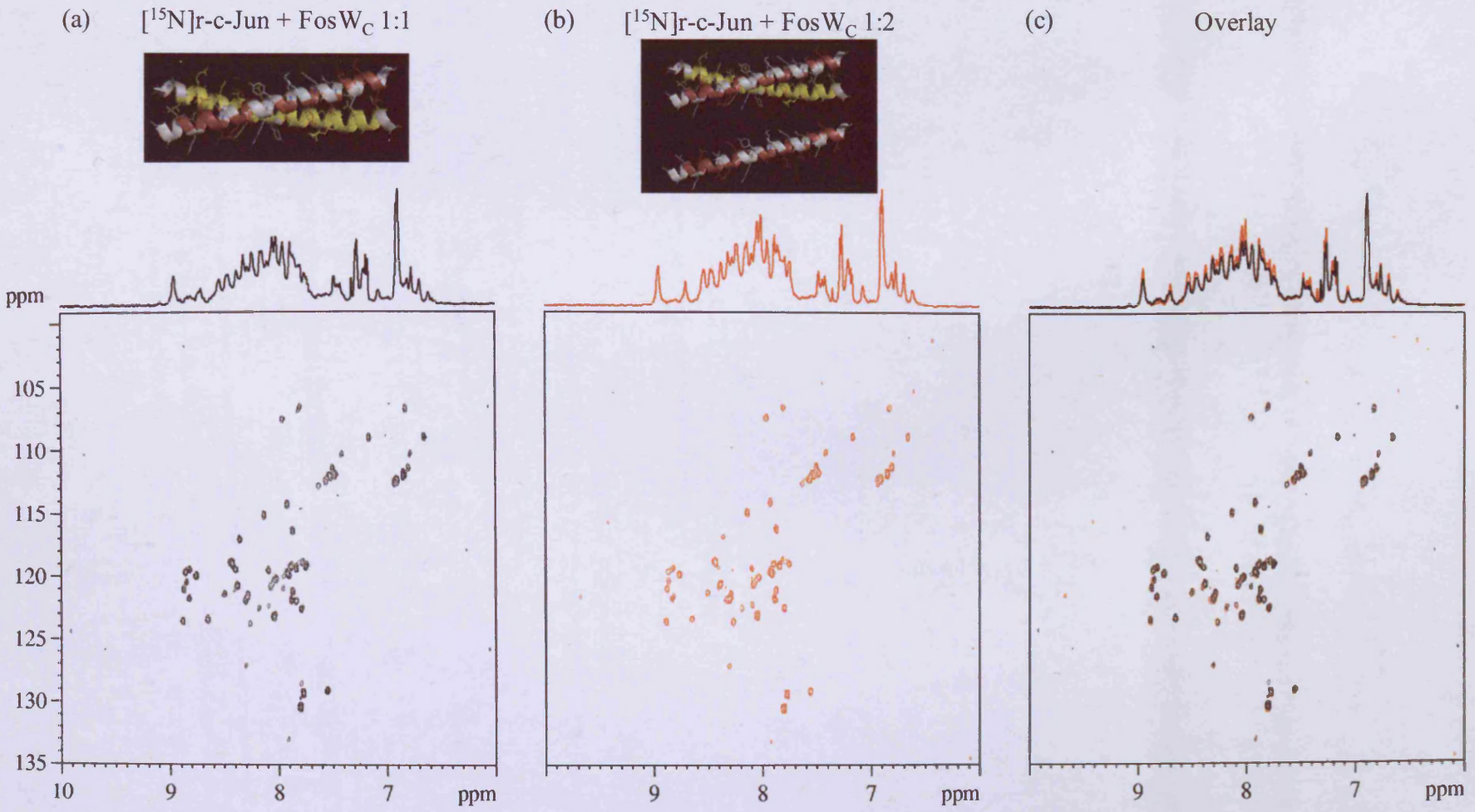

Figure 5.31 2D ^{15}N HSQC characterisation of the [^{15}N]r-c-Jun : $FosW_C$ coiled-coil complex at a 1:1 and 1:2 ratios. Panel (a) shows [^{15}N]r-c-Jun + unlabelled $FosW_C$ (1:1), panel (b) shows [^{15}N]r-c-Jun + unlabelled $FosW_C$ (1:2) and panel (c) shows the overlaid spectra. Samples were prepared at peptide concentrations of 75 μM.

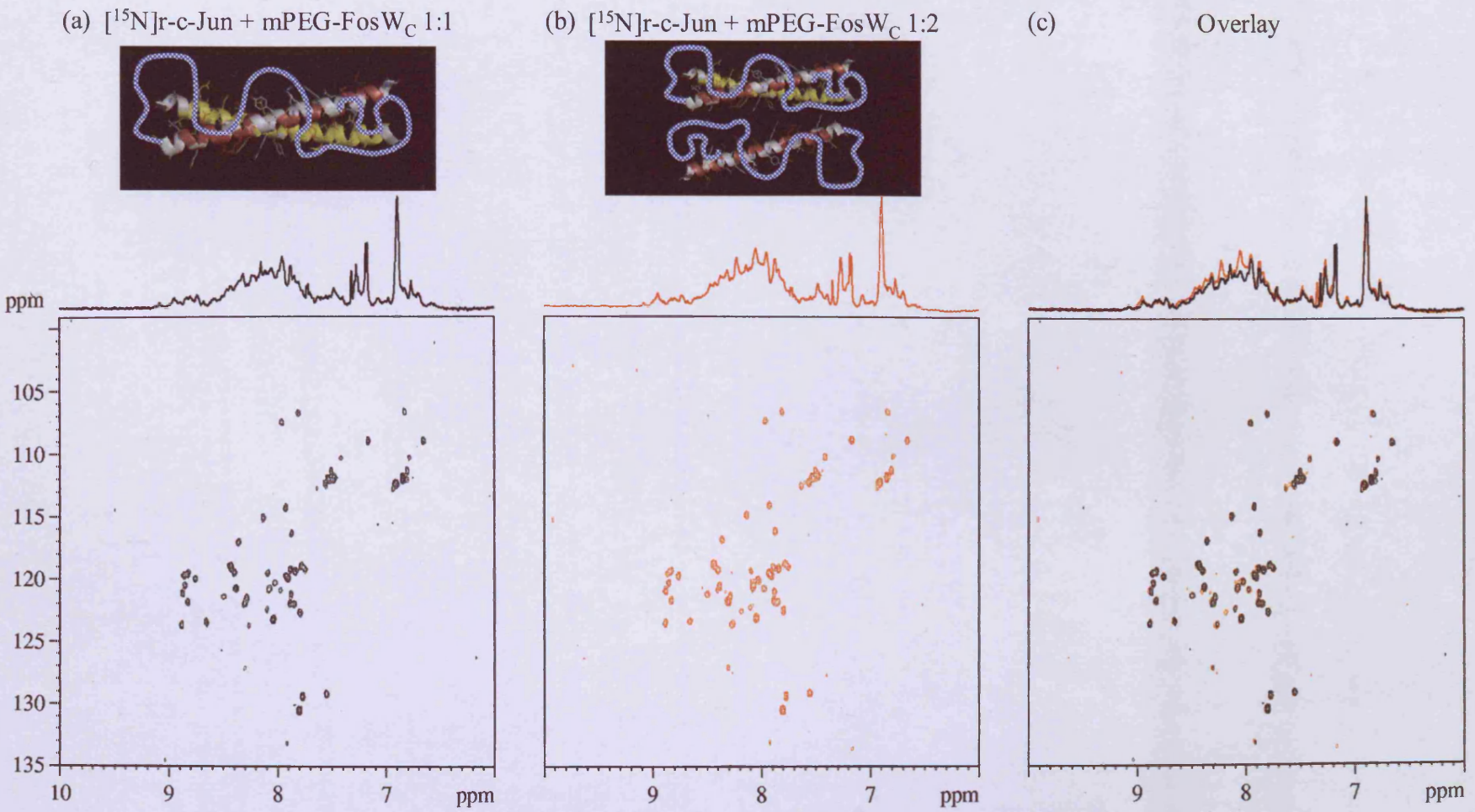

Figure 5.32 2D ^{15}N HSQC characterisation of the [^{15}N]r-c-Jun : mPEG-FosW$_C$ coiled-coil complex at a 1:1 and 1:2 ratios. Panel (a) shows [^{15}N]r-c-Jun + unlabelled mPEG-FosW$_C$ (1:1), panel (b) shows [^{15}N]r-c-Jun + unlabelled mPEG-FosW$_C$ (1:2) and panel (c) shows the overlaid spectra. Samples were prepared at peptide concentrations of 75 μM.

undergoes target hybridisation. The task of testing this hypothesis was a challenging one. Firstly it was necessary have a good model of the target, either a protein or peptide domain, subsequently it was necessary to develop CD and NMR spectroscopy techniques to conduct the proposed analyses.

5.4.1 Comparative Merits of the Model Targets Used to Study Phb : E2F1 and $FosW_C$: c-Jun Hybridisation

Use of E2F1 Derived Peptides and rhE2F1

Unlike previous studies by Wang *et al*, (1999) where co-immunoprecipitation techniques were used to study the PHB : E2F1 interaction, this study sought to characterise spectroscopically whether hybridisation was driven by a hetero-oligomeric coiled-coil. CD and NMR spectroscopy required larger quantities (mg *cf.* μg) of target material due to the lower sensitivities of the techniques and greater sample volumes needed.

Use of the peptides, E2F1a and E2F1b, which corresponded to the Phb-binding domain in the E2F1 protein was first proposed due to the difficulty in obtaining full-length protein. The advantage of this approach was twofold, first it was possible to synthesise large quantities of either peptide using Fmoc-SPPS (Chapter 3) to a high level of purity (> 95 %). Moreover, it was proposed that the small size of the peptides would facilitate characterisation by CD and or NMR spectroscopy. However, it was not known whether the peptides E2F1a and E2F1b would form a similar structure to the Phb-binding domain in the E2F1 protein. Furthermore, occasionally other sequences within the protein have been shown to be necessary to facilitate/trigger coiled-coil formation (Steinmetz *et al*, 1998).

Therefore, on balance use of full-length E2F1 protein for hybridisation studies was considered the optimal approach. Since E2F1 was too large to synthesise by conventional Fmoc-SPPS (Chan & White, 2000) the recombinant approach summarised in section 5.1.1 was used.

The original studies using GST-rhE2F1 do not describe in detail the methods used to clone or to express the protein (Bandara *et al*, 1993; Girling *et al*, 1993). The BL21 (DE3) *E.coli* strain was suggested as a suitable strain in a personal communication by La Thangue *et al*, however, in this study successful over-expression of GST-rhE2F1 was only observed using the BL21 (DE3) pLysS *E.coli* strain. As the T7 high-level expression system in the BL21 (DE3) *E.coli* strain is well known to allow

some basal expression prior to induction with IPTG, lack of GST-rhE2F1 overexpression would suggest that the protein is toxic to *E.coli.* The pLysS plasmid solved this problem by suppressing basal level expression of GST-rhE2F1 *via* reduction of T7 RNA polymerase expression (Moffatt & Studier, 1987). Unfortunately it was not possible to achieve the end goal of expressing sufficient rhE2F1 to enable characterisation by CD/NMR spectroscopy as a mechanical method of lysing the cells was not available in the Welsh School of Pharmacy.

Use of [^{15}N]r-c-Jun and Synthetic c-Jun Peptides

With the characterisation of the plasmid encoding r-c-Jun completed by a collaborator (Dr A.K. Schott) it was possible to focus attention on optimising the expression and purification protocols. The successful expression of the [^{15}N]r-c-Jun peptide enabled a detailed study of mPEG-$FosW_C$: c-Jun interaction by 2D ^{1}H, ^{15}N HSQC spectroscopy. The product was pure (> 90 %) and had the expected molecular weight by MALDI-TOF MS.

Monitoring each step of an expression protocol usually relies solely on the use of denaturing SDS-PAGE (Chapter 2, section 2.2.1.3). However, in the case of [^{15}N]r-c-Jun, the orange/red colour of the cytb5 tag (adapted from Mitra *et al*, 2003) made it possible to qualitatively assess each step of the expression and purification protocols.

A disadvantage of recombinant preparation was that a N-terminal "GT" sequence was left following TEV protease cleavage. Furthermore, it was not possible to neutralise the charged N- and C-termini by selective amidation and acetylation as performed during Fmoc-SPPS of the peptides described in Chapter 3. When c-Jun (synthetic) was compared with r-c-Jun at 37 °C, both far UV CD spectra indicated a random coil structure. This was expected since the T_m of the c-Jun peptide as determined by CD spectroscopy was 24 °C (Mason *et al*, 2006), moreover, early NMR studies of the c-Jun homodimer necessitated low pH (3.6) buffers to induce coiled-coil structure. In this study, when cooled to 4 °C, r-c-Jun remained as a random coil, whereas synthetic c-Jun underwent a transition to an α-helix, possibly a homodimeric coiled-coil. The most likely explanation for this observation is that the charged termini of the recombinant peptide prevented parallel association of the two peptides and so a similar transition did not occur. As such, [^{15}N]r-c-Jun was only used in experiments conducted at 37 °C, whilst the synthetic c-Jun was used in later CD and NMR experiments requiring study over a wider range of temperatures.

5.4.2 Challenges of Verifying Coiled-Coil Driven Target Hybridisation

Study of Phb : E2F1 Using CD Spectroscopy

CD spectra showed that at temperatures below 20 °C the PHB derived peptides $Phb_{185\text{-}214}$ and $Phb_{Y185\text{-}214}$ adopted α-helical structures. This may suggest that given the right environment the peptides could form a coiled-coil structure, in agreement with the studies by Joshi *et al*, (2003) where PHB was shown to form homodimers driven by the putative coiled-coil domain.

In subsequent studies where the interaction of $Phb_{Y185\text{-}214}$ and the peptides E2F1a and E2F1b was investigated no evidence of either heterodimeric or heterotrimeric coiled-coil formation was observed. Due to the short length of the E2F1 derived peptides it may be that there were too few heptads to enable the formation of a coiled-coil or alternatively, that other sequences within the E2F1 protein may have been necessary to facilitate/trigger coiled-coil formation (Steinmetz *et al*, 1998).

One proposal is that the putative coiled-coil domain in the PHB protein drives homodimerisation and holds it in an inactive state. In response to an unknown stimuli the protein then switches to the active (monomeric) form whereby the putative coiled-coil domain is exposed and can interact with E2F1 and suppress transcription. Further studies would be required to investigate this hypothesis further. Ideally these should use full-length E2F1 and PHB proteins in combination with the $Phb_{Y185\text{-}214}$ peptide prepared here.

Study of the c-Jun : $FosW_C$ and c-Jun : mPEG-$FosW_C$ Interaction

The far-UV CD spectra of c-Jun and c-Fos related peptides are well documented so this study did not seek to repeat the many spectra published in the literature (Mason *et al*, 2006; John *et al*, 1996). However it was important to show that coiled-coil formation did occur when c-Jun and mPEG-$FosW_C$ were combined under physiological conditions.

Far UV CD spectra of c-Jun : mPEG-$FosW_C$ at equimolar concentrations (7.5 μM each) acquired using a tandem cell confirmed α-helical structures at 37 °C. Furthermore, the increase in the $[\theta]_{208}/[\theta]_{222}$ ratio post-mixing suggested the formation of a coiled-coil. The ratio of the CD intensities for dimeric coiled-coils $[\theta]_{208}/[\theta]_{222} \sim 1$ is indicative for tertiary interactions between helices: whereas the n-π* transition

(222nm) mainly reflects on the α-helical content, the π-π* band (208nm) polarizes parallel to the helix axis and therefore reports on tertiary contacts.

Subsequently, far UV CD spectra for both c-Jun : $FosW_C$ and c-Jun : mPEG-$FosW_C$ at higher concentrations (75 μM each) equivalent to those used in the study by Mason *et al*, (2006) confirmed α-helical, coiled-coil structures for both complexes at 37 °C and 4 °C. The thermal denaturation studies showed that a clear preference remained for the heterodimers at physiological temperature (37 °C). However, the T_m for the c-Jun : mPEG-$FosW_C$ complex was 45.5 °C, substantially lower than seen for the c-Jun : $FosW_C$ complex (70.1 °C) possibly as a result of temperature inducing increased mobility of the mPEG chain. The T_m determined by Mason *et al*, (2006) for the c-Jun : FosW complex was 63°C; this was 7 °C lower than measured in this study. Other than the N-terminal cysteine tag (in the case of $FosW_C$), the only differences between the peptides were the C-terminal proline residues, which had been omitted in this study. It is pertinent to realise however that the T_m determined by Mason *et al*, (2006) for the wild-type c-Jun : c-Fos complex was much lower (16 °C) than either T_m value determined for the c-Jun : mPEG-$FosW_C$ (45.5 °C) and c-Jun : $FosW_C$ (70.1 °C) complexes. Thus, while the mPEG chain appears to reduce the affinity of $FosW_C$ for the target peptide c-Jun, it is still markedly more stable than the wild-type complex. This suggests that mPEG-$FosW_C$ could act effectively as a competitive inhibitor of AP-1 by sequestering wild-type c-Jun and preventing coiled-coil driven heterodimerisation of c-Jun : c-Fos.

1D ^{1}H-NMR spectra were acquired with the intention of corroborating the findings shown by CD spectroscopy. However, the maximum temperature at which spectra could be recorded with the instrument was 49 °C, this was below the T_m of most of the complexes and so the study was limited to characterisation of just the individual peptides/conjugate (c-Jun, $FosW_C$ and mPEG-$FosW_C$). Interestingly, the data acquired for the c-Jun homodimer corroborate the T_m of 24 °C determined by Mason *et al*, (2006). This indicates that by monitoring the disappearance of the amide peaks in the 1D ^{1}H-NMR one can successfully determine the T_m of a coiled-coil complex. The level of accuracy with which this can be achieved would necessitate further study.

While not of great importance here, the advantages of the NMR approach are that analyses can be conducted with buffers and salts not compatible with CD e.g. carboxylate, 4-(2-hydroxyethyl)-1-piperazineethanesulfonic acid (HEPES) and 3-(N-morpholino) propanesulfonic acid (MOPS). The acquisition of far UV CD spectra

between pH 4-6 (lysosomal-late endosomal range) is normally problematic due to the need for these buffers. Moreover, modifying the ionic strength with Cl^- is problematic since it absorbs strongly at $\lambda \leq 195$ (Dr. K. Beck, personal communication), hence F^- (NaF) was used in this study. In NMR analyses Cl^- could be used; advantageous if low pH (< 7) studies were required since under acidic conditions NaF may be converted to HF which can damage (etch) the expensive quartz cells or NMR tubes.

2D ^{15}N HSQC spectroscopy demonstrated that at 37 °C the [^{15}N]r-c-Jun peptide alone has very little structure, but subsequent addition of an equimolar concentration of mPEG-$FosW_C$ induced structural changes consistent with an induced fit theory of coiled-coil heterodimerisation. The spectral changes were equivalent to those seen when $FosW_C$ was added so it can be concluded that site-specific conjugation of mPEG did not change the manner of heterodimerisation. Furthermore, the observation that doubling the concentration of both $FosW_C$ and mPEG-$FosW_C$ (relative to [^{15}N]r-c-Jun peptide) did not induce further spectral changes suggests that a stable heterodimer is fully formed at equimolar concentrations. This also underlines the preference for heterodimerisation rather than potential homodimerisation of either $FosW_C$ or [^{15}N]r-c-Jun.

General Considerations for the Study of Protein Interactions in a Model Environment

It is pertinent to consider that while the temperature and pH of the buffered solution within which the samples were analysed was adjusted to model physiological conditions i.e. 37 °C, pH 7.4, the local environment found within the cell is likely to be very different, in particular, the ionic strength, concentration and type of counter-ions. Furthermore, hybridisation may be dependent or at least affected by the presence of chaperone proteins, in the case of E2F1, binding proteins such as Brg-1 and Brm (Wang *et al*, 2002). Therefore, approaches where NMR may be used to study interactions in a real, living cell have great promise (Inomata *et al*, 2009; Sakakibara *et al*, 2009; Burz *et al*, 2006).

5.4.3 Conclusions

With the synthesis of well-characterised peptides and conjugates (Chapters 3 and 4, respectively) and the [^{15}N]r-c-Jun peptide prepared here, it was possible to

investigate $FosW_C$/mPEG-$FosW_C$: c-Jun target hybridisation using 2D ^1H, ^{15}N-HSQC, CD and ^1H-NMR spectroscopy.

In conclusion, these studies demonstrate for the first time that an mPEG-$FosW_C$ conjugate is able to heterodimerise *via* the formation of a coiled-coil with r-c-Jun in a similar manner as for $FosW_C$. No N-H signal shifts were recorded in the 2D-HSQC spectra, nor were any significant changes in peak intensity observed. Furthermore, CD spectroscopy corroborated the formation of a coiled-coil structure for both $FosW_C$ and mPEG-$FosW_C$: c-Jun complexes. While mPEG reduced the T_m of the coiled-coil complex, it remained three times that determined for the wild-type in previous studies.

Progress was made regarding study of the Phb : E2F1 interaction, however it was not possible to achieve the end goal of expressing sufficient rhE2F1 to enable characterisation by CD/NMR spectroscopy. Nonetheless it was possible to successfully characterise the plasmid encoding GST-rhE2F1 then determine the optimal *E.coli* strain and expression conditions. Further investigation and detailed charcterisation of the interaction would make a very exciting continuation of this thesis.

Moving forward, it was considered essential to begin to investigate the biological activity of such novel polymer therapeutics in a cellular environment. Therefore, studies in Chapter 6 began to study the therapeutic potential of the $Phb_{Y185-214}$ and $FosW_C$ coiled-coil motifs and their respective mPEG conjugates using cell-based assays to determine cytotoxicity, biocompatibility and cellular uptake.

CHAPTER 6

Investigation of the Cellular Uptake and Cytotoxicity of mPEG-Phb$_{CY185-214}$ and mPEG-FosW$_C$ in MCF-7 Cells *In Vitro*

6.1 Introduction

As described in Chapter 1, $FosW_C$, $Phb_{Y185-214}$ and their respective mPEG-conjugates were designed as potential anti-cancer agents. In both instances, the protein targets c-Jun (Pekarsky *et al*, 2008) and E2F1 (Fusaro *et al*, 2003) are localised in the cytosol and/or nucleus. Therefore, in order to exert a cytotoxic effect by their proposed mechanisms (section 1.4) they would need to be able to gain cytosolic access. In the previous study (Chapter 5) the ability of $FosW_C$ and mPEG-$FosW_C$ to hybridise with the target, c-Jun, was demonstrated in a model environment. The aims of these preliminary studies were to determine whether mPEG-$FosW_C$ and/or mPEG-$Phb_{Y185-214}$ could show cytotoxicity *in vitro*.

Experimental Overview

Cellular cytotoxicity was assessed in the human breast cancer cell line, MCF-7, using the MTT assay. Previous research by Joshi *et al,* (2003) showed that a 41-residue peptide (from which $Phb_{Y185-214}$ was derived) was able to mediate cytotoxicity without the need for a transfection reagent. Therefore studies with $Phb_{Y185-214}$ and mPEG-$Phb_{CY185-214}$ were conducted without the cationic lipid Tfx™-50 used to deliver $FosW_C$ and mPEG-$FosW_C$. The use of Tfx™-50 for the delivery of c-Fos derived peptides was shown to be essential in earlier studies by Yao *et al*, (1998). In light of their work, it was first necessary to determine the cytotoxicity of this reagent alone, then optimise the Tfx™-50 : $FosW_C$/mPEG-$FosW_C$ ratio.

Further studies using flow cytometry were conducted to assess cellular uptake and of both $Phb_{Y185-214}$/mPEG-$Phb_{CY185-214}$ and $FosW_C$/mPEG-$FosW_C$ (± Tfx™-50) at 37 °C. In order to perform these latter experiments it was first necessary to synthesise fluorescently labelled (OG) peptides and conjugates. Although the above relates to the chronological order of these studies, for the purpose of clarity here, the synthesis, characterisation and cellular uptake studies of OG-labelled peptides/conjugates are presented first, followed by preliminary cytotoxicity and haematotoxicity studies (**Figure 6.1**). A brief background to the rationale and use of each of these experiments is described in the following sections.

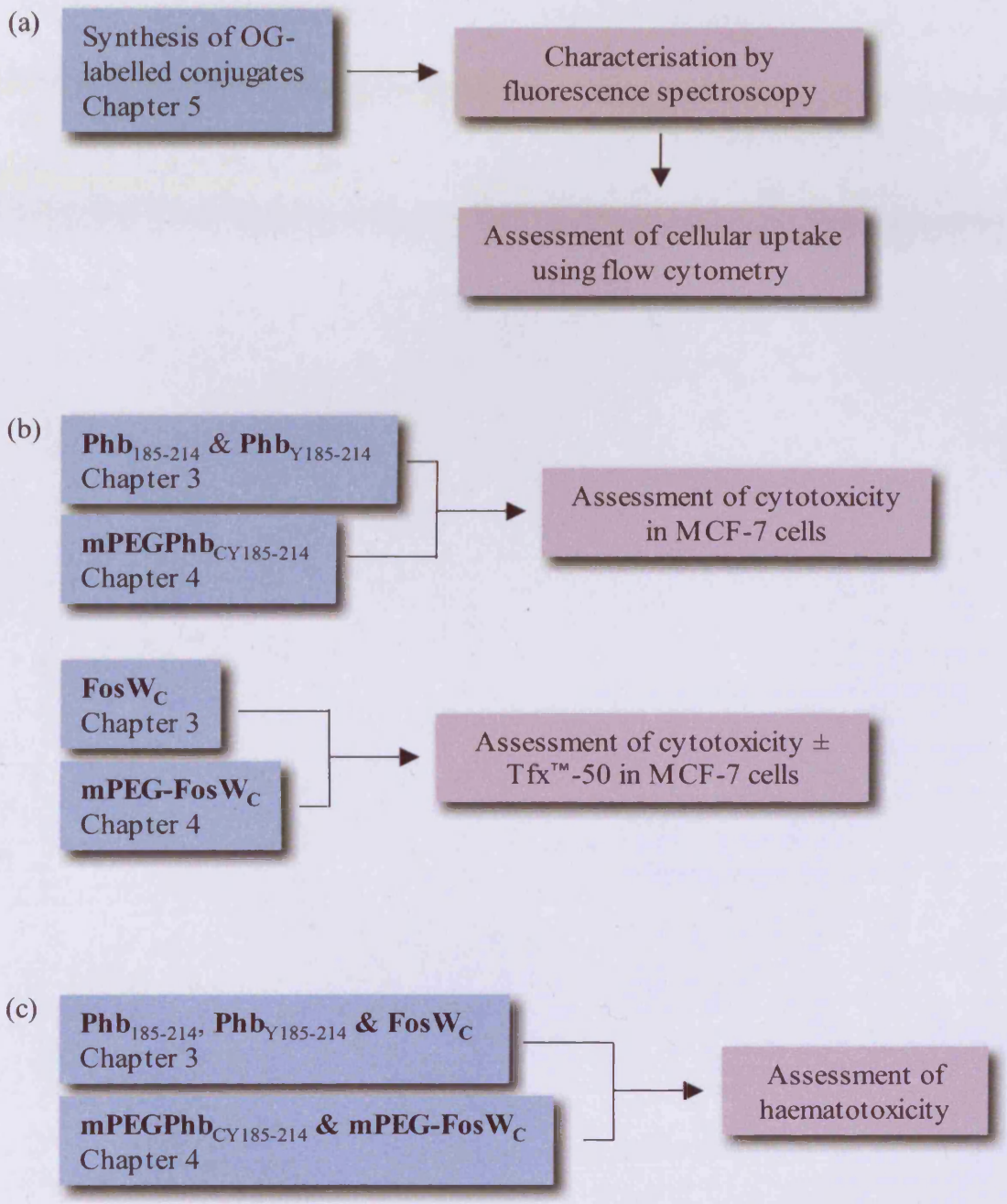

Figure 6.1 Schematic overview of the experiments conducted in this study.

6.1.1 Flow Cytometry as a Tool to Study Cellular Uptake of OG-Labelled Conjugates

In this study, flow cytometry was used to monitor and quantitate cell uptake of fluorescently labelled peptides, conjugates and controls. This technique enables the analysis of thousands of cells per second, by passing the cells through a laser beam and measuring the discrete measurements of cellular fluorescence and light scattering (Melamed *et al*, 1990). Following statistical analysis of the data using flow cytometry software one may deduce cellular features and characteristics such as size, granularity, phenotype, health and cell-associated fluorescence. Furthermore, it is also possible to study the cellular uptake of fluorescent drugs e.g. doxorubicin (Dordal *et al*, 1995; Greco *et al*, 2007) and non-fluorescent compounds, labelled with an appropriate fluorophore e.g. OG. Such modification has made it possible be to monitor the cellular uptake of polymers (Richardson *et al*, 2008; Seib *et al*, 2007; Shukla *et al*, 2006), peptides (López de Saro *et al*, 2003) and many other molecules of interest (Seye *et al*, 2004). Flow cytometry has a number of key advantages over other cell imaging techniques, for example, it does not just give a measurement of cell-associated fluorescence for the entire population of cells but instead allows the user to define a population range. This is particularly useful to enable dead cells to be excluded from measurements, or to determine if there are differences in uptake by different populations (e.g. transfected and non-transfected) of cells in a given sample. A further advantage is that the cells may be imaged live without the need for fixing or digestion (Ramanathan, 1997), both of which have the potential to introduce artefacts into the measurements. However, flow cytometry does not enable one to discern the intracellular localisation of polymer therapeutics by imaging of individual cells made possible with confocal fluorescence microscopy (Richardson *et al*, 2008). Moreover, quantitative analysis of fluorescence can be hindered by the variable output of the fluorescent probe, a problem not seen with a combined radio-labelling and sub-cellular fractionation approach (Seib *et al*, 2006; Manunta *et al*, 2007).

6.1.2 Choice of Fluorescent Probe

To establish whether Tfx™-50 was effectively facilitating the uptake of either $FosW_C$ or mPEG-$FosW_C$, studies were conducted using flow cytometry (reviewed in section 6.1.1 above). Studies were also planned to assess the relative uptake of Phb_{Y185-}

$_{214}$ and mPEG-$Phb_{Y185-214}$ (though not in conjunction with Tfx™-50). In order to conduct these studies it was first necessary to label each compound with a suitable fluorescent probe. Prior to conjugation, it was necessary to consider (i) the choice of fluorophore, (ii) possible site of attachment to the peptide or polymer, and (iii) the linking chemistry.

Oregon Green (OG)

A wide-range of fluorophores are commercially available for the purpose of labelling peptides, polymers or other molecules. Oregon green (OG) was identified as the fluorophore of choice for use in this study. In previous studies it has been used to label polymers such as dextrin and HPMA co-polymer conjugates (Richardson *et al*, 2008), dendrimers and both linear and branched PEI (Seib *et al*, 2007). Other fluorophores, such as fluorescein have been widely used in the past, however, despite similar fluorescence excitation and emission wavelengths (λ_{ex} = 488 nm and λ_{em} = 520 nm), fluorescein has been shown to be less photostable. Furthermore, a marked quenching of the fluorescence output has been reported at pH < 7 (Lanz *et al*, 1997). The increased photostability of OG facilitates its use in a practical sense, and theoretically reduces the concentration of fluorophore required for detection. However, more significant is the reduced quenching observed with OG in the pH range 5.5 to 7.4 compared with fluorescein (Seib *et al*, 2007). As discussed in Chapter 1, any compound that undergoes endocytosis and subsequent transport to lysosomal vesicles will experience a drop in local pH; approximately 6.5 in early endosomes, while dropping further to 5.5 in late endosomes and lysosomes. As such, if a fluorophore were subject to pH related quenching it would not be suitable to accurately assess either qualitatively or quantitatively cellular uptake.

Conjugation Site(s) and Linking Chemistry

The peptides $FosW_C$ and $Phb_{Y185-214}$ were synthesised using only naturally occurring amino-acid residues, therefore the only reactive side-chains that could be used for OG-conjugation were R-COOH, R-NH_2 and R-SH (**Figure 6.2**). As discussed in Chapter 4, the R-SH group of the cysteine residue is the most potent electrophile and is therefore a useful way of ensuring site-specific conjugation. However, since the mPEG-conjugates were prepared using this same approach, neither mPEG-$FosW_C$ nor mPEG-$Phb_{Y185-214}$ possessed any reactive cysteine residues that could be targeted.

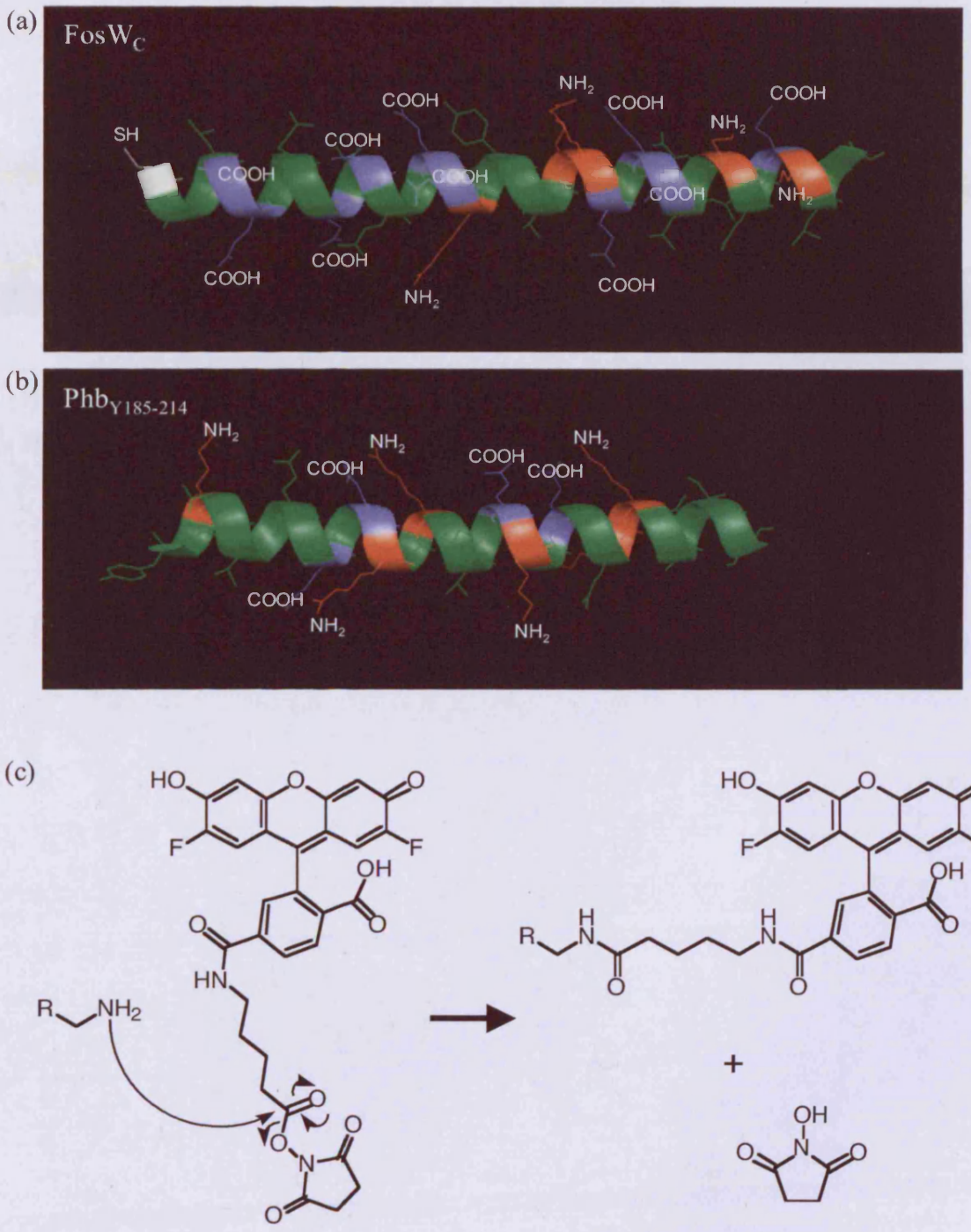

Figure 6.2 Possible sites of conjugating OG to peptides $FosW_C$ and $Phb_{Y185-214}$ and reaction scheme for OGSE488-X with a reactive amine side-chain. Panels (a) and (b) show COOH sides-chains coloured blue, NH_2 side-chains red and SH white. The latter was not reactive in the PEGylated peptides. Panel (c) shows the structure of OGSE488-X and its reaction mechanism with an amine side-chain. N.B. R-SH could react in the same manner. Protein structure file was obtained from the PDB, DOI:10.2210/pdb1fos/pdb and edited/rendered accordingly using MacPyMOL.

To facilitate later analyses with fluorescence spectroscopy and flow cytometry, it was important that exactly the same fluorophore, and linking chemistry, was used to prepare both the OG-labelled peptides and mPEG-conjugates. The ideal approach would have utilised a heterobifunctional PEG chain, whereby OG could be conjugated to one end and either $FosW_C$ or $Phb_{CY185-214}$ to the other. However, the cost of PEG reagents needed to perform such a synthesis were prohibitive, furthermore this approach would have required new conjugates to be synthesised. Instead, the use of an OG derivative such as OGSE488-X would make it possible to label each compound in a similar manner, i.e. same fluorophore, same linking chemistry. The only possible difference was the exact site of conjugation, since each peptide possessed multiple arginine and lysine residues. To ensure the same site of conjugation it would have been necessary to re-synthesise the coiled-coil motif peptides with protecting groups that could be selectively removed i.e. with differing concentrations of TFA. Re-synthesis was not a feasible option; therefore, the random amine-labelling approach as described above was used. The most significant disadvantage of this approach was that conjugation of OGSE488-X to an amine side-chain would likely disrupt the α-helical structure of the peptides and probably prevent coiled-coil formation with their respective targets. Furthermore, it was hypothesised that changes to the secondary structure of the coiled-coil motif peptides may affect their intracellular uptake and trafficking. However, the random amine-labelling approach was the only option available which would allow the preliminary uptake studies to be conducted with the time and materials that were available. Prior to conducting the synthesis of OG-labelled peptides and conjugates, optimisation of the protocol was conducted using mPEG-NH_2 (Chapter 2, section 2.2.7).

6.1.3 Methods of Investigating *In Vitro* Cell Viability

The assessment of *in vitro* cell viability is an essential step in the pre-clinical study of any compound if considered as a potential future therapeutic. To best characterise candidate compounds, a cell viability assay must be reproducible and able to report accurately changes in viability, furthermore it is imperative that the assay is a good predictor of *in vivo* and/or clinical outcomes.

A myriad of techniques are available, including measuring (i) mitochondrial respiration using the MTT assay (Mosmann, 1983), (ii) the incorporation of

radiolabelled DNA precursors e.g. [^{3}H]-thymidine (Amirghofran *et al*, 2007) and (iii) lactate dehydrogenase (LDH) release as a measure of membrane integrity (Korzeniewski and Callewaert, 1983).

The MTT assay, first described by Mosmann (1983) has been routinely used to screen polymer-anticancer agents (Alley *et al*, 1998) to detect changes in cytotoxicity, proliferation or activation. The main advantages of this colorimetric assay were its "...rapidity and precision, and the lack of any [requirement for a] radioisotope" (Mosmann, 1987). Furthermore, in an evaluation of the clinical usefulness of preclinical assessment using the MTT assay, the prediction rate for anti-tumour therapy was shown to be 86.4 % (Furukawa *et al*, 1991). Thus this assay was chosen to measure the cytotoxicity of $Phb_{Y185-214}$ and mPEG-$Phb_{Y185-214}$ and subsequently $FosW_C$ and mPEG-$FosW_C$.

Rationale for Use of the MCF-7 Cell Line

As mentioned above (section 6.1), a peptide similar to $Phb_{Y185-214}$ was previously shown to have a pro-apoptotic effect in four different cell lines including MCF-7 (Joshi *et al*, 2003). These observations were made without the use of a transfection reagent and the MCF-7 cell line was found to be most sensitive, with 46 % of cells in an apoptotic state (TUNEL assay) at a peptide concentration of 15 μM. In this study, experiments were conducted using the MTT assay to determine whether a similar effect could be observed for either $Phb_{Y185-214}$ or mPEG-$Phb_{Y185-214}$.

Previous work had also demonstrated that c-Fos derived peptides were cytotoxic in the MCF-7 cell line, albeit when delivered with the transfection reagent Tfx™-50 (Yao *et al*, 1998). Experiments conducted without the use of Tfx™-50 had failed to show any cytotoxicity up to a concentration of 100 μM (Yao *et al*, 1998). In light of this work, a review of the use of Tfx™-50 and other methods for the transfection of peptides was conducted.

6.1.4 Transfection of Peptide/Polymer Therapeutics

A diverse range of methods and reagents have been developed with the aim of delivering macromolecules including peptides/proteins, polymers and DNA into cells. Commonly used techniques for facilitating intracellular delivery include the use of calcium phosphate precipitation, peptides, cationic polymers e.g. polyethyleneimine

Table 6.1 Choice of reagents considered to aid intracellular delivery of FosW_C and mPEG-FosW_C.

Reagent Name	Description	Reference(s)
Chariot™	Intracellular-delivery demonstrated for a wide-range of macromolecules in many different cell lines, including delivery of green fluorescent protein (GFP) in MCF-7 cells. Reported to be non-cytotoxic, transfection is serum independent. Used for the intracellular delivery of a PHB derived peptide.	Morris *et al*, 1999; Morris *et al*, 2001; Joshi *et al*, 2003
DeliverX™	Virus derived ampipathic peptides that form nano-particles capable of passing through plasma membranes avoiding the endocytic pathway. Purported delivery of a peptide inhibitor of cyclin dependent kinase 2 (Cdk2) in HeLa cells.	Simeoni *et al*, 2003
Pro-Ject™	Cationic lipid used to successfully transfect a range of macromolecules including, GFP, high and low molecular weight dextran sulfate and caspase enzymes. Protocol advises to transfect in serum free media.	Thermo Scientific, www.piercenet.com
PULSin™	Cationic amphiphile, forms non-covalent complexes with proteins. Said complexes are delivered following binding with anionic cell adhesion receptors. Used for wide range of proteins in many cell types, though not including MCF-7.	Weill *et al*, 2008; Cortez *et al*, 2007
Tfx™-50	Cationic lipid marketed for the transfection of DNA, however, successful transfection of c-Fos derived peptides demonstrated in the MCF-7 cell line. Works in presence of serum.	Yao *et al*, 1998
TransPass™ P	Reagent that delivers proteins and peptides into cells via endocytosis. Successfully used in MCF-7 cell line. Very little other information available.	New England BioLabs (www.neb.com)

(PEI) (Boussif *et al*, 1995), cationic liposomes (Felgner *et al*, 1987), electroporation (Chu *et al*, 1987), micro-injection (Capecchi, 1980) and viral methods (Graham and Van der Eb, 1973).

The use of viral vectors, or access to electroporation and/or micro-injection techniques was not possible during the course of this study. As such the relative pros and cons of the remaining reagents were assessed, with particular regard to the peptide and cationic lipid reagents (**Table 6.1**).

The cationic liposome Tfx™-50 was of particular interest since its use with Fos derived peptides had shown promise in previous work (Yao et al, 1998). Furthermore, it was commercially available, substantially cheaper than the peptide reagents (therefore a greater range of experiments could be conducted) and could be used to perform transfections in the presence of serum (Schenborn *et al*, 1995).

Structure of Tfx ™-50 and Proposed Mechanism of Action

The cationic lipid component of the Tfx™-50 reagent is N, N, N', N'-tetramethyl-N, N'-bis(2-hydroxyethyl)-2, 3, -dioleoyloxy-1, 4-butane diammonium iodide (Schenborn *et al*, 1995). Whilst the exact mechanism by which the reagent is purported to facilitate transfection is unknown, it is postulated that the cationic head groups of the lipid molecule form an ionic complex with the anionic groups of the target molecule (Schenborn *et al*, 1995), in this case the peptide. As discussed in Chapter 1 (section 1.4), the cell membrane presents a charged surface by virtue of the anioic phosphate groups positioned at the outer edges of the lipid bilayer. It is thought that by conveying an overall cationic charge to the peptide (or mPEG-peptide conjugate) the complex will be able to make contact with the cell membrane surface, and an unknown fusion-type event follow, allowing the complex to be internalised into the cell (Zhou and Huang, 1994; Remy *et al*, 1994).

6.1.5 RBC Lysis as a Tool to Study Haematotoxicity

The overall aim of this research was to develop novel polymer-coiled-coil motif conjugates with therapeutic potential as novel nanomedicines for clinical use. With this approach in mind, it was necessary to ascertain whether non-specific toxicity (e.g. membrane damage) was likely to arise following parenteral administration of any of the

compounds described in this study. It was essential that the compounds did not induce lysis of cellular membranes, as such an effect would preclude further study.

The RBC lysis assay is a well-established method of investigating whether polymers, proteins and other biomacromolecules exert a membrane destabilising effect (Duncan *et al*, 1994; Lavignac *et al*, 2005; Vandermeulen *et al*; 2005). It was used in conjunction with well-established positive and negative controls, PEI and mPEG-NH_2 respectively.

6.16 Experimental Aims

In summary, the aims of this study were to:

For Flow Cytometry Studies:

- Synthesise, purify and characterise OG-labelled peptides ($FosW_C$-OG and $Phb_{Y185-214}$-OG) and mPEG-peptide conjugates (mPEG-$FosW_C$-OG and mPEG-$Phb_{CY185-214}$-OG).

- Study the effect of OG conjugation and complexation with Tfx™-50 on (i) the fluorescence excitation and emission spectra and (ii) the fluorescence intensity at the $\lambda_{ex\ (max)}$ and $\lambda_{em\ (max)}$ using fluorescence spectroscopy.

- Investigate the effect of pH (in the physiological range - 5.5 to 7.4) on the fluorescence emission intensity of each of the OG-labelled compounds. If quenching did occur, to estimate the degree to which it occurred and whether it was likely to affect the data obtained from flow cytometry measurements.

- Measure the uptake of OG-labelled peptides and conjugates at 37 °C using flow cytometry. Firstly to assess the uptake of $Phb_{Y185-214}$-OG and mPEG-$Phb_{CY185-214}$-OG relative to mPEG-OG. Secondly, to quantify the uptake of the compounds $FosW_C$-OG and mPEG-$FosW_C$-OG relative to their respective Tfx-50 complexes.

For Assessment of Cytotoxicity:

- Study the effect of each of the unlabelled peptides and conjugates on cell viability in the MCF-7 cell line using the MTT assay. Investigate the use of the

transfection reagent Tfx™-50 to deliver FosW$_C$ and mPEG-FosW$_C$ and determine by means of the MTT assay whether the complex is more cytotoxic than either compound in isolation.

For Assessment of Haematotoxicity:

- Determine whether the unlabelled peptides and conjugates induced haemolysis using the red blood cell lysis assay as a means of assessing likely biocompatibility.

6.2 Methods

The coiled-coil motif peptides, FosW$_C$ and Phb$_{Y185-214}$, and mPEG-coiled-coil motif conjugates, mPEG-FosW$_C$ and mPEG-Phb$_{CY185-214}$, used in this study were prepared as described in Chapters 3 (section 3.2.2) and 4 (section 4.2.2), respectively. The molecular weight and peptide sequence for each compound is provided in Appendix 1.

General methods relating to cell culture and characterisation of the OG-conjugates prepared in this study are described in Chapter 2. In particular, use of UV spectroscopy to determine sample concentration (section 2.2.1.1), packing of Sephadex® G-15 chromatography columns (section 2.2.2.1), purification and analysis of OG-labelled conjugates (section 2.2.2.2), and flow cytometry (section 2.2.4.3).

The methods in this Chapter are divided into two sections; the first describes the synthesis and characterisation of the OG-labelled conjugates and cellular uptake studies using flow cytometry, while the second describes the haemolysis, MTT and transfection assays.

6.2.1 Preparation of OG-Labelled Probes

Prior to conducting any cell-uptake experiments with flow cytometry it was first necessary to prepare and characterise OG-labelled peptides (FosW$_C$-OG and Phb$_{Y185-214}$-OG), conjugates (mPEG-FosW$_C$-OG and mPEG-Phb$_{CY185-214}$-OG) and as a control mPEG-OG. The methods used to prepare the probes used in this study were optimised in earlier work with mPEG-OG and are summarised in Chapter 2 (section 2.2.2.2).

Table 6.2 Summary of Reactants Used for Preparation of the OG-Labelled Probes.

Sample ID	Peptide/Conjugate[†]		Volume of OG[#]
	(mg)	μmoles	(μL)
$FosW_C$-OG	10	2.29	71
mPEG- $FosW_C$-OG	10	2.29	71
$Phb_{Y185-214}$-OG	5	1.42	44
mPEG-$Phb_{CY185-214}$-OG	5	1.38	43

[†]For each of the mPEG-conjugates, quantities were determined using the peptide molecular weight.

[#][Stock solution] = 5 mg mL^{-1}.

6.2.1.1 Synthesis, Purification and Analysis of OG-Labelled Probes

This method describes the preparation of mPEG-OG; all OG conjugates were prepared in the same manner. For reference, the quantities of reactants used in the preparation of the other four OG-labelled conjugates are summarised in **Table 6.2.**

mPEG-NH_2 (5,000 g mol^{-1}, 11 mg, 2.2 μmoles) was dissolved in sodium bicarbonate buffer, pH 8.3 (0.5 mL). OGSE488-X was dissolved in methanol to a concentration of 5 mg mL^{-1}. An aliquot (68 μL, 0.25 mol. eq.) of this solution was added to the reaction flask. The flask was wrapped in foil and the reaction left to proceed for 4 h at room temperature in the dark. Progress of the reaction was monitored at t = 0, 1, 2 and 4 h, by thin layer chromatography (TLC) using methanol as the mobile phase, once dry the plates were visualised using a UV lamp.

SEC with a PD-10 desalting column was used to purify the crude reaction mixture; ddH_2O was used as the mobile phase. An aliquot (25 μL) of the purified sample was dissolved in ddH_2O and the purity checked using a PD-10 desalting column equilibrated in PBS. Aliquots (100 μL) from each fraction collected (500 μL) were assayed using a fluorescence plate reader (FLUOstar OPTIMA) to determine the ratio of free to bound OG-SE (detailed in section 2.2.7). UV spectroscopy was used to determine the peptide and OG concentrations where appropriate (section 2.2.1).

6.2.1.2 Effect of OG-Conjugation on Fluorescence Excitation and Emission Spectra

To investigate whether the fluorescence spectra were changed as a result of conjugation, excitation and emission spectra were measured for each of the OG-conjugates prepared in section 6.2.1.1. Each sample was prepared at an OGSE488-X concentration of 1.5 μg mL^{-1} (determined by UV spectroscopy) in PBS, pH 7.4, total volume 120 μL. To determine the appropriate gain setting, the emission intensity for each of the samples was first measured using a fluorescence plate reader (FLUOstar OPTIMA) with excitation and emission filters set at λ_{ex} = 485 nm and λ_{em} = 520 nm, respectively. These filters were chosen as they were closest available to the published $\lambda_{ex\,(max)}$ and $\lambda_{em\,(max)}$ for OGSE488-X (www.invitrogen.com).

The sample with the highest emission intensity at λ_{em} = 520 nm (mPEG-OG) was then measured first with a fluorometer (SIM-AMICO) and the gain adjusted such that the $\lambda_{ex\,(max)}$ was set to 60 % of the maximum detection limit. Spectra were acquired for each sample using a quartz cuvette, pathlength 1 cm. The instrument settings were

as follows: λ range of 350 to 550 nm for excitation scans and a λ range of 450 to 650 nm for emission scans, resolution was 2 nm, integration time 1 s and monochromator band pass 4 nm. All spectra were saved and exported as .txt files.

6.2.1.3 Effect of pH and Concentration on the Fluorescence Emission Intensity of the OG-Labelled Conjugates

Prior to conducting cell-uptake experiments with flow cytometry it was first necessary to determine whether the fluorescence emission intensity of the OG-conjugates changed in response to pH and/or concentration; and in the case of FosW$_C$ and mPEG-FosW$_C$ following complexation with the cationic lipid, Tfx™-50, transfection reagent.

Stock solutions (100 μg mL^{-1}) of OGSE488-X and each OG-labelled conjugate were prepared in PBS, pH 7.4 and diluted with either, PBS (pH 7.4), PBS (pH 6.5) or citrate buffer (pH 5.5) to provide 5 samples (0.1, 0.5, 0.75, 1.0 and 1.5 μg mL^{-1}) of each probe for each pH. The total volume of each sample was 120 μL. All of the samples were prepared directly into black, polypropylene 96-well plates suitable for fluorescence spectroscopy. Aliquots (120 μL) of each buffer were also added to the respective plates as a negative control. The fluorescence emission intensity at 520 nm was measured using a fluorescence plate reader (FLUOstar OPTIMA) with excitation and emission filters set at λ_{ex} = 485 nm and λ_{em} = 520 nm, respectively. The gain was adjusted such that the fluorescence emission for the sample of highest intensity (mPEG-OG, 1.5 μg mL^{-1}, pH 7.4) was set to 90 % of the maximum detection limit. This gain value (1223) was used in the acquisition of data for all three plates. Immediately prior to acquiring the emission data, each plate was shaken for 10 s inside the plate reader. Post-acquisition, all data were saved and exported as .xls files.

6.2.2 Study of Cellular Uptake Using Flow Cytometry

6.2.2.1 Cell Uptake Studies Using OG-Labelled Peptides and Conjugates

The general method used to analyse the cellular uptake of OG-conjugates by flow cytometry analysis was described in Chapter 2, section 2.2.8. In the experiments conducted in this study all samples were standardised to an [OG] of 1.5 μg mL^{-1}; this was the same concentration used to conduct the fluorescent spectroscopy experiments described earlier (section 6.2.1). Wells were seeded with MCF-7 cells at a

concentration of 5 x 10^5 cells mL^{-1} and incubated for 24 h at 37 °C, 5 % CO_2 to allow cells to adhere before adding test compounds.

For studies with mPEG-OG, $Phb_{Y185-214}$-OG and mPEG-$Phb_{CY185-214}$-OG, uptake at time points of 0, 1, 3 and 5 h were measured relative to control (untreated) cells. In each experiment samples were prepared in triplicate and the data from three experiments collated.

For studies with $FosW_C$-OG, mPEG-$FosW_C$-OG and their respective, Tfx™-50 complexes, uptake was measured at time points of 0, 1 and 2 h relative to control (untreated) and Tfx™-50 treated cells. The 2 h time-point samples were prepared by incubating the cells with test compounds for 1 h, then removing and adding fresh complete media for a further 1 h; thus replicating the protocol used in the earlier cell viability studies (section 6.2.3). Samples were added in reverse time order such that all samples were ready to analyse with the flow cytometer at the same time. In each experiment samples were prepared in triplicate and the data from two experiments collated.

All data were analysed and exported in two formats (i) dot-plots (x-axis: forward scatter, y-axis: side scatter) and (ii) histograms (x-axis: fluorescence - FL-1, y-axis: counts), data were later processed using GraphPad Prism v4.0 to generate the bar charts presented (x-axis: time, y-axis: fluorescence).

6.2.2.2 Stability of OG-Conjugates Post-Incubation with MCF-7 Cells

An important control was to determine whether significant amounts of OGSE488-X were cleaved from each of the respective OG-conjugates during incubation with the cells over the course of the flow cytometry experiments. Liberation of large amounts of OGSE488-X, either by acid or enzymatic hydrolysis would likely, introduce artefacts into the fluorescence data obtained (due to differences in rate of uptake and transport of free OGSE488-X compared with the macromolecular form). As such, cell media, post-incubation at each of the time points measured (1 and 2 h) was analysed using PD-10 columns filled with Sephadex® G-15 media (see section 2.2.6 for preparation and use). Analysis of each sample by fluorescence spectroscopy was conducted as described in section 2.2.2.2.

6.2.3 Assessment of Cell Viability Using the MTT Assay

This assay was described in Chapter 2, section 2.2.3. Detailed here are specific references to the test compounds under study. In all instances cells were seeded in 96-well plates at a density of 40,000 cells mL^{-1} using clear complete media (100 µL / well) and incubated for 72 h at 37 °C, 5 % CO_2 prior to addition of test compound to ensure that the cells were in their exponential growth phase.

6.2.3.1 Cytotoxicity of $Phb_{185-214}$, $Phb_{Y185-214}$ and mPEG-$Phb_{CY185-214}$

In the first three experiments $Phb_{185-214}$ was used as the test compound; as it did not possess a strong UV-sensitive choromophore e.g. tyrosine, concentrations were determined gravimetrically as for the polymers PEI and mPEG-NH_2 used as positive and negative controls, respectively. Solutions of PEI (70,000 g mol^{-1}), $Phb_{185-214}$ (3531 g mol^{-1}) and mPEG-NH_2 (5,000 g mol^{-1}) were prepared at concentrations of 0, 0.01, 0.05, 0.1, 0.5 and 1 mg mL^{-1} in clear complete media. Aliquots (100 µL) of each in replicates of 6 were added to the respective wells. Plates were then incubated (37 °C, 5 % CO_2) for a total of 72 h; the remainder of the assay was conducted as described in Chapter 2, section 2.2.4.2.

Further studies made use of the peptide $Phb_{Y185-214}$ along with the conjugate mPEG-$Phb_{CY185-214}$ as test compounds, since both contained the tyrosine chromophore that made accurate determination of concentration by UV spectroscopy possible. Each of these experiments was conducted using the same protocol as described for $Phb_{185-214}$.

6.2.3.2 Cytotoxicity of $FosW_C$ and mPEG-$FosW_C$ ± Tfx™-50

Initial studies were conducted to investigate cytotoxicity of $FosW_C$ and mPEG-$FosW_C$ without the use of the transfection reagent Tfx™-50. Three separate experiments were conducted using the same protocol as described for the Phb derivatives above.

In light of data published by Yao *et al*, (1998) suggesting the need to use a transfection reagent (Tfx™-50) to deliver Fos derived peptides, subsequent studies were conducted using this reagent. Optimisation of the transfection protocol was conducted using only the peptide $FosW_C$ to minimise the amount of Tfx™-50 reagent required. Comparative studies using mPEG-$FosW_C$ were performed later.

Approaches to Calculating the Amount of Tfx™-50 Reagent to Complex with $FosW_C$

It was necessary to determine the amount of Tfx-50 reagent to use to form a complex with the peptide $FosW_C$. In the work by Yao *et al,* (1998) a charge ratio of 2:1 (peptide : Tfx™-50) was used. However the authors did not mention whether this ratio was calculated using the summed negative charge/molecule of the peptides studied, or the overall charge, i.e. summed negative charges/molecule minus the sum of positive charges/molecule. $FosW_C$ has a total of ten negatively charged and five positively charged functional groups. A preliminary experiment was conducted to evaluate whether there was any difference between the complexes prepared using either approach to the calculation. For clarity, a 2:1 charge ratio using a negative charge of -10/molecule of $FosW_C$ is equivalent to a 1:2.5 (peptide : Tfx™-50) molar ratio; a negative charge of -5/molecule equates to a 1:1.25 molar ratio.

Furthermore, it is important to note that in these experiments concentrations were prepared using molar, rather than mass units in contrast to earlier studies, this decision was taken to facilitate comparison of the data with that obtained by Yao *et al,* (1998).

6.2.3.3 Preparation and Reconstitution of Tfx ™-50 Reagent

Complexes were prepared in accordance with the manufacturers instructions, summarised in **Figure 6.3a**; all work was conducted in an aseptic suite. In brief, a vial of Tfx™-50 reagent was warmed to room temperature at least the day prior to each experiment. Nuclease-free water (400 µL) was added to the contents of each vial to produce a lipid suspension of concentration, 1 mM (1 nmol μL^{-1}). The sample was vortexed vigorously (10 s) to suspend the lipid film, then incubated at 65 °C in a water bath for 1 min. Care was taken to ensure that the water level was above that of the lipid suspension in the vial and that the rubber septum did not "pop" off during incubation. The suspension was vortexed a second time (10-15 s) then stored overnight at - 20 °C. When required, the suspension was thawed at room temperature and vortexed (10-15 s). Once reconstituted the suspension was used within 8 weeks or discarded in accordance with the manufacturers advice.

6.2.3.4 $FosW_C$ / mPEG-$FosW_C$: Tfx ™-50 Complex Preparation

$FosW_C$ / mPEG-$FosW_C$: Tfx™-50 complexes were prepared immediately prior to use in each experiment. An illustration is provided in **Figure 6.3b**. Sample solution

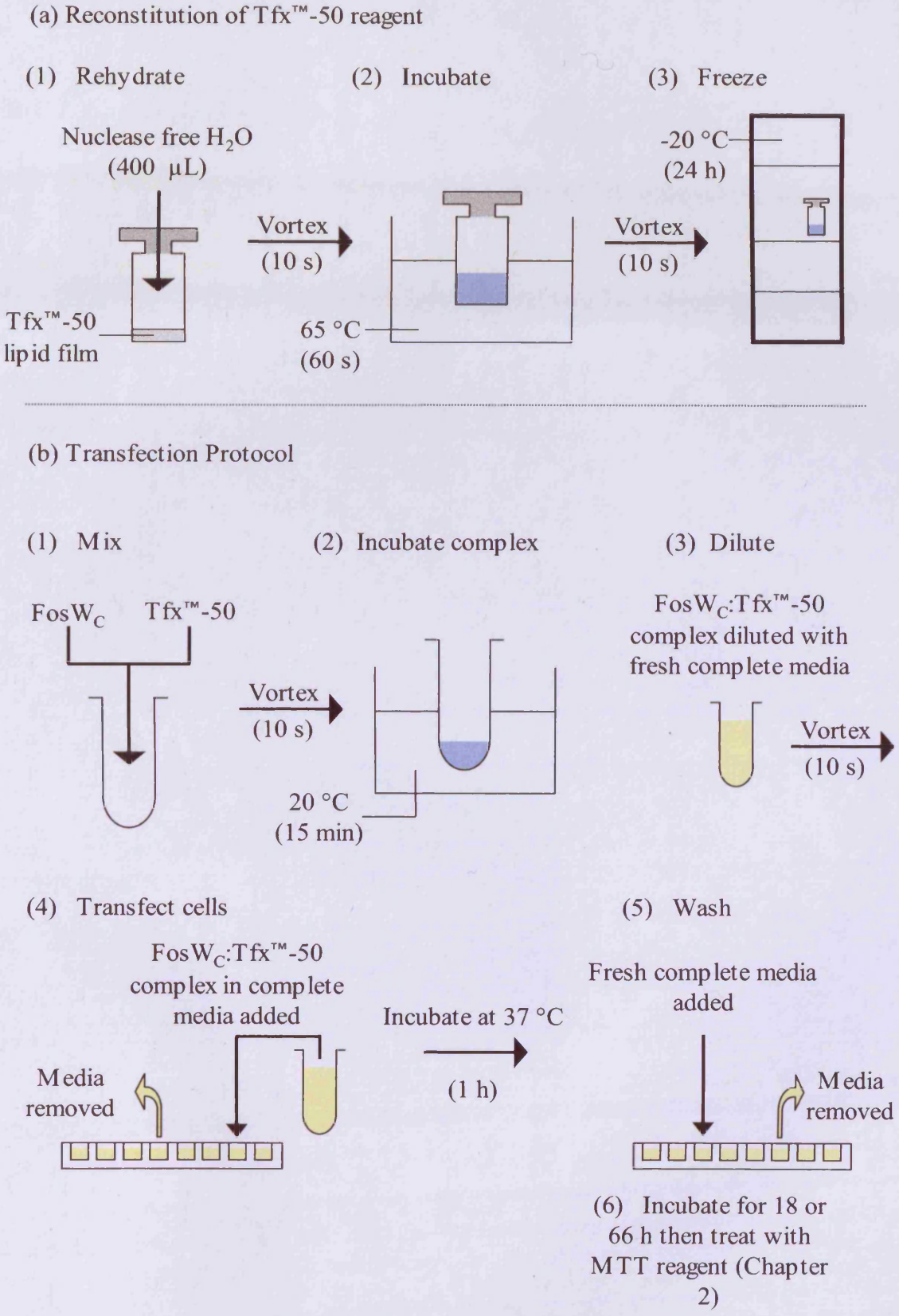

Figure 6.3 Reconstiution and use of Tfx™-50 reagent. Panel (a) shows the reconstitution of Tfx™-50 reagent. Panel (b) shows transfection of MCF-7 cells using $FosW_C$, Tfx™-50 controls were prepared using PBS in replacement of $FosW_C$.

($FosW_C$ or mPEG-$FosW_C$ in PBS) and Tfx™-50 reagent were combined in sterile plastic Eppendorf™ tubes (2 mL). The tubes were sealed and vortexed (10-15 s) then incubated for 15 min at room temperature (20 °C). The samples were then ready to be added to the cells, see individual experiment descriptions below.

6.2.3.5 Assessment of $FosW_C$: Tfx™-50 Molar Ratio and MTT Assay Incubation Time

The first assay was performed using samples of $FosW_C$: Tfx™-50 prepared using a 1:1.25 molar ratio, the second using a 1:2.5 molar ratio. In each assay, a 5-log concentration range was used to construct a dose response curve to compare the cytotoxicity of the $FosW_C$: Tfx™-50 complex relative to Tfx™-50 alone. The test compounds were incubated with the cells for a total of 72 h and the MTT assay performed as described in Chapter 2, section 2.2.3. A third assay was conducted using a 1:2.5 molar ratio, however with a 24 h incubation time as used by Yao *et al*, (1998). In all three assays, samples were prepared at each concentration in triplicate.

6.2.3.6 Determination of the Optimal $FosW_C$: Tfx™-50 Charge Ratio

In all further cell viability studies experiments were conducted using a fixed peptide concentration of 10 μM and with and incubation time of 24 h. A 10 μM concentration was chosen since it was at this concentration that the greatest difference between the cytotoxicity of the $FosW_C$: Tfx™-50 complex and the Tfx™-50 control was observed in all three assays. This experiment investigated whether a charge ratio of 2:1 (calculated on the basis of a molar ratio of 1:2.5) was optimal. Complexes and Tfx™-50 controls at equivalent concentrations were prepared in triplicate to investigate the effect on cell viability at charge ratios of 2:1, 1:1, 1:2, 1:4 and 1:8 ($FosW_C$: Tfx™-50). The incubation time was kept at 24 h.

6.2.3.7 Assessment of the Cytotoxicty of $FosW_C$ /mPEG-$FosW_C$: Tfx™-50 Complexes Using a 2:1 Charge Ratio (1:2.5 Molar Ratio)

Four assays were conducted, in each instance using a fixed peptide concentration of 10 μM. The first assay was performed using only the peptide $FosW_C$ and was conducted with three controls: (i) untreated cells, (ii) Tfx™-50 alone and (iii) $FosW_C$, each at equivalent concentrations to those used in the $FosW_C$: Tfx™-50 complex. The remaining three assays were conducted with Tfx™-50 complexes of both

FosW$_C$ and mPEG-FosW$_C$ and three controls as above. To improve the power of the data, in each assay samples were prepared in replicates of six. Data from the three separate assays were combined to generate an n of 18.

6.2.4 Investigation of Haemolytic Activity Using the RBC Lysis Assay

Prior to preparation of the RBC suspension, samples (100 μL) of the positive and negative-controls, PEI (70,000 g mol^{-1}) and mPEG-NH$_2$ (5,000 g mol^{-1}), respectively were added to "v-bottomed" 96-well plates in pentuplicate. It was important to note that the concentration of sample prepared in each well was doubled, since it was to be diluted 2-fold by the addition of RBC suspension (100 μL). For each sample, a 3-log range of concentrations was prepared such that the final concentrations were 0.001, 0.01, 0.1 and 1 mg mL^{-1}. Since neither of the polymers had a chromophore from which the concentration could be determined using UV spectroscopy, concentrations were determined gravimetrically. Two additional lanes (5 wells each) were included in each experiment, a "blank" lane of PBS, pH 7.4 and a second, consisting of Triton X-100 (1 % w/v). The latter was used as a 100 % haemolysis control so that all other data could be expressed as a percentage of this value. All plates were then chilled to 4 °C, while the RBC suspension was prepared.

The method used to prepare the RBCs was described previously by Duncan *et al,* (1994). In brief, male Wistar rats (c.a. 250-300 g body weight) were killed by CO_2 asphyxiation. Blood (6-8 mL / rat) was obtained by cardiac puncture using a large bore needle (18 G) and syringe and rapidly transferred to Li-Hep Vacutainer™ tubes (pre-weighed) on ice (c.a. 4 °C). PBS, pH 7.4 (1-2 mL / tube) was added to make the volume up to 5 mL following which, the tubes were centrifuged at 1500 g for 10 min at 4 °C. The supernatant was removed, fresh PBS, pH 7.4 was added (up to 5 mL / tube) and the sample centrifuged a second time. This process was repeated a third time and the mass of the pellet determined such that the volume of PBS, pH 7.4 required to make a 2 % w/v RBC suspension could be calculated. This suspension was freshly prepared for each experiment and stored on ice (c.a. 4 °C) while in use.

Aliquots (100 μL) of RBC suspension were added to each of the sample wells in the 96-well plate. The plate was then placed in an incubator for 1 h at 37 °C. Following incubation, the plate was centrifuged at 1500 g for 10 min at 4 °C. Aliquots (100 μL) of supernatant were then carefully removed from each well and transferred to

a "flat-bottomed" 96-well plate. The UV absorbance at $\lambda_{550\ nm}$ was determined using a microtitre plate reader (Tecan Sunrise). The mean absorbance of the "blank" lane was subtracted from all of the sample values and the data expressed as a % (± SD) of the haemoglobin released relative to Triton X-100.

Once the protocol was optimised using the positive and negative-controls, further assays were conducted with samples (100 µL) of $FosW_C$, mPEG-$FosW_C$, $Phb_{Y185-214}$ and mPEG-$Phb_{CY185-214}$. Sample concentrations were prepared in the same 3-log range, however a maximum concentration of 0.5 mg mL^{-1} was used for each test compound sample to conserve material. The experiment was conducted three times, each time a fresh RBC suspension was prepared with blood from a new rat. The data were collated and expressed as described above.

6.3 Results

6.3.1 Synthesis and Characterisation of OG-Labelled Conjugates

The OG-labelling protocol optimised in Chapter 2, section 2.2.2.2 was successfully applied to the synthesis of $Phb_{Y185-214}$-OG, mPEG-$Phb_{CY185-214}$-OG, $FosW_C$-OG and mPEG-$FosW_C$-OG for use in this study. TLC was used to monitor the progress of each reaction; in each case, after 2 h a bright fluorescent spot was visible on the baseline of the TLC plate for the reaction mixture. After 4 h, there was no further change in the appearance of the TLC. However, the efficiency of the reaction was well below 100 %, as judged by the fluorescent spot remaining in the reaction mixture lane for each sample with a RF similar to that of the free (un-reacted) OGSE control.

Analysis of the crude reaction mixture by SEC corroborated the observations made by TLC (**Figures 6.4 and 6.5**). In each instance, peaks corresponding to un-reacted OGSE488-X eluted between 5 and 15 mL, while the OG-labelled peptides and OG-labelled conjugates in the void volume (0.5 - 5 mL). Analyses conducted post purification by SEC, demonstrated the effectiveness of this technique at removing free OGSE488-X as only peaks corresponding to macromolecular-OG were observed in each analytical run (**Figures 6.4 and 6.5**). The first OG-labelled peptide prepared, $Phb_{Y185-214}$-OG, eluted slightly later than the other samples suggesting the possibility of a higher % of free OG contaminant. Free OG was higher in this sample (2.97 %)

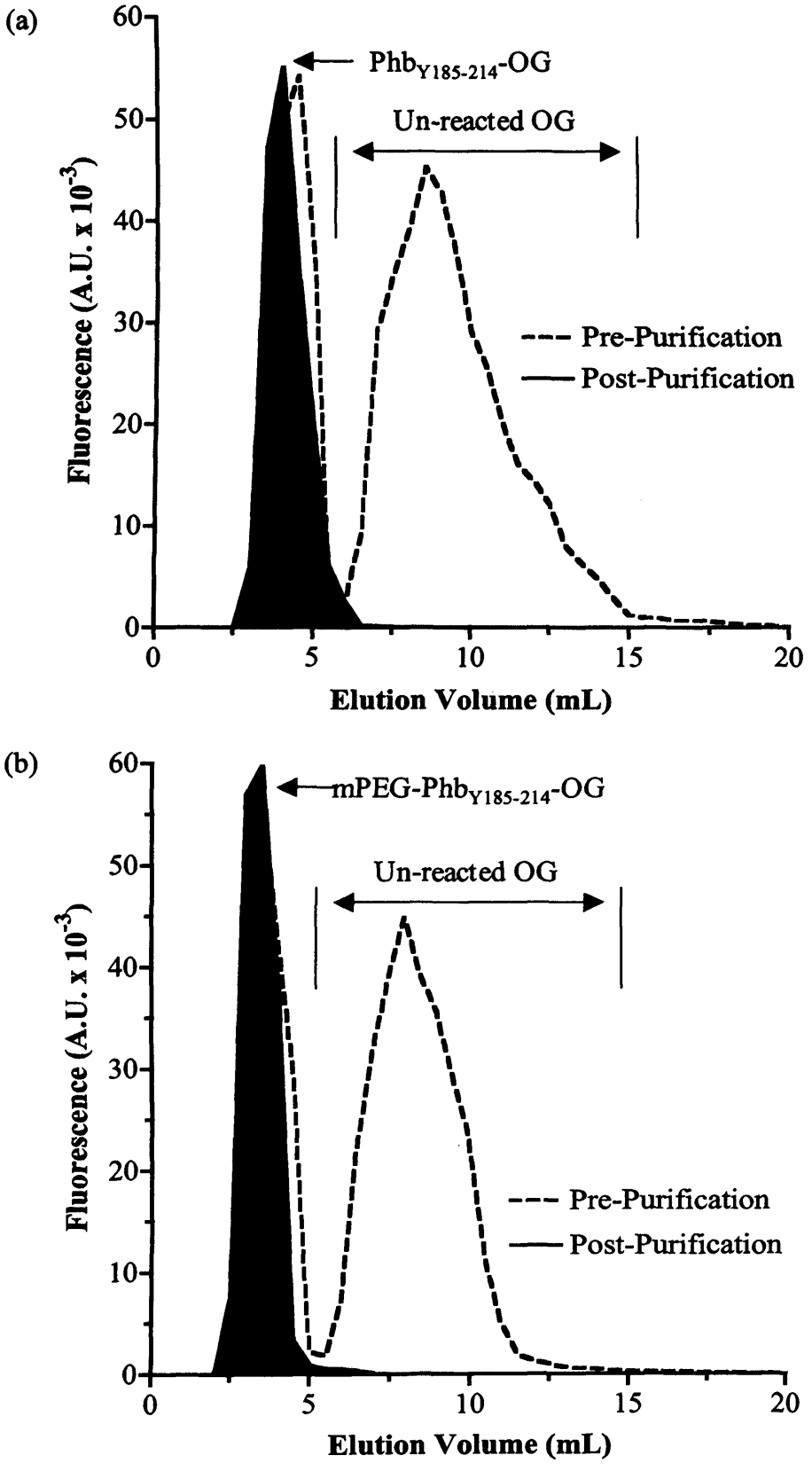

Figure 6.4 Evaluation of reaction efficiency and purity using SEC of OG-labelled conjugates $Phb_{Y185-214}$-OG and mPEG-$Phb_{Y185-214}$-OG. PD-10 columns containing Sephadex® G-25 media were used for purification and analysis of mPEG-$Phb_{Y185-214}$-OG while G-15 filled columns were used for $Phb_{Y185-214}$-OG.

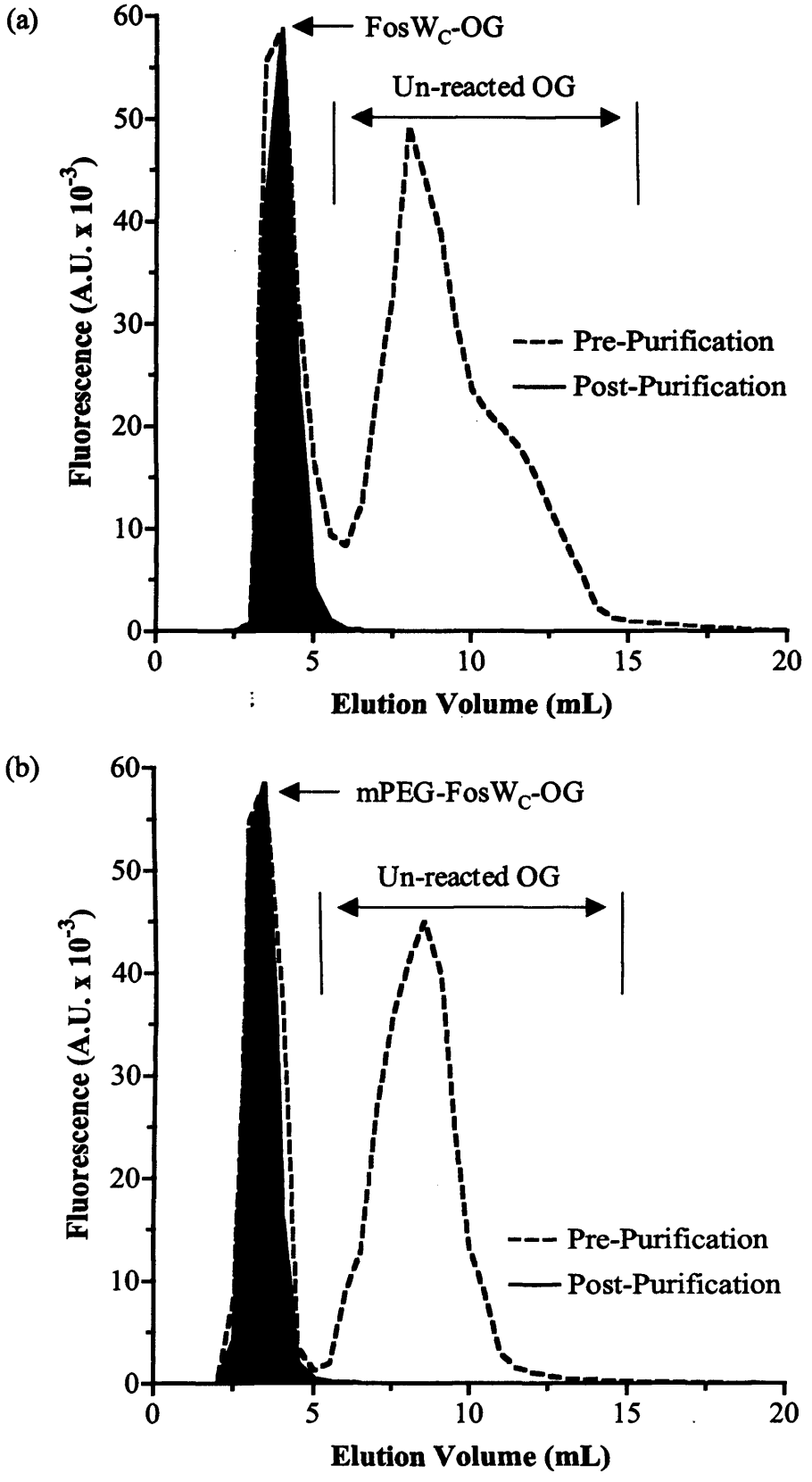

Figure 6.5 Evaluation of reaction efficiency and purity using SEC of OG-labelled conjugates $FosW_C$-OG and mPEG-$FosW_C$-OG. PD-10 columns containing Sephadex® G-25 media was used for purification and analysis of mPEG-$FosW_C$-OG while G-15 media was used for the peptide $FosW_C$-OG.

Table 6.3 Characterisation of OG-labelled peptides, polymer and conjugates.

Sample ID	Molar Ratio (OG : peptide/ polymer/conjugate)	Specific Activity (μg OG mg^{-1} conjugate)	Purity† (% Free OG)
mPEG-OG	0.38	04.20	2.90
$Phb_{Y185-214}$-OG	0.56	21.31	2.97
mPEG-$Phb_{CY185-214}$-OG	0.23	21.07	0.88
$FosW_C$-OG	0.17	18.94	0.85
mPEG-$FosW_C$-OG	0.16	19.80	0.24

†Determined by AUC

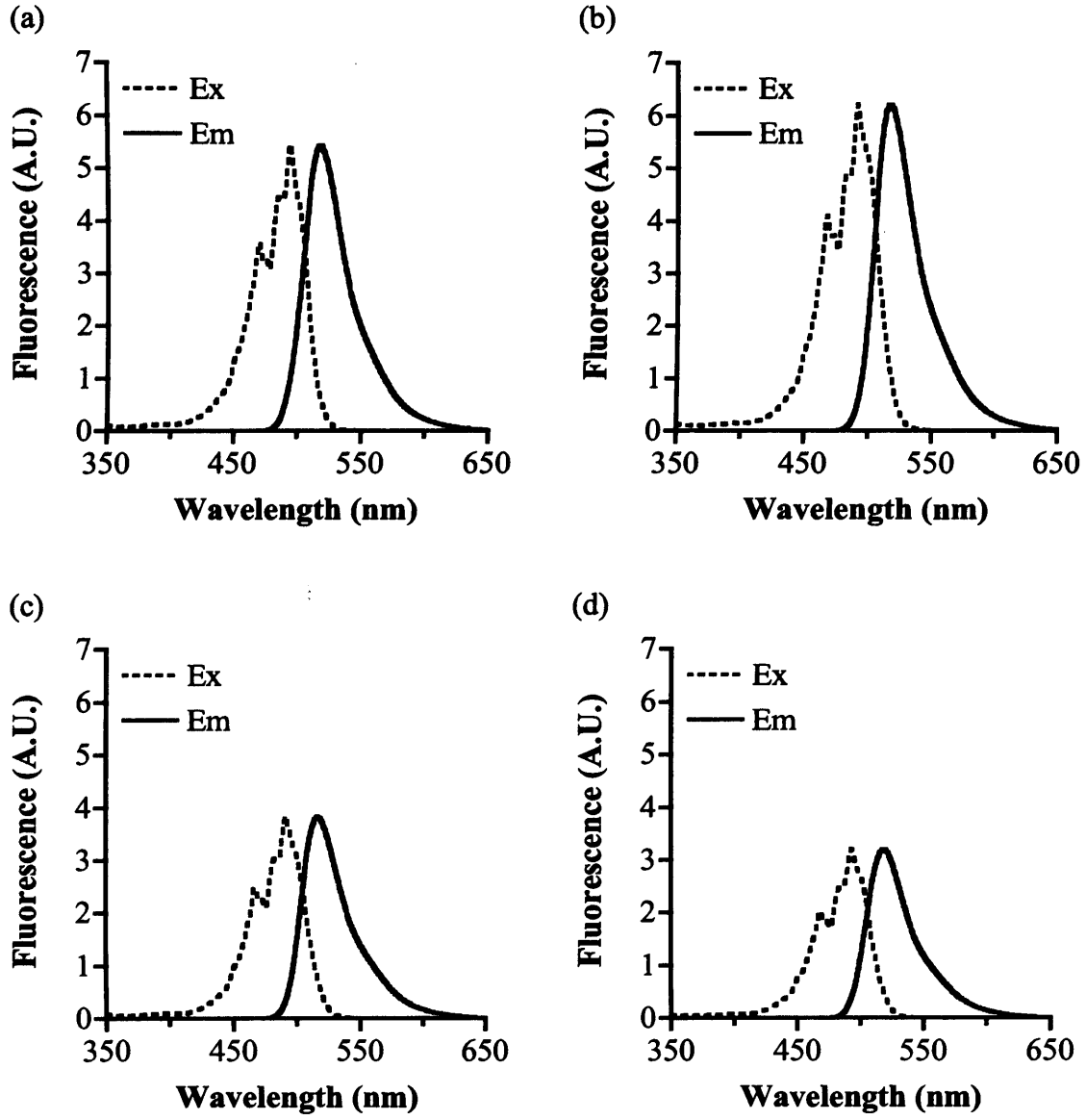

Figure 6.6 Characterisation of OG fluorescence excitation and emission spectra. Panels show (a) OGSE488-X, (b) mPEG-OG, (c) Phb$_{Y185-214}$-OG and (d) mPEG-Phb$_{CY185-214}$-OG. All samples were prepared at equi-molar concentrations of OG (1.5 $\mu g\,mL^{-1}$) in PBS, pH 7.4.

compared with 0.88, 0.85 and 0.24 % for mPEG-$Phb_{CY185-214}$-OG, $FosW_C$-OG and mPEG-$FosW_C$-OG, respectively (**Table 6.3**). With the exception of mPEG-OG, all OG-labelled conjugates had similar specific activities in the range of 20 μg OG / mg conjugate (**Table 6.3**).

Fluorescence Excitation and Emission Spectra of OG Pre and Post Conjugation

The fluorescence excitation and emission spectra for OGSE488-X are shown in **Figure 6.6a**. $\lambda_{ex\ (max)}$ and $\lambda_{em\ (max)}$ were 492 and 517 nm, respectively. Following conjugation there was no change in the $\lambda_{ex\ (max)}$ and $\lambda_{em\ (max)}$ values, however, in every case changes in the intensity of both the excitation and emission spectra were observed. For mPEG-OG (**Figure 6.6b**) the intensity of both spectra increased by approximately 14 %; it is possible that this small difference may be accounted for, at least in part by errors in determining the concentration of the sample. More marked changes were observed however when the fluorophore was conjugated to $Phb_{Y185-214}$-OG (**Figure 6.6c**); the fluorescence intensity decreased by 33 % and for mPEG-$Phb_{Y185-214}$-OG, the decrease was greater at approximately 41 %. A similar pattern was observed for $FosW_C$-OG (**Figure 6.7a**) and mPEG-$FosW_C$-OG (**Figure 6.7b**), with decreases of 30 and 36 % respectively.

When complexed with Tfx™-50 even greater quenching was observed. The fluorescence output of the $FosW_C$-OG : Tfx™-50 complex (**Figure 6.7c**) decreased by 91 %. The decrease was less pronounced for the mPEG-$FosW_C$-OG : Tfx™-50 complex (**Figure 6.7d**) at 57 %. However spikes in both the fluorescence excitation and emission spectra were detected for this sample. These may be suggestive of light scattering. Spectra were also acquired for an equi-molar concentration of Tfx™-50 as a control (**Figure 6.7e**), spikes, as seen for the mPEG-$FosW_C$-OG : Tfx™-50 complex were observed at the same λ_{ex} and λ_{em} values. Furthermore the excitation peak was of higher wavelength than the emission peak, again suggestive of light scattering rather than fluorescence, possibly indicative of micellar structures.

When normalised with respect to maximal fluorescence emission intensity at 517 nm (**Figure 6.8**), the excitation and emission spectra were almost identical in shape, both pre and post-conjugation. The only difference observed was a small change in the excitation spectra at 483 nm; the fluorescence intensity post conjugation (of all OG-labelled samples) decreased by approximately 4 % relative to free OG.

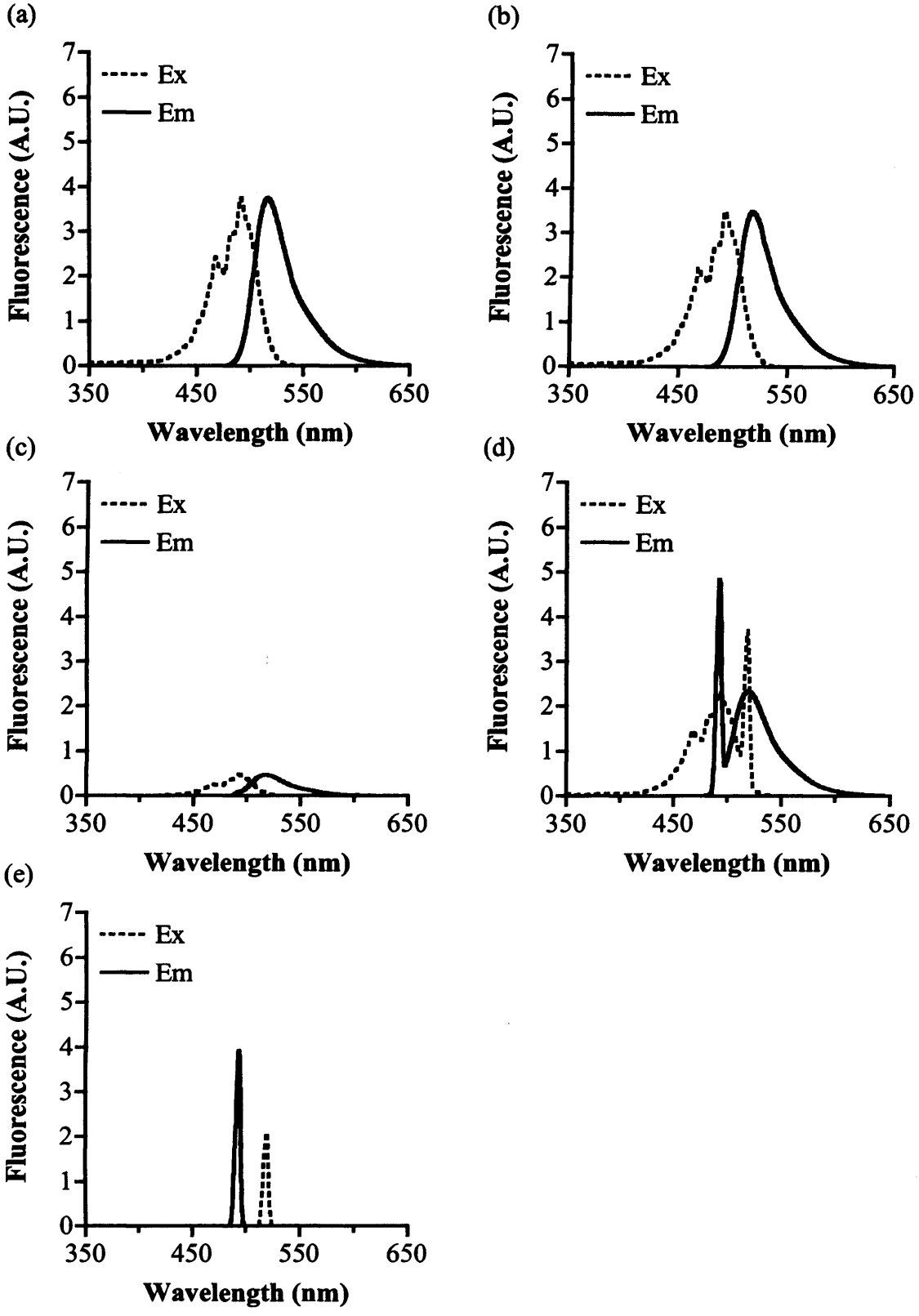

Figure 6.7 Characterisation of OG fluorescence excitation and emission spectra (continued). Panels show (a) FosW$_C$-OG, (b) mPEG-FosW$_C$-OG, (c) FosW$_C$-OG : Tfx™-50, (d) mPEG-FosWc-OG : Tfx™-50, (e) Tfx™-50. All samples were prepared at equi-molar concentrations of OG (1.5 μg mL^{-1}) in PBS, pH 7.4.

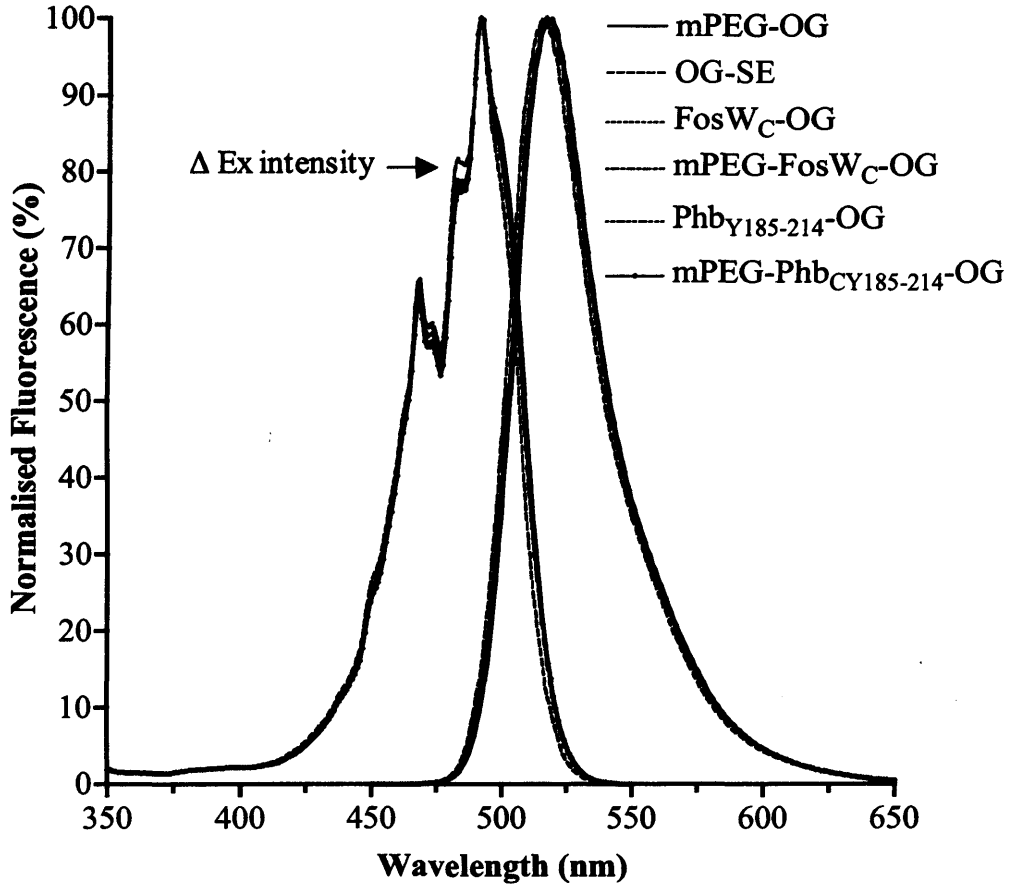

Figure 6.8 Overlay of the normalised fluorescence excitation and emission spectra of OGSE488-X and OG-labelled peptides and mPEG-conjugates. All samples were prepared at equi-molar concentrations of OG (1.5 μg mL^{-1}) in PBS, pH 7.4.

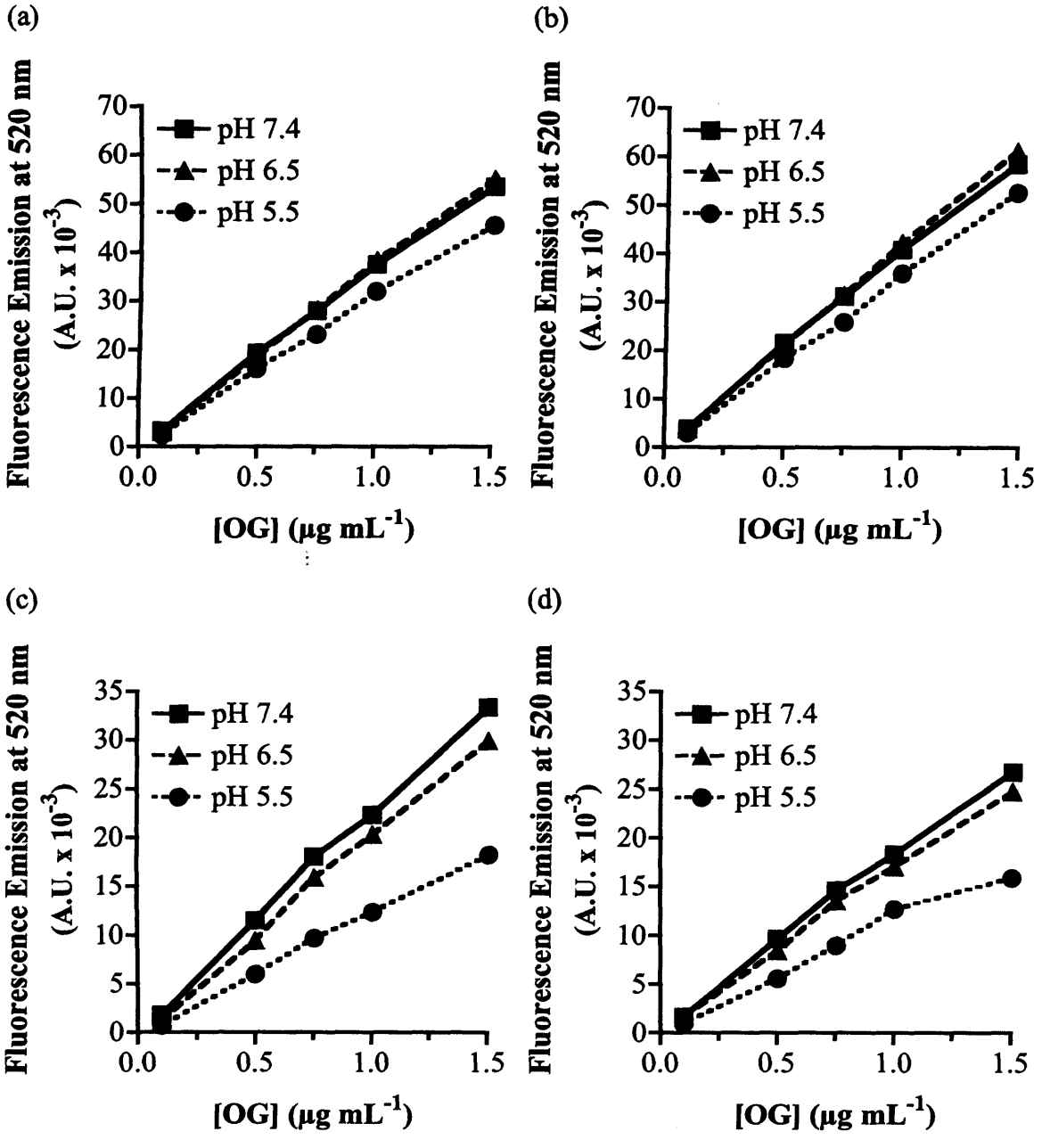

Figure 6.9 Determination of the pH sensitivity of OG fluorescence emission before and after conjugation. Panels show (a) OGSE488-X, (b) mPEG-OG, (c) $Phb_{Y185-214}$-OG and (d) mPEG- $Phb_{CY185-214}$-OG.

pH Sensitivity of OGSE488-X and OG-Labelled Peptides, Conjugates and Tfx-50 Complexes

Further characterisation at pH 7.4, 6.5 and 5.5 demonstrated the different degrees of fluorescence quenching seen for each of the OG-labelled compounds compared with free OGSE488-X. No change in fluorescence emission intensity was observed for OGSE488-X between pH 7.4 and 6.5 (**Figure 6.9a**). However a 15 % reduction was observed at pH 5.5 between OGSE488-X concentrations of 0.5 – 1.5 μg mL^{-1}. A similar pattern was observed for mPEG-OG (**Figure 6.9b**). Greater pH sensitivity was observed for $Phb_{Y185-214}$-OG, with a 10 % decrease at pH 6.5 and a 45 % decrease at ph 5.5 in the same concentration range (**Figure 6.9c**). For mPEG-$Phb_{Y185-214}$-OG the quenching was less at pH 6.5 (8 %), however at pH 5.5 ranged between 30 % at 1.0 μg mL (OGSE488-X) and 40 % at 1.5 μg mL (OGSE488-X) (**Figure 6.9d**); this was suggestive of a non-linear relationship between fluorescence emission and OGSE488-X concentration at pH 5.5. All other data had suggested a linear relationship in the ranges measured.

In subsequent experiments with $FosW_C$-OG, mPEG-$FosW_C$-OG and their respective Tfx™-50 complexes, similar patterns of pH dependent fluorescence quenching were observed (**Figure 6.10**). The decreased fluorescence at pH 6.5 for $FosW_C$-OG was approximately 14 %, while a 45 % decrease was observed at pH 5.5 (**Figure 6.10a**). Little pH sensitivity was observed for the $FosW_C$-OG : Tfx™-50 complex, however this may be due to the very low output for all measurements (**Figure 6.10b**). The trend for mPEG-$FosW_C$-OG was very similar to mPEG-$Phb_{Y185-214}$-OG with a 5 % decrease at pH 6.5 and a greater, 37 % decrease at pH 5.5 though the relationship between fluorescence output and OGSE488-X concentration was linear at all three pH values (**Figure 6.10c**). The mPEG-$FosW_C$-OG : Tfx™-50 complex showed no pH quenching up to an OG concentration of 0.75 μg mL^{-1} (**Figure 6.10d**). Between 0.75 and 1.5 μg mL^{-1} no quenching was observed between pH 7.4 and 6.5, however a 23 % decrease was observed at pH 5.5.

6.3.2 Cellular Uptake of OG-Labelled Conjugates

Cellular Uptake of $Phb_{Y185-214}$-OG and mPEG-$Phb_{CY185-214}$-OG

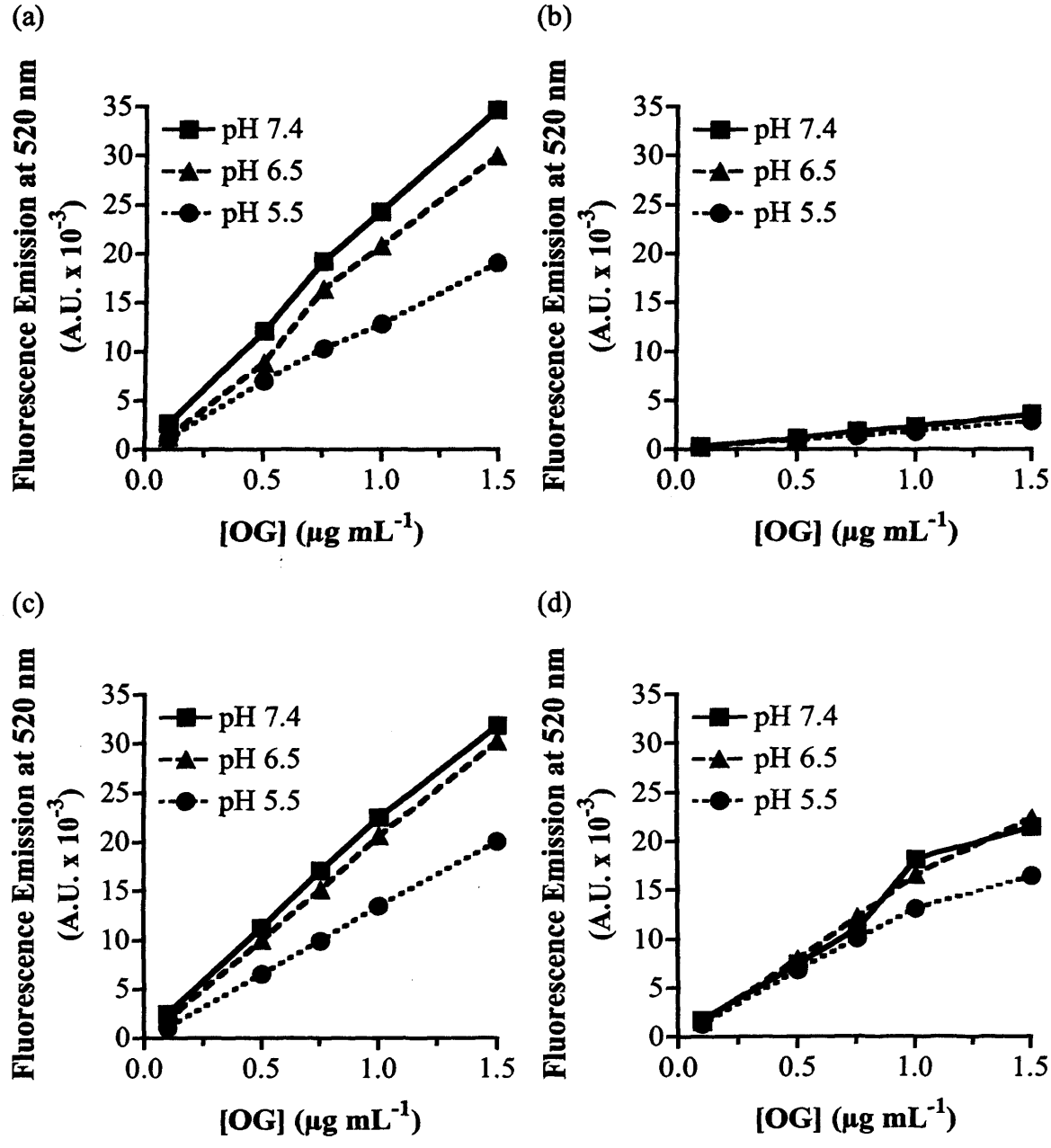

Figure 6.10 Determination of the pH sensitivity of OG fluorescence emission (continued). Panels show (a) FosW$_C$-OG, (b) FosW$_C$-OG : Tfx™-50 complex (c) mPEG-FosW$_C$, (d) mPEG-FosW$_C$: Tfx™-50 complex.

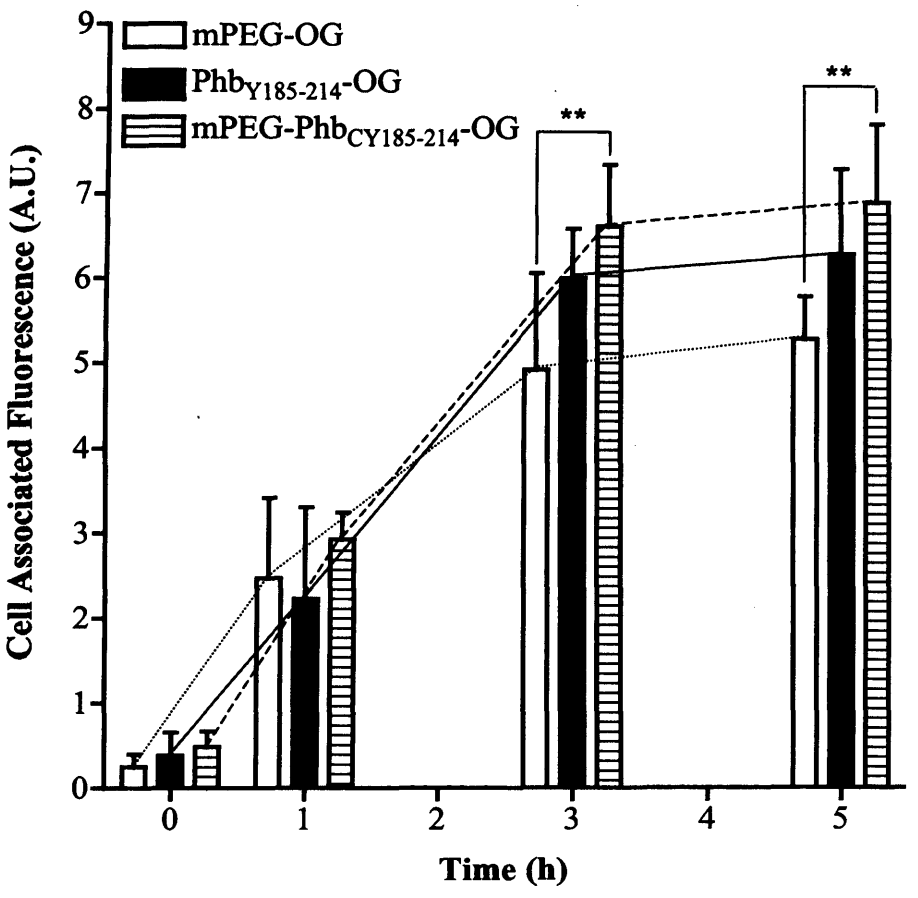

Figure 6.11 Uptake of $Phb_{Y185-214}$-OG and mPEG-$Phb_{Y185-214}$-OG relative to mPEG-OG at 37 °C in MCF-7 cells over 5 h. Data represent the mean (n=6) ± SD obtained from two separate experiments. Statistical analysis represents a two-way ANOVA, ** = $p < 0.01$, all others were n.s.

Cell-associated fluorescence increased almost linearly from 0 to 3 h for each of the three compounds (**Figure 6.11**). No statistically significant ($p > 0.05$) difference was observed between $Phb_{Y185-214}$-OG, mPEG-$Phb_{CY185-214}$-OG or the control mPEG-OG at 1 h, however, at 3 h the uptake of mPEG-$Phb_{CY185-214}$-OG was significantly ($p < 0.01$) greater than that of the mPEG-OG control. This suggested that the coiled-coil peptide motif was responsible for increasing the cellular uptake/binding to the cell membrane. Between 3 and 5 h the rate of uptake had reached a plateau suggesting a state of equilibrium had been reached between cellular uptake and exocytosis. At 5 h, the uptake of mPEG-$Phb_{CY185-214}$-OG remained significantly ($p < 0.01$) greater than that of the mPEG-OG control however, no statistically significant ($p > 0.05$) difference was observed between $Phb_{Y185-214}$-OG and mPEG-$Phb_{CY185-214}$-OG. The stability of the OG-conjugates was determined by SEC (PD-10) at 5 h and in each instance the free OGSE488-X found to be < 10 % of the total fluorescence, compared with < 3 % prior to incubation indicating that a small amount of OGSE488-X had been cleaved.

Cellular Uptake of $FosW_C$ and mPEG-$FosW_C$ ± Tfx™-50

Statistically significant ($p < 0.001$) differences in cell-associated fluorescence were observed between $FosW_C$-OG/mPEG-$FosW_C$-OG and the Tfx™-50 complexed samples at t = 1 and 3 h (**Figure 6.12**). In each instance there was very little instantaneous binding between the probes and the cell membrane as judged by the fluorescence at 0 h. No statistically significant ($p > 0.05$) difference was seen for any of the OG-conjugates at t = 0 h, however the cell-associated fluorescence of the cells treated with Tfx™-50 alone was markedly greater than that of the untreated, control cells at 0 h. After an incubation time of 1 h this difference diminished.

At 1 h, there was a 25-fold increase in the cell-associated fluorescence of the cells treated with the Tfx™-50 complexes compared with either $FosW_C$-OG or mPEG-$FosW_C$-OG alone. Though no statistically significant ($p > 0.05$) difference was observed between the complexes $FosW_C$-OG : Tfx™-50 and mPEG-$FosW_C$-OG : Tfx™-50 at 1 h. After the 1 h "chase" phase (t = 2 h), a significant difference ($p < 0.001$) was observed for the two samples in respect of both magnitude and trend. The cell-associated fluorescence of $FosW_C$-OG : Tfx™-50 doubled at t = 2 h c.f. t = 1 h, while that for mPEG-$FosW_C$-OG : Tfx™-50 decreased by approximately 40 %. A similar trend was observed upon comparison of $FosW_C$-OG and mPEG-$FosW_C$-OG, though the

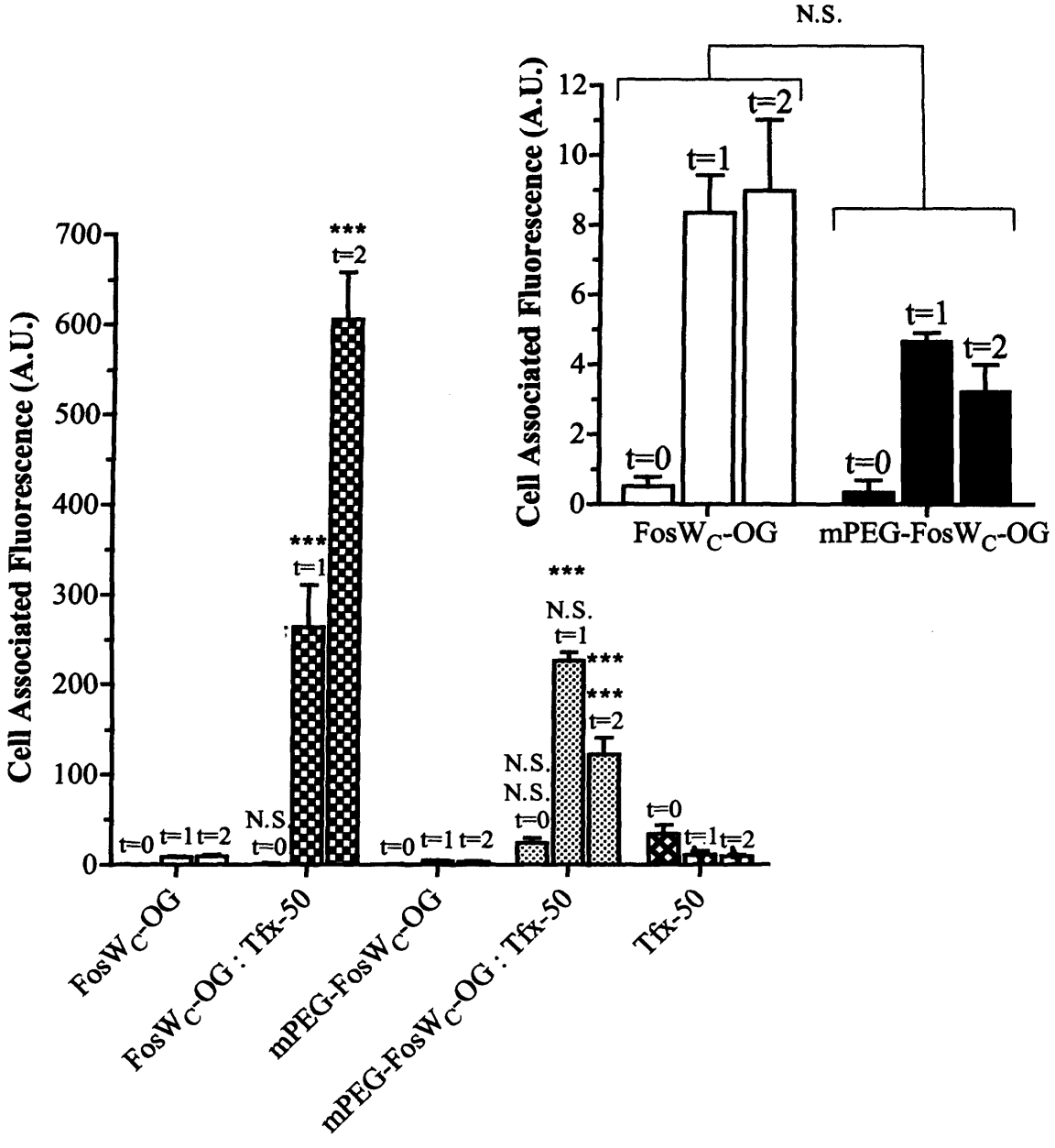

Figure 6.12 Uptake of FosW$_C$-OG, FosW$_C$-OG : Tfx™-50, mPEG-FosW$_C$ OG, mPEG-FosW$_C$-OG : Tfx™-50 and Tfx™-50 alone over the first 2 h of the transfection protocol. Data show cell associated fluorescence determined by flow cytometry and represents the mean (n=6) ± SD of two separate experiments. Inset shows the uptake of FosW$_C$ and mPEG- FosW$_C$ without Tfx™-50 on a magnified y-axis. Time (h) is shown above each bar. Statistical significance determined using a two-way ANOVA with Bonferroni post hoc test. N.S. represents no significant difference, ** = $p < 0.01$, *** = $p < 0.001$. Black shows difference ± Tfx-50, blue shows difference between FosW$_C$-OG : Tfx™-50 and mPEG-FosW$_C$-OG : Tfx™-50 complexes.

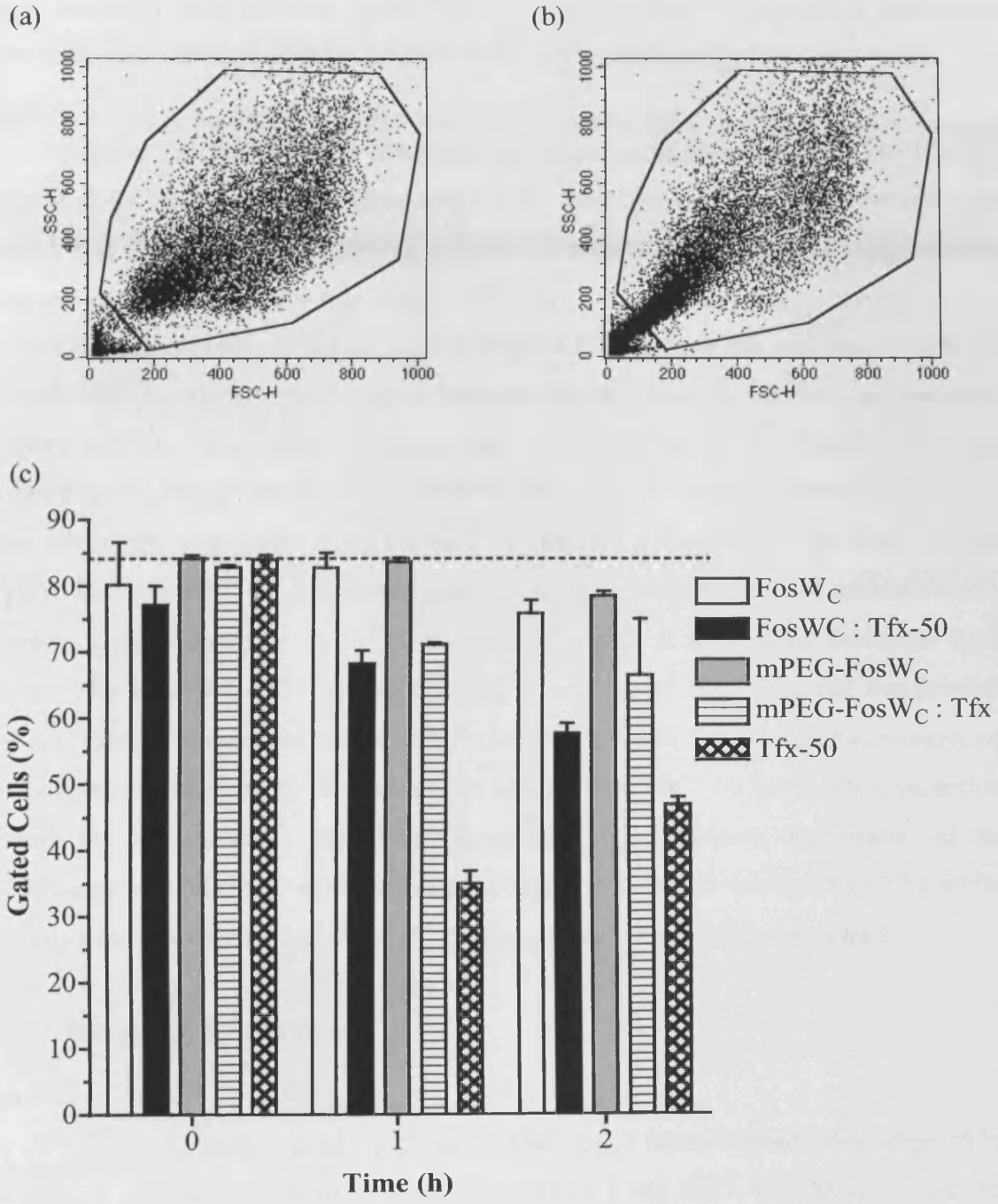

Figure 6.13 Change in acquisition pattern of cells and gated population during the course of flow cytometry analysis. Panels (a) and (b): Dot plots show change in acquisition pattern, data represent treatment with Tfx™-50 at 0 h and 1 h as examples. In panel (c) bars show number of cells in gate as a % of the total number of cells acquired. Data represent mean (n=6) ± SD. Dotted line indicates mean % gated cells in the untreated control.

magnitude of the difference was much reduced (**Figure 6.12 inset**). At 2 h the stability of the OG-conjugates was determined by SEC (PD-10) and in each instance the free OG found to be < 7 % of the total fluorescence, compared with < 1 % prior to incubation indicating that a small amount of OGSE488-X had been cleaved.

During analysis by flow cytometry the acquisition pattern in the dot-plot was monitored for each sample, in most cases there was little change. However the cells treated with Tfx™-50 alone exhibited a distinct change in morphology as judged by the decrease in the forward and side-scatter (FSC and SSC, respectively) measurements of the cell population (**Figure 6.13**). At 0 h (**Figure 6.13a**), the cells appeared indifferent to those treated with the other samples, however the change after 1 h was quite dramatic (**Figure 6.13b**). The flow cytometry data corroborated visual observations of a morphological change during Tfx™-50 treatment. The bar chart summarises the % of cells within the acquisition gate for each of the test compounds over time (**Figure 6.13c**). The non-Tfx™-50 complexed samples had no effect on the % of gated cells at 1 h, while a small decrease *circa* 10 % was noted after 2 h. Linear decreases were observed for each of the Tfx™-50 complexes. The effect of Tfx™-50 alone was greatest at 1 h with a 58 % decrease, while at 2 h recovery towards the original % commenced with a lesser decrease of 40 %. These data suggest that Tfx™-50 has a cytotoxic action towards the cells, possibly due to membrane damage. However, the "health" of the cells treated with Tfx™-50 alone appeared to improve after the wash phase (2 h), while the cells treated with either of the Tfx™-50 complexes continued to deteriorate.

6.3.3 Biological Assessment

Cytotoxicity of $Phb_{185-214}$, $Phb_{Y185-214}$ and mPEG-$Phb_{CY185-214}$

The first assay conducted with $Phb_{185-214}$ demonstrated dose-dependent cytotoxicity over a concentration range of 0.001 to 1 mg mL^{-1} with an IC_{50} value of approximately 0.8 mg mL^{-1} (**Figure 6.14a**). Statistically significant cytotoxicity c.f. mPEG-NH_2 was determined at 0.05 mg mL^{-1} ($p < 0.05$) and 0.1-1 mg mL^{-1} ($p < 0.001$). A repeat of this experiment failed to show any cytotoxicity up to 1 mg mL^{-1} (**Figure 6.14b**). A second repeat showed statistically significant cytotoxicity c.f. mPEG-NH_2 between 0.05 mg mL^{-1} ($p < 0.05$) 1 mg mL^{-1} ($p < 0.001$). At a $Phb_{185-214}$ concentration of 1 mg mL^{-1} cell growth was reduced by 34 % (**Figure 6.14c**).

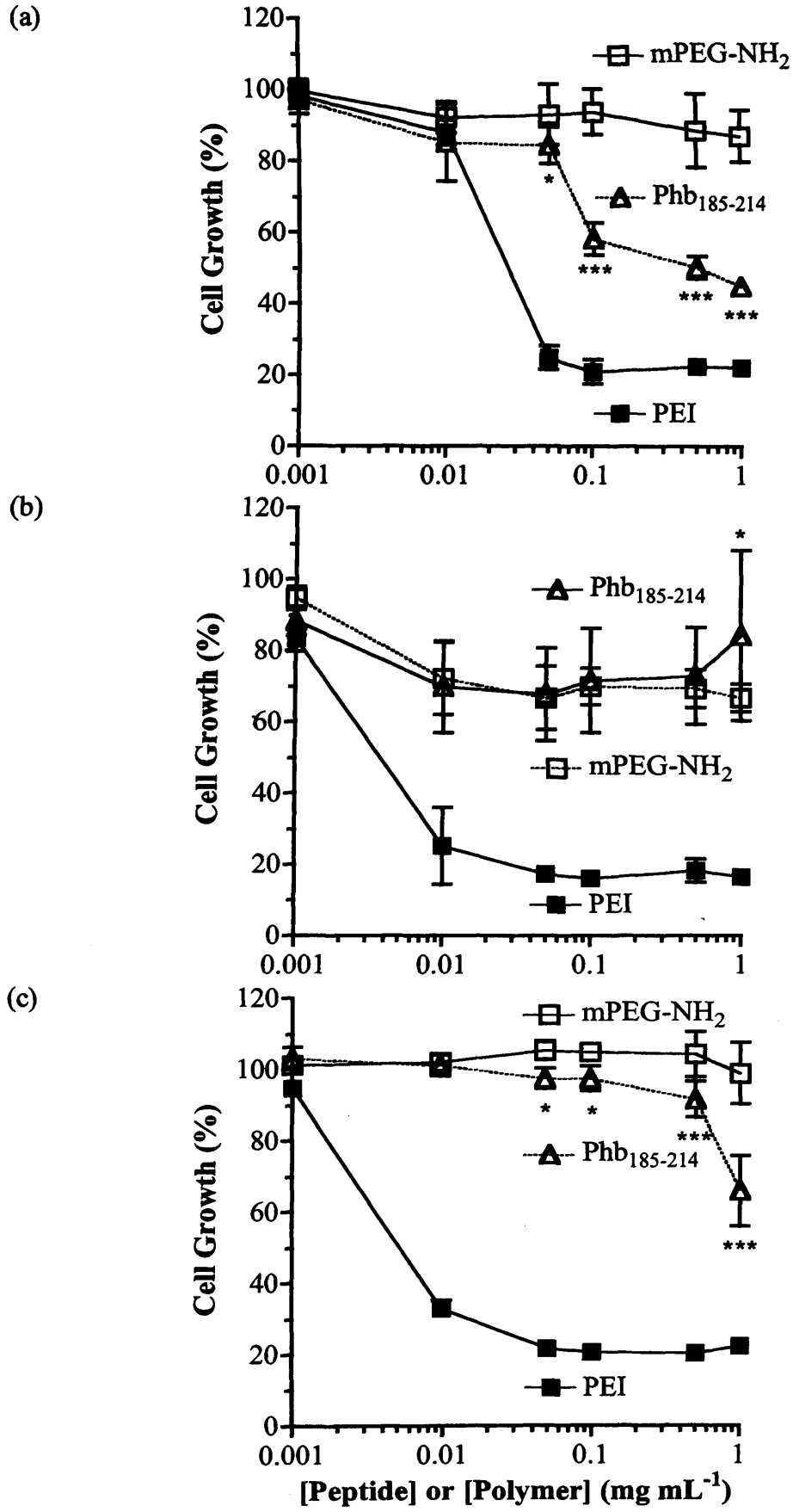

Figure 6.14 Cytotoxicity of Phb$_{Y185-214}$ and mPEG-Phb$_{CY185-214}$ relative to mPEG-NH$_2$ and PEI in MCF-7 cells, over 72 h. Each panel denotes a separate experiment, data represent cell viability as a % of untreated cells ± SD, n = 6. Statistical significance determined using a two-way ANOVA with Bonferroni post hoc test

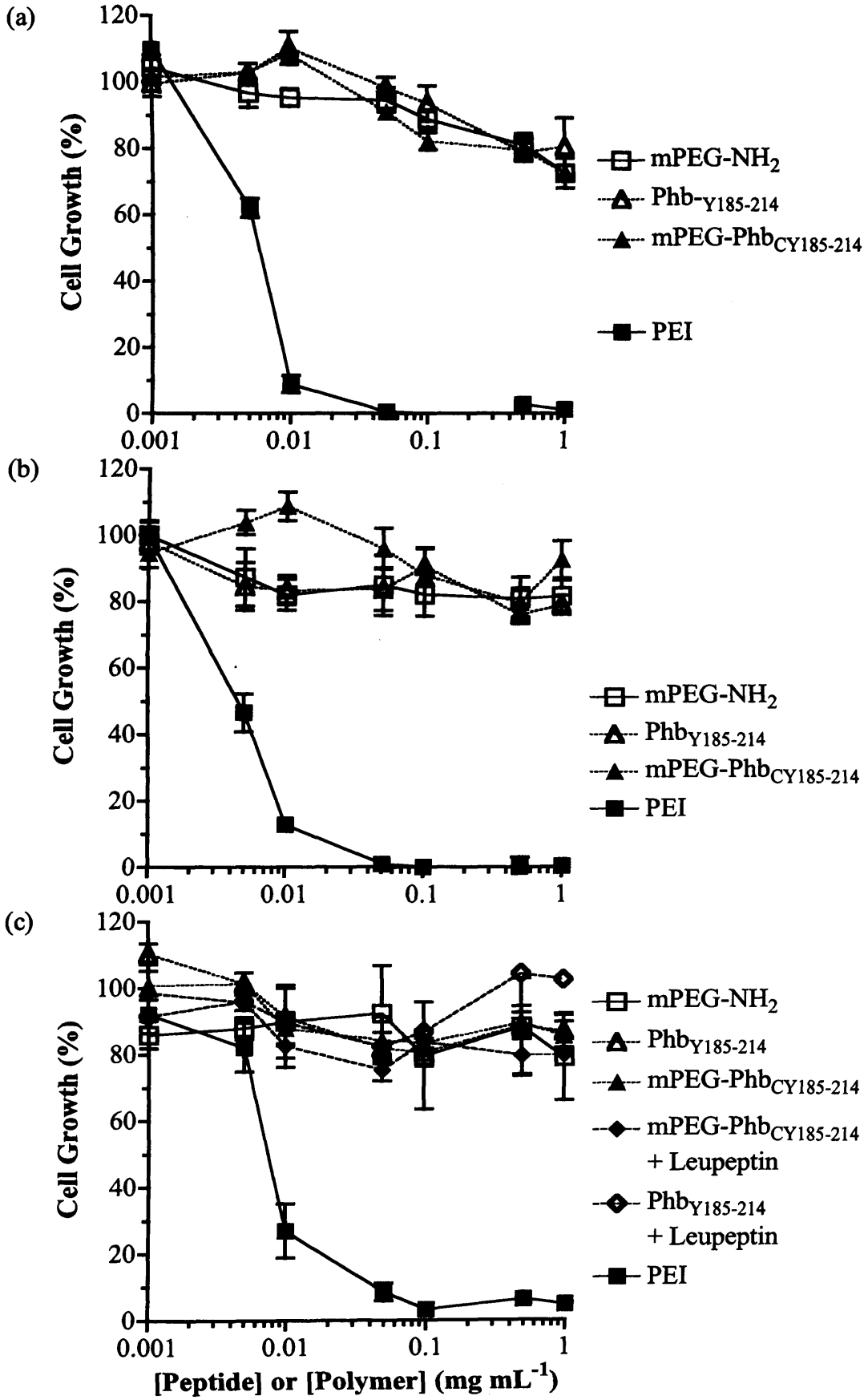

Figure 6.15 Cytotoxicity of Phb$_{Y185-214}$ and mPEG-Phb$_{CY185-214}$ relative to mPEG-NH$_2$ and PEI in MCF-7 cells over 72 h. Each panel denotes a separate experiment, data represent cell viability as a % of untreated cells ± SD, n = 6. No statistical significance determined (two-way ANOVA & Bonferroni post hoc test).

To investigate whether the differences observed in the three assays may have been the result of error in determining the peptide concentration, a further three assays were conducted using $Phb_{Y185-214}$, since concentration could be calculated by UV-spectroscopy using the tyrosine chromophore. In these experiments $Phb_{Y185-214}$ was found to be no more toxic than the mPEG-NH_2 negative control (**Figure 6.15a, b and c**). In parallel, the cytotoxicity of mPEG-$Phb_{CY185-214}$ was studied and in all three assays the conjugate was shown to be non-cytotoxic up to the maximum concentration used of 1 mg mL^{-1}. To determine whether the lack of cytotoxicity could be attributed to the proteolytic degradation of the peptides, in the third repeat of the assay $Phb_{Y185-214}$ and mPEG-$Phb_{CY185-214}$ were incubated in the presence of the protease inhibitor leupeptin (**Figure 6.15c**). No cytotoxic activity was observed up to the maximum concentration tested (1 mg mL^{-1}).

Cytotoxicity of $FosW_C$ and mPEG-$FosW_C$

No dose-dependent cytotoxicity was observed in two repeats of the MTT assay for either $FosW_C$ or mPEG-$FosW_C$ (**Figure 6.16 a and b**). However, in the second assay a statistically significant increase in toxicity relative to mPEG-NH_2 was determined at 1 mg mL^{-1} ($p < 0.001$) for both $FosW_C$ and mPEG-$FosW_C$. In the third assay, incubation with either $FosW_C$ or mPEG-$FosW_C$ reduced cell viability by approximately 15-20 % at concentrations of between 0.01 and 0.5 mg mL^{-1} compared with the negative control mPEG-NH_2 (**Figure 6.16c**). However, while these differences were determined to be statistically significant ($p < 0.001$) the absolute decrease in cell viability was modest.

Cytotoxicity of $FosW_C$ and mPEG-$FosW_C$ ± Tfx™-50

Initial experiments were conducted to determine the concentration at which the greatest divergence between $FosW_C$: Tfx™-50 and Tfx™-50 alone occurred. When $FosW_C$ was complexed with Tfx™-50 at a molar ratio of 1:1.25 divergent trends between the complex and the Tfx™-50 control were observed at peptide concentrations in the range of 0.01 and 10 μM with a statistically significant ($p < 0.01$) difference observed at the 10 μM concentration (**Figure 6.17a**). A repeat of this assay using a molar ratio of 1:1.2.5 showed again a significant ($p < 0.01$) difference between the cytotoxicity of the control and the complex at 10 μM (peptide concentration), though

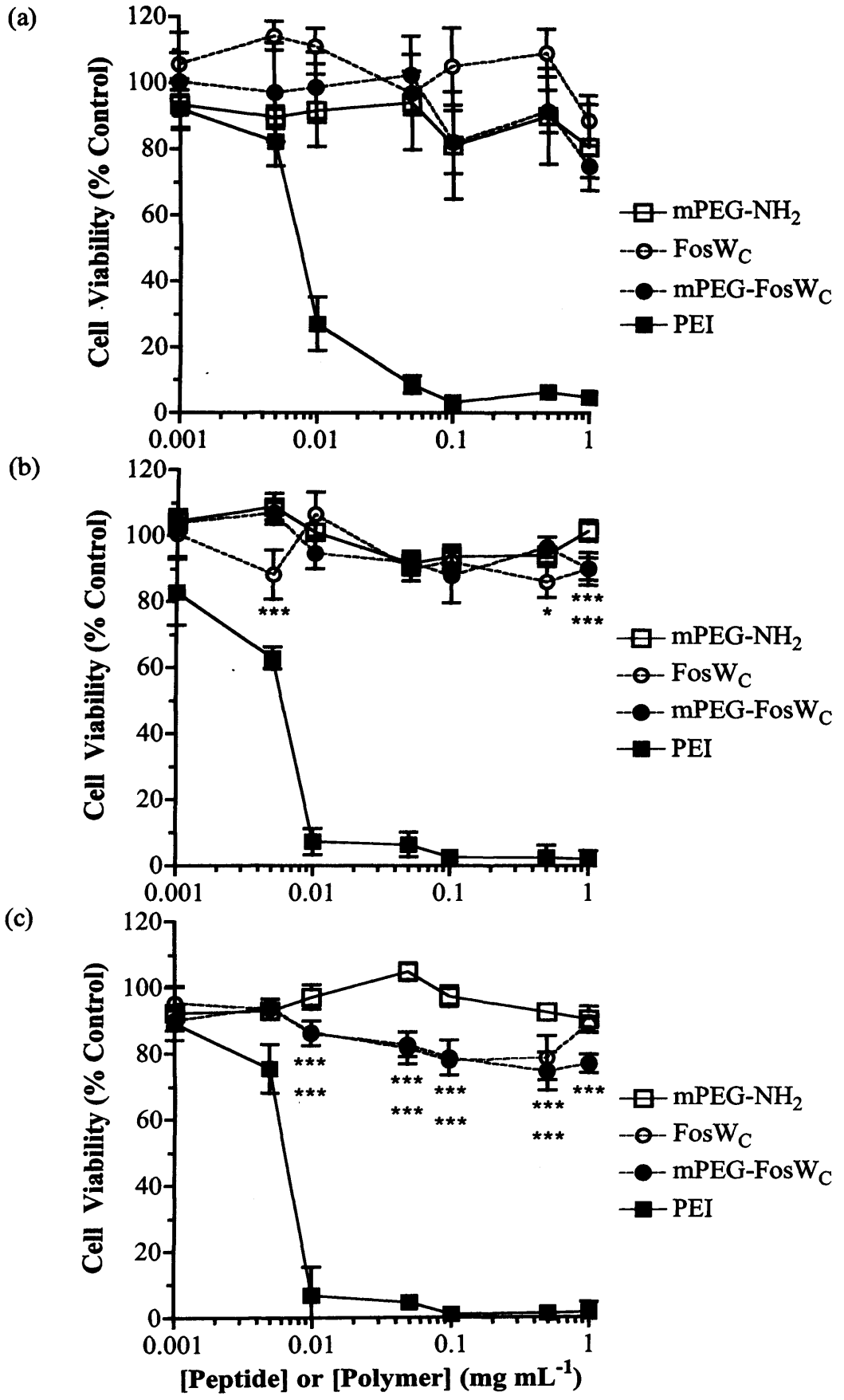

Figure 6.16 Cytotoxicity of FosW$_C$ and mPEG-FosW$_C$ relative to mPEG-NH$_2$ and PEI in MCF-7 cells over 72 h. Each panel denotes a separate experiment, data represent cell viability as a % of untreated cells ± SD, n = 6. Statistical significance determined using a two-way ANOVA with Bonferroni post hoc test.

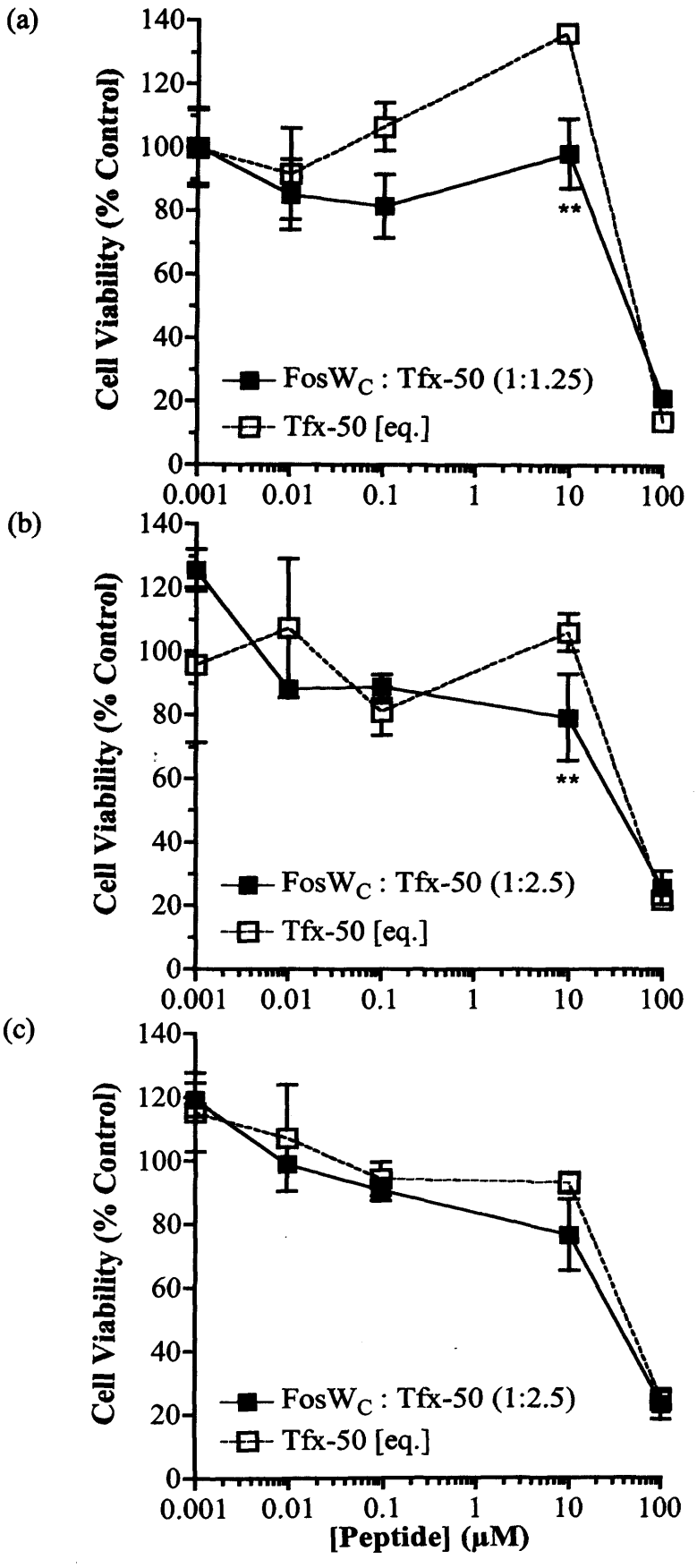

Figure 6.17 Determination of the optimal molar ratio of FosW$_C$: Tfx™-50 over 24 and 72 h in MCF-7 cells using the MTT assay. Panels show (a) 1:1.25 molar ratio, 72 h incubation, (b) 1:2.5 molar ratio, 72 h incubation, (c) 1:2.5, 24 h incubation. All data represent mean (n=3) ± SD. Statistical significance determined using a two-way ANOVA with Bonferroni post hoc test.

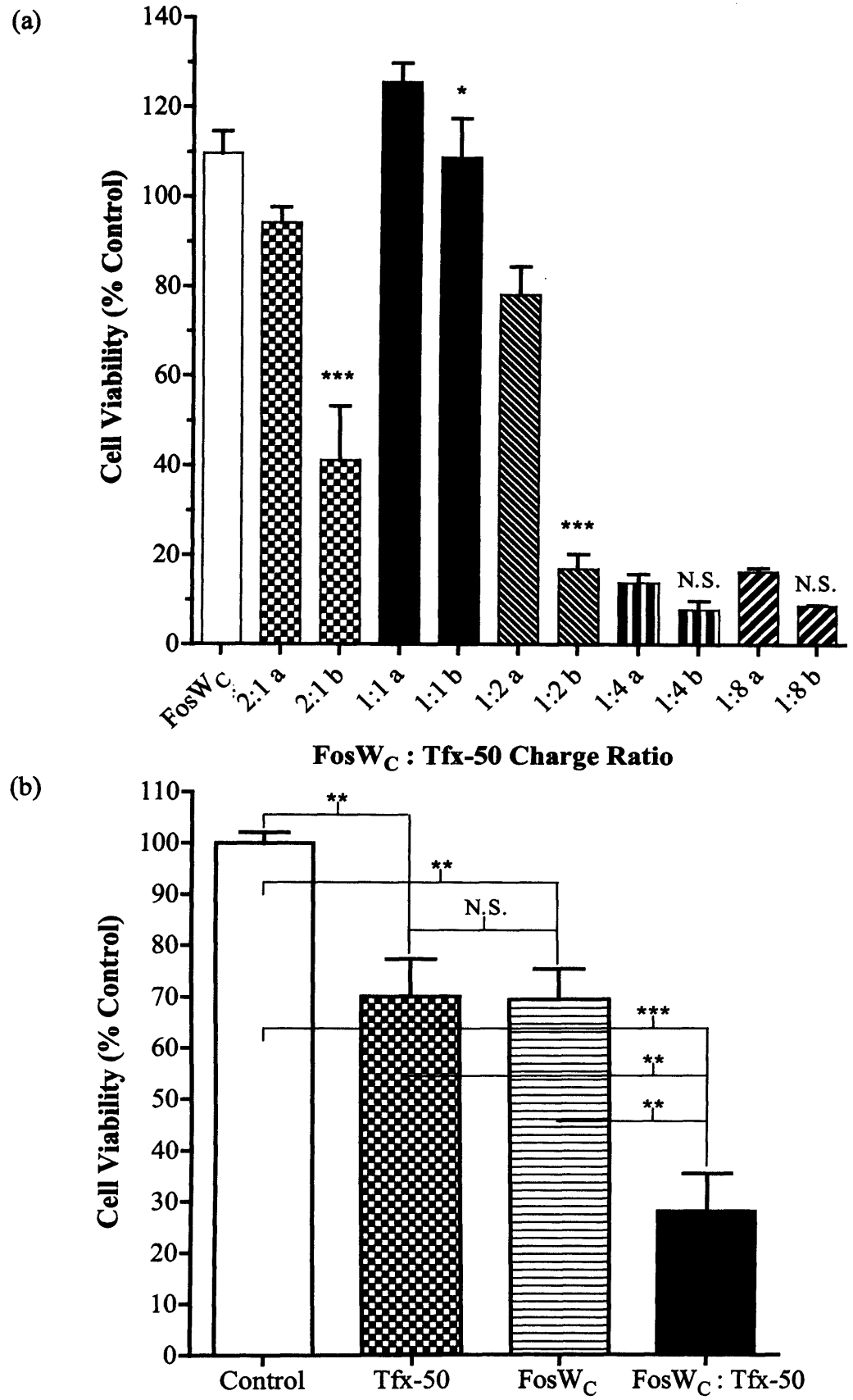

Figure 6.18 Effect of charge ratio on the cytotoxicity of the FosW$_C$: Tfx™-50 complex in MCF-7 cells using the MTT assay. In panel (a) the first column in each pair represents Tfx™-50 alone, and the second the complex. Panel (b) shows a repeat with the 2:1 charge ratio. Data represent mean (n=3) ± SD. Statistical significance determined using a one-way ANOVA with Bonferroni post hoc test.

not at lower concentrations (**Figure 6.17b**). The assay was repeated with a shorter incubation period (24 h, rather than 72 h) using a molar ratio of 1:2.5 and a similar observation was made (**Figure 6.17b**).

The second study assessed the optimal charge ratio, in all instances the complex was found to be more cytotoxic than the Tfx™-50 control (**Figure 6.18a**). However, this difference was not statistically significant ($p > 0.05$) at charge ratios of 1:4 and 1:8 ($FosW_C$: Tfx™-50). The greatest difference (without toxicity from the equimolar Tfx™-50 control) was observed at a charge ratio of 2:1 ($FosW_C$: Tfx™-50) as used in the previous study (**Figure 6.17**). However, the cytotoxic effect observed here was significantly greater ($p < 0.001$) as cell viability was reduced to 40 % of the untreated control compared with 80 % in the previous studies. A repeat of this experiment, using only the 2:1 charge ratio corroborated this result (**Figure 6.18b**). Further experiments conducted using Tfx™-50 complexes of $FosW_C$ and mPEG-$FosW_C$ demonstrated a similar trend (**Figure 6.19**). However, while statistically significant ($p < 0.001$) increases in cytotoxicity were observed between both $FosW_C$ ± Tfx™-50 and mPEG-$FosW_C$ ± Tfx™-50 no statistically significant ($p > 0.05$) reduction in cell viability was determined when a comparison was made between either $FosW_C$: Tfx™-50 or mPEG-$FosW_C$: Tfx™-50 and the Tfx™-50 control.

RBC Lysis

PEI was found to be very haemolytic at concentrations above 0.001 mg mL^{-1} while no lysis was observed for mPEG-NH_2 at concentrations up to 1 mg mL^{-1} (**Figure 6.20a**). In subsequent experiments the peptides $FosW_C$, $Phb_{Y185-214}$ and conjugates mPEG-$Phb_{CY185-214}$, and mPEG-$FosW_C$ were found to be no more haemolytic than the negative control, mPEG-NH_2 up to the maximum concentrations tested (0.5 mg mL^{-1}) (**Figure 6.20b**).

6.4 Discussion

6.4.1 Challenges of Using Fluorescence to Investigate Cellular Uptake

Assessing cellular uptake can be investigated using either a direct approach i.e. monitoring of the molecule of interest or an indirect approach i.e. monitoring of a cellular response. The disadvantage of the latter is that failure to illicit the expected

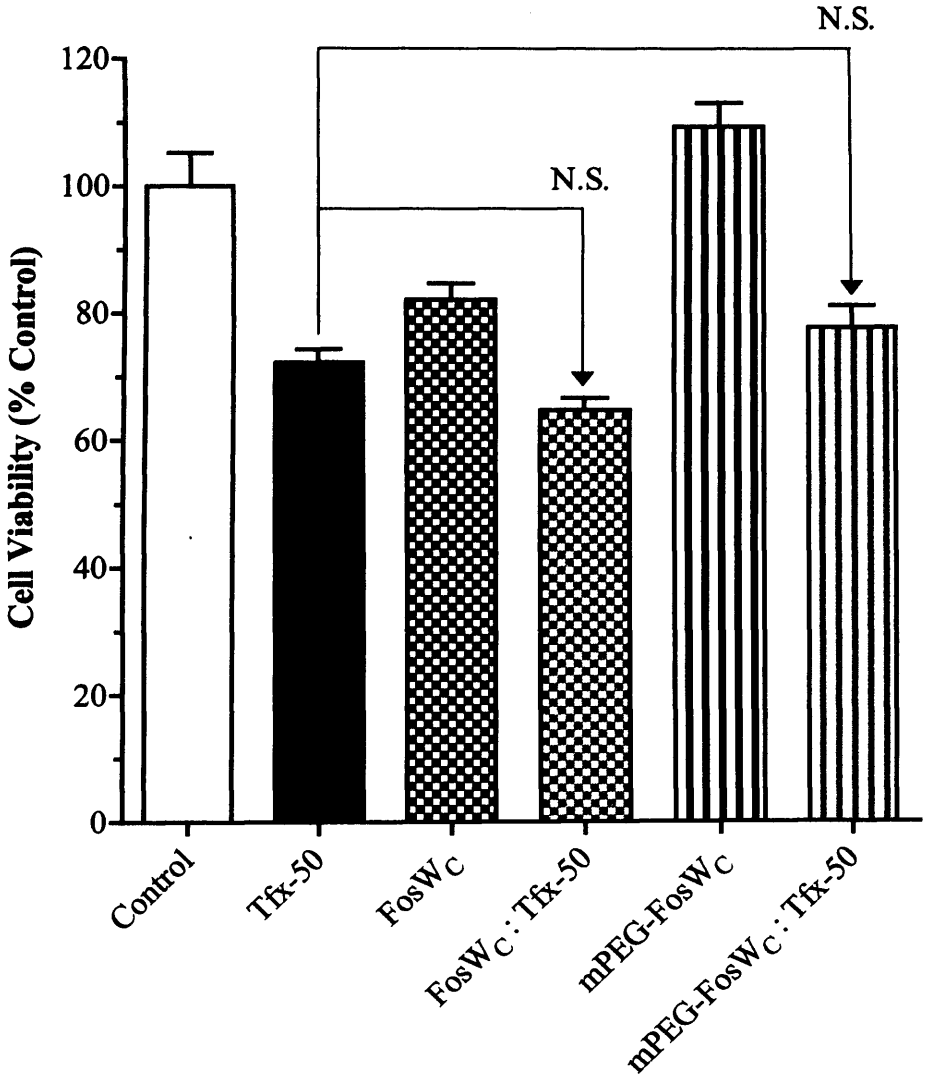

Figure 6.19 Cytotoxicity of $FosW_C$, $FosW_C$: Tfx™-50 complex, mPEG-$FosW_C$, and mPEG-$FosW_C$: Tfx™-50 complex in MCF-7 cells using the MTT assay. Charge ratio = 2:1 (peptide/conjugate : Tfx™-50). Data represent the mean of three experiments (n=18), error ± SD. No statistical significance determined using a two-way ANOVA with Bonferroni/Tukey post hoc test.

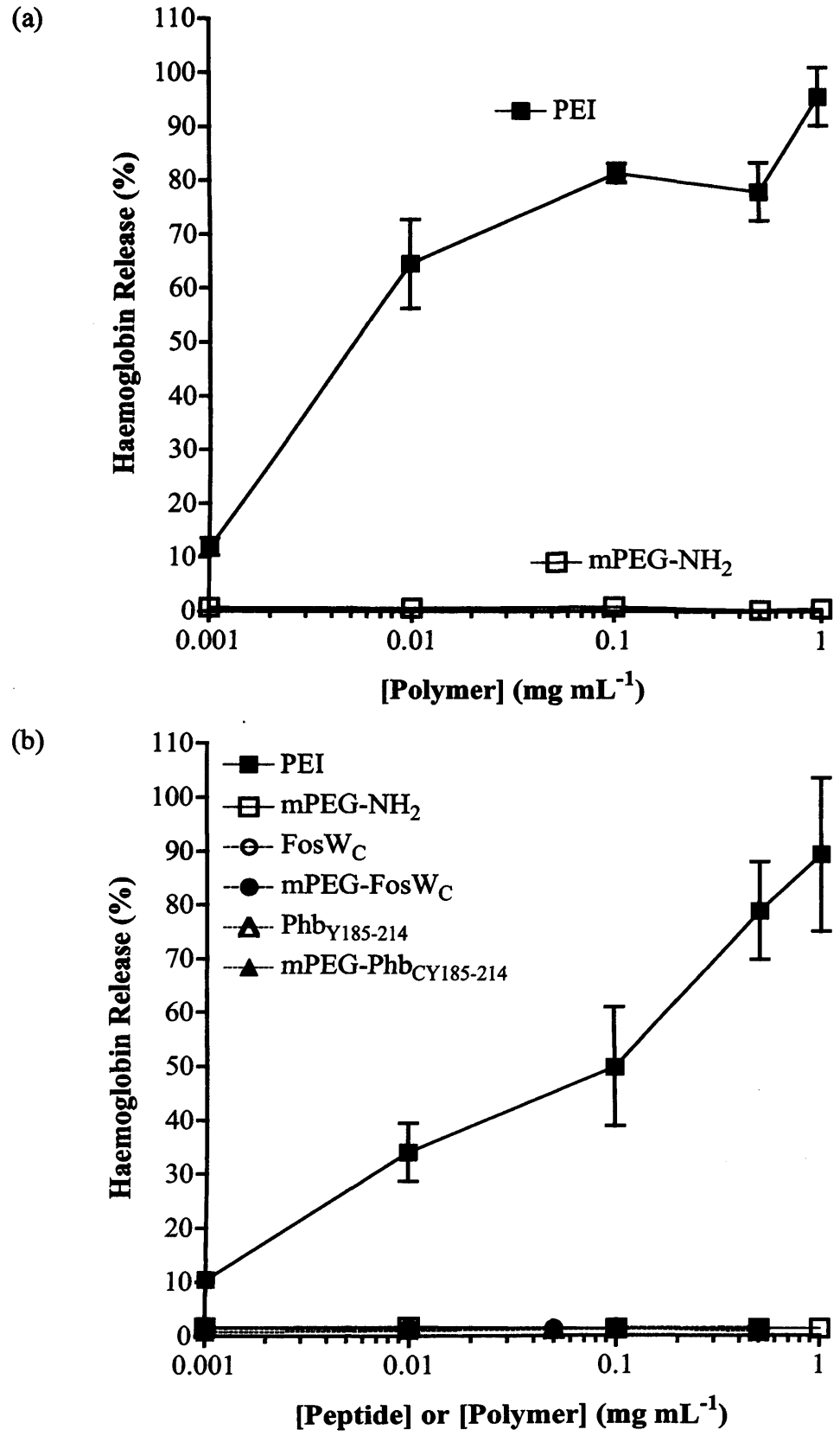

Figure 6.20 Haematotoxicity of the polymer controls, $Phb_{Y185-214}$ and $FosW_C$ peptides and mPEG-$Phb_{Y185-214}$ and mPEG-$FosW_C$ conjugates. Panel (a) shows haemoglobin release (%) post incubation (1 h) for the polymer controls and panel (b) shows test compounds relative to controls. Data shown represents the mean of three experiments (n = 15), error reported as ± SD.

response raises the question "did the molecule enter the cell and fail to show activity, or did it simply not enter".

Since it was not known for certain whether any of the coiled-coil motif peptides or mPEG-conjugates under investigation would successfully illicit the desired response i.e. downregulation of E2F1 or AP1 regulated transcription, a "direct approach" using fluorescence to assess cellular uptake was used in this study. As neither the coiled-coil peptide motifs, nor mPEG-coiled-coil motif conjugates possessed any inherent fluorescence it was necessary to label each compound with an appropriate fluorophore, as such, OGSE488-X was used.

It was possible to successfully synthesise OG-labelled coiled-coil motif peptides ($Phb_{Y185-214}$ and $FosW_C$) and mPEG-conjugates using succinimidyl ester chemistry so that the fluorophore was attached *via* an amine side-chain. Purification using either Sephadex® G-15 or G-25 SEC media yielded OG-conjugates with < 3 % free OGSE488-X. Previous studies have demonstrated a shift in the fluorescence emission spectra for fluorophores post-conjugation to peptides (Delmotte & Delmas, 1999). This was not seen with the OGSE488-X fluorophore used in this study and may be due to the $-(CH_2-)_5$ spacer positioning the molecule sufficiently far from the conjugated molecule to prevent a shift in the fluorescence emission spectrum (**Figure 6.21**). However, a small decrease (4 % cf. OGSE488-X) in the excitation spectrum at 483 nm was observed post-conjugation, in future studies this could be used as an analytical fingerprint to confirm that OGSE488-X has been successfully conjugated.

As macromolecules are usually excluded from entering cells *via* passive diffusion or direct translocation it was envisaged that cellular uptake would occur *via* endocytosis (discussed in Chapter 1, section 1.4). It was therefore important to investigate whether the emission fluorescence of the OGSE488-X fluorophore was sensitive to changes in pH. As a fluorinated analogue of fluorescein (**Figure 6.21**), OGSE488-X has a lower pK_a (4.7 cf. 6.4 of fluorescein), which should render the probe insensitive to changes in pH in the physiological range (http://www.invitrogen.com/site/us/en/home/References/Molecular-Probes-The-Handbook.html). However, in this study it was shown that the fluorescence characteristics of OGSE488-X changed following conjugation. Like many fluorophores, the fluorescence output of fluorescein derivatives have been shown to be quenched by proteins, it has been speculated that this is due to charge-transfer interactions with aromatic amino-acids (http://www.invitrogen.com/site/

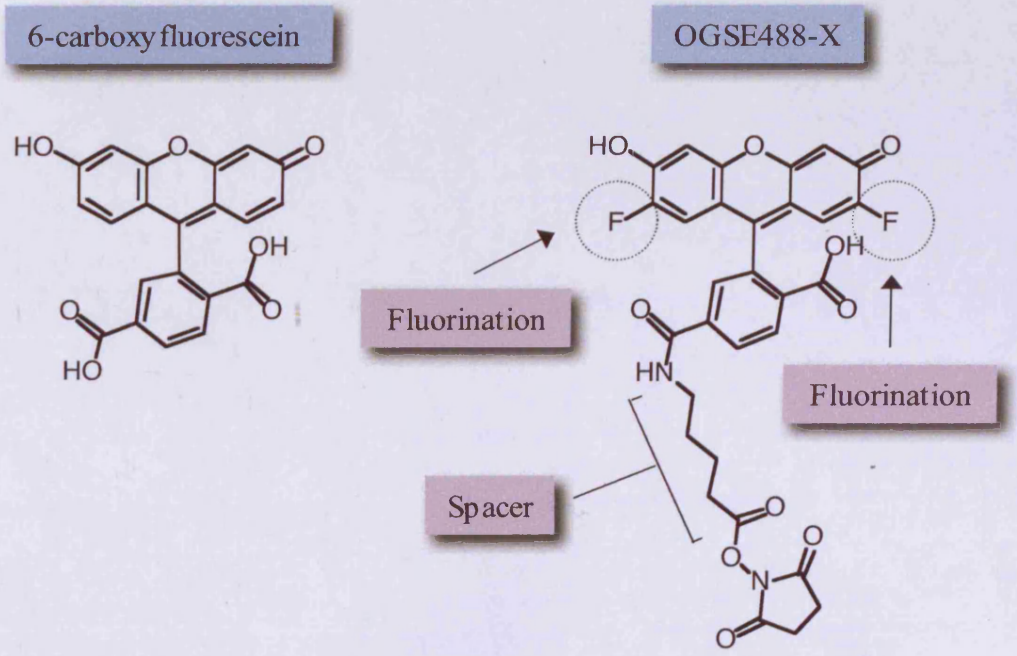

Figure 6.21 Structures of 6-carboxyfluorescein and OGSE488-X.

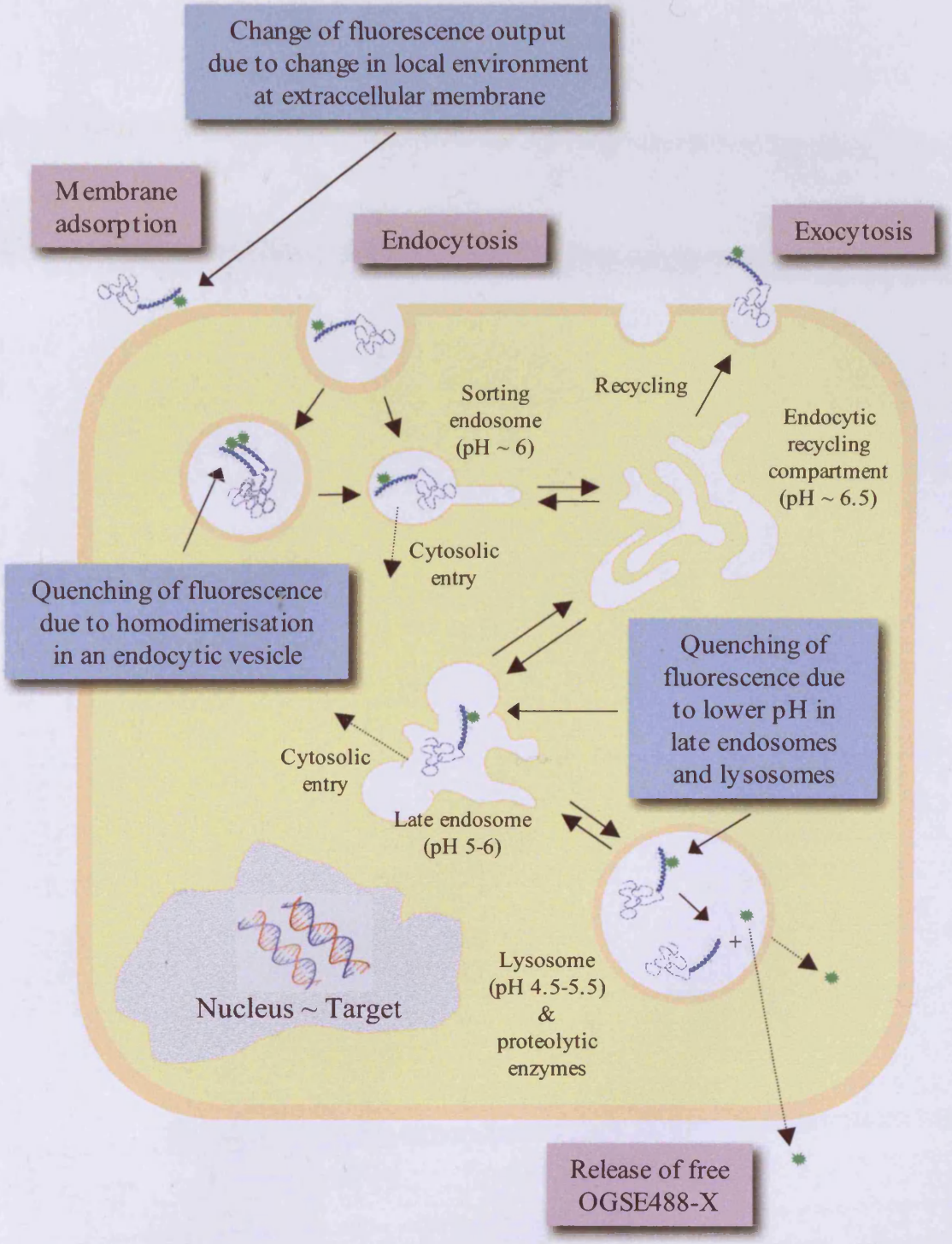

Figure 6.22 Possible cellular fates of OG-conjugates and the challenges faced with the use of fluorescence probes.

us/en/home/References/Molecular-Probes-The-Handbook.html). Both peptides $Phb_{Y185-214}$ and $FosW_C$ have arginine/lysine residues in close proximity to the aromatic tyrosine tags (**Figure 6.2**) therefore, this could offer an explanation for the observed quenching which was not seen following conjugation to mPEG-NH_2. An alternative explanation may be that at low pH (5.5-6.5) $Phb_{Y185-214}$ and $FosW_C$ may homodimerise resulting in the positioning of OGSE488-X molecules in close proximity and thus lead to self-quenching (Chen & Knutson, 1988) (**Figure 6.22**). Such speculation can be supported by previous studies whereby the fluorescence of the drug doxorubicin has been shown to be self-quenched when conjugated to the polymer HPMA at high concentrations (Greco *et al*, 2007). Unfortunately, the homodimerisation at low pH (5.5-6.5) of either peptide, or either mPEG-conjugate was not investigated in Chapter 5. Further studies with CD or NMR spectroscopy could offer clarification.

The most dramatic quenching of OGSE488-X emission fluorescence was seen following complexation of $FosW_C$-OG with Tfx™-50. While quenching was seen for the mPEG-$FosW_C$-OG : Tfx™-50 complex it was of a much lesser magnitude suggesting that the OGSE488-X molecules were positioned in a rather different local environment. As discussed earlier (section 6.1.4) Tfx™-50 is a cationic lipid and therefore could create a hydrophobic environment around the OGSE488-X fluorophore. Previous studies have shown that hydrophobic solvents or micellar environments may increase the emission fluorescence output of a similar OG derivative (Delmotte & Delmas, 1999), however, the opposite effect was seen here. Furthermore, in view of the different spectral shapes observed for the $FosW_C$-OG : Tfx™-50 and mPEG-$FosW_C$-OG : Tfx™-50 complexes (**Figure 6.7**) i.e. the presence of spikes for the latter it is likely that the 3D arrangement of the complexes is very different. Further analyses using light scattering techniques would be useful to investigate these differences further.

In light of the challenges posed by the differing fluorescence characteristics, in particular the sensitivity of OGSE488-X to environmental factors such as, pH, proximity/concentration and possibly solvent/complex polarity, extensive studies were not undertaken with flow cytometry. The flow cytometry experiments were standardised by using the same concentration of OGSE488-X (1.5 $\mu g\ mL^{-1}$) since absorption spectra and extinction coefficients are reported to be much less sensitive to changes in local environment compared with fluorescence characteristics (http://www.in

vitrogen.com/site/us/en/home/References/Molecular-Probes-The-Handbook.html). Whilst is was considered more important to standardise with respect to [OGSE488-X] it is worth noting that it was not possible to keep the concentrations of the peptides and conjugates exactly the same due to the small differences in specific activity of each OG-conjugate (see **Table 6.3**).

Preliminary studies with $Phb_{Y185-214}$-OG, mPEG-$Phb_{CY185-214}$-OG and mPEG-OG showed that the rates of uptake were similar. A statistically significant difference in the cell-associated fluorescence of mPEG-$Phb_{CY185-214}$-OG cf. mPEG-OG was seen at 3 and 5 h suggesting that the putative coiled-coil peptide motif ($Phb_{CY185-214}$) increased cellular uptake when conjugated to mPEG. Without conducting extensive studies including inhibiting mechanisms of endocytosis and actively removing membrane bound OG-conjugates (e.g. *via* acid washing) it is impossible to conclude with confidence whether the increased cell-associated fluorescence is indicative of increased uptake or simply binding to the extracellular membrane. The plateau in the cell-associated fluorescence for each of the OG-conjugates between 3 and 5 h is indicative of an equilibrium state between uptake/binding and exocytosis, quenching of OGSE488-X fluorescence and release of OGSE488-X following enzymatic degradation of the peptide or cleavage of the amide bond (**Figure 6.22**). The latter is unlikely within the time-course of the experiment due to the biological stability of the amide bond (Banks & Paquette, 1995), however, if either $Phb_{Y185-214}$-OG or mPEG-$Phb_{CY185-214}$-OG are trafficked to lysosomal compartments degradation of the putative coiled-coil peptide motif would be probable. Free OGSE488-X was < 10 % at 5 h, this equated to approximately a 3-fold increase suggesting that some $Phb_{Y185-214}$-OG/mPEG-$Phb_{CY185-214}$-OG was entering lysosomal compartments and being degraded.

Flow cytometry studies with $FosW_C$-OG and mPEG-$FosW_C$-OG ± Tfx™-50 showed clearly that complexation with Tfx™-50 dramatically increased cell-associated fluorescence. Whether this was due to increased binding of $FosW_C$-OG or mPEG-$FosW_C$-OG to the extracellular membrane or endocytosis cannot be concluded from this experiment. Only small increases in the amount of free OGSE488-X (< 10 % at 2 h) were observed suggesting that some $FosW_C$-OG and mPEG-$FosW_C$-OG was entering lysosomal compartments and being degraded rather than staying on the extracellular membrane (**Figure 6.22**).

The most interesting observations in this experiment were the differences in the cell-associated fluorescence at 2 h between the $FosW_C$-OG and mPEG-$FosW_C$-OG Tfx™-50 complexes. In the case of the $FosW_C$-OG : Tfx™-50 complex, cell-associated fluorescence doubled 1 h after the wash, since no more $FosW_C$-OG could have been taken up by the cell from the extracellular media increased fluorescence could only arise from $FosW_C$-OG escaping the $FosW_C$-OG : Tfx™-50 complex. This data suggests that at the second time-point $FosW_C$-OG is being effectively delivered, however it is not known whether it is liberated inside an endocytic vesicle or into the cystosol. A decrease in the cell-associated fluorescence at the same time-point for the mPEG-$FosW_C$-OG : Tfx™-50 complex suggests that OGSE488-X is either being quenched as a result of localisation in late-endocytic or lysosomal vesicles or that mPEG-$FosW_C$-OG is being exocytosed.

To answer the many questions arising from these initial studies would require the focus of a whole new Ph.D. thesis. This study has highlighted the many challenges of using fluorescence tagging to assess cellular uptake, in particular, the variable output of the fluorescent probe depending upon the local environment. Moreover, coupling of the hydrophobic OGSE488-X molecule may affect the structure of the coiled-coil peptide motif and/or intracellular trafficking, therefore future studies must utilise analytical approaches that do not introduce additional artefacts into the experimental design. Quantitative assessments should be conducted using radio-labelled peptides and conjugates with sub-cellular fraction methods to elucidate the intracellular localisation (Manunta *et al*, 2007; Seib *et al*, 2006). This approach should be combined with the recent advances in NMR spectroscopy to enable "in cell" target hybridisation studies to be conducted (Inomata *et al*, 2009; Sakakibara *et al*, 2009; Burz *et al*, 2006).

6.4.2 Assessing Biological Activity and the Challenges of Intracellular Delivery of mPEG-Coiled-Coil Motif Therapeutics

Targeting E2F1 Mediated Transcription with $Phb_{185-214}$, $Phb_{Y185-214}$ and mPEG-$Phb_{CY185-214}$

The design of the putative coiled-coil peptide motif $Phb_{185-214}$ was inspired by a study by Joshi *et al*, (2003) (discussed in Chapter 1, section 1.5 and Chapter 3, section 3.3.2.1). $Phb_{185-214}$ initially demonstrated dose-dependent cytotoxicity with an

estimated IC_{50} value of 0.8 mg mL^{-1} (238 μM). In the study by Joshi *et al*, (2003) the similar 41-residue peptide induced apoptosis in approximately 40 % of MCF-7 cells at a concentration of 15 μM. At an equivalent concentration (0.05 mg mL^{-1}), $Phb_{185-214}$ reduced cell growth by approximately 10 %. However, it was difficult to make direct comparisons since the TUNEL assay used by Joshi *et al*, (2003) measured % apoptotic cells, whereas the MTT assay used here assessed cell viability. Subsequent repeats of the MTT assay yielded inconsistent results with the first showing no cytotoxicity relative to mPEG-NH_2 and the second showing activity only at the highest concentrations tested. To determine whether the inconsistent data was due to variability in sample concentration further studies were conducted with $Phb_{Y185-214}$ and the mPEG-$Phb_{CY185-214}$ conjugate. Both failed to show any evidence of cytotoxicity. To see whether this could be attributed to proteolytic degradation of the putative coiled-coil motif samples were incubated with the protease inhibitor leupeptin. However, no cytotoxic activity was observed.

The study by Joshi *et al*, (2003) does not actually specify the sequence of the 41-residue peptide, rather it states that it was derived from the putative coiled-coil domain of the PHB protein. Therefore, it is difficult to make any comparison with regard to structure. It is possible that the extra 11-residues aided intracellular delivery of the peptide and hence explain the higher activity cf. $Phb_{185-214}$. A satisfactory explanation for the differences in cytotoxicity observed between $Phb_{185-214}$ and $Phb_{Y185-214}$ in this study remains elusive.

Targeting c-Jun Mediated Transcription with $FosW_C$ and mPEG-$FosW_C$

Initial studies with $FosW_C$ and mPEG-$FosW_C$ failed to show consistent, dose-dependent cytotoxicity over a 3-log concentration range (0.001 to 1 mg mL^{-1} ~ 0.23 to 230 μM) with only one experiment showing marginal cytotoxic activity for either $FosW_C$ or mPEG-$FosW_C$. Previous studies by Yao *et al*, (1998) with a number of c-Fos derived peptides had demonstrated similarly that the peptides were not active against MCF-7 cells unless used in conjunction with the transfection reagent Tfx™-50. As the study by Yao *et al*, (1998) did not show the toxicity of the Tfx™-50 reagent first studies here compared the cell viability of the $FosW_C$: Tfx™-50 complex with Tfx™-50 alone and found that the greatest difference was at a peptide concentration of 10 μM. In the study by Yao *et al*, (1998) the cytotoxic concentrations of the transfected peptides were in the same magnitude (6 to 48 μM). The optimal charge ratio was found to be the

Table 6.4 Comparison of c-Fos derived peptide sequences and charges.

Peptide	Sequence	No. of Residues (+ve)	No. of Residues (-ve)	Net Charge	Length (residues)	Net Charge (%)
c-Fos	**ELTDTLQAETDQLEDE**K**SALQTEIANLL**K**E**K**E**K**LEF**	4	11	-7	36	19
FosW$_C$	**CASLDELQAEIEQLEE**R**NYAL**RK**EIED**LQ**K**Q**LE**K**LGA**	5	10	-5	37	14
Fos-32	**TDTLQAETDQLEDE**K**SALQTEIANLL**K**E**K**E**K**L**	4	9	-5	32	16
Fos-N25	**TDTLQAETDQLEDE**K**SALQTEIANL**	1	7	-6	25	24
Fos-N18	**TDTLQAETDQLEDE**K**SAL**	1	6	-5	18	28
Fos-C25	**TDQLEDE**K**SALQTEIANLL**K**E**K**E**K**L**	4	7	-3	25	12
Fos-C18	K**SALQTEIANLL**K**E**K**E**K**L**	4	3	+1	18	6
Fos-15	**LQAETDQLEDE**K**SAL**	1	5	-4	15	27
Fos-14	**LQAETDQLEDE**K**SA**	1	5	-4	14	29

N.B. Positive residues are shown in bold font-type and negative residues are underlined.

same as that used in the study by Yao *et al*, (1998). This was perhaps unsurprising upon comparison of the relative net charge ratios of $FosW_C$ with the most active peptides Fos-32, Fos-15 and Fos-14 used by Yao *et al*, (1998) (**Table 6.4**).

A repeat of the initial experiment showed that the cell viability was reduced by 70 % following incubation with the $FosW_C$: Tfx™-50 complex, compared with a reduction of 30 % with either $FosW_C$ or Tfx™-50 alone. However, upon collation of three separate experiments no statistically significant difference was found between either the $FosW_C$: Tfx™-50 complex or mPEG-$FosW_C$: Tfx™-50 complex the Tfx™-50 control. As for the studies with the $Phb_{185-214}$ peptides and mPEG-conjugate a satisfactory explanation for the differences in the cytotoxicty observed between the assays in this study remains elusive.

General Considerations

Failure to achieve intracellular delivery of the coiled-coil peptide motifs and mPEG-coiled-coil motif conjugates is probably the reason for the low or non-existent cytotoxic activity shown in this study. In the second study the use of the transfection reagent Tfx™-50 failed to solve this issue satisfactorily. Furthermore, the toxicity of the reagent made it impossible to accurately discern whether the toxicity of the complexes was due to the effect of $FosW_C$/mPEG-$FosW_C$ or Tfx™-50 itself. Morphological changes in the appearance of the cells following incubation with Tfx™-50 or the $FosW_C$/mPEG-$FosW_C$: Tfx™-50 complexes was possibly suggestive of apoptosis, as such further investigations may benefit from use of the TUNEL assay as used by Joshi *et al*, (2003). However, to have real potential as novel polymer therapeutics it is essential that the compounds show activity without the use of tranfection reagents or artificial techniques such as microinjection or microporation. These techniques could be of use to see whether the compounds are active following intracellular delivery, however, re-design of the construct e.g. use of an endosomolytic polymer (Lavignac *et al*, 2004; Pattrick *et al*, 2001) would then be necessary to develop a therapeutic that could mediate its own delivery.

6.4.3 Conclusions

Fluorescence Studies

OG-labelled coiled-coil motif peptides ($Phb_{Y185-214}$ and $FosW_C$) and mPEG-conjugates were successfully synthesised using succinimidyl ester chemistry, and purified using either Sephadex® G-15 or G-25 SEC media to yield OG-conjugates with < 3 % free OG. A subtle, yet reproducible change in the OGSE488-X fluorescence emission spectrum was seen post-conjugation, which, in future studies could be used as an analytical fingerprint to confirm that OGSE488-X has been successfully conjugated.

Significant pH-dependent quenching of OGSE488-X emission fluorescence (up to 45 %), particularly post-conjugation to either coiled-coil peptide motifs or mPEG-coiled-coil motif conjugates was observed. Furthermore, complexation of Tfx™-50 with $FosW_C$ almost completely quenched OGSE488-X emission fluorescence at pH 7.4, 6.5 and 5.5. These observations demonstrated that fluorescence output was highly dependent upon the local environment and varied from one OG-conjugate to another, it was therefore not an ideal tool with which to assess cellular uptake. Future studies should be conducted using radiolabelled peptides/conjugates and cellular uptake assessed using a sub-cellular fractionation methodology.

Flow cytometry studies suggested that Tfx™-50 significantly increased the cellular uptake of both $FosW_C$-OG and mPEG-$FosW_C$-OG relative to peptide or mPEG-conjugate alone. In light of the earlier studies, which demonstrated the pH sensitivity of the fluorescence output, it is likely that the differences recorded are underestimates and the real values could be far greater than shown here.

Assessment of Biological Activity

None of the compounds tested were found to be haemolytic, however, the accurate assessment of cytotoxicity was impeded by significant assay-assay variability.

Preliminary investigations with $Phb_{185-214}$ showed evidence of dose-dependent cytotoxicity, however efforts to repeat these initial observations yielded inconsistent data. No dose-dependent cytotoxicity was observed for either $Phb_{Y185-214}$ or mPEG-$Phb_{CY185-214}$. In one study statistically significant cytotoxicity was measured for $FosW_C$ and mPEG-$FosW_C$ relative to mPEG-NH_2 however, this data was not reproducible.

Initial studies demonstrated increased cytotoxicity of $FosW_C$ when complexed with Tfx™-50 over Tfx™-50 alone. However, in further studies the Tfx™-50 reagent was found to be too toxic at the concentrations used to make it possible to accurately determine the effect of $FosW_C$ or mPEG-$FosW_C$ conjugate on cells.

CHAPTER 7

General Discussion

7.1 General Discussion

In recent years, the growing potential of nanomedicine has been widely acknowledged starting with the European Science Foundation report "Forward Look on Nanomedicine" (ESF, 2005) and latterly the US National Institute of Health's Nanomedicine Roadmap (http://nihroadmap.nih.gov/nanomedicine). In Europe, the ESF Summer Schools of 2007 and 2009 have promoted the exchange and development of ideas between researchers from backgrounds as diverse as chemistry, engineering, biology, pharmaceutics, medicine and ethics. This thesis is testament to the potential of highly successful, interdisciplinary collaborative research with studies conducted at Cardiff University (UK), EPFL (Switzerland) and CIPF (Spain).

Polymer therapeutics has been shown to be the most productive field of nanomedicine in terms of translating laboratory research into clinical products, with more than ten therapeutic agents in clinical use and many more in development (reviewed in Duncan, 2003; Duncan, 2006). PEGylation now over 30 years old has proven the most successful and popular approach and has been the subject of a number of excellent reviews (Davis, 2002; Harris & Chess, 2003; Parveen & Sahoo, 2006; Veronese & Harris, 2008; Pasut *et al*, 2008). While much progress has been made of late towards the use of biodegradable polymers in particular dextrin (Hreczuk-Hirst *et al*, 2001; Ferguson & Duncan, 2008; Hardwicke *et al*, 2008; Duncan *et al*, 2008), PEG is likely to remain at the forefront of clinically approved polymer therapeutics for a number of years yet. A paradigm shift towards the use of alternative (biodegradable) polymer materials is most likely to be realised in the advent of the development of polymer therapeutics for the treatment of chronic rather than acute diseases where repeated, possibly life-long injections are required.

Opening the Gateway for the Development of Coiled-Coil Motif Therapeutics

Increased understanding of the 3D structure of proteins and its role in the assembly of multi-protein complexes that regulate biological pathways has provided attractive new targets for drug development (reviewed in Dev, 2004). For example, the initial step of HIV-1 cellular entry involves binding of the trimeric viral envelope glycoprotein gp120/gp41 to cell surface receptor CD4 and its chemokine co-receptor CXCR4 or CCR5. This triggers conformational changes in the envelope proteins such

that gp120 dissociates from gp41, allowing fusion peptide insertion into the plasma membrane then cellular entry (Gallo *et al*, 2003). In the last decade we have observed the clinical approval of the first large (36-residue) peptide therapeutic (enfuvirtide/Fuzeon) designed for the treatment of HIV-1 by inhibiting this process as "association between the fusion inhibitor and gp41 prevents the successful completion of gp41 zipping" (Fletcher, 2003; Matthews *et al*, 2004). Although Fuzeon is acting at the C-terminus of the gp41 trimeric coiled-coil it has not been described as an inhibitor of coiled-coil formation. The requirement for large-scale (multi-tonne) production of Fuzeon, as a by-product has resulted in peptide synthesis reagent costs dropping dramatically, worldwide, thus markedly reducing reagent costs for laboratory scale synthesis. Today, Fmoc-SPPS has become a readily available tool for the preparation of peptides, used in thousands of laboratories from industry to academia. Moreover, recombinant technology has allowed design of coiled-coil based protein biomaterials, bioresponsive hybrid hydrogels and epitope displays (reviewed in Tang *et al*, 2001).

7.2 Summary of the Strategy of this Thesis and Key Results, Successes and Challenges

Polymer conjugates of coiled-coil peptides designed as molecular switches to modulate physiological protein heterodimerisation are particularly attractive as a new therapeutic strategy. Using an appropriately tailored polymer (in respect of molecular weight and physico-chemical nature depending on the sub-cellular location of its complementary molecular target), the polymer therapeutic approach has the potential to efficiently deliver the peptide to an extracellular, cell surface, endocytic or, more challengingly, an intracellular location (**Figure 1.7**).

Earlier studies used a novel LAEIEAK-based coiled-coil sequence to systematically study the effect alterations in peptide primary structure have on the self-assembly properties of PEG-*b*-peptide hybrid block copolymers and provided a platform for this Ph.D. thesis (**Figure 7.1**). Despite differences in peptide primary structure, all peptides and PEG-conjugates retained their ability to form coiled coils. However, CD spectroscopy and other techniques showed that self-organisation could be described as a two-state equilibrium between discrete monomers and dimeric coiled-coil aggregates. The key aim of this study was to develop an mPEG-coiled-coil motif

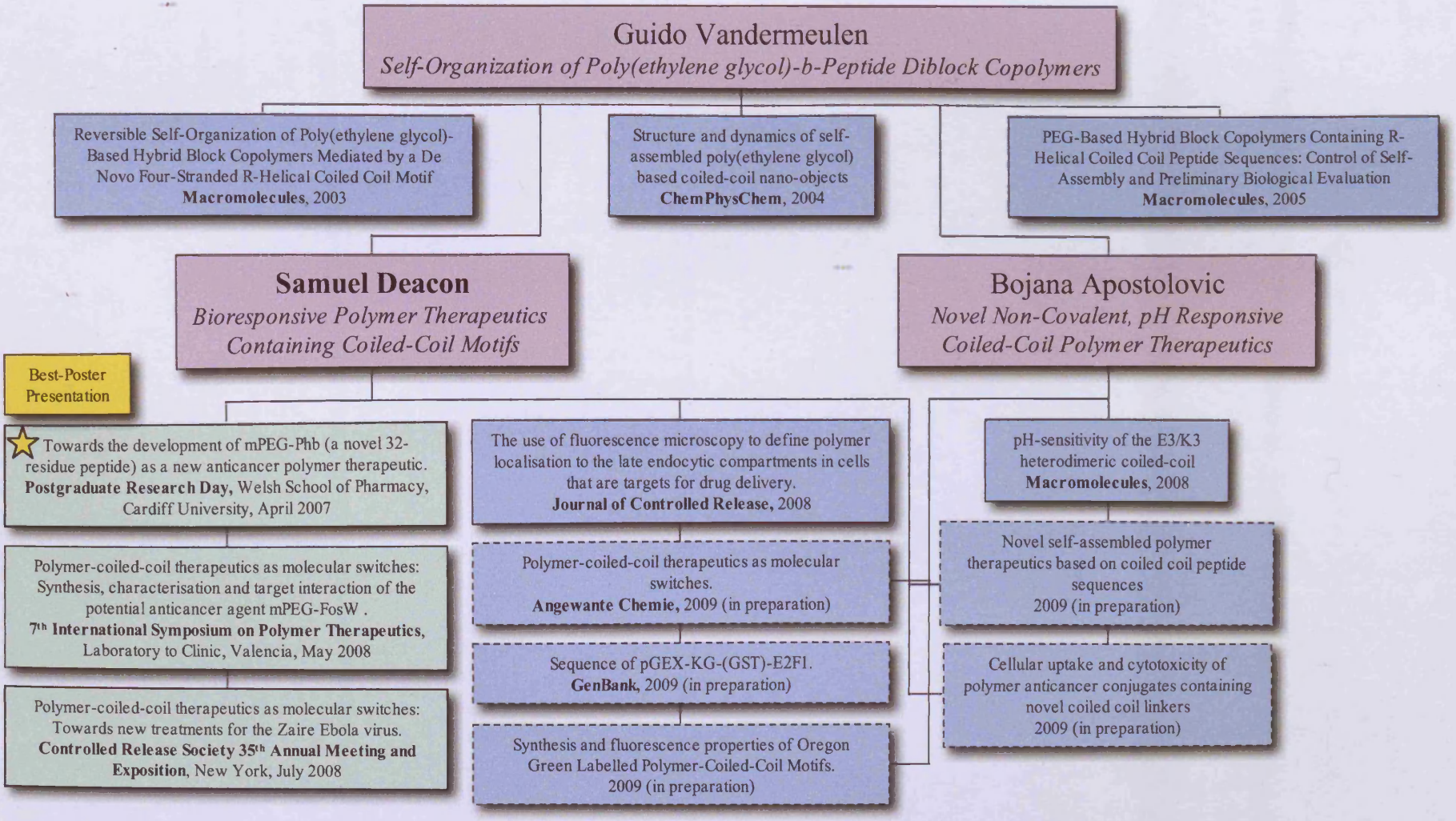

Figure 7.1 Schematic showing selected publications leading to and emanating from this Ph.D. thesis. Italic font type denotes thesis title, blue boxes show papers (dashed-lines denote papers that are in preparation) and green boxes show posters/presentations.

conjugate that would preferentially hybridise with its target whilst not forming macro-molecular homoligomeric aggregates.

Synthesis and Characterisation

The ability to design and successfully synthesise a range of putative coiled-coil peptides was demonstrated using Fmoc-SPPS in Chapter 3. This study also highlighted the large degree of variability seen with using computational software to predict the existence of a coiled-coil domain; this observation should serve as a caveat to the shortcomings of this approach. Unfortunately, not all of the peptides designed were easily solubilised. The most problematic were EbGP2 and EbVP35 derived coiled-coil motif peptides. Whilst the difficulties were overcome with EbGP2 and two peptides were synthesised it was not possible to prepare soluble EbVP35 derived peptides.

The solution phase thiol-directed method of PEGylation described in Chapter 4 was a very efficient and rapid yet simple approach, which yielded four site-specific mono-PEGylated conjugates designed to target the proteins E2F1, c-Jun and EbGP2. Ellman's assay provided a useful means of monitoring the progress of each reaction and ion-exchange chromatography, once optimised for each conjugate proved an excellent method of purification. In particular, because it enabled the removal of both unreacted mPEG-Mal and free coiled-coil motif peptide, separation of the former being something not oft reported for the synthesis of polymer therapeutics. Thus, the final samples were of very high purity and suitable for further study by NMR and CD spectroscopy to determine whether target hybridisation by coiled-coil formation would be achievable.

The challenge of characterising the purified mPEG-coiled-coil motif conjugates by MALDI-TOF MS was an aspect of this thesis that was not fully solved. The indisputable advantage of characterisation by MALDI-TOF MS was that it could not give a "false positive" result. Therefore, the existence of the peaks in the expected mass-range was conclusive proof that mono-PEGylated conjugates had been successfully synthesised. Coupled with the greater resolution and more rapid analysis that it afforded over SDS-PAGE or similar techniques, meant that a considerable amount of time was allocated to optimising the method of sample preparation. Using a minor modification to the optimised spotting protocol described by Meier and Schubert, (2003) it was possible to confirm the expected molecular weights of mPEG-EbGP2$_{609-630}$ and mPEG-FosW$_C$. However, the acquisition of spectra confirming the expected

molecular weights of the conjugates mPEG-$Phb_{CY185-214}$ and mPEG-$EbGP2_{CY566-589}$ was not achieved and thus demonstrates that further optimisation of the sample preparation method is required.

In Vitro Study of Target Hybridisation

Proof of concept was successfully demonstrated using the well-characterised coiled-coil driven heterodimerisation of the AP-1 transcription factor as a model target. These studies demonstrated for the first time that an mPEG-$FosW_C$ conjugate was able to heterodimerise with r-c-Jun in exactly the same manner as for $FosW_C$.

The [^{15}N]r-c-Jun peptide synthesised using a recombinant methodology adapted from Mitra *et al*, (2005) enabled a detailed study of the $FosW_C$/mPEG-$FosW_C$: c-Jun interaction by 2D ^{1}H, ^{15}N HSQC spectroscopy. At 37 °C the [^{15}N]r-c-Jun peptide alone had very little structure, but subsequent addition of an equimolar concentration of mPEG-$FosW_C$ induced structural changes consistent with an induced fit model of coiled-coil heterodimerisation. The spectral changes were equivalent to those seen when $FosW_C$ was added, so it can be concluded that site-specific conjugation of mPEG did not impair heterodimerisation. Furthermore, the observation that doubling the concentration of both $FosW_C$ and mPEG-$FosW_C$ (relative to the [^{15}N]r-c-Jun peptide) did not induce further spectral changes suggested that a stable heterodimer was fully formed at equimolar concentrations. This also underlined the preference for heterodimerisation rather than potential homodimerisation of $FosW_C$ or [^{15}N]r-c-Jun. Under the same conditions, further characterisation by CD spectroscopy corroborated the formation of a coiled-coil structure.

Lesser progress was made towards characterisation of the Phb : E2F1 interaction as it was not possible to express sufficient rhE2F1 to enable characterisation by CD/NMR spectroscopy. Nonetheless, it was possible to successfully characterise the plasmid encoding GST-rhE2F1 and determine the optimal *E.coli* strain and expression conditions. Further investigation and detailed charcterisation of the interaction would make a very exciting continuation of this thesis.

Biological Evaluation

In preliminary studies, the successful demonstration of reproducible biological activity in a cellular model was not realised for either of the anti-cancer mPEG-coiled-coil motif conjugates prepared. This was probably due to difficulties in achieving

intracellular delivery rather than inactivity of the coiled-coil motif. As shown in Chapter 6, initial observations of $Phb_{185-214}$ cytotoxic activity in the MCF-7 cell line were not routinely reproducible. A satisfactory explanation could not be found and subsequent experiments with the tyrosine tagged and PEGylated coiled-coil motif failed to show any activity.

In studies involving $FosW_C$/mPEG-$FosW_C$ initial experiments demonstrated increased cytotoxicity of $FosW_C$ when complexed with Tfx™-50 over Tfx™-50 alone. However, in further studies the Tfx™-50 reagent was found to be too toxic at the concentrations used to make it possible to accurately determine the effect of $FosW_C$ or mPEG-$FosW_C$ conjugate on cells. Further studies are warranted to elucidate accurately whether $FosW_C$/mPEG-$FosW_C$ or $Phb_{Y185-214}$/mPEG-$Phb_{CY185-214}$ are not active because they are not reaching their target proteins, c-Jun and E2F1, respectively

The challenges of using fluorescence to assess cellular uptake were amply demonstrated by the control studies in Chapter 6. Should further investigations be conducted, they would benefit greatly from using radiolabelled peptides/polymers and a quantitative approach such as sub-cellular fractionation.

7.3 Potential Applications of this Concept

An overview of the many projects that could emanate from this thesis are summarised in **Figure 7.2** while a selection are discussed at greater length below. The answer to the question "is there a future for coiled-coils as molecular switches?" is undoubtedly "yes". The most exciting opportunity for further research lies with the development of mPEG-coiled-coil motif conjugates as fusion inhibitors for the treatment of Ebola HF. The preliminary evaluation of biological activity could be conducted using the conjugates prepared in Chapter 4. However, these would require new collaborations to be established. The use of "live" Ebola virus requires class 4 biocontainment facilities and as such discussion should be sought with the Ministry of Defence (MoD) laboratories at Porton, Salisbury. Alternatively, proof of concept studies could be conducted using a less dangerous Ebola virus model such as that designed by Watanabe *et al*, (2000).

Further development of this approach could be conducted towards the development of polymer therapeutics for the treatment of many other infectious diseases

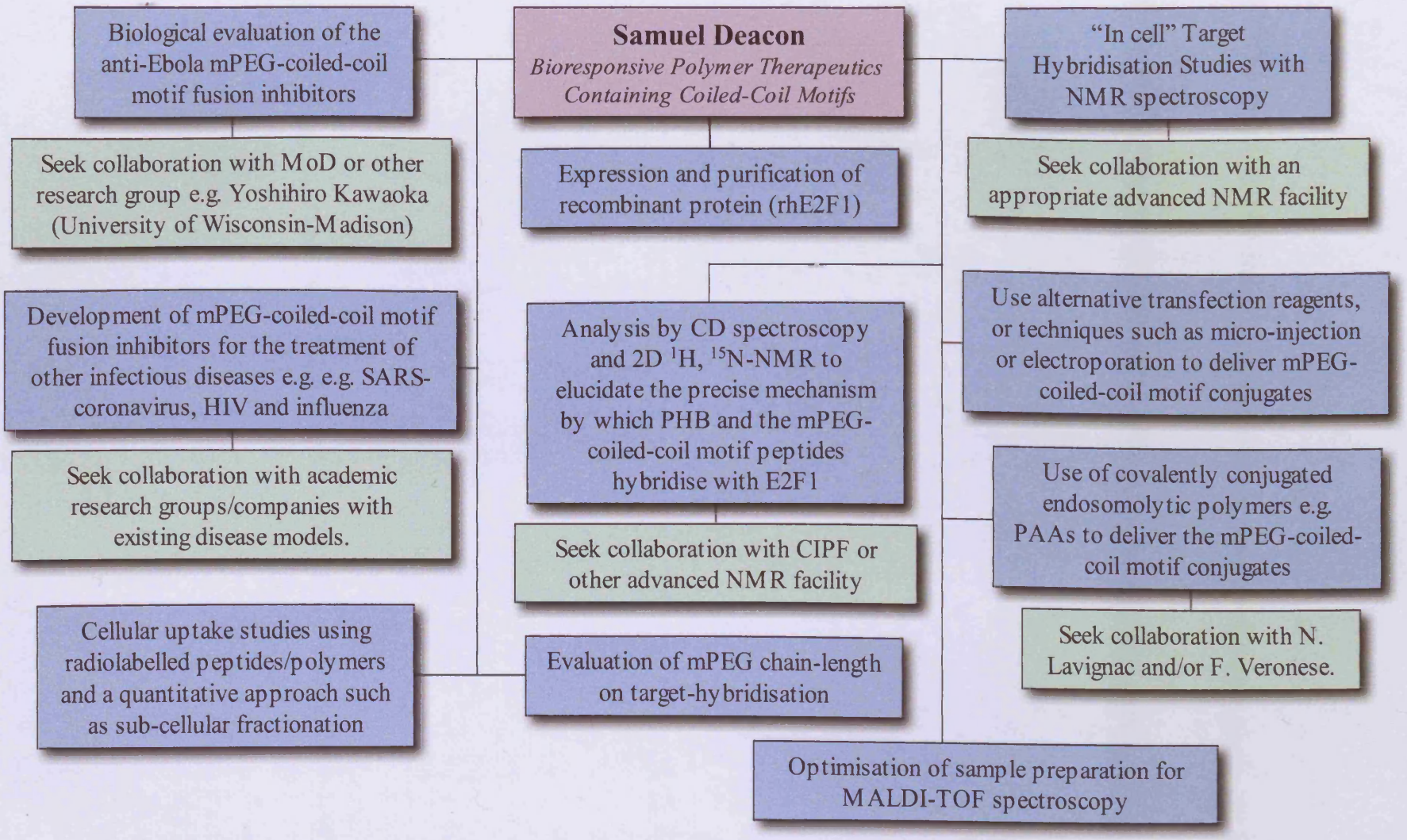

Figure 7.2 Schematic showing potential research projects that could be conducted as a continuation of this Ph.D. thesis.

e.g. SARS-coronavirus, HIV and influenza since these viruses rely upon similar mechanisms of gaining cellular entry.

The challenge of targeting the intracellular transcription factors AP-1 and E2F1 was one that could not be completed during the course of this study. Therefore, more extensive investigations could be conducted towards the development of novel anti-cancer polymer therapeutics.

In the case of the E2F1 transcription factor, further studies should focus initially on the expression of recombinant protein (rhE2F1), then conduct extensive analyses to elucidate the precise mechanism by which PHB and the coiled-coil motif peptides hybridise. Such studies would benefit from the characterisation by CD and NMR spectroscopy presented in Chapter 5 using mPEG-FosW_C and c-Jun

The power, scope and applications of NMR spectroscopy have grown enormously since the start of this thesis in 2005. Most significantly, the characterisation of "in cell" mPEG-coiled-coil motif : target hybridisation is theoretically possible. This would be a challenging, yet very exciting continuation of this work particularly of conducted alongside the biological assays proposed below.

It is possible that the challenge of intracellular delivery may be solved by the mass of research being conducted towards delivery of siRNA. However, in the meanwhile further studies could be conducted as discussed in Chapter 6 using alternative transfection reagents, or techniques such as micro-injection or electroporation to deliver the mPEG-coiled-coil motif conjugates.

7.4 General Conclusions

As we are facing new healthcare challenges and the potential threat of bioterrorism in the 21st century we wished to investigate whether this concept might be more widely applicable to diseases without any effective current treatment.

These studies have demonstrated the potential of mPEG-coiled-coil motifs as therapeutic agents. However, the demonstration of reproducible biological activity was not possible with the intracellular targets. As discussed in Chapter 1 (section 1.5) infection by the Ebola virus results in severe haemorrhagic fever in humans and primates. Statistics from the World Health Organisation indicate that fatality ensues in 50-90 % of cases. There is no anti-viral treatment or vaccine available. Investigating

the biological activity of the conjugates designed to target the extra-cellular Ebola virus fusion proteins remains an exciting prospect. GP2 is a particularly interesting target since the trimeric coiled-coil is thought to be key to fusion of the virus with the host cell membrane and therefore the target of inhibition is extracellular. Therefore circumventing the need to modify the design of the polymer-coiled-coil conjugate for intracellular delivery.

If the significant challenges of intracellular delivery can be overcome, therapeutic agents such as mPEG-$Phb_{CY185-214}$ or mPEG-$FosW_C$ that are capable of down-regulating either E2F1 or AP-1 mediated transcription have enormous potential, not only in oncology but for a whole raft of other proliferative disorders.

Fortunately, it would appear thus far that the field of Nanomedicine has avoided the disastrous public response as seen with genetically modified (GM) foodstuffs. Nanomedicine has the potential to contribute the most sophisticated therapeutics and diagnostic tools ever created. It is therefore essential that these overwhelming benefits are effectively communicated to investors, policy makers and the general public. A fantastic example of the latter are the animated videos, "The Adventure of Nano" (http://www.nanonet.go.jp/english/kids/video) produced by the Nanotechnology Researchers Network Center of Japan. Education and most importantly, inspiration of the next generation of scientists will help realise the many challenges in healthcare and medicine and hopefully solve a few.

"Every day you may make progress. Every step may be fruitful. Yet there will stretch out before you an ever-lengthening, ever-ascending, ever-improving path. You know you will never get to the end of the journey. But this, so far from discouraging, only adds to the joy and glory of the climb."

"Now this is not the end. It is not even the beginning of the end. But it is, perhaps, the end of the beginning."

Sir Winston Churchill

Bibliography

Abe S, Otsuki M (2002) Styrene maleic acid neocarzinostatin treatment for hepatocellular carcinoma. *Current Medicinal Chemistry Anti-Cancer Agents* **2:** 715-26

Abegunde D, Beaglehole, R, Durivage, S, Epping-Jordan, J, Mathers, C, Shengelia, B, Strong, K, Tukuitonga, C, Unwin, N. (2005) Preventing chronic diseases : a vital investment. *WHO global report.* Beaglehole R (ed). Geneva: World Health Organisation

Abuchowski A, Kazo GM, Verhoest CR, van Es T, Kafkewitz D, Nucci ML, Viau AT, Davis FF (1984) Cancer therapy with chemically modified enzymes. I. Antitumor properties of polyethylene glycol-asparaginase conjugates. *Cancer Biochem Biophys* **7:** 175-86

Alberts B, Shamoo AE, Johnson A, Khin-Maung-Gyi FA, Lewis J, Raff M, Roberts K (2002) *Molecular Biology of the Cell*, 4th edn.: Garland Science

Alley MC, Scudiero DA, Monks A, Hursey ML, Czerwinski MJ, Fine DL, Abbott BJ, Mayo JG, Shoemaker RH, Boyd MR (1988) Feasibility of drug screening with panels of human tumor cell lines using a microculture tetrazolium assay. *Cancer Res* **48:** 589-601

Ameyar-Zazoua M, Wisniewska MB, Bakiri L Wagner EF, Yaniv M, Weitzman JB (2005) AP-1 dimers regulate transcription of the p14/p19 ARF tumor suppressor gene. *Oncogene* **24**: 2298–2306

Amirghofran Z, Bahmani M, Azadmehr A, Javidnia K (2007) Immunomodulatory and apoptotic effects of Stachys obtusicrena on proliferative lymphocytes. *Med Sci Monit* **13:** BR145-50

Amon MA, Ali M, Bender V, Hall K, Aguilar MI, Aldrich-Wright J, Manolios N (2008) Kinetic and conformational properties of a novel T-cell antigen receptor transmembrane peptide in model membranes. *J Pept Sci.* **14**(6): 714-24

Anderson RG, Brown MS, Goldstein JL (1977) Role of the coated endocytic vesicle in the uptake of receptor-bound low density lipoprotein in human fibroblasts. *Cell* **10:** 351-64

Angel P, Karin M (1991) The role of Jun, Fos and the AP-1 complex in cell-proliferation and transformation. *Biochimica et Biophysica Acta* **1072:** 129-57

Arnau J, Lauritzen C, Petersen GE, Pedersen J (2006) Current strategies for the use of affinity tags and tag removal for the purification of recombinant proteins. *Protein Expression and Purification* **48:** 1-13

Arndt KM, Muller KM, Pluckthun A (2001) Helix-stabilized Fv (hsFv) antibody fragments: substituting the constant domains of a Fab fragment for a heterodimeric coiled-coil domain. *J Mol Biol* **312:** 221-8

Bakin AV, Curran T (1999) Role of DNA 5-methylcytosine transferase in cell transformation by fos. *Science* **283:** 387-90

Bakiri L, Lallemand D, Bossy-Wetzel E, Yaniv M (2000) Cell cycle-dependent variations in c-Jun and JunB phosphorylation: a role in the control of cyclin D1 expression. *The EMBO Journal* **19**: 2056-68

Balan S, Choi JW, Godwin A, Teo I, Laborde CM, Heidelberger S, Zloh M, Shaunak S, Brocchini S (2007) Site-specific PEGylation of protein disulfide bonds using a three-carbon bridge. *Bioconjugate Chemistry* **18:** 61-76

Bandara LR, Buck VM, Zamanian M, Johnston LH, La Thangue NB (1993) Functional synergy between DP-1 and E2F-1 in the cell cycle-regulating transcription factor DRTF1/E2F. *The EMBO Journal* **12**: 4317-24

Banks PR, Paquette DM (1995) Comparison of three common amine reactive fluorescent probes used for conjugation to biomolecules by capillary zone electrophoresis. *Bioconjugate Chemistry* **6:** 447-58

Bareford LM, Swaan PW (2007) Endocytic mechanisms for targeted drug delivery. *Advanced Drug Delivery Reviews* **59:** 748-58

Barjat H, Morris GA, Smart S, Swanson AG, Williams SCR (1995) High-Resolution Diffusion-Ordered 2D Spectroscopy (HR-DOSY)-A New Tool for the Analysis of Complex Mixtures. *Journal of Magnetic Resonance* **108**: 170-72

Barr FA, Short B (2003) Golgins in the structure and dynamics of the Golgi apparatus. *Curr Opin Cell Biol* **15:** 405-13

Basler CF, Mikulasova A, Martinez-Sobrido L, Paragas J, Muhlberger E, Bray M, Klenk HD, Palese P, Garcia-Sastre A (2003) The Ebola virus VP35 protein inhibits activation of interferon regulatory factor 3. *J Virol* **77:** 7945-56

Basler CF, Wang X, Muhlberger E, Volchkov V, Paragas J, Klenk HD, Garcia-Sastre A, Palese P (2000) The Ebola virus VP35 protein functions as a type I IFN antagonist. *Proc Natl Acad Sci U S A* **97:** 12289-94

Beard M, Satoh A, Shorter J, Warren G (2005) A cryptic Rab1-binding site in the p115 tethering protein. *J Biol Chem* **280:** 25840-8

Bedford J, Hyde C, Johnson T, Jun W, Owen D, Quibell M, Sheppard RC (1992) Amino acid structure and "difficult sequences" in solid phase peptide synthesis. *Int J Pept Protein Res* **40:** 300-7

Berger B (1995) Algorithms for protein structural motif recognition. *J Comput Biol* **2:** 125-38

Berger B, Singh M (1997) An iterative method for improved protein structural motif recognition. *J Comput Biol* **4:** 261-73

Berger B, Wilson DB, Wolf E, Tonchev T, Milla M, Kim PS (1995) Predicting coiled coils by use of pairwise residue correlations. *Proc Natl Acad Sci USA* **92:** 8259-63

Bianchi E, Finotto M, Ingallinella P, Hrin R, Carella AV, Hou XS, Schleif WA, Miller MD, Geleziunas R, Pessi A (2005) Covalent stabilization of coiled coils of the HIV gp41 N region yields extremely potent and broad inhibitors of viral infection. *Proc Natl Acad Sci U S A* **102:** 12903-8

Bjorndal AS, Szekely L, Elgh F (2003) Ebola virus infection inversely correlates with the overall expression levels of promyelocytic leukaemia (PML) protein in cultured cells. *BMC Microbiol* **3:** 6

Bodenhausen G, Ruben DJ (1980) Natural abundance nitrogen-15 NMR by enhanced heteronuclear spectroscopy. *Chem Phys Letters* **69**: 185-89

Borges-Walmsley MI, Beauchamp J, Kelly SM, Jumel K, Candlish D, Harding SE, Price NC, Walmsley AR (2003) Identification of oligomerization and drug-binding domains of the membrane fusion protein EmrA. *J Biol Chem* **278:** 12903-12

Bossy-Wetzel E, Bakiri L, Yaniv M (1997) Induction of apoptosis by the transcription factor c-Jun. *The EMBO Journal* **16**: 1695-1709

Boussif O, Lezoualc'h F, Zanta MA, Mergny MD, Scherman D, Demeneix B, Behr JP (1995) A versatile vector for gene and oligonucleotide transfer into cells in culture and in vivo: polyethylenimine. *Proc Natl Acad Sci USA* **92:** 7297-301

Bowen ET, Lloyd G, Harris WJ, Platt GS, Baskerville A, Vella EE (1977) Viral haemorrhagic fever in southern Sudan and northern Zaire. Preliminary studies on the aetiological agent. *Lancet* **1:** 571-3

Bradford MM (1976) A rapid and sensitive method for the quantitation of microgram quantities of protein utilizing the principle of protein-dye binding. *Anal Biochem* **72:** 248-54

Brand T, Cabrita EJ, Berger S (2005) Intermolecular interaction as investigated by NOE and diffusion studies. *Progress in Nuclear Magnetic Resonance Spectroscopy* **46**: 159-196

Bray M (2003) Defense against filoviruses used as biological weapons. *Antiviral Res* **57:** 53-60

Bukowski R, Ernstoff MS, Gore ME, Nemunaitis JJ, Amato R, Gupta SK, Tendler CL (2002) Pegylated interferon alfa-2b treatment for patients with solid tumors: a phase I/II study. *J Clin Oncol* **20:** 3841-9

Bulaj G, Kortemme T, Goldenberg DP (1998) Ionization-reactivity relationships for cysteine thiols in polypeptides. *Biochemistry* **37:** 8965-72

Burz DS, Dutta K, Cowburn D, Shekhtman A (2006) Mapping structural interactions using in-cell NMR spectroscopy (STINT-NMR). *Nat Meth* **3:** 91-3

Cao Z, Klebba PE (2002) Mechanisms of colicin binding and transport through outer membrane porins. *Biochimie* **84:** 399-412

Capecchi MR (1980) High efficiency transformation by direct microinjection of DNA into cultured mammalian cells. *Cell* **22:** 479-88

Carpino LA, Han GY (1972) 9-Fluorenylmethoxycarbonyl amino-protecting group. *The Journal of Organic Chemistry* **37:** 3404-3409

Carrington JC, Dougherty WG (1988) A viral cleavage site cassette: identification of amino acid sequences required for tobacco etch virus polyprotein processing. *Proc Natl Acad Sci USA* **85:** 3391-5

Chakraborty M, Qiu SG, Vasudevan KM, Rangnekar VM (2001) Par-4 drives trafficking and activation of Fas and Fasl to induce prostate cancer cell apoptosis and tumor regression. *Cancer Res* **61:** 7255-63

Chan DC, Chutkowski CT, Kim PS (1998) Evidence that a prominent cavity in the coiled coil of HIV type 1 gp41 is an attractive drug target. *Proc Natl Acad Sci USA* **95:** 15613-7

Chan SY, Speck RF, Ma MC, Goldsmith MA (2000) Distinct mechanisms of entry by envelope glycoproteins of Marburg and Ebola (Zaire) viruses. *J Virol* **74:** 4933-7

Chan WC, White PD (Eds) (2000) *Fmoc Solid Phase Peptide Synthesis*edn. New York: Oxford University Press Inc.

Chang DK, Cheng SF, Trivedi VD, Lin KL (1999) Proline affects oligomerization of a coiled coil by inducing a kink in a long helix. *J Struct Biol* **128:** 270-9

Chapman AP, Antoniw P, Spitali M, West S, Stephens S, King DJ (1999) Therapeutic antibody fragments with prolonged in vivo half-lives. *Nat Biotechnol* **17:** 780-3

Chaudhary AK, Critchley G, Diaf A, Beckman EJ, Russell AJ (1996) Characterization of synthetic-polymers using matrix-assisted laser desorption/ionization-time-of-Flight mass-spectrometry. *Macromolecules* **29**: 2213–21

Chen CP, Park Y, Rice KG (2004) An improved large-scale synthesis of PEG-peptides for gene delivery. *J Pept Res* **64:** 237-43

Chen RF, Knutson JR (1988) Mechanism of fluorescence concentration quenching of carboxyfluorescein in liposomes: energy transfer to nonfluorescent dimers. *Anal Biochem* **172:** 61-77

Chu G, Hayakawa H, Berg P (1987) Electroporation for the efficient transfection of mammalian cells with DNA. *Nucleic Acids Research* **15:** 1311-26

Claas EC, Osterhaus AD, van Beek R, De Jong JC, Rimmelzwaan GF, Senne DA, Krauss S, Shortridge KF, Webster RG (1998) Human influenza A H5N1 virus related to a highly pathogenic avian influenza virus. *Lancet* **351:** 472-7

Collier HB (1973) Letter: A note on the molar absorptivity of reduced Ellman's reagent, 3-carboxylato-4-nitrothiophenolate. *Anal Biochem* **56:** 310-1

Conner SD, Schmid SL (2003) Regulated portals of entry into the cell. *Nature* **422:** 37-44

Cornish J, Callon KE, Lin CQ, Xiao CL, Mulvey TB, Cooper GJ, Reid IR (1999) Trifluoroacetate, a contaminant in purified proteins, inhibits proliferation of osteoblasts and chondrocytes. *Am J Physiol* **277:** E779-83

Cortez DM, Feldman MD, Mummidi S, Valente AJ, Steffensen B, Vincenti M, Barnes JL, Chandrasekar B (2007) IL-17 stimulates MMP-1 expression in primary human cardiac fibroblasts via p38 MAPK- and ERK1/2-dependent C/EBP-beta , NF-kappaB, and AP-1 activation. *Am J Physiol Heart Circ Physiol* **293:** H3356-65

Crick FHC (1953) The packing of α-Helices: Simple Coiled-Coils. *Acta Crystallographica* **6:** 685-697

Cross TJ, Antoniades CG, Harrison PM (2008) Current and future management of chronic hepatitis C infection. *Postgraduate Medical Journal* **84:** 172-6

Dai Y, Whittal RM, Li L (1999) Two-layer sample preparation: a method for MALDI-MS analysis of complex peptide and protein mixtures. *Anal Chem* **71:** 1087-91

Davis FF (2002) The origin of pegnology. *Advanced Drug Delivery Reviews* **54:** 457-8

DeGregori J (2002) The genetics of the E2F family of transcription factors: shared functions and unique roles. *Biochimica et Biophysica Acta* **1602:** 131-50

Delmotte C, Delmas A (1999) Synthesis and fluorescence properties of Oregon Green 514 labeled peptides. *Bioorg Med Chem Lett* **9:** 2989-94

Dev KK (2004) Making protein interactions druggable: targeting PDZ domains. *Nat Rev Drug Discov* **3:** 1047-56

Devleeschouwer N, Body JJ, Legros N, Muquardt C, Donnay I, Wouters P, Leclercq G (1992) Growth factor-like activity of phenol red preparations in the MCF-7 breast cancer cell line. *Anticancer Research* **12:** 789-94

Dimova DK, Dyson NJ (2005) The E2F transcriptional network: old acquaintances with new faces. *Oncogene* **24:** 2810-26

Doherty DH, Rosendahl MS, Smith DJ, Hughes JM, Chlipala EA, Cox GN (2005) Site-specific PEGylation of engineered cysteine analogues of recombinant human granulocyte-macrophage colony-stimulating factor. *Bioconjugate Chemistry* **16:** 1291-8

Donaruma LG (1975) Synthetic biologically active polymers. *Progress in Polymer Science* **4:** 1-25

Dordal MS, Ho AC, Jackson-Stone M, Fu YF, Goolsby CL, Winter JN (1995) Flow cytometric assessment of the cellular pharmacokinetics of fluorescent drugs. *Cytometry* **20:** 307-14

Dosio F, Arpicco S, Adobati E, Canevari S, Brusa P, De Santis R, Parente D, Pignanelli P, Negri DR, Colnaghi MI, Cattel L (1998) Role of cross-linking agents in determining the biochemical and pharmacokinetic properties of Mgr6-clavin immunotoxins. *Bioconjugate Chemistry* **9:** 372-81

Duncan R (1992) Drug-polymer conjugates: potential for improved chemotherapy. *Anti-Cancer Drugs* **3:** 175-210

Duncan R (2003) The dawning era of polymer therapeutics. *Nat Rev Drug Discov* **2:** 347-60

Duncan R (2005) *Encyclopedia of Molecular Cell Biology and Molecular Medicine.* Vol. 14. Weinheim: WILEY-VCH Verlag GmbH & Co. KGaA

Duncan R (2006) Polymer conjugates as anticancer nanomedicines. *Nat Rev Cancer* **6:** 688-701

Duncan R, Ferruti P, Sgouras D, Tuboku-Metzger A, Ranucci E, Bignotti F (1994) A polymer-Triton X-100 conjugate capable of PH-dependent red blood cell lysis: a model system illustrating the possibility of drug delivery within acidic intracellular compartments. *Journal of Drug Targeting* **2:** 341-7

Duncan R, Gilbert HRP, Carbajo RJ, Vicent MJ (2008) Polymer masked-unmasked protein therapy. 1. Bioresponsive dextrin-trypsin and-melanocyte stimulating hormone conjugates designed for alpha-amylase activation. *Biomacromolecules* **9**: 1146-54

Duncan R, Kopecek J (1984) Soluble synthetic polymers as potential drug carriers. In *Polymers in Medicine* Vol. 57, pp 53-101. Berlin: Springer

Ebihara Y, Miyamoto M, Shichinohe T, Kawarada Y, Cho Y, Fukunaga A, Murakami S, Uehara H, Kaneko H, Hashimoto H, Murakami Y, Itoh T, Okushiba S, Kondo S, Katoh H (2004) Over-expression of E2F-1 in esophageal squamous cell carcinoma correlates with tumor progression. *Dis Esophagus* **17:** 150-4

Echt S, Bauer S, Steinbacher S, Huber R, Bacher A, Fischer M (2004) Potential anti-infective targets in pathogenic yeasts: structure and properties of 3,4-dihydroxy-2-butanone 4-phosphate synthase of Candida albicans. *J Mol Biol* **341:** 1085-96

Eferl R, Wagner EF (2003) AP-1: a double-edged sword in tumorigenesis. *Nat Rev Cancer* **3:** 859-68

Eggermont AM, Suciu S, Santinami M, Testori A, Kruit WH, Marsden J, Punt CJ, Salès F, Gore M, Mackie R, Kusic Z, Dummer R, Hauschild A, Musat E, Spatz A, Keilholz U, Group EM (2008) Adjuvant therapy with pegylated interferon alfa-2b versus observation alone in resected stage III melanoma: final results of EORTC 18991, a randomised phase III trial. *Lancet* **372:** 117-26

Eichelberger L (2007) SARS and New York's Chinatown: the politics of risk and blame during an epidemic of fear. *Social Science & Medicine (1982)* **65:** 1284-95

El-Guendy N, Rangnekar VM (2003) Apoptosis by Par-4 in cancer and neurodegenerative diseases. *Exp Cell Res* **283:** 51-66

El-Guendy N, Zhao Y, Gurumurthy S, Burikhanov R, Rangnekar VM (2003) Identification of a unique core domain of par-4 sufficient for selective apoptosis induction in cancer cells. *Mol Cell Biol* **23:** 5516-25

Ellman GL (1959) Tissue sulfhydryl groups. *Archives of Biochemistry and Biophysics* **82:** 70-7

Enright MC, Robinson DA, Randle G, Feil EJ, Grundmann H, Spratt BG (2002) The evolutionary history of methicillin-resistant Staphylococcus aureus (MRSA). *Proc Natl Acad Sci U S A* **99:** 7687-92

ESF (2005) European Science Foundation Forward Look on Nanomedicine

Feber A, Clark J, Goodwin G, Dodson AR, Smith PH, Fletcher A, Edwards S, Flohr P, Falconer A, Roe T, Kovacs G, Dennis N, Fisher C, Wooster R, Huddart R, Foster CS, Cooper CS (2004) Amplification and overexpression of E2F3 in human bladder cancer. *Oncogene* **23:** 1627-30

Felgner PL, Gadek TR, Holm M, Roman R, Chan HW, Wenz M, Northrop JP, Ringold GM, Danielsen M (1987) Lipofection: a highly efficient, lipid-mediated DNA-transfection procedure. *Proc Natl Acad Sci USA* **84:** 7413-7

Ferguson EL, Duncan R (2009) Dextrin-Phospholipase A(2): Synthesis and Evaluation as a Bioresponsive Anticancer Conjugate. *Biomacromolecules* **9**: 1146-54

Fialka I, Schwarz H, Reichmann E, Oft M, Busslinger M, Beug H (1996) The estrogen-dependent c-JunER protein causes a reversible loss of mammary epithelial cell polarity involving a destabilization of adherens junctions. *J Cell Biol* **132:** 1115-32

Fields CG, VanDrisse VL, Fields GB (1993) Edman degradation sequence analysis of resin-bound peptides synthesized by 9-fluorenylmethoxycarbonyl chemistry. *Pept Res* **6:** 39-47

Fields GB, Noble RL (1990) Solid phase peptide synthesis utilizing 9-fluorenylmethoxycarbonyl amino acids. *Int J Pept Protein Res* **35:** 161-214

Fletcher CV (2003) Enfuvirtide, a new drug for HIV infection. *Lancet* **361:** 1577-8

Foster CS, Falconer A, Dodson AR, Norman AR, Dennis N, Fletcher A, Southgate C, Dowe A, Dearnaley D, Jhavar S, Eeles R, Feber A, Cooper CS (2004) Transcription factor E2F3 overexpressed in prostate cancer independently predicts clinical outcome. *Oncogene* **23:** 5871-9

França LTC, Carrilho E, Kist TBL (2002) A review of DNA sequencing techniques. *Quarterly Reviews of Biophysics* **35**: 69-200

Frank S, Lustig A, Schulthess T, Engel J, Kammerer RA (2000) A distinct seven-residue trigger sequence is indispensable for proper coiled-coil formation of the human macrophage scavenger receptor oligomerization domain. *J Biol Chem* **275:** 11672-7

Fuertges F, Abuchowski A (1990) The clinical efficacy of poly (ethylene glycol)-modified proteins. *J Control Release* **11:** 139-148

Fujiwara Y, Akaji K, Kiso Y (1994) Racemization-free synthesis of C-terminal cysteine-peptide using 2-chlorotrityl resin. *Chem Pharm Bull* **42:** 724-6

Furukawa T, Kubota T, Suto A, Takahara T, Yamaguchi H, Takeuchi T, Kase S, Kodaira S, Ishibiki K, Kitajima M (1991) Clinical usefulness of chemosensitivity testing using the MTT assay. *Journal of Surgical Oncology* **48:** 188-93

Fusaro G, Dasgupta P, Rastogi S, Joshi B, Chellappan S (2003) Prohibitin induces the transcriptional activity of p53 and is exported from the nucleus upon apoptotic signaling. *J Biol Chem* **278:** 47853-61

Gallo SA, Finnegan CM, Viard M, Raviv Y, Dimitrov A, Rawat SS, Puri A, Durell S, Blumenthal R (2003) The HIV Env-mediated fusion reaction. *Biochimica et Biophysica Acta* **1614:** 36-50

Garcia BA, Heaney PJ, Tang K (2002) Improvement of the MALDI-TOF analysis of DNA with thin-layer matrix preparation. *Anal Chem* **74:** 2083-91

Garner J, Harding MM (2007) Design and synthesis of alpha-helical peptides and mimetics. *Organic & Biomolecular Chemistry* **5:** 3577-85

Garnett MC, Kallinteri P (2006) Nanomedicines and nanotoxicology: some physiological principles. *Occupational Medicine (Oxford, England)* **56:** 307-11

Gillingham AK, Munro S (2003) Long coiled-coil proteins and membrane traffic. *Biochimica et Biophysica Acta* **1641:** 71-85

Girling R, Partridge JF, Bandara LR, Burden N, Totty NF, Hsuan JJ, La Thangue NB (1993) A new component of the transcription factor DRTF1/E2F. *Nature* **362**: 83-87

Glasel JA (1995) Validity of nucleic acid purities monitored by 260nm/280nm absorbance ratios. *BioTechniques* **18:** 62-3

Glover JN, Harrison SC (1995) Crystal structure of the heterodimeric bZIP transcription factor c-Fos-c-Jun bound to DNA. *Nature* **373:** 257-61

Goodson RJ, Katre NV (1990) Site-directed pegylation of recombinant interleukin-2 at its glycosylation site. *Biotechnology (NY)* **8:** 343-6

Gorgoulis VG, Zacharatos P, Mariatos G, Kotsinas A, Bouda M, Kletsas D, Asimacopoulos PJ, Agnantis N, Kittas C, Papavassiliou AG (2002) Transcription factor E2F-1 acts as a growth-promoting factor and is associated with adverse prognosis in non-small cell lung carcinomas. *J Pathol* **198:** 142-56

Graham FL, van der Eb AJ (1973) Transformation of rat cells by DNA of human adenovirus 5. *Virology* **54:** 536-9

Graham ML (2003) Pegaspargase: a review of clinical studies. *Advanced Drug Delivery Reviews* **55:** 1293-302

Grant, GA (ed) (1992) *Synthetic Peptides*, 1st Edn. New York: W.H. Freeman and Company

Gräslund S, Nordlund P, Weigelt J, Bray J, Gileadi O, Knapp S, Oppermann U, Arrowsmith C, Hui R, Ming J, Dhe-Paganon S, Park H, Savchenko A, Yee A, Edwards A, Vincentelli R, Cambillau C, Kim R, Kim S, Rao Z, Shi Y, Terwilliger T, Kim C, Hung L, Waldo G, Peleg Y, Albeck S, Unger T, Dym O, Prilusky J, Sussman J, Stevens R, Lesley S, Wilson I, Joachimiak A, Collart F, Dementieva I, Donnelly M, Eschenfeldt W, Kim Y, Stols L, Wu R, Zhou M, Burley S, Emtage J, Sauder J, Thompson D, Bain K, Luz J, Gheyi T, Zhang F, Atwell S, Almo S, Bonanno J, Fiser A, Swaminathan S, Studier F, Chance M, Sali A, Acton T, Xiao R, Zhao L, Ma L, Hunt J, Tong L, Cunningham K, Inouye M, Anderson S, Janjua H, Shastry R, Ho C, Wang D, Wang H, Jiang M, Montelione G, Stuart D, Owens R, Daenke S, Schütz A, Heinemann U, Yokoyama S, Büssow K, Gunsalus K (2008) Protein production and purification. *Nat Meth* **5:** 135-146

Greco A, Fusetti L, Miranda C, Villa R, Zanotti S, Pagliardini S, Pierotti MA (1998) Role of the TFG N-terminus and coiled-coil domain in the transforming activity of the thyroid TRK-T3 oncogene. *Oncogene* **16:** 809-16

Greco F, Vicent MJ, Gee S, Jones AT, Gee J, Nicholson RI, Duncan R. (2007) Investigating the mechanism of enhanced cytotoxicity of HPMA copolymer-Dox-AGM in breast cancer cells. *J Control Release* **117**: 28-39

Greenfield NJ (2006) Using circular dichroism spectra to estimate protein secondary structure. *Nat Protoc* **1:** 2876-90

Guo Q, Fu W, Xie J, Luo H, Sells SF, Geddes JW, Bondada V, Rangnekar VM, Mattson MP (1998) Par-4 is a mediator of neuronal degeneration associated with the pathogenesis of Alzheimer disease. *Nat Med* **4:** 957-62

Guo Q, Xie J (2004) AATF inhibits aberrant production of amyloid beta peptide 1-42 by interacting directly with Par-4. *J Biol Chem* **279:** 4596-603

Guy CA, Fields GB (1997) Trifluoroacetic acid cleavage and deprotection of resin-bound peptides following synthesis by Fmoc chemistry. *Meth Enzymol* **289:** 67-83

Hanton SD (2001) Mass spectrometry of polymers and polymer surfaces. *Chem Rev* **101:** 527-69

Hardwicke J, Ferguson EL, Moseley R, Stephens P, Thomas DW, Duncan R (2008) Dextrin-rhEGF conjugates as bioresponsive nanomedicines for wound repair. *J Control Release* **130:** 275-83

Harris JM, Chess RB (2003) Effect of pegylation on pharmaceuticals. *Nat Rev Drug Discov* **2:** 214-21

Helling RB, Goodman HM, Boyer HW (1974) Analysis of endonuclease R-EcoRI fragments of DNA from lambdoid bacteriophages and other viruses by agarose-gel electrophoresis. *J Virol* **14:** 1235-44

Hennigan RF, Hawker KL, Ozanne BW (1994) Fos-transformation activates genes associated with invasion. *Oncogene* **9:** 3591-600

Hensley LE, Young HA, Jahrling PB, Geisbert TW (2002) Proinflammatory response during Ebola virus infection of primate models: possible involvement of the tumor necrosis factor receptor superfamily. *Immunol Lett* **80:** 169-79

Hermanson GT (2008) Bioconjugate Techniques. 2nd Edn. Burlington: Academic Press

Hicks MR, Holberton DV, Kowalczyk C, Woolfson DN (1997) Coiled-coil assembly by peptides with non-heptad sequence motifs. *Fold Des* **2:** 149-58

Hidaka S, Konecke V, Osten L, Witzgall R (2004) PIGEA-14, a novel coiled-coil protein affecting the intracellular distribution of polycystin-2. *J Biol Chem* **279:** 35009-16

Hreczuk-Hirst D, Chicco D, German L, Duncan R (2001) Dextrins as potential carriers for drug targeting: tailored rates of dextrin degradation by introduction of pendant groups. *International Journal of Pharmaceutics* **230:** 57-66

Hu E, Mueller E, Oliviero S, Papaioannou VE, Johnson R, Spiegelman BM (1994) Targeted disruption of the c-fos gene demonstrates c-fos-dependent and -independent pathways for gene expression stimulated by growth factors or oncogenes. *The EMBO Journal* **13:** 3094-103

Hu YF, Li R (2002) JunB potentiates function of BRCA1 activation domain 1 (AD1) through a coiled-coil-mediated interaction. *Genes Dev* **16:** 1509-17

Hu YF, Miyake T, Ye Q, Li R (2000) Characterization of a novel trans-activation domain of BRCA1 that functions in concert with the BRCA1 C-terminal (BRCT) domain. *J Biol Chem* **275:** 40910-5

Inomata K, Ohno A, Tochio H, Isogai S, Tenno T, Nakase I, Takeuchi T, Futaki S, Ito Y, Hiroaki H, Shirakawa M (2009) High-resolution multi-dimensional NMR spectroscopy of proteins in human cells. *Nature* **457:** 106-109

Itakura K, Hirose T, Crea R, Riggs AD, Heyneker HL, Bolivar F, Boyer HW (1977) Expression in Escherichia coli of a chemically synthesized gene for the hormone somatostatin. *Science* **198:** 1056-63

Ivanov VN, Bhoumik A, Krasilnikov M, Raz R, Owen-Schaub LB, Levy D, Horvath CM, Ronai Z (2001) Cooperation between STAT3 and c-jun suppresses Fas transcription. *Mol Cell* **7:** 517-28

Iwai K, Maeda H, Konno T (1984) Use of oily contrast medium for selective drug targeting to tumor: enhanced therapeutic effect and X-ray image. *Cancer Res* **44:** 2115-21

John M, Leppik R, Busch SJ, Granger-Schnarr M, Schnarr M (1996) DNA binding of Jun and Fos bZip domains: homodimers and heterodimers induce a DNA conformational change in solution. *Nucleic Acids Res* **24:** 4487-94

Jooss KU, Muller R (1995) Deregulation of genes encoding microfilament-associated proteins during Fos-induced morphological transformation. *Oncogene* **10**: 603-08

Joshi B, Ko D, Ordonez-Ercan D, Chellappan SP (2003) A putative coiled-coil domain of prohibitin is sufficient to repress E2F1-mediated transcription and induce apoptosis. *Biochem Biophys Res Commun* **312:** 459-66

Junius FK, O'Donoghue SI, Nilges M, Weiss AS, King GF (1996) High resolution NMR solution structure of the leucine zipper domain of the c-Jun homodimer. *J Biol Chem* **271:** 13663-7

Kabanov AV, Felgner PL, Seymour LW (1998) Self-assembling Complexes for Gene Delivery. From Laboratory to Clinical Trial. Chichester: Willey

Kasibhatla S, Brunner T, Genestier L, Echeverri F, Mahboubi A, Green DR (1998) DNA damaging agents induce expression of Fas ligand and subsequent apoptosis in T lymphocytes via the activation of NF-kappa B and AP-1. *Mol Cell* **1:** 543-51

Kinstler OB, Brems DN, Lauren SL, Paige AG, Hamburger JB, Treuheit MJ (1996) Characterization and stability of N-terminally PEGylated rhG-CSF. *Pharm Res* **13:** 996-1002

Kogan TP (1992) The synthesis of substituted methoxy-poly (ethyleneglycol) derivatives suitable for selective protein modification. *Synthetic Communications* **22**: 2417-24

Kohler G, Milstein C (1975) Continuous cultures of fused cells secreting antibody of predefined specificity. *Nature* **256:** 495-7

Kolb HC, Finn MG, Sharpless KB (2001) Click Chemistry: Diverse Chemical Function from a Few Good Reactions. *Angewandte Chemie (International ed)* **40:** 2004-2021

Konno T, Maeda H (1987) Neoplasms of the liver. In, Okada K, Ishak KG (eds), pp 343-352. New York: Springer-Verlag

Korzeniewski C, Callewaert DM (1983) An enzyme-release assay for natural cytotoxicity. *J Immunol Methods* **64:** 313-20

Kuhn K, Campbell-Lendrum D, Haines A, Cox J (2005) *Using climate to predict infectious disease epidemics*. Geneva: WHO Document Production Services

Lamb RF, Hennigan RF, Turnbull K, Katsanakis KD, MacKenzie ED, Birnie GD, Ozanne BW (1997) AP-1-mediated invasion requires increased expression of the hyaluronan receptor CD44. *Mol Cell Biol* **17:** 963-76

Landon LA, Zou J, Deutscher SL (2004) Is phage display technology on target for developing peptide-based cancer drugs? *Curr Drug Discov Technol* **1:** 113-32

Lau SY, Taneja AK, Hodges RS (1984) Synthesis of a model protein of defined secondary and quaternary structure. Effect of chain length on the stabilization and formation of two-stranded alpha-helical coiled-coils. *J Biol Chem* **259:** 13253-61

Lavignac N, Lazenby M, Foka P, Malgesini B, Verpilio I, Ferruti P, Duncan R (2004) Synthesis and endosomolytic properties of poly(amidoamine) block copolymers. *Macromolecular Bioscience* **4:** 922-9

Lavignac N, Lazenby M, Franchini J, Ferruti P, Duncan R (2005) Synthesis and preliminary evaluation of poly(amidoamine)-melittin conjugates as endosomolytic polymers and/or potential anticancer therapeutics. *International Journal of Pharmaceutics* **300:** 102-12

Linnemayr K, Vana P, Allmaier G (1998) Time-delayed extraction matrix-assisted laser desorption/ionization time-of-flight mass spectrometry of polyacrylnitrile and other synthetic polymers with the matrix-4-hydroxybenzylidene malononitrile. *Rapid Commun Mass Spectrom* **12**: 1344-50

López de Saro FJ, Georgescu RE, O'Donnell M (2003) A peptide switch regulates DNA polymerase processivity. *Proc Natl Acad Sci USA* **100:** 14689-94

Lu C, Shen Q, DuPré E, Kim H, Hilsenbeck S, Brown PH (2005) cFos is critical for MCF-7 breast cancer cell growth. *Oncogene* **24**: 6516-24

Lupas A (1996) Coiled coils: new structures and new functions. *Trends Biochem Sci* **21:** 375-82

Lupas A, Van Dyke M, Stock J (1991) Predicting coiled coils from protein sequences. *Science* **252:** 1162-4

Luzio JP, Pryor PR, Bright NA (2007) Lysosomes: fusion and function. *Nat Rev Mol Cell Biol* **8:** 622-32

Ma J, Zhang T, Novotny-Diermayr V, Tan AL, Cao X (2003) A novel sequence in the coiled-coil domain of Stat3 essential for its nuclear translocation. *J Biol Chem* **278:** 29252-60

Mach H, Middaugh CR, Lewis RV (1992) Statistical determination of the average values of the extinction coefficients of tryptophan and tyrosine in native proteins. *Anal Biochem* **200:** 74-80

Maeda H, Konno T (1997) Neocazinostatin: The Past, Present, and Future of an Anticancer Drug. In, Maeda H, Edo K, Ishida N (eds), pp 227-267. Berlin: Springer-Verlag

Mant CT, Chen Y, Yan Z, Popa TV, Kovacs JM, Mills JB, Tripet BP, Hodges RS (2007) HPLC analysis and purification of peptides. *Methods Mol Biol* **386:** 3-55

Manunta M, Izzo L, Duncan R, Jones AT (2007) Establishment of subcellular fractionation techniques to monitor the intracellular fate of polymer therapeutics II. Identification of endosomal and lysosomal compartments in HepG2 cells combining single-step subcellular fractionation with fluorescent imaging. *Journal of Drug Targeting* **15:** 37-50

Marconcini L, Marchio S, Morbidelli L, Cartocci E, Albini A, Ziche M, Bussolino F, Oliviero S (1999) c-fos-induced growth factor/vascular endothelial growth factor D induces angiogenesis in vivo and in vitro. *Proc Natl Acad Sci USA* **96:** 9671-6

Martin SJ, Green DR (1995) Protease activation during apoptosis: death by a thousand cuts? *Cell* **82:** 349-52

Mason JM, Schmitz MA, Muller KM, Arndt KM (2006) Semirational design of Jun-Fos coiled coils with increased affinity: Universal implications for leucine zipper prediction and design. *Proc Natl Acad Sci U S A* **103:** 8989-94

Masters JRW, Twentyman P, Arlett C, Dyer S, Davis J, Daley R, Freshney I, Galphine A, Harrison M, Hurst H, Kelland L, Stacey G, Stratford I, Ward T, Doyle A (1999) UKCCCR Guidelines for the Use of Cell Lines in Cancer Research (First Edition). London: United Kingdom Co-Ordinating Committee On Cancer Research

Matsumura Y, Maeda H (1986) A new concept for macromolecular therapeutics in cancer chemotherapy: mechanism of tumoritropic accumulation of proteins and the antitumor agent smancs. *Cancer Res* **46:** 6387-92

Matthews T, Salgo M, Greenberg M, Chung J, DeMasi R, Bolognesi D (2004) Enfuvirtide: the first therapy to inhibit the entry of HIV-1 into host CD4 lymphocytes. *Nat Rev Drug Discov* **3:** 215-25

Maxfield FR, McGraw TE (2004) Endocytic recycling. *Nat Rev Mol Cell Biol* **5**: 121-132

McDonnell AV, Jiang T, Keating AE, Berger B (2006) Paircoil2: improved prediction of coiled coils from sequence. *Bioinformatics* **22:** 356-8

McEwen CN, Peacock PM (2002) Mass Spectrometry of Chemical Polymers. *Analytical Chemistry* **74:** 2743-2748

Meier MAR, Schubert US (2003) Evaluation of a new multiple-layer spotting technique for matrix-assisted laser desorption/ionization time-of-flight mass spectrometry of synthetic polymers. *Rapid Commun Mass Spectrom* **17**: 713-16

Melamed MR (1990) Flow cytometry detection and evaluation of bladder tumors. *Journal of Occupational Medicine* **32:** 829-33

Merrifield RB (1964) Solid-phase peptide synthesis. 3. An improved synthesis of bradykinin. *Biochemistry* **3:** 1385-90

Merrifield RB (1963) Solid-phase peptide synthesis. I. The synthesis of a tetrapeptide. *Journal of the American Chemical Society* **85**: 2149-54

Middaugh CR, Evans RK, Montgomery DL, Casimiro DR (1998) Analysis of plasmid DNA from a pharmaceutical perspective. *Journal of Pharmaceutical Sciences* **87:** 130-46

Milde-Langosch K (2005) The Fos family of transcription factors and their role in tumourigenesis. *Eur J Cancer* **41:** 2449-61

Miliotis T, Kjellström S, Nilsson J, Laurell T, Edholm LE, Marko-Varga G (2002) Ready-made matrix-assisted laser desorption/ionization target plates coated with thin matrix layer for automated sample deposition in high-density array format. *Rapid Commun Mass Spectrom* **16:** 117-26

Miron T, Wilchek M.(1993) A simplified method for the preparation of succinimidyl carbonate polyethylene glycol for coupling to proteins. *Bioconjugate Chemistry* **4:** 568-9

Mitra A, Chakrabarti KS, Shahul Hameed MS, Srinivas KV, Senthil Kumar G, Sarma SP (2005) High level expression of peptides and proteins using cytochrome b5 as a fusion host. *Protein Expression and Purification* **41:** 84-97

Moffatt BA, Studier FW (1987) T7 lysozyme inhibits transcription by T7 RNA polymerase. *Cell* **49:** 221-7

Mohanty AK, Bishop CM, Bishop TC, Wimley WC, Wiener MC (2003) Enzymatic E-colicins bind to their target receptor BtuB by presentation of a small binding epitope on a coiled-coil scaffold. *J Biol Chem* **278:** 40953-8

Morishita R, Gibbons GH, Horiuchi M, Ellison KE, Nakama M, Zhang L, Kaneda Y, Ogihara T, Dzau VJ (1995) A gene therapy strategy using a transcription factor decoy of the E2F binding site inhibits smooth muscle proliferation in vivo. *Proc Natl Acad Sci USA* **92:** 5855-9

Morpurgo M, Veronese FM, Kachensky D, Harris JM (1996) Preparation of characterization of poly(ethylene glycol) vinyl sulfone. *Bioconjugate Chemistry* **7:** 363-8

Morris MC, Depollier J, Mery J, Heitz F, Divita G (2001) A peptide carrier for the delivery of biologically active proteins into mammalian cells. *Nat Biotechnol* **19:** 1173-6

Morris MC, Robert-Hebmann V, Chaloin L, Mery J, Heitz F, Devaux C, Goody RS, Divita G (1999) A new potent HIV-1 reverse transcriptase inhibitor. A synthetic peptide derived from the interface subunit domains. *J Biol Chem* **274:** 24941-6

Mosmann T (1983) Rapid colorimetric assay for cellular growth and survival: application to proliferation and cytotoxicity assays. *J Immunol Methods* **16**:55-63

Murgasova R, Hercules DM (2002) Polymer characterization by combining liquid chromatography with MALDI and ESI mass spectrometry. *Analytical and Bioanalytical Chemistry* **373:** 481-9

Nelson R (2003) Antibiotic development pipeline runs dry. New drugs to fight resistant organisms are not being developed, experts say. *Lancet* **362:** 1726-7

Nevins JR (2001) The Rb/E2F pathway and cancer. *Hum Mol Genet* **10:** 699-703

Nielen MWF (1999) MALDI time-of-flight mass spectrometry of synthetic polymers. *Mass Spectrometry Reviews* **18**: 309-44

O'Shea EK, Rutkowski R, Stafford WF, Kim PS (1989) Preferential heterodimer formation by isolated leucine zippers from fos and jun. *Science* **245:** 646-8

Oeggerli M, Tomovska S, Schraml P, Calvano-Forte D, Schafroth S, Simon R, Gasser T, Mihatsch MJ, Sauter G (2004) E2F3 amplification and overexpression is associated with invasive tumor growth and rapid tumor cell proliferation in urinary bladder cancer. *Oncogene* **23:** 5616-23

Office for National Statistics. 2008. *Cancer statistics, registrations of cancer diagnosed in 2005, England: Series MB1 no. 36.* Newport

Otting G, Wüthrich K (1990) Heteronuclear filters in two-dimensional [1H,1H]-NMR spectroscopy: combined use with isotope labelling for studies of macromolecular conformation and intermolecular interactions. *Quarterly Reviews of Biophysics* **23:** 39-96

Ozanne BW, Spence HJ, McGarry LC, Hennigan RF (2007) Transcription factors control invasion: AP-1 the first among equals. *Oncogene* **26:** 1-10

Pace CN, Vajdos F, Fee L, Grimsley G, Gray T (1995) How to measure and predict the molar absorption coefficient of a protein. *Protein Sci* **4:** 2411-23

Park YG, Nesterova M, Agrawal S, Cho-Chung YS (1999) Dual blockade of cyclic AMP response element- (CRE) and AP-1-directed transcription by CRE-transcription factor decoy oligonucleotide. gene-specific inhibition of tumor growth. *J Biol Chem* **274:** 1573-80

Parkinson C, Scarlett JA, Trainer PJ (2003) Pegvisomant in the treatment of acromegaly. *Advanced Drug Delivery Reviews* **55:** 1303-14

Parveen S, Sahoo SK (2006) Nanomedicine: clinical applications of polyethylene glycol conjugated proteins and drugs. *Clinical Pharmacokinetics* **45:** 965-88

Pasch H, Schrepp W (2003) MALDI-TOF mass spectrometry of synthetic polymers. Berlin: Springer-Verlag p 298

Passegué E, Wagner EF (2000) JunB suppresses cell proliferation by transcriptional activation of p16(INK4a) expression. *The EMBO Journal* **19:** 2969-79

Pasut G, Guiotto A, Veronese F (2004) Protein, peptide and non-peptide drug PEGylation for therapeutic application. *Expert Opinion on Therapeutic Patents* **14**: 791-804

Pasut G, Sergi M, Veronese FM (2008) Anti-cancer PEG-enzymes: 30 years old, but still a current approach. *Advanced Drug Delivery Reviews* **60:** 69-78

Pasut G, Veronese F (2007) Polymer–drug conjugation, recent achievements and general strategies. *Progress in Polymer Science* **32:** 933-961

Pattrick NG, Richardson SC, Casolaro M, Ferruti P, Duncan R (2001) Poly(amidoamine)-mediated intracytoplasmic delivery of ricin A-chain and gelonin. *J Control Release* **77:** 225-32

Pauling L, Corey RB (1953) Compound helical configurations of polypeptide chains: structure of proteins of the alpha-keratin type. *Nature* **171:** 59-61

Pekarsky Y, Palamarchuk A, Maximov V, Efanov A, Nazaryan N, Santanam U, Rassenti L, Kipps T, Croce CM (2008) Tcl1 functions as a transcriptional regulator and is directly involved in the pathogenesis of CLL. *Proc Natl Acad Sci USA* **105:** 19643-8

Perczel A, Hollósi M, Tusnády G, Fasman GD (1991) Convex constraint analysis: a natural deconvolution of circular dichroism curves of proteins. *Protein Eng* **4:** 669-79

Peters CJ (2005) Marburg and Ebola--arming ourselves against the deadly filoviruses. *The New England Journal of Medicine* **352:** 2571-3

Peters CJ, LeDuc JW (1999) An introduction to Ebola: the virus and the disease. *J Infect Dis* **179 Suppl 1:** ix-xvi

Peti W, Page R (2007) Strategies to maximize heterologous protein expression in Escherichia coli with minimal cost. *Protein Expression and Purification* **51:** 1-10

Rajender Reddy K, Modi MW, Pedder S (2002) Use of peginterferon alfa-2a (40 KD) (Pegasys) for the treatment of hepatitis C. *Advanced Drug Delivery Reviews* **54:** 571-86

Ramanathan M (1997) Flow cytometry applications in pharmacodynamics and drug delivery. *Pharm Res* **14:** 1106-14

Ramaswamy S, Ross K, Lander E, Golub T (2003) A molecular signature of metastasis in primary solid tumors. *Nat Genet* **33:** 49-54

Rashidzadeh H, Wang Y, Guo B (2000) Matrix effects on selectivities of poly(ethylene glycol)s for alkali metal ion complexation in matrix-assisted laser desorption/ionization. *Rapid Commun Mass Spectrom* **14:** 439-43

Rebollo A, Dumoutier L, Renauld JC, Zaballos A, Ayllón V, Martínez-A C (2000) Bcl-3 expression promotes cell survival following interleukin-4 deprivation and is controlled by AP1 and AP1-like transcription factors. *Mol Cell Biol* **20:** 3407-16

Reed J, Reed TA (1997) A set of constructed type spectra for the practical estimation of peptide secondary structure from circular dichroism. *Anal Biochem* **254**: 36-40

Regelson W, Parker G (1986) The routinization of intraperitoneal (intracavitary) chemotherapy and immunotherapy. *Cancer Invest* **4:** 29-42

Reichmann E, Schwarz H, Deiner EM, Leitner I, Eilers M, Berger J, Busslinger M, Beug H (1992) Activation of an inducible c-FosER fusion protein causes loss of epithelial polarity and triggers epithelial-fibroblastoid cell conversion. *Cell* **71:** 1103-16

Reid SP, Cardenas WB, Basler CF (2005) Homo-oligomerization facilitates the interferon-antagonist activity of the ebolavirus VP35 protein. *Virology* **341:** 179-89

Remy JS, Sirlin C, Vierling P, Behr JP (1994) Gene transfer with a series of lipophilic DNA-binding molecules. *Bioconjugate Chemistry* **5:** 647-54

Richard JP, Melikov K, Vives E, Ramos C, Verbeure B, Gait MJ, Chernomordik LV, Lebleu B (2003) Cell-penetrating peptides. A reevaluation of the mechanism of cellular uptake. *J Biol Chem* **278:** 585-90

Richardson SC, Wallom KL, Ferguson EL, Deacon SP, Davies MW, Powell AJ, Piper RC, Duncan R (2008) The use of fluorescence microscopy to define polymer localisation to the late endocytic compartments in cells that are targets for drug delivery. *J Control Release* **127:** 1-11

Rihova B, Riha I (1985) Immunological problems of polymer-bound drugs. *Critical Reviews in Therapeutic Drug Carrier Systems* **1:** 311-74

Ringsdorf H (1975) Structure and properties of pharmacologically active polymers. *Journal of Polymer Science: Polymer Symposia* **51**: 135-53

Rink H (1987) Solid-phase synthesis of protected peptide fragments using a trialkoxy-diphenyl-methylester resin. *Tetrahedron Letters* **28:** 3787-3790

Roberts MJ, Bentley MD, Harris JM (2002) Chemistry for peptide and protein PEGylation. *Advanced Drug Delivery Reviews* **54:** 459-76

Robinson BV, Sullivan FM, Borzelleca JF, Schwartz SL (1990) *PVP: A Critical Review of the Kinetics and Toxicology of Polyvinylpyrrolidone (Povidone)*: CRC Press

Rösler A, Klok HA, Hamley IW, Castelletto V, Mykhaylyk OO (2003) Nanoscale structure of poly(ethylene glycol) hybrid block copolymers containing amphiphilic beta-strand peptide sequences. *Biomacromolecules* **4:** 859-63

Rousselle P, Golbik R, van der Rest M, Aumailley M (1995) Structural requirement for cell adhesion to kalinin (laminin-5). *J Biol Chem* **270:** 13766-70

Sakakibara D, Sasaki A, Ikeya T, Hamatsu J, Hanashima T, Mishima M, Yoshimasu M, Hayashi N, Mikawa T, Wälchli M, Smith BO, Shirakawa M, Güntert P, Ito Y (2009) Protein structure determination in living cells by in-cell NMR spectroscopy. *Nature* **457:** 102-105

Sanz L, Garcia-Bermejo L, Blanco FJ, Kristensen P, Feijoo M, Suarez E, Blanco B, Alvarez-Vallina L (2003) A novel cell binding site in the coiled-coil domain of laminin involved in capillary morphogenesis. The *EMBO Journal* **22:** 1508-17

Satchi R, Connors TA, Duncan R (2001) PDEPT: polymer-directed enzyme prodrug therapy. I. HPMA copolymer-cathepsin B and PK1 as a model combination. *Br J Cancer* **85:** 1070-6

Sato AK, Viswanathan M, Kent RB, Wood CR (2006) Therapeutic peptides: technological advances driving peptides into development. *Current Opinion in Biotechnology* **17:** 638-42

Sato T, Saito H, Swensen J, Olifant A, Wood CR, Danner D, Sakamoto T, Takita K, Kasumi F, Miki Y (1992) The human prohibitin gene located on chromosome 17q21 is mutated in sporadic breast cancer. *Cancer Res* **52:** 1643-6

Sato T, Sakamoto T, Takita K, Saito H, Okui K, Nakamura Y (1993) The human prohibitin (PHB) gene family and its somatic mutations in human tumors. *Genomics* **17:** 762-4

Schenborn E, Oler J, Goiffon V, Balasubramaniam R, Bennett MJ, Aberle AM, Nantz MH, Malone RW (1995) Tfx™-50 reagent: A new transfection reagent for eukaryotic cells. *Promega Notes* **52:** 02-06

Seaman MNJ, Luzio JP (2001) *Lysosomes and other late compartments of the endocytic pathway*. New York: Oxford University Press

Seib FP, Jones AT, Duncan R (2006) Establishment of subcellular fractionation techniques to monitor the intracellular fate of polymer therapeutics I. Differential centrifugation fractionation B16F10 cells and use to study the intracellular fate of HPMA copolymer - doxorubicin. *Journal of Drug Targeting* **14:** 375-90

Seib FP, Jones AT, Duncan R (2007) Comparison of the endocytic properties of linear and branched PEIs, and cationic PAMAM dendrimers in B16f10 melanoma cells. *J Control Release* **117:** 291-300

Sela M, Fuchs S, Arnon R (1962) Studies on the chemical basis of the antigenicity of proteins. 5. Synthesis, characterization and immunogenicity of some multichain and linear polypeptides containing tyrosine. *Biochem J* **85:** 223-35

Selo I, Negroni L, Creminon C, Grassi J, Wal JM (1996) Preferential labeling of alpha-amino N-terminal groups in peptides by biotin: application to the detection of specific anti-peptide antibodies by enzyme immunoassays. *J Immunol Methods* **199:** 127-38

Seye CI, Knaapen MW, Daret D, Desgranges C, Herman AG, Kockx MM, Bult H (2004) 7-Ketocholesterol induces reversible cytochrome c release in smooth muscle cells in absence of mitochondrial swelling. *Cardiovasc Res* **64:** 144-53

Shafer D (2000) Reaction of Tris(2-carboxyethyl)phosphine (TCEP) with Maleimide and α-Haloacyl Groups: Anomalous Elution of TCEP by Gel Filtration. *Anal Biochem* **282:** 161-164

Shaulian E, Karin M (2002) AP-1 as a regulator of cell life and death. *Nature Cell Biology* **4:** E131-6

Shaulian E, Schreiber M, Piu F, Beeche M, Wagner EF, Karin M (2000) The mammalian UV response: c-Jun induction is required for exit from p53-imposed growth arrest. *Cell* **103:** 897-907

Shukla R, Thomas TP, Peters JL, Desai AM, Kukowska-Latallo J, Patri AK, Kotlyar A, Baker JR (2006) HER2 specific tumor targeting with dendrimer conjugated anti-HER2 mAb. *Bioconjugate Chemistry* **17:** 1109-15

Sieber P (1987) A new acid-labile anchor group for the solid-phase synthesis of C-terminal peptide amides by the Fmoc method. *Tetrahedron Letters* **28:** 2107-2110

Simeoni F, Morris MC, Heitz F, Divita G (2003) Insight into the mechanism of the peptide-based gene delivery system MPG: implications for delivery of siRNA into mammalian cells. *Nucleic Acids Res* **31:** 2717-24

Steinmetz MO, Stock A, Schulthess T, Landwehr R, Lustig A, Faix J, Gerisch G, Aebi U, Kammerer RA (1998) A distinct 14 residue site triggers coiled-coil formation in cortexillin I. The *EMBO Journal* **17:** 1883-91

Stevaux O, Dyson NJ (2002) A revised picture of the E2F transcriptional network and RB function. *Curr Opin Cell Biol* **14:** 684-91

Stroher U, West E, Bugany H, Klenk HD, Schnittler HJ, Feldmann H (2001) Infection and activation of monocytes by Marburg and Ebola viruses. *J Virol* **75:** 11025-33

Studier FW, Rosenberg AH, Dunn JJ, Dubendorff JW (1990) Use of T7 RNA polymerase to direct expression of cloned genes. *Meth Enzymol* **185:** 60-89

Suzuki K, Doi T, Imanishi T, Kodama T, Tanaka T (1997) The conformation of the alpha-helical coiled coil domain of macrophage scavenger receptor is pH dependent. *Biochemistry* **36:** 15140-6

Szabowski A, Maas-Szabowski N, Andrecht S, Kolbus A, Schorpp-Kistner M, Fusenig NE, Angel P (2000) c-Jun and JunB antagonistically control cytokine-regulated mesenchymal-epidermal interaction in skin. *Cell* **103:** 745-55

Takada A, Robison C, Goto H, Sanchez A, Murti KG, Whitt MA, Kawaoka Y (1997) A system for functional analysis of Ebola virus glycoprotein. *Proc Natl Acad Sci USA* **94:** 14764-9

Takeuchi K, Wagner G (2006) NMR studies of protein interactions. *Current Opinion in Structural Biology* **16:** 109-117

Tam J, Lu Y (1995) Coupling difficulty associated with interchain clustering and phase transition in solid phase peptide synthesis. *Journal of the American Chemical Society* **117:** 12058-12063

Tam JP, Xu J, Eom KD (2001) Methods and strategies of peptide ligation. *Biopolymers* **60:** 194-205

Tang A, Wang C, Stewart RJ, Kopecek J (2001) The coiled coils in the design of protein-based constructs: hybrid hydrogels and epitope displays. *J Control Release* **72:** 57-70

Tom I, Lee V, Dumas M, Madanat M, Ouyang J, Severs J, Andersen J, Buxton JM, Whelan JP, Pan CQ (2007) Reproducible production of a PEGylated dual-acting peptide for diabetes. *American Association of Pharmaceutical Scientists Journal* **9**: 227-234

Toft DJ, Rosenberg SB, Bergers G, Volpert O, Linzer DI (2001) Reactivation of proliferin gene expression is associated with increased angiogenesis in a cell culture model of fibrosarcoma tumor progression. *Proc Natl Acad Sci USA* **98:** 13055-9

Tunggal P, Smyth N, Paulsson M, Ott MC (2000) Laminins: structure and genetic regulation. *Microsc Res Tech* **51:** 214-27

Ungchusak K, Auewarakul P, Dowell SF, Kitphati R, Auwanit W, Puthavathana P, Uiprasertkul M, Boonnak K, Pittayawonganon C, Cox NJ, Zaki SR, Thawatsupha P, Chittaganpitch M, Khontong R, Simmerman JM, Chunsutthiwat S (2005) Probable person-to-person transmission of avian influenza A (H5N1). *The New England Journal of Medicine* **352:** 333-40

Valeur E, Bradley M (2009) Amide bond formation: beyond the myth of coupling reagents. *Chemical Society Reviews* **38:** 606-31

van Dam H, Castellazzi M (2001) Distinct roles of Jun : Fos and Jun : ATF dimers in oncogenesis. *Oncogene* **20:** 2453-64

Vandermeulen GW, Hinderberger D, Xu H, Sheiko SS, Jeschke G, Klok HA (2004) Structure and dynamics of self-assembled poly(ethylene glycol) based coiled-coil nano-objects. *Chemphyschem* **5:** 488-94

Vandermeulen GWM, Tziatzios C, Duncan R, Klok H-A (2005) PEG-Based Hybrid Block Copolymers Containing α-Helical Coiled Coil Peptide Sequences: Control of Self-Assembly and Preliminary Biological Evaluation *Macromolecules* **38:** 761-769

Vandermeulen GWM, Tziatzios C, Klok H-A (2003) Reversible Self-Organisation of Poly(ethylene glycol)-Based Hybrid Block Copolymers Mediated by a De Novo Four Stranded α-Helical Coiled Coil Motif. *Macromolecules* **36:** 4107-4114

Vellodi A (2005) Lysosomal storage disorders. *Br J Haematol* **128:** 413-31
Veronese FM, Harris JM (2008) Peptide and protein PEGylation III: advances in chemistry and clinical applications. *Advanced Drug Delivery Reviews* **60:** 1-2

Villinger F, Rollin PE, Brar SS, Chikkala NF, Winter J, Sundstrom JB, Zaki SR, Swanepoel R, Ansari AA, Peters CJ (1999) Markedly elevated levels of interferon (IFN)-gamma, IFN-alpha, interleukin (IL)-2, IL-10, and tumor necrosis factor-alpha associated with fatal Ebola virus infection. *J Infect Dis* **179 Suppl 1:** S188-91

Vogt PK (2002) Fortuitous convergences: the beginnings of JUN. *Nat Rev Cancer* **2:** 465-9

Wagstaff KM, Jans DA (2006) Protein transduction: cell penetrating peptides and their therapeutic applications. *Curr Med Chem* **13:** 1371-87

Wahl-Jensen VM, Afanasieva TA, Seebach J, Ströher U, Feldmann H, Schnittler HJ (2005) Effects of Ebola virus glycoproteins on endothelial cell activation and barrier function. *J Virol* **79:** 10442-50

Wang H, Birkenbach M, Hart J (2000) Expression of Jun family members in human colorectal adenocarcinoma. *Carcinogenesis* **21:** 1313-7

Wang S, Nath N, Fusaro G, Chellappan S (1999) Rb and prohibitin target distinct regions of E2F1 for repression and respond to different upstream signals. *Mol Cell Biol* **19:** 7447-60

Wang YS, Youngster S, Grace M, Bausch J, Bordens R, Wyss DF (2002) Structural and biological characterization of pegylated recombinant interferon alpha-2b and its therapeutic implications. *Advanced Drug Delivery Deviews* **54:** 547-70

Watanabe S, Takada A, Watanabe T, Ito H, Kida H, Kawaoka Y (2000) Functional importance of the coiled-coil of the Ebola virus glycoprotein. *J Virol* **74:** 10194-201

Watts C (1985) Rapid endocytosis of the transferrin receptor in the absence of bound transferrin. *J Cell Biol* **100:** 633-7

Weidner S, Kuhn G, Friedrich J (1998) Infrared-matrix-assisted laser desorption/ionization and infrared-laser desorption/ionization investigations of synthetic polymers. *Rapid Commun Mass Spectrom* **12**: 1373-81

Weill CO, Biri S, Adib´ A, Erbacher P (2008) A practical approach for intracellular protein delivery. *Cytotechnology* **56:** 41-8

Weissenhorn W, Carfi A, Lee KH, Skehel JJ, Wiley DC (1998) Crystal structure of the Ebola virus membrane fusion subunit, GP2, from the envelope glycoprotein ectodomain. *Mol Cell* **2:** 605-16

Whitfield J, Neame SJ, Paquet L, Bernard O, Ham J (2001) Dominant-negative c-Jun promotes neuronal survival by reducing BIM expression and inhibiting mitochondrial cytochrome c release. *Neuron* **29:** 629-43

Whittal RM, Schriemer DC, Li L (1997) Time-lag focusing MALDI time-of-flight mass spectrometry for polymer characterization: oligomer resolution, mass accuracy, and average weight information. *Anal Chem* **69:** 2734-41

WHO. 2008. *World Health Statistics*. World Health Organisation Press, Geneva.

WHO. 2006. *Fact Sheet No. 297*. World Health Organisation Press, Geneva.

Woghiren C, Sharma B, Stein S (1993) Protected thiol-polyethylene glycol: a new activated polymer for reversible protein modification. *Bioconjugate Chemistry* **4:** 314-8

Wolf E, Kim PS, Berger B (1997) MultiCoil: a program for predicting two- and three-stranded coiled coils. *Protein Sci* **6:** 1179-89

Wool-Lewis RJ, Bates P (1998) Characterization of Ebola virus entry by using pseudotyped viruses: identification of receptor-deficient cell lines. *J Virol* **72:** 3155-60

Woolfson DN (2005) The design of coiled-coil structures and assemblies. *Adv Protein Chem* **70:** 79-112

Xie J, Guo Q (2005) PAR-4 is involved in regulation of beta-secretase cleavage of the Alzheimer amyloid precursor protein. *J Biol Chem* **280:** 13824-32

Yang ZY, Duckers HJ, Sullivan NJ, Sanchez A, Nabel EG, Nabel GJ (2000) Identification of the Ebola virus glycoprotein as the main viral determinant of vascular cell cytotoxicity and injury. *Nat Med* **6:** 886-9

Yao S, Brickner M, Pares-Matos EI, Chmielewski J (1998) Uncoiling c-Jun coiled coils: inhibitory effects of truncated Fos peptides on Jun dimerization and DNA binding in vitro. *Biopolymers* **47:** 277-83

Yokoyama M, Miyauchi M, Yamada N, Okano T, Sakurai Y, Kataoka K, Inoue S (1990) Polymer micelles as novel drug carrier: adriamycin-conjugated poly (ethylene glycol)-poly (aspartic acid) block copolymer. *J Control Release* **11:** 269-278

Yoo C, Suckau D, Sauerland V, Ronk M, Ma M (2009) Toward top-down determination of PEGylation site using MALDI in-source decay MS analysis. *J Am Soc Mass Spectrom* **20:** 326-33

Zalipsky S, Seltzer R, Menon-Rudolph S (1992) Evaluation of a new reagent for covalent attachment of polyethylene glycol to proteins. *Biotechnol Appl Biochem* **15:** 100-14

Zenz R, Scheuch H, Martin P, Frank C, Eferl R, Kenner L, Sibilia M, Wagner EF (2003) c-Jun regulates eyelid closure and skin tumor development through EGFR signaling. *Dev Cell* **4:** 879-89

Zgurskaya HI, Nikaido H (1999) Bypassing the periplasm: reconstitution of the AcrAB multidrug efflux pump of Escherichia coli. *Proc Natl Acad Sci U S A* **96:** 7190-5

Zhang T, Kee WH, Seow KT, Fung W, Cao X (2000) The coiled-coil domain of Stat3 is essential for its SH2 domain-mediated receptor binding and subsequent activation induced by epidermal growth factor and interleukin-6. *Mol Cell Biol* **20:** 7132-9

Zhou M, Veenstra T (2008) Mass spectrometry: m/z 1983-2008. *BioTechniques* **44:** 667-8, 670

Zhou X, Huang L (1994) DNA transfection mediated by cationic liposomes containing lipopolylysine: characterization and mechanism of action. *Biochimica et Biophysica Acta* **1189:** 195-203

Zuiderweg ER (2002) Mapping protein-protein interactions in solution by NMR spectroscopy. *Biochemistry* **41:** 1-7

WEB SITES

All checked for accessibility on 29th May 2009:

Cancer Research UK Web Site. Available at http://info.cancerresearchuk.org/cancerstats/incidence/commoncancers/?a=5441

ExPASy proteomics server of the Swiss Institute of Bioinformatics. Available at http://www.expasy.org

Herceptin Web Site. Available at http://www.herceptin.com

Innovagen Peptide Property Calculator Web Site. Available at http://www.innovagen.se/custom-peptide-synthesis/peptide-property-calculator/peptide-property-calculator.asp

Invitrogen Molecular Probes The Handbook Web Site. Available at http://www.invitrogen.com/site/us/en/home/References/Molecular-Probes-The-Handbook.html

Invitrogen Molecular Probes Web Site. Available at http://www.invitrogen.com

COILS Server. Available at http://www.ch.embnet.org/software/COILS_form.html

Invitrogen OligoPerfect™ Custom Primer Designer Web Site. Available at https://tools.invitrogen.com/content.cfm?pageid=9716

LearnCoil-VMF Server. Available at http://groups.csail.mit.edu/cb/learncoil-vmf/cgi-bin/vmf.cgi

MultiCoil Server. Available at http://groups.csail.mit.edu/cb/multicoil/cgi-bin/multicoil.cgi

National Institute of Health Web Site. Available at http://nihroadmap.nih.gov/nanomedicine

Nektar Therapeutics Web Site. Available at http://www.nektar.com

New England BioLabs Web Site. Available at http://www.neb.com

Nobel Foundation Web Site. Available at http://nobelprize.org/nobel_prizes/lists/all

NOF Corporation Web Site. Available at http://www.peg-drug.com

Paircoil Server. Available at http://groups.csail.mit.edu/cb/paircoil/cgi-bin/paircoil.cgi

Paicoil2 Server. Available at http://groups.csail.mit.edu/cb/paircoil2/paircoil2.html

Rapp-Polymere Web Site. Available at http://www.rapp-polymere.com

Stratagene Web Site. Available at http://www.stratagene.com

The Adventure of Nano Web Site. Available at http://www.nanonet.go.jp/english/kids/video

Thermo Scientific Website. Available at http://www.piercenet.com

Appendix I

Table I Summary of peptide sequences and molecular weights for the peptides and mPEG-conjugates synthesised in this study.

Peptide	Sequence abcdefgabcdefgabcdefgabcdefgabcdef	Length (residues)	Molecular Weight[#*] (g mol^{-1})
E2F1 and PHB derived peptides			
$Phb_{185-214}$	**AKQVAQQEAERARFVVEKAEQQKKAAIISA**	30	3368
$Phb_{Y185-214}$	**YAKQVAQQEAERARFVVEKAEQQKKAAIISA**	31	3531
$Phb_{CY185-214}$	**CYAKQVAQQEAERARFVVEKAEQQKKAAIISA**	32	3634
mPEG-$Phb_{CY185-214}$	mPEG-**CYAKQVAQQEAERARFVVEKAEQQKKAAIISA**	32	9322
E2F1a[†]	**YPGKTPSQEVTSEEENRA**	18	2063
E2F1b[†]	**YLTTDPSQSLLSLEQEGG**	18	1979
c-Jun and c-Fos derived peptides			
c-Jun[†]	**ASIARLEEKVKTLKAQNYELASTANMLREQVAQLGA**	36	3988
$FosW_C$	**CASLDELQAEIEQLEERNYALRKEIEDLQKQLEKLGA**	37	4359
mPEG-$FosW_C$	mPEG-**CASLDELQAEIEQLEERNYALRKEIEDLQKQLEKLGA**	37	10047

[†] Peptides that represent target domains for use in *in-vitro* binding assays.

[#] Theoretical molecular weight based upon the average isotopic abundance of naturally occurring elements.

[*] For mPEG-conjugates the molecular weight shown is Mw.

N.B. Apolar residues in positions "a" and "d" are shown in bold type font.

Table I Summary of peptide sequences and molecular weights for the peptides and mPEG-conjugates synthesised in this study.

Peptide	Sequence abcdefgabcdefgabcdefgabcdefgabcdefgab	Length (residues)	Molecular Weight[#*] ($g\ mol^{-1}$)
EbVP35 derived peptides			
$EbVP35_{82\text{-}119}$	SFEEVVQTLASLATVVQQQTIASESLEQRITSLENGLK	38	4190
$EbVP35_{CY88\text{-}119}$	CYQTLASLATVVQQQTIASESLEQRITSLENGLK	34	3697
EbGP2 derived peptides	abcdefg abcdefgabcdefgabcdefgabcdef		
$EbGP2_{609\text{-}630}$[*]	CIEPHDWTKNITDKIDQIIHDF	22	2723
mPEG-$EbGP2_{609\text{-}630}$	mPEG-CIEPHDWTKNITDKIDQIIHDF	22	8411
$EbGP2_{CY557\text{-}589}$	CYGLRQLANETTQALQLFLRATTELRTFSILNRKA	35	4083
$EbGP2_{CY557\text{-}595}$	CYGLRQLANETTQALQLFLRATTELRTFSILNRKAIDFLLQ	41	4813
$EbGP2_{CY566\text{-}589}$	CYTQALQLFLRATTELRTFSILNRKA	26	3100
mPEG-$EbGP2_{CY566\text{-}589}$	mPEG-CYTQALQLFLRATTELRTFSILNRKA	26	8788

[#] Theoretical molecular weight based upon the average isotopic abundance of naturally occurring elements.

[*] For mPEG-conjugates the molecular weight shown is Mw.

N.B. Apolar residues in positions "a" and "d" are shown in bold type font ([*]heptad positions are not assigned for peptide $EbGP2_{609\text{-}630}$ as it is an α-helical peptide, not strictly a coiled-coil motif).